

Alterations in expression, proteolysis and intracellular localizations of clusterin in esophageal squamous cell carcinoma

Hong-Zhi He, Zhen-Mei Song, Kun Wang, Liang-Hong Teng, Fang Liu, You-Sheng Mao, Ning Lu, Shang-Zhong Zhang, Min Wu, Xiao-Hang Zhao

Hong-Zhi He, Liang-Hong Teng, Fang Liu, You-Sheng Mao, Ning Lu, Min Wu, Xiao-Hang Zhao, National Laboratory of Molecular Oncology, Department of Thoracic Surgery and Department of Pathology, Cancer Institute and Hospital, Chinese Academy of Medical Sciences and Peking Union Medical College, Beijing 100021, China

Zhen-Mei Song, Shang-Zhong Zhang, Qilu Hospital, School of Medicine, Shandong University, Qindao 250012, Shandong Province, China

Kun Wang, Xiao-Hang Zhao, Beijing Yanjing Hospital, Beijing 100037, China

Supported by National Natural Science Foundation, No.30225045, No.39990570, No.30171049 and No.30370713, and National High Tech and Major State Basic R & D Program of China, No.G1998051205 and No.2001AA227091

Co-first-authors: Hong-Zhi He and Zhen-Mei Song

Correspondence to: Xiao-Hang Zhao, M.D., Ph.D. National Laboratory of Molecular Oncology, Cancer Institute and Hospital, Chinese Academy of Medical Sciences and Peking Union Medical College, Beijing 100021, China. zhaoxh@pubem.cicams.ac.cn

Telephone: +86-10-67709015 **Fax:** +86-10-67709015

Received: 2004-01-09 **Accepted:** 2004-02-24

Abstract

AIM: To investigate biogenesis and intracellular localizations of clusterin to elucidate the potential molecular mechanisms implicated in tumorigenesis of esophageal mucosa.

METHODS: Semi-quantitative RT-PCR for multi-region alteration analysis, Western blot for different transcriptional forms and immunohistochemical staining for intracellular localizations of clusterin were carried out in both tissues and cell lines of ESCC.

RESULTS: The N-terminal deletions of the clusterin gene and the appearance of a 50-53 ku nuclear clusterin, an uncleaved, nonglycosylated, and disulfide-linked isoform, were the major alterations in cancer cells of esophagus. Naturally the 40 ku clusterin was located in the connective tissue of the lamina *propria* of epithelial mucosa and right under the basal membrane of epithelia, but it was disappeared in stromal mucosa of esophagus and the pre-matured clusterin was found positive in cancerous epithelia.

CONCLUSION: The N-terminal deletion of clusterin may be essential for its alterations of biogenesis in ESCC.

He HZ, Song ZM, Wang K, Teng LH, Liu F, Mao YS, Lu N, Zhang SZ, Wu M, Zhao XH. Alterations in expression, proteolysis and intracellular localizations of clusterin in esophageal squamous cell carcinoma. *World J Gastroenterol* 2004; 10(10): 1387-1391
<http://www.wjgnet.com/1007-9327/10/1387.asp>

INTRODUCTION

Clusterin, a 70-80 ku heterodimeric, disulfide-linked glycoprotein is expressed in a wide variety of tissues and secreted in all

human fluids^[1-3]. Human clusterin is encoded by a single copy gene located on chromosome 8p12 and 8p21 with nine exons and eight introns, spanning approximately 17 kb^[4,5]. Clusterin gene has a single functional promoter and a single transcript mRNA, 1.6 kb in length, containing an N-terminal hydrophobic leader sequence. There are two forms of clusterin: one set of proteins is directly for secreted into humour, and the other forms are expressed in the cytoplasm and nucleus. The secretory form of the clusterin protein is produced by translation on membrane-bound ribosomes from the first AUG codon of the full-length clusterin mRNA and is targeted to the endoplasmic reticulum (ER) by an initial leader peptide. Subsequently, this -60 ku pre-clusterin protein containing 427 amino acids has to be further glycosylated in the ER and proteolytically cleaved between R205 and S206 into a mature protein discrete α - and β -chains, held together by disulfide bonds in Golgi^[1,6]. External secretory clusterin is a 70-80 ku heterodimeric glycoprotein that appears as a -40 ku α - and β -subunits smear by sodium dodecyl sulfate-polyacrylamide gel (SDS-PAGE) electrophoresis under reducing conditions^[7-9]. Recent data suggest that secretory clusterin acts as a molecular chaperone to scavenge denatured proteins and cellular debris outside cells following specific stress-induced injury such as heat shock^[10-14].

Clusterin has been found highly conserved and implicated in a variety of biological processes including lipid transport, epithelial cell differentiation, transformation, and regulation of apoptosis in numerous models of epithelial cells during hormone ablation^[15-20]. It is induced during regression of most hormone-dependent secretory epithelial cells as one of the most potent proteins of the rat ventral prostate or mammary gland^[9,20-23]. Overexpression of secretory clusterin in human cancer cells caused drug resistance and protection against certain cytotoxic agents that induce apoptosis^[24-26]. In human prostate cancer cells, overexpression of clusterin provides protection against TNF α -induced cell death and oligonucleotide directed antisense inhibition enhances spontaneous cell death in untreated cultures^[24]. Clusterin may have a cytoprotective role in epithelial cell death. There are significant alterations in the biogenesis of clusterin during apoptosis, which lead to the appearance of a 50-53 ku uncleaved, nonglycosylated, disulfide-linked isoform that accumulates in the nucleus of MCF-7 cells^[20]. Nuclear clusterin synthesis is a product of alternative splicing, in which the exon II, containing the first AUG and encoding the ER-targeting peptide, was omitted. This "death" form of the clusterin protein was proposed to be synthesized from a second in-frame AUG codon in exon III as translation start site. The short mRNA produces the 49 ku precursor nuclear clusterin which overexpression acts as a pro-death signal, inhibiting cell growth and survival^[27-29].

Clusterin mRNA and protein was recently shown to be down-regulated in esophageal squamous cell carcinoma (ESCC), the major malignant tumor occurred in epithelium of esophagus^[7]. Thus, to the author's knowledge, it is unclear whether alternative splicing clusterin is also involved and the possible roles of clusterin in process of the ESCC. We additionally studied, by multi-regional RT-PCR, Western blot

and immunohistochemical staining, the levels of expression and cellular distribution of clusterin in both tissues and cell lines of human ESCC.

MATERIALS AND METHODS

Tissue sample

The esophageal specimens were obtained from patients diagnosed with ESCC by the pathologists that assisted in our previous work in Cancer Hospital of Chinese Academy of Medical Sciences and Beijing Yanjing Hospital^[7]. The study was approved by the Institutional Review Board. Briefly, immediately the specimens were dissected manually into several aliquots (about 0.3 cm³ in size), quickly frozen in the liquid nitrogen and, then stored at -80 °C until analysis. Carcinoma tissues were obtained from poorly, moderate, and well differentiated ESCC. The corresponding normal tissues were obtained from the distant edge of dissected esophagus. For immunohistochemical (IHC) staining, tissues were fixed in 700 mL/L ethanol or 40 mg/L neutral formalin and embedded in paraffin.

Cell lines

Human ESCC cell lines, EC0156 and EC0132, were generated in our laboratory from ESCC tissues.

RNA isolation and semi-quantative RT-PCR

Total RNAs were isolated from ESCC specimens and cell lines with RNeasy MinElute cleanup kit (QIAGEN, Valencia, CA) according to the manufacture's instruction. RNA quality was assessed on agarose gel electrophoresis and spectrophotometric analysis. Reverse transcription reactions were performed on 5 µg of total RNAs using SuperScript™ First-Strand synthesis for RT-PCR II kit (Invitrogen, Carlsbad, CA) at 42 °C for 80 min, and 0.5-1 µg aliquots of the cDNA were then subjected to RT-PCR. Based on probable splice sites, the following primers were used to investigate different regions whether alternative splice forms or deleted fragments of clusterin could be found (Table 1).

The PCR step was performed using Taq DNA polymerase (Invitrogen, Carlsbad, CA). As an internal control, *GAPDH* was amplified to ensure cDNA quality and quantity for each RT-PCR reactions. The amplified multiproducts were analyzed on 12-20 g/L agarose gels. Each PCR reaction was down triplicate.

Protein extraction and western blot

The tumor tissues and cell lines were lysed in the lysis buffer (50mmol/L Tris-HCl, pH 7.4, 150mmol/L NaCl, 10 g/L TritonX-100, 1 g/L SDS, 1 mmol/L AEBSF, 20 µg/mL Approtinin and 20 µg/mL Leupeptin) for soluble protein extraction or in the extraction/labeling buffer (BD Biosciences, San Jose, CA) for whole

proteins extraction, and then placed on ice for 20 min. Then they were sonicated and centrifuged at 12 000 g at 4 °C for 30 min. The supernatants were transferred and the protein concentration was measured by Bradford method^[30].

Equal amount of proteins were separated on 100 g/L of SDS-PAGE gels and transferred to polyvinylidene difluoride (PVDF) membranes. After being blocked with 10 g/L non-fat milk, the membranes were incubated with anti-clusterin monoclonal antibody B-5 (sc-5289, Santa Cruz Biotechnology, Santa Cruz, CA) (1:1 000 dilution) at 4 °C overnight. After washing for 3 times, the membranes were incubated with rabbit anti-mouse IgG at room temperature for 1 h. The signals were developed with the ECL kit (Amersham Pharmacia Biotechnology, Piscataway, NJ) and using anti-α-tubulin antibody (Santa Cruz Biotechnology, Santa Cruz, CA) as an internal loading control.

Rabbit anti-human clusterin polyclonal H-330 antibody (sc-8354, Santa Cruz Biotechnology, Santa Cruz, CA) was used to detect the truncated forms of clusterin in whole extracts from EC0156 and EC0132 cells and tissues. A 1:500 dilution of primary H-330 antibody was used, followed by a 1:3 000 dilution of horseradish peroxidase-conjugated anti-rabbit secondary antibody (Santa Cruz Biotechnology, Santa Cruz, CA).

Immunohistochemical analysis

The streptavidin-peroxidase method was used for the immunohistochemical staining of clusterin. Briefly, after deparaffinization in xylene and rehydration in grade ethanol, endogenous peroxidase activity was blocked by incubation with 30 mL/L hydrogen peroxide for 10 min. Tissue sections were then heated at 100 °C in citrate buffer (10 mmol/L, pH 6.0) to retrieve antigens for 10 min. After being incubated with anti-human clusterin monoclonal/polyclonal antibodies, clusterin was visualized by adding biotinylated secondary antibody and streptavidin-horseradish peroxidase (Zymed Laboratories, South San Francisco, CA). Counterstaining was performed with hematoxylin and 3,3'-diaminobenzidine used as a chromogen. Negative controls, made by PBS excluding mono- or polyclonal anti-human clusterin antibodies from the reaction, showed no specific staining and. Experiments performed using polyclonal and monoclonal anti-human clusterin antibodies from the same commercial source gave the same pattern of specific distributions. Cover slips were mounted with Eukitt (O. Kindler GmbH & Co., Freiburg, Germany).

RESULTS

N-terminal deletions of the clusterin transcription in ESCC

To detect the alterations of clusterin expression, a multi-region cDNA fragments of ESCC were analyzed by semi-quantitative

Table 1 Primers and PCR reactions for multi-region amplifications of clusterin

Amplified fragments (bp)	Sense primers	Antisense primers	PCR conditions
1-1 350	5'-CCGGATCCTTATGATGA AGACTCTGCTGCTG-3'	5'-GCCTCGAGTCACTCC CGCTGCTTTTGTG-3'	95 °C for 40 s, 62 °C for 40 s, and 72 °C for 90 s
1-1 056	5'-CCGGATCCTTATGATG AAGACTCTGCTGCTG-3'	5'-GTGTTGAGCATCTTCC ACTG-3'	95 °C for 30 s, 60 °C for 40 s, and 72 °C for 60 s
1-321	5'-CCGGATCCTTATGATGA AGACTCTGCTGCTG-3'	5'-CATCATGGTCTCATT GCACAC-3'	95 °C for 30 s, 56 °C for 30 s, and 72 °C for 30 s
437-1 056	5'-GAGCTCGCCCTTCTACTTCT-3'	5'-GTGTTGAGCATCTTCCACTG-3'	95 °C for 30 s, 56 °C for 30 s, and 72 °C for 30 s
437-1 350	5'-GAGCTCGCCCTTCTACTTCT-3'	5'-GCCTCGAGTCACTC CCGCTGCTTTTGTG-3'	95 °C for 40 s, 60 °C for 40 s, and 72 °C for 60 s
1 120-1 350	5'-ACCTCACGCAAGGC GAAGACC-3'	5'-TCTCACTCCTCCCGGTGCTT-3'	95 °C for 30 s, 56 °C for 25 s, and 72 °C for 25 s
GAPDH	5'-ACCACAGTCCATGCCATCAC-3'	5'-TCCACCACCCTGTTGCTGTA-3'	

RT-PCR (Figure 1). The clusterin cDNA derived from the total RNA of both ESCC tissues and their matched dissected normal esophageal mucosa. The results of various fragments are shown in Figure 2. Comparing with the tumor matched normal epithelia of esophagus, the expressions of full-length and N-terminal fragment (1-320 bp) of clusterin were deleted obviously, however, there were no differences between the middle (437-1 056 bp) and C-terminal fragments (1 120-1 350 bp). By this approach, additionally using the primer containing the start codon of clusterin and the -3' end of the middle fragment obtained the same result with the one from full-length (1-1 056 bp), and also found the same expression level between the cancer tissue and normal epithelia from 437 to the end of clusterin (437-1 350 bp). The exceptional transcription area of clusterin was narrowed in the region of 1-437 bp, which contained the abnormal translation start site of the "death" form clusterin (nuclear clusterin) and omitted the region encoding the endoplasmic reticulum (ER)-targeting peptide of clusterin protein. These results indicated that clusterin was truncated at 5' end of gene.

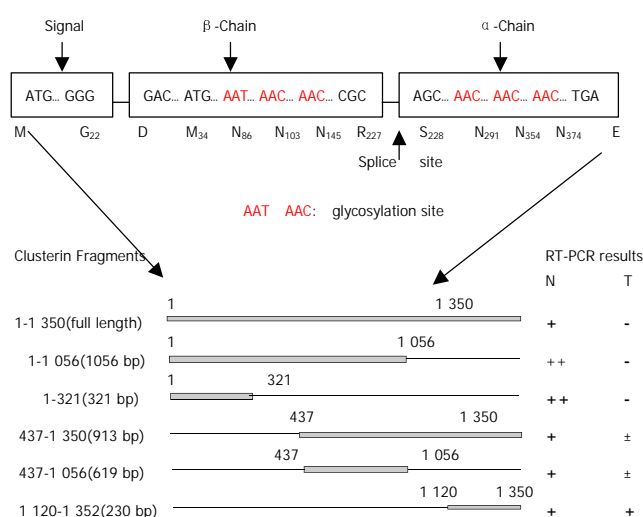


Figure 1 Schematic diagram of analyzed fragments of clusterin. A: structural map of the human clusterin protein. Letters and boxes signify the following: ER-targeting signal, endoplasmic reticulum-targeting hydrophobic leader peptide; splice site, α/β -cleavage site (amino acid 205 and 206) of cytoplasmic -60 ku pre-secreted clusterin which was glycosylated and cleaved into α and β chains to form an 80 ku matured secretory clusterin protein; rectangles, hydrophobic leader peptide (N-terminal 66 bp encode aa M1 to G22, 22 aa), β -chain (5' end) and α -chain (3' end); Red letters, the glycosylation sites. B: Schematic diagram of analyzed fragments of clusterin and their RT-PCR results.

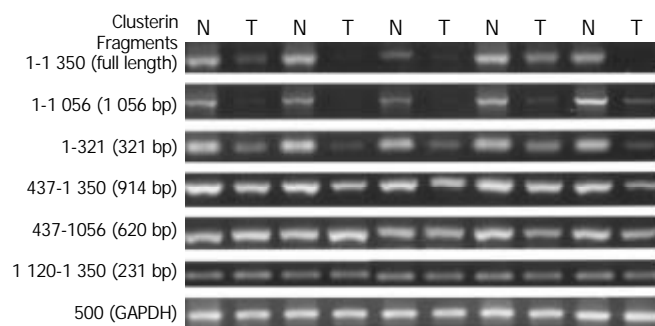


Figure 2 N-terminal truncated clusterin was analyzed by RT-PCR. GAPDH was used as internal control. N: tumor matched far edge normal esophageal mucosa. T: ESCC specimens. The expression of full-length and different of clusterin fragments

were analyzed comparing with the tumor matched normal esophageal mucosa. The truncated region was narrowed down at the 5' end of clusterin (1-437 bp).

Down-regulation of nuclear clusterin and secreted clusterin in ESCC

According to the results of RT-PCR, anti-clusterin antibodies were used to detect the expression of clusterin protein both in the tissues and cell lines of ESCC (Figure 3). The predominant form of clusterin in tumor tissues was the secreted heterodimeric glycoprotein with MW of 75-80 ku (37-40 ku smear in reducing SDS-PAGE), which was down-regulated in ESCC tissues compared with the normal epithelia of esophagus (100%, 21/21), but was absent in the ESCC cell lines (EC0516 and EC0132). The results confirmed our previous data that the clusterin gene is generally down-regulated in esophageal cancer^[7]. Meanwhile, an about 50 ku nuclear clusterin was appeared in both the ESCC tissues (100%, 21/21) and cell lines (100%, 2/2), and sometimes in normal epithelia. It was highly expressed in the tumor tissues and cells. Additionally, an about 35 ku band was detected by anti-clusterin antibody H-330 in the EC0132 cell line. Under these experimental conditions, it must be noticed that, as shown in Figure 3, the monoclonal antibody used (Clusterin- β , B-5 from Santa Cruz Biotechnology, Santa Cruz, CA) might react with the carboxy terminus of clusterin β chain of human origin and not react with uncleaved nuclear clusterin. However, the polyclonal antibody used (Clusterin- α/β , H-330 from Santa Cruz Biotechnology Inc., Santa Cruz, CA) recognized the major part of clusterin from 120 to 449 amino acids at the carboxy terminus of clusterin- α/β chains, including the 60 ku precursor (cytoplasmic clusterin), from which all clusterin isoforms are supposed to be derived, uncleaved nuclear clusterin (-50 ku) and the matured secreted clusterin (-37-40 ku, cleaved in $-\alpha$ and $-\beta$ chains).

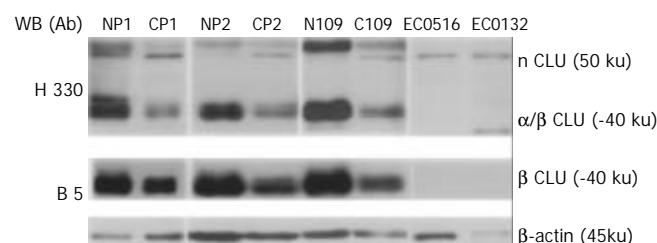


Figure 3 Western blot analysis of expression of multiple forms of clusterin in ESCC. nCLU: the nonglycosylated uncleaved nuclear clusterin; α/β CLU: cleaved and glycosylated secreted clusterin protein; β CLU: cleaved and glycosylated clusterin β chain; B-5: monoclonal antibody (Santa Cruz Biotechnology, Santa Cruz, CA) reacted with the C-terminus of clusterin- β of human origin and did not react with the nuclear clusterin; H-330: polyclonal antibody (Santa Cruz Biotechnology, Santa Cruz, CA) recognized the major part of clusterin from 120 to 449 aa at the C-terminus of clusterin- α/β chains including uncleaved nuclear clusterin (-50 ku) and the matured secreted clusterin (-37-40 ku); Np: pooled normal esophageal mucosa from 10 cases; Cp: pooled ESCC tumor tissues from 10 cases; N109: normal esophageal mucosa from a single individual; C109: ESCC tumor tissue from a single individual. β -actin was used as loading control.

Intracellular localizations of clusterin in ESCC

Immunohistochemistry analysis was performed in the tissue sections of ESCC specimen and matched normal counterparts using the same antibody (B 5, Santa Cruz Biotechnology, Santa Cruz, CA) as previously used for Western blot analysis (Figure 4). In normal esophageal mucosa, clusterin protein localized prevalently to the stroma of esophageal mucosa, while the squamous epithelial cells and basal lamina were negative. Very

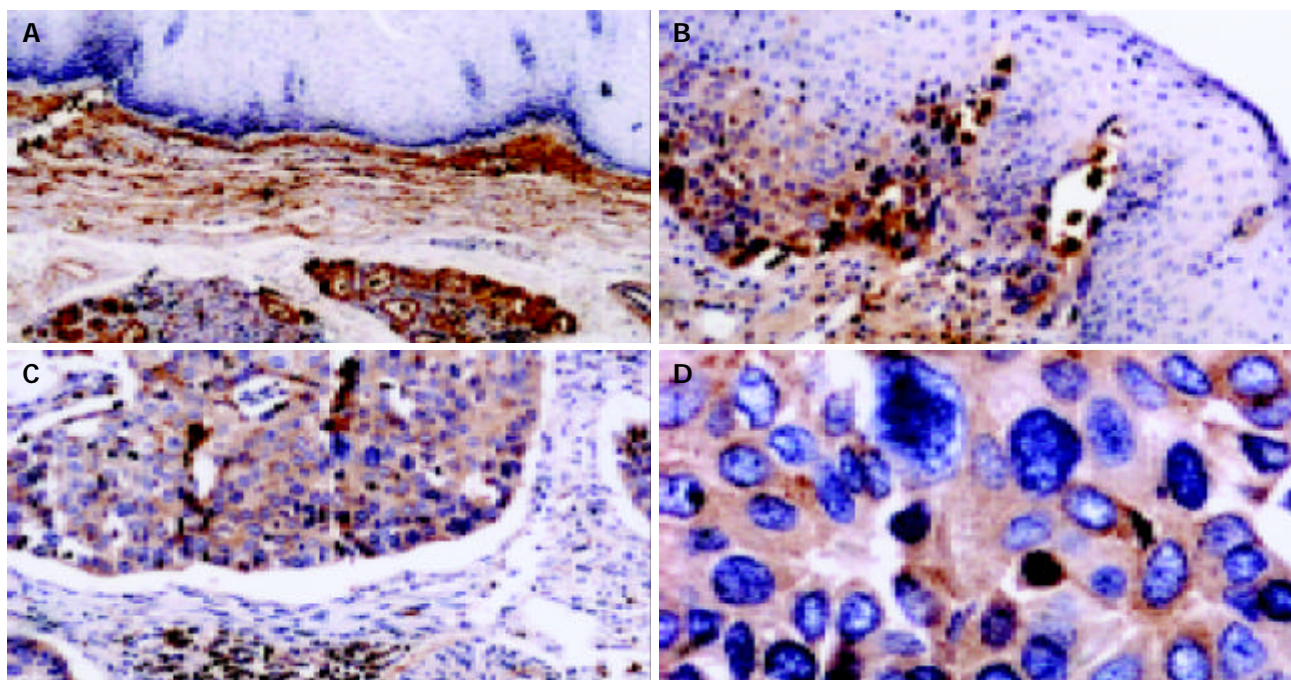


Figure 4 Detection of clusterin protein in tissue sections of human ESCC by immunohistochemistry. In normal esophageal mucosa, the expression of clusterin in squamous epithelial cells and basal lamina was negative, while clusterin immunostaining was visualized obviously in the stroma of epithelial mucosa (A, 100 \times); clusterin was positive in middle dysplasia, while the vast majority of stromal cells were negative in normal squamous epithelia of esophagus (B, 100 \times); clusterin was strong positive in the remnants of stromal extracellular matrix invaded by tumor cells in well-differentiated ESCC (C, 100 \times). D show that stromal and basal membrane are almost completely disrupted and invaded by tumor cells. (D, same section, different field of that of C, 400 \times). Counterstaining was performed with hematoxylin.

high levels of clusterin expression were found in the connective tissue of the lamina *propria* of epithelial mucosa, in which clusterin was confined to what appeared to be the remnants of the extra cellular matrix right under the basal membrane of epithelia, the cytoplasm of esophageal glandular cells, plasma membrane and cytoplasm of duct glandular epithelia, and plasma membrane and cytoplasm of lymphocytes in lymphatic follicle were detected positive by IHC (Figure 4A). During tumorigenesis the intracellular localizations of clusterin was translocated from stroma to the squamous epithelial cells at very early states. It was even found positive in middle dysplasia, a kind of very early lesion of esophagus versus negative in normal squamous epithelia (Figure 4B). However, clusterin and its pre-matured form were distributed in cancerous epithelia of ESCC (the antibody B 5 is able to detect the 60-ku secretory clusterin precursor by Western blot analysis, data not show here) and then, disappeared in stromal mucosa of esophagus (Figure 4C and D).

DISCUSSION

Based on our previous data, clusterin is markedly down-regulated in both serum and tissues of ESCC^[7]. To further clarify the mechanisms of clusterin alterations during tumorigenesis, we first analyzed the gene transcription using semi-quantitative RT-PCR by amplifying different regions from 5' end to 3' end of the gene. We found the same expression results from 437 to 1 350 bp of clusterin between cancer and their matched normal. However, comparing with the cDNA reverse-transcribed from the total mRNA of normal epithelial mucosa, using the cDNA of tumor tissues, no fragment was amplified completely by the N-terminus of 5' -primer which contains the start codon located in the first exon (see underline sequences of the primer 5' - CCGGATCCTTATGATGAAGACTCTGCTGCTG-3'). Those suggested that there was an N-terminal deletion or miss splicing located on 1-437 bp that induced a wrong transcription

forms of the clusterin in ESCC. A miss splicing site repeated in breast cancer cell line MCF 7 was right in this area^[29]. At protein expression level, this region is naturally corresponding to the β chain of clusterin protein. According this rationale, an N-terminal truncated form of clusterin protein would be also detectable. The different protein forms of clusterin in ESCC also describe the biogenesis of multi-transcription forms of clusterin.

The significance of alterations of clusterin gene expression during tumorigenesis remains a mystery. Our data indicated that human esophageal epithelial cells synthesized at least two forms of clusterin, secretory and nuclear clusterins, and their expression levels were changed during tumorigenesis. The secretory clusterin was down-regulated both in serum and tissues of ESCC; while, nuclear clusterin was induced in tumor cells. We also found a 60 ku secretory clusterin precursor protein in ESCC and normal epithelial cells (data not shown). Previous data indicated the existence of a mature about 55 ku nuclear clusterin protein, as a cell death protein and lack ER-signaling peptides, which did not appear to be either glycosylated or cleaved at its α/β site, a site cleaved during maturation of the 60 ku secretory clusterin precursor protein^[12,28,29]. Yang *et al*^[27], described nuclear clusterin was induced by relatively high levels of cytotoxic stress in direct proportion to lethality after growth stimulation of ionizing radiation (IR). Utilization of an in-framed secondary downstream AUG as a translation start site was proposed to result in the synthesis of an about 50 ku precursor nuclear clusterin protein that resided in cytoplasm of undamaged cells by confocal microscopy. Overexpression of this nuclear clusterin, even without IR treatment, caused cell death^[12]. In our immunoblotting results, an about 50 ku nuclear clusterin was detected in both ESCC tissues and cell lines, and occasionally in normal esophageal epithelia using H-330 anti-clusterin antibody. This form of nuclear clusterin could not be detected with B-5 anti-clusterin antibody. As Leskov *et al*^[29] used, H-330 anti-clusterin antibody recognizes the major part of clusterin from 120 to 449 amino acid at the

carboxy terminus of clusterin α/β chains, including the 60 ku precursor and a -49 ku nuclear clusterin precursor (pnCLU). These results were consistent with our findings by RT-PCR that deletion at 5' end or appearance of a splicing at different sites of clusterin gene resulted in N-terminal truncated forms of clusterin transcription. These abnormal forms of clusterin undergo alien post-translational modification compared to secretory clusterin.

Nuclear clusterin is associated with Ku70^[8], a DNA double-strand break repair protein. Its Ku70 binding activity was localized to the C-terminal coiled-coil domain of nuclear clusterin^[30]. The C-terminal coiled-coil domain of nuclear clusterin was the minimal region required for Ku binding and apoptosis. We also found that Ku70 altered in ESCC (data not shown). Although we do not yet know whether nuclear clusterin binding to Ku70 is essential for lethality, we could speculate that enhanced clusterin binding to Ku70 may hinder the formation of Ku70/Ku80 heterodimer, consequently interfere with non-homologous DNA repair, resulting in genomic instability or cell death.

Our studies suggested, on the other hand, the alterations of the localizations and intracellular localizations of clusterin. It was translocated from stroma to the epithelial cells by disrupting the basal membrane of epithelial mucosa during carcinogenesis.

In general, our results demonstrated that the alterations in the expression, proteolysis and intracellular localizations of clusterin and an N-terminus truncated form of clusterin were found in ESCC. Its possible roles in cell survival, cell death and neoplastic transformation remain an additional debate.

ACKNOWLEDGEMENTS

Professor Xin-Yu Zhang and Dr. Li-Yong Zhang are thanked for their help with clusterin primers design.

REFERENCES

- Trougakos IP**, Gonos ES. Clusterin/apolipoprotein J in human aging and cancer. *Int J Biochem Cell Biol* 2002; **34**: 1430-1448
- Polihronis M**, Paizis K, Carter G, Sedal L, Murphy B. Elevation of human cerebrospinal fluid clusterin concentration is associated with acute neuropathology. *J Neurol Sci* 1993; **115**: 230-233
- Law GL**, Griswold MD. Activity and form of sulfated glycoprotein 2 (clusterin) from cultured Sertoli cells, testis, and epididymis of the rat. *Biol Reprod* 1994; **50**: 669-679
- Purrello M**, Bettuzzi S, Di Pietro C, Mirabile E, Di Blasi M, Rimini R, Grzeschik KH, Ingletti C, Corti A, Sichel G. The gene for SP-40, 40, human homolog of rat sulfated glycoprotein 2, rat clusterin, and rat testosterone-repressed prostate message 2, maps to chromosome 8. *Genomics* 1991; **10**: 151-156
- Wong P**, Taillefer D, Lakins J, Pineault J, Chader G, Tenniswood M. Molecular characterization of human TRPM-2/clusterin, a gene associated with sperm maturation, apoptosis and neurodegeneration. *Eur J Biochem* 1994; **221**: 917-925
- Kapron JT**, Hilliard GM, Lakins JN, Tenniswood MP, West KA, Carr SA, Crabb JW. Identification and characterization of glycosylation sites in human serum clusterin. *Protein Sci* 1997; **6**: 2120-2133
- Zhang LY**, Ying WT, Mao YS, He HZ, Liu Y, Wang HX, Liu F, Wang K, Zhang DC, Wang Y, Wu M, Qian XH, Zhao XH. Loss of clusterin both in serum and tissue correlates with the tumorigenesis of esophageal squamous cell carcinoma via proteomics approaches. *World J Gastroenterol* 2003; **9**: 650-654
- Yang CR**, Yeh S, Leskov K, Odegaard E, Hsu HL, Chang C, Kinsella TJ, Chen DJ, Boothman DA. Isolation of Ku70-binding proteins (KUBs). *Nucleic Acids Res* 1999; **27**: 2165-2174
- Wong P**, Pineault J, Lakins J, Taillefer D, Leger J, Wang C, Tenniswood M. Genomic organization and expression of the rat TRPM-2 (clusterin) gene, a gene implicated in apoptosis. *J Biol Chem* 1993; **268**: 5021-5031
- Humphreys DT**, Carver JA, Easterbrook-Smith SB, Wilson MR. Clusterin has chaperone-like activity similar to that of small heat shock proteins. *J Biol Chem* 1999; **274**: 6875-6881
- Clark AM**, Griswold MD. Expression of clusterin/sulfated glycoprotein-2 under conditions of heat stress in rat Sertoli cells and a mouse Sertoli cell line. *J Androl* 1997; **18**: 257-263
- Kimura K**, Asami K, Yamamoto M. Effect of heat shock treatment on the production of variant testosterone-repressed prostate message-2 (TRPM-2) mRNA in culture cells. *Cell Biochem Funct* 1997; **15**: 251-257
- Michel D**, Chatelain G, North S, Brun G. Stress-induced transcription of the clusterin/apoJ gene. *Biochem J* 1997; **328**(Pt 1): 45-50
- Viard I**, Wehrli P, Jornot L, Bullani R, Vechietti JL, Schifferli JA, Tschopp J, French LE. Clusterin gene expression mediates resistance to apoptotic cell death induced by heat shock and oxidative stress. *J Invest Dermatol* 1999; **12**: 290-296
- Witte DP**, Aronow BJ, Dry JK, Harmony JA. Temporally and spatially restricted expression of apolipoprotein J in the developing heart defines discrete stages of valve morphogenesis. *Dev Dyn* 1994; **201**: 290-296
- Wunsche W**, Tenniswood MP, Schneider MR, Vollmer G. Estrogenic regulation of clusterin mRNA in normal and malignant endometrial tissue. *Int J Cancer* 1998; **76**: 684-688
- Correa-Rotter R**, Ibarra-Rubio ME, Schwachau G, Cruz C, Silksens JR, Pedraza-Chaverri J, Chmielewski D, Rosenberg ME. Induction of clusterin in tubules of nephrotic rats. *J Am Soc Nephrol* 1998; **9**: 33-37
- Calvo EL**, Mallo GV, Fiedler F, Malka D, Vaccaro MI, Keim V, Morisset J, Dagorn JC, Iovanna JL. Clusterin overexpression in rat pancreas during the acute phase of pancreatitis and pancreatic development. *Eur J Biochem* 1998; **254**: 282-289
- May PC**. Sulfated glycoprotein-2: an emerging molecular marker for neurodegeneration. *Ann N Y Acad Sci* 1993; **679**: 235-244
- O'Sullivan J**, Whyte L, Drake J, Tenniswood M. Alterations in the post-translational modification and intracellular trafficking of clusterin in MCF-7 cells during apoptosis. *Cell Death Differ* 2003; **10**: 914-927
- Guenette RS**, Corbeil HB, Leger J, Wong K, Mezil V, Mooibroek M, Tenniswood M. Induction of gene expression during involution of the lactating mammary gland of the rat. *J Mol Endocrinol* 1994; **12**: 47-60
- Bettuzzi S**, Hiipakka RA, Gilna P, Liao ST. Identification of an androgen-repressed mRNA in rat ventral prostate as coding for sulphated glycoprotein 2 by cDNA cloning and sequence analysis. *Biochem J* 1989; **257**: 293-296
- Strange R**, Li F, Saurer S, Burkhardt A, Friis RR. Apoptotic cell death and tissue remodelling during mouse mammary gland involution. *Development* 1992; **115**: 49-58
- Sensibar JA**, Sutkowski DM, Raffo A, Buttyan R, Griswold MD, Sylvester SR, Kozlowski JM, Lee C. Prevention of cell death induced by tumor necrosis factor alpha in LNCaP cells by overexpression of sulfated glycoprotein-2 (clusterin). *Cancer Res* 1995; **55**: 2431-2437
- Steinberg J**, Oyasu R, Lang S, Sintich S, Rademaker A, Lee C, Kozlowski JM, Sensibar JA. Intracellular levels of SGP-2 (Clusterin) correlate with tumor grade in prostate cancer. *Clin Cancer Res* 1997; **3**: 1707-1711
- Miyake H**, Nelson C, Rennie PS, Gleave ME. Acquisition of chemoresistant phenotype by overexpression of the antiapoptotic gene testosterone-repressed prostate message-2 in prostate cancer xenograft models. *Cancer Res* 2000; **60**: 2547-2554
- Yang CR**, Leskov K, Hosley-Eberlein K, Criswell T, Pink JJ, Kinsella TJ, Boothman DA. Nuclear clusterin/XIP8, an x-ray-induced Ku70-binding protein that signals cell death. *Proc Natl Acad Sci U S A* 2000; **97**: 5907-5912
- Reddy KB**, Jin G, Karode MC, Harmony JA, Howe PH. Transforming growth factor beta (TGF beta)-induced nuclear localization of apolipoprotein J/clusterin in epithelial cells. *Biochemistry* 1996; **35**: 6157-6163
- Leskov KS**, Klovov DY, Li J, Kinsella TJ, Boothman DA. Synthesis and functional analyses of nuclear clusterin, a cell death protein. *J Biol Chem* 2003; **278**: 11590-11600
- Bradford MM**. A rapid and sensitive method for the quantitation of microgram quantities of protein utilizing the principle of protein-dye binding. *Anal Biochem* 1976; **72**: 248-254

Effects of *c9,t11*-conjugated linoleic acid on adhesion of human gastric carcinoma cell line SGC-7901

Bing-Qing Chen, Yan-Mei Yang, Qi Wang, Yan-Hui Gao, Jia-Ren Liu, Jing-Shu Zhang, Xuan-Lin Wang, Rui-Hai Liu

Bing-Qing Chen, Qi Wang, Jia-Ren Liu, Jing-Shu Zhang, Xuan-Lin Wang, Department of Nutrition and Food Hygiene, Public Health College, Harbin Medical University, Harbin 150001, Heilongjiang Province, China

Yan-Mei Yang, Medical College of Shantou University, Shantou 515031, Guangdong Province, China

Yan-Hui Gao, Chinese Center for Disease Control and Prevention, the Center for Endemic Disease Control, Beijing, China

Rui-Hai Liu, Food Science and Toxicology, Department of Food Science, 108 Stocking Hall, Cornell University, Ithaca, NY 14853-7201, USA

Supported by the National Natural Science Foundation of China, No. 30070658

Correspondence to: Professor Bing-Qing Chen, Department of Nutrition and Food Hygiene, Public Health College, Harbin Medical University, Harbin 150001, Heilongjiang Province, China. bingqingchen@sina.com

Telephone: +86-451-3608014 **Fax:** +86-451-3648617

Received: 2003-10-08 **Accepted:** 2003-12-08

Abstract

AIM: To investigate the effect of *c9,t11*-conjugated linoleic acid (*c9,t11*-CLA) on the adhesion of human gastric carcinoma cell line (SGC-7901).

METHODS: SGC-7901 cells were at first treated with different concentrations (25, 50, 100, 200 $\mu\text{mol/L}$) of *c9,t11*-CLA and 1 mL/L ethanol (as a negative control) for 24 h. Using adhesion assay and Western blot, we investigated the ability of SGC-7901 cells to adhere to intracellular matrix and examined the expression of E-cadherin (ECD), α -catenin, intercellular adhesion molecule 1 (ICAM-1) and vascular cell adhesion molecule 1 (VCAM-1) in these cells.

RESULTS: The attachment rate to laminin of SGC-7901 cells treated with different concentrations of *c9,t11*-CLA (0, 25, 50, 100, and 200 $\mu\text{mol/L}$) was 100.0 ± 3.3 , 95.7 ± 4.0 , 89.2 ± 4.6 , 87.9 ± 6.1 , and 65.9 ± 5.8 , respectively. The attachment rate to fibronectin was 100.0 ± 4.7 , 96.8 ± 3.8 , 94.5 ± 4.1 , 76.5 ± 4.3 , and 61.8 ± 4.8 , respectively. The attachment rate to Matrigel was 99.9 ± 6.6 , 91.4 ± 6.8 , 85.5 ± 7.4 , 79.3 ± 5.6 , and 69.6 ± 5.1 , respectively. Besides, *c9,t11*-CLA could increase the level of ECD and α -catenin, and decrease the level of ICAM-1 and VCAM-1 in SGC-7901 cells.

CONCLUSION: *c9,t11*-CLA can reduce the adhesion of human gastric carcinoma cells to laminin, fibronectin and Matrigel. *c9,t11*-CLA can increase the level of ECD and α -catenin, and decrease the level of ICAM-1 and VCAM-1 in human gastric carcinoma cells.

Chen BQ, Yang YM, Wang Q, Gao YH, Liu JR, Zhang JS, Wang XL, Liu RH. Effects of *c9,t11*-conjugated linoleic acid on adhesion of human gastric carcinoma cell line SGC-7901. *World J Gastroenterol* 2004; 10(10): 1392-1396
<http://www.wjgnet.com/1007-9327/10/1392.asp>

INTRODUCTION

Although the incidence of gastric cancer is decreasing worldwide, it remains one of the most common tumors in China^[1-4] and is a major cause of cancer deaths in some countries^[5,6]. Most of gastric cancer patients die from metastasis. Although the mechanism of gastric cancer metastasis is not fully elucidated, the abnormal adhesion ability of cells has been reported to play a pivotal role. Cell-cell and cell-matrix adhesions are essential for establishing and maintaining normal cell morphology and function. Disturbance of cell adhesion may result in the malignant transformation of cells. Furthermore, cell adhesion molecules are important ingredients in maintaining cell-cell adhesion and cell-matrix interactions. The abnormality of cell adhesion molecules closely correlates with neoplastic transformation and metastasis^[7,8]. Cell adhesion molecules mediate tumor cell-cell, tumor cell-endothelial cell and tumor cell-matrix interactions. In tumor metastasis, cell-cell and cell-matrix interactions are determined by functional status of cell adhesion molecules. Glycoproteins are the cell adhesion molecules and can be classified into several classes according to their structure: cadherins, selectins, CD44, immunoglobulin family, and integrin family.

Conjugated linoleic acid (CLA) is a class of positional and stereoisomers of octadecadienoate (18:2) with conjugated double bonds. The predominant isomer in foods is the *c9,t11*-CLA isomer^[9-16]. In 1979, Pariza *et al.*^[17] detected mutagenic inhibitory activity in both cooked and uncooked ground beef. Then in 1985, they observed that the crude extracts could protect rats against tumors^[18]. In 1987, Ha *et al.*^[19] identified four isomers of CLA from cooked beef. In several animal models of chemical carcinogenesis, it has been reported that CLA was a potent cancer preventive agent. For example, CLA could inhibit skin papillomas^[18,20], forestomach neoplasia^[21-23], mammary tumors^[24-30], and colon aberrant crypt foci^[31]. Moreover, CLA was also effective in reducing the size and metastasis of transplanted human breast cancer cells and prostate cancer cells in SCID mice^[32,33]. Several studies^[34-43] suggested that CLA was cytostatic and cytotoxic to a variety of human cancer cells *in vitro*, including hepatoma, malignant melanoma, colorectal cancer, breast carcinoma, and gastric cancer.

One of our previous studies showed that *c9,t11*-CLA could inhibit the invasion of mouse melanoma cells (B16-MB) through reducing their adhesion ability to extracellular matrix^[44]. Two other studies of ours showed that *c9,t11*-CLA could decrease the invasive ability of human gastric carcinoma cells (SGC-7901)^[45,46]. However, it is unclear whether CLA influences the adhesive ability of SGC-7901 cells and the expression of their adhesion molecules. Therefore, in this study, we investigated the effect of *c9,t11*-CLA on the adhesive ability of SGC-7901 cells and detected the expression of E-cadherin (ECD), α -catenin, intercellular adhesion molecule 1 (ICAM-1) and vascular cell adhesion molecule 1 (VCAM-1) in SGC-7901 cells using adhesion and Western blot assays.

MATERIALS AND METHODS

Materials

c9,t11-CLA with 98% purity, was provided by Dr. Rui-Hai

Liu at Food Science and Toxicology, Department of Food Science, Cornell University, Ithaca, NY, USA. The *c9,t11*-CLA was dissolved in ethanol, then diluted to the following concentrations: 25, 50, 100, and 200 $\mu\text{mol/L}$.

To examine the expression of ECD, α -catenin, ICAM-1, and VCAM-1, we used four primary antibodies: rabbit polyclonal antibody for ECD, mouse monoclonal antibody for α -catenin, and goat polyclonal antibodies for ICAM-1 and VCAM-1, respectively. These antibodies were purchased from Zhongshan Co., China.

Methods

Cell culture Human gastric adenocarcinoma cells (SGC-7901), purchased from Cancer Research Institute of Beijing (China), were cultured in RPMI 1640 (Gibco) medium, supplemented with 100 mL/L fetal calf serum (FCS), 100×10^3 U/L penicillin, 100 mg/L streptomycin and 2 mmol/L L-glutamine under 50 mL/L CO_2 in a humidified incubator. The pH was maintained at 7.2–7.4 and the temperature at 37 °C. After sub-cultured with EDTA, the SGC-7901 cells were incubated with different concentrations (25, 50, 100, and 200 $\mu\text{mol/L}$) of *c9,t11*-CLA and 1 mL ethanol (as a negative control) for 24 h.

Cell adhesion assay A total of 96-well plates (Nunc. Co.) were incubated at 37 °C with laminin, fibronectin or Matrigel for 1 h and then blocked with phosphate-buffered saline (PBS) containing 100 g/L BSA at the same temperature for another 1 h. After exposed to different concentrations (25, 50, 100, and 200 $\mu\text{mol/L}$) of *c9,t11*-CLA for 24 h, the SGC-7901 cells were suspended in serum-free medium at a density of 8×10^5 cells/mL. Then, 0.1 mL of SGC-7901 cells suspension was added to each well and incubated at 37 °C for 1 h. The plates were washed three times with PBS to remove unattached cells. The remaining SGC-7901 cells in 96-well plates were reacted with MTT for 4 h at 37 °C, then solved with DMSO. The absorbance of each well was measured at 570 nm with an ELX800 microplate reader (Bio-TEK Co.). Results were expressed as the percentage of total cells assuming that the adhesion of cells in control was 100%.

Protein extract and western blot The SGC-7901 cells treated with different concentrations of *c9,t11*-CLA were harvested, washed twice times with PBS and lysed at 4 °C in lysis buffer containing 150 mmol/L NaCl, 1 mL/L NP-40, 5 mg/L sodium deoxycholate, 100 g/L SDS, 50 mmol Tris (pH 7.4), 1 mmol/L DTT, 0.5 mmol/L Na_3VO_4 , 10 mmol/L phenylmethylsulfonyl fluoride (PMSF), 10 mg/L aprotinin, and 5 mg/L leupeptin. Following the centrifugation of 10 000 *g* for 30 min at 4 °C, the amount of protein in the supernatant was determined using DUR 640 nucleic acid and protein analyzer. Equal amount of protein was separated on SDS-polyacrylamide gel electrophoresis and transferred to nitrocellulose membrane (Gibco BRL, USA) overnight. Blocked with 50 g/L defatted milk, the membrane was hybridized with rabbit anti-E-cadherin, mouse anti- α -catenin, goat anti-ICAM-1 and goat anti-VCAM-1 antibody, then incubated with horseradish peroxidase-conjugated IgG. Finally, the immunoreactive bands were detected using diaminobenzidine tetrahydrochloride (DAB) substrate and analyzed with a ChemiImager™ 4000 low light imaging system (Alpha Innotech Corporation). At the same time GAPDH was used as house-keeping protein.

RESULTS

Effect of *c9,t11*-CLA on adhesion of SGC-7901 cells

As shown in Table 1, *c9,t11*-CLA could reduce the cell attachment to FN, LN or Matrigel in a dose dependent manner after SGC-7901 cells were pre-incubated for 24 h with different concentrations of *c9,t11*-CLA.

Table 1 Effects of *c9,t11*-CLA on adhesion of SGC-7901 cells (*n*=3)

Doses ($\mu\text{mol/L}$)	Attachment rate to LN (%)	Attachment rate to FN (%)	Attachment rate to matrigel (%)
200	100.0 \pm 3.3	100.0 \pm 4.7	99.9 \pm 6.6
100	95.7 \pm 4.0	96.8 \pm 3.8	91.4 \pm 6.8
50	89.2 \pm 4.6 ^b	94.5 \pm 4.1	85.5 \pm 7.4 ^a
25	87.9 \pm 6.1 ^b	76.5 \pm 4.3 ^b	79.3 \pm 5.6 ^b
Negative control group	65.9 \pm 5.8 ^b	61.8 \pm 4.8 ^b	69.6 \pm 5.1 ^b

^a*P*<0.05 vs negative control, ^b*P*<0.01 vs negative control.

Effect of *c9,t11*-CLA on ECD and α -catenin in SGC-7901 cells

As shown in Figure 1, the level of ECD and α -catenin protein in SGC-7901 cells treated with different concentrations of *c9,t11*-CLA was increased in comparison with that in the negative control group. The level of ECD and α -catenin protein in SGC-7901 cells treated with 200 $\mu\text{mol/L}$ *c9,t11*-CLA increased 65.9% and 80.5% respectively, compared with those in the negative control group.

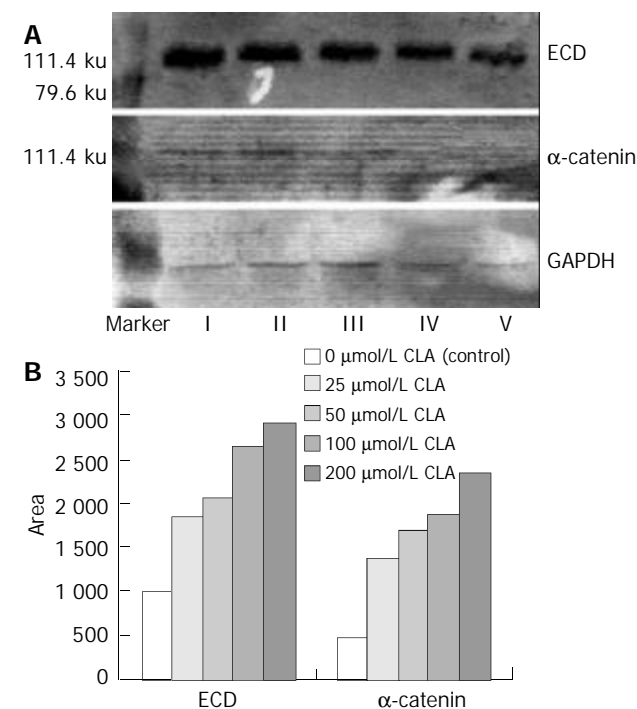


Figure 1 Effect of *c9,t11*-CLA on ECD and α -catenin in SGC-7901 cells detected by Western blot. A: Top: The expression of ECD in SGC-7901 cells treated with different concentrations of *c9,t11*-CLA. Middle: The expression of α -catenin protein in SGC-7901 cells treated with different concentrations of *c9,t11*-CLA. I - IV are 200, 100, 50, 25 $\mu\text{mol/L}$ *c9,t11*-CLA; V is the control group. B: the result of quantitation of ECD and α -catenin levels in SGC-7901 cells by ChemiImager™ 4000 digital system.

Effect of *c9,t11*-CLA on ICAM-1 and VCAM-1 in SGC-7901 cells

As shown in Figure 2, the expression of ICAM-1 and VCAM-1 protein in SGC-7901 cells treated with different concentrations of *c9,t11*-CLA was decreased in comparison with that in the negative control group. Analyzed by ChemiImager 4000 digital system, the level of ICAM-1 and VCAM-1 protein in SGC-7901 cells treated with 200 $\mu\text{mol/L}$ *c9,t11*-CLA increased 70.2% and 65.4% respectively, compared with that in the negative control group.

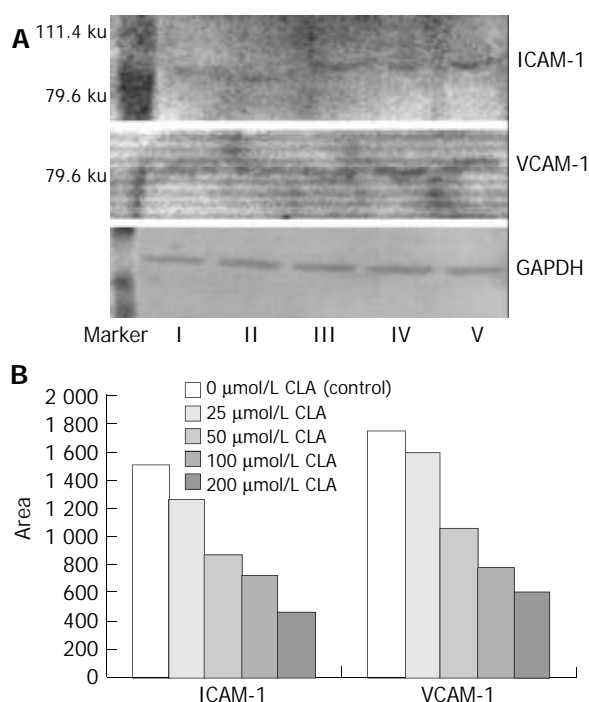


Figure 2 Effect of *c9,t11*-CLA on ICAM-1 and VCAM-1 in SGC-7901 cells detected by Western blot. A: Top: The expression of ICAM-1 in SGC-7901 cells treated with different concentrations of *c9,t11*-CLA. Middle: The expression of VCAM-1 in SGC-7901 cells treated with different concentrations of *c9,t11*-CLA. I-IV are 200, 100, 50, 25 $\mu\text{mol/L}$ *c9,t11*-CLA, respectively; V is the control group. B: the result of quantitation of ICAM-1 and VCAM-1 levels in SGC-7901 cells by ChemiImagerTM 4000 digital system.

DISCUSSION

Many researches have indicated the importance of cancer cell-extracellular matrix (ECM) interaction in tumor metastasis. Cell and matrix interactions could promote cell migration, proliferation, and ECM degradation^[47-51]. It also has been shown that prevention of tumor cell adhesion and migration is related to inhibition of tumor cell invasion into the basement membrane. Laminin (LN), fibronectin (FN) and type IV collagen are the principal components of ECM. The *in vitro* assays of FN, LN, or Matrigel that mainly contain FN, LN and type IV collagen can better simulate the *in vivo* adhesive process. It was shown that agents that inhibited cell attachment *in vitro* decreased the invasion and metastatic potential of tumor cells *in vivo*. Therefore, cell adhesion assay not only is employed in determining the adhesive interaction between tumor cells and matrix components, but also is suitable in screening agents that can inhibit adhesion and metastasis of tumor cell. We demonstrated in our current study that after incubation with 200, 100, and 50 $\mu\text{mol/L}$ of *c9,t11*-CLA for 1 h, the attachment to extracellular matrix components of SGC-7901 cells was significantly reduced. The result was consistent with the findings in our previous study^[44]. Therefore, we could conclude that *c9,t11*-CLA could inhibit the attachment to extracellular matrix components of tumor cells and this process might be a mechanism for the inhibition of tumor invasion.

Before they can invade or metastasize, tumor cells have to dissociate from primary neoplasms. A loss of cell-cell adhesive interaction is required for the detachment. Thus, adhesion molecules play an important role in metastatic process. Cadherins have been found to be a class of calcium dependent cell adhesion molecules involved in homotypic cell-cell adhesion^[7,8]. E-cadherin is a member of the cadherin family that is expressed in all epithelial cells and is essential to the

maintenance of cell morphology, cell movement and cell adhesive function. Because E-cadherin can maintain cell adhesion, its abnormalities may be associated with tumorigenesis. It was proved that abnormalities of E-cadherin mRNA and E-cadherin protein expression existed in various human primary cancers, such as gastric, colon, pancreas, esophagus, liver, prostate, bladder, breast, and head and neck tumors^[52]. Recent studies showed that gene mutations or loss of heterozygous E-cadherin occurred in gastric carcinomas, ovary cancer, and cervix cancer. It was found that E-cadherin had strong expression in well-differentiated noninvasive cancers with tight cell-cell adhesion, and had markedly reduced, heterogeneous, or even no expression in undifferentiated invasive cancers with lack of cell-cell adhesion. Several studies have offered the evidence that reduction or structural alternation of E-cadherin expression plays a causal role in metastasis of gastric and colon cancers. The role of E-cadherin in metastasis and invasion was further demonstrated by the fact that the invasion of epithelial tumor cell lines was inhibited *in vitro* by transfection and expression of E-cadherin cDNA, and induced again by exposure to anti-E-cadherin monoclonal antibodies^[53]. Through its cytoplasmic sequence, E-cadherin was associated with a group of proteins called catenins, which are necessary for E-cadherin function^[54]. Dysfunction of catenin can cause instability of homotypic cell-cell adhesion mediated by E-cadherin. Therefore, in tumors with normal E-cadherin expression, alteration of cell adhesion may result from abnormal expression of catenins. Catenins have been classified into α -catenin, β -catenin, and γ -catenin. α -catenin links E-cadherin with cytoskeleton. Expression of α -catenin is essential to the function of E-cadherin in normal cells. Thus, in cancers with normal E-cadherin expression, decreased expression of α -catenin leads to impaired cell adhesion. Downregulation of α -catenin and E-cadherin expression in several cancer tissues has been found to be associated with differentiation degree, invasion and metastasis of cancer cells^[55-57]. Our current study demonstrated that after incubation with different concentrations of *c9,t11*-CLA for 24 h, expression of E-cadherin and catenin in SGC-7901 cells increased. Through upregulation of expression of E-cadherin and catenin, *c9,t11*-CLA also increased homotypic adhesion of cancer cells.

ICAM-1 is a 70-110 ku glycoprotein belonging to the immunoglobulin superfamily and is also a ligand for leukocyte-function associated antigen-1 (LFA-1). It has been reported that ICAM-1 could express on the surface of tumor cells, endothelial cells, keratinocytes, and mediate heterotypic cell-cell interaction^[58]. Several studies indicated that high expression of ICAM-1 in melanoma cells was associated with tumor metastasis, and expression on the surface of metastasizing cancer cells in lymph node increased significantly^[59]. It is suggested that high expression of ICAM-1 on the surface of metastasizing cancer cells in lymph node plays a role in evading immune destruction, thus helping these cancer cells retain in lymphatic sinus to form metastasis. VCAM-1 is a 90 ku cell surface glycoprotein belonging to the immunoglobulin superfamily. Studies also showed that VCAM-1 in renal cell carcinoma, melanoma, and malignant sarcoma linked tumor cells to endothelial cells via binding to integrin $\alpha_4\beta_1$, and contributed to penetration into blood vessels^[60]. We demonstrated here that different concentrations of *c9,t11*-CLA could decrease expression of ICAM-1 and VCAM-1 in SGC-7901 cells after incubation for 24 h and also decrease heterotypic adhesion of cancer cells via downregulation of expression of ICAM-1 and VCAM-1.

In conclusion, *c9,t11*-CLA can inhibit cell-matrix component interactions, increase expression of E-cadherin and catenin and reduce expression of ICAM-1 and VCAM-1 in

SGC-7901 cells. Through these effects, *c9,t11*-CLA may inhibit the invasion of SGC-7901 cells.

REFERENCES

- Liu LX, Liu ZH, Jiang HC, Qu X, Zhang WH, Wu LF, Zhu AL, Wang XQ, Wu M. Profiling of differentially expressed genes in human Gastric carcinoma by cDNA expression array. *World J Gastroenterol* 2002; **8**: 580-585
- Song ZJ, Gong P, Wu YE. Relationship between the expression of iNOS, VEGF, tumor angiogenesis and gastric cancer. *World J Gastroenterol* 2002; **8**: 591-595
- Shi XY, Zhao FZ, Dai X, Ma LS, Dong XY, Fang J. Effect of jianpiyiwei capsule on gastric precancerous lesions in rats. *World J Gastroenterol* 2002; **8**: 608-612
- Zhao AG, Zhao HL, Jin XJ, Yang JK, Tang LD. Effects of Chinese Jianpi herbs on cell apoptosis and related gene expression in human gastric cancer grafted onto nude mice. *World J Gastroenterol* 2002; **8**: 792-796
- Fuchs CS, Mayer RJ. Gastric carcinoma. *N Engl J Med* 1995; **333**: 32-41
- Hansson LE, Sparen P, Nyren O. Survival in stomach cancer is improving: results of a nationwide population-based Swedish study. *Ann Surg* 1999; **230**: 162-169
- Takeichi M. Cadherin cell adhesion receptors as a morphogenetic regulator. *Science* 1991; **251**: 1451-1455
- Hirohashi S. Inactivation of the E-cadherin-mediated cell adhesion system in human cancers. *Am J Pathol* 1998; **153**: 333-339
- Sebedio JL, Gnaedig S, Chardigny JM. Recent advances in conjugated linoleic acid research. *Curr Opin Clin Nutr Metab Care* 1999; **2**: 499-506
- Pariza MW, Park Y, Cook ME. Mechanisms of action of conjugated linoleic acid: evidence and speculation. *Proc Soc Exp Biol Med* 2000; **223**: 8-13
- Pariza MW, Park Y, Cook ME. Conjugated linoleic acid and the control of cancer and obesity. *Toxicol Sci* 1999; **52**(2 Suppl): 107-110
- Whigham LD, Cook ME, Atkinson RL. Conjugated linoleic acid: implications for human health. *Pharmacol Res* 2000; **42**: 503-510
- MacDonald HB. Conjugated linoleic acid and disease prevention: a review of current knowledge. *J Am Coll Nutr* 2000; **19**(2 Suppl): 111S-118S
- Banni S. Conjugated linoleic acid metabolism. *Curr Opin Lipidol* 2002; **13**: 261-266
- Belury MA. Dietary conjugated linoleic acid in health: physiological effects and mechanisms of action. *Annu Rev Nutr* 2002; **22**: 505-531
- Belury MA. Inhibition of carcinogenesis by conjugated linoleic acid: potential mechanisms of action. *J Nutr* 2002; **132**: 2995-2998
- Pariza MW, Ashoor SH, Chu FS, Lund DB. Effects of temperature and time on mutagen formation in pan-fried hamburger. *Cancer Lett* 1979; **7**: 63-69
- Pariza MW, Hargraves WA. A beef-derived mutagenesis modulator inhibits initiation of mouse epidermal tumors by 7,12-dimethylbenz[a]anthracene. *Carcinogenesis* 1985; **6**: 591-593
- Ha YL, Grimm NK, Pariza MW. Anticarcinogens from fried ground beef: heat-altered derivatives of linoleic acid. *Carcinogenesis* 1987; **8**: 1881-1887
- Belury MA, Nickel KP, Bird CE, Wu Y. Dietary conjugated linoleic acid modulation of phorbol ester skin tumor promotion. *Nutr Cancer* 1996; **26**: 149-157
- Ha YL, Storkson J, Pariza MW. Inhibition of benzo(a)pyrene-induced mouse forestomach neoplasia by conjugated dienoic derivatives of linoleic acid. *Cancer Res* 1990; **50**: 1097-1101
- Zhu Y, Qiou J, Chen B. The inhibitory effect of CLA on mice forestomach neoplasia induced by B(a). *Zhonghua Yufang Yixue Zazhi* 2001; **35**: 19-22
- Chen BQ, Xue YB, Liu JR, Yang YM, Zheng YM, Wang XL, Liu RH. Inhibition of conjugated linoleic acid on mouse forestomach neoplasia induced by benzo(a)pyrene and chemopreventive mechanisms. *World J Gastroenterol* 2003; **9**: 44-49
- Ip C, Jiang C, Thompson HJ, Scimeca JA. Retention of conjugated linoleic acid in the mammary gland is associated with tumor inhibition during the post-initiation phase of carcinogenesis. *Carcinogenesis* 1997; **18**: 755-759
- Ip C, Singh M, Thompson HJ, Scimeca JA. Conjugated linoleic acid suppresses mammary carcinogenesis and proliferative activity of the mammary gland in the rat. *Cancer Res* 1994; **54**: 1212-1215
- Ip C, Banni S, Angioni E, Carta G, McGinley J, Thompson HJ, Barbano D, Bauman D. Conjugated linoleic acid-enriched butter fat alters mammary gland morphogenesis and reduces cancer risk in rats. *J Nutr* 1999; **129**: 2135-2142
- Thompson H, Zhu Z, Banni S, Darcy K, Loftus T, Ip C. Morphological and biochemical status of the mammary gland as influenced by conjugated linoleic acid: implication for a reduction in mammary cancer risk. *Cancer Res* 1997; **57**: 5067-5072
- Banni S, Angioni E, Casu V, Melis MP, Carta G, Corongiu FP, Thompson H, Ip C. Decrease in linoleic acid metabolites as a potential mechanism in cancer risk reduction by conjugated linoleic acid. *Carcinogenesis* 1999; **20**: 1019-1024
- Kimoto N, Hirose M, Futakuchi M, Iwata T, Kasai M, Shirai T. Site-dependent modulating effects of conjugated fatty acids from safflower oil in a rat two-stage carcinogenesis model in female Sprague-Dawley rats. *Cancer Lett* 2001; **168**: 15-21
- Ip C, Ip MM, Loftus T, Shoemaker S, Shea-Eaton W. Induction of apoptosis by conjugated linoleic acid in cultured mammary tumor cells and premalignant lesions of the rat mammary gland. *Cancer Epidemiol Biomarkers Prev* 2000; **9**: 689-696
- Liew C, Schut HA, Chin SF, Pariza MW, Dashwood RH. Protection of conjugated linoleic acids against 2-amino-3-methylimidazo[4,5-f]quinoline-induced colon carcinogenesis in the F344 rat: a study of inhibitory mechanisms. *Carcinogenesis* 1995; **16**: 3037-3043
- Visonneau S, Cesano A, Tepper SA, Scimeca JA, Santoli D, Kritchevsky D. Conjugated linoleic acid suppresses the growth of human breast adenocarcinoma cells in SCID mice. *Anticancer Res* 1997; **17**: 969-973
- Cesano A, Visonneau S, Scimeca JA, Kritchevsky D, Santoli D. Opposite effects of linoleic acid and conjugated linoleic acid on human prostatic cancer in SCID mice. *Anticancer Res* 1998; **18**: 1429-1434
- Shultz TD, Chew BP, Seaman WR, Lueddecke LO. Inhibitory effect of conjugated dienoic derivatives of linoleic acid and beta-carotene on the *in vitro* growth of human cancer cells. *Cancer Lett* 1992; **63**: 125-133
- Igarashi M, Miyazawa T. Newly recognized cytotoxic effect of conjugated trienoic fatty acids on cultured human tumor cells. *Cancer Lett* 2000; **148**: 173-179
- Igarashi M, Miyazawa T. The growth inhibitory effect of conjugated linoleic acid on a human hepatoma cell line, HepG2, is induced by a change in fatty acid metabolism, but not the facilitation of lipid peroxidation in the cells. *Biochim Biophys Acta* 2001; **1530**: 162-171
- Park Y, Allen KG, Shultz TD. Modulation of MCF-7 breast cancer cell signal transduction by linoleic acid and conjugated linoleic acid in culture. *Anticancer Res* 2000; **20**: 669-676
- O'Shea M, Devery R, Lawless F, Murphy J, Stanton C. Milk fat conjugated linoleic acid (CLA) inhibits growth of human mammary MCF-7 cancer cells. *Anticancer Res* 2000; **20**: 3591-3601
- O'Shea M, Stanton C, Devery R. Antioxidant enzyme defence responses of human MCF-7 and SW480 cancer cells to conjugated linoleic acid. *Anticancer Res* 1999; **19**: 1953-1959
- Cunningham DC, Harrison LY, Shultz TD. Proliferative responses of normal human mammary and MCF-7 breast cancer cells to linoleic acid, conjugated linoleic acid and eicosanoid synthesis inhibitors in culture. *Anticancer Res* 1997; **17**: 197-203
- Schonberg S, Krokan HE. The inhibitory effect of conjugated dienoic derivatives (CLA) of linoleic acid on the growth of human tumor cell lines is in part due to increased lipid peroxidation. *Anticancer Res* 1995; **15**: 1241-1246
- Liu J, Chen B, Liu R, Lu G. Inhibitory effect of conjugated linoleic acid on human gastric carcinoma cell line. *Weisheng Yanjiu* 1999; **28**: 353-355
- Liu JR, Li BX, Chen BQ, Han XH, Xue YB, Yang YM, Zheng YM, Liu RH. Effect of *cis*-9, *trans*-11-conjugated linoleic acid on cell cycle of gastric adenocarcinoma cell line (SGC-7901). *World J Gastroenterol* 2002; **8**: 224-229
- Xue Y, Chen B, Zheng Y, Yuan L. Effects of conjugated linoleic

- acid on the metastasis of mouse melanoma B16-MB. *Weisheng Yanjiu* 2001; **30**: 37-39
- 45 **Yang Y**, Chen B, Xue Y, Zheng Y. Effects of c9, t11-conjugated linoleic acid on the metastasis of human gastric carcinoma cell line. *Weisheng Yanjiu* 2003; **32**: 117-119
- 46 **Yang YM**, Chen BQ, Zheng YM, Wang XL, Liu JR, Xue YB, Liu RH. The effects of conjugated linoleic acid on the expression of invasiveness and metastasis-associated gene of human gastric carcinoma cell line. *Zhonghua Yufang Yixue Zazhi* 2003; **37**: 26-28
- 47 **Yoon SO**, Kim MM, Chung AS. Inhibitory effect of selenite on invasion of HT1080 tumor cells. *J Biol Chem* 2001; **276**: 20085-20092
- 48 **Ara T**, Deyama Y, Yoshimura Y, Higashino F, Shindoh M, Matsumoto A, Fukuda H. Membrane type 1-matrix metalloproteinase expression is regulated by E-cadherin through the suppression of mitogen-activated protein kinase cascade. *Cancer Lett* 2000; **157**: 115-121
- 49 **Seftor RE**, Seftor EA, Gehlsen KR, Stetler-Stevenson WG, Brown PD, Ruoslahti E, Hendrix MJ. Role of the alpha v beta 3 integrin in human melanoma cell invasion. *Proc Natl Acad Sci U S A* 1992; **89**: 1557-1561
- 50 **Nakahara H**, Nomizu M, Akiyama SK, Yamada Y, Yeh Y, Chen WT. A mechanism for regulation of melanoma invasion. Ligation of alpha6beta1 integrin by laminin G peptides. *J Biol Chem* 1996; **271**: 27221-27224
- 51 **Giancotti FG**, Ruoslahti E. Integrin signaling. *Science* 1999; **285**: 1028-1032
- 52 **Dogan A**, Wang ZD, Spencer J. E-cadherin expression in intestinal epithelium. *J Clin Pathol* 1995; **48**: 143-146
- 53 **Chan AO**, Lam SK, Chu KM, Lam CM, Kwok E, Leung SY, Yuen ST, Law SY, Hui WM, Lai KC, Wong CY, Hu HC, Lai CL, Wong J. Soluble E-cadherin is a valid prognostic marker in gastric carcinoma. *Gut* 2001; **48**: 808-811
- 54 **Jawhari A**, Farthing M, Pignatelli M. The importance of the E-cadherin-catenin complex in the maintenance of intestinal epithelial homeostasis: more than intercellular glue? *Gut* 1997; **41**: 581-584
- 55 **Jiang WG**. E-cadherin and its associated protein catenins, cancer invasion and metastasis. *Br J Surg* 1996; **83**: 437-446
- 56 **Yu J**, Ebert MP, Miehke S, Rost H, Lendeckel U, Leodolter A, Stolte M, Bayerdorffer E, Malferteiner P. Alpha-catenin expression is decreased in human gastric cancers and in the gastric mucosa of first degree relatives. *Gut* 2000; **46**: 639-644
- 57 **Shiozaki H**, Iihara K, Oka H, Kadowaki T, Matsui S, Gofuku J, Inoue M, Nagafuchi A, Tsukita S, Mori T. Immunohistochemical detection of α -catenin expression in human cancers. *Am J Pathol* 1994; **144**: 667-674
- 58 **Schwaeble W**, Kerlin M, Meyer zum Buschenfelde KH, Dippold W. De novo expression of intercellular adhesion molecule 1 (ICAM-1, CD54) in pancreas cancer. *Int J Cancer* 1993; **53**: 328-333
- 59 **Natali P**, Nicotra MR, Cavaliere R, Bigotti A, Romano G, Temponi M, Ferrone S. Differential expression of intercellular adhesion molecule 1 in primary and metastatic melanoma lesions. *Cancer Res* 1990; **50**: 1271-1278
- 60 **Tomita Y**, Saito T, Saito K, Oite T, Shimizu F, Sato S. Possible significance of VLA-4 ($\alpha 4 \beta 1$) for hematogenous metastasis of renal-cell cancer. *Int J Cancer* 1995; **60**: 753-758

Edited by Chou LF and Wang XL **Proofread by** Xu FM

Diagnosis and surgical treatments of hepatocellular carcinoma with tumor thrombosis in bile duct: Experience of 34 patients

Lun-Xiu Qin, Zeng-Chen Ma, Zhi-Quan Wu, Jia Fan, Xin-Da Zhou, Hui-Chuan Sun, Qing-Hai Ye, Lu Wang, Zhao-You Tang

Lun-Xiu Qin, Zeng-Chen Ma, Zhi-Quan Wu, Jia Fan, Xin-Da Zhou, Hui-Chuan Sun, Qing-Hai Ye, Lu Wang, Zhao-You Tang, Liver Cancer Institute and Zhongshan Hospital, Fudan University former Shanghai Medical University, Shanghai 200032, China

Correspondence to: Zhao-You Tang, M.D., Professor and Chairman, Liver Cancer Institute, Fudan University, 136 Yi Xue Yuan Road, Shanghai 200032, China. zytang@srcap.stc.sh.cn

Telephone: +86-21-64037181 **Fax:** +86-21-64037181

Received: 2003-10-15 **Accepted:** 2003-12-16

Abstract

AIM: Hepatocellular carcinoma (HCC) with bile duct tumor thrombosis (BDT) is a rare event. The prognosis of this type of patients is very dismal. The aim of this study was to share the experience in the diagnosis and treatment of HCC with BDT, to further improve the prognosis of these patients.

METHODS: Thirty-four patients of HCC with BDT received surgical treatment in authors' institute from July 1987 to January 2003 were reviewed retrospectively. The experience in the diagnosis and treatment, and the outcome of this type of HCC patients were summarized.

RESULTS: Thirty of the 34 patients (88.2%) were positive for alpha-fetoprotein (AFP) ($>20 \mu\text{g/L}$), and 12 patients (35.3%) were found having obstructive jaundice before operation, 18 cases were suspected of "obstruction of bile duct" preoperatively. The primary tumors were frequently located at the left medial (13 cases) or right anterior lobe (14 cases). Thirty-one patients received liver resections and removal of BDT, while the other 3 patients received removal of BDT combined with hepatic artery ligation and cannulation (HAL+HAI), or only removal of BDT because their liver function reservation and general condition could not tolerate the primary tumor resection. The 1-year survival rate was 71.4%(20/28). The longest disease-free survival was over 15 years. The intrahepatic tumor recurrence within 1 year after operation was found in 14 patients (14/28, 50.0%).

CONCLUSION: Surgical removal of primary tumors and BDT is safe and beneficial to the HCC patients with BDT. Early detection, diagnosis, and surgical treatment are the key points to prolong the survival time of patients.

Qin LX, Ma ZC, Wu ZQ, Fan J, Zhou XD, Sun HC, Ye QH, Wang L, Tang ZY. Diagnosis and surgical treatments of hepatocellular carcinoma with tumor thrombosis in bile duct: Experience of 34 patients. *World J Gastroenterol* 2004; 10(10): 1397-1401
<http://www.wjgnet.com/1007-9327/10/1397.asp>

INTRODUCTION

Obstructive jaundice as the main presenting clinical feature is uncommon in patients with hepatocellular carcinoma (HCC). Only 1-12% of patients with HCC manifest obstructive jaundice as the initial complaint^[1-3]. Mallory *et al.* described

the first such case in 1947, in which HCC invaded the cystic duct and gave rise to obstructive jaundice caused by the tumor thrombosis^[4]. These kinds of patients were clinically classified as "icteric-type hepatoma"^[5] or "cholestatic type of HCC"^[6].

Tumor thrombus in bile duct (BDT) is one of the main reasons for obstructive jaundice. The incidence was 1.2-9% in previous reports^[2,3,5-8]. However, Huang *et al.* found the incidence was only 0.53%^[9]. It is usually difficult to make diagnosis before operation, because of the low incidence rate, ignorance of this disease, and the difficulty for the imaging diagnosis to find the BDT preoperatively. The prognosis of this type of HCC patients is very dismal, but is better than those with jaundice caused by hepatic insufficiency. Identification of this group of patients is clinically important, because surgical treatment may be beneficial. In this study, we summarized our experience in the diagnosis and treatment of 34 cases of this type of HCC during the past 15 years.

MATERIALS AND METHODS

Patients' information

From July 1987 to January 2003, totally 4 324 patients suffering from HCC received surgical treatment in Liver Cancer Institute and Zhongshan Hospital, Fudan University (former Shanghai Medical University), and 34 cases (0.79%) were found having tumor thrombosis in bile duct. Among of them, 28 cases were male, and 6 cases were female. The mean age of patients was 48.5 years (32-76 years). The history of hepatitis B virus (HBV) infection or HBsAg positive was found in all of the patients, and liver cirrhosis in 94.1%(32/34) of patients. Thirty of them (30/34, 88.2%) were positive for alpha-fetoprotein (AFP) ($>20 \mu\text{g/L}$), and the highest was over 2 000 $\mu\text{g/L}$. Preoperative obstructive jaundice was found in 12 patients (12/34, 35.3%), and 2 of them had the history of "transient cholangitis" with the manifestation of transient jaundice. The history of "hemorrhage of upper digestive system" was found in 2 patients. Four patients had the history of preoperative transcatheter arterial chemoembolization (TACE) (Table 1).

Imaging diagnostic features

Ultrasonography (US) and CT scan were performed in all of the patients. Magnetic resonance cholangiography (MRCP) was also done in 12 patients in recent 3 years. (Figures 1, 2) Eighteen cases were suspected of "obstruction of bile duct" because of the occurrence of preoperative jaundice (12 cases), and/or dilation of intrahepatic bile duct shown in imaging diagnosis (in 6 cases without obstructive jaundice). Only 9 cases of them were obviously shown tumor thrombosis in the bile duct by US, CT scan or MRI preoperatively. One case with neoplasm in the bile duct, while no obvious intrahepatic lesion, was misdiagnosed as cholangiocarcinoma, in spite of the positive AFP.

Characteristics of the primary tumors and BDT

The size of primary tumors was 6.4 ± 2.5 cm in diameter (2-15 cm). All of the primary tumors had no capsule, with unclear tumor margin, and invasive pattern of growth. The primary tumors

were located at the segment IV in 13 cases, right anterior section (segments V and VIII) in 14 cases, segment I (caudate lobe) in 1 case, segment II-III in 4 cases, and segment VI in 2 cases. The tumor thrombus located at left hepatic duct (LHD) in 5 cases, LHD to common hepatic duct (CHD)/common bile duct (CBD) in 9 cases, right hepatic bile duct (RHD) in 5 cases, RHD to CHD/CBD in 8 cases, and CBD in 7 cases. According to Ueda classification^[10], 2 cases belonged to type I, 8 cases type II, 16 cases type IIIa, 1 case type IIIb, and 7 cases type IV. In 2 cases, the BDT was as long as 6 cm, and 9 cm, respectively (Table 1, Figure 1).

Treatment strategies

All of the patients received surgical treatment. Thirty-one patients received liver resection and removal of the tumor thrombosis (or thrombectomy). Among them, 12 patients received left hemihepatectomy, 2 cases received left lateral sectionectomy, 11 cases received limited partial resection of the liver, 5 cases received right hemihepatectomy, and 1 case received resection of the left lobe and caudate lobe of liver, and CHD, and RHD-jejunum anastomosis. Two patients received removal of CBD thrombosis combined with hepatic artery ligation and cannulation (HAL+HAI), and 1 patient

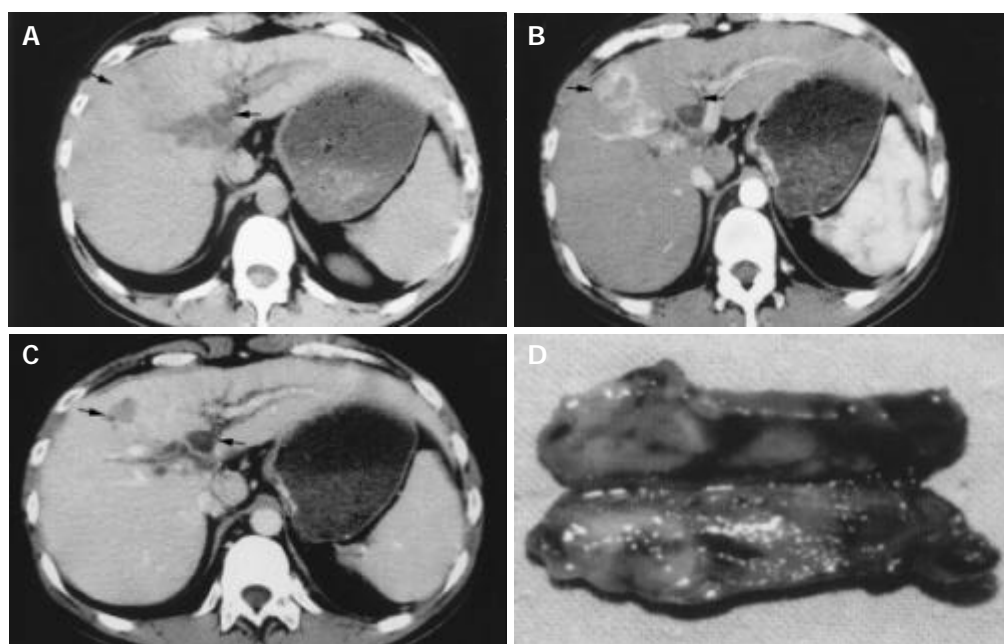


Figure 1 The hepatocellular carcinoma (HCC) with tumor thrombosis in common bile duct. A-C: The three phases of CT scan. One small HCC with rich arterial blood flow is shown in the left medial lobe of liver (arrow), with the intrahepatic bile duct of both sides and common hepatic duct dilated obviously (arrow). D: The tumor thrombosis removed from the common bile duct of this HCC patient.

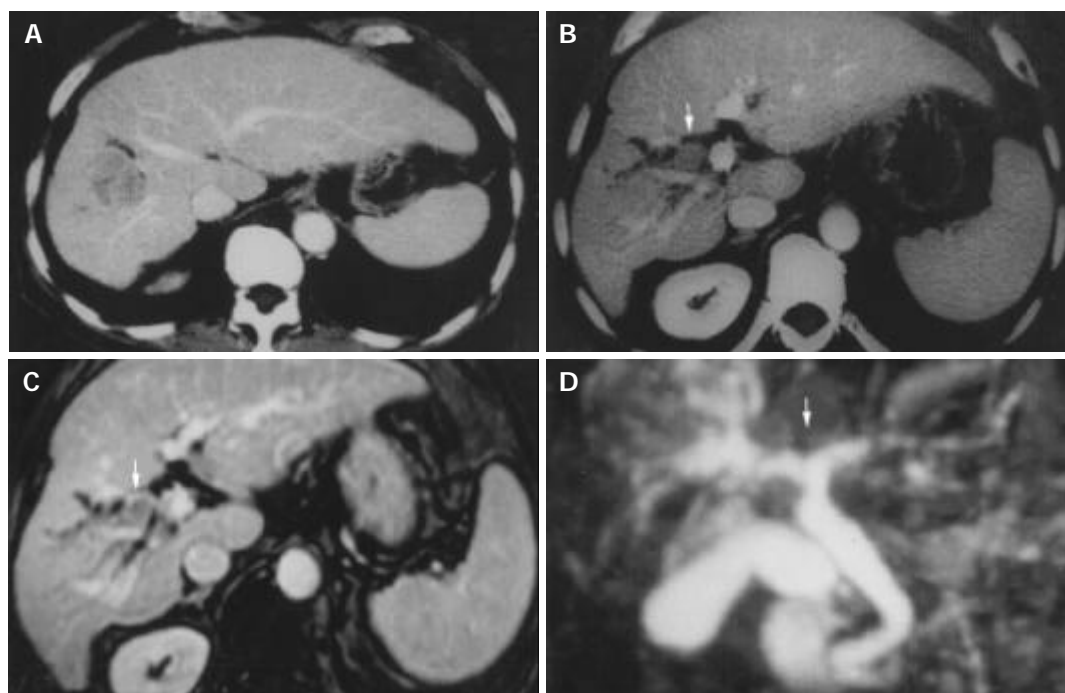


Figure 2 The imaging diagnosis of hepatocellular carcinoma with thrombosis in bile duct. A and B are pictures of CT scan, C and D are pictures of magnetic resonance cholangiography (MRCP). These pictures show the primary tumor in right anterior lobe of the liver, with tumor thrombosis in common hepatic duct (arrow).

received removal of BDT only because their liver function reservation and general condition could not tolerate the primary tumor resection.

The tumor thrombi were removed by the exploration of CBD in 14 cases, from the cut end of the bile duct after liver resection in 15 cases, and *en bloc* removal with the primary tumor in 5 patients. Intraoperative active bleeding from the CHD after removal of the thrombosis happened in 1 patient, and hemostasis was achieved finally by infusing noradrenalin in normal saline into the bile duct and oppressing locally.

The operations were well tolerated. After operation, the obstructive jaundice due to BDT was successfully relieved in all but 2 patients. One patient with severe liver cirrhosis and preoperative obstructive jaundice (the total serum bilirubin was 182 $\mu\text{mol/L}$) received partial resection of the right liver lobe, and died of liver failure at the 35th d after the operation. Another patient with severe preoperative obstructive jaundice (total serum bilirubin was 320 $\mu\text{mol/L}$, and the direct bilirubin was 210 $\mu\text{mol/L}$) received right hemihepatectomy and removal of thrombosis in CBD, the total serum bilirubin did not decrease although the general condition of the patient was good, the patient himself chose to give up the treatment and left the hospital at the 40th d after the operation. A third patient with obstructive jaundice (preoperative total serum bilirubin was 156 $\mu\text{mol/L}$) due to BDT in the CBD received left hemihepatectomy and removal of BDT. His total serum bilirubin rose to over 700 $\mu\text{mol/L}$ in 2 wk after operation, and finally returned to normal in 3 mo. By now, this patient has survived for 11 mo.

Table 1 The clinical information of the 34 HCC patients with tumor thrombosis in bile duct

Items	Cases (%)
Sex	
Male	28 (82.4%)
Female	6
HBV infection	
HBsAg+	34 (100%)
Liver cirrhosis	32 (94.1%)
AFP	
>20 $\mu\text{g/L}$	30 (88.2%)
≤20 $\mu\text{g/L}$	4
Obstructive jaundice	
+	12 (12, 35.3%)
-	
Ueda classification	
Type I	2
Type II	8
Type IIIa	16
Type IIIb	1
Type IV	7
Treatment	
Surgical resection	31 (91.2%)
Removal of BDT +HAL+HAI	2
Only removal of BDT	1
Survival	
>1 yr	20 (20/28, 71.4%)
>3 yr	3
>15 yr	1
HCC recurrence	
Within 1 yr	14 (14/28, 50.0%)
Within 3 mo	9 (9/31, 29.0%)

Survivals

The follow-up was up to February of 2003. Twenty-eight patients

were followed-up over 1 year. Twenty patients survived over 1 year. One-year survival rate was 71.4%(20/28). The longest disease-free survival time was over 15 years. It occurred in one female patient who received left hemihepatectomy and removal of the tumor thrombosis in CBD (Ueda type IV) in July of 1987. She was still alive without recurrence of cancer up to the last follow-up. Another female patient who received partial resection of right lobe and removal of BDT from the RHD (Ueda type II) in August of 1993 had survived over 9 years without recurrence. The third female patient received right hemihepatectomy and removal of CHD thrombosis (Ueda type IIIa) in May of 1995, and received the second operation due to HCC recurrence 3.5 years later. One male patient who received right hemihepatectomy in September of 1999 (Type II) had also survived over 2 years without recurrence. Fourteen patients (14/28, 50.0%) were found intrahepatic HCC recurrence within 1 year after operation. Nine of them (9/31, 29.0%) were found intrahepatic recurrence within 3 mo after operations. The survival times of the 3 patients received biliary decompression were only 2, 3, and 3.5 mo, respectively (Table 1).

DISCUSSION

Obstructive jaundice caused by BDT, especially as the initial presentation of HCC, is a rare event. And little is known about this type of HCC. However, there are more and more reports about this type of disease, and the incidence is increasing in patients with HCC^[11]. In this study, only 34 out of the 4 324 HCC patients who received surgical treatment in authors' institute were found BDT. The incidence was only 0.79%. And more, most of them (26/34, 76.5%) were treated in recent 5 years. This might be due to the increased understanding of this type of HCC, further improvement of diagnosis (particularly the imaging diagnosis), and more positive attitude towards the treatment to this kind of patients.

HCC invades into bile duct through the following different mechanisms: a distal tumor may grow continuously until it fills the entire extrahepatic biliary system; a fragment of necrotic tumor may separate from the proximal intraductal growth, migrate to the distal common bile duct and cause an obstruction; hemorrhage from the tumor may partially or completely fill the biliary tract with tumor-containing blood clots^[2,3,7-9,12,13]. These produce different types of BDT which will also affect the patients' prognosis^[10]. In this series, 4 patients without any obvious evidence of BDT at initial diagnosis were found BDT after TACE treatment, which suggested that TACE might increase the possibility of BDT^[11]. The exact mechanism is not clear yet.

Just as other types of HCC, no specific symptoms could be found in the early stage. Only when intraductal tumor growth occurs in the CHD and/or CBD does obstructive jaundice become a clinical concern. The common clinical features include high level of serum AFP, the history of cholangitis with dilation of intrahepatic bile duct, aggravating jaundice and rapidly developing into liver dysfunction. Unexplained hemobilia could be the initial complaint without any manifestation of primary tumor. And "hemorrhage of upper digestive system", which might be due to the hemorrhage of bile duct (hemobilia), could also be the first manifestation. The most important point is that we should think about the possibility of BDT when these manifestations are found in HCC patients.

There are still difficult and challenging problems in differential diagnosis of this type of HCC before operation. Despite remarkable recent improvements in the imaging techniques for diagnosis of HCC, such cases were still incorrectly diagnosed as cholangiocarcinoma or choledocholithiasis^[2,7-14]. In this series, only 9 out of the 18 cases suspected of "obstruction

of bile duct" were obviously shown BDT with US or CT scan preoperatively. The others were misdiagnosed as "bile duct stone" or cholangiocarcinoma, even though "neoplasm in CBD" was found. All of these suggest that deeper understanding of this type of disease is the key to further improving the diagnosis preoperatively. Further advanced imaging examination should be performed if the intrahepatic bile duct of one lobe or around the tumor is found dilated. The existence of tumor thrombosis in bile duct should be considered when an occupying lesion is found within bile duct. Fortunately, in recent years, more correct preoperative diagnosis could be made in this type of patients.

MR cholangiography (MRCP) is an absolutely noninvasive imaging modality, which has been shown to be superior to ERCP in detecting the presence of biliary obstruction. Both primary liver tumors and dilatation of biliary system could be demonstrated in MRCP^[15]. Presence of intraluminal soft tissue at the bile duct, and enhancement of the intraluminal soft tissue in the arterial phase are 2 typical features of HCC with BDT (Figure 2). However, these characteristic cholangiographic features should be differentially diagnosed with papillary type cholangiocarcinoma, intraductal polyps or mucin-hypersecreting intrahepatic biliary neoplasm, or intrahepatic cholangiocarcinoma with invasion of extrahepatic bile duct, and even the bile duct stones^[16]. It still relies on other information, such as the presence of liver cirrhosis, hepatitis markers, tumor markers (AFP, CEA), the fluctuation of jaundice, and hemobilia.

The prognosis of this type of HCC is generally dismal, particularly for those with obstructive jaundice^[2,3]. However, the prognosis of these patients is better than those HCC patients who have jaundice caused by hepatic insufficiency, which is closely related to the stage of disease, the location and extent of BDT. Different therapies also influence the prognosis of this type of patients. Surgical resection is the only way that possibly cures the patients. Jaundice is not necessarily a harbinger of advanced disease and a contraindication for surgery. The goals of operative intervention are biliary decompression with removal of tumor debris or tumor-containing blood clots, and, if possible, curative resection of the hepatic tumor. The usually used operative methods are lobectomy (including the primary tumor and the tumor thrombosis in bile duct), hepatectomy combined with thrombectomy, biliary decompression and drainage (choledochotomy with T-tube drainage alone, internal biliary stenting, or biliary diversion). The ideal treatment is hepatic resections^[17-19]. Patients who received curative liver resection had a much better survival rate than those without resection^[20-24]. In our series, the postoperative 1-year survival rate of patients was 71.4%, 1-year disease-free survival rate was 21.4%, and one patient has survived over 15 years. These are better than that of previous reports. It might be attributed to active attitude of the doctors and appropriate procedures of treatment taken. All of the 4 long-term survivors received major liver resection (hemihepatectomy) and removal of BDT, while the 3 patients who received biliary decompression only survived 2, 3, and 3.5 mo, respectively. So, to improve survival, if the patient's liver function and general condition could tolerate, it is suggested to perform major liver resection with removal of BDT. However, it should be very careful to perform major liver resection for those patients with both severe liver cirrhosis and severe obstructive jaundice, because their liver function reservation is very poor. In this series, one patient died of liver failure postoperatively even though his liver function test was good (except for obstructive jaundice). If hepatic resection cannot be accomplished with bile duct resection due to limited liver function, non-surgical modalities should be considered instead of surgery.

Surgical intervention is very effective to relieve the

obstruction of bile duct in this type of patients. It could take a long time (such as 3 mo in one case of this study) for the serum bilirubin of patients with obstructive jaundice to return to normal, or even transiently increase in short time after operation though the obstruction in bile duct has been dispelled completely. The altering pattern and the duration for the serum bilirubin to return to normal after operation, especially for those with severe preoperative obstructive jaundice, still need further studying.

The ideal way to remove BDT is *en bloc* resection with the primary tumor. It is also relatively easy to remove BDT either with the exploration of CBD or from the cut-end of bile duct after hepatectomy. However, active hemorrhage occurred during operation in some cases, possibly because of the continuity of the intraductal tumor debris with the main intrahepatic tumor. In this study, we met one patient with active bleeding during the operation after removing the thrombosis from the common hepatic duct. The hemostasis was achieved finally by infusing noradrenalin in normal saline into the bile duct and oppressing locally. Suturing, electrocauterization, compression, Pringle's maneuver, or hepatic arterial ligation are some alternative ways to achieve hemostasis.

BDT often grows faster than the primary cancer. We found in 2 cases, the BDT was as long as 6 cm, and 9 cm, respectively, while their primary HCC less than 6 cm. The primary tumor often has no capsule, with unclear tumor margin, and invasive growth. The infiltrative nature of this particular type of HCC may in part explain their invasion of the biliary tree early in their growth without regard to tumor size or type^[25,26], which might also be one of the reasons that the prognosis of this type of patients was very poor. In this series, the 1-year recurrence rate was 50.0%, and as high as 29.0% of the patients were found having tumor recurrence within 3 mo after operation. This might also indicate the poor malignant phenotype of this type of HCC. Combined chemotherapy or chemoembolization might be helpful to control the postoperative recurrence^[27].

In summary, HCC with tumor thrombosis in bile duct, particularly with obstructive jaundice as the main presenting clinical feature, is uncommon. The prognosis of this type of HCC is generally dismal, but is better than those HCC patients who have jaundice caused by hepatic insufficiency. Jaundice is not necessarily a harbinger of advanced disease and a contraindication for surgery. If appropriate procedures are selected and carried out safely, it can result in long-term relief of symptoms and occasional long-term survival. Deeper understanding, and active attitude to treatment of this type of disease are the keys to further improving survival of these patients.

REFERENCES

- 1 Kew MC, Paterson AC. Unusual presentations of hepatocellular carcinoma. *Trop Gastroenterol* 1985; **6**: 10-22
- 2 Kojiro M, Kawabata K, Kawano Y, Shirai F, Takemoto N, Nakashima T. Hepatocellular carcinoma presenting as intrabiliary duct tumor growth. A clinicopathological study of 24 cases. *Cancer* 1982; **49**: 2144-2147
- 3 Qin LX, Tang ZY. Hepatocellular carcinoma with obstructive jaundice: diagnosis, treatment and prognosis. *World J Gastroenterol* 2003; **9**: 385-391
- 4 Mallory TB, Castleman B, Parris EE. Case records of the Massachusetts General Hospital. *N Eng J Med* 1947; **237**: 673-676
- 5 Lin TY, Chen KM, Chen YR, Lin WS, Wang TH, Sung JL. Icteric type hepatoma. *Med Chi Dig* 1975; **4**: 267-270
- 6 Okuda K. Clinical aspects of hepatocellular carcinoma: analysis of 134 cases. In: Okuda K, Peters RL, eds. *Hepatocellular carcinoma*. New York: John Wiley 1976: 387-436
- 7 Jan YY, Chen MF. Obstructive jaundice secondary to hepatocellular carcinoma rupture into the common bile duct: choledochoscopic findings. *Hepatogastroenterology* 1999; **46**: 157-161
- 8 Lau WY, Leung JW, Li AK. Management of hepatocellular carcinoma

- noma presenting as obstructive jaundice. *Am J Surg* 1990; **160**: 280-282
- 9 **Huang JF**, Wang LY, Lin ZY, Chen SC, Hsieh MY, Chuang WL. Incidence and clinical outcome of icteric type hepatocellular carcinoma. *J Gastroenterol Hepatol* 2002; **17**: 190-195
- 10 **Ueda M**, Takeuchi T, Takayasu T, Takahashi K, Okamoto S, Tanaka A. Classification and surgical treatment of hepatocellular carcinoma (HCC) with bile duct thrombi. *Hepatogastroenterology* 1994; **41**: 349-354
- 11 **Spahr L**, Frossard JL, Felley C, Brundler MA, Majno PE, Hadengue A. Biliary migration of hepatocellular carcinoma fragment after transcatheter arterial chemoembolization therapy. *Eur J Gastroenterol Hepatol* 2000; **12**: 243-244
- 12 **Afroudakis A**, Bhuta SM, Ranganath KA, Kaplowitz N. Obstructive jaundice caused by hepatocellular carcinoma. *Dig Dis* 1978; **23**: 609-617
- 13 **Buckmaster MJ**, Schwartz RW, Carnahan GE, Strodel WE. Hepatocellular carcinoma embolus to the common hepatic duct with no detectable primary hepatic tumor. *Am Surg* 1994; **60**: 699-702
- 14 **Wang JH**, Chen TM, Tung HD, Lee CM, Changchien CS, Lu SN. Color Doppler sonography of bile duct tumor thrombi in hepatocellular carcinoma. *J Ultrasound Med* 2002; **21**: 767-772
- 15 **Fulcher AS**, Turner MA, Capps GW, Zfass AM, Baker KM. Half-Fourier RARE MR cholangiopancreatography: experience in 300 subjects. *Radiology* 1998; **207**: 21-32
- 16 **Yeh TS**, Jan YY, Tseng JH, Chiu CT, Chen TC, Hwang TL, Chen MF. Malignant perihilar biliary obstruction: magnetic resonance cholangiopancreatographic findings. *Am J Gastroenterol* 2000; **95**: 432-440
- 17 **Chen MF**, Jan YY, Jeng LB, Hwang TL, Wang CS, Chen SC. Obstructive jaundice secondary to ruptured hepatocellular carcinoma into the common bile duct. *Cancer* 1994; **73**: 1336-1340
- 18 **Jan YY**, Chen MF, Chen TJ. Long term survival after obstruction of the common bile duct by ductal hepatocellular carcinoma. *Eur J Surg* 1995; **161**: 771-774
- 19 **Tantawi B**, Cherqui D, Tran van Nhieu J, Kracht M, Fagniez PL. Surgery for biliary obstruction by tumour thrombus in primary liver cancer. *Br J Surg* 1996; **83**: 1522-1525
- 20 **Lau WY**, Leung KL, Leung TW, Liew CT, Chan MS, Yu SC, Li AK. A logical approach to hepatocellular carcinoma presenting with jaundice. *Ann Surg* 1997; **225**: 281-285
- 21 **Wang HJ**, Kim JH, Kim WH, Kim MW. Hepatocellular carcinoma with tumor thrombi in the bile duct. *Hepatogastroenterology* 1999; **46**: 2495-2499
- 22 **Hu J**, Pi Z, Yu MY, Li Y, Xiong S. Obstructive jaundice caused by tumor emboli from hepatocellular carcinoma. *Am Surg* 1999; **65**: 406-410
- 23 **Lau WY**, Leung KL, Leung TW, Ho S, Chan M, Liew CK. Obstructive jaundice secondary to hepatocellular carcinoma. *Surg Oncol* 1995; **4**: 303-308
- 24 **Nishio H**, Miyata K, Hanai M, Kato M, Yoneyama F, Kobayashi Y. Resection of an icteric type hepatoma with tumor thrombi filling the right posterior bile duct. *Hepatogastroenterology* 2002; **49**: 1682-1685
- 25 **Huang GT**, Sheu JC, Lee HS, Lai MY, Wang TH, Chen DS. Icteric type hepatocellular carcinoma: revisited 20 years later. *J Gastroenterol* 1998; **33**: 53-56
- 26 **Tseng JH**, Hung CF, Ng KK, Wan YL, Yeh TS, Chiu CT. Icteric-type hepatoma: magnetic resonance imaging and magnetic resonance cholangiographic features. *Abdom Imaging* 2001; **26**: 171-177
- 27 **Fukuda S**, Okuda K, Imamura M, Imamura I, Eriguchi N, Aoyagi S. Surgical resection combined with chemotherapy for advanced hepatocellular carcinoma with tumor thrombus: report of 19 cases. *Surgery* 2002; **131**: 300-310

Edited by Zhu LH Proofread by Xu FM

Construction of human liver cancer vascular endothelium cDNA expression library and screening of the endothelium-associated antigen genes

Xing Zhong, Yu-Liang Ran, Jin-Ning Lou, Dong Hu, Long Yu, Yu-Shan Zhang, Zhuan Zhou, Zhi-Hua Yang

Xing Zhong, Yu-Liang Ran, Dong Hu, Long Yu, Yu-Shan Zhang, Zhuan Zhou, Zhi-Hua Yang, Department of Cell and Molecular Biology, Cancer Institute (Hospital), Chinese Academy of Medical Sciences and Peking Union Medical College, Beijing, 100021, China
Jin-Ning Lou, Institute of Clinical Medical Sciences, China-Japan Friendship Hospital, Beijing 100029, China

Supported by the National 863 Program, No.2001AA221251 and the National Natural Science Foundation of China, No.30230150

Correspondence to: Professor Zhi-Hua Yang, Department of Cell and Molecular Laboratory, Cancer Institute (Hospital), Chinese Academy of Medical Sciences and Peking Union Medical College, Panjiayuan, Chaoyang Qu PO Box, Beijing, 100021, China. zhyang@public.bta.net.cn

Telephone: +86-10-87771740 **Fax:** +86-10-67713359

Received: 2003-10-15 **Accepted:** 2003-12-02

Abstract

AIM: To gain tumor endothelium associated antigen genes from human liver cancer vascular endothelial cells (HLCVECs) cDNA expression library, so as to find some new possible targets for the diagnosis and therapy of liver tumor.

METHODS: HLCVECs were isolated and purified from a fresh hepatocellular carcinoma tissue sample, and were cultured and proliferated *in vitro*. A cDNA expression library was constructed with the mRNA extracted from HLCVECs. Anti-sera were prepared from immunized BALB/c mice through subcutaneous injection with high dose of fixed HLCVECs, and were then tested for their specificity against HLCVECs and angiogenic effects *in vitro*, such as inhibiting proliferation and inducing apoptosis of tumor endothelial cells, using immunocytochemistry, immunofluorescence, cell cycle analysis and MTT assays, etc. The identified xenogeneic sera from immunized mice were employed to screen the library of HLCVECs by modified serological analyses of recombinant cDNA expression libraries (SEREX). The positive clones were sequenced and analyzed by bio-informatics.

RESULTS: The primary cDNA library consisted of 2×10^6 recombinants. Thirty-six positive clones were obtained from 6×10^5 independent clones by immunoscreening. Bio-informatics analysis of cDNA sequences indicated that 36 positive clones represented 18 different genes. Among them, 3 were new genes previously unreported, 2 of which were hypothetical genes. The other 15 were already known ones. Series analysis of gene expression (SAGE) database showed that *ERP70*, *GRP58*, *GAPDH*, *SSB*, *S100A6*, *BMP-6*, *DVS27*, *HSP70* and *NAC alpha* in these genes were associated with endothelium and angiogenesis, but their effects on HLCVECs were still unclear. *GAPDH*, *S100A6*, *BMP-6* and *hsp70* were identified by SEREX in other tumor cDNA expression libraries.

CONCLUSION: By screening of HLCVECs cDNA expression library using sera from immunized mice with HLCVECs,

the functional genes associated with tumor endothelium or angiogenesis were identified. The modified SEREX, xenogeneic functional serum screening, was demonstrated to be effective for isolation and identification of antigen genes of tumor endothelium, and also for other tumor cell antigen genes. These antigen genes obtained in this study could be a valuable resource for basic and clinical studies of tumor angiogenesis, thus facilitating the development of anti-angiogenesis targeting therapy of tumors.

Zhong X, Ran YL, Lou JN, Hu D, Yu L, Zhang YS, Zhou Z, Yang ZH. Construction of human liver cancer vascular endothelium cDNA expression library and screening of the endothelium-associated antigen genes. *World J Gastroenterol* 2004; 10 (10): 1402-1408

<http://www.wjgnet.com/1007-9327/10/1402.asp>

INTRODUCTION

Angiogenesis is a critical event in solid tumor growth, invasion, and metastasis. Recently, more attractive targets are thought to be vasculature of tumor compared with tumor cells themselves in the therapy of solid tumor^[1]. Tumor endothelium is a key mediator during the complex process of tumor angiogenesis. There will not form new blood vessels in tumor if tumor vascular endothelia are lacking of the functions of proliferation, activation, adhering, migration and vessel formation. To date, the morphology, phenotype, functional aspects and gene expression observed in tumor-derived endothelial cells (TEC) were proven to be different from normal-derived endothelial cells (NEC)^[2,3]. Virtually, the therapeutic strategy of solid tumors targeting for tumor vasculature makes use of these differences. Various methods have been developed to identify the differences between TEC and NEC, such as serial analysis of gene expression (SAGE)^[4], suppression subtractive hybridization (SSH)^[5], antibody target^[6], immunohistochemical analysis of known endothelial adhesion molecules^[7] phage display peptide library^[8], and cDNA microarray^[9], etc. Due to the difficulty of isolating highly purified TEC, most studies now selected activated endothelial cells as a substitute, however, the activated endothelial cells cannot completely represent TEC.

SEREX has recently emerged as a powerful method for serological identification of tumor associated antigens (TAAs) and/or tumor rejection antigens (TRAs). Up to date, more than 1 000 candidate tumor antigens in various cancers have been identified^[10,11]. Tumor antigens identified by SEREX could provide valuable targets for cancer diagnosis, therapy and the study of cancer vaccines. Similarly, the proliferation-associated antigens on tumor endothelial cells may be more useful candidates for antiangiogenic therapy/vascular targeting therapy of tumor. However, up to the present, no data are available that associated antigen genes have been isolated from TEC.

The goal of this study was to define tumor endothelium associated antigen genes by the method of modified SEREX.

Therefore, we constructed and screened the HLCVECs cDNA expression library with murine immunosera of anti-HLCVECs, and identified 18 HLCVECs associated antigen genes. These genes may not only provide a valuable tool for study on the roles of endothelial cells in tumor angiogenesis, but also some potent candidate targets for antiangiogenic therapy of cancer. Our results in this report also indicated that the approach of screening cDNA expression library with functional xenogeneic sera, a modified SEREX, could be an effective strategy for isolation and identification of tumor endothelium associated antigen genes.

MATERIALS AND METHODS

Tumor tissue samples and cells

Human tumor tissue was obtained from therapeutic surgical resection of one patient with hepatocellular carcinoma (HCC) at the Cancer Hospital of Peking Union Medical College. After surgical removal, the tissue sample was immediately transferred to the laboratory in cold culture medium (DMEM, GIBCO) with penicillin (400 U/mL) and EDTA (1 g/L) and was isolated for 2 h. Human umbilical vein endothelial cells (HUVECs) were isolated as described^[12]. HUVECs were stimulated to generate activated HUVECs with endothelium growth medium (Clontech) containing EC growth factors and tumor tissues homogenate prepared in our laboratory.

Isolation, purification and culturing of HLCVECs

Isolation, purification and culturing of HLCVECs were performed by previously described method^[13,14] with some modifications. Briefly, the liver cancer tissue from patient with HCC was finely minced with curved scissors into approximately 2 mm×2 mm×2 mm pieces, then was re-suspended in 20 mL of 1 g/L trypsin (type II, Sigma) in DMEM containing 1 g/L EDTA and incubated for 10 min at 37 °C. After digestion, the whole suspension was filtered through a 200 µm melt mesh sieve and the filtrate was washed twice in DMEM by centrifugation at 450 r/min for 5 min at room temperature. The pellet was re-suspended in 5 mL of DMEM + 100 g/L FCS (Hyclon) added to 25 mL of 200 g/L percoll (Pharmacia Biotech) in DMEM and centrifuged at 1500 g for 15 min at 4 °C. Again, the cell pellet was washed twice. The isolated cells were resuspended in complete culture medium (DMEM containing 200 mL/L FCS, 2 mmol/L L-glutamin (GIBCO), 100 µg/mL antibiotic (penicillin/streptomycin), 100 µg/mL endothelial cell growth supplement and 40 U/mL heparin). The cells were seeded into a 20 g/L gelatin-coated 6-well plate (FALCON), and cultured at 37 °C in 50 mL/L CO₂ incubator and the medium was changed every 3 d, the purification could be carried out by the way of sub-cell colonies after 1 wk. The cells were cultured and proliferated in gelatin-coated T75 plastic tissue culture flasks (Falcon), and passaged by 1 g/L trypsin (1 g/L EDTA). The purified endothelial cells were identified by immunocytochemistry for von Willebrand factor (vWF), CD31 and uptake of Ac-LDL. Fenestration was demonstrated by transmission electron microscopy.

Preparation of the anti-HLCVECs immunosera

Female BALB/c mice (6-8 wk) were purchased from Experimental Animal Center of Peking Union Medical College. Six mice were immunized with HLCVECs (immunized), and 4 mice were treated with PBS alone (non-immunized). All studies on mice were approved by the institute's Animal Care and Use Committee.

Sera were obtained as described^[15]. For the generation of immunosera, mice were immunized subcutaneously with 1-6×10⁶ HLCVECs fixed with 30 g/L paraformaldehyde in PBS or PBS alone once weekly for 8 continuous weeks. Serum was obtained from each mouse of immunized and non-immunized on d 21, 28, 35, 42, 49 and 56 after the first immunization. Serum from each

mouse of immunized and non-immunized groups was serially diluted, and the reactivity against HLCVECs was examined by immunocytochemistry.

Immunofluorescence

To determine the reactivity of sera from immunized and non-immunized mice reacting to different endothelium, HLCVECs, HUVECs and activated HUVECs were seeded onto glass coverslips in 6-cm plates, then fixed in cold acetone and incubated with serially diluted sera isolated from immunized or non-immunized mice at 37 °C for 1 h, fluorescein-conjugated goat-anti-mouse IgG (H+L) (Sigma) was subsequently applied to them and incubated for another 1h, then to be restained by 0.1 g/L Evens Blue and washed 3 times by PBS. The results were observed under fluorescence microscope (Nicon)^[16].

MTT assay

Approximately 8×10³ cells in 200 µL DMEM were seeded in triplicate into each well of the 96-well tissue culture plates, and immunized or non-immunized sera diluted at 1:30, 1:90, 1:270, 1:810, 1:2430, 1:7290 and 1:21870 were added to corresponding wells. After 72 h of incubation, 10 µL MTT (100 mg/mL) reagent was added to each well (5 g/L), and incubated for 4 h at 37 °C, 50 mL/L CO₂. Subsequently, 180 µL medium was pipetted out from each well and 50 µL DMSO was added to it. The absorbency A₅₇₀, which correlates to the number of cells, was measured with micro-plate reader (Model 450, Bio-Rad)^[17].

Cell cycle analysis by flow cytometry

HLCVECs were serum starved for 24 h and then treated with immunized and non-immunized sera diluted at 1:100 for 6 h. Cells were trypsinized, washed twice in PBS. Totally 1×10⁶ cells were resuspended in 500 µL PBS and stained with 500 µL propidium iodide (10 µg/mL, Sigma) for 30 min. Flow Cytometry (Becton) was performed to determine DNA content and apoptosis^[18].

Construction of cDNA expression library

The mRNA was directly extracted from HLCVECs with mRNA extraction kit (mRNA Poly(A) Tract System 1 000, Promega, Madison, WI), Oligo (dT)-primed double-stranded cDNA was synthesized from 6 µg purified mRNA and ligated into the ZAP phage expression vector DNA according to the user's manual (including THERMO Script™ RT-PCR System Kit, ZAP-cDNA synthesis kit, ZAP-cDNA Gigapack III Gold Mrna Cloning kit, Stratagene).

Screening the HLCVECs cDNA expression library with immunosera

Immunoscreening of the HLCVECs cDNA expression library was performed as described previously^[19] with the following modifications. Sera from immunized mice were diluted 1:10 and preabsorbed with lysate from *Escherichia coli* (*E.coli*) strain XL-1 coupled to Sepharose 4B to remove antibodies reacting with *E.coli* components. X-L1 infected with recombinant phage vectors containing HLCVECs cDNA were plated onto NZY-tetracycline-agar plates. After induction of protein synthesis in *E.coli*, we transferred the expressed polypeptides onto nitrocellulose membranes (Gelman) and incubated them with 1:500 diluted pre-absorbed sera overnight at 4 °C in the first screening. After being washed, the filters were incubated with a 1:10 000 dilution of alkaline phosphatase-conjugated goat-anti-mouse IgG (H+L) (Secondary Ab, Sigma) for 1-2 h at room temperature. Reactive clones were visualized with 5-bromo-4-chloro-3-indolyl-phosphate/nitro blue tetrazolium tablets (BCIP/NBT, Sigma). Only clones that appeared blue were considered serum positive. The positive clones were picked out and plated on NZY-tetracycline agar plates for secondary screening with

1:5 000 diluted pre-absorbed immunosera. Subsequently, positive clones were subcloned 2 times to obtain monoclonality.

Sequence analyses of the reactive clones

Identified and subcloned positive clones were converted to pBluescript phagemid forms by *in vitro* excision, plasmid was purified and subjected to *EcoR* I and *Xho* I restriction enzyme digestion. Clones representing different cDNA inserts were sequenced with T3 primers by the dideoxy chain termination method using the Big Dye Terminator Cycle Sequencing Kit (PE Applied Biosystems, Foster city, CA) and an ABI PRISM automated DNA sequencer (Perkin-Elmer, Norwalk, CT). DNA and predicted amino acid sequences were compared with sequences in the GenBank and other public databases by using the BLAST program.

RESULTS

Identification of HLCVECs

The heterogeneity of human TEC is detectable at different levels and differentiates the behavior between different tumor tissues. HLCVECs here belong to micro-vascular ECs, and they grow in a monolayer and exhibit contact inhibition properties. Using electron microscopy, surface fenestrations and Weibel-Palade (W-P) bodies were observed in HLCVECs. Immunofluorescence staining showed that these cells expressed vWF, CD31 and took up large amounts of Ac-LDL (Figure 1). These results demonstrated that isolated and purified HLCVECs expressing specific markers of endothelial cells, especially fenestration, a tumor endothelium-specific structure, were also found in HLCVECs.

Detection of antibodies against endothelial cells in immunosera

The antibody titer in sera from immunized mice with HLCVECs are shown in Table 1. Titer of antibody reached 1:1 000 at 21 d after the first immunization, 1:9 000 at 42 d and 1:27 000 at 49 d as well as at 56 d. In contrast, the sera from non-immunized

mice were negative for anti-HLCVECs response. A similar antibody response, with a minimal variation in titer, was seen in all six immunized mice.

To determine whether differences existed in reactivity of sera from mice immunized with HLCVECs with human TEC versus NEC, immunofluorescence was applied to detect the reaction of anti-HLCVECs sera with HLCVECs, HUVECs and activated HUVECs. The results indicated that 1:500 dilution of the immunized serum showed the same degree fluorescence staining in HLCVECs and activated HUVECs, but the staining in HUVECs was distinctly weaker than that of the other 2 kinds of cells. The 1:5 000 dilutions of immunosera showed markedly stronger staining with HLCVECs than with activated HUVECs (Figures 2A and 2B), whereas the staining of HUVECs was completely negative in this dilution (Figure 2C). By comparison, the staining of all the 3 kinds of cells was negative when reacting with sera from non-immunized mice. Simultaneously, the fluorescence staining was observed in the membrane of positive endothelial cells. These data indicated that the murine anti-HLCVECs sera contained the specific antibodies with a high titer against TECs.

Table 1 Titer of anti-HLCVECs antibody in immunized animals

	D21	D28	D35	D42	D49	D56
HLCVEC	1:1 000	1:3 000	1:9 000-	1:9 000	1:27 000	1:27 000+

1:9 000- indicates that the titer is lower than 1:9 000, 1:27 000+ indicates that the titer is 1:27 000 or higher.

Identification of the effect of immunosera on ECs growth

To investigate whether the immunosera have any effects on the proliferation of HLCVECs, HLCVECs were treated with variously diluted sera isolated from mice immunized or non-immunized with HLCVECs. MTT assay demonstrated that the growth and proliferation of HLCVECs were apparently inhibited by the sera from immunized mice with HLCVECs, and there was

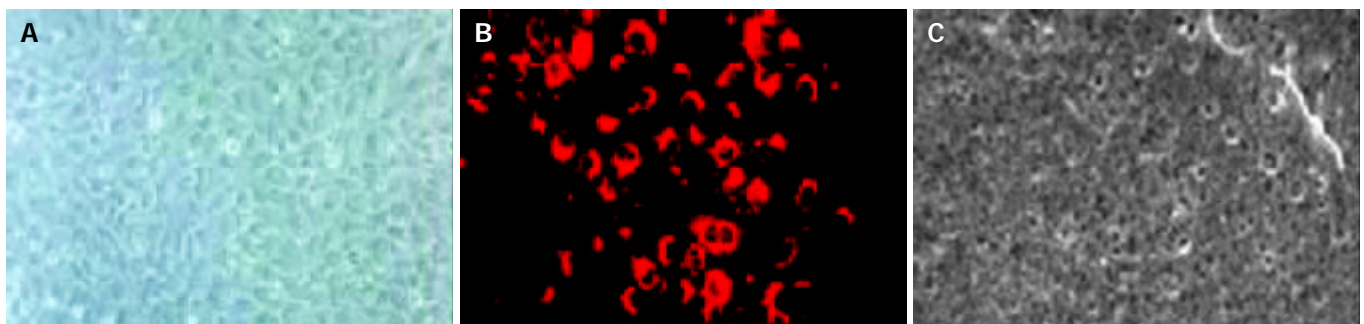


Figure 1 Cultured human liver cancer vascular endothelial cells. A: Morphology of cultured human liver cancer vascular endothelial cells; B: Uptake of Ac-LDL; C: Electron microscope for fenestration.

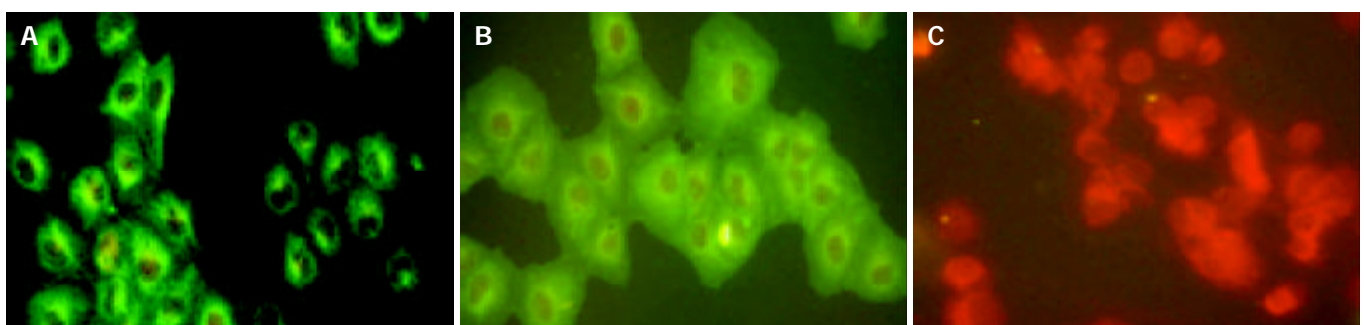


Figure 2 Immunofluorescence analysis of endothelial cells stained with the sera diluted 1:5 000 isolated from the mice immunized with HLCVECs. A: HLCVECs; B: Activated HUVECs; C: HUVECs.

Table 2 Construction of HLCVECs libraries in λ -ZAP expression vector and the number of SEREX-identified antigens

Patient	Age (years)	Primary size	Screening serum	Clones screened	Positive clones	cDNA fragment	Known genes	Unknown gene
HCC	56	2×10^6	immunized	6×10^5	36	18	15	3

Table 3 Results of immunoscreening of HLCVECs cDNA expression library by immunized BALB/C sera screening

Clone	Size (bp)	Gene	Localization	Identity	Accession number
EC19	2 100	HS.Protein disulfide isomerase related protein	7q35	99%	NM 004911.2
EC24	700	HS.Glucose regulated protein	15q15	98%	NM 005313.3
EC26	1 000	HS.Chemokine ligand 1	4q12-q13	99%	BC 011976
EC29	1 600	HS.Inner membrane protein	2p11.2	99%	NM 006839.1
EC30	1 800	HS.Hypothetical protein Loc283241	11q12.3	99%	XM 208579.1
EC31	1 700	HS.genomic DNA, clone	11q	98%	AP 002340.3
EC35	700	HS.BMP-6	15q13-q15	98%	NM 013372.1
EC36	2 200	HS.Glycerol dehyde-3-phosphate dehydrogenase	12p13.31	98%	BC 004109
EC38	1 900	HS.Replication factor C5	12q24.2	99%	NM 007370.2
EC39	2 100	HS.BAC, CloneRP11-1591120		99%	AC 010974.9
EC40	800	HS.Sjogren syndrome antigen B	2q31.1	98%	BC 020818
EC42	2 400	HS.X-ray repair complementing defective repair in Chinese	12q23	99%	AY 034001.1
EC51	400	HS.S100 calcium-binding protein A6	1q21	100%	BC 009017
EC52	1 500	HS.Protein kinase C	19p1.1	98%	NM 002743.1
EC53	1 700	HS.Heat shock 70 ku protein4	5q31.3	99%	XM 114482.2
EC59	1 900	HS.DVS27 related protein	9p24.1	99%	BC 04785.1
EC62	1 500	HS.NAC alpha mRNA	12q2	99%	AY 034001.1
EC63	1 500	HS.Hypothetical protein DJ1042k10.2	2 213.1	100%	HS1042k10

a dose dependent response from 1:30 to 1:2 430 dilution of the murine immunosera, while no inhibitory effects were observed in sera from non-immunized mice. Figure 3 shows the results of serum from one of six immunized mice and one of 4 non-immunized mice.

Using MTT assay, we observed that human TEC growth was inhibited when they were incubated with the immunosera, however, the underlying mechanism was unknown. We therefore studied further the effects of the sera on cell cycle of human TEC with Flow Cytometry. The results showed that the amount of apoptotic cells were increased in the group of immunosera compared with the group of non-immunosera at 6 h after treatment (Figure 4). Approximately 20.1% apoptotic cells were seen in the group of immunized serum and only 4.9% apoptotic cells were observed in the group of non-immunized serum. The results further indicated that, in terms of specificity and the effects on human TEC, the immunized sera were suitable to screen the HLCVECs cDNA expression library to obtain endothelium associated antigen genes.

Isolation of HLCVECs associated antigens genes by modified SEREX

HLCVEC cDNA expression library with 2×10^6 primary clones was established (Table 2). The 6×10^5 clones were immunoscreened with pooled sera from six immunized BALB/c mice collected on d 56 after inoculation of HLCVECs. Primary screening with 1:500 diluted pooled immunosera yielded 153 positive clones (named EC1 to EC153). After secondary screening with 1:5 000 immunosera and subcloning, a total of 36 positive clones were obtained (Figure 5). These 36 clones were then excised, to phagemide forms and purified *in vitro*. The size of inserts of these positive clones were determined by restriction enzyme digestion with *Eco*R I and *Xho*I, which yielded inserts sized from 900 bp to 3 600 bp, with an average of about 1 500 bp (Figure 6).

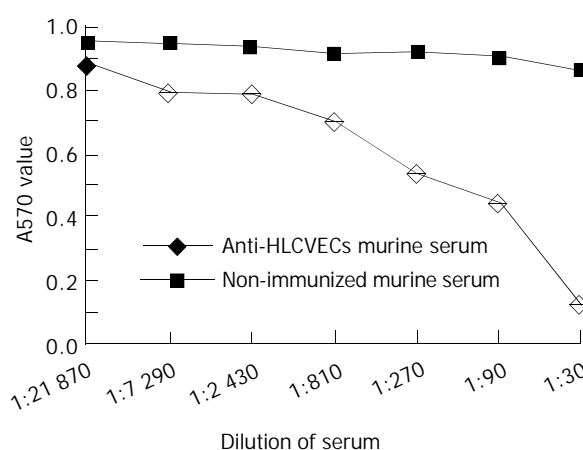


Figure 3 Inhibition of the HLCVECs proliferation by HLCVECs immunized murine serum from 1 of 6 immunized mice and 1 of 4 non-immunized mice. Points are the average of three wells.

Sequence analysis of the positive clones

Nucleotide sequences of cDNA inserts of 36 positive clones were sequenced. Sequence alignments were analyzed with DNASIS and BLAST software on EMBL and GeneBank. These 36 positive clones represented 18 different antigen genes (Table 3). EC36 was represented by 11 overlapping clones, EC42 by 6 overlapping clones, EC 62 by 4 overlapping clones and the others by a single clone. Of these 18 clones, 3 clones were new unknown genes, 2 of which may be functional genes encoding hypothetical proteins. The other 15 genes were known. However, all of them were first isolated and reported in the endothelial cells of human HCC here. By SAGE database analysis, the 15 genes can be grouped into different classes: (1) 9 of these genes are associated with endothelium and angiogenesis, such

as EC26, EC52, EC59, *etc.* (2) 4 of these genes have been reported previously as tumor antigen genes, such as NAPDH, S100A6, BMP-6 and hsp70, (3) The other genes are involved in genes transcription, protein translation and cell mitosis, such as inner membrane protein gene (IMMT).

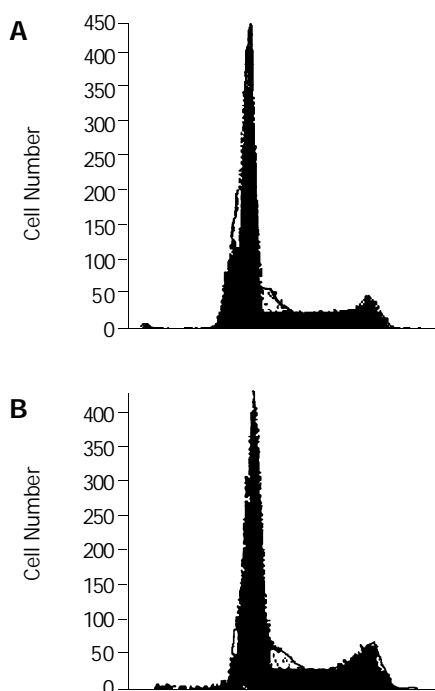


Figure 4 Cell cycle analysis of HLCVECs after treatment with immune sera or non-immune sera. A: HLCVECs treated with immune sera for 6 h; B: HLCVECs treated with non-immune sera for 6 h.

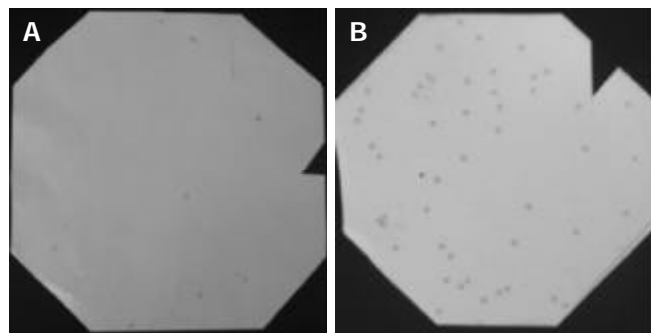


Figure 5 Positive dots of phage clone of screening by immune sera. A: The first cycle of screening by immune sera; B: The second cycle of screening by immune sera.

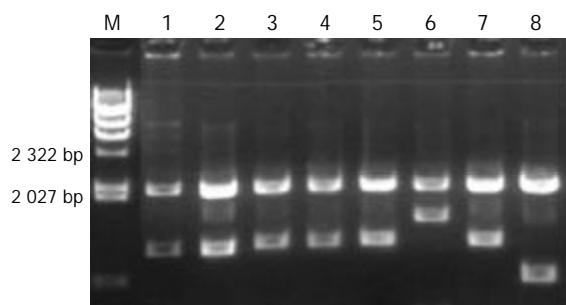


Figure 6 Electrophoresis analysis of enzymatic digestion of SEREX positive clones. M, λ Hind III marker, from above to below: 20 130, 9 416, 6 557, 4 316, 2 322, 2 027, 564 bp; Lanes 1-8, positive clones digested with *EcoR* I and *Xho* I.

DISCUSSION

Tumor angiogenesis is dependent on biochemical processes mediating the formation and development of the blood capillary network that supplies the tumor. In recent years, increasing evidence has indicated that targeting tumor vasculature is a very promising strategy for the therapy of solid tumor. Identifying molecular markers, target genes and antigen on endothelial cells of tumor vessels, in turn, is critical for the antiangiogenic therapeutic strategy of tumor. A number of researchers have gained some endothelia associated genes from activated HUVECs with cell growth factors and supernatant of cultured tumor cells. But it is difficult to determine tumor specific endothelial genes by these ways, because activated endothelium cannot completely represent tumor endothelium. In 2000, Croix^[4] first reported in *Science* that they successfully isolated tumor endothelium from human colorectal cancer and gained tumor endothelium associated genes by the method of SAGE. In the present study, to obtain specific endothelium genes of human liver cancer vascular endothelial cells, we isolated and purified endothelial cells from liver tumor tissue of the patients with HCC. These endothelial cells were confirmed to have characteristics of endothelial cells with expressing vWF, CD31, W-P bodies and taking up high level of Ac-LDL, *etc.*, and also have the structure of fenestrations found only in tumor endothelial cells. From cDNA expression library constructed with above purified HLCVECs, we isolated 18 endothelia associated genes. Some of them were related to human TEC. Up to date, there have been no reports about the successful isolation of human liver cancer vascular endothelial cells and their specific genes.

Over the past years, efforts have been made to isolate and identify the proliferating TEC genes, including the methods of phage display peptide libraries, SSH and SAGE analysis, *etc.* However, the genes identified using these methods, in terms of their specificity and functions were rarely known. Therefore, in this study, to isolate and identify functional TEC associated antigen genes, we modified traditional SEREX and used it to screen cDNA expression library of HLCVECs. SEREX has recently emerged as a powerful method for identification of human tumor-associated antigen. The identification of tumor antigens with SEREX was based on the existence of autoantibodies in sera of patients^[10]. It is not unexpected that the method is applicable to only a limited number of patients because autoantibodies against most antigens can only be detected in 10-30% patients who bear tumors expressing the corresponding antigens. Therefore, a number of modifications have been made since the introduction of SEREX methodology to expand the range of antigens identified. These modifications include using established cell lines instead of tumor specimen to construct the cDNA library, and using allogeneic sera or xenogeneic sera instead of autologous sera as the antibody source. Hideho *et al.*, introduced the "cytokine-assisted SEREX (CAS)", which resulted in an enhanced capacity to identify glioma tumor associated antigens (TAAs) with characteristics similar to TAAs identified by traditional SEREX^[19-21]. Despite extensive screening of various tumor cDNA libraries with sera from tumor patients, however, identification of human tumor endothelium associated antigens by SEREX have not been reported up to date. To develop a method to screen the endothelium associated functional genes, we first immunized BALB/c mice by injection subcutaneously with high dose purified HLCVECs. Sera from the immunized mice were identified with several fixed methods for their specificity against HLCVECs and the effects on endothelial cells. For example, detection by immunocytochemistry and immunofluorescence showed that the ability of immunosera to bind HLCVECs were higher compared with activated HUVECs when sera were diluted at 1:5 000, whereas the staining of unactivated HUVECs were completely negative. These data

indicated that the immunosera still contained specific antibodies directed against HLCVECs in this dilution. By MTT assay and cell cycles analysis, we have also demonstrated that the growth and proliferation of HLCVECs were significantly inhibited when treated with anti-HLCVECs immunosera in range of 1:30-1:2430 dilution, while this inhibitory effect of sera from non-immunized (only injected by PBS) mice was not observed. To identify the possible mechanism about anti-HLCVECs proliferation activity of immunosera, we employed Flow Cytometry to analyse cell cycle of HLCVECs treated with the immunosera. The results showed that there was a 4-fold increase in the amount of apoptotic cells compared with the group of non-immunosera. These findings suggested that the anti-sera obtained from mice immunized with high dose of fixed HLCVECs presented some functional immunoglobulin with potent antiangiogenic activity. Similar results were also observed by Scappaticci *et al.*^[18], who recently demonstrated that vaccination of rabbits with murine endothelial cells yielded immunized sera with antiangiogenic effects *in vitro* and that the mechanism of antiangiogenic effect was proven to be through induction of apoptosis of ECs by polyclonal immunoglobulin in this serum. Furthermore, Wei *et al.*^[15] reported also that vaccination of mice with human ECs could induce a specific antiangiogenic immune response with broad anti-tumor activity. In our study, using xenogeneic functional anti-sera from mice immunized with HLCVECs to screen cDNA expression library of HLCVECs, a modified xenogeneic SEREX, we first isolated endothelium associated antigen genes from human liver cancer vascular endothelium.

To isolate TEC associated functional antigens genes, we immunoscreened HLCVECs cDNA expression library by a modified xenogeneic SEREX. Thirty-six positive clones were identified after screening of 6×10^5 clones. Sequencing analysis for homology with the GeneBank and other public databases indicated that these clones represented 18 different genes which were first isolated and identified to be the endothelial genes from human HCC tissues. Three of them were previously not reported new genes, 2 of which may be functional gene encoding hypothetical proteins. There other 15 genes were known. SAGE analysis revealed that 9 of the 15 genes, have been reported as endothelium associated genes and some of them were involved in the proliferation, migration of endothelial cells and the process of angiogenesis. For example, EC26 has 99% homology with chemokine ligand 1(CXCL1), which was implicated having effects on endothelial cells in angiogenesis^[22]. EC35 has 99% homology with bone morphogenetic protein-6 (BMP-6), which stimulates angiogenesis and induces migration^[23,24]. EC52 may be one of the factors that up-regulate VEGF gene expression during hypoxia^[25-27]. The expression of EC59 gene was mostly highly up-regulated in cerebral arteries^[28]. Camby *et al.* found that the level of EC51 expression differed markedly in the blood vascular walls according to whether these vessels originated from low- or high-grade astrocyte tumors^[29,30]. EC53 had 99% homology with heat shock 70 ku protein (HSP70) and is expressed in human microvascular endothelial cells. The expression of HSP70 is known to increase endothelial cells survival and growth^[31-33]. These data indicated that the genes identified in this study using specific and functional antiserum from mice immunized with human TEC, may be functional genes for human endothelial cells and angiogenesis. Furthermore, this approach through screening cDNA expression library with xenogeneic serum containing specific antibodies may serve as an effective strategy for isolation and identification of human TEC genes, which will provide useful marker and targets for tumor anti-angiogenesis therapy.

In summary, the screening of HLCVECs cDNA expression library by using murine immunosera of anti-tumor endothelium yielded 18 functional antigen genes associated with tumor endothelium. These antigen genes may be related to the

proliferation, migration and vessel formation of tumor vascular endothelium. Further exploration of these genes and their relationship with tumor angiogenesis would provide a valuable resource for basic and clinical studies of anti- angiogenesis targeting therapy of tumor.

REFERENCES

- 1 **Folkman J.** Angiogenesis inhibitors generated by tumors. *Mol Med* 1995; **1**: 120-122
- 2 **Hashizume H,** Baluk P, Morikawa S, Mclean JW, Thurston G, Roberge S, Jain RK, McDonald DM. Openings between defective endothelial cells explain tumor vessel leakiness. *Am J Pathol* 2000; **156**: 1363-1380
- 3 **Alessandri G,** Chirivi RG, Fiorentini S, Dossi R, Bonardelli S, Giulini SM, Zanetta G, Landoni F, Graziotti PP, Turano A, Caruso A, Zardi L, Giavazzi R, Bani MR. Phenotypic and functional characteristics of tumour-derived microvascular endothelial cells. *Clin Exp Metastasis* 1999; **17**: 655-662
- 4 **St Croix B,** Rago C, Velculescu V, Traverso G, Romans KE, Montgomery E, Lal A, Riggins GJ, Lengauer C, Vogelstein B, Kinzler KW. Genes expressed in human tumor endothelium. *Science* 2000; **289**: 1197-1203
- 5 **Liu C,** Zhang L, Shao ZM, Beatty P, Sartippour M, Lane TF, Barsky SH, Livingston E, Nguyen M. Identification of a novel endothelial-derived gene EG-1. *Biochem Biophys Res Commun* 2002; **290**: 602-612
- 6 **Huang X,** Molema G, King S, Wakins L, Edgington TS, Thorpe PE. Tumor infarction in mice by antibody-directed targeting of tissue factor to tumor vasculature. *Science* 1997; **275**: 547-550
- 7 **Nguyen M,** Corless CL, Kraling BM, Tran C, Atha T, Bischoff J, Barsky SH. Vascular expression of E-selectin is increased in estrogen-receptor-negative breast cancer: a role for tumor-cell-secreted interleukin-1 alpha. *Am J Pathol* 1997; **150**: 1307-1310
- 8 **Koivunen E,** Arap W, Valtanen H, Rainisalo A, Medina OP, Heikkila P, Kantor C, Gahmberg CG, Salo T, Kontinen YT, Sorsa T, Ruoslahti E, Pasqualini R. Tumor targeting with a selective gelatinase inhibitor. *Nat Biotechnol* 1999; **17**: 768-774
- 9 **Lee MJ,** Van Brocklyn JR, Thangada S, Liu CH, Hand AR, Menzeleev R, Spiegel S, Hla T. Sphingosine-1-phosphate as a ligand for the G protein-coupled receptor EDG-1. *Science* 1998; **279**: 1552-1555
- 10 **Chen YT.** Cancer vaccine: identification of human tumor antigens by SEREX. *Cancer J* 2000; **6**(Suppl 3): S208-S217
- 11 **Wang Y,** Han KJ, Pang XW, Vaughan HA, Qu W, Dong XY, Peng JR, Zhao HT, Rui JA, Leng XS, Cebon J, Burgess AW, Chen WF. Large scale identification of human hepatocellular carcinoma-associated antigens by autoantibodies. *J Immunol* 2002; **169**: 1102-1109
- 12 **Martinez J,** Rich E, Barsigian C. Transglutaminase-mediated cross-linking of fibrinogen by human umbilical vein endothelial cells. *J Biol Chem* 1989; **264**: 20502-20508
- 13 **Rupnick MA,** Carey A, Williams SK. Phenotypic diversity in cultured cerebral microvascular endothelial cells. *In Vitro Cell Dev Biol* 1988; **24**: 435-444
- 14 **Lou J,** Buhler L, Deng S, Mentha G, Montesano R, Grau GE, Morel P. Inhibition of leukocyte adherence and transendothelial migration in cultured human liver vascular endothelial cells by prostaglandin E1. *Hepatology* 1998; **27**: 823-828
- 15 **Wei YQ,** Wang QR, Zhao X, Yang L, Tian L, Lu Y, Kang B, Lu CJ, Huang MJ, Lou YY, Xiao F, He QM, Shu JM, Xie XJ, Mao YQ, Lei S, Luo F, Zhou LQ, Liu CE, Zhou H, Jiang Y, Peng F, Yuan LP, Li Q, Wu Y, Liu JY. Immunotherapy of tumors with xenogeneic endothelial cells as a vaccine. *Nat Med* 2000; **6**: 1160-1166
- 16 **Lou JN,** Mili N, Decrind C, Donati Y, Kossodo S, Spiliopoulos A, Ricou B, Suter PM, Morel DR, Morel P, Grau GE. An improved method for isolation of microvascular endothelial cells from normal and inflamed human lung. *In Vitro Cell Dev Biol Anim* 1998; **34**: 529-536
- 17 **Xin L,** Xu R, Zhang Q, Li TP, Gan RB. Kringle 1 of human hepatocyte growth factor inhibits bovine aortic endothelial cell proliferation stimulated by basic fibroblast growth factor and causes cell apoptosis. *Biochem Biophys Res Commun* 2000; **277**:

- 186-190
- 18 **Scappaticci FA**, Contreras A, Boswell CA, Lewis JS, Nolan G. Polyclonal antibodies to xenogeneic endothelial cells induce apoptosis and block support of tumor growth in mice. *Vaccine* 2003; **21**: 2667-2677
- 19 **Okada H**, Attanucci J, Giezeman-Smits KM, Brissette-Storkus C, Fellows WK, Gambotto A, Pollack LF, Pogue-Geile K, Lotze MT, Bozik ME, Chambers WH. Immunization with an antigen identified by cytokine tumor vaccine-assisted SEREX (CAS) suppressed growth of the rat 9L glioma *in vivo*. *Cancer Res* 2001; **61**: 2625-2631
- 20 **Chen YT**, Gure AO, Tsang S, Stockert E, Jager E, Knuth A, Old LJ. Identification of multiple cancer/testis antigens by allogeneic antibody screening of a melanoma cell line library. *Proc Natl Acad Sci U S A* 1998; **95**: 6919-6923
- 21 **Ono T**, Sato S, Kimura N, Tanaka M, Shibuya A, Old LJ, Nakayama E. Serological analysis of BALB/C methylcholanthrene sarcoma Meth A by SEREX: identification of a cancer/testis antigen. *Int J Cancer* 2000; **88**: 845-851
- 22 **Dhawan P**, Richmond A. Role of CXCL1 in tumorigenesis of melanoma. *Leukoc Biol* 2002; **72**: 9-18
- 23 **Valdimarsdottir G**, Goumans MJ, Rosendahl A, Brugman M, Itoh S, Lebrin F, Sideras P, ten Dijke P. Stimulation of Id1 expression by bone morphogenetic protein is sufficient and necessary for bone morphogenetic protein-induced activation of endothelial cells. *Circulation* 2002; **106**: 2263-2270
- 24 **Deckers MM**, van Bezooijen RL, van der Horst G, Hoogendam J, van Der Bent C, Papapoulos SE, Lowik CW. Bone morphogenetic proteins stimulate angiogenesis through osteoblast-derived vascular endothelial growth factor A. *Endocrinology* 2002; **143**: 1545-1553
- 25 **Zhou Z**, Yang XM, Xie YZ, Yin ZY. Vascular endothelial growth factor gene expression regulated by protein kinase C pathway in endothelial cells during hypoxia. *Space Med Med Eng* 2002; **15**: 322-326
- 26 **Siflinger-Birnboim A**, Johnson A. Protein kinase C modulates pulmonary endothelial permeability: a paradigm for acute lung injury. *Am J Physiol Lung Cell Mol Physiol* 2003; **284**: L435-451
- 27 **Feener EP**, King GL. Endothelial dysfunction in diabetes mellitus: role in cardiovascular disease. *Heart Fail Monit* 2001; **1**: 74-82
- 28 **Onda H**, Kasuya H, Takakura K, Hori T, Imaizumi T, Takeuchi T, Inoue I, Takeda J. Identification of genes differentially expressed in canine vasospastic cerebral arteries after subarachnoid hemorrhage. *J Cereb Blood Flow Metab* 1999; **19**: 1279-1288
- 29 **Ilg EC**, Schafer BW, Heizmann CW. Expression pattern of S100 calcium-binding proteins in human tumors. *Int J Cancer* 1996; **68**: 325-332
- 30 **Camby I**, Lefranc F, Titeca G, Neuci S, Fastrez M, Dedeken L, Schafer BW, Brotchi J, Heizmann CW, Pochet R, Salmon I, Kiss R, Decaestecker C. Differential expression of S100 calcium-binding proteins characterizes distinct clinical entities in both WHO grade II and III astrocytic tumours. *Neuropathol Appl Neurobiol* 2000; **26**: 76-90
- 31 **Oehler R**, Schmieder B, Zellner M, Prohaska R, Roth E. Endothelial cells downregulate expression of the 70 kDa heat shock protein during hypoxia. *Biochem Biophys Res Commun* 2000; **274**: 542-547
- 32 **Piura B**, Rabinovich A, Yavelsky V, Wolfson M. Heat shock proteins and malignancies of the female genital tract. *Harefuah* 2002; **141**: 969-972
- 33 **Gain P**, Thuret G, Chiquet C, Dumollard JM, Mosnier JF, Campos L. *In situ* immunohistochemical study of Bcl-2 and heat shock proteins in human corneal endothelial cells during corneal storage. *Br J Ophthalmol* 2001; **85**: 996-1000

Edited by Zhu LH and Xu FM

Effects of endostatin-vascular endothelial growth inhibitor chimeric recombinant adenoviruses on antiangiogenesis

Xin Pan, Yong Wang, Min Zhang, Wei Pan, Zhong-Tian Qi, Guang-Wen Cao

Xin Pan, Min Zhang, Wei Pan, Zhong-Tian Qi, Department of Microbiology, Second Military Medical University, Shanghai 200433, China

Yong Wang, Department of Ophthalmology of Changhai Hospital, Second Military Medical University, Shanghai 200433, China

Guang-Wen Cao, Department of Epidemiology, Second Military Medical University, Shanghai 200433, China

Supported by The National Natural Science Foundation of China, No. 30170891 and No.39970819

Correspondence to: Xin Pan, Department of Microbiology, Second Military Medical University, Shanghai 200433, China. panxinpx@yahoo.com

Telephone: +86-21-25070314 **Fax:** +86-21-25070312

Received: 2003-10-08 **Accepted:** 2003-12-06

Abstract

AIM: To investigate the inhibitory effects of endostatin-vascular endothelial growth inhibitor (VEGI₁₅₁) recombinant adenoviruses on neovascularization.

METHODS: We used recombinant adenoviruses to treat human vascular endothelial cell line ECV304, human hepatocellular carcinoma cell line HepG2, and murine fibroblast cell line L929, in order to study the chimeric gene expression in these cell lines. Chick chorioallantoic membrane (CAM) model, rabbit inflammatory corneal neovascularization (CNV) model, and liver cancer-bearing nude mice model were employed to investigate the negative biological effect of fusion molecules on neovascularization *in vivo*.

RESULTS: Western blot showed that the molecular weight of fusion protein was about 41kD after infection of ECV304, HepG2 and L929 cells with supernatant of AdhENDO-VEGI₁₅₁. The fusion protein showed a specific inhibitory effect on the proliferation of ECV304 cells, but no inhibitory effect on the growth of HepG2 and L929 cells ($F=13112.13$, $P=0.0001$). In the chick chorioallantoic membrane (CAM) assay, the expressed fusion protein significantly inhibited neovascularization. Rabbit inflammatory corneal neovascularization (CNV) induced by intrastromal sutures resulted in a uniform neovascular response. In this model, direct subconjunctival injection of AdhENDO-VEGI₁₅₁ expressed the fusion protein *in vivo* and suppressed the development of CNV. Topical application of AdhENDO-VEGI₁₅₁ led to a significant suppression of CNV ($F=1413.11$, $P=0.0001$), as compared with the control group of AdLacZ. Immunohistochemical staining showed the fusion protein dominantly expressed in corneal epithelium. Compared with the control group of AdLacZ ($4075.9 \pm 1849.9 \text{ mm}^3$), the average tumor size of group AdhENDO-VEGI₁₅₁ reduced in size ($487.7 \pm 241.2 \text{ mm}^3$) ($F=14.80$, $P=0.0085$), with an inhibition rate of 88.03%. Immunohistochemical staining showed the adenoviruses carried the fusion gene expressed on liver cancer cell membrane. MVD decreased more significantly in treated mice ($30.75 \pm 3.31\%$) than in AdLacZ control ($50.25 \pm 8.65\%$) ($F=17.72$, $P=0.0056$) with an inhibition rate of 39%.

CONCLUSION: Fusion protein expressed by recombinant adenoviruses has a significant inhibitory effect on neovascularization.

Pan X, Wang Y, Zhang M, Pan W, Qi ZT, Cao GW. Effects of endostatin-vascular endothelial growth inhibitor chimeric recombinant adenoviruses on antiangiogenesis. *World J Gastroenterol* 2004; 10(10): 1409-1414

<http://www.wjgnet.com/1007-9327/10/1409.asp>

INTRODUCTION

Neovascularization plays a critical role in solid tumor growth and corneal opacification. Researches indicated that angiogenesis inhibitors were highly potent in suppressing angiogenesis which could enable the tumor mass to remain in a dormant state^[1-4] and inhibit the development of corneal neovascularization^[5-7]. Endostatin could cause G(1) cell cycle arrest in endothelial cells, inhibit endothelial cell proliferation and migration, and promote apoptosis^[8]. Vascular endothelial cell growth inhibitor (VEGI) belongs to the tumor necrosis factor superfamily. VEGI is another endothelial cell-specific gene and a potent inhibitor of endothelial cell proliferation, angiogenesis^[9]. VEGI could mediate early G(1) arrest in G(0)/G(1) endothelial cells responding to growth stimuli, and programmed death in proliferating endothelial cells^[10]. In our laboratory two recombinant proteins have been used to treat tumor-bearing nude mice, but the inhibitory effect was not satisfactory. A few groups have demonstrated that antiangiogenic gene therapy with viral vectors is a potentially useful approach for inhibiting tumor growth in mouse models^[11-15]. In the current study, we acquired recombinant adenoviruses carrying endostatin-vascular endothelial growth inhibitor fusion gene to investigate its inhibitory effect *in vitro* on endothelial cells and antiangiogenic activity *in vivo* on chicken chorioallantoic membrane, inflammatory corneal neovascularization (CNV) in rabbit and liver cancer in nude mice.

MATERIALS AND METHODS

Materials

AdhENDO-VEGI₁₅₁ and AdLacZ were prepared in our laboratory. Endostatin polyclonal antibody was a gift from Dr. Stanker (Hanover, Germany). VEGI polyclonal antibody was prepared in our laboratory. Ad5-transformed human embryo renal cell line 293, human vascular endothelial cell line ECV304, human hepatocellular carcinoma cell line HepG2, and murine fibroblast cell line L929 were purchased from the Institute of Cell Biology, Chinese Academy of Sciences. Cell culture media were obtained from GIBCO. Nine-day-old fertilized white Leghorn eggs, New Zealand white rabbits, liver cancer-bearing nude mice SMMC-LTNM, and BALB/c nude mice were purchased from the Center of Experiment Animals, Second Military Medical University (Shanghai, China). All cell lines and animals were maintained under standard conditions.

Methods

Recombinant adenovirus infectivity examination AdhENDO-

VEGI₁₅₁ and AdLacZ were acquired as described previously^[16,17]. In a 24-well plate, 6×10^5 293 cells were infected with 50 μ L of identified recombinant adenoviruses AdhENDO-VEGI₁₅₁ or AdLacZ in 150 μ L of Dulbecco's modified Eagle's medium (DMEM) containing 100 mL/L fetal bovine serum (200 μ L in total) for 72 h. The cells showed evidence of cytopathic effect (CPE) and its supernatant was harvested. After three freeze/thaw cycles, the mixtures were passed through a 0.45 μ m millipore filter. The filtrate was frozen at -70 °C and stored. TCID₅₀ was used to determine the titer of recombinant adenoviruses^[18]. Ten thousand ECV304 cells were incubated in a 96-well plate for 5 h. Cells were infected with AdLacZ, covering a proper multiplicity of infection (MOI) range (0.1, 5, 10, 20, 50 and 100 MOI), and incubated for 48 h. X-gal staining was performed and blue stained cells were counted under a microscope.

Western blotting analysis Ad5-transformed human embryo renal cell line 293, human vascular endothelial cell line ECV304, human hepatocellular carcinoma cell line HepG2, and murine fibroblast cell line L929 were used in this assay. In a 6-well plate, 1×10^6 cells were infected with recombinant adenoviruses at an MOI of 20 for 4 h, then the medium containing recombinant adenoviruses was replaced with 1 mL of normal medium and cells were incubated for 24 h. Cell extracts were separated by 100 g/L sodium dodecyl sulfate-polyacrylamide gel electrophoresis under reducing conditions and electroblotted onto nitrocellulose membrane followed by treatment with blocking buffer containing 50 g/L nonfat dry milk in TBST (20 mmol/L Tris [pH8.0], 150 mmol/L NaCl, 1 g/L Tween-20) for 1 h. The electroblotted membranes were incubated with rabbit polyclonal antibodies against VEGI proteins, then subsequently incubated with peroxidase horseradish-conjugated anti-rabbit immunoglobulin for 1 h at 37 °C. The immune complexes were visualized with diaminobenzidine (DAB) staining.

In vitro bioactivity of fusion gene products One $\times 10^3$ cells were incubated in the 96-well plates, cells were infected with recombinant adenoviruses at an MOI of 20 for 4 h. The cell lines were ECV304, HepG2, and L929, respectively. The recombinant adenoviruses were AdhENDO-VEGI₁₅₁ and AdLacZ, respectively. The medium containing recombinant adenoviruses was replaced with 100 μ L of normal medium and cells were incubated at 37 °C for an appropriate period of time. The medium containing recombinant adenoviruses was removed, murine fibroblast cell line L929 was incubated with a normal medium containing 0.5 μ g/mL actinomycin D. Cell viability was determined by crystal violet vital staining^[19]. Cell viability (%) = (AdhENDO-VEGI₁₅₁ infected group $A_{570/630}$ / AdLacZ control group $A_{570/630}$) $\times 100$.

Inhibition of chick embryonic chorioallantoic membrane angiogenesis by recombinant adenoviruses A 1 cm \times 1 cm window in the shell was drilled over the air sac at the end of 9-day-old eggs. Chick embryonic chorioallantoic membrane was exposed by tearing up the egg membrane with a tip. A disk of methylcellulose was put on CAM, and 10 μ L recombinant adenoviruses was added at a titer of 1×10^{12} TCID₅₀/L. The windows were sealed with aseptic tapes and the eggs were incubated for 3 d. The membrane was cut around the air sac, which was turned upside down and observed by a stereomicroscope.

Suppression of rabbit inflammatory corneal neovascularization In this study, 4 female New Zealand white rabbits, weighing 4-5 kg, were used. Inflammatory CNV in rabbits induced by placement of intrastromal sutures resulted in a uniform neovascular response as described^[20]. On the first day after suturation, four rabbits were divided into AdlacZ control group and AdhENDO-VEGI₁₅₁ group. One hundred microliters of each recombinant adenovirus at a titer of 1×10^{12} TCID₅₀/L was injected into subconjunctiva. Then, gentamicin ointment was applied to the eyes once per day. Eyes were examined daily by

a slit-lamp biomicroscope and a surgical microscope was used to monitor angiogenic responses to recombinant adenoviruses. The area of corneal neovascularization was determined by measuring the vessel length (L) from the limbus and the number of clock hours (C) of limbus involved^[21-24]. Only the uniform contiguous band of neovascularization adjacent to the suture was measured. A formula was used to determine the area^[25]: $C/12 \times 3.1416 \times [r^2 - (r-L)^2]$, where $r=6$ mm (the measured radius of rabbit cornea). Rabbits were sacrificed on d 21. Rabbits' eyes were enucleated and inflammatory cornea was fixed in 40 g/L paraformaldehyde for 24 h.

Immunohistochemical staining of fusion protein in inflammatory cornea of rabbits Buffered formaldehyde fixed tissues were embedded in paraffin, 4- μ m thick sections were treated with 3 mL/L H₂O₂ in methanol for 20 min, and blocked with normal rabbit serum (1:20 dilution) for 20 min at room temperature. Then, the sections were incubated with rabbit polyclonal anti-endostatin (1:50 dilution) for 1 h at room temperature, followed by incubation with biotinylated goat anti-rabbit antibody IgG for 30 min and horseradish peroxidase-conjugated streptavidin at room temperature for 30 min. After completion of conjugation reaction, the slides were stained using 3,3'-diaminobenzidine (DAB)-H₂O₂. The sections were counterstained with hematoxylin, and viewed using a light microscope.

Treatment of liver cancer-bearing nude mice with recombinant adenoviruses Three SMMC-LTNM nude mice with liver cancer were sacrificed, and skin overlying the tumor was cleaned with ethanol. The tumors were resected under aseptic conditions. A suspension of tumor cells in Hank's was made by passage of viable tumor tissues small hypodermic needles. The final concentration was adjusted to 2×10^7 cells/mL. Female Balb/c nude mice, 3 wk of age, received injections sc into the dorsal midline in a 200 μ L volume. Tumors appeared approximately 10 d after implantation. The animals were randomized into 2 groups, and each group had four mice with comparable tumor size within and among the groups. Five hundred microliters of recombinant adenoviruses AdhENDO-VEGI₁₅₁ or AdLacZ at a titer of 1×10^{12} TCID₅₀/L was administered 10 times by sc every other day. The mice were sacrificed 24 h after the last injection, tumors from each mouse were removed and fixed in 40 g/L neutral buffered formaldehyde. Tumor size in all groups was measured, tumor volume was determined using the formula $\pi \times \text{width}^2 \times \text{length} / 6$. Tumor weight, inhibition rate and expression of target gene were evaluated, respectively.

Immunohistochemical staining of fusion protein in liver cancer of nude mice Tissues from liver cancer of nude mice were fixed in 40 g/L neutral buffered formaldehyde, embedded in paraffin, and sectioned into 4 μ m. The sections were treated with PBS, blocked with normal rabbit serum, incubated with rabbit polyclonal anti-endostatin (1:100 dilution) overnight at 4 °C, washed with PBS, incubated with HRP-conjugated goat anti-rabbit antibody (1:500 dilution) for 1 h at 37 °C, and stained using 3,3'-diaminobenzidine (DAB)-H₂O₂, counterstained with hematoxylin, and examined by a light microscope.

Determination of intratumor microvessel density Determination of microvessel density was carried out as described^[26-28]. Briefly, intratumor microvessels were immunostained with rat anti-human CD34 monoclonal antibody, and visualized with a biotinylated anti-rat IgG antibody by the Strept Avidin-Biotin Complex method. The sections were examined under low power to identify most vascular areas of the tumor. Within these areas, a maximum of 3 fields at $\times 200$ magnification was examined, and the mean values were calculated.

Statistical analysis Data were expressed as mean \pm SD. An analysis of variance was performed with Statview 4.0 statistical analysis software, and $P < 0.05$ was considered statistically significant.

RESULTS

Recombinant adenovirus infectivity

The titer of amplification of these two kinds of recombinant adenoviruses was 1×10^{12} TCID₅₀/L. When ECV304 cells were infected with AdLacZ at an MOI of 0.1, 20% cells showed LacZ-positive staining. If MOI was 20, 100% cells were stained blue (Figure 1). This result suggested recombinant adenoviruses had the highly efficient gene delivery.

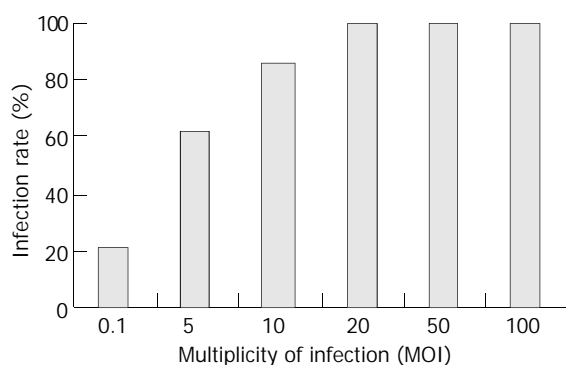


Figure 1 Infection efficiency of AdLacZ with different MOI.

Fusion protein expression of AdhENDO-VEGI₁₅₁ *in vitro*

Four kinds of cell lines infected with AdhENDO-VEGI₁₅₁ were immunoblotting stained with polyclonal antibodies against VEGI and visualized with DAB system. The results demonstrated that the fusion gene carried by AdhENDO-VEGI₁₅₁ could be *in vitro* expressed in all the cell lines, and the specific bands were located at about 41 ku, which was the expected size of ENDO-VEGI₁₅₁ fusion protein (Figure 2).

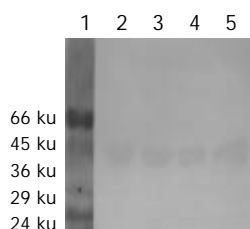


Figure 2 Western blot analysis of expressed fusion protein by AdhENDO-VEGI₁₅₁ with polyclonal antibody against VEGI₁₅₁. Lane 1: protein marker; lane 2: 293 cell; lane 3: ECV304 cell; lane 4: HepG2 cell; lane 5: L929 cell.

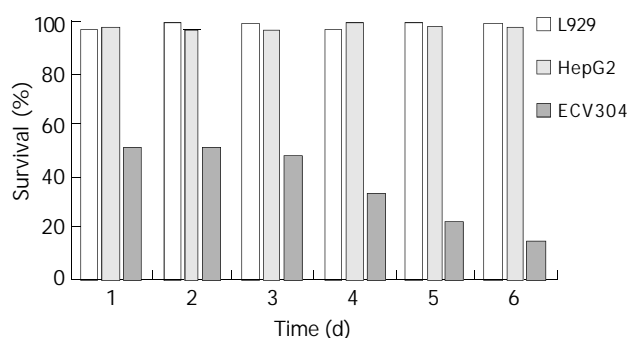


Figure 3 Viability of cells infected with AdhENDO-VEGI₁₅₁.

In vitro bioactivity of fusion gene on different cell lines

Human vascular endothelial cells ECV304 were sensitive to AdhENDO-VEGI₁₅₁, and cell proliferation was significantly inhibited. In contrast, no inhibitory activities on HepG2 and L929 *in vitro* growth were observed following AdhENDO-

VEGI₁₅₁ infection (Figure 3). Further analysis of variance showed there was a significant difference in viability between ECV304 cells and non-endothelial cells (HepG2 cells and L929 cells) ($F=13112.13$, $P=0.0001$). At different time points, there was a significant difference between the two groups ($F=72.75$, $P=0.0001$). There was no significant difference in viability between HepG2 cells and L929 cells neither for the hypothesis of no time effect ($F=7.17$, $P=0.0554$) nor at different time point ($F=1.74$, $P=0.2424$).

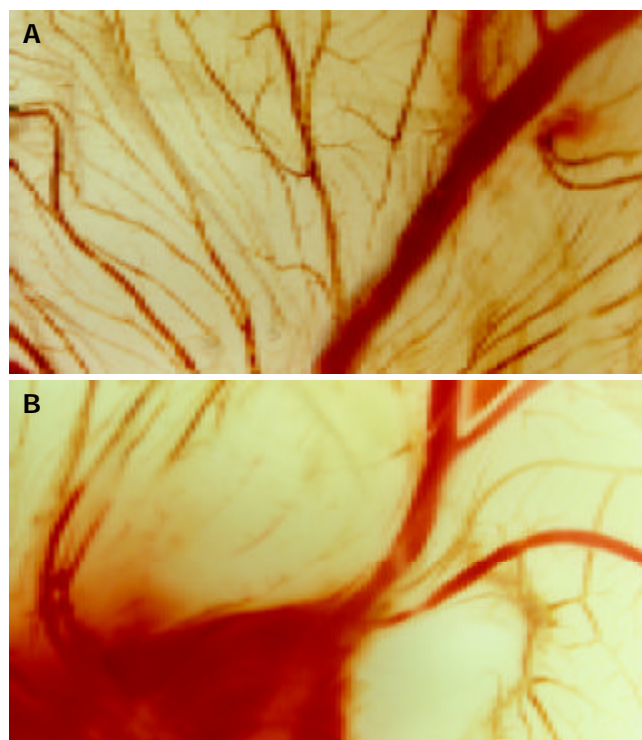


Figure 4 Inhibition of chick embryonic chorioallantoic membrane angiogenesis ($\times 7$). A: AdLacZ control; B: AdhENDO-VEGI₁₅₁.

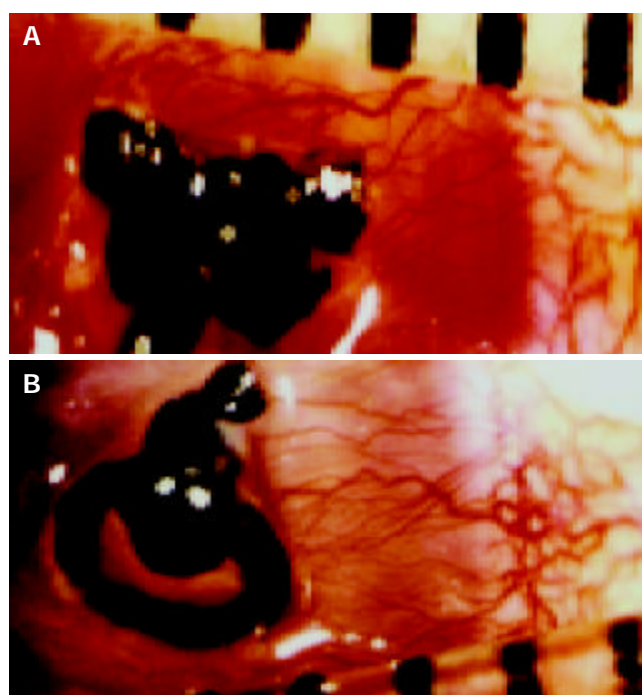


Figure 5 Suppression of rabbit corneal neovascularization ($\times 7$), CNV was examined on day 21. A: AdLacZ control; B: AdhENDO-VEGI₁₅₁.

Angiogenesis inhibition by AdhENDO-VEGI₁₅₁ in CAM

Nine-day old chick embryos were incubated with filter disks infected with AdhENDO-VEGI₁₅₁, or AdLacZ. The effect of AdhENDO-VEGI₁₅₁ on CAM angiogenesis was analyzed 3 d after incubation, by excising the membrane around the air sac and microscopy (Figure 4). At doses of 10-20 μ L/disc at a titer of 1×10^{12} TCID₅₀/L, there was a potent inhibition of angiogenesis of AdhENDO-VEGI₁₅₁ on the tested CAMs ($n=4$ /group). In contrast, AdLacZ failed to suppress angiogenesis in CAM. There was no evidence of toxicity in any chick embryos tested.

Vessel inhibition in inflammatory cornea of rabbits

After direct subconjunctival injection of recombinant adenoviruses, rabbit eyes were examined by a surgical microscope daily. A few small capillary buds that arose from engorged limbal arcades were observed. CNV increased gradually, peaked on d 12-14, and degenerated on day 15 after suture induction. So we chose d 7, 10, 13, or 16 as time points to determine the number and length of vessels, and the area of neovascularization. Analysis of the CNV area found that local application of AdhENDO-VEGI₁₅₁ resulted in a significant suppression of CNV (Figure 5, Figure 6). Repeated measurement of two factors and multilevel analysis of variance showed there were significant differences between AdhENDO-VEGI₁₅₁ group and AdLacZ group ($F=1413.11$, $P=0.0001$) for the hypothesis of no time effect. At different time points, there was a significant difference between the two groups ($F=15517.87$, $P=0.0001$).

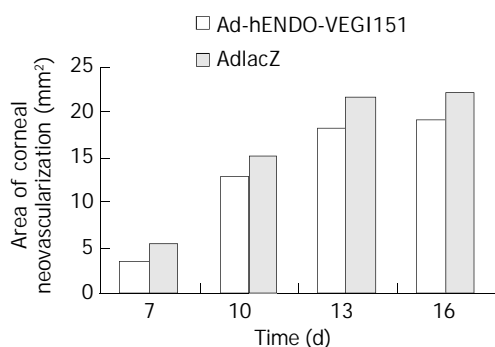


Figure 6 Comparison of corneal neovascularization in 2 groups.

AdhENDO-VEGI₁₅₁ expression in inflammatory cornea of rabbits

The fusion gene expression in inflammatory cornea of rabbits was detected by immunohistochemistry. Corneal endothelium was stained brown in AdLacZ group, others were stained negative. Corneal endothelium and epithelium were stained brown in AdhENDO-VEGI₁₅₁ group (Figure 7), and lasted for 21 d.

AdhENDO-VEGI₁₅₁ inhibited growth of liver cancer

Twenty-one days after therapy, the mice were sacrificed. Compared with AdLacZ control group ($4\,075.9 \pm 1\,849.9$ mm³), the average tumor size of AdhENDO-VEGI₁₅₁ group had confirmed regression (487.7 ± 241.2 mm³) ($F=14.80$, $P=0.0085$) with an inhibition rate of 88.03%.

Immunohistochemical features in liver cancer of nude mice

When we examined the sections stained by rabbit polyclonal anti-endostatin by a light microscope, strongly positive staining of fusion molecules presented in all cases of animals treated with AdhENDO-VEGI₁₅₁. The recombinant adenoviruses carrying chimeric gene could be expressed in liver cancer. Brown staining was mainly located on the membrane of liver cancer cells (Figure 8). There was no positive staining in tumor tissues of the control animals.

Determination of intratumor microvessel density

The antiangiogenesis effect of fusion protein producing adenoviruses was evaluated in tumor model. Tumor microvessel density (MVD) was reduced by the production of hENDO-VEGI₁₅₁ fusion gene. The MVD was decreased ($30.75 \pm 3.31\%$) more significantly in treated mice than in control ($50.25 \pm 8.65\%$) ($F=17.72$, $P=0.0056$).

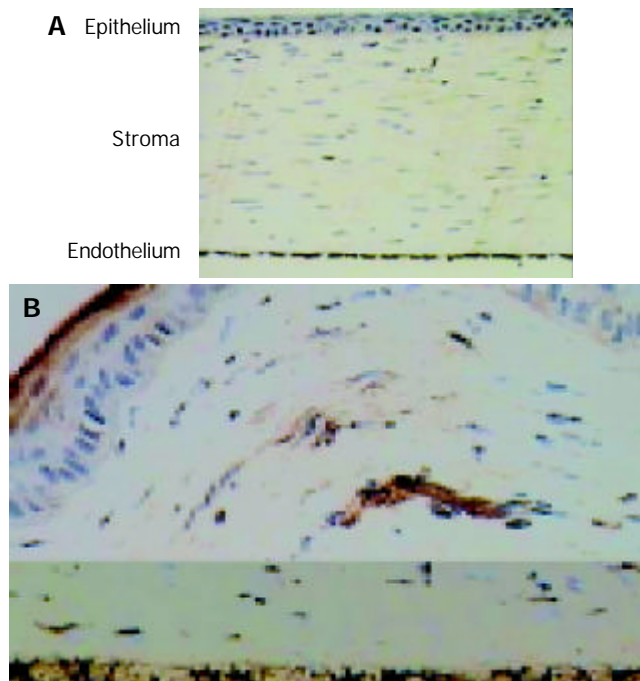


Figure 7 Immunohistochemical staining of rabbit cornea with polyclonal antibody against endostatin ($\times 200$). A: AdLacZ control; B: AdhENDO-VEGI₁₅₁.

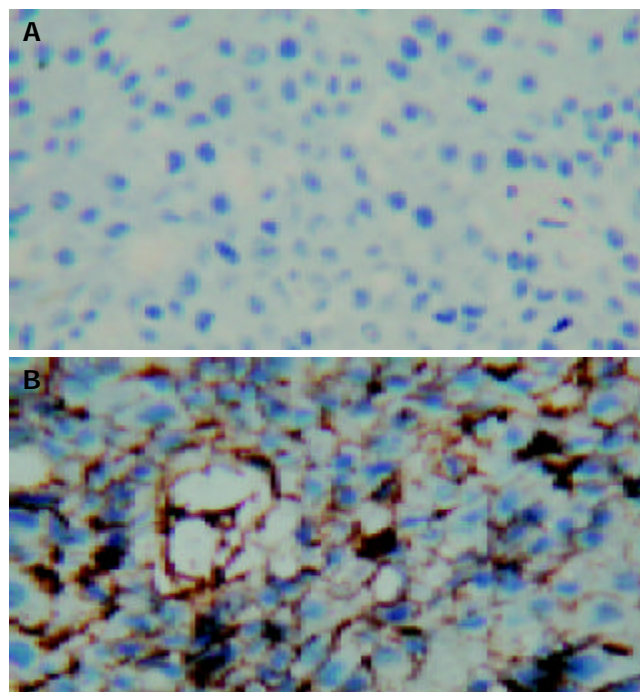


Figure 8 Immunohistochemical staining of nude mice liver cancer with polyclonal antibody against endostatin ($\times 200$). A: AdLacZ control; B: AdhENDO-VEGI₁₅₁.

DISCUSSION

Endostatin and vascular endothelial growth inhibitor are

endogenous angiostatic molecules. Both of them are angiogenesis inhibitors that could suppress the growth of endothelial cells^[29,30]. To achieve effectiveness, antiangiogenic therapy with endostatin or VEGI in tumor-bearing mice required prolonged administration and high doses of recombinant proteins^[31,32]. Production of functional polypeptides has proven difficult, perhaps because of its physical properties or variations in the purification procedures in different laboratories^[33,34]. In our laboratory (Department of Microbiology, Second Military Medical University, Shanghai, China) these two recombinant proteins were used respectively to treat tumor-bearing nude mice, but their bioactivities were not satisfactory. So we performed antiangiogenic gene therapy with adenoviral vectors. The results suggested recombinant adenoviruses AdhENDO-VEGI₁₅₁ could express fusion protein about 41 ku in ECV304, HepG2, L929 and 293 cells, and showed a specific inhibition on the proliferation of ECV304 cells, the inhibition rate reached 49% in 24 h and 86% in 144 h, respectively. But the AdhENDO-VEGI₁₅₁ showed no suppression on growth of HepG2 cells. VEGI belongs to the tumor necrosis factor (TNF) superfamily^[35] and was constitutively expressed in endothelial cells. Since murine fibroblast cell line L929 was used to determine the bioactivity of TNF, we also used this cell line to test the bioactivity of AdhENDO-VEGI₁₅₁. The results showed it had no suppression on growth of L929 cells, suggesting that fusion protein expressed by AdhENDO-VEGI₁₅₁ infection had no cytotoxicity to non-endothelial cells. Chick choriocallant membrane assay showed that fusion protein expressed by AdhENDO-VEGI₁₅₁ infection could significantly inhibit angiogenesis, and form no vessel regions. Because CAM was formed during embryogenic period, it was difficult to distinguish new vessels from previously established vascular networks. On the other hand, inflammatory CNV assay could avoid any confusion between new vessels and previously existed vessels, and any vessels penetrating into the corneal stroma could be identified as newly formed, as the cornea was avascular. For CNV was the main reason for corneal opacification, and also the main risk factor of immunologic rejection in allogeneous corneal transplantation, we tried to use AdhENDO-VEGI₁₅₁ as a safe and effective agent to inhibit CNV. We used intrastromal sutures to induce inflammatory CNV in rabbits. Neovascularization began sprouting into the corneal stroma from the limbus to the site of sutures within a few days after direct subconjunctival injection. Since small capillary vessels subsided gradually 16 d after suture induction, we selected d 7, 10, 13, or 16 as time points to measure vessel length and clock hours of circumferential neovascularization. Analysis of CNV area found there were significant differences between AdhENDO-VEGI₁₅₁ group and AdLacZ group. Local application of AdhENDO-VEGI₁₅₁ led to significant suppression of CNV, the inhibition rate was 36%, 16%, 17%, or 13% in turn. Our results suggested that in order to sustain the angiogenesis inhibition, AdhENDO-VEGI₁₅₁ should be administrated every 7 d. Immunohistochemical staining showed that the positive reaction was predominant in corneal epithelium of AdhENDO-VEGI₁₅₁ group. These results suggested that the expression of recombinant adenoviruses was related with the site of injection. Positive staining in corneal endothelium was observed in two groups. This phenomenon might be caused by the endogenous endostatin expression of corneal endothelial cells. Compared with AdLacZ control group, the average tumor size of AdhENDO-VEGI₁₅₁ group was reduced with an inhibition rate of 88.03%. The gene of interest in adenoviruses could express in liver cancer. Since the fusion gene included IL-3 signal peptide coding sequence, the fusion protein might secrete out of the membrane of liver cancer cells. MVD was decreased more significantly in treated mice than that in control, the inhibition rate was 39%. These findings in combination with

the results of cell assay suggested that the antitumor activity of AdhENDO-VEGI₁₅₁ was not due to a direct effect on tumor cells, interference with the development of tumor microvessel density was responsible for tumor regression. However, up to now, we do not know whether the combination is more potent or not. Comparison of the effectiveness of fusion molecules with individual molecules has been under investigation.

REFERENCES

- 1 **Kleinman HK**, Liao G. Gene therapy for antiangiogenesis. *J Natl Cancer Inst* 2001; **93**: 965-967
- 2 **Tomanek RJ**, Schattman GC. Angiogenesis: new insights and therapeutic potential. *Anat Rec* 2000; **261**: 126-135
- 3 **Kim CW**, Lee HM, Lee TH, Kang C, Kleinman HK, Gho YS. Extracellular membrane vesicles from tumor cells promote angiogenesis via sphingomyelin. *Cancer Res* 2002; **62**: 6312-6317
- 4 **Oehler MK**, Bicknell R. The promise of anti-angiogenic cancer therapy. *Br J Cancer* 2000; **82**: 749-752
- 5 **Lai CM**, Brankov M, Zaknich T, Lai YK, Shen WY, Constable IJ, Kovesdi I, Rakoczy PE. Inhibition of angiogenesis by adenovirus-mediated sFlt-1 expression in a rat model of corneal neovascularization. *Hum Gene Ther* 2001; **12**: 1299-1310
- 6 **Lai CM**, Spilsbury K, Brankov M, Zaknich T, Rakoczy PE. Inhibition of corneal neovascularization by recombinant adenovirus mediated antisense VEGF RNA. *Exp Eye Res* 2002; **75**: 625-634
- 7 **Ambati BK**, Jousen AM, Ambati J, Moromizato Y, Guha C, Javaherian K, Gillies S, O'Reilly MS, Adamis AP. Angiostatin inhibits and regresses corneal neovascularization. *Arch Ophthalmol* 2002; **120**: 1063-1068
- 8 **Hanai J**, Dhanabal M, Karumanchi SA, Albanese C, Waterman M, Chan B, Ramchandran R, Pestell R, Sukhatme VP. Endostatin causes G1 arrest of endothelial cells through inhibition of cyclin D1. *J Biol Chem* 2002; **277**: 16464-16469
- 9 **Zhang M**, Wang L, Wang HW, Pan X, Pan W, Qi ZT. Effect of N-terminal deletion on biological activity of vascular endothelial cell growth inhibitor. *Shengwu Huaxue Yu Shengwu Wuli Xuebao* 2003; **35**: 133-137
- 10 **Yu J**, Tian S, Metheny-Barlow L, Chew LJ, Hayes AJ, Pan H, Yu GL, Li LY. Modulation of endothelial cell growth arrest and apoptosis by vascular endothelial growth inhibitor. *Circ Res* 2001; **89**: 1161-1167
- 11 **Tanaka T**, Cao Y, Folkman J, Fine HA. Viral vector-targeted antiangiogenic gene therapy utilizing an angiostatin complementary DNA. *Cancer Res* 1998; **58**: 3362-3369
- 12 **Hampel M**, Tanaka T, Albert PS, Lee J, Ferrari N, Fine HA. Therapeutic effects of viral vector-mediated antiangiogenic gene transfer in malignant ascites. *Hum Gene Ther* 2001; **12**: 1713-1729
- 13 **Nguyen JT**. Adeno-associated virus and other potential vectors for angiostatin and endostatin gene therapy. *Adv Exp Med Biol* 2000; **465**: 457-466
- 14 **Nguyen JT**, Wu P, Clouse ME, Hlatky L, Terwilliger EF. Adeno-associated virus-mediated delivery of antiangiogenic factors as an antitumor strategy. *Cancer Res* 1998; **58**: 5673-5677
- 15 **Cao GW**, Qi ZT, Pan X, Zhang XQ, Miao XH, Feng Y, Lu XH, Kuriyama S, Du P. Gene therapy for human colorectal carcinoma using human CEA promoter controlled bacterial ADP-ribosylating toxin genes human CEA: PEA & DTA gene transfer. *World J Gastroenterol* 1998; **4**: 388-391
- 16 **Li Z**, Pan X, Pan W, Cao GS, Wen ZZ, Fang GE, Qi ZT, Bi JW, Hua JD. Packaging and identification of recombinant adenovirus carrying endostatin-soluble vascular endothelial growth inhibitor gene. *Shijie Huaren Xiaohua Zazhi* 2003; **11**: 741-744
- 17 **Pan X**, Li Z, Zhang M, Wang Y, Pan W, Qi ZT. Therapeutic effect of endostatin-vascular endothelial growth inhibitor recombinant adenoviruses on gastric carcinoma in nude mice. *Shijie Huaren Xiaohua Zazhi* 2003; **11**: 1282-1285
- 18 **Nyberg-Hoffman C**, Shabram P, Li W, Giroux D, Aguilar-Cordova E. Sensitivity and reproducibility in adenoviral infectious titer determination. *Nat Med* 1997; **3**: 808-811
- 19 **Michie J**, Akudugu J, Binder A, Van Rensburg CE, Bohm L.

- Flow cytometric evaluation of apoptosis and cell viability as a criterion of anti-tumour drug toxicity. *Anticancer Res* 2003; **23**: 2675-2679
- 20 **Zhao CS**, Zhang L, Shen YP. A preventive and therapeutic study of experimental corneal neovascularization. *Tongji Yike Daxue Xuebao* 1996; **25**: 399-401
- 21 **Cao Y**, Linden P, Farnebo J, Cao R, Eriksson A, Kumar V, Qi JH, Claesson Welsh L, Alitalo K. Vascular endothelial growth factor C induces angiogenesis *in vivo*. *Proc Natl Acad Sci U S A* 1998; **95**: 14389-14394
- 22 **Saita N**, Fujiwara N, Yano I, Soejima K, Kobayashi K. Trehalose 6,6'-dimycolate (cord factor) of *Mycobacterium tuberculosis* induces corneal angiogenesis in rats. *Infect Immun* 2000; **68**: 5991-5997
- 23 **Volpert OV**, Fong T, Koch AE, Peterson JD, Waltenbaugh C, Tepper RI, Bouck NP. Inhibition of angiogenesis by interleukin 4. *J Exp Med* 1998; **188**: 1039-1046
- 24 **Amin MA**, Volpert OV, Woods JM, Kumar P, Harlow LA, Koch AE. Migration inhibitory factor mediates angiogenesis via mitogen-activated protein kinase and phosphatidylinositol kinase. *Circ Res* 2003; **93**: 321-329
- 25 **Seo K**, Choi J, Park M, Rhee C. Angiogenesis effects of nerve growth factor (NGF) on rat corneas. *J Vet Sci* 2001; **2**: 125-130
- 26 **Chew LJ**, Pan H, Yu J, Tian S, Huang WQ, Zhang JY, Pang S, Li LY. A novel secreted splice variant of vascular endothelial cell growth inhibitor. *FASEB J* 2002; **16**: 742-744
- 27 **Nor JE**, Christensen J, Liu J, Peters M, Mooney DJ, Strieter RM, Polverini PJ. Up-Regulation of Bcl-2 in microvascular endothelial cells enhances intratumoral angiogenesis and accelerates tumor growth. *Cancer Res* 2001; **61**: 2183-2188
- 28 **Olewniczak S**, Chosia M, Kwas A, Kram A, Domagala W. Angiogenesis and some prognostic parameters of invasive ductal breast carcinoma in women. *Pol J Pathol* 2002; **53**: 183-188
- 29 **Wang L**, Pan W, Zhu FL, Jiao BH, Lou YH, Xiao Y, Qi ZT. Cloning, expression and biological activity of VEGI(151), a novel vascular endothelial cell growth inhibitor. *Shengwu Huaxue Yu Shengwu Wuli Xuebao* 2000; **32**: 485-489
- 30 **Cao MM**, Pan W, Chen QL, Ma ZC, Ni ZJ, Wu XL, Wu WB, Pan X, Cao GW, Qi ZT. Construction of the eukaryotic expression vector expressing the fusion protein of human endostatin protein and IL₃ signal peptide. *Shijie Huaren Xiaohua Zazhi* 2001; **9**: 43-46
- 31 **O'Reilly MS**, Boehm T, Shing Y, Fukai N, Vasios G, Lane WS, Flynn E, Birkhead JR, Olsen BR, Folkman J. Endostatin: an endogenous inhibitor of angiogenesis and tumor growth. *Cell* 1997; **88**: 277-285
- 32 **Zhai Y**, Yu J, Iruela-Arispe L, Huang WQ, Wang Z, Hayes AJ, Lu J, Jiang G, Rojas L, Lippman ME, Ni J, Yu GL, Li LY. Inhibition of angiogenesis and breast cancer xenograft tumor growth by VEGI, a novel cytokine of the TNF superfamily. *Int J Cancer* 1999; **82**: 131-136
- 33 **Dhanabal M**, Volk R, Ramchandran R, Simons M, Sukhatme VP. Cloning, expression, and *in vitro* activity of human endostatin. *Biochem Biophys Res Commun* 1999; **258**: 345-352
- 34 **Ding I**, Sun JZ, Fenton B, Liu WM, Kimsely P, Okunieff P, Min W. Intratumoral administration of endostatin plasmid inhibits vascular growth and perfusion in MCA-4 murine mammary carcinomas. *Cancer Res* 2001; **61**: 526-531
- 35 **Zhai Y**, Ni J, Jiang GW, Lu J, Xing L, Lincoln C, Carter KC, Janat F, Kozak D, Xu S, Rojas L, Aggarwal BB, Ruben S, Li LY, Gentz R, Yu GL. VEGI, a novel cytokine of the tumor necrosis factor family, is an angiogenesis inhibitor that suppresses the growth of colon carcinomas *in vivo*. *FASEB J* 1999; **13**: 181-189

Edited by Wang XL and Xu FM

Changes of tumor microcirculation after transcatheter arterial chemoembolization: First pass perfusion MR imaging and Chinese ink casting in a rabbit model

Jun-Gong Zhao, Gan-Sheng Feng, Xiang-Quan Kong, Xin Li, Ming-Hua Li, Ying-Sheng Cheng

Jun-Gong Zhao, Ming-Hua Li, Ying-Sheng Cheng, Department of Radiology, Sixth Affiliated Hospital of Shanghai Jiaotong University, Shanghai 200233, China

Gan-Sheng Feng, Xiang-Quan Kong, Xin Li, Department of Radiology, Union Hospital, Tongji Medical College, Huazhong University of Science and Technology, Wuhan 430022, Hubei Province, China

Correspondence to: Dr. Jun-Gong Zhao, Department of Radiology, Sixth Affiliated Hospital of Shanghai Jiaotong University, Shanghai 200233, China. zhaojun_gong@sohu.com

Telephone: +86-21-64369181 Ext 8882

Received: 2003-09-09 **Accepted:** 2003-10-22

Abstract

AIM: To observe the change of tumor microcirculation after transcatheter arterial chemoembolization (TACE) with *bletilla* microspheres by using first pass perfusion MR imaging (FP) and Chinese ink casting.

METHODS: VX2 carcinoma cells were surgically implanted into the left and right lobes of liver of 30 New Zealand white rabbits, which were divided into 3 groups at random. Emulsion of lipiodol mixed with mitomycin C, and 5-FU *bletilla* microspheres were injected into the hepatic artery respectively, and saline was used as control agent. MR imaging was performed with turbo-flash sequence 14 d after tumor implantation and 7 d after interventional therapy. The steepest slopes (SS) of the signal intensity versus time curves were created for quantitative analysis, 7.5% Chinese ink gelatin solution was injected through ascending artery (17 cases) or portal vein (2 cases) for lesion microvessel area (MVA) measurement after the last MRI examination. The correlation between perfusion imaging and MVA was studied blindly.

RESULTS: The SS values at the rim of tumor in lipiodol group (mean, 49% per second) and *bletilla* group (mean, 35% per second) were significantly decreased ($P < 0.05$) as compared with control group (mean, 124% per second), no difference was found between lipiodol and *bletilla* groups ($P > 0.05$). In lipiodol group, the MVAs ($24\ 974 \pm 11\ 836\ \mu\text{m}^2$) in the center of the tumor were significantly smaller than those of the control group ($35\ 510 \pm 15\ 675\ \mu\text{m}^2$) ($P < 0.05$), while the MVAs ($80\ 031 \pm 22\ 745\ \mu\text{m}^2$) around the tumor were significantly increased because small and dense plexuses appeared around the tumor which correlated to intense reaction of granulation tissue. None of the vessels was seen in the tumor in *bletilla* group, the peripheral MVAs of the tumor were significantly smaller than those of the control group ($P < 0.05$) and lipiodol group ($P < 0.05$). There was a good correlation between SS and MVAs in control group ($r_s, 0.985, P < 0.0001$) and *bletilla* group ($r_s, 0.743, P < 0.05$), the correlation was not significant in lipiodol group ($r_s, 0.527, P > 0.05$).

CONCLUSION: TACE with *bletilla* microspheres may

enhance its anti-tumor effect by inhibiting the angiogenesis, and FP-MRI provides useful information to assess the TACE effect by depicting tumor vascularization and perfusion.

Zhao JG, Feng GS, Kong XQ, Li X, Li MH, Cheng YS. Changes of tumor microcirculation after transcatheter arterial chemoembolization: First pass perfusion MR imaging and Chinese ink casting in a rabbit model. *World J Gastroenterol* 2004; 10(10): 1415-1420

<http://www.wjgnet.com/1007-9327/10/1415.asp>

INTRODUCTION

Transcatheter arterial chemoembolization (TACE) has been widely used and is considered to be an effective conservative treatment for hepatocellular carcinoma^[1,2]. Rapid development of small vessels after TACE resulting in incomplete necrosis, however, reduces therapeutic effectiveness^[1-9]. Therefore, inhibition of the development of arterial collaterals may be important in enhancing the therapeutic efficacy of this treatment. Recently, TACE with microspheres, microcapsules, cyanoacrylate and *bletilla* has been shown to improve the therapeutic results^[1,3,10-12]. *Bletilla* microspheres have also been shown to improve the therapeutic results because of its embolization of the hepatic artery and portal vein as well as controlled release systems, although changes at the level of hepatic microcirculation are not completely elucidated.

The purpose of this study was to observe the change of tumor microcirculation after TACE with *bletilla* microspheres by using first pass perfusion MR imaging (FP) and Chinese ink casting.

MATERIALS AND METHODS

Animals and tumor models

The VX2 tumor model used in this study was initially a virus-induced papilloma first seen in domestic rabbit in 1937. With sequential transplantations, the tumor line became increasingly anaplastic^[13]. VX2 carcinoma (Department of Radiology, Union Hospital, Tongji Medical College, Huazhong University of Science and Technology, Wuhan, China) was retained for approximately 4 years by repeated passage of tumor every 14-21 d by way of intramuscular or subcutaneous implantation into the thighs of male New Zealand white rabbits.

Twenty-five male and five female New Zealand white rabbits (Laboratory Center, Tongji Medical College) weighing 1-1.5 kg were used. Prior to all procedures, including tumor implantation and imaging, rabbits received an intramuscular injection of 1.0 mL/kg of body weight of ketamine hydrochloride injection (Shanghai Sino-west Pharmaceutical Company), intravenous access was then acquired via a marginal ear vein. Anesthesia was maintained by using the same dose of intravenously administered ketamine hydrochloride.

The technique for tumor implantation was basically similar to that described by Li *et al*^[14]. Briefly, the liver was exposed

by performing midline laparotomy, VX2 tumor fragments of approximately 1 mm³ were injected intraparenchymally into the right and left lobes of the rabbit liver. Thirty New Zealand white rabbits with tumors were divided into three groups at random. They were group A (control group, 8 rabbits), group B (lipiodol group, 12 rabbits) and group C (*bletilla* group, 10 rabbits). All three groups received their interventional therapy 14-21 d after tumor inoculation when MRI confirmed the successful implantation.

Interventional therapy

A polyethylene catheter (inner diameter 0.3 mm, outer diameter 0.5 mm) was retrogradely inserted into the gastroduodenal artery, the following agents were manually injected into the gastroduodenal artery, namely, saline only into group A, 0.4-0.6 mL lipiodol (Aulnay Sous-Bios, France) emulsion (lipiodol mixed with MMC) into group B, 0.3 mL ultravist mixed with 10 mg *bletilla* microspheres (Department of Radiology, Union Hospital, Wuhan, China, 40-200 µm in diameter, combined with 5-FU) into group C.

MR imaging and data analysis

Fourteen days after tumor implantation and 7 d after interventional therapy, MR imaging was undertaken by using a 1.5 T system (Magnetom Vision, Siemens Medical Systems) with a head coil. Transverse spin-echo T1-weighted images (repetition time was 525 ms, the echo time was 14 ms) and HASTE T2-weighted images (repetition time was 4.4 ms, the echo time was 90 ms) were obtained by using a 3 mm thick section, 0.5 mm intersection space, and four signals were acquired.

For the FP, a strongly T1-weighted, turbo-FLASH sequence was used with a high temporal resolution of 1.196 s per section, a single image was acquired sequentially with 65 repetitions, which resulted in an acquisition time of 2 min. The repetition time was 3.3 ms, the echo time was 1.4 ms, and time interval was 300 ms. At the end of the fourth acquisition, a dose of 0.1 mmol/kg body weight of gadopentetate dimeglumine (Bellona, Beijing, China) was administered via a marginal ear vein.

To quantitatively analyze FP, four circular ROIs were hand drawn, covering the center and rim of the lesion, signal intensity time curve was obtained over ROIs, and the steepest slope of the curve (SS) was calculated according to the previously described method^[15].

Evaluation of anti-tumor effect

Tumor size was measured with calipers. The size of each tumor on the liver surface was measured immediately before treatment and seven days after treatment on MR imaging. We evaluated the anti-tumor effect based on the tumor volume, which was calculated as follows: tumor volume (mm³)=0.5×*a*×*b*², where *a* is the length of major axis and *b* is the length of minor axis measured with calipers.

Chinese ink casting and histological evaluation

The tumor microvessels were demonstrated by perfusion of 75 g/L Chinese ink (Beijing Chinese Ink Company) gelatin solution into the ascending artery (17 cases) or portal vein (2 cases) after the last MR imaging examination. Before perfused with 75 g/L Chinese ink gelatin solution, 500 units of heparin was administered intravenously. After the rabbits were killed, the livers were removed and stored at -20 °C for 24 h. The specimens were immersed in 250-995 mL/L ethyl alcohol at increasing concentrations, and finally in a solution of methyl salicylate. When the oil penetrated the tissue, the specimens became transparent. The sections (50 µm) were observed first under a low power microscope (×40), then the sections with most dense area of microvessels were selected and observed under a high

power (×200). Micro-vessels filled with Chinese ink gelatin were evaluated under a microscope, micro-vessel areas (MVAs) in the center and rim of the lesion were calculated by an imaging analysis system (Beijing Aeronautic University). A 5 µm sections of the same specimens were stained with hematoxylin and eosin for light microscopy.

Statistical analysis

All data were expressed as mean±SD, the statistical differences between different groups were analyzed by ANOVA, and the correlation between SS and MVA was assessed by Spearman correlation analysis. Significance was accepted when *P*<0.05.

RESULTS

MR imaging

MR imaging depicted all tumors on pretreatment images. All untreated tumors had a low signal intensity on T1-weighted images and an intermediate signal intensity on T2-weighted images. Central areas of high signal intensity on T2-weighted images and low signal intensity on T1-weighted images were compatible with the central necrosis when tumors were larger than 1 cm. T1-weighted images after injection of gadolinium showed a slight enhancement in the center of lesion and a rim enhancement around the center of lesion in all tumors (Figure 1). No significant difference in tumor volume was observed among the three groups before therapy.

Tumor volumes in the lipiodol group and *bletilla* group after TACE were significantly decreased compared with the control group on d 7 after treatment, no significant difference in tumor volumes was observed between lipiodol group and *bletilla* group (Figure 2, Table 1). The central slight enhancement area was larger, and the peripheral arterial phase rim enhancement in the two groups was thinner. The SS values at the rim of tumor in lipiodol group (mean, 49% per second) and *bletilla* group (mean, 35% per second) were significantly decreased (*P*<0.05), as compared with the control group (mean, 124% per second), no difference was found between lipiodol group and *bletilla* one (*P*>0.05) (Table 2).

Table 1 Tumor volumes pre- and post-treatment (cm³)

Group	Pre-treatment	Post treatment
Control	0.430±0.067	1.620±0.327
Lipiodol	0.465±0.120	0.971±0.285 ^a
Bletilla	0.402±0.171	0.736±0.145 ^a

^a*P*<0.05 vs control.

Table 2 SS values at the rim of tumor in different groups

Group	SS (%·s ⁻¹)	<i>F</i>	<i>P</i>
Control	124±62		
Lipiodol	49±15	11.08	0.004 ^a
Bletilla	35±9	6.88	0.019 ^a

^a*P*<0.05 vs control.

Table 3 Correlation between SS values and MVA in different groups

Group	SS (%·s ⁻¹)	MVA (µm ²)	<i>r</i> _s	<i>P</i>
Control	124±62	35 510±15 675	0.985	<0.05
Lipiodol	49±15	80 031±22 745	0.527	>0.05
Bletilla	35±9	15 530±7 973	0.743	<0.05

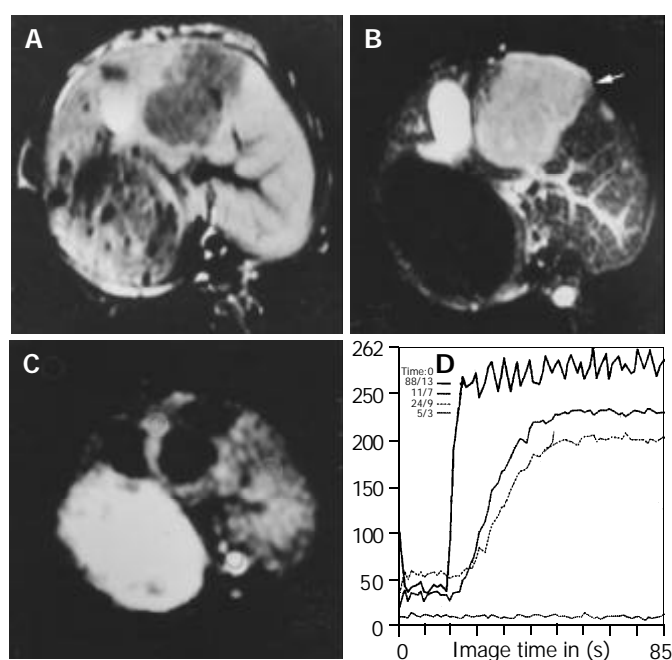


Figure 1 Images obtained before treatment in control group. A: T1WI shows hypointense lesions in left lobe of the liver. B: T2WI shows homogeneous hyperintense lesions in left lobe of the liver. C: FP T1-weighted image with gadolinium shows rim enhancement and no enhancement in the center of lesion. D: Signal intensity time curve derived from FP, SS of the curve in the border of the lesion is steeper than that of the normal liver.

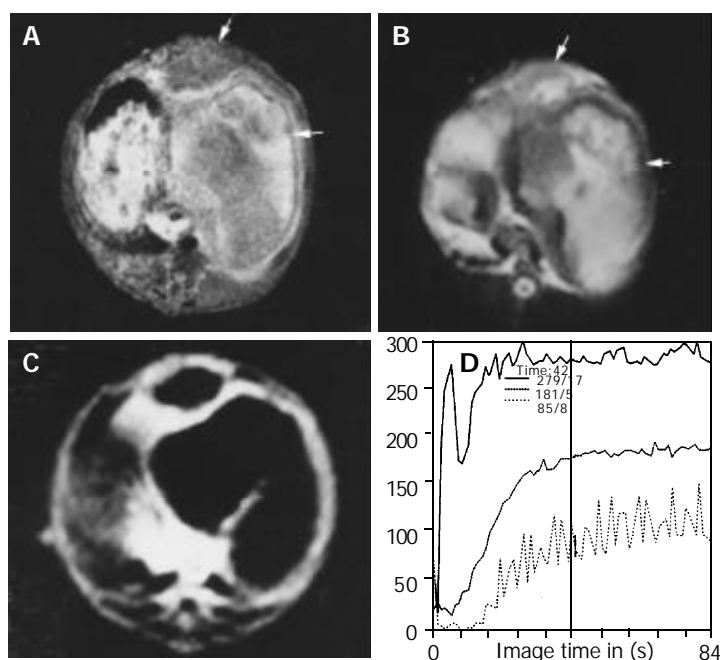


Figure 2 Images obtained after treatment in lipiodol group. Inhomogeneous hyperintense lesions with intermediate intense rim (arrow head) can be seen on T1WI (A) and T2WI (B), indicating the necrosis of the lesion and intratumor retention of lipiodol. (C) FP T1-weighted image with gadolinium shows thinner rim enhancement and no enhancement in the center of the lesion compared with control group although the lesion volume is increased. (D) SS of the curve in center of the lesion is decreased compared with those of the border.

Chinese ink casting

Investigation under microscope ($\times 40$) of the livers filled with Chinese ink in control group revealed networks of vessels or plexuses of dilated and tortuous course around and within the tumor originated from the arterioles, some sinusoid vessels were observed in the tumors, all these vessels were clearly distinct from the lobular architecture. In lipiodol group after TACE, the MVAs within the tumor ($24\,974 \pm 11\,836\ \mu\text{m}^2$) were significantly smaller than those of the control group ($35\,510 \pm 15\,675\ \mu\text{m}^2$) ($P < 0.05$), while the MVAs around the tumor ($80\,031 \pm 22\,745\ \mu\text{m}^2$) were significantly increased, as

compared with the control group ($35\,510 \pm 15\,675\ \mu\text{m}^2$) ($P < 0.05$). Small and dense plexuses appeared around the tumor, with unknown origin. None of the vessels was seen in the tumor in *bletilla* group after TACE (Figure 3). The peripheral MVAs of the tumor ($15\,530 \pm 7\,973\ \mu\text{m}^2$) in *bletilla* group were significantly smaller than those of the control group ($35\,510 \pm 15\,675\ \mu\text{m}^2$) ($P < 0.05$) and lipiodol group ($80\,031 \pm 22\,745\ \mu\text{m}^2$) ($P < 0.05$). There was a good correlation between SS and MVA at the rim of tumor in control group ($r_s, 0.985, P < 0.0001$) and *bletilla* group ($r_s, 0.743, P < 0.05$), the correlation was not significant in lipiodol group ($r_s, 0.527, P > 0.05$) (Table 3).

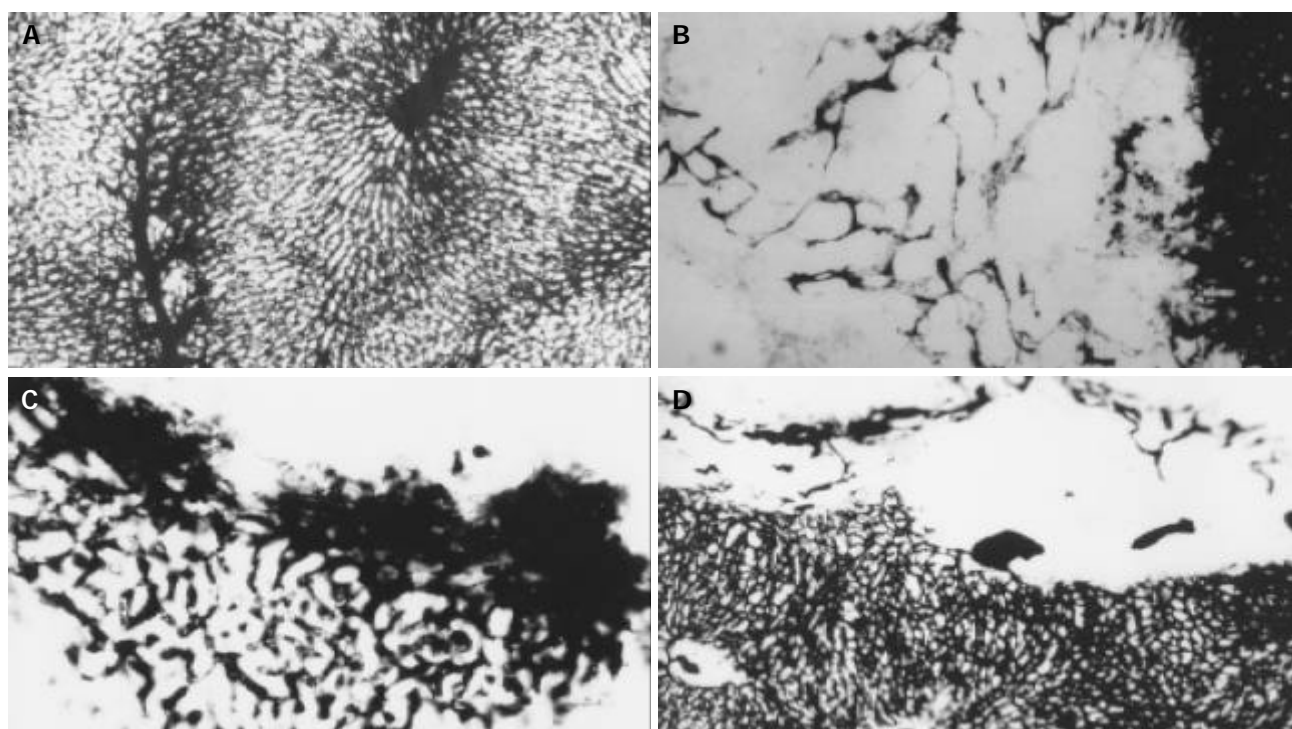


Figure 3 Micro-vessel casting with Chinese ink through ascending artery. A: The specimens show a lobular architecture of normal liver, magnification $\times 100$. B: In control group, hepatic artery perfusion shows networks of micro-vessels or plexuses of dilated and tortuous course around and within the tumor originated from the arterioles, some sinusoid vessels can be observed in this tumor, magnification $\times 100$. C: The original micro-vessels of the tumor are remarkably diminished, small and dense new plexuses appear around the tumor in lipiodol group, which are correlated to intense reaction of granulation tissue, magnification $\times 100$. D: micro-vessels are decreased in *betilla* group, no new micro-vessels can be seen at all, magnification $\times 100$.

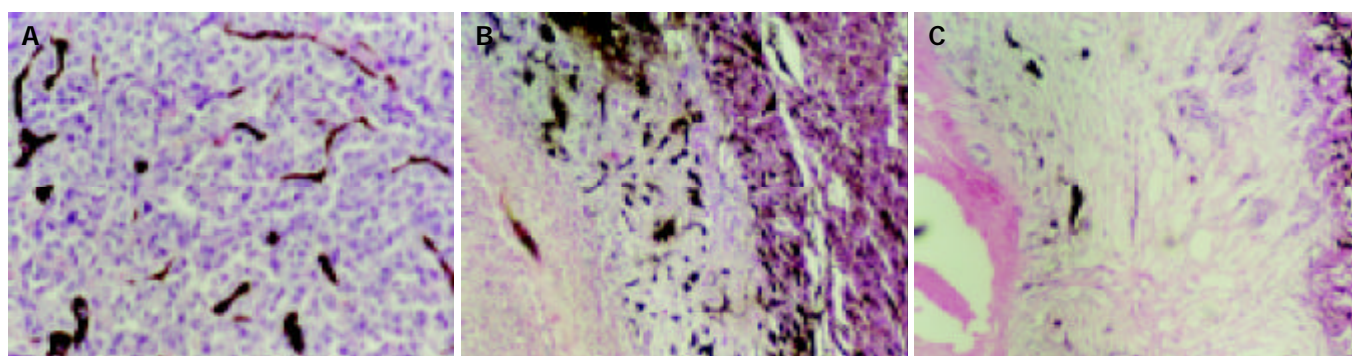


Figure 4 Histological examinations of hepatic lesion before and after treatment. A: HE stain shows nidal arrangement of VX2 cells as well as micro-vessels filled with Chinese ink before treatment, magnification $\times 200$. B: In lipiodol group, histological examination shows coagulation necrosis at the center of lesion, very few micro-vessels can be seen within this zone, residual tumor cells are seen at the periphery of the lesion, moreover, an intense reaction of granulation tissue is seen within this area, small dense vessels are scattered at border of the lesion, and congested sinusoids are seen in the periphery of the tumor, magnification $\times 200$. C: Coagulation necrosis as well as large infarcts involving multiple adjacent lobules is seen in *betilla* group, few vessels are seen at the border of the lesion, magnification $\times 200$.

Pathologic correlation

The specimens did not show necrosis or infarct when the lesion was less than 1 cm in control group. In lipiodol group none lesions underwent complete necrosis, coagulation necrosis was demonstrated at the center of all lesions. Viable or residual cancerous tissues as well as an intense reaction of granulation tissue were seen at the periphery of all lesions in lipiodol groups after TACE, small and dense vessels were scattered at the border of the lesions, correlating with the irregular thick rim enhancement on MR image. In *betilla* group after TACE, all lesions demonstrated complete coagulation necrosis, large infarcts involving multiple adjacent lobules were seen as well, few vessels were seen at the border of the lesion, no granulation tissue was seen (Figure 4).

DISCUSSION

Bletilla inhibition of tumor micro-vessels

A previous study reported an intense reaction of granulation tissue at the periphery of all lesions in lipiodol group^[16], the dense angiogenic plexus in the granulation tissue is, to our knowledge, a new finding. Granulation tissue which resulted in capillary proliferation and permeability increase was correlated to arterial phase rim enhancement on MR image. Angiogenesis was central to tumor stroma formation and offered nutrition to the remaining viable tumor cells, which limited lipiodol embolization and anti-tumor effect. As a result, local tumor recurrence would occur sooner or later^[7-9,16].

TNP-470, cyanoacrylate and Plcg-mitomycin-microsphere have been used to inhibit capillary networks or to prolong

first-pass effect and to enhance the anti-tumor effect of TACE^[11,17-20]. Our experimental study indicated that *bletilla* could enhance the anti-tumor effect of TACE as well. *Bletilla*, as an anti-tumor and anti-inflammation agent, is a Chinese medicine^[10,12]. Its microspheres (mixed with 5-FU, 40-200 μm in diameter) can result in dual embolization (embolization of hepatic arterial and portal venous blood supply) and inhibit the microvessels around and in the tumor completely. The reason why no microvessels developed after TACE was partly due to its anti-tumor and anti-inflammation effect, partly through inhibition of the binding of vascular endothelial growth factor to its receptor^[10]. As a result, treatment with *bletilla* could necrose the tumor thoroughly. This was why *bletilla* could enhance the anti-tumor effect of TACE even the lesion was very large^[12].

VX2 microcirculation morphology

Many materials, including Chinese ink and microfil, have been used to demonstrate the vascular morphology of tumors^[17,21]. Among them, microfil is commonly used because of its different colors, which could identify the origin of vessels. But microfil was too viscous to get into the sinusoid, no vessel was visible inside the tumors less than 0.25 mm in diameter^[17]. So we selected less viscous materials to reveal microvessel morphology of VX2. Three percent of Chinese ink gelatin solution was used to explore the vascular architecture of cheek pouch carcinoma^[21]. To avoid overfilling the microvessels, we added gelatin to increase the viscosity of the solution to obtain 7.5% solution. As a result, all the microvessels of normal liver including arterioles and sinusoid were filled with black Chinese ink, so did those of tumor. Moreover, the pathologic change of the other part of the same specimens stained with HE could be observed. So microvessel casting correlating with pathologic change could assess the changes of tumor microcirculation at the same time. We believe that Chinese ink gelatin solution casting may be used as the golden standard to evaluate the microvessels in perfusion study with CT and MR imaging.

Value of FP-MRI

Although power Doppler US has been used to assess vascularity of tumors^[23-25], before contrast enhanced harmonic power Doppler US has widely been used, the major problems in the use of power Doppler are as follows. The detected velocities were too slow in the tumor, there were too many blooming artifacts associated with micro-bubble injection, the duration of enhancement was short and there were artifacts resulted from respiration^[23]. So the vascularity of tumors could not be evaluated in detail by power Doppler US. FP-MRI, with a high time resolution, can monitor the contrast agent first passing the target tissue by using signal intensity time curve, the steepest slope of which (SS, i.e. the maximum upward slope of the curve) correlates linearly with flow velocity and angiogenesis, and has been successfully used to quantify the myocardial perfusion reserve and to depict the tumor vascularization^[15,22], but no study has assessed the tumor microcirculation after TACE by FP^[26,27]. Our experimental result revealed that areas with the fastest contrast medium uptake (SS) colocalized significantly with focal hot spots of MVA in control group and *bletilla* group, but no significant correlation was observed between SS and MVA in lipiodol group, suggesting that factors beyond the MVA are involved in the gadopentetate dimeglumine-related signals enhanced in microvessels. We believed that the discrepancy could reflect the difference between small dense vessels newly developed at the border of the lesion after lipiodol treatment and tumor microvessels before treatment. The new vessels were hyperpermeable^[28], part of the small molecular contrast media (gadopentetate dimeglumine) might leak out of microvessels even at first pass

course. On the other hand, the new vessels might be too small to have the same flow velocity like those before treatment. So we believed that when the same categoric vessels were assessed by FP, the flow velocity might be constant, the SS was correlated linearly with MVA. When different categoric vessels were evaluated by FP, the flow velocity and permeability were different, and not dependent only on MVA.

In this study, *bletilla* microspheres were administered for 7 d only, and further studies of extended duration are needed. We conclude that tumor microvessels can be markedly inhibited by using *bletilla* microspheres in combination with 5-FU, which can explain and confirm its effectiveness in clinic. The SS derived from FP has a good correlation with MVA and may be used as a noninvasive method to quantitatively evaluate tumor angiogenesis after TACE.

REFERENCES

- 1 **Loewe C**, Cejna M, Schoder M, Thurnher MM, Lammer J, Thurnher SA. Arterial embolization of unresectable hepatocellular carcinoma with use of cyanoacrylate and lipiodol. *J Vasc Interv Radiol* 2002; **13**: 61-69
- 2 **Pacella CM**, Bizzarri G, Cecconi P, Caspani B, Magnolfi F, Bianchini A, Anelli V, Pacella S, Rossi Z. Hepatocellular carcinoma: long-term results of combined treatment with laser thermal ablation and transcatheter arterial chemoembolization. *Radiology* 2001; **219**: 669-678
- 3 **Tancredi T**, McCusky PA, Kan Z, Wallace S. Changes in rat liver microcirculation after experimental hepatic arterial embolization: comparison of different embolic agents. *Radiology* 1999; **211**: 177-181
- 4 **Park SI**, Lee do Y, Won JY, Lee JT. Extrahepatic collateral supply of hepatocellular carcinoma by the intercostal arteries. *J Vasc Interv Radiol* 2003; **14**: 461-468
- 5 **Tan LL**, Li YB, Chen DJ, Li SX, Jiang JD, Li ZM. Helical dual-phase CT scan in evaluating blood supply of primary hepatocellular carcinoma after transcatheter hepatic artery chemoembolization with lipiodol. *Zhonghua Zhongliu Zazhi* 2003; **25**: 82-84
- 6 **Won JY**, Lee do Y, Lee JT, Park SI, Kim MJ, Yoo HS, Suh SH, Park SJ. Supplemental transcatheter arterial chemoembolization through a collateral omental artery: treatment for hepatocellular carcinoma. *Cardiovasc Intervent Radiol* 2003; **26**: 136-140
- 7 **Yi J**, Liao X, Yang Z, Li X. Study on the changes in microvessel density in hepatocellular carcinoma following transcatheter arterial chemoembolization. *J Tongji Med Univ* 2001; **21**: 321-322
- 8 **Shao G**, Wang J, Zhou K, Yan Z. Intratumoral microvessel density and expression of vascular endothelial growth factor in hepatocellular carcinoma after chemoembolization. *Zhonghua Ganzangbing Zazhi* 2002; **10**: 170-173
- 9 **Huang J**, He X, Lin X, Zhang C, Li J. Effect of preoperative transcatheter arterial chemoembolization on tumor cell activity in hepatocellular carcinoma. *Chin Med J* 2000; **113**: 446-448
- 10 **Feng GS**, Li X, Zheng CS, Zhou CK, Liu X, Wu HP. Mechanism of inhibition of tumor angiogenesis by Bletilla colloid: an experimental study. *Zhonghua Yixue Zazhi* 2003; **83**: 412-416
- 11 **Furuse J**, Ishii H, Satake M, Onaya H, Nose H, Mikami S, Sakai H, Mera K, Maru Y, Yoshino M. Pilot study of transcatheter arterial chemoembolization with degradable starch microspheres in patients with hepatocellular carcinoma. *Am J Clin Oncol* 2003; **26**: 159-164
- 12 **Feng GS**, Zheng CS, Zhou RM, Liang B, Zhang YF. Arterial embolization of hepatocellular carcinoma with use of bletilla and gelatin powder. *Zhonghua Fangshexue Zazhi* 1996; **30**: 135-137
- 13 **Kuszyk BS**, Boitnott JK, Choti MA, Blumke DA, Sheth S, Magee CA, Horton KM, Eng J, Fishman EK. Local tumor recurrence following hepatic cryoablation: radiologic-histopathologic correlation in a rabbit model. *Radiology* 2000; **217**: 477-486
- 14 **Li X**, Zheng CS, Feng GS, Zhuo CK, Zhao JG, Liu X. An implantable rat tumor model for experimental chemoembolization therapy and its imaging features. *World J Gastroenterol* 2002; **8**: 1035-1039
- 15 **Verstraete KL**, De Deene Y, Roels H, Dierick A, Uyttendaele D, Kunnen M. Benign and malignant musculoskeletal lesions: dy-

- namic contrast-enhanced MR imaging-parametric "first-pass" images depict tissue vascularization and perfusion. *Radiology* 1994; **192**: 835-843
- 16 **Han GH**, Guo QL, Huang GS, Guo YL. Distribution of lipiodol in hepatocellular carcinoma after hepatic arterial injection and its significance. *Zhonghua Fangshexue Zazhi* 1993; **27**: 828-831
- 17 **Mugitani T**, Taniguchi H, Takada A, Yamaguchi A, Masuyama M, Hoshima M, Takahashi T. TNP-470 inhibits collateralization to complement the anti-tumor effect of hepatic artery ligation. *Br J Cancer* 1998; **77**: 638-642
- 18 **Tanaka H**, Taniguchi H, Mugitani T, Koishi Y, Masuyama M, Higashida T, Koyama H, Suganuma Y, Miyata K, Takeuchi K, Takahashi T. Intra-arterial administration of the angiogenesis inhibitor TNP-470 blocks liver metastasis in a rabbit model. *Br J Cancer* 1995; **72**: 650-653
- 19 **Lund EL**, Bastholm L, Kristjansen PE. Therapeutic synergy of TNP-470 and ionizing radiation: effect on tumor growth, vessel morphology, and angiogenesis in human glioblastoma multiforme xenografts. *Clin Cancer Res* 2000; **6**: 971-978
- 20 **Qian J**, Truebenbach J, Graepler F, Pereira P, Huppert P, Eul T, Wiemann G, Claussen C. Application of poly-lactide-co-glycolide-microspheres in the transarterial chemoembolization in an animal model of hepatocellular carcinoma. *World J Gastroenterol* 2003; **9**: 94-98
- 21 **Zhou ZT**, Jin ZG, Zhang SL, Wang Z, Li WG. A morphic study on erigeron breviscapus (vant) hand-mazz affecting angiogenesis of golden hamster cheek pouch. *Linchuang Kouqiang Yixue Zazhi* 2000; **16**: 166-169
- 22 **Wilke N**, Jerosch-Herold M, Wang Y, Huang Y, Christensen BV, Stillman AE, Ugurbil K, McDonald K, Wilson RF. Myocardial perfusion reserve: assessment with multisection, quantitative, first-pass MR imaging. *Radiology* 1997; **204**: 373-384
- 23 **Du WH**, Yan WX, Wang X, Xiong XQ, Zhou Y, Li T. Vascularity of hepatic VX2 tumors of rabbits: assessment with conventional power Doppler US and contrast enhanced harmonic power Doppler US. *World J Gastroenterol* 2003; **9**: 258-261
- 24 **Kubota K**, Hira N, Nishikawa T, Fujiwara Y, Murata Y, Itoh S, Yoshida D, Yoshida S. Evaluation of hepatocellular carcinoma after treatment with transcatheter arterial chemoembolization: comparison of Lipiodol-CT, power Doppler sonography, and dynamic MRI. *Abdom Imaging* 2001; **26**: 184-190
- 25 **Hosoki T**, Yosioka Y, Matsubara T, Minamitani K, Higashi M, Ohtani M, Choi S, Mitomo M, Tono T. Power Doppler sonography of hepatocellular carcinoma treated by transcatheter arterial chemoembolization. Assessment of the therapeutic effect. *Acta Radiol* 1999; **40**: 639-643
- 26 **Tsui EY**, Chan JH, Cheung YK, Cheung CC, Tsui WC, Szeto ML, Lau KW, Yuen MK, Luk SH. Evaluation of therapeutic effectiveness of transarterial chemoembolization for hepatocellular carcinoma: correlation of dynamic susceptibility contrast-enhanced echoplanar imaging and hepatic angiography. *Clin Imaging* 2000; **24**: 210-216
- 27 **Chan JH**, Tsui EY, Luk SH, Yuen MK, Cheung YK, Wong KP. Detection of hepatic tumor perfusion following transcatheter arterial chemoembolization with dynamic susceptibility contrast-enhanced echoplanar imaging. *Clin Imaging* 1999; **23**: 190-194
- 28 **Du JR**, Jiang Y, Zhang YM, Fu H. Vascular endothelial growth factor and microvascular density in esophageal and gastric carcinoma. *World J Gastroenterol* 2003; **9**: 1604-1606

Edited by Wang XL and Zhu LH Proofread by Xu FM

Expression of angiostatin cDNA in human hepatocellular carcinoma cell line SMMC-7721 and its effect on implanted carcinoma in nude mice

Kai-Shan Tao, Ke-Feng Dou, Xing-An Wu

Kai-Shan Tao, Ke-Feng Dou, Department of Hepatobiliary Surgery, Xijing Hospital, Fourth Military Medical University, Xi'an 710032, Shaanxi Province, China

Xing-An Wu, Department of Microbiology, Faculty of Basic Medicine, Fourth Military Medical University, Xi'an 710032, Shaanxi Province, China

Correspondence to: Kai-Shan Tao, Department of Hepatobiliary Surgery, Xijing Hospital, Fourth Military Medical University, Xi'an 710032, Shaanxi Province, China. tkaishan@fmmu.edu.cn

Telephone: +86-29-83375259 **Fax:** +86-29-83375255

Received: 2004-02-11 **Accepted:** 2004-02-21

Abstract

AIM: To transfect murine angiostatin cDNA into human hepatocellular carcinoma cell line SMMC-7721 and to investigate its effects on implanted carcinoma in nude mice.

METHODS: A eukaryotic expression vector of pcDNA3.1-mAST containing murine angiostatin was constructed. Then pcDNA3.1-mAST plasmid was transfected into cell line SMMC-7721 by Lipofectamine. The resistant clone was screened by G418 filtration and identified by RT-PCR and Western blotting. Nude mice were divided into three groups of 10 each. Mice in blank control group were only injected with SMMC-7721 cells. Mice in vector control group were injected with SMMC-7721 cells transfected with pcDNA3.1 (+) vector, whereas mice in angiostatin group were injected with SMMC-7721 cells transfected with pcDNA3.1-mAST plasmid. Volume, mass and microvessel density (MVD) of the tumors in different groups were measured and compared.

RESULTS: Murine angiostatin cDNA was successfully cloned into the eukaryotic expression vector pcDNA3.1 (+). pcDNA3.1-mAST was successfully transfected into SMMC-7721 cell line and showed stable expression in this cell line. No significant difference was observed in the growth speed of SMMC-7721 cells between groups transfected with and without angiostatin cDNA. Tumor volume, mass and MVD in the angiostatin group were significantly lower than those in the blank control group and vector control group ($P < 0.01$). The inhibitory rate of tumor reached 78.6%. Mass and MVD of the tumors only accounted for 34.6% and 48.9% respectively of those in the blank control group.

CONCLUSION: Angiostatin cDNA could be stably expressed in human hepatocellular carcinoma cell line SMMC-7721 without obvious inhibitory effects on the growth of SMMC-7721 cells. When implanted into nude mice, SMMC-7721 cells transfected with angiostatin cDNA show a decreased tumorigenic capability. It suggests that angiostatin can inhibit tumor growth through its inhibition on angiogenesis in tumors.

Tao KS, Dou KF, Wu XA. Expression of angiostatin cDNA in human hepatocellular carcinoma cell line SMMC-7721 and its effect on

implanted carcinoma in nude mice. *World J Gastroenterol* 2004; 10(10): 1421-1424

<http://www.wjgnet.com/1007-9327/10/1421.asp>

INTRODUCTION

The growth and metastasis of a tumor depend on the growth of blood vessels^[1-5], so anti-angiogenesis becoming a new way in treatment of tumors^[6-9]. Recently, angiostatin has been found to be one of the most effective inhibitory genes of angiogenesis. It can inhibit specifically the proliferation and migration of endothelial cells of blood vessels, and has been regarded as a very useful target gene in anti-angiogenesis-based cancer treatment^[10]. Liver cancer is one kind of cancers rich in blood vessels, so therapeutic angiogenesis represents a potential option in the therapy of primary liver cancer. We investigated the construction of an expression vector containing angiostatin cDNA and evaluated its effect on implanted tumor in nude mice.

MATERIALS AND METHODS

Transfection of pcDNA3.1-mAST into SMMC-7721

Eukaryotic expression vector of pcDNA3.1 (+) (Invitrogen, USA) and plasmid pRC-mAST containing full-length of angiostatin gene (a gift from Dr. Zhang DX in Folkman Laboratory, Yale University, USA) were digested by restriction enzymes *Xba* I and *Hind* III. The digested vector and angiostatin cDNA fragment were ligated. Recombinant clones were identified by *Xba* I and *Hind* III double digestion. Positive clones named pcDNA3.1-mAST were further confirmed by sequencing.

Cultured SMMC-7721 cells were divided into three groups: transfected with recombinant pcDNA3.1-mAST (group A), transfected with pcDNA3.1 (+) vector (group B), not transfected with pcDNA3.1 (+) vector (group C). Transfection was performed according to the instructions of Lipofectamine TM2000 reagent kit (Gibco). Cells were cultured in RPMI 1640 medium containing 200 mL/L fetal calf serum and 350 mg/L G418. Resistant clones could be detected two weeks later. Cell growth curve was also made.

RT-PCR and Western blotting

Total RNA was extracted following reversal transcriptase PCR. Primers used in PCR were designed according to the reported angiostatin cDNA sequence^[7]. The primer sequences were as follows: 5' end: 5'-ATGGACCATAAGGAAGTAA-3'; 3' end: 5'-GGTGGGCAATTCCACAAACA-3'. The products of PCR were identified on 10 g/L agarose gel electrophoresis.

Cultured cells in the three groups were treated by adding 500 L solution containing 500 g/L lysine-Sepharose and 50 mmol/L Tris-HCl (pH 8.0) into the culture medium. Western blotting was then performed according to the reported methods^[11]. The primary antibody was anti-rabbit HA-tagged antibody (a gift from Dr. Zhang DX in Yale University).

Animal experiment

Thirty Balb/c nu/nu male mice aged 4-6 wk (body mass 18-20 g) were bred under SPF conditions. They were randomly divided into three groups of 10 each. The mice in blank control group were injected only with SMMC-7721 cells, the mice in vector-treated control group were injected with SMMC-7721 cells transfected with pcDNA3.1 (+) vector, the mice in angiostatin group received an injection of SMMC-7721 cells transfected with recombinant pcDNA3.1-mAST. After cancer cells were cultured into the stage of logarithmic growth phase, they were digested with trypsin to make cancer cell suspension of $5 \times 10^{10}/L$. Then, 0.2 mL of each suspension was subcutaneously injected into the right back of nude mice.

Tumor volume measurement

The survival of nude mice was observed every day. Tumor volume and inhibitory rate were measured on days 7, 14, 21, 28 and 35 after injection.

Tumor volume = $\pi/6 \times (\text{long radius} \times \text{short radius}^2)^{1/2}$.

Inhibition rate = (tumor volume of blank control group - tumor volume of angiostatin group) / tumor volume of blank control group $\times 100\%$.

Microvessel density counting

Thirty-five days after cancer cell injection, the nude mice were killed and their tumors were removed. The surrounding fatty tissues were dissected and the tumors were weighed. CD34 immunohistochemical staining was carried out according to the previously reported methods^[11] to label endothelial cells of blood vessels. Five areas with the highest microvessel density (MVD) in each section were selected under $40 \times$ subjective lens. The number of blood vessels in each area was counted under a magnification of 200 fields ($0.708 \text{ mm}^2/\text{field}$). The data from 5 areas were averaged and the value was regarded as the tumor MVD of each nude mouse. The average MVD from 10 mice in each group was regarded as the MVD of implanted tumor of that group^[13].

Statistical analysis

All data were expressed as mean \pm SD and analyzed by Student's *t* test. A *P* value less than 0.05 was considered statistically significant.

RESULTS

Identification of recombinant plasmid pcDNA3.1-mAST

After digestion by *Xba* I and *Hind* III, bands at 1.4 kb could be detected for positive clones (Figure 1), which suggested that mAST fragment was inserted into the pcDNA3.1 (+) vector, named recombinant plasmid pcDNA3.1-mAST.

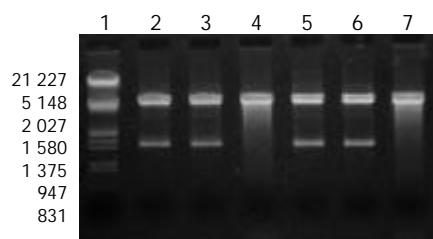


Figure 1 Restriction enzyme digestion of recombinant plasmid pcDNA3.1-mAST by *Xba* I and *Hind* III. Lane 1: DNA/*Eco*R I + *Hind* III Marker; Lanes 2, 3, 5, 6: positive clones; Lanes 4, 7: negative clones.

pcDNA3.1-mAST plasmid DNA was prepared and performed for sequencing. The sequence obtained was the same as the reported sequence of angiostatin cDNA, indicating that

the murine angiostatin gene was successfully cloned into the eukaryotic expression vector pcDNA3.1 (+).

Screening of angiostatin gene-transfected cells

No significant differences between the morphological characteristics of transfected cells and normal SMCC-7721 cells (Figure 2) were observed. No differences were detected in their growth rates (Figure 3).

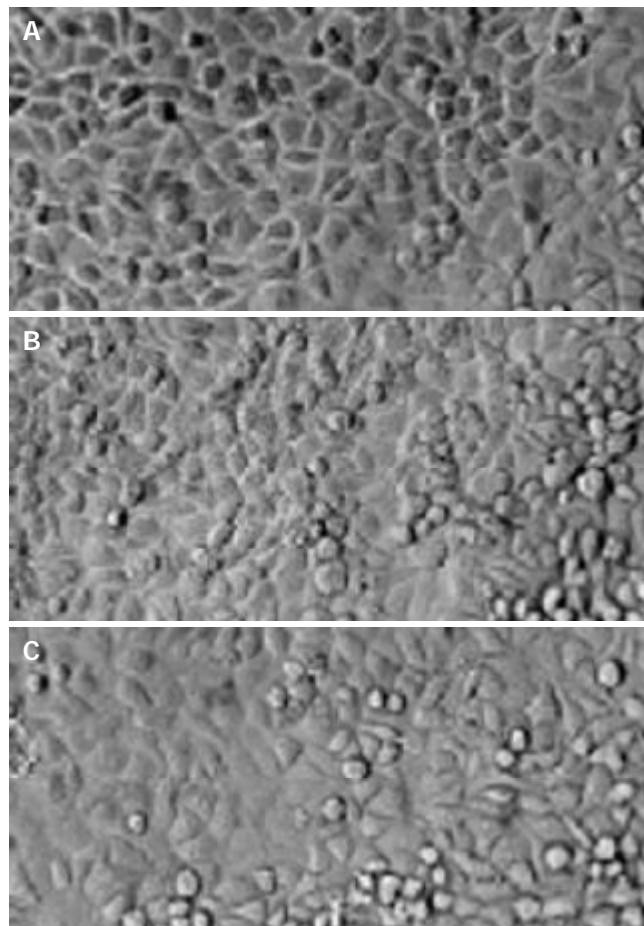


Figure 2 Morphology of HCC cells. A: SMMC-7721 cells; B: SMCC-7721 cells transfected with pcDNA3.1(+); C: SMCC-7721 cells transfected with pcDNA3.1-mAST.

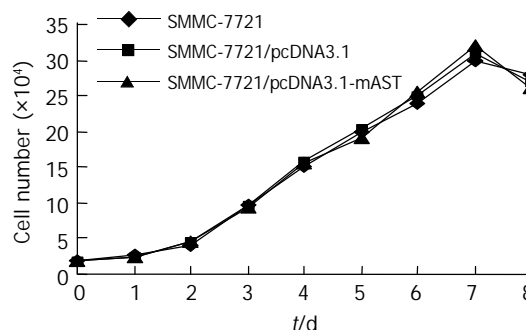


Figure 3 Growth curve of SMCC-7721 cells.

RT-PCR and Western blotting of angiostatin expression in transfected cells

SMMC-7721 cells transfected with pcDNA3.1-mAST were prepared and used as the template. By using angiostatin primers, a band was detected at 1.4 kb with PCR, indicating the presence of angiostatin cDNA in SMMC-7721 liver cancer cells (Figure 4).

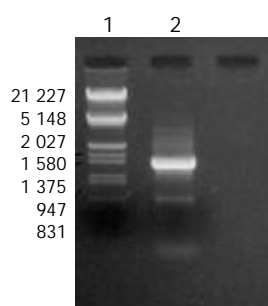


Figure 4 RT-PCR of transfected cells. Lane 1: DNA/*EcoR* I + *Hind* III Markers; Lane 2: positive clones.

Supernatants of cultured cells in three groups were collected and analyzed by Western blotting. A band in a molecular mass of 58 000 was detected with rabbit anti-HA-tagged antibody from the cells transfected with pcDNA3.1-mAST, but no bands were detected from blank control group or vector control group (Figure 5).

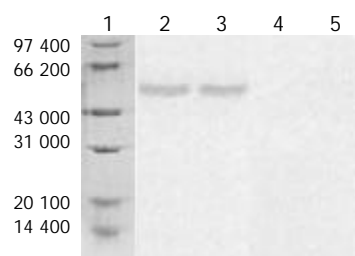


Figure 5 Western blotting of angiostatin expression. Lane 1: Marker protein; Lanes 2, 3: SMMC-7721/pcDNA3.1-mAST; Lane 4: SMMC-7721/pcDNA3.1 (+); Lane 5: SMMC-7721.

Tumor growth in nude mice

Tumors were observed in the nude mice just 5 d after they were implanted with cells in blank control group or vector control group. There was no significant difference in tumor volume between blank control group and vector control group ($t=1.53$, $P>0.05$). Mice had a visible tumor 10 d after cell injection in pcDNA3.1-mAST transfection group, and the tumor grew slowly. Tumor volumes among three groups were quite different, and a significant difference was observed when compared angiostatin group with blank control group or vector control group ($t=13.07$ and $t=12.91$, respectively, $P<0.01$, Table 1).

Table 1 Volume of implanted tumors in nude mice of three groups (mm³)

Group	Time after implantation (d)				
	7	14	21	28	35
Blank control	20±5	91±25	624±139	1 631±363	3 538±643
Vector control	19±6	85±24	653±149	1 542±358	3 128±547
Angiostatin	0	23±6	112±20	237±46	755±198 ^b

^b $P<0.01$ vs blank control and vector control group.

On the 35th day, the tumor growth inhibition rate in angiostatin group reached 78.6% vs the control group. In addition, the speed of tumor growth in angiostatin group was significantly slower than that in blank control or vector control group (Figure 6).

On the other hand, the tumor mass in three groups was measured on day 35. It was found that the tumor mass in angiostatin group (2.1 ± 0.5 g) was significantly smaller than

that in blank control (6.0 ± 0.7 g) or vector control (5.9 ± 0.5 g) group ($t=14.98$ and 16.14 , respectively, $P<0.01$), whereas there was no significant difference in tumor mass between the blank control and vector control groups ($t=0.59$, $P>0.05$).

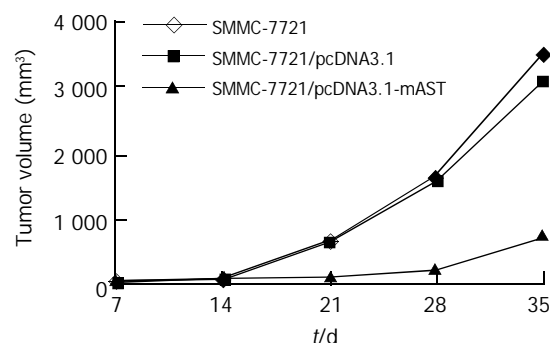


Figure 6 Growth curve of tumors.

MVD

Blood vessels were visualized by CD34 immunohistochemistry and endothelial cells were stained in brown color (Figure 7). There were no significant differences of MVD between the vector control group (49 ± 7 , mm²) and the blank control group (52 ± 6 , mm²) ($t=0.92$, $P>0.05$). But the tumor MVD in the angiostatin group (26 ± 4 , mm²) was significantly lower than that in other two control groups ($t=9.33$, 10.94 , respectively, $P<0.01$), and was about 48.9% of that in the blank control group.

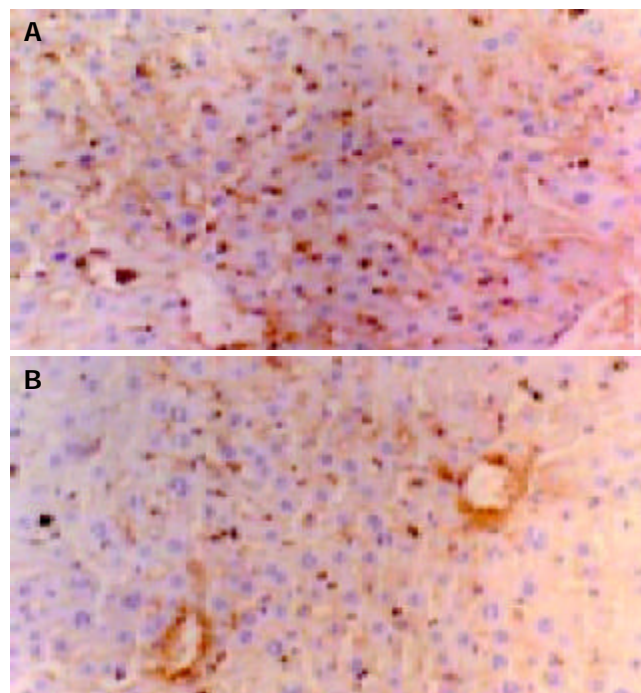


Figure 7 Immunohistochemical analysis of MVD in tumor tissue (×200). A: blank control group; B: angiostatin group

DISCUSSION

The growth and metastasis of a tumor depend upon the growth of blood vessels. Therefore, inhibition of blood vessel growth is a potential therapy for primary tumors, and it has become an important way to treat tumors by increasing the expression of inhibitory factors of angiogenesis in the tumor area. Angiostatin is one of the endogenous angiogenesis inhibitory factors^[10] and has been proved *in vitro* to inhibit the proliferation of endothelial cells. *In vivo* studies also confirmed

that angiostatin could inhibit the angiogenesis in solid tumors that could result in the inhibition of tumor growth^[14-20].

In the present study, we constructed a target fragment that contained a sequence encoding a secretory signal (SS) and a preactivation peptide (PA), the N-terminal kringle1-4 sequence of plasminogen and 11 amino acids in the C-terminal HA-tagged gene. The target gene fragment of 1.4 kb in length was cloned into *Xba* I and *Hind* III restriction sites of eukaryotic expression vector pcDNA3.1(+). Restriction digestion and sequencing analysis for positive clones indicated that a recombinant eukaryotic expression vector containing the angiostatin gene was successfully constructed. This recombinant vector was then transfected into human liver cancer cell line SMMC-7721 and screened by G418. The result of RT-PCR showed that the recombinant plasmid was stably integrated into the cells. By Western blotting, a protein ($M_r=38\ 000$) was detected, indicating that angiostatin protein was expressed in transfected SMMC-7721 cells. Furthermore, the growth curve showed that there was no significant difference in growth rate between transfected and non-transfected SMMC-7721 cells. This indicated that angiostatin had no inhibitory effect on the growth of SMMC-7721 cells.

CD34 is specifically located in endothelial cells. It was reported that CD34 could be regarded as a good marker of endothelial cells in liver cancer because of its high sensibility and specificity. Therefore, the expression of CD34 can reflect the angiogenesis of primary liver cancer and implanted liver tumors. So in this experiment we used CD34 antibody to label endothelial cells.

In this experiment, SMMC-7721 cells that stably expressed angiostatin cDNA (angiostatin group), SMMC-7721 cells alone (blank control group) and SMMC-7721 cells transfected with pcDNA3.1 (+) vector (vector control group) were subcutaneously implanted into nude mice respectively. We found that the implanted tumors appeared later in the angiostatin group, and the mass and volume of the tumor were significantly lower and smaller than those of the other two groups. The inhibitory rate reached 78.6%, and the mass was only 34.6% of that of the blank control group. These results suggested that angiostatin could significantly inhibit the growth of primary tumors. The MVD of the tumor in the angiostatin group was much less than that in the other two groups ($P<0.01$). These data indicated that angiostatin could upregulate the expression of angiogenic inhibitory factors and/or downregulate the expression of angiogenic stimulus factors after its cDNA was transfected into SMMC-7721 cells. This would change the balance between angiogenesis stimulus factors and angiogenic inhibitory factors, thus inhibiting of the angiogenesis and growth of tumors.

Gene therapy, concerning the special angiogenic inhibitory factor of endothelial cells of tumor tissue, is a new way of cancer treatment. We believe that this treatment in combination with chemotherapy and radiotherapy would definitely improve the effect of cancer treatment. Because liver cancer is more prevalent in the world^[21-23], especially in China^[24], our results have the significance in further research.

REFERENCES

- Compagni A, Christofori G. Recent advances in research on multistage tumorigenesis. *Br J Cancer* 2000; **83**: 1-5
- Detmar M. Tumor angiogenesis. *J Invest Dermatol Symp Proc* 2000; **5**: 20-23
- Maehara Y, Kabashima A, Koga T, Tokunaga E, Takeuchi H, Kakeji Y, Sugimachi K. Vascular invasion and potential for tumor angiogenesis and metastasis in gastric carcinoma. *Surgery* 2000; **128**: 408-416
- Gervaz P, Scholl B, Mainguene C, Poitry S, Gillet M, Wexner S. Angiogenesis of liver metastases: role of sinusoidal endothelial cells. *Dis Colon Rectum* 2000; **43**: 980-986
- Sabo E, Boltenko A, Sova Y, Stein A, Kleinhaus S, Resnick MB. Microscopic analysis and significance of vascular architectural complexity in renal cell carcinoma. *Clin Cancer Res* 2001; **7**: 533-537
- Carmeliet P, Jain RK. Angiogenesis in cancer and other diseases. *Nature* 2000; **407**: 249-257
- Cao Y, O'Reilly MS, Marshall B, Flynn E, Ji RW, Folkman J. Expression of angiostatin cDNA in a murine fibrosarcoma suppresses primary tumor growth and produces long-term dormancy of metastases. *J Clin Invest* 1998; **101**: 1055-1063
- Luo YQ, Wu MC, Cong WM. Gene expression of hepatocyte growth factor and its receptor in HCC and nontumorous liver tissues. *World J Gastroenterol* 1999; **5**: 119-121
- Barinaga M. Designing therapies that target tumor blood vessels. *Science* 1997; **275**: 482-484
- O'Reilly MS, Holmgren L, Shing Y, Chen C, Rosenthal RA, Moses M, Lane WS, Cao Y, Sage EH, Folkman J. Angiostatin: a novel angiogenesis inhibitor that mediates the suppression of metastases by a Lewis lung carcinoma. *Cell* 1994; **79**: 315-328
- Towbin H, Staehelin T, Gordon T. Electrophoretic transfer of proteins from polyacrylamide gels to nitrocellulose sheets: procedure and some applications. *Proc Natl Acad Sci U S A* 1979; **76**: 4350-4354
- Hanahan D, Folkman J. Patterns and emerging mechanisms of the angiogenic switch during tumorigenesis. *Cell* 1996; **86**: 353-364
- Araya M, Terashima M, Takagane A, Abe K, Nishizuka S, Yonezawa H, Irinoda T, Nakaya T, Saito K. Microvessel count predicts metastasis and prognosis in patients with gastric cancer. *J Surg Oncol* 1997; **65**: 232-236
- O'Reilly MS, Holmgren L, Shing Y, Chen C, Rosenthal RA, Cao Y, Moses M, Lane WS, Sage EH, Folkman J. Angiostatin: a circulating endothelial cell inhibitor that suppresses angiogenesis and tumor growth. *Cold Spring Harb Symp Quant Biol* 1994; **59**: 471-482
- Stack MS, Gately S, Bafetti LM, Enghild JJ, Soff GA. Angiostatin inhibits endothelial and melanoma cellular invasion by blocking matrix-enhanced plasminogen activation. *Biochem J* 1999; **340** (Pt 1): 77-84
- Hari D, Beckett MA, Sukhatme VP, Dhanabal M, Nodzenski E, Lu H, Mauceri HJ, Kufe DW, Weichselbaum RR. Angiostatin induces mitotic cell death of proliferating endothelial cell. *Mol Cell Biol Res Commun* 2000; **3**: 277-282
- Ijland SA, Jager MJ, Heijdra BM, Westphal JR, Peek R. Expression of angiogenic and immunosuppressive factors by uveal melanoma cell lines. *Melanoma Res* 1999; **9**: 445-450
- Matsuda KM, Madoiwa S, Hasumi Y, Saga Y, Kume A, Mano H, Ozana K, Matsuda M. A novel strategy for the tumor angiogenesis-targeted gene therapy: generation of angiostatin from endogenous plasminogen by protease gene transfer. *Cancer Gene Ther* 2000; **7**: 589-596
- Volm M, Mattern J, Koomagi R. Angiostatin expression in non-small cell lung cancer. *Clin Cancer Res* 2000; **6**: 3236-3240
- Wu J, Shi YQ, Wu KC, Zhang DX, Yang JH, Fan DM. Angiostatin up-regulation in gastric cancer cell SGC7901 inhibits tumorigenesis in nude mice. *World J Gastroenterol* 2003; **9**: 59-64
- El-Serag HB, Davila JA, Petersen NJ, McGlynn KA. The continuing increase in the incidence of hepatocellular carcinoma in the United States: an update. *Ann Intern Med* 2003; **139**: 817-823
- Regimbeau JM, Abdalla EK, Vauthey JN, Lauwers GY, Durand F, Nagorney DM, Ikai I, Yamaoka Y, Belghiti J. Risk factors for early death due to recurrence after liver resection for hepatocellular carcinoma: results of a multicenter study. *J Surg Oncol* 2004; **85**: 36-41
- Ku Y, Iwasaki T, Tominaga M, Fukumoto T, Takahashi T, Kido M, Ogata S, Takahashi M, Kuroda Y, Matsumoto S, Obara H. Reductive surgery plus percutaneous isolated hepatic perfusion for multiple advanced hepatocellular carcinoma. *Ann Surg* 2004; **239**: 53-60
- Lin GY, Chen ZL, Lu CM, Li Y, Ping XJ, Huang R. Immunohistochemical study on p53, H-rasp21, c-erbB-2 protein and PCNA expression in HCC tissues of Han and minority ethnic patients. *World J Gastroenterol* 2000; **6**: 234-238

Expression and altered subcellular localization of the cyclin-dependent kinase inhibitor p27^{Kip1} in hepatocellular carcinoma

Ke-Jun Nan, Zhao Jing, Ling Gong

Ke-Jun Nan, Zhao Jing, Department of Medical Oncology, First Hospital of Xi'an Jiaotong University, Xi'an 710061, Shaanxi Province, China

Ling Gong, Department of Infectious Diseases, First Hospital of Xi'an Jiaotong University, Xi'an 710061, Shaanxi Province, China

Correspondence to: Ke-Jun Nan, Department of Medical Oncology, First Hospital of Xi'an Jiaotong University, 1 Jiankang Xilu, Xi'an 710061, Shaanxi Province, China. jz96329@163.com

Telephone: +86-29-5324086 **Fax:** +86-29-5324086

Received: 2003-09-18 **Accepted:** 2003-12-08

Abstract

AIM: To investigate p27 expression in hepatocellular carcinoma (HCC), adjacent nontumoral and normal liver tissues, and to verify whether the subcellular localization of p27 was altered in HCC.

METHODS: The level of p27 in tumoral, nontumoral, and normal liver tissues were assessed by immunohistochemical (IHC) analysis. Parallel immunostaining was done for proliferating cell nuclear antigen (PCNA) to evaluate cell proliferation.

RESULTS: The labeling index (LI) of p27 in tumoral lesions was significantly lower than that in adjacent nontumoral lesions ($t=2.444$, $P=0.017$) and normal controls ($t=2.268$, $P=0.029$). The LI of p27 significantly decreased in patients with massive type ($t=2.227$, $P=0.037$) and infiltration ($t=2.197$, $P=0.036$). The prognosis of patients with higher p27 LI was longer than that of patients with lower p27 LI ($P=0.0247$, log-rank test). The LI of PCNA was significantly higher in HCC than that in adjacent nontumoral lesions ($t=2.092$, $P=0.041$) and normal controls ($t=3.533$, $P=0.002$). There was no significant correlation between p27 expression and cell proliferation in tumor samples. The level of p27 in the cytoplasmic fraction was higher in tumoral and nontumoral liver tissues, and was associated with clinical stage ($t=2.520$, $P=0.029$) and the degree of invasion ($t=2.640$, $P=0.019$). Survival analysis showed that p27 was an independent prognosis marker for HCC patients.

CONCLUSION: These results suggest that p27 underexpressing in patients with HCC is closely associated with infiltration, metastasis, and prognosis. Alterations in the subcellular localization of p27 protein may occur early during hepatocarcinogenesis.

Nan KJ, Jing Z, Gong L. Expression and altered subcellular localization of the cyclin-dependent kinase inhibitor p27^{Kip1} in hepatocellular carcinoma. *World J Gastroenterol* 2004; 10 (10): 1425-1430

<http://www.wjgnet.com/1007-9327/10/1425.asp>

INTRODUCTION

Abnormalities in various regulators of cell cycle frequently

occur in human cancers^[1-4]. Cell cycle is tightly controlled by the regulators, including cyclins, cyclin-dependent kinases (CDKs), and their inhibitors. Cyclin-dependent kinase inhibitors (CKIs) are potent negative regulators of cell cycle, and have two families on the basis of sequence homology. The inhibitors of CDK4 (INK4) family, including p16^{Ink4a}, p15^{Ink4b}, p18^{Ink4c}, and p19^{Ink4}, specifically binds to CDK4 and CDK6, and inhibits cyclin D binding. The Cip/Kip family, including p21^{Cip1}, p27^{Kip1}, and p57^{Kip2}, binds to and inhibits cyclin-bound CDKs^[5]. Among CKIs, p27 is thought to have crucial^[6] and important roles in a variety of fundamental cellular processes^[7-10]. The underexpression of p27 assessed by IHC analysis has been associated with more severe tumor grade and a negative prognostic marker in different carcinomas^[11-16].

Furthermore, studies showed that reduced p27 expression was correlated with advanced tumor stages and poorer disease-free survival in patients with HCC at a variety of evolutionary stages^[17-20]. However, most precious investigations are based on immunostaining of tumoral liver samples without comparing with surrounding nontumoral liver, which should be the best control tissue to be used for comparison.

In addition, p27 functions at the nuclear level by binding to and inhibiting cyclin/CDK complexes. It was recently reported that cytoplasmic displacement was an alternative way to inhibit p27 activity and might also play a role in tumor development^[21]. Indeed, positive immunostaining of cytoplasmic p27 has been previously reported in various human cancers^[22-25]. To address this hypothesis, the expression of p27 in tumoral, adjacent nontumoral, and normal liver tissues was evaluated by IHC analysis in patients with HCC, and the subcellular distribution of p27 was also investigated in this study.

MATERIALS AND METHODS

Patients and tumor samples

From January 2000 to December 2001, 32 liver samples were collected from patients who had HCC and underwent surgery in our institution. All liver tumors were histologically diagnosed. Tumor gross type and stage were diagnosed using Eggel's classification and Union International Contre Cancer (UICC) criteria. Tumor cellular differentiation was identified by Edmondson's classification. No patient received pre-operative chemotherapy or chemoembolization. The clinicopathologic characteristics of 32 patients with HCC are listed in Table 1. Normal livers were prepared from 10 patients who were died from the accident as the controls.

After curative surgery, all patients were followed up every 3 mo till death. They were followed from 2 to 32 mo (mean 15.2 mo). Actuarial survival was measured from the day of surgical operation to that of death or last follow-up.

Immunohistochemical study

Liver samples were routinely fixed in 40 g/L formaldehyde solution and embedded in paraffin. After slicing into 4 μ m-thick sections, IHC analysis was performed using Dako ElivisionTM plus two-step System. In brief, the sections were dewaxed in xylene, and rinsed in alcohol and graded alcohol/water mixtures. Then, 30 mL/L hydrogen peroxide was applied to block

endogenous peroxidase activity. The sections were subsequently treated in a microwave oven twice for 5 min in citrate buffer (pH 6.0) at high power. After blocking with goat serum, the mouse monoclonal antibodies against p27 (ZM-0340) and PCNA (ZM-0213) (Zymed Biotechnology, Zymed, CA) were applied on the slides at the dilution of 1:120 and 1:50, respectively. After rising, staining was performed by the Elivision™ plus two-step System (kit-9902, Dako, Carpinteria, CA). The color was developed by reacting with 3,3-diaminobenzidine. Slides were then counterstained with hematoxylin, dehydrated, cleared, and mounted. Negative controls were performed by replacing the primary antibody with nonimmune mouse serum or PBS (Figure 1). A human breast cancer specimen and the reactive tonsil were used as positive controls for p27 (Figure 2) and PCNA, respectively.

Table 1 Clinicopathologic characteristics of 32 Patients

Clinicopathologic parameters	Number	%
Age		
≤45 years	14	43.8
>45 years	18	56.2
Gender		
Male	26	81.2
Female	6	18.8
Gross type		
Massive	15	46.9
Nodular	17	53.1
Tumor size		
≤5 cm	5	15.6
>5 cm	27	84.4
Cellular differentiation		
I	4	12.5
II	17	53.1
III	5	15.6
IV	6	18.8
Degree of invasion		
T ₁ +T ₂	12	37.5
T ₃ +T ₄	20	62.5
Stage		
I+II	10	31.2
III+IV	22	68.8
Lymph node metastasis		
Present	4	87.5
Absent	28	12.5
Portal invasion		
With	3	9.4
Without	29	90.6
Infiltration		
Present	12	37.5
Absent	20	62.5

Immunostaining evaluation

Slides were mounted independently by 2 investigators without notifying any clinical or pathological information. The positive cells for p27 and PCNA were measured by counting at least 1 000 HCC cells from at least 5 randomly selected fields under the microscope. Then, LI was calculated as a percentage for each protein.

Statistical analysis

Values were expressed as mean±SD. The Student's *t* test was performed to analyze the relationship between the expression of the proteins and various clinicopathologic parameters. The

cumulative survival rate was computed and actuarial survival curves were constructed by the Kaplan-Meier method. The cumulative survival rate was compared between groups using the log-rank test. Relevant prognostic factors were identified by univariate and multivariate Cox proportional hazard regression analyses. Tests were considered significant when the *P* values were <0.05.

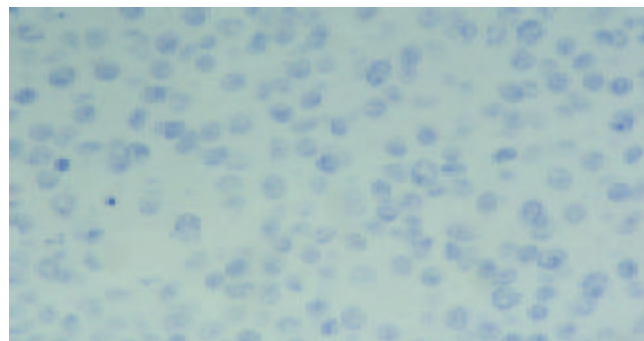


Figure 1 Negative control of p27 (×400).

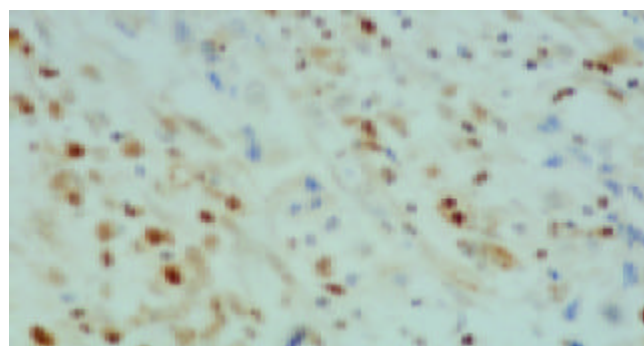


Figure 2 Positive control of p27 (×400).

RESULTS

Reduced expression of p27 in HCC

The mean LI of p27 in HCC was 27.7±19.9%, which was lower than that in adjacent nontumoral lesions (42.3±21.4%, *t*=2.444, *P*=0.017) and that in normal controls (39.1±17.5%, *t*=2.268, *P*=0.029). Furthermore, the LI of p27 in adjacent nontumoral lesions was not significantly different from that in normal controls (Figure 3). Table 2 shows the relationship between p27 expression and clinicopathologic characteristics. The LI of p27 significantly decreased in patients with massive type (*t*=2.227, *P*=0.037) and infiltration (*t*=2.197, *P*=0.036).

Proliferating activity in HCC

The mean LI of PCNA was 49.5±14.2% in HCC, which was higher than that in adjacent nontumoral lesions (42.8±11.2%, *t*=2.092, *P*=0.041) and normal controls (36.2±8.9%, *t*=3.533, *P*=0.002). The LI of PCNA in adjacent nontumoral lesions was not significantly different from that in normal controls (Figure 4). The LI of PCNA significantly increased in cases with poor differentiation (*t*=2.259, *P*=0.031, Table 2). The patients were divided into low p27 and high p27 groups with the cut-off value of the median LI. The LI of PCNA was 51.2±15.6% and 48.1±13.0% in low p27 and high p27 groups, respectively. There was no significant difference between these two groups (*t*=0.578, *P*=0.568).

Altered subcellular localization of p27 in HCC

The cytoplasmic expression of p27 was found in the HCC,

adjacent nontumoral, and normal liver tissues. Therefore, the cytoplasmic displacement of p27 might not be a specific phenomenon of tumor cells. However, the cytoplasmic sequestration of p27 was more frequent in HCC and adjacent nontumoral lesions (Figure 3).

The mean LI of cytoplasmic p27 was $31.0 \pm 12.6\%$ in adjacent nontumoral lesions, which was higher than that in HCC ($21.6 \pm 18.2\%$, $t=2.378$, $P=0.021$) and normal controls ($13.9 \pm 5.6\%$, $t=5.994$, $P<0.001$). The LI of cytoplasmic p27 in HCC was higher than that in normal controls ($t=2.106$, $P=0.042$).

Whereas, the nuclear LI in normal controls ($31.3 \pm 12.6\%$) was higher than that in HCC ($12.5 \pm 9.7\%$, $t=4.968$, $P<0.001$) and nontumoral lesions ($16.5 \pm 10.4\%$, $t=3.731$, $P=0.001$). Altered subcellular localization of p27 was correlated with clinical stage ($t=2.520$, $P=0.029$) and the degree of invasion ($t=2.640$, $P=0.019$) (Table 2).

Expression of p27 and PCNA and survival

The survival rate of 6, 12, and 24 mo was 71.9%, 47.8%, and 25.1%, respectively. The patients were divided into 2 groups according

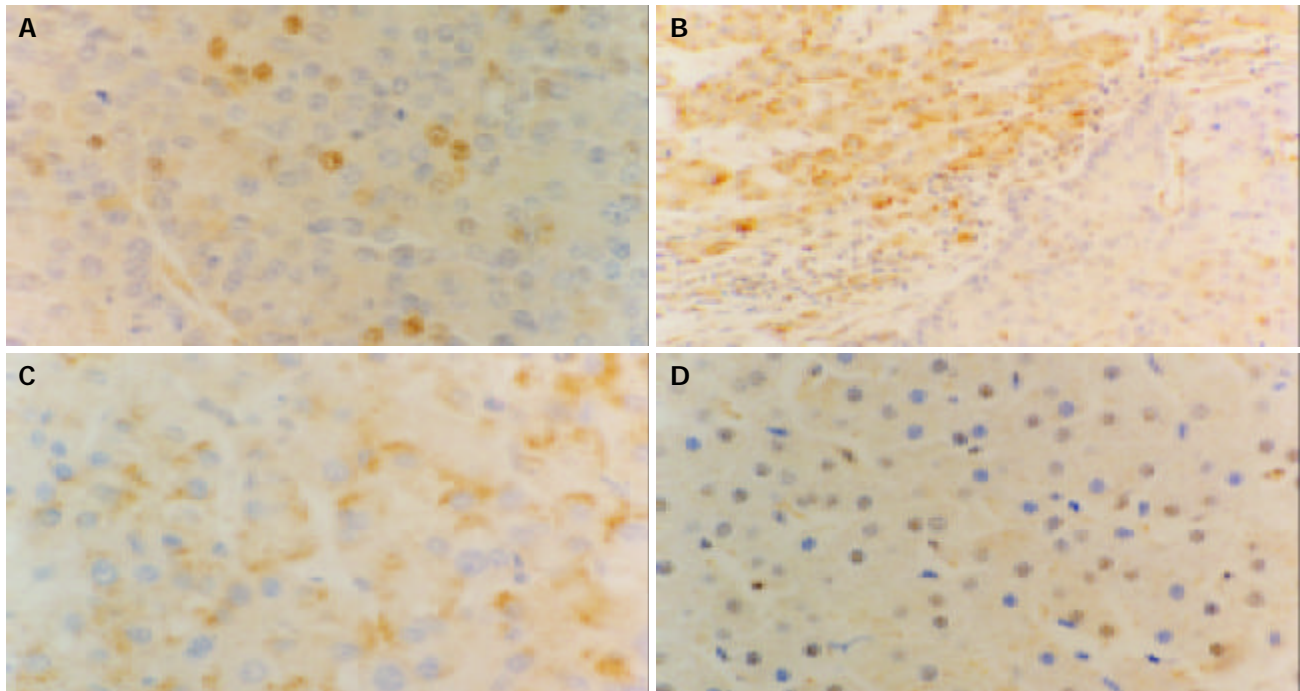


Figure 3 Immunohistochemical staining of p27 in different liver tissues(Elivision), A: p27 expression is decreased in HCC $\times 400$, B: Decreased p27 expression in HCC (right), the p27 expression is mostly located in the cytoplasm in nontumoral liver tissues (left) $\times 200$, C: Some tumor cells show cytoplasmic staining of p27 $\times 400$, D: p27 staining in normal controls is mostly located in nuclear $\times 400$.

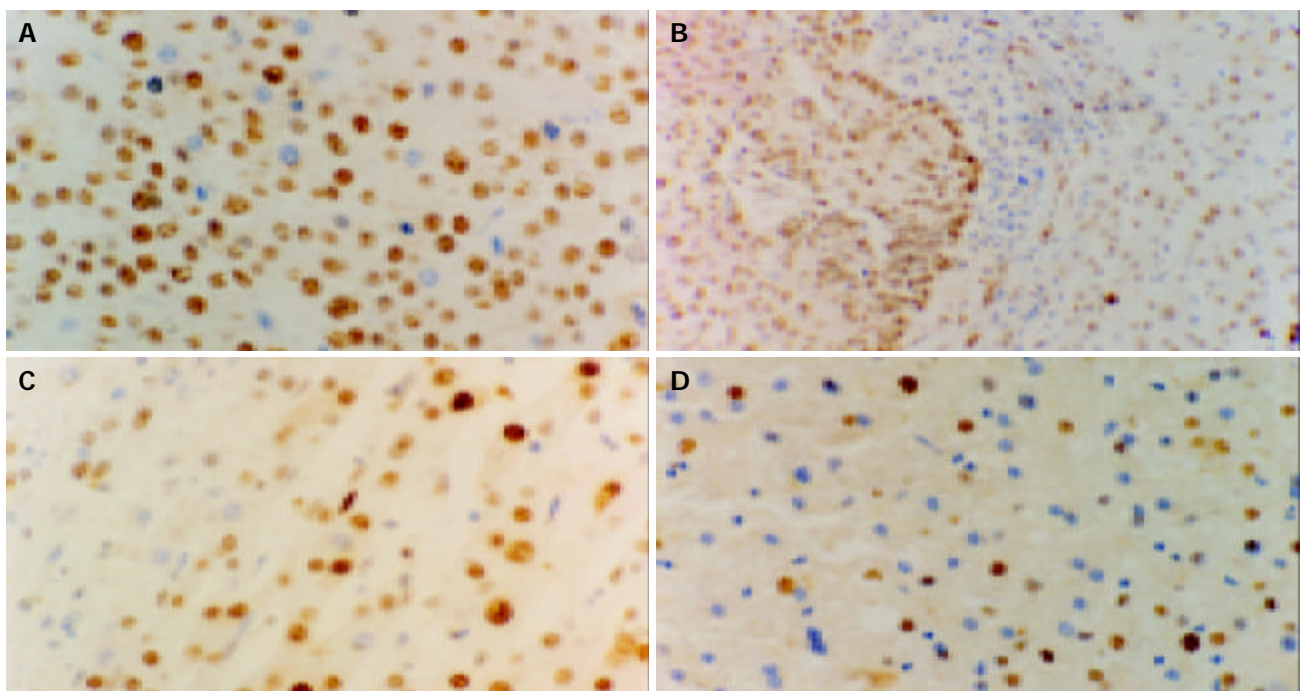
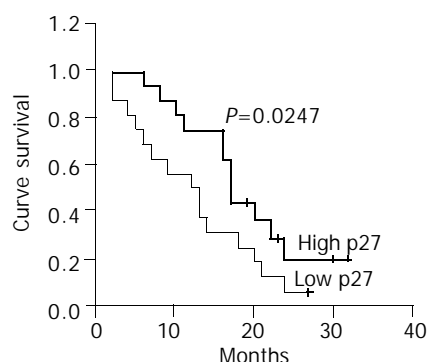


Figure 4 Expression of PCNA in different liver tissues(Elivision), A: Expression of PCNA in HCC $\times 400$, B: Expression of PCNA in HCC(left) and in nontumoral liver tissues(right) $\times 200$, C: Expression of PCNA in nontumoral liver tissues $\times 400$, D: in normal controls $\times 400$.

Table 2 Relationship among p27, PCNA, and cytoplasmic p27staining with clinicopathologic features

Parameters	p27 LI (%)	<i>P</i>	PCNA LI (%)	<i>P</i>	Cytoplasmic p27 LI (%)	<i>P</i>
Gross type						
Massive	20.5±13.1	0.037	46.4±13.4	0.249	25.9±18.9	0.221
Nodular	35.7±23.4		52.3±14.7		17.9±17.3	
Tumor size						
≤5 cm	23.8±14.4	0.645	38.1±10.7	0.047	27.0±24.1	0.481
>5 cm	28.4±20.9		51.7±13.9		20.6±17.4	
Cellular differentiation						
Well or moderate	29.7±21.4	0.438	45.7±13.8	0.031	23.2±18.0	0.498
Poor	23.8±17.1		56.9±12.6		18.6±19.1	
Degree of invasion						
T ₁ +T ₂	32.6±23.3	0.285	51.1±14.7	0.64	33.0±22.3	0.019
T ₃ +T ₄	24.7±17.5		48.6±14.4		14.8±11.1	
Stage						
I+II	33.6±25.6	0.261	48.0±12.9	0.688	35.3±23.9	0.029
III+IV	24.9±16.7		50.2±15.0		15.4±10.7	
Infiltration						
Present	18.3±18.8	0.036	44.4±12.3	0.117	19.0±18.3	0.536
Absent	33.3±18.7		52.6±14.7		23.2±18.5	
Lymphocyte metastasis						
With	25.5±2.6	0.565	56.0±14.9	0.339	16.0±10.6	0.518
Without	27.9±21.3		48.6±14.2		22.4±19.1	
Portal invasion						
Present	14.3±12.7	0.229	58.3±12.0	0.267	13.0±11.8	0.398
Absent	29.1±20.1		48.6±14.3		22.5±18.7	

to the median LI of p27, cytoplasmic p27, and PCNA. The survival analysis was performed on 32 patients and took into account for the following variables: age, gender, gross type, tumor size, UICC tumor stage, Edmondson's grade, portal invasion, lymph node metastasis, depth of invasion, infiltration, p27 LI, cytoplasmic p27 LI, and PCNA LI. In univariate analysis, a significant correlation with short survival was found only for present portal invasion ($P=0.021$) and low p27 expression ($P=0.033$). The prognosis of patients with higher p27 LI was longer than that of patients with lower p27 LI ($P=0.0247$, log-rank test, Figure 5). Multivariate analysis was performed by Cox proportional hazard regression model, age ≥ 45 years ($P=0.016$) and low p27 expression ($P=0.009$) were significantly associated with shorter survival. In addition, there was a trend of present lymphocyte metastasis ($P=0.05$) and advanced stage ($P=0.08$) correlated with poor prognosis (Table 3). For gross type, tumor size, Edmondson grade, depth of invasion, infiltration, cytoplasmic p27 LI, and PCNA LI, no significant correlations with overall survival were found.

**Figure 5** Kaplan-Meier curve for actuarial survival of patients in low p27 and high p27 groups.**Table 3** Univariate and multivariate analyses of individual parameters

Variables	<i>P</i> Values	
	Univariate	Multivariate
Age	0.150	0.016
Tumor size	0.513	0.678
Carcinoma differentiation	0.415	0.628
Stage	0.200	0.080
Lymphocyte metastasis	0.821	0.050
Infiltration	0.317	0.849
Portal invasion	0.021	0.619
p27	0.033	0.009
Cytoplasmic p27	0.114	0.624
PCNA	0.915	0.282

DISCUSSION

Hepatocellular carcinoma is one of the most common malignant tumors in China, and the incidence of HCC has increased in recent years^[26]. Cell proliferating activity is one of the prominent parameters for evaluating the biological aggressiveness of tumors. The study in cell proliferating status of HCC is very important for evaluating the biological aggressiveness^[27,28], because distant and lymph node metastasis are not very common.

The protein p27 is an important member of CKI family. It regulates G1 progression by binding to and inhibiting cyclin/CDKs^[29,30]. Loss or reduced expression of p27 has been found in a variety of human cancers and associated with more aggressive tumor behavior. The present study showed that p27 expression significantly decreased in HCC. The finding of p27 underexpression in HCC was similar to the previous reports^[31]. This study showed that the expression of p27 in

HCC was associated with gross type and direct liver invasion. Univariate analysis showed that portal invasion and p27 LI were related to survival in this study. In multivariate analysis, p27 expression was the strongest predictor of survival for HCC patients, which was independent of the other variables. Similar findings have also been observed in other cancers^[32-34]. It is therefore suggested that p27 should work as a negative regulator during hepatocarcinogenesis and may exert a useful prognostic marker. Interestingly, as reported by Milde-Langosch^[35], there was no correlation between p27 expression and proliferating level, indicating that reduced expression of p27 did not merely reflect high proliferating activity during tumor progression.

To our knowledge, this was the first study to report the altered subcellular localization of p27 in HCC. The protein p27 can bind to and inhibit the active cyclin/CDK complexes in the nucleus, so the cytoplasmic displacement may play an important role in inactivating this protein in tumor cells and in contributing to tumor development. Indeed, cytoplasmic localization of p27 immunostaining has been reported in various types of human cancers. In our study, we found that the cytoplasmic localization of p27 was more frequent in HCC and surrounding nontumoral livers. Furthermore, the cytoplasmic staining for p27 was more frequently accompanied with nuclear staining in normal controls. However, the increase in the cytoplasmic staining for p27 was often observed in the absence of a concomitant increase in the nuclear staining and was sometimes associated with a decrease in the nuclear staining. Some tumors expressed an increased level of p27 mainly because of an increase in the cytoplasmic level of this protein. The increase in the amount of cytoplasmic p27 was more frequent in early stage (I and II) tumors. Altered subcellular localization of p27 was also reported in Barrett's associated adenocarcinoma and colon cancer^[22,23]. In agreement with our results, cytoplasmic localization of p27 was an early event during carcinogenesis.

Although the mechanism responsible for the abnormal subcellular localization was not known, it may be due to loss of the tuberous sclerosis complex gene-2 (TSC2), the HER/Grb2/MAPK pathway which leads to nuclear export of p27^[36], overexpression of cyclin D3 which contributes to retaining p27 in the cytoplasm^[37], or PKB/Akt which phosphorylates p27 to impair its nuclear import^[38-40].

In conclusion, our results suggest that underexpression of p27 can contribute to the development of HCC. Cytoplasmic displacement is an alternative mechanism of inactivating p27 that acts early during hepatocarcinogenesis. Furthermore, studies on a large number of cases will reveal the significance of p27 subcellular localization in hepatocarcinogenesis and its relationship with clinicopathologic and prognostic parameters.

REFERENCES

- 1 **Ho A**, Dowdy SF. Regulation of G(1) cell-cycle progression by oncogenes and tumor suppressor genes. *Curr Opin Genet Dev* 2002; **12**: 47-52
- 2 **Sanchez-Beato M**, Sanchez-Aguilera A, Piris MA. Cell cycle deregulation in B-cell lymphomas. *Blood* 2003; **101**: 1220-1235
- 3 **Todd R**, Hinds PW, Munger K, Rustgi AK, Opitz OG, Suliman Y, Wong DT. Cell cycle dysregulation in oral cancer. *Crit Rev Oral Biol Med* 2002; **13**: 51-61
- 4 **Fiano V**, Ghimenti C, Schiffer D. Expression of cyclins, cyclin-dependent kinases and cyclin-dependent kinase inhibitors in oligodendrogliomas in humans. *Neurosci Lett* 2003; **347**: 111-115
- 5 **Polak J**, Pekova S, Schwarz J, Kozak T, Haskovec C. Expression of cyclin-dependent kinase inhibitors in leukemia. *Cas Lek Cesk* 2003; **142**: 25-28
- 6 **Slingerland J**, Pagano M. Regulation of the cdk inhibitor p27 and its deregulation in cancer. *J Cell Physiol* 2000; **183**: 10-17
- 7 **Philipp-Staheli J**, Payne SR, Kemp CJ. p27(Kip1): regulation and function of a haploinsufficient tumor suppressor and its misregulation in cancer. *Exp Cell Res* 2001; **264**: 148-168
- 8 **Tsukiyama T**, Ishida N, Shirane M, Minamishima YA, Hatakeyama S, Kitagawa M, Nakayama K, Nakayama K. Down-regulation of p27Kip1 expression is required for development and function of T cells. *J Immunol* 2001; **166**: 304-312
- 9 **Muraoka RS**, Lenferink AE, Simpson J, Brantley DM, Roebuck LR, Yakes FM, Arteaga CL. Cyclin-dependent kinase inhibitor p27(Kip1) is required for mouse mammary gland morphogenesis and function. *J Cell Biol* 2001; **153**: 917-932
- 10 **Alexander K**, Hinds PW. Requirement for p27(KIP1) in retinoblastoma protein-mediated senescence. *Mol Cell Biol* 2001; **21**: 3616-3631
- 11 **Nitti D**, Belluco C, Mammano E, Marchet A, Ambrosi A, Mencarelli R, Segato P, Lise M. Low level of p27(Kip1) protein expression in gastric adenocarcinoma is associated with disease progression and poor outcome. *J Surg Oncol* 2002; **81**: 167-175
- 12 **Hu YX**, Watanabe H, Li P, Wang Y, Ohtsubo K, Yamaguchi Y, Sawabu N. An immunohistochemical analysis of p27 expression in human pancreatic carcinomas. *Pancreas* 2000; **21**: 226-230
- 13 **Filipits M**, Puhalla H, Wrba F. Low p27Kip1 expression is an independent prognostic factor in gallbladder carcinoma. *Anticancer Res* 2003; **23**: 675-679
- 14 **Anastasiadis AG**, Calvo-Sanchez D, Franke KH, Ebert T, Heydthausen M, Schulz WA, Burchardt M, Gerharz CD. p27KIP1-expression in human renal cell cancers: implications for clinical outcome. *Anticancer Res* 2003; **23**: 217-221
- 15 **Tannapfel A**, Grund D, Katalinic A, Uhlmann D, Kockerling F, Haugwitz U, Wasner M, Hauss J, Engeland K, Wittekind C. Decreased expression of p27 protein is associated with advanced tumor stage in hepatocellular carcinoma. *Int J Cancer* 2000; **89**: 350-355
- 16 **Yue H**, Song FL, Zhang N, Feng XL, An TY, Yu JP. Expression of p27(kip1), Rb protein and proliferating cell nuclear antigen and its relationship with clinicopathology in human pancreatic cancer. *Hepatobiliary Pancreat Dis Int* 2003; **2**: 142-146
- 17 **Fiorantino M**, Altamari A, D'Errico A, Cukor B, Barozzi C, Loda M, Grigioni WF. Acquired expression of p27 is a favorable prognostic indicator in patients with hepatocellular carcinoma. *Clin Cancer Res* 2000; **6**: 3966-3972
- 18 **Zhou Q**, He Q, Liang LJ. Expression of p27, cyclin E and cyclin A in hepatocellular carcinoma and its clinical significance. *World J Gastroenterol* 2003; **9**: 2450-2454
- 19 **Qin LF**, Ng IO. Expression of p27(KIP1) and p21(WAF1/CIP1) in primary hepatocellular carcinoma: clinicopathologic correlation and survival analysis. *Hum Pathol* 2001; **32**: 778-784
- 20 **Ito Y**, Matsuura N, Sakon M, Miyoshi E, Noda K, Takeda T, Umeshita K, Nagano H, Nakamori S, Dono K, Tsujimoto M, Nakahara M, Nakao K, Taniguchi N, Monden M. Expression and prognostic roles of the G1-S modulators in hepatocellular carcinoma: p27 independently predicts the recurrence. *Hepatology* 1999; **30**: 90-99
- 21 **Blagosklonny MV**. Are p27 and p21 cytoplasmic oncoproteins? *Cell Cycle* 2002; **1**: 391-393
- 22 **Sgambato A**, Ratto C, Faraglia B, Merico M, Ardito R, Schinzari G, Romano G, Cittadini AR. Reduced expression and altered subcellular localization of the cyclin-dependent kinase inhibitor p27(Kip1) in human colon cancer. *Mol Carcinog* 1999; **26**: 172-179
- 23 **Singh SP**, Lipman J, Goldman H, Ellis FH Jr, Aizenman L, Cangi MG, Signoretti S, Chiau DS, Pagano M, Loda M. Loss or altered subcellular localization of p27 in Barrett's associated adenocarcinoma. *Cancer Res* 1998; **58**: 1730-1735
- 24 **Masciullo V**, Sgambato A, Pacilio C, Pucci B, Ferrandina G, Palazzo J, Carbone A, Cittadini A, Mancuso S, Scambia G, Giordano A. Frequent loss of expression of the cyclin-dependent kinase inhibitor p27 in epithelial ovarian cancer. *Cancer Res* 1999; **59**: 3790-3794
- 25 **Masciullo V**, Susini T, Zamparelli A, Bovicelli A, Minimo C, Massi D, Taddei G, Maggiano N, De Iaco P, Ceccaroni M, Bovicelli L, Amunni G, Mancuso S, Scambia G, Giordano A. Frequent loss of expression of the cyclin-dependent kinase inhibitor p27(Kip1) in estrogen-related endometrial adenocarcinomas. *Clin Cancer Res* 2003; **9**: 5332-5338

- 26 **Tang ZY**. Hepatocellular carcinoma-cause, treatment and metastasis. *World J Gastroenterol* 2001; **7**: 445-454
- 27 **Qin LX**, Tang ZY. The prognostic significance of clinical and pathological features in hepatocellular carcinoma. *World J Gastroenterol* 2002; **8**: 193-199
- 28 **Zeng WJ**, Liu GY, Xu J, Zhou XD, Zhang YE, Zhang N. Pathological characteristics, PCNA labeling index and DNA index in prognostic evaluation of patients with moderately differentiated hepatocellular carcinoma. *World J Gastroenterol* 2002; **8**: 1040-1044
- 29 **Lloyd RV**, Erickson LA, Jin L, Kulig E, Qian X, Cheville JC, Scheithauer BW. p27kip1: a multifunctional cyclin-dependent kinase inhibitor with prognostic significance in human cancers. *Am J Pathol* 1999; **154**: 313-323
- 30 **McIntyre M**, Desdouets C, Senamaud-Beaufort C, Laurent-Winter C, Lamas E, Brechot C. Differential expression of the cyclin-dependent kinase inhibitor P27 in primary hepatocytes in early-mid G1 and G1/S transitions. *Oncogene* 1999; **18**: 4577-4585
- 31 **Armengol C**, Boix L, Bachs O, Sole M, Fuster J, Sala M, Llovet JM, Rodes J, Bruix J. p27(Kip1) is an independent predictor of recurrence after surgical resection in patients with small hepatocellular carcinoma. *J Hepatol* 2003; **38**: 591-597
- 32 **Zhang H**, Sun XF. Loss of p27 expression predicts poor prognosis in patients with Dukes' B stage or proximal colorectal cancer. *Int J Oncol* 2001; **19**: 49-52
- 33 **Hayashi H**, Ogawa N, Ishiwa N, Yazawa T, Inayama Y, Ito T, Kitamura H. High cyclin E and low p27/Kip1 expressions are potentially poor prognostic factors in lung adenocarcinoma patients. *Lung Cancer* 2001; **34**: 59-65
- 34 **Haitel A**, Wiener HG, Neudert B, Marberger M, Susani M. Expression of the cell cycle proteins p21, p27, and pRb in clear cell renal cell carcinoma and their prognostic significance. *Urology* 2001; **58**: 477-481
- 35 **Milde-Langosch K**, Hagen M, Bamberger AM, Loning T. Expression and prognostic value of the cell-cycle regulatory proteins, Rb, p16MTS1, p21WAF1, p27KIP1, cyclin E, and cyclin D2, in ovarian Cancer. *Int J Gynecol Pathol* 2003; **22**: 168-174
- 36 **Yang HY**, Zhou BP, Hung MC, Lee MH. Oncogenic signals of HER-2/neu in regulating the stability of the cyclin-dependent kinase inhibitor p27. *J Biol Chem* 2000; **275**: 24735-24739
- 37 **Baldassarre G**, Belletti B, Bruni P, Boccia A, Trapasso F, Pentimalli F, Barone MV, Chiappetta G, Vento MT, Spiezia S, Fusco A, Viglietto G. Overexpressed cyclin D3 contributes to retaining the growth inhibitor p27 in the cytoplasm of thyroid tumor cells. *J Clin Invest* 1999; **104**: 865-874
- 38 **Liang J**, Zubovitz J, Petrocelli T, Kotchetkov R, Connor MK, Han K, Lee JH, Ciarallo S, Catzavelos C, Beniston R, Franssen E, Slingerland JM. PKB/Akt phosphorylates p27, impairs nuclear import of p27 and opposes p27-mediated G1 arrest. *Nat Med* 2002; **8**: 1153-1160
- 39 **Shin I**, Yakes FM, Rojo F, Shin NY, Bakin AV, Baselga J, Arteaga CL. PKB/Akt mediates cell-cycle progression by phosphorylation of p27(Kip1) at threonine 157 and modulation of its cellular localization. *Nat Med* 2002; **8**: 1145-1152
- 40 **Viglietto G**, Motti ML, Bruni P, Melillo RM, D'Alessio A, Califano D, Vinci F, Chiappetta G, Tsichlis P, Bellacosa A, Fusco A, Santoro M. Cytoplasmic relocation and inhibition of the cyclin-dependent kinase inhibitor p27(Kip1) by PKB/Akt-mediated phosphorylation in breast cancer. *Nat Med* 2002; **8**: 1136-1144

Edited by Chao JCJ Proofread by Xu FM

Loss of heterozygosity on chromosome 1 in sporadic colorectal carcinoma

Chong-Zhi Zhou, Guo-Qiang Qiu, Fang Zhang, Lin He, Zhi-Hai Peng

Chong-Zhi Zhou, Guo-Qiang Qiu, Fang Zhang, Zhi-Hai Peng,
Department of General Surgery, Shanghai Jiaotong University, First
People's Hospital, Shanghai 200080, China

Lin He, Shanghai Institute for Biological Science, Chinese Academy
of Sciences, Shanghai 200031, China

Supported by the National Natural Science Foundation of China,
No. 30080016

Correspondence to: Dr. Zhi-Hai Peng, Department of General
Surgery, Shanghai Jiaotong University, First People's Hospital, 85
Wujin Road, Shanghai 200080, China. pengpzhb@online.sh.cn

Telephone: +86-21-63240090 Ext 3102

Received: 2003-06-10 **Accepted:** 2003-08-16

Abstract

AIM: Loss of heterozygosity (LOH) on tumor suppressor genes is believed to play a key role in carcinogenesis of colorectal cancer. When it occurs at a tumor suppressor gene locus with abnormal allele, neoplastic transformation happens. In this study, we analyzed the LOH at 21 loci on chromosome 1 in sporadic colorectal cancer to identify additional loci involved in colorectal tumorigenesis.

METHODS: Twenty-one polymorphic micro-satellite DNA markers were analyzed with PCR both in 83 cases of colorectal cancer and in normal tissues. PCR products were electrophoresed on an ABI 377 DNA sequencer. Genescan 3.1 and Genotype 2.1 software were used for LOH scanning and analysis. χ^2 test was used to compare LOH frequency with clinicopathological data. $P < 0.05$ was considered as statistically significant.

RESULTS: The average LOH frequency of chromosome 1, short arm and long arm was 19.83%, 18.00% and 21.66%, respectively. The 2 highest LOH loci with a frequency of 36.54% and 32.50% were identified on D1S468 (1p36.33-p36.31) and D1S413 (1q31.3), respectively. On D1S2726 locus, LOH frequency of rectal cancer was 28.57% (6/21), which was higher than that of colon cancer (0.00%, 0/33) ($P = 0.002$), suggesting that the mechanism of carcinogenesis was different in both groups.

CONCLUSION: Putative tumor suppressor genes on chromosome 1 may relate to sporadic colorectal carcinomas. Tumor-suppressor-genes might locate on 1p36.33-36.31 and/or 1q31.3.

Zhou CZ, Qiu GQ, Zhang F, He L, Peng ZH. Loss of heterozygosity on chromosome 1 in sporadic colorectal carcinoma. *World J Gastroenterol* 2004; 10(10): 1431-1435

<http://www.wjgnet.com/1007-9327/10/1431.asp>

INTRODUCTION

Colorectal cancer is one of the three leading causes of cancer mortality worldwide. The progression of the cancer is due to an accumulation of genetic alteration in controlling growth

and proliferation at numerous loci. As a model for both multistep and multipathway carcinogenesis, colorectal neoplastic progression provides paradigms of both oncogenes and tumor suppressor genes^[1,2]. The loss of heterozygosity (LOH) on tumor suppressor genes is believed as one of the key steps to carcinogenesis of colorectal cancer^[3]. The loss of one allele at a specific locus is caused by a deletion mutation or loss of a chromosome from a chromosome pair^[4]. When this occurs at a tumor suppressor gene with an abnormal allele, neoplastic transformation occurs. In colorectal cancers, frequent allelic loss has been identified in chromosome 5q (30%), 8p (40%), 17p (75-80%), 18q (80%), and 22q (20-30%)^[5,6]. Tumor suppressor genes APC, p53, and DCC were found to be located on chromosome 5q, 17p, and 18q, respectively. LOH analysis became an effective way to find informative loci candidate tumor suppressor genes afterwards^[7,8]. In this study we analyzed the LOH at 21 loci on chromosome 1 in sporadic colorectal cancers to identify additional loci involved in colorectal tumorigenesis.

MATERIALS AND METHODS

Materials

From 1998 to 1999, 83 consecutively collected tumors were treated surgically at Surgical Department of First People's Hospital in Shanghai Jiaotong University. There were 40 males and 43 females with a median age of 66 years (range 31-84). The diagnosis was verified pathologically. The number of Dukes stages A, B, C, D was 8, 21, 40 and 14, respectively. The number of proximal colon cancer, distal colon cancer, and rectal cancer was 33, 21 and 29, respectively. Well-differentiated adenocarcinomas, moderately differentiated adenocarcinomas and poorly differentiated adenocarcinomas were 23, 39 and 6, respectively, and mucinous adenocarcinomas were 15. HNPCC patients were ruled out by Amsterdam criteria^[9,10]. Informed consent to use surgical specimens in this study was obtained from patients.

Methods

DNA extraction Thirty min after surgery, fresh cancerous and adjacent normal tissues were cut into approximately 2 mm³ and immediately frozen in liquid nitrogen. DNA was extracted using standard method with proteinase K digestion and phenol/chloroform purification.

Microsatellite markers and PCR Twenty-one fluorescence-labeled primers for polymorphic microsatellite markers (Perkin-Elmer, USA), at a density of approximately one marker every 10 cm (Figure 1), were used to amplify DNAs from normal and tumor tissues for LOH analysis. PCR for DNAs from normal and tumor tissue was done to analyze the polymorphic microsatellite markers. PCR conditions were as follows: 5 μ L total volume with approximately 1.4 ng of DNA as a template with 10 \times standard buffer, 0.3 μ L Mg²⁺, 0.8 μ L deoxynucleotide triphosphates, 0.3 unit of Hot-start taq polymerase and 0.06 μ L of each oligonucleotide primer, with the forward primer fluorescence labeled with HEX, FAM or NED. Cycling conditions consisted of 3 stages: an initial

denaturation at 96 °C for 12 min in stage I; 14 cycles each at 94 °C for 20 s, at 63-56 °C for 1 min (0.5 °C decreased per cycle), at 72 °C for 1 min in stage II; 35 cycles each at 94 °C for 20 s, at 56 °C for 1 min, at 72 °C for 1 min in stage III^[11-13].

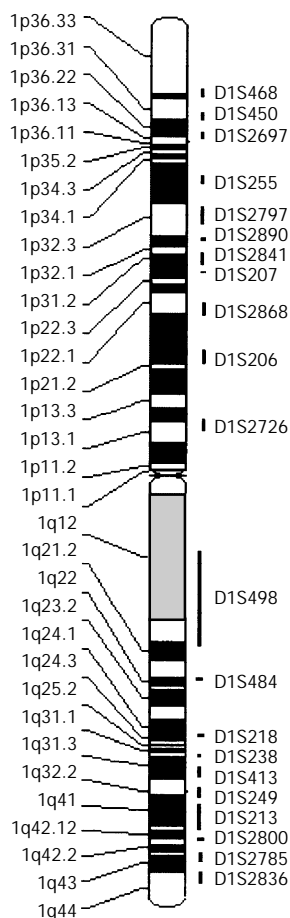


Figure 1 Twenty-one microsatellite markers on chromosome 1.

LOH analysis PCR product (0.5 µL) was mixed with 0.1 µL of Genescan 500 size standard (PE Applied Biosystems, USA) and 0.9 µL of formamide loading buffer. After denaturation

at 96 °C for 5 min, products were electrophoresed on 50 g/L polyacrylamide gels on an ABI 377 DNA sequencer (PE Applied Biosystems, USA) for 3 h. Genotype 2.1 software displayed individual gel lanes as electropherograms with a given size, height, and area for each detected fluorescent peak. Stringent criteria were used to score the samples. Alleles were defined as the two highest peaks within the expected size range. A ratio of T1:T2/N1:N2 less than 0.67 or greater than 1.50 was scored as a loss of heterozygosity (Figure 2). Most amplifications of normal DNA producing two PCR products indicated preserve of heterozygosity. A single fragment amplified from normal DNA (homozygote) and fragments not clearly amplified from PCR reactions were scored as not informative. The LOH frequency of a locus was equal to the ratio of the number between allelic loss and informative cases. The average LOH frequency of chromosome 1 was the mean of the LOH frequency in all loci^[14-17].

Statistics χ^2 test was used to compare LOH with clinicopathological data. $P < 0.05$ was considered statistically significant.

RESULTS

LOH of 21 microsatellite markers on chromosome 1

The average LOH frequency at chromosome 1, short arm and long arm was 19.83%, 18.00% and 21.66%, respectively. The two highest LOH loci with a frequency of 36.54% and 32.50% were identified on D1S468 (1p36.33-36.31) and D1S413 (1q31.3). Other loci also exhibited higher LOH frequencies, including D1S255 (1p34.1-32.3), D1S2868 (1p22.1), D1S218 (1q24.1-24.3), D1S249 (1q32.2), D1S2800 (1q42.12-42.2) and D1S2836 (1q43-44) (Table 1).

Relationship of clinicopathological features and LOH on chromosome 1

On D1S2726 locus, LOH frequency of rectal cancer was 28.57% (6/21), which was higher than that of colon cancer (0%, 0/33) ($P = 0.002$). No association between LOH of each marker on chromosome 1 and other clinicopathological data (patient sex, age, tumor size, growth pattern or Dukes stage) was observed. It indicated that LOH on chromosome 1 was a common phenomenon in all kinds of sporadic colorectal cancers (Tables 2A, 2B).

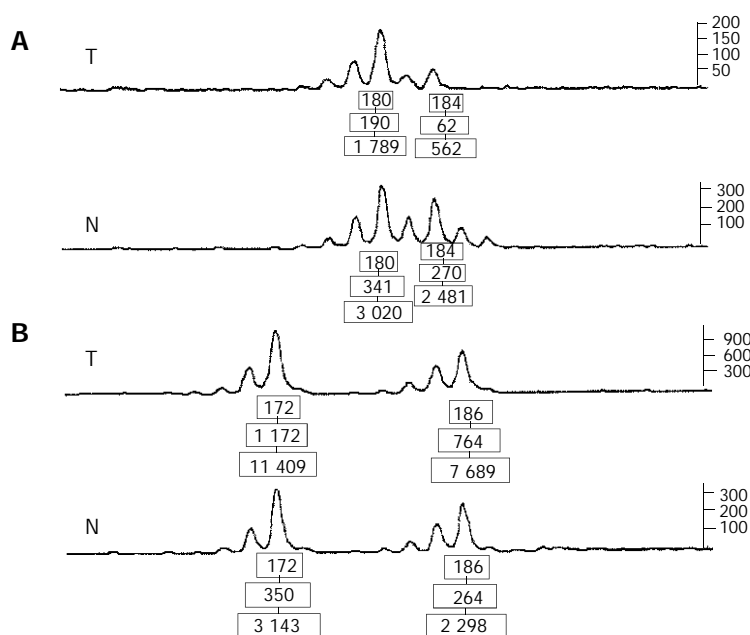


Figure 2 Typical peak and normal peak of LOH3. A: Typical peak of LOH: Allele ratio=(T1/T2)/(N1/N2)=(190/62)/(341/270)=2.43>1.5, B: The normal peak (no LOH): Allele ratio=(T1/T2)/(N1/N2)=(1172/764)/(350/264)=1.15, T: Tumor, N: Normal.

Table 1 LOH frequency of 21 microsatellite markers on chromosome 1

Locus	Location	LOH case	Normal case	LOH rate (%)	Informative rate (%)
D1S468	1p36.33-36.31	19	33	36.54	62.65
D1S450	1p36.31	7	41	14.58	57.83
D1S2697	1p36.22-36.13	5	25	16.67	36.14
D1S255	1p34.1-32.3	11	43	20.37	65.06
D1S2797	1p32.3	8	46	14.81	65.06
D1S2890	1p32.3-32.1	6	48	11.11	65.06
D1S2841	1p31.2	11	46	19.30	68.67
D1S207	1p31.2-22.3	5	63	7.35	81.93
D1S2868	1p22.1	10	39	20.41	59.04
D1S206	1p22.1-21.2	7	33	17.50	48.19
D1S2726	1p13.3-13.1	6	48	11.11	65.06
D1S498	1q12-21.2	11	48	18.64	71.08
D1S484	1q22	10	55	15.38	78.31
D1S218	1q24.1-24.3	16	42	27.59	69.88
D1S238	1q31.1	3	38	7.32	49.40
D1S413	1q31.3	13	27	32.50	48.19
D1S249	1q32.2	10	36	21.74	55.42
D1S213	1q41-42.12	8	41	16.33	59.04
D1S2800	1q42.12-42.2	12	45	21.05	68.67
D1S2785	1q43	10	48	17.24	69.88
D1S2836	1q43-44	12	36	25.00	57.83

Table 2a Relationship between clinicopathological features and LOH of 11 loci on short arm of chromosome 1

		D1S468		D1S450		D1S2697		D1S255		D1S2797		D1S2890		D1S2841		D1S207		D1S2868		D1S206		D1S2726	
		N	L	N	L	N	L	N	L	N	L	N	L	N	L	N	L	N	L	N	L	N	L
Gender	Male	18	8	20	4	13	2	19	7	20	5	21	4	20	6	31	2	15	3	17	3	19	5
	Female	15	11	21	3	12	3	24	4	26	3	27	2	26	5	32	3	24	7	16	4	29	1
Age (yr)	>60	26	13	30	7	19	4	32	8	36	7	37	6	34	11	46	5	32	7	27	5	33	6
	≤60	7	6	11	0	6	1	11	3	10	1	11	0	12	0	17	0	7	3	6	2	15	0
Location	Proximal colon	12	9	12	2	13	2	14	5	19	2	22	3	21	4	24	2	13	6	11	1	20	0
	Distal Colon	7	5	10	1	4	2	12	2	8	3	11	1	9	4	17	1	13	2	8	4	13	0
	Rectum	14	5	19	4	8	1	17	4	19	3	15	2	16	3	22	2	13	2	14	2	15	6 ¹
Gross pattern	Massive	15	9	16	2	10	1	15	7	21	3	17	5	20	4	23	2	17	3	17	1	19	2
	Ulcerative	13	5	16	3	9	3	22	4	19	3	20	1	18	4	27	3	15	3	10	3	20	3
	Encroaching	5	5	9	2	6	1	6	0	6	2	11	0	8	3	13	0	7	4	6	3	9	1
Size	≥5 (cm)	18	8	21	5	13	1	19	8	24	4	27	2	23	4	31	1	19	5	13	5	24	3
	<5 (cm)	15	11	20	2	12	4	24	3	22	4	21	4	23	7	32	4	20	5	20	2	24	3
LN metastasis	LN (+)	24	10	26	5	17	4	29	4	28	6	31	5	26	9	38	5	22	8	20	5	28	4
	LN (-)	9	9	15	2	8	1	14	7	18	2	17	1	20	2	25	0	17	2	13	2	20	2
Differentiation	Well	8	7	14	1	5	1	10	3	20	1	15	0	12	4	16	2	13	2	14	3	18	0
	Moderately	16	10	19	5	12	4	21	5	14	7	19	5	22	5	31	3	16	5	13	2	18	6
	Poorly	3	0	4	1	2	0	5	0	4	0	5	0	2	0	6	0	3	1	0	2	5	0
	Mucinous	6	2	4	0	6	0	7	3	8	0	9	1	10	2	10	0	7	2	6	0	7	0
Dukes stage	A	3	3	4	0	1	0	4	1	3	2	4	0	7	0	7	0	5	0	2	1	5	0
	B	6	6	11	2	7	1	10	6	15	0	13	1	13	2	18	0	12	2	11	1	15	2
	C	17	8	20	3	11	2	21	3	20	5	23	5	18	7	26	5	16	7	18	3	20	4
	D	7	2	6	2	6	2	8	1	8	1	8	0	8	2	12	0	6	1	2	2	8	0

¹P=0.002, LOH frequency of rectal cancer vs colon cancer.

Table 2b Relationship between clinicopathological features and LOH of 10 loci on long arm of chromosome 1

		D1S498		D1S484		D1S218		D1S238		D1S413		D1S249		D1S213		D1S2800		D1S2785		D1S2836	
		N	L	N	L	N	L	N	L	N	L	N	L	N	L	N	L	N	L	N	L
Gender	Male	25	6	25	7	22	6	20	1	14	7	16	6	17	3	19	9	25	3	19	5
	Female	23	5	30	3	20	10	18	2	13	6	20	4	24	5	26	3	23	7	17	7
Age (yr)	>60	37	10	43	6	30	14	28	3	18	10	28	7	33	6	33	10	39	10	26	9
	≤60	11	1	12	4	12	2	10	0	9	3	8	3	8	2	12	2	9	0	10	3
Location	Proximal colon	14	6	20	4	16	5	15	1	10	6	17	3	15	2	15	6	18	6	16	5
	Distal colon	14	3	14	4	14	4	10	1	7	3	4	2	12	3	14	1	14	2	6	5
	Rectum	20	2	21	2	12	7	13	1	10	4	15	5	14	3	16	5	16	2	14	2
Gross pattern	Massive	22	4	23	3	18	11	12	2	14	5	13	4	17	4	17	3	20	6	16	5
	Ulcerative	17	5	24	3	15	4	19	1	9	5	13	5	19	4	18	6	20	3	12	5
	Encroaching	9	2	8	4	9	1	7	0	4	3	10	1	5	0	10	3	8	1	8	2
Size	≥5 (cm)	21	7	27	7	22	6	18	3	11	6	16	5	21	4	21	8	23	7	17	8
	<5 (cm)	27	4	28	3	20	10	20	0	16	7	20	5	20	4	24	4	25	3	19	4
LN Metastasis	LN (+)	31	6	36	4	26	11	23	2	16	6	22	6	28	5	30	7	31	7	25	5
	LN (-)	17	5	19	6	16	5	15	1	11	7	14	4	13	3	15	5	17	3	11	7
Differentiation	Well	12	4	15	3	11	3	8	1	7	3	10	2	13	2	13	5	16	2	10	5
	Moderately	26	4	27	4	22	7	19	0	12	6	17	4	18	5	21	5	18	7	18	6
	Poorly	2	0	6	0	3	2	3	0	2	1	2	3	4	0	4	1	4	0	2	1
	Mucinous	8	3	7	3	6	4	8	2	6	3	7	1	6	1	7	1	10	1	6	0
Dukes stage	A	4	0	5	2	3	2	5	1	3	2	2	1	3	1	4	0	4	1	2	3
	B	13	5	14	4	13	3	10	0	8	5	12	3	10	2	11	5	13	2	9	4
	C	22	5	26	4	18	9	18	1	12	4	15	5	21	5	21	6	23	6	17	2
	D	9	1	10	0	8	2	5	1	4	2	7	1	7	0	9	1	8	1	8	3

DISCUSSION

During tumorigenesis, loss of wild-type alleles (inherited from the non-mutation-carrying parents) is frequently observed. Loss of heterozygosity (LOH) on tumor suppressor genes played a key role in colorectal cancer transformation, and LOH analysis of sporadic colorectal cancers could help discover unknown tumor suppressor genes^[7,8]. In this study, LOH scanning was analyzed by Genotyper software in 83 sporadic colorectal cancer samples with 21 highly polymorphic markers, the ratio of the fluorescence intensity of alleles was studied to identify additional loci involved in colorectal tumorigenesis.

In this study, the average LOH frequency at chromosome 1 (19.83%), short arm (18.00%) and long arm (21.66%) was consistent with the previous study^[5]. The two highest LOH loci with a frequency of 36.54% and 32.50% was identified on D1S468 (1p36.33-36.31) and D1S413 (1q31.3). There were few reports about the relationship between the long arm of chromosome 1 and colorectal cancer. But some previous studies showed that the 1q31-32 region frequently presented allelic loss in breast cancers and medulloblastomas. Pietsch *et al.*^[18] found that 36% of medulloblastomas showed loss of heterozygosity (LOH) on chromosome 1q. The study of Benitez J showed more than 60% of breast tumors exhibited allelic loss in the 1q31-32 region^[19]. These results suggested that putative tumor suppressor genes might locate on the 1q31-32 region. Our study also found that D1S413(1q31.3) exhibited a higher LOH frequency and that the LOH frequency of long arm of chromosome 1 was higher than that of short arm^[5]. If D1S413 could be excluded, the LOH frequency of long arm was nearly equal to that of short arm. Thus, we hypothesized that the higher LOH frequency of D1S413 might be the reason why the LOH frequency of long arm of chromosome 1 was higher than that of short arm, suggesting the presence of a tumor suppressor gene in this region. This gene might be involved in the neoplastic process of colorectal cancer, breast cancer and medulloblastoma.

Previous studies showed that the 1p36 region frequently presented allelic loss in various cancers, such as colon cancer^[20], neuroblastoma^[21], hepatocellular carcinomas^[22], lung cancer^[23], and breast cancer^[24]. But only NB gene was confirmed to be the tumor suppressor gene of neuroblastomas. In 1993, Tanaka *et al.* believed that a normal chromosome 1p36 might contain a tumor suppressor gene of colon carcinogenesis^[25]. By database referring, we found TP73 gene (1p36) might be the known candidate tumor-suppressor genes related to colon cancer in this region. TP73, a novel family member of p53, was predicted to encode a protein with significant amino acid sequence similarity to p53^[29]. TP73 could inhibit cell growth in a p53-like manner by inducing apoptosis^[27]. Kaghad *et al.*^[26] regarded TP73 as a tumor suppressor gene. But Sunahara found that allelic loss of p73 occurred only in 17% of colorectal carcinomas, and suggested that p73 might not play a role as a tumor suppressor in colorectal carcinoma at least not in a classic Knudson manner^[28]. In our study, the highest LOH frequency was exhibited in 1p36.33-36.31, and colorectal cancer related tumor suppressor gene (s) might locate in the region. TP73 gene is a member of p53 family, its effect on colorectal carcinogenesis is not certain and requires further study. Due to many genes located in the region of 1p36.33-36.31, further LOH scanning with high-density microsatellite markers in the region is necessary in order to find new candidate genes.

No association between LOH markers on chromosome 1 and the clinicopathological data was found, indicating that LOH was a common phenomenon in all sporadic colorectal cancers. However, we found that on D1S2726 locus, LOH frequency of rectal cancer was high, no LOH was found in colon cancer. In 2001, Kapiteijn *et al.*^[29] proposed that rectal cancer had more significant expression of p53 and more nuclear beta-catenin than colon cancer, and considered that the mechanism of carcinogenesis in distal colon was different from that in proximal colon. Our results could show that the mechanism of carcinogenesis in distal colon and rectum was not completely the same as in proximal colon.

In conclusion, colorectal cancer associated candidate genes are likely to locate on D1S468 and D1S413. Further LOH scanning with high-density microsatellite markers in the region may provide much more genetic information and discover novel tumor suppressor genes.

REFERENCES

- 1 **Fearon ER**, Vogelstein B. A genetic model for colorectal tumorigenesis. *Cell* 1990; **61**: 759-767
- 2 **Hardy RG**, Meltzer SJ, Jankowski JA. ABC of colorectal cancer: Molecular basis for risk factors. *BMJ* 2000; **321**: 886-889
- 3 **Kataoka M**, Okabayashi T, Johira H, Nakatani S, Nakashima A, Takeda A, Nishizaki M, Orita K, Tanaka N. Aberration of p53 and DCC in gastric and colorectal cancer. *Oncol Rep* 2000; **7**: 99-103
- 4 **Lengauer C**, Kinzler KW, Vogelstein B. Genetic instabilities in human cancers. *Nature* 1998; **396**: 643-649
- 5 **Vogelstein B**, Fearon ER, Kern SE, Hamilton SR, Preisinger AC, Nakamura Y, White R. Allelotype of colorectal carcinomas. *Science* 1989; **244**: 207-211
- 6 **Weber TK**, Conroy J, Keitz B, Rodriguez-Bigas M, Petrelli NJ, Stoler DL, Anderson GR, Shows TB, Nowak NJ. Genome-wide allelotyping indicates increased loss of heterozygosity on 9p and 14q in early age of onset colorectal cancer. *Cytogenet Cell Genet* 1999; **86**: 142-147
- 7 **Baker SJ**, Fearon ER, Nigro JM, Hamilton SR, Preisinger AC, Jessup JM, vanTuinen P, Ledbetter DH, Barker DF, Nakamura Y. Chromosome 17 deletions and p53 gene mutations in colorectal carcinomas. *Science* 1989; **244**: 217-221
- 8 **Kinzler KW**, Nilbert MC, Vogelstein B, Bryan TM, Levy DB, Smith KJ, Preisinger AC, Hamilton SR, Hedge P, Markham A. Identification of a gene located at chromosome 5q21 that is mutated in colorectal cancers. *Science* 1991; **251**: 1366-1370
- 9 **Vasen HF**, Mecklin JP, Khan PM, Lynch HT. The International Collaborative Group on Hereditary Non-Polyposis Colorectal Cancer (ICG-HNPCC). *Dis Colon Rectum* 1991; **34**: 424-425
- 10 **Vasen HF**, Watson P, Mecklin JP, Lynch HT. New clinical criteria for hereditary nonpolyposis colorectal cancer (HNPCC, Lynch syndrome) proposed by the International Collaborative group on HNPCC. *Gastroenterology* 1999; **116**: 1453-1456
- 11 **Zhou CZ**, Peng ZH, Zhang F, Qiu GQ, He L. Loss of heterozygosity on long arm of chromosome 22 in sporadic colorectal carcinoma. *World J Gastroenterol* 2002; **8**: 668-673
- 12 **Peng Z**, Zhou C, Zhang F, Ling Y, Tang H, Bai S, Liu W, Qiu G, He L. Loss of heterozygosity of chromosome 20 in sporadic colorectal cancer. *Chin Med J* 2002; **115**: 1529-1532
- 13 **Zhang F**, Zhou C, Ling Y, Qiu G, Bai S, Liu W, He L, Peng Z. Allelic analysis on chromosome 5 in sporadic colorectal cancer patients. *Zhonghua Zhongliu Zazhi* 2002; **24**: 458-460
- 14 **Xu SF**, Peng ZH, Li DP, Qiu GQ, Zhang F. Refinement of heterozygosity loss on chromosome 5p15 in sporadic colorectal cancer. *World J Gastroenterol* 2003; **9**: 1713-1718
- 15 **Peng Z**, Zhang F, Zhou C, Qiu G, Bai S, Liu W, He L. Loss of heterozygosity analysis to define putative region involved in tumor differentiation and metastases in sporadic colorectal cancer patients. *Zhonghua Waiké Zazhi* 2002; **40**: 776-779
- 16 **Peng Z**, Ling Y, Bai S. Loss of heterozygosity on chromosome 3 in sporadic colorectal carcinoma. *Zhonghua Yixue Zazhi* 2001; **81**: 336-339
- 17 **Zhang F**, Zhou C, Ling Y, Bai S, Liu W, Qiu G, He L, Peng Z. High frequency of LOH on chromosome 18 in Chinese sporadic colorectal cancer patients. *Zhonghua Shiyān Waiké Zazhi* 2002; **19**: 320-321
- 18 **Pietsch T**, Koch A, Wiestler OD. Molecular genetic studies in medulloblastomas: evidence for tumor suppressor genes at the chromosomal regions 1q31-32 and 17p13. *Klin Padiatr* 1997; **209**: 150-155
- 19 **Benitez J**, Osorio A, Barroso A, Arranz E, Diaz-Guillen MA, Robledo M, Rodriguez de Cordoba S, Heine-Suner D. A region of allelic imbalance in 1q31-32 in primary breast cancer coincides with a recombination hot spot. *Cancer Res* 1997; **57**: 4217-4220
- 20 **Praml C**, Finke LH, Herfarth C, Schlag P, Schwab M, Amler L. Deletion mapping defines different regions in 1p34.2-pter that may harbor genetic information related to human colorectal cancer. *Oncogene* 1995; **11**: 1357-1362
- 21 **White PS**, Maris JM, Beltinger C, Sulman E, Marshall HN, Fujimori M, Kaufman BA, Biegel JA, Allen C, Hilliard C. A region of consistent deletion in neuroblastoma maps within human chromosome 1p36.2-36.3. *Proc Natl Acad Sci USA* 1995; **92**: 5520-5524
- 22 **Yeh SH**, Chen PJ, Chen HL, Lai MY, Wang CC, Chen DS. Frequent genetic alterations at the distal region of chromosome 1p in human hepatocellular carcinomas. *Cancer Res* 1994; **54**: 4188-4192
- 23 **Nomoto S**, Haruki N, Tatematsu Y, Konishi H, Mitsudomi T, Takahashi T, Takahashi T. Frequent allelic imbalance suggests involvement of a tumor suppressor gene at 1p36 in the pathogenesis of human lung cancers. *Genes Chromosomes Cancer* 2000; **28**: 342-346
- 24 **Bieche I**, Khodja A, Lidereau R. Deletion mapping of chromosomal region 1p32-pter in primary breast cancer. *Genes Chromosomes Cancer* 1999; **24**: 255-263
- 25 **Tanaka K**, Yanoshita R, Konishi M, Oshimura M, Maeda Y, Mori T, Miyaki M. Suppression of tumorigenicity in human colon carcinoma cells by introduction of normal chromosome 1p36 region. *Oncogene* 1993; **8**: 2253-2258
- 26 **Kaghad M**, Bonnet H, Yang A, Creancier L, Biscan JC, Valent A, Minty A, Chalon P, Lelias JM, Dumont X, Ferrara P, McKeon F, Caput D. Monoallelically expressed gene related to p53 at 1p36, a region frequently deleted in neuroblastoma and other human cancers. *Cell* 1997; **90**: 809-819
- 27 **Jost CA**, Marin MC, Kaelin WG Jr. p73 is a human p53-related protein that can induce apoptosis. *Nature* 1997; **389**: 191-194
- 28 **Sunahara M**, Ichimiya S, Nimura Y, Takada N, Sakiyama S, Sato Y, Todo S, Adachi W, Amano J, Nakagawara A. Mutational analysis of the p73 gene localized at chromosome 1p36.3 in colorectal carcinomas. *Int J Oncol* 1998; **13**: 319-323
- 29 **Kapiteijn E**, Liefers GJ, Los LC, Kranenbarg EK, Hermans J, Tollenaar RA, Moriya Y, van de Velde CJ, van Krieken JH. Mechanisms of oncogenesis in colon versus rectal cancer. *J Pathol* 2001; **195**: 171-178

Edited by Ren SY and Wang XL Proofread by Xu FM

Effect of Hejie decoction on T cell immune state of chronic hepatitis B patients

Shi-Jun Zhang, Ze-Xiong Chen, Shao-Xian Lao, Bi-Jun Huang

Shi-Jun Zhang, Ze-Xiong Chen, Department of Traditional Chinese Medicine, First Affiliated Hospital, Sun Yat-Sen University, Guangzhou 510080, Guangdong Province, China

Shao-Xian Lao, Institute of Digestive Diseases, Traditional Chinese Medicine University of Guangzhou, Guangzhou 510405, Guangdong Province, China

Bi-Jun Huang, Institute of Cancer, Sun Yat-Sen University, Guangzhou 510080, Guangdong Province, China

Supported by Guangdong Administrative Bureau of TCM and Chinese Drugs, No.98374 and No.100108

Correspondence to: Shi-Jun Zhang, Department of Traditional Chinese Medicine, First Affiliated Hospital, Sun Yat-Sen University, Guangzhou 510080, Guangdong Province, China. zhsjun1967@hotmail.com

Telephone: +86-20-87334505 **Fax:** +86-20-87334505

Received: 2003-08-06 **Accepted:** 2003-09-01

Abstract

AIM: To explore the effect of Hejie decoction (HJD) (mediation decoction) on T cellular immune state of chronic hepatitis B patients.

METHODS: Sixty-five patients with chronic hepatitis B were randomly divided into 2 groups. Forty patients in the treatment group were treated by HJD, and 25 patients in the control group were treated by routine Western medicine. The TCRV β_7 gene expression, T lymphocyte subsets (CD $_3^+$, CD $_4^+$, CD $_8^+$, CD $_4$ /CD $_8^+$) levels were observed before and after treatment.

RESULTS: The level of CD $_4^+$ cells was lower whereas the level of CD $_8^+$ cells was higher in patients than in the normal group. There was no significant difference between the levels of CD $_3^+$ cells in patients and normal persons. After 6 months of treatment, ALT, AST, TB levels of the 2 groups were obviously decreased, and the level of CD $_4^+$ cells was increased whereas the level of CD $_8^+$ cells was decreased in the treatment group. However, the level of CD $_4^+$ cells and CD $_8^+$ cells had no significant difference in the control group. TCRV β_7 expressions were detected in 6 patients of the treatment group, whose HBV-DNA and HBeAg turned negative and ALT became normal. HBeAg in another 3 patients turned negative while HBV-DNA did not, and TCRV β_7 expressions were not detectable. TCRV β_7 expression could not be detected in the control group, HBV-DNA of the control group did not turn negative. HBeAg in 1 patient turned negative while HBV-DNA did not, and TCRV β_7 expressions were not detectable. The total effective rate was not significantly different between the 2 groups and the markedly effective rate was significantly different ($P < 0.01$).

CONCLUSION: HJD is effective for treating chronic hepatitis B, and its effect seems to relate with the improvement of the TCRV β_7 expression of chronic hepatitis B patients, thus activating T cells and eliminating HBV. T cellular immune function plays an important role in HBV infection and virus elimination.

Zhang SJ, Chen ZX, Lao SX, Huang BJ. Effect of Hejie decoction on T cell immune state of chronic hepatitis B patients. *World J Gastroenterol* 2004; 10(10): 1436-1439
<http://www.wjgnet.com/1007-9327/10/1436.asp>

INTRODUCTION

T cells take charge of recognizing the cells infected with bacilli and virus, as well as cancer cells^[1]. Recent studies have demonstrated that the stimulating signal would be transferred to the inside of cells by CD $_3$ molecules when antigens are recognized by T cell receptor (TCR), sequentially activating T lymphocyte cells. TCR plays a crucial role in exerting T cellular immune function. Therefore it is very important to investigate the relation of T cellular function and clinical effect by studying the function of T cell receptor^[2-4]. We treated chronic hepatitis B patients with HJD from June 1999 to March 2003, and observed the relation between clinical effects and T lymphocyte subsets, TCRV β_7 gene expression. The results are reported as follows.

MATERIALS AND METHODS

Materials

All the 65 patients with chronic hepatitis B enrolled were outpatients from the special clinics of liver diseases, and were divided into 2 groups according to random number table. The 40 patients in the treatment group were 22 males and 18 females, aged 18-60 years, averaged 38.6 \pm 9.8 years, with an average course of illness of 0.8-12.5, 3.5 \pm 1.2 years. The 25 patients in the control group were 14 males and 11 females, aged 18-60 years, averaged 39.0 \pm 8.9 years, with an average course of illness of 0.6-11.1, 3.2 \pm 1.1 years. The difference of clinical data between the 2 groups was insignificant, so the 2 groups were comparable. Ten age-matched healthy donors from the Blood Center of our hospital were assigned as normal group.

Diagnostic criteria

The patient had a history of hepatitis B or HBsAg carrier for at least 6 mo and still had the symptoms and signs of hepatitis and abnormal liver function at the time when they were included in the trial. Their HBsAg, HBeAg and HBVDNA were positive.

Criteria of enrollment

The patients were aged 18-60 years, their serum levels of alanine aminotransferase (ALT) were between 80 U/L and 240 U/L, their serum HBeAg and HBV-DNA (quantitative PCR) were positive. The diagnostic criteria of hepatitis B were in accordance with the standards for chronic viral hepatitis issued in the Fifth National Conference on Infectious Diseases and Parasitosis in China (Beijing, China, 1995)^[5].

Criteria of exclusion

The patients who were over 60, or less than 18 years old, and those who were pregnant or in breast-feeding period, those who were complicated with hepatitis C or other hepatic viral infection, suspicious of autoimmune hepatitis, and drug hepatitis or alcoholic hepatitis, as well as those who had severe

complications of cardiovascular, renal or hematopoietic systems and mental diseases were excluded from the trial.

Methods

The treatment group was treated with Hejie decoction, consisting of Radix Bupleuri 10 g, Radix Scutellariae 12 g, Rhizoma Pinelliae 9 g, Radix Codonopsis Pilosulae 30 g, Radix Glycyrrhizae Praeparata 6 g, Fructus Ziziphi Jujubae 9 g, Rhizoma Polygoni Cuspidati 30 g, Radix Morindae Officinalis 8 g, Herba Hedyotis Diffusae 30 g. One dose was taken per day for 6 mo. The control group was treated with compound vitamin B₂, 2 tablets, vitamin C 100 mg, vitamin E 50 mg, Wuzhi capsules, 2 tablets, 3 times a day for 6 mo. Patients who had normal serum ALT, HBeAg and HBV DNA (quantitative PCR) after treatment were defined as responders, while those with negative results were taken as non-responders.

Patients' symptoms and signs were recorded in detail using "Clinical Observation Table" once a month before and during the treatment. HBV-M and anti-HAV, anti-HCV, anti-HDV and anti-EBV marks: Enzyme linked immunosorbent assay (ELISA) kit was obtained from Shanghai Kehua Corporation. HBV-DNA: Quantitative polymerized chain reaction (PCR) kit was from Diagnostic Center of Sun Yat-Sen University.

The patients had liver function examination (American Experiment Instrument Corporation) every month during the treatment, including contents of serum proteins, total bilirubin (TB), and activities of ALT and AST (aspartate aminotransferase). The kit was a product of American Experiment Instrument Corporation.

T-lymphocyte subsets were detected using single clone antibody APAAP method, the kits were purchased from Wuhan Boster Biological Technology Co. Ltd.

Peripheral blood mononuclear cells (PBMC) were prepared from 8 mL of freshly, heparinized blood by centrifugation at 400 r/min through a Ficoll-hypaque density gradient, washed 3 times with 10 g/L BSA in PBS and resuspended in 5 g/L BSA in PBS, stored on ice or at -70 °C for extraction of RNA.

Total cellular RNA was extracted from fresh PBMC with acid guanidinium thiocyanate-phenol-chloroform extraction according to the manufacturer's instructions, RNAs were purchased from Promega Corporation.

The primers were synthesized on an applied biosystems DNA synthesizer (Shanghai Shengong Company, China), and the sequences^[6] were (5' -3'): CCTGAATGCCCAACAGCTCTC,

expanding length: 235. β -actin was prepared as an internal standard to quantify the products. Three micrograms of total RNA was used to synthesize first-strand cDNA. RT-PCR was carried out according to the manufacturer's instructions (Promega, USA). The amplified products were then electrophoresed on 20 g/L agarose gel. The electrophoresis images were scanned by Fluor-S MultiImager (Bio-Rad, USA) and analyzed according to the V β / β -actin ratios by computing densitometer and Image Quant software.

Statistical analysis

All statistics were performed by using statistical procedure of social science (SPSS), including chi-square test and Wilcoxon rank sum test. The probability values less than 0.05 were considered significant.

RESULTS

Standard for efficacy evaluation

The clinical efficacy of treatment was evaluated according to the following standards formulated by authors: (1) Markedly effective: Chief symptoms including right upper abdomen pain, poor appetite and abdominal distention disappeared, HBeAg and HBV-DNA turned negative, serum levels of ALT, AST, TBIL restored to normal. (2) Effective: Chief symptoms were alleviated or improved, the level of HBV-DNA decreased, HBeAg did not turn negative, serum levels of ALT, AST, TBIL decreased by >1/2 of the original levels. (3) Ineffective: Neither the chief symptoms nor the serum levels of ALT, AST and TBIL or HBeAg, HBV-DNA showed any improvement.

Clinical efficacy of treatment

In the treated group, the treatment was markedly effective in 6 cases, effective in 33 and ineffective in 1, the total effective rate was 97.5%. In the control group, the treatment was markedly effective in 0 cases, effective in 22 and ineffective in 3, the total effective rate was 88.0%. The difference of total effective rate was insignificant between the 2 groups ($P>0.05$) and that of markedly effective rate was significant ($P<0.01$).

ALT, AST, TB and HBVDNA levels before and after treatment, as well as TCRV β gene expression

After 6 mo of treatment, the ALT, AST, TB levels of the 2 groups

Table 1 ALT, AST, TB and HBVDNA levels before and after treatment (mean \pm SD)

	<i>n</i>	ALT (U/L)	AST (U/L)	TB (μ mol/L)	HBVDNA (copy/mL)
Normal	10	27.80 \pm 8.65	19.07 \pm 8.50	12.55 \pm 5.52	0
Treatment					
Pre-T	40	213.66 \pm 10.30	134.66 \pm 9.82	41.03 \pm 4.36	(1.52 \pm 0.72) \times 10 ^{8.25}
Post-T	40	37.01 \pm 9.75 ^b	29.07 \pm 8.97 ^b	20.55 \pm 5.52 ^b	(4.25 \pm 1.90) \times 10 ^{6.02 a}
Control					
Pre-T	25	195.70 \pm 11.11	125.12 \pm 9.21	40.87 \pm 6.78	(1.32 \pm 0.89) \times 10 ^{8.12}
Post-T	25	36.01 \pm 9.75 ^b	69.88 \pm 8.97 ^b	30.55 \pm 5.52 ^b	(6.95 \pm 2.39) \times 10 ^{7.82}

n: number; normal: normal group; treatment: treatment group; control: control group; Pre-T: before treatment; Post-T: after treatment; ^a $P<0.05$, vs before treatment in the same group, ^b $P<0.01$, vs before treatment in the same group.

Table 2 T lymphocyte subsets before and after treatment (mean \pm SD)

	<i>n</i>	CD ₃ (%)	CD ₄ (%)	CD ₈ (%)	CD ₄ /CD ₈
Normal	10	67.80 \pm 8.65	39.07 \pm 8.50	30.55 \pm 5.52	1.62 \pm 0.46
Treatment					
Pre-T	40	65.97 \pm 8.45	34.76 \pm 4.82 ^b	34.08 \pm 4.36 ^b	1.04 \pm 0.32
Post-T	40	67.01 \pm 9.75	37.39 \pm 8.97 ^a	32.35 \pm 5.52 ^a	1.20 \pm 0.30 ^a
Control					
Pre-T	25	65.70 \pm 9.11	35.02 \pm 5.21 ^b	34.87 \pm 6.78 ^b	1.02 \pm 0.29
Post-T	25	66.01 \pm 9.75	35.88 \pm 8.97	34.15 \pm 5.52	1.09 \pm 0.39

n: number; normal: normal group; treatment: treatment group; control: control group; Pre-T: before treatment; Post-T: after treatment; ^a $P<0.05$, vs before treatment in the same group, ^b $P<0.01$, vs control.

were obviously decreased ($P<0.01$), HBVDNA levels of the treatment group were obviously decreased ($P<0.05$, Table 1). TCRV β_7 expressions were detected in 6 patients of the treated group, and their HBV-DNA and HBeAg turned negative, and HBeAg in another 3 patients turned negative, but HBV-DNA did not turn negative, and TCRV β_7 expressions were not detectable. The TCRV β_7 expression could not be detected in the control group, HBV-DNA of the control group did not turn negative. HBeAg in 1 patient turned negative in the control group, but HBV-DNA did not turn negative, and TCRV β_7 expressions were not detectable. In patients without HBeAg negative conversion, or patients with HBeAg negative conversion and positive HBV-DNA and normal liver function, TCRV β_7 expression could not be detected.

T lymphocyte subsets before and after treatment

The level of CD $_4^+$ cells was lower whereas the level of CD $_8^+$ cells was higher in the patients than in the normal group ($P<0.01$), there was no significant difference between the levels of CD $_3^+$ cells of the patients and normal persons. After 6 mo of treatment, the level of CD $_4^+$ cells increased whereas the level of CD $_8^+$ cells decreased ($P<0.05$) in the treated group. However, the level of CD $_4^+$ cells and CD $_8^+$ cells had no significant difference in the control group ($P>0.05$, Table 2).

Table 3 T lymphocyte subsets of responders and non-responders in treatment group before and after treatment (mean \pm SD)

		<i>n</i>	CD $_3$ (%)	CD $_4$ (%)	CD $_8$ (%)
Responders	Pre-T	6	66.62 \pm 8.86	35.10 \pm 4.76 ^b	34.02 \pm 4.86 ^b
	Post-T	6	66.80 \pm 9.11	38.85 \pm 8.85 ^a	30.15 \pm 5.82 ^a
Non-responders	Pre-T	34	65.86 \pm 9.08	34.62 \pm 6.30 ^b	34.17 \pm 6.56 ^b
	Post-T	34	66.09 \pm 9.35	35.72 \pm 8.70	33.85 \pm 5.52
Normal		10	67.80 \pm 8.65	39.07 \pm 8.50	30.55 \pm 5.52

n: number; responders: patients who had normal ALT and HBeAg and HBV DNA after treatment; non-responders: patients who had abnormal ALT, HBeAg and HBV DNA after treatment; normal: normal group; Pre-T: before treatment; Post-T: after treatment; ^a $P<0.05$, vs before treatment in the same group, ^b $P<0.01$, vs normal group.

T lymphocyte subsets of responders and non-responders in treatment group before and after treatment

The level of CD $_3^+$, CD $_4^+$, CD $_8^+$ cells in the 2 groups had no significant difference before treatment ($P>0.05$). The level of CD $_4^+$ cells increased whereas the level of CD $_8^+$ cells decreased in the responders' group ($P<0.01$). The level of CD $_4^+$ and CD $_8^+$ cells in the non-responders' group had no significant difference after treatment ($P>0.05$, Table 3).

DISCUSSION

Although the pathogenesis of chronic hepatitis B has not been fully studied, the importance of cellular immune in the occurrence of chronic HBV infection and elimination of HBV has received more and more attention^[7]. CD $_3^+$, CD $_4^+$ and CD $_8^+$ are the major function subsets of T cells, many studies have discovered that CD $_3^+$, CD $_4^+$ of chronic hepatitis B with serum HBV positive are lower than those of chronic hepatitis B with serum HBV negative, and the higher the quantity of HBVDNA is, the lower the T cellular immune function is. Antiviral cellular immune response of CD $_4^+$ and CD $_8^+$ is the important mechanism of hepatocyte injury induced by HBV, the specific response of CD $_4^+$ and CD $_8^+$ to the virus antigen is closely related with the elimination of the virus. It is suggested that T cells could play a critical role in response to HBV infection, and their level and mutual relationship could be used to identify the cellular immune

level and could serve as one of the valuable immunologic targets to forecast the change of patients' condition^[8-12]. Some studies on chronic hepatitis B showed that T cell receptor function was the important cause of the obstacle to T cells, sequentially bringing about HBV escaping immune response, and finally resulting in standing HBV infection^[2,3,13-16]. Therefore, it is very important to study the antiviral effect of T cells starting with immune identification.

TCR has been found to be the receptor of T lymphocyte surface recognising extra antigen and the major histocompatibility complex I (MHC I), as well as the specific sign of T cells^[17-19]. The genes of the α and β chains which promote TCR α β reset formation of large amount of specific TCR to recognise the extra antigen when they meet antigen. TCR and CD $_3$ would inosculate on the surface cells and form TCRCD3 compounds, the stimulating signals would be transferred to the inside of cells by CD3 molecules when antigens were recognised by TCR, activating T lymphocyte cells^[20-26]. Some studies have indicated that the priority expression and employment of TCRV β_7 were related with the specific immune reaction of chronic hepatitis B^[27-29]. Therefore, It is a meaningful pathway to eliminate HBV and decrease the occurrence of liver cancer by screening experimental recipes to activate T cells by improving T cell recognising function under the present circumstances of low cure ratio and high recurrence. We discovered that in the outbreak period of chronic hepatitis B, TCRV β_7 gene expression was low. The level of CD $_4^+$ cells was lower whereas the level of CD $_8^+$ cells was higher in patients than in the normal group ($P<0.01$). The serum TCRV β_7 gene expressions of non-responders were low, the level of CD $_4^+$ cells of non-responders was lower in patients than in normal persons whereas the level of CD $_8^+$ cells of non-responders was higher in patients than in the normal persons. After treatment, the TCRV β_7 gene expression was high in patients with the conversion of HBV-DNA and HBeAg, and the liver function, the level of CD $_4^+$ and CD $_8^+$ cells resumed to normal. The levels of CD $_4^+$ and CD $_8^+$ cells in the treatment group were significantly different from those before treatment ($P<0.01$). The results showed that TCRV β_7 participated in the elimination of HBV and cytotoxic function, and the occurrence of chronic hepatitis B was related to the low expression of TCRV β_7 . The CTL could not be effectively activated to kill or injure HBV due to the obstacle of T cell receptor function, sequentially bringing about stable reproduction of HBV and resulting in chronic inflammation of hepatocytes. At the same time, we also discovered that TCRV β_7 expression of some patients in the palliating period was still low, indicating that recurrence might increase.

When HBeAg in chronic hepatitis B patients transforms to Anti-HBe, hepatocyte injury aggravates, which is considered to be mediated by CTL antiviral cellular immune response. The dynamic observation of 6 cases whose TCRV β_7 gene expressions were positive showed that the TCRV β_7 gene expression related with the HBeAg serum conversion, the decreased quantity of HBVDNA, and ALT levels experienced a period of acute exacerbation in the course of descending, suggesting that TCRV β_7 participated in the elimination of HBV and cytotoxic function. ALT fluctuation in patients with TCRV β_7 negative was small, and there was no obvious decrease in HBVDNA, or obvious HBeAg serum conversion, suggesting the cellular immune response of the patients was feeble. Thus TCRV β_7 might be an index to evaluate the cellular immune state of hepatitis B patients.

HBeAg is a good index that reflects the HBV replication. When HBeAg transforms to Anti-HBe, the reproduction of HBV will obviously weaken or cease, along with the relief of the state of illness. Among the 10 patients with HBeAg serum conversion, the quantity of HBVDNA in some patients did not alleviate or vanish after HBeAg serum conversion, and the

state of illness fluctuated, which should be treated continually. HJD is a proved recipe for treating hepatitis, in which cold and warm drugs are used to eliminate evils and restore healthy energy. Previous researches indicated that HJD had the effect to protect the liver, as well as the function of antiviral and immune regulation^[30-33]. We discovered that HJD could meliorate liver function, regulate TCRV β 7 gene expression, improve T cellular immune function of chronic hepatitis B in this study. The results suggest that the clinical effects of HJD on chronic hepatitis B, especially on the elimination of HBV, might relate with the improvement of TCR identifying function, and effectively activate CTL. However, HJD could not interrupt immune endurance of some patients, resulting in the failure of treatment, which needs further study to explore the cause and resolving methods.

REFERENCES

- 1 **Wang YX**, Ruan CP, Li L, Shi JH, Kong XT. Clinical significance of changes of perioperative T cell and expression of its activated antigen in colorectal cancer patients. *World J Gastroenterol* 1999; **5**: 181-182
- 2 **Guo Y**, Wu H, Li SY, Yan H. T cell receptor gene rearrangement of peripheral blood mononuclear cells from patients with chronic hepatitis B. *Zhonghua Chuanranbing Zazhi* 2000; **18**: 88-90
- 3 **Sugyo S**, Yuh K, Nakamura K, Emi K, Shijo H, Iida T, Kimura N, Tamura K. An analysis of T cell antigen receptor variable beta genes during the clinical course of patients with chronic hepatitis B. *J Gastroenterol Hepatol* 1999; **14**: 333-338
- 4 **Pardigon N**, Cambouris C, Bercovici N, Lemaître F, Liblau R, Kourilsky P. Delayed and separate costimulation *in vitro* supports the evidence of a transient "excited" state of CD8⁺ T cells during activation. *J Immunol* 2000; **164**: 4493-4499
- 5 The infectious and parasitic disease institute of Chinese medical association. Diagnostic criteria of virus hepatitis. *Zhonghua Chuanranbing Zazhi* 1995; **13**: 242-247
- 6 **Yang LJ**, Li YQ, Chen SH, Han SF, Chen ST, Zhang XL, Zhang T. Comparison of the clonal expansion of TCR β T cells in patients with acute promyelocytic leukemia *in vivo* and *in vitro*. *Zhongguo Shiyang Xueyue Zazhi* 2003; **11**: 499-502
- 7 **Li L**, Gu CH, Li X. The significance of activation-induced cell death (AICD) in pathogenesis of hepatitis B. *Zhonghua Yixue Zazhi* 2003; **83**: 1146-1149
- 8 **Wang KX**, Peng JL, Wang XF, Tian Y, Wang J, Li CP. Detection of T lymphocyte subsets and mIL-2R on surface of PBMC in patients with hepatitis B. *World J Gastroenterol* 2003; **9**: 2017-2020
- 9 **Wang JP**, Li XH, Zhu Y, Wang AL, Lian JQ, Jia ZS, Xie YM. Detection of serum sIL-2R, IL-6, IL-8, TNF- α and lymphocytes subsets, mIL-2R in patients with chronic hepatitis B. *Shijie Huaren Xiaohua Zazhi* 2000; **8**: 763-766
- 10 **Crispe IN**. Hepatic T cells and liver tolerance. *Nat Rev Immunol* 2003; **3**: 51-62
- 11 **Sing GK**, Li D, Chen X, Macnaughton T, Lichanska AM, Butterworth L, Ladham A, Cooksley G. A molecular comparison of T lymphocyte populations infiltrating the liver and circulating in the blood of patients with chronic hepatitis B: evidence for antigen-driven selection of a public complementarity-determining region 3 (CDR3) motif. *Hepatology* 2001; **33**: 1288-1298
- 12 **Zhang MX**, Zhang XY, Jin SG, Dong HF, Chen JJ, Wang LT. The changes of peripheral blood CD⁺28T from patients with liver diseases. *Shijie Huaren Xiaohua Zazhi* 2000; **8**: 1432-1433
- 13 **Maru Y**, Yokosuka O, Imazeki F, Saisho H, Omata M. Analysis of T cell receptor variable regions and complementarity determining region 3 of infiltrating T lymphocytes in the liver of patients with chronic type B hepatitis. *Intervirology* 2003; **46**: 277-288
- 14 **Huang S**, Cao M, Luo L. Hepatitis B virus antigen-induced specific TCR V beta gene subfamily amplifications and their diversity. *Zhonghua Shiyang He Linchuang Bingdixue Zazhi* 1998; **12**: 318-321
- 15 **Soroosh P**, Shokri F, Azizi M, Jeddi-Tehrani M. Analysis of T-cell receptor beta chain variable gene segment usage in healthy adult responders and nonresponders to recombinant hepatitis B vaccine. *Scand J Immunol* 2003; **57**: 423-431
- 16 **Suzuki T**, Yamauchi K, Kuwata T, Hayashi N. Characterization of hepatitis B virus surface antigen-specific CD4⁺ T cells in hepatitis B vaccine non-responders. *J Gastroenterol Hepatol* 2001; **16**: 898-903
- 17 **Hodges E**, Krishna MT, Pickard C, Smith JL. Diagnostic role of tests for T cell receptor (TCR) genes. *J Clin Pathol* 2003; **56**: 1-11
- 18 **Hughes MM**, Yassai M, Sedy JR, Wehrly TD, Huang CY, Kanagawa O, Gorski J, Sleckman BP. T cell receptor CDR3 loop length repertoire is determined primarily by features of the V(D)J recombination reaction. *Eur J Immunol* 2003; **33**: 1568-1575
- 19 **Rezvan MR**, Jeddi-Tehrani M, Wigzell H, Osterborg A, Mellstedt H. Leukemia-associated monoclonal and oligoclonal TCR-BV use in patients with B-cell chronic lymphocytic leukemia. *Blood* 2003; **101**: 1063-1070
- 20 **Jiang H**, Curran S, Ruiz-Vazquez E, Liang B, Winchester R, Chess L. Regulatory CD8⁺ T cells fine-tune the myelin basic protein-reactive T cell receptor V beta repertoire during experimental autoimmune encephalomyelitis. *Proc Natl Acad Sci U S A* 2003; **100**: 8378-8383
- 21 **Hohn H**, Neukirch C, Freitag K, Necker A, Hitzler W, Seliger B, Maeurer MJ. Longitudinal analysis of the T-cell receptor (TCR)-VA and -VB repertoire in CD8⁺ T cells from individuals immunized with recombinant hepatitis B surface antigen. *Clin Exp Immunol* 2002; **129**: 309-317
- 22 **Vigan I**, Jouvin-Marche E, Leroy V, Pernollet M, Tongiani-Dashan S, Borel E, Delachanal E, Colomb M, Zarski JP, Marche PN. T lymphocytes infiltrating the liver during chronic hepatitis C infection express a broad range of T-cell receptor beta chain diversity. *J Hepatol* 2003; **38**: 651-659
- 23 **Turner SJ**, Diaz G, Cross R, Doherty PC. Analysis of clonotype distribution and persistence for an influenza virus-specific CD8⁺ T cell response. *Immunity* 2003; **18**: 549-559
- 24 **Raaphorst FM**, Schelonka RL, Rusnak J, Infante AJ, Teale JM. TCRBV CDR3 diversity of CD4⁺ and CD8⁺ T-lymphocytes in HIV-infected individuals. *Hum Immunol* 2002; **63**: 51-60
- 25 **Mitarnun W**, Saechan V, Pradutkanchana J, Suwiwat S, Takao S, Ishida T. Epstein-Barr virus-associated peripheral T-cell lymphoma with gastrointestinal tract involvement. *J Med Assoc Thai* 2003; **86**: 816-828
- 26 **König R**, Zhou W. Signal transduction in T helper cells: CD4 coreceptors exert complex regulatory effects on T cell activation and function. *Curr Issues Mol Biol* 2004; **6**: 1-15
- 27 **Abbott WG**, Geursen A, Fraser JD, Marbrook J, Skinner MA, Tan PL. The influence of a maternal chronic hepatitis B virus infection on the repertoire of transcribed T-cell receptor beta chain variable region genes in human cord blood. *Hepatology* 1995; **22**: 1034-1039
- 28 **Chen XH**, Cooksley G, Sing G. Distinct patterns of T cell receptor distribution of peripheral blood CD8⁺ cells during different stages of chronic infection with hepatitis B virus. *Human Immunol* 1998; **59**: 199-211
- 29 **Dou HY**, Wu JC, Peng WL, Chang C, Chi WK, Chu YD, Hu CP. Analysis of T cell receptor Vbeta gene usage during the course of disease in patients with chronic hepatitis B. *J Biomed Sci* 1998; **5**: 428-434
- 30 **Zhang SJ**, Chen ZX, Huang BJ. Effect of hejie decoction on T-cell receptor V beta 7 gene expression in patients of chronic hepatitis B. *Zhongguo Zhongxiyi Jiehe Zazhi* 2002; **22**: 499-500
- 31 **Zhang SJ**, Chen ZX, Huang JB, Li JB. Clinical study on the He Jie Decoction in keeping HBeAg negative conversion states of chronic hepatitis B patients after HBeAg negative conversion. *Zhongguo Zhongxiyi Jiehe Xiaohua Zazhi* 2001; **9**: 92-93
- 32 **Zhang SJ**, Chen ZX. Clinical study of He Jie Decoction on 37 chronic hepatitis B patients with HBeAg positive. *Shiyong Zhongyi Zazhi* 1999; **15**: 16-17
- 33 **Zhang SJ**, Chen ZX, Huang JB, Li JB, Qin J, Huang BJ, Huang DX, Liu XQ. Clinical study of He Jie Decoction on IL-8, sIL-2R of chronic hepatitis B patients. *Zhonghua Shiyong Zhongxiyi Zazhi* 2001; **14**: 725-726

Differential expression of cholangiocyte and ileal bile acid transporters following bile acid supplementation and depletion

N. Sertac Kip, Konstantinos N. Lazaridis, Anatoliy I. Masyuk, Patrick L. Splinter, Robert C. Huebert, Nicholas F. LaRusso

N. Sertac Kip, Konstantinos N. Lazaridis, Anatoliy I. Masyuk, Patrick L. Splinter, Robert C. Huebert, Nicholas F. LaRusso, Center for Basic Research in Digestive Diseases, Division of Gastroenterology and Hepatology, Department of Internal Medicine, Mayo Medical School, Clinic and Foundation, Rochester, MN 55905, USA
Nicholas F. LaRusso, Department of Biochemistry and Molecular Biology, Mayo Medical School, Clinic and Foundation, Rochester, MN, 55905, USA

Correspondence to: Nicholas F. LaRusso M.D., Center for Basic Research in Digestive Diseases, Mayo Clinic, 200 First Street, SW Rochester, MN 55905, USA. larusso.nicholas@mayo.edu

Telephone: +1-507 284-1006 **Fax:** +1-507 284-0762

Received: 2004-03-23 **Accepted:** 2004-04-09

ASBT and t-ASBT in cholangiocytes is regulated by a negative feedback loop while the expression of these transporters in terminal ileum is modified via positive feedback. Thus, while transcriptional regulatory mechanisms in response to alterations in bile acid pool size are operative in both cholangiocytes and ileocytes, each cell type responds differently to bile acid supplementation and depletion.

Kip NS, Lazaridis KN, Masyuk AI, Splinter PL, Huebert RC, LaRusso NF. Differential expression of cholangiocyte and ileal bile acid transporters following bile acid supplementation and depletion. *World J Gastroenterol* 2004; 10(10): 1440-1446 <http://www.wjgnet.com/1007-9327/10/1440.asp>

Abstract

AIM: We have previously demonstrated that cholangiocytes, the epithelial cells lining intrahepatic bile ducts, encode two functional bile acid transporters via alternative splicing of a single gene to facilitate bile acid vectorial transport. Cholangiocytes possess ASBT, an apical sodium-dependent bile acid transporter to take up bile acids, and t-ASBT, a basolateral alternatively spliced and truncated form of ASBT to efflux bile acids. Though hepatocyte and ileal bile acid transporters are in part regulated by the flux of bile acids, the effect of alterations in bile acid flux on the expression of t-ASBT in terminal ileocytes remains unclear. Thus, we tested the hypothesis that expression of ASBT and t-ASBT in cholangiocytes and ileocytes was regulated by bile acid flux.

METHODS: Expression of ASBT and t-ASBT message and protein in cholangiocytes and ileocytes isolated from paired rats given control (C) and 1% taurocholate (TCA) or 5% cholestyramine (CY) enriched diets, were assessed by both quantitative RNase protection assays and quantitative immunoblotting. The data obtained from each of the control groups were pooled to reflect the changes observed following TCA and CY treatments with respect to the control diets. Cholangiocyte taurocholate uptake was determined using a novel microperfusion technique on intrahepatic bile duct units (IBDUs) derived from C, TCA and CY fed rats.

RESULTS: In cholangiocytes, both ASBT and t-ASBT message RNA and protein were significantly decreased in response to TCA feeding compared to C diet. In contrast, message and protein of both bile acid transporters significantly increased following CY feeding compared to C diet. In the ileum, TCA feeding significantly up-regulated both ASBT and t-ASBT message and protein compared to C diet, while CY feeding significantly down-regulated message and protein of both bile acid transporters compared to C diet. As anticipated from alterations in cholangiocyte ASBT expression, the uptake of taurocholate in microperfused IBDUs derived from rats on TCA diet decreased 2.7-fold, whereas it increased 1.7-fold in those on CY diet compared to C diet fed groups.

CONCLUSION: These data demonstrate that expression of

INTRODUCTION

Bile acids are synthesized in hepatocytes from cholesterol, conjugated to either taurine or glycine, secreted into bile and reach the small intestine via the bile ducts to facilitate lipid absorption^[1]. Subsequently, bile acids are reclaimed at the terminal ileum, returned to the liver via the portal circulation, and resecreted into bile accomplishing their enterohepatic circulation^[1]. At the cellular level, this recycling of bile acids, important for conservation of the bile acid pool, is achieved by the coordinated activities of a series of apical and basolateral membrane bile acid transporters expressed on the epithelial cells of the terminal ileum and liver^[2].

The active recovery of conjugated bile acids in the terminal ileum is mediated by a Na⁺ driven bile acid transporter, ASBT, located at the luminal domain of the ileocyte^[2]. Following uptake into the ileocytes, bile acids bind to the intestinal bile acid binding protein (I-BABP) in the cytoplasm to be directed across the cell to the basolateral membrane where they enter into the portal venous circulation by a Na⁺-independent mechanism^[2]. Subsequently, the majority of conjugated bile acids are efficiently reabsorbed from portal vein blood into hepatocytes, mainly via the Na⁺-taurocholate cotransporter (ntcp)^[3] and then are secreted into the biliary system primarily via ATP-dependent export pumps located on the apical (*i.e.*, canalicular) domain of hepatocytes^[3].

As bile percolates through the intrahepatic bile ducts, it undergoes numerous modifications due to both secretory and absorptive activities of cholangiocytes. We and others, have previously shown that biliary epithelia can take up conjugated bile acids via ASBT^[4,5] expressed on the cholangiocyte apical membrane, a protein identical to that cloned from rat ileum and kidney^[6,7]. We have also recently identified an alternatively spliced and truncated transcript of ASBT, designated t-ASBT that allows cholangiocytes and possibly other bile-acid transporting epithelia (*i.e.*, ileum and kidney) to extrude bile acids at the basolateral domain^[8].

Despite these advances in our understanding of the physiology of bile acid transport, little is known about the regulation of ASBT and t-ASBT in bile acid transporting epithelia, especially in cholangiocytes. While recent studies have assessed the effects of ursodeoxycholic acid supplementation^[9], bile acid depletion and repletion in bile duct ligated rats^[10,11]

and bile acid feeding on different physiologic responses by cholangiocytes, including in some instances ASBT expression^[12]. No studies have addressed the regulation of t- ASBT or systematically compared the responses of the liver and ileum to bile acid expansion or depletion. We, therefore, designed the present study to further investigate the role of bile acids in the regulation of ASBT and t- ASBT in both the biliary tree and terminal ileum. For this purpose, we performed studies in non-surgically manipulated rats to determine the message and protein levels of ASBT and t- ASBT in both cholangiocytes and ileocytes following well-accepted experimental perturbations to either expand (*i.e.*, taurocholate feeding) or deplete (*i.e.*, cholestyramine feeding) the bile acid pool. To ensure that our molecular observations were physiologically relevant, we also employed functional studies using microperfusion of rat intrahepatic bile duct units (IBDUs), a technique recently developed in our laboratory.

MATERIALS AND METHODS

Materials

[α -³²P] UTP (specific activity 800 Ci/mmol) of >95% purity was purchased from Amersham (Arlington Heights, IL), taurocholate (TCA) of 98% purity was obtained from Calbiochem-Novabiochem Corp (La Jolla, CA). MAXIscript SP6/T7 high specific activity transcription kit and RPA III kit were purchased from Ambion Inc (Austin, TX). All sodium dodecyl sulfate-polyacrylamide gel reagents were purchased from Biorad (Hercules, CA). The ASBT antibody used in immunoblotting was a generous gift of Paul Dawson^[2]. The t-ASBT antibody was produced as described previously^[8]. The secondary antibody (goat anti-rabbit), a horseradish peroxidase (HRP) conjugate, was obtained from Biosource International. Enhanced chemiluminescence (ECL) Western blotting detection reagents were bought from Amersham (Arlington Heights, IL). X-ray films were purchased from Eastman Kodak Co (Rochester, NY). For measurement of biliary phospholipids and cholesterol, commercial kits were purchased from Wako Chemicals (Richmond, VA) and Boehringer Mannheim (Indianapolis, IN). All other commercially available reagents, including cholestyramine, were obtained from Sigma Chemical Co (St. Louis, MO).

Animals

All procedures involving rats were in compliance with guidelines of the Mayo Foundation Animal Care Committee, which approved the experimental protocols. Male Fischer 344 rats (225–275 g) purchased from Harlan Sprague Dawley Inc (Indianapolis, IN) were maintained in a temperature-controlled environment (22 °C) with alternating 12-h light-dark cycles. Rats had free access to water but were pair-fed for 10 d, either control diet (C), or diets enriched with 1% taurocholate (TCA) (wt/wt) or 5% cholestyramine (CY) (wt/wt) prepared by Dyets Inc (Bethlehem, PA). The feeding studies were conducted in two paired groups (*i.e.*, control and test) and four sets of rats (TCA vs C and CY vs C). However for data analysis, results from each of the control groups with respect to the message and protein data were pooled. To ensure equal chow consumption between the pair-fed groups, each rat was kept in an individual cage and its food intake and weight were monitored daily. According to the pair-feeding protocol, the amount of chow consumed by each one of the TCA or CY designated rats one day was provided the following day to the corresponding pair-fed C animal as control chow. At the end of each feeding study, rats were anesthetized with sodium pentobarbital (50 mg/kg) intraperitoneally, the common bile duct was cannulated and bile was collected continuously in timed aliquots to determine bile flow rate. Bile samples were extracted with 4 volumes of isopropanol and immediately frozen in liquid nitrogen for later

measurements of biliary bile acids, phospholipids and cholesterol. Subsequently, rats were euthanized consistently between 8 and 9 am to control possible circadian variation in ASBT and t- ASBT expression.

Isolation of cholangiocytes

Freshly isolated, highly purified cholangiocytes (>95%) were prepared from the livers of C, TCA, and CY fed rats using collagenase perfusion, enzymatic digestion, mechanical disruption and immunopurification as described^[13]. Cholangiocytes derived from animals of the same feeding group were pooled and kept at -70 °C until used for mRNA or protein extraction.

Isolation of ileocytes

The small intestine was prepped and 15 cm of terminal ileum was excised, flushed with cold 9 g/L NaCl solution and the luminal surface was scraped to harvest the epithelial cells. Ileocytes collected from animals of the same feeding group were pooled, centrifuged at 2 000 rpm for 5 min, and the pellet was kept at -70 °C until used for mRNA isolation and protein extraction.

Quantitative ribonuclease protection assay (Q-RPA)

Following extraction of total cellular RNA from freshly isolated cholangiocytes and ileocytes^[14], ASBT and t- ASBT mRNA were determined by Q-RPA using the RPA III kit, as previously described^[8]. Yeast and kidney RNA were used as a negative and positive control, respectively. Following RPA, the ASBT or t- ASBT mRNA content of the samples was measured both by scanning the X-ray film of the protected bands corresponding to either ASBT or t- ASBT and by comparing their arbitrary densitometric units to those obtained from their respective standard curves as described^[8]. The comparability of the total RNA used in this assay was determined both spectrophotometrically and by ultraviolet detection of the intensity of 28S and 14S ribosomal bands on ethidium bromide stained gels.

Quantitative immunoblotting (Q-IB)

Following cholangiocyte immunoisolation, the cells were sonicated twice for 7 s, using a Sonifier cell disrupter (Heat Systems-Ultrasonic, Inc. Plainview, NY) in a buffer containing 50 mmol/L Tris-HCl (pH 7.4), 50 mmol/L EDTA, 100 μ mol/L leupeptin, 1 μ mol/L pepstatin and 0.2 mmol/L PMSF. Cell fragments attached to immunomagnetic beads were removed by applying the samples to a magnet. The remaining cell lysate was centrifuged at 4 °C for 10 min at 2 500 rpm. Subsequently, the cholangiocyte post nuclear supernatant (PNS) was collected, protein concentration was determined and stored at -70 °C until used. To obtain PNS from ileocytes of the terminal ileum, the scraped ileocytes were sonicated in the same buffer and centrifuged as indicated above. In the PNS fraction of ileocytes, protein concentration was calculated and then it was stored at -70 °C until used.

Cholangiocyte and ileal PNS were run on a 120 g/L SDS-polyacrylamide gel. Electrophoresis was done at 100 volts (V) in the presence of a prestained low molecular range protein as a size marker (Biorad) and 40 μ g of kidney PNS as a positive control. Proteins were transferred overnight at 4 °C at 25 V onto nitrocellulose membranes (Micron Separations Inc., Westboro, MA) as described^[4]. Immunoblotting of ASBT and t- ASBT was performed using the well-characterized, specific, rabbit anti rat, polyclonal anti- ASBT^[6] and anti-t- ASBT^[8] antibodies. In brief, membranes were blocked in 50 mL/L milk and incubated at room temperature for 2 h with ASBT antibody (1:4 000) or t- ASBT antibody (1:1 000). Subsequently, membranes were washed 3 times and exposed to horseradish peroxidase conjugated secondary (goat anti-rabbit) antibody (1:7 000) for

1 h at room temperature. Following three additional washings of the membrane, the immunoreactive ASBT (48 kDa) and t-ASBT (19 kDa) bands were detected by enhanced chemiluminescence detection system (ECL).

Immunoblotting for β -actin (41 kDa), a housekeeping protein, was employed to demonstrate equal protein loading. Quantitative comparisons among experimental groups were made by determining the immunoreactive areas by densitometry using an imaging densitometer (Model GS-700) and the Molecular Analyst software program (Bio-Rad Laboratories, Hercules, CA) to calculate the ratios of ASBT or t-ASBT to that of β -actin. The immunoblotting data were also evaluated using another technique to exclude possible risk of β -actin being altered by any of the experimental perturbations. For this purpose, arbitrary densitometric units of each immunoreactive band were divided by the μ g of protein loaded and this value was further divided by the exposure time of the autoradiograph. The specificity of ASBT and t-ASBT antibodies and the bands observed in the immunoblots were evaluated by stripping the membranes and reprobing them with ASBT and t-ASBT antibodies (3 mg/mL) previously blocked with their respective peptides (2 mg/mL) for 1 h at 37°C^[4,8].

Isolation and microperfusion of rat intrahepatic bile duct units (IBDUs)

Isolation and microperfusion of IBDUs were performed, as previously described^[15]. Microperfusion of an IBDU was carried out using Ringer-HCO₃ (KRB solution) containing 40 mmol/L taurocholate at a perfusion rate of 436 nl/min and bile acid (*i.e.*, taurocholate) uptake by individual microperfused IBDU was calculated as published previously^[15].

Protein concentration

Concentrations of proteins were measured by the fluorescamine method using bovine serum albumin (BSA) as standard^[16]. Data were confirmed using the colorimetric Bradford method where vendor's (Sigma) instructions were applied. No differences were observed in protein recovery in TCA or CY groups when compared to controls for a specific cell type.

Measurements of biological samples

Biliary phospholipids and cholesterol were analyzed spectrophotometrically using commercial kits from Wako Chemicals and Boehringer Mannheim, respectively. Biliary bile acid concentration was determined spectrophotometrically according to the vendor's instructions (Sigma). Bile acid concentration of samples was derived from a calibration curve prepared using bile acid of known concentrations: 5, 10, 50, 100 and 200 μ mol/L.

Statistical analysis

All data were expressed as mean \pm SE. Statistical differences were analyzed by Student's *t*-test, and results were considered to be statistically different at $P < 0.05$.

RESULTS

Effect of TCA and CY feeding on body mass, bile flow, and biliary bile acids, phospholipids and cholesterol

The effects of TCA and CY feeding on rat body mass, bile flow and biliary lipid composition compared to C diet are provided in Table 1. Though an approximate 6% weight loss was observed following TCA and CY feedings, the differences in total body masses in experimental groups vs C diet were not significant. Bile flow was significantly higher (2.2-fold) in the TCA group, but similar in the CY group compared to the C group. As expected, the biliary bile acids in the TCA fed rats

were 3.2-fold higher, but 2-fold lower in the CY fed rats compared to the C fed rats. Biliary phospholipids of the TCA fed rats were significantly greater. In the CY group, biliary phospholipids were significantly lower than in the C group. Finally, biliary cholesterol levels of both the TCA and CY groups were similar compared to the C rats. These data indicated that the diets employed significantly altered bile flow and the biliary lipid parameters as anticipated.

Table 1 Alterations of weight and biliary constituents after TCA and CY feeding

	Control	TCA	CY
Body mass (g)	261(\pm 7)	247(\pm 3)	246(\pm 9)
Bile flow (μ L/min)	9.2(\pm 0.4)	19.8(\pm 0.3) ^a	9.7(\pm 0.8)
Biliary bile acids (mmol/L)	20(\pm 2)	65(\pm 3) ^a	10(\pm 1) ^a
Biliary phospholipids (mg/dL)	248(\pm 60)	470(\pm 87) ^a	127(\pm 76) ^a
Biliary cholesterol (g/L)	0.16(\pm 0.03)	0.16(\pm 0.01)	0.15(\pm 0.03)

^a $P < 0.05$.

Effect of TCA and CY feeding on ASBT and t-ASBT messages in cholangiocytes

Using Q-RPA, ASBT mRNA levels were significantly lower (2.3-fold) in cholangiocytes of the TCA fed rats than in cholangiocytes of the C fed rats (0.0035 \pm 0.002 ng mRNA/ μ g total RNA and 0.0081 \pm 0.002 ng mRNA/ μ g total RNA, respectively, $P = 0.009$) (Figure 1). Parallel to the down-regulation of ASBT in the TCA fed rats, t-ASBT mRNA of the same group was also 4.3-fold lower compared to the C fed rats (0.003 \pm 0.001 ng mRNA/ μ g total RNA and 0.013 \pm 0.003 ng mRNA/ μ g total RNA, respectively, $P = 0.01$) (Figure 1). ASBT mRNA levels were 1.5-fold higher in cholangiocytes of the CY fed rats than in those of the C fed rats (0.012 \pm 0.002 ng mRNA/ μ g total RNA and 0.0081 \pm 0.002 ng, RNA/ μ g total RNA, respectively, $P = 0.04$) (Figure 1). Corresponding to the upregulation of ASBT in the CY fed rats, t-ASBT mRNA of the same group was also 1.3-fold greater compared to the C fed rats. However, this was not statistically significant (0.015 \pm 0.004 ng mRNA/ μ g total RNA and 0.013 \pm 0.003 ng mRNA/ μ g total RNA, respectively, $P = 0.4$) (Figure 1). The insignificant increase in the t-ASBT message and the significant increase in the protein levels of t-ASBT (Figure 2) following CY treatment might indicate post-transcriptional modifications.

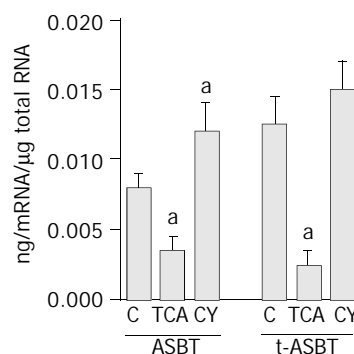


Figure 1 Q-RPA data demonstrating down-regulation of ASBT and t-ASBT message following TCA feeding and up-regulation of their expression following CY feeding in cholangiocytes. Bar graphs demonstrating ASBT and t-ASBT mRNA expression, in which 40 μ g total cellular RNA isolated from cholangiocytes obtained from rats fed regular chow (C), 1% TCA or 5% CY incorporated diets were used. Densitometric values shown here are expressed as mean \pm SE and represent 3 feeding studies in which 30 rats in total were analyzed per group (^a $P < 0.05$).

Effect of TCA and CY feeding on ASBT and t-ASBT proteins in cholangiocytes

ASBT protein in the TCA group decreased 2.2-fold compared to the C fed rats and that was statistically significant ($P=0.006$) (Figure 2). Protein levels of t-ASBT were also repressed 2.4-fold following TCA feeding compared to C fed rats that was also statistically significant ($P=0.004$) (Figure 2). The protein quantitative data were also analyzed using an additional approach to verify the above findings. In this case, to exclude the possibility of β -actin being affected by the bile acid feeding, quantitative analysis was made by determining the arbitrary densitometric units of each immunoreactive band and further dividing it by the amount of protein loaded and exposure time of the autoradiograph. Using this alternative approach, cholangiocyte ASBT protein from the TCA group was shown to be downregulated 2.2-fold compared to C fed rats. This finding reassured us about the accuracy of the data we obtained by the first quantitative method and provided evidence that actin was not affected by TCA feeding. In addition, following CY feeding, the ASBT protein was 2.3-fold higher and statistically significant compared to C fed rats ($P=0.003$) (Figure 2). Moreover, after CY feeding, the t-ASBT protein was also increased 2.4-fold compared to C fed rats ($P=0.04$) (Figure 2).

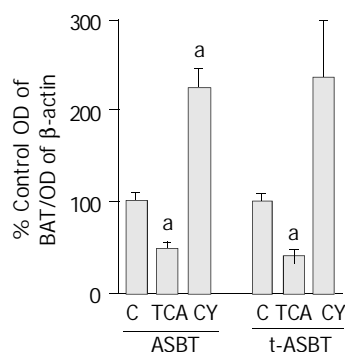


Figure 2 Effect of TCA and CY feeding on the expression of ASBT and t-ASBT protein in cholangiocytes. Bar graphs showing densitometric ratios of ASBT and t-ASBT standardized to β -actin in PNS fractions of freshly isolated cholangiocytes from rats fed control (C), 1% TCA or 5% CY incorporated diet. A 80 μ g for ASBT and 120 μ g for t-ASBT PNS protein were subjected to SDS-PAGE, immunoblotted for ASBT (48 kDa), t-ASBT (19 kDa) and β -Actin (41 kDa) and the bands were then visualized using enhanced chemiluminescence techniques. Densitometric values shown here are expressed as mean \pm SE ($^aP<0.05$) and represent 3 feeding studies for ASBT protein analyses of the TCA and CY groups. Similarly, 3 feeding studies were performed to reflect the data obtained on t-ASBT protein following CY feeding, but only 2 feeding studies were done for t-ASBT protein analysis of the TCA group. Ten rats per group were analyzed in each of these feeding studies, thus a total of 30 rats per feeding study were used in all of the above groups, whereas 20 rats were incorporated into the analysis of t-ASBT in the TCA group.

Effect of TCA and CY feeding on ASBT and t-ASBT messages in ileum

Using Q-RPA, ASBT mRNA levels in ileum of the TCA fed rats were 2.1-fold higher than those in ileum of the C fed rats (0.073 ± 0.01 ng mRNA/ μ g total RNA and 0.036 ± 0.01 ng mRNA/ μ g total RNA, respectively, $P=0.01$) (Figure 3). Parallel to upregulation of ASBT message, t-ASBT mRNA of the TCA group was also 1.9 fold higher compared to the C fed rats (0.076 ± 0.015 ng mRNA/ μ g total RNA and 0.040 ± 0.004 ng mRNA/ μ g total RNA, respectively, $P=0.01$) (Figure 3). In addition, the ileal ASBT mRNA levels of the CY fed rats were 1.4-fold less and statistically

significant than those of the C fed rats (0.026 ± 0.003 ng mRNA/ μ g total RNA and 0.036 ± 0.007 ng mRNA/ μ g total RNA, respectively, $P=0.07$) (Figure 3). Corresponding to these findings, t-ASBT mRNA levels of the CY fed rats were 1.3-fold lower and statistically significant compared to the C fed rats (0.031 ± 0.002 ng mRNA/ μ g total RNA and 0.040 ± 0.004 ng mRNA/ μ g total RNA, $P=0.01$) (Figure 3).

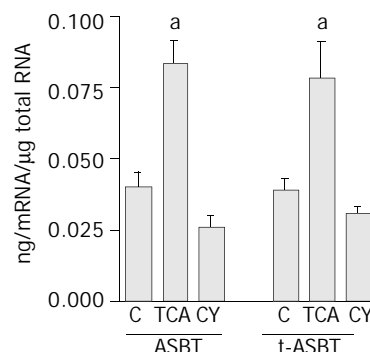


Figure 3 Q-RPA data demonstrating upregulation of ASBT and t-ASBT message following TCA feeding and downregulation of their message following CY feeding in ileum. Bar graphs demonstrating ASBT and t-ASBT mRNAs, in which 40 μ g total cellular RNA isolated from cholangiocytes obtained from rats fed regular chow (C), 1% TCA or 5% CY incorporated diets were used. Densitometric values demonstrated here are expressed as mean \pm SE and represent $n=3$ feeding studies in which 30 rats in total were analyzed for each group ($^aP<0.05$).

Effect of TCA and CY feeding on ASBT and t-ASBT proteins in ileum

Parallel to increased ASBT transcript observed following bile acid feeding, ASBT protein expression was also 2.3-fold higher and statistically significant in the TCA fed rats compared to the C fed rats ($P=0.001$) (Figure 4). Moreover, the t-ASBT protein expression was also supportive of the mRNA data, t-ASBT protein was 2.7-fold higher and statistically significant in the TCA fed rats compared to the C fed rats ($P=0.02$) (Figure 4). Furthermore, following CY feeding, and parallel to decreased ASBT transcript, ileal ASBT protein was also 2.1-fold significantly down-regulated ($P=0.008$) compared to the C fed rats (Figure 4). Finally, the ileal t-ASBT protein was also in support of the message results for this transporter. Indeed, t-ASBT protein was 2.3-fold significantly decreased in the CY fed rats compared to the C fed rats ($P=0.01$) (Figure 4).

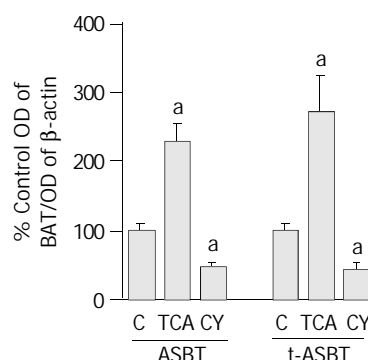


Figure 4 Effect of TCA and CY feeding on the amount of ASBT and t-ASBT protein in ileum. Bar graphs showing ratios of ASBT/ β -actin and t-ASBT/ β -Actin in PNS of ileal scrapings obtained from rats fed C, TCA and CY diets. Forty and 80 μ g of protein were subjected to SDS-PAGE and immunoblotted to visualize ASBT and t-ASBT, respectively. Data shown here are representative of $n=3$ feeding studies were analyzed per group

and expressed as mean \pm SE ($^aP<0.05$). For the analysis of ASBT and t-ASBT in the TCA treated groups, 7 and 3 rats in total were used, respectively. Whereas, the number of animals analyzed in the CY groups totaled 10 and 3 for ASBT and t-ASBT, respectively. Hence, the number of control rats was 17 for ASBT and 6 for t-ASBT in total.

Effect of TCA and CY feeding on bile acid uptake by IBDUs

To further verify and extend our observations at the functional level, taurocholate uptake was measured in IBDUs isolated from rats fed either TCA or CY diets and compared to those obtained from C fed animals using a novel microperfusion technique. Specifically, taurocholate uptake by IBDUs derived from the C diet group was 1.1 ± 0.2 nmol/min/mm². Taurocholate uptake was significantly lower in the TCA group (0.4 ± 0.1 nmol/min/mm², $P=0.002$, $n=4$ IBDU, 2 feeding studies) and significantly higher in CY group (1.95 ± 0.3 nmol/min/mm², $P=0.007$) (Figure 5).

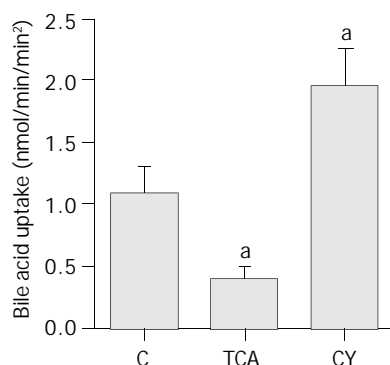


Figure 5 Effect of TCA and CY feeding on taurocholate uptake by ASBT in rat IBDUs. Bar graphs showing 2.7-fold decrease and 1.7-fold increase in taurocholate uptake in TCA and CY fed rats, respectively, compared to controls. Data shown here, and expressed as mean \pm SE, were obtained from $n=3$ feeding studies in which 11 control, 4 TCA and 5 CY IBDUs were analyzed ($^aP<0.05$).

DISCUSSION

The major findings described here are TCA feeding downregulates but CY feeding upregulates both ASBT and t-ASBT in cholangiocytes and TCA feeding upregulates whereas CY feeding downregulates both ASBT and t-ASBT in terminal ileum. Our findings suggested that both ASBT and t-ASBT in a specific cell type underwent parallel modes of regulation. On the other hand, reciprocal changes were observed between cholangiocytes and ileocytes in terms of ASBT and t-ASBT expression, suggesting organ-specific differences in regulation of these bile acid transporters.

Regulation of transporter expression to accommodate altered substrate loads is a well-recognized physiologic phenomenon. For example, adaptive up- or down-regulation of hepatic and ileal bile acid transporters occurred in response to changes in bile acid pool size^[3]. Moreover, a limited number of very recent studies addressed the problem of whether the same adaptive events could operate in cholangiocytes with respect to ASBT^[9-12]. However, no data exist regarding the regulation of t-ASBT in the liver or terminal ileum after bile acid supplementation or depletion. Regarding ASBT expression in terminal ileum, prior investigations have shown evidence of transcriptional regulation by bile acids^[17-19]. Nevertheless, results of these studies appeared to be species-specific given reported differences in ASBT regulation. For example, Lillienau *et al.* reported a negative feedback regulation of the ileal bile acid transporter in the guinea pig based on whole organ, ileal perfusion studies^[17]. Following cloning of ASBT in rats, Stravitz *et al.* described a positive

feedback regulatory mechanism of the ileal ASBT. These authors demonstrated induction of both mRNA and protein levels of ASBT after cholic acid feeding including supportive functional studies using ileal brush border membrane vesicles^[18]. More recently, Arrese *et al.* reported no change in ASBT expression and function following bile duct ligation and intestinal sequestration of bile acids^[19].

In the present study, we demonstrated that in cholangiocytes compared to C fed rats, TCA feeding downregulated both ASBT transcript and protein abundance as well as t-ASBT transcript and protein expression. On the other hand, CY feeding upregulated both ASBT transcript and protein abundance as well as t-ASBT transcript and protein expression compared to C fed rats. To support these molecular findings, microperfusion studies in rat IBDUs compared to C fed animals revealed 2.7-fold decrease and 1.7-fold increase in taurocholate uptake by IBDUs derived from TCA or CY fed rats, respectively. In terminal ileum, TCA feeding upregulated both ASBT transcript and protein abundance as well as t-ASBT transcript and protein expression. In contrast, CY feeding downregulated both ileal ASBT transcript and protein abundance as well as t-ASBT transcript and protein expression compared to C fed rats.

The pathophysiological significance of ASBT and t-ASBT adaptive changes in biliary epithelia and terminal ileum in response to bile acid pool perturbations described in this paper are intriguing. It appears that bile acid transporting epithelia of different organs (*i.e.*, bile ducts and ileum) respond differently to bile acid supplementation or depletion. ASBT and t-ASBT transcriptional down-regulation in cholangiocytes upon TCA feeding could diminish the cholehepatic shunt of conjugated bile acids. This pathway is believed to play a role in reclamation of bile acids from bile back to liver. Thus, during bile acid feeding, decreased expression of bile acid transporters in cholangiocytes and the ensuing reduction of bile acid shunting may provide protection to cholangiocytes and subsequently hepatocytes from the deleterious effects of excessive intracellular accumulation of bile acids. In fact, this protective mechanism became even more relevant given the fact that bile acid feeding increased the expression of bile acid transporters in terminal ileum as shown in the present and other studies^[18] and thus enhancing the uptake capacity of ileum for bile acids for delivery to the liver, perhaps to compensate the decreased cholehepatic shunt, and thus keeping the bile acid synthesis at a balance.

We have also observed that in CY fed rats, cholangiocyte ASBT and t-ASBT were up-regulated. These data should be reviewed in parallel with the reciprocal findings in the terminal ileum where CY feeding caused upregulation of both ASBT and t-ASBT. The potential pathophysiologic relevance of ASBT and t-ASBT induction in cholangiocytes after CY feeding may relate to increasing the biliary bile acid return to the liver via an enhanced cholehepatic shunt. This condition would potentially assist maintaining cholesterol homeostasis, given the concurrent observation of diminished expression of bile acid transporters in distal intestine and thus reducing absorption of bile acids from the terminal ileum. The experimental effect of CY on the expression of cholangiocyte bile acid transporters is analogous to the bile duct ligated (BDL) model, in which the enterohepatic circulation of bile acids is interrupted due to mechanical obstruction of the common bile duct. To this end, our observations in cholangiocytes were comparable to those reported by Lee *et al.*^[11]. These authors reported adaptive up-regulation and down-regulation of ASBT in biliary epithelia and kidney, respectively, in BDL rats, postulating that these changes might accommodate alternative pathways for secretion of excessive bile acids in cholestasis^[11]. However, others have shown in both BDL^[9,10] and bile acid fed rats^[12] that bile acid depletion and repletion could decrease and increase the expression of ASBT, respectively, in cholangiocytes. Differences

in results may very well reflect differences in study design (e.g., feeding rats in a paired vs non-paired manner, feeding them until the surgical procedure vs fasting them overnight, feeding for 10 d vs 7 d, the age of the animals 225–275 g vs 125–150 g starting masses).

In our ileal studies, a significant increase in ASBT and t-ASBT occurred after TCA feeding, whereas a decrease in message and protein levels of both transporters was seen in bile acid depleted rats. These data suggest that changes in bile acid pool size could result in marked alterations in these bile acid carrier molecules. Our data agree with the work of Stravitz *et al.*^[18] who also reported a positive feedback mechanism on the regulation of ASBT in ileum. Arrese *et al.* reported that neither the pharmacological sequestration of bile acids nor common bile duct ligation affected the expression and function of ileal ASBT^[19]. Whether the different pharmacological agents used for bile acid depletion by Arrese (*i.e.*, the novel sequestrant GT31-104)^[19], and in our work, the well-established cholestyramine, accounted for these differences is unclear^[18].

Recently, the promoter region of the ASBT gene has been extensively analyzed^[20]. It appears that two AP-1 consensus sites have been identified in the proximal promoter of ASBT. At least four nuclear binding proteins, designated ABP 1-4, interacting with AP-1 sites, have been described. Of interest, formation of the ABP2 nuclear binding protein complex appeared to be correlated with regional and developmental stage-specific expression of ASBT in the rat intestine^[20]. In a study clarifying the transcriptional mechanisms involved in cytokine-mediated repression of rat ASBT, the authors observed reductions in ileal ASBT message and protein following proinflammatory cytokine and IL-1 beta treatment of IEC-6 and Caco-2 cells, along with significant increases in c-fos expression^[22]. The proinflammatory cytokines and interleukin-1 beta have thus been shown to repress the activity of the ASBT promoter via serine phosphorylation, and nuclear translocation of c-fos. Inflammation, associated with up-regulation, phosphorylation, and nuclear translocation of c-fos, which then represses ASBT promoter activity via binding to the 3' AP-1 element by a c-fos/c-jun heterodimer, may be operative following bile acid treatment, a stimulus known to increase inflammation in cholangiocytes. The inflammatory influence of bile acids might occur following directly activating eosinophils and inducing their effector functions^[23], or triggering interferon-gamma and tumor necrosis factor alpha production, which might in turn stimulate superoxide and interleukin release that resulted in disruption of the tight junctions in cholangiocytes^[24]. Bile acids, with the potential of altering the profile of cytokines, chemokines, and proinflammatory stimuli, which in turn were likely to activate fibrogenesis, stimulate apoptotic and proliferative responses, seemed to be important players in the pathophysiology of chronic cholestatic disorders^[25]. It is therefore imperative to begin to investigate the role of AP-1, ABP 1-4 and c-fos expression in bile acid transporting epithelia hoping to shed light on the adaptive and reciprocal expression of ASBT and t-ASBT. In a recent study, decreased expression of ileal ASBT protein and mRNA in mice following bile acid treatment was related to the presence of a potential liver receptor homologue-1 (LRH-1) cis acting element in the bile acid responsive region of the mouse but not the rat promoter. The mouse but not the rat promoter was activated by LRH-1 and this correlated with nuclear protein binding to the mouse but not rat LRH-1 element. Thus, species-specific negative feedback regulation of ASBT by bile acids was mediated by FXR via SHP-dependent repression of LRH-1 activation of the ASBT promoter^[21]. It is possible, therefore that, the reciprocal regulation pattern we have observed between cholangiocytes and ileocytes may reflect the role of FXR and LRH-1 in cholangiocytes.

In conclusion, we present data demonstrate that a bile acid enriched diet can down-regulate ASBT and t-ASBT in cholangiocytes but upregulate both transporters in terminal ileum. Conversely, bile acid depletion by sequestration can upregulate ASBT and t-ASBT in cholangiocytes, but down-regulate both transporters in terminal ileum. To have a better understanding of the mechanism (s) affecting the expression of bile acid transporters in relevant epithelia, a systematic comparative evaluation of their regulatory elements in different tissues known to be involved in bile acid homeostasis is required. Unraveling the presumed cell-specific regulatory mechanisms that affect bile acid transporter expression and function will help to develop novel rational options to treat cholestasis and chronic cholestatic liver diseases.

REFERENCES

- 1 **Hofmann AF.** Intestinal absorption of bile acids and biliary constituents: the intestinal component of the enterohepatic circulation and the integrated system. In: Physiology of the gastrointestinal tract, edited by LR Johnson. New York: Raven 1994; 1845-1865
- 2 **Dawson PA, Oelkers P.** Bile Acid transporters. *Curr Opin Lipidol* 1995; **6**: 109-114
- 3 **St-Pierre MV, Kullak-Ublick GA, Hagenbuch B, Meier PJ.** Transport of bile acids in hepatic and non-hepatic tissues. *J Exp Biol* 2001; **204**: 1673-1686
- 4 **Lazaridis KN, Pham T, Tietz P, Marinelli RA, deGroen PC, Levine S, Dawson PA, LaRusso NF.** Rat cholangiocytes absorb bile acids at their apical domain via the ileal sodium dependent bile acid transporter. *J Clin Invest* 1997; **100**: 2714-2721
- 5 **Alpini G, Glaser SS, Rodgers R, Phinizy JL, Robertson WE, Lasater J, Caligiuri A, Tretjak Z, Lesage GD.** Functional expression of the apical Na⁺-dependent bile acid transporter in large but not small rat cholangiocytes. *Gastroenterology* 1997; **113**: 1734-1740
- 6 **Shneider BL, Dawson PA, Christie DM, Hardikar W, Wong MH, Suchy FJ.** Cloning and molecular characterization of the ontogeny of a rat ileal sodium-dependent bile acid transporter. *J Clin Invest* 1995; **95**: 745-754
- 7 **Christie DM, Dawson PA, Thevananther S, Shneider BL.** Comparative analysis of the ontogeny of a sodium-dependent bile acid transporter in rat kidney and ileum. *Am J Physiol* 1996; **271**: G377-G385
- 8 **Lazaridis KN, Tietz P, Wu T, Kip S, Dawson PA, LaRusso NF.** Alternative splicing of the rat sodium/bile acid transporter changes its cellular localization and transport properties. *Proc Natl Acad Sci U S A* 2000; **97**: 11092-11097
- 9 **Alpini G, Baiocchi L, Glaser S, Ueno Y, Marzioni M, Francis H, Phinizy JL, Angelico M, Lesage G.** Ursodeoxycholate and tauroursodeoxycholate inhibit cholangiocyte growth and secretion of BDL rats through activation of PKC alpha. *Hepatology* 2002; **35**: 1041-1052
- 10 **Alpini G, Glaser S, Alvaro D, Ueno Y, Marzioni M, Francis H, Phinizy JL, Angelico M, Lesage G.** Bile acid depletion and repletion regulate cholangiocyte growth and secretion by a phosphatidylinositol 3-kinase-dependent pathway in rats. *Gastroenterology* 2002; **123**: 1226-1237
- 11 **Lee J, Azzaroli F, Wang L, Soroka CJ, Gigliozi A, Setchell KD, Kramer W, Boyer JL.** Adaptive regulation of bile salt transporters in kidney and liver obstructive cholestasis in the rat. *Gastroenterology* 2001; **121**: 1473-1484
- 12 **Alpini G, Ueno Y, Glaser SS, Marzioni M, Phinizy, Francis JL, LeSage G.** Bile acid feeding increased proliferative activity and apical bile acid transporter expression in both small and large rat cholangiocytes. *Hepatology* 2001; **34**: 868-876
- 13 **Alpini G, Philips JO, Vroman B, LaRusso NF.** Recent advances in the isolation of liver cells. *Hepatology* 1994; **20**: 494-514
- 14 **Chomczynski P, Sacchi N.** The single-step method of RNA isolation by acid guanidium thiocyanate phenol-chloroform extraction. *Anal Biochem* 1987; **162**: 156-159

- 15 **Masyuk AI**, Gong AY, Kip S, Burke MJ, LaRusso NF. Perfused rat intrahepatic bile ducts secrete and absorb water, solute, and ions. *Gastroenterology* 2000; **119**: 1672-1680
- 16 **Udenfriend S**, Stein S, Bohlen P, Dairman W, Leimgruber W, Weigle M. Fluorescamine: a reagent for assay of amino acids, peptides, proteins and primary amines in the picomole range. *Science* 1972; **178**: 871-872
- 17 **Lillienau J**, Crombie DL, Munoz J, Longmire-Cook SJ, Hagey LR, Hofmann AF. Negative feedback regulation of the ileal bile acid transport system in rodents. *Gastroenterology* 1993; **104**: 38-46
- 18 **Stravitz RT**, Sanyal AJ, Pandak WM, Vlahcevic ZR, Beets JW, Dawson PA. Induction of sodium dependent bile acid transporter messenger RNA, protein, and activity in rat ileum by cholic acid. *Gastroenterology* 1997; **113**: 1599-1608
- 19 **Arrese M**, Trauner M, Sacchiero RJ, Crossman MW, Shneider BL. Neither intestinal sequestration of bile acids nor common bile duct ligation modulate the expression and function of the rat ileal bile acid transporter. *Hepatology* 1998; **28**: 1081-1087
- 20 **Chen F**, Ma L, Al-Ansari N, Shneider BL. The role of AP-1 in the transcriptional regulation of the rat apical sodium-dependent bile acid transporter. *J Biol Chem* 2001; **276**: 38703-38714
- 21 **Chen F**, Ma L, Dawson PA, Sinal CJ, Sehayek E, Gonzalez FJ, Breslow J, Ananthanarayanan M, Shneider BL. Liver-receptor homologue-1 mediates species and cell-line specific bile acid dependent negative feedback regulation of the apical sodium dependent bile acid transporter. *J Biol Chem* 2003; **278**: 19909-19916
- 22 **Chen F**, Ma L, Sartor RB, Li F, Xiong H, Sun AQ, Shneider B. Inflammatory-mediated repression of the rat ileal sodium-dependent bile acid transporter by c-fos nuclear translocation. *Gastroenterology* 2002; **123**: 2005-2016
- 23 **Yamazaki K**, Gleich GJ, Kita H. Bile acids induce eosinophil degranulation by two different mechanisms. *Hepatology* 2001; **33**: 582-590
- 24 **Hanada S**, Harada M, Koga H, Kawaguchi T, Taniguchi E, Kumashiro R, Ueno T, Ueno Y, Ishii M, Sakisaka S, Sata M. Tumor necrosis factor-alpha and interferon-gamma directly impair epithelial barrier function in cultured mouse cholangiocytes. *Liver Int* 2003; **23**: 3-11
- 24 **Strazzabosco M**. Transport systems in cholangiocytes: their role in bile formation and cholestasis. *Yale J Biol Med* 1997; **70**: 427-434

Edited by Wang XL Proofread by Xu FM

Transcriptional regulation of human $\alpha 1(I)$ procollagen gene in dermal fibroblasts

Chun-Fang Gao, Hao Wang, Ai-Hua Wang, Wei-Dong Wan, Yan-Aan Wu, Xian-Tao Kong

Chun-Fang Gao, Hao Wang, Ai-Hua Wang, Wei-Dong Wan, Yan-Aan Wu, Xian-Tao Kong, Department of Laboratory Medicine, Changzheng Hospital, Second Military Medical University, Shanghai 200003, China

Supported by the Natural Science Foundation of China, No. 39870301, No.30270605 and Project “208” of Shanghai Changzheng Hospital
Correspondence to: Dr. Chun-Fang Gao, Department of Laboratory Medicine, Changzheng Hospital, 415 Fengyang Road, Shanghai 200003, China. wanggaob@online.sh.cn

Telephone: +86-21-63610109-73641 **Fax:** +86-21-63520020

Received: 2003-12-10 **Accepted:** 2004-01-12

Abstract

AIM: To clarify the fractional activity of promoters from human $\alpha 1(I)$ procollagen gene, the interaction between cis-elements and consensus DNA-binding proteins responsible for high promoter activity, and the potential application of promoter competitors as well as cytokines for antifibrogenesis.

METHODS: Sequence between 2 483 bp upstream of the start of transcription and 42 bp downstream of this site was investigated with serial 5' -deletion. The 5' -deleted promoters recombined with chloramphenicol acetyltransferase (CAT) as reporter gene were transiently transfected to human dermal fibroblasts. Electrophoretic mobility shift assay was performed to show the DNA-protein binding capacity of the promoter sequence. Cytokines including tumor necrosis factor α (TNF α) and interferons (IFNs) were added to the culture medium of transiently transfected fibroblasts. Competitor DNA for the binding sites of Sp-1, Ap-1 and NF-1 was individually cotransfected transiently in order to block the promoter-driven CAT expression.

RESULTS: Sequences of -2 483 to +42 bp and -268 to +42 bp of human $\alpha 1(I)$ procollagen gene had high activity as promoters. Binding sites for Ap-1 and Sp-1 were among the cis-regulatory elements recognizing consensus transcription factors responsible for basal promoter activity of sequence -268 to +42 bp. TNF α , IFN α , IFN β showed inhibitory effects on sequence -2 483 to +42 bp as promoter with activities 43%, 62% and 60% of control respectively. Transfection of the promoter competitors could reverse the promoter activity of -268 to +42 bp 40-60%.

CONCLUSION: Sequences of -2 483 to +42 bp recombined with reporter gene provide an ideal construction for transcriptional study of $\alpha 1(I)$ procollagen gene. The anti-collagen capacity of TNF α and IFNs is associated with their transcriptional regulation. Ap-1 and Sp-1 mediate the basal transcriptional activation of human $\alpha 1(I)$ procollagen gene in dermal fibroblasts. Competitors for highly active promoters might be a novel potential candidate in fibrotic blockade.

Gao CF, Wang H, Wang AH, Wan WD, Wu YA, Kong XT. Transcriptional regulation of human $\alpha 1(I)$ procollagen gene in dermal fibroblasts. *World J Gastroenterol* 2004; 10(10): 1447-1451
<http://www.wjgnet.com/1007-9327/10/1447.asp>

INTRODUCTION

Excessive accumulation of extracellular matrix (ECM) following chronic impairment of tissue gives rise to the development of fibrosis which might occur in skin and other organs, such as liver, kidney and lung^[1]. Scarring or cirrhosis with the progression of fibrosis can cause functional failure of the organ due to the distortion of the structure. Type I collagen, composed of two chains of $\alpha 1(I)$ and one chain of $\alpha 2(I)$, is the most abundant component of ECM in most fibrotic tissues^[1]. The expression of genes coding for the $\alpha 1(I)$ and $\alpha 2(I)$ chains of type I collagen is regulated coordinatively^[2]. Researches on the expression of type I collagen in the past decades have been ascribed to fluctuations under various pathophysiological conditions at transcriptional and translational levels^[3]. Most of the recent available evidence suggest that the principal mechanisms operate at the level of transcription, although control and changes in mRNA processing and stability may also play a role^[4-7]. The mechanisms of transcriptional activation of collagen genes are poorly understood till now. Several putative regulatory elements that may determine the transcriptional efficiency of type I collagen gene have been identified in their corresponding promoters^[8-11]. Fine mapping of the cis-acting elements as well as the identification of their consensus DNA-binding proteins involved in the modulation of collagen gene expression is crucial for understanding the pathological regulation of collagen accumulation. In our previous work, we analyzed the promoter activity from mouse $\alpha 2(I)$ procollagen gene as well as its modulation by cytokines^[12,13]. In this study, we investigated the fractional activity of promoter from human $\alpha 1(I)$ procollagen gene and the interaction between cis-elements and consensus DNA-binding proteins responsible for high promoter activity. Sequence between 2 500 bp upstream of the start of transcription and 42 bp downstream of this site was studied with serial 5' -deletion. We report that regions from -2 483 to +42 bp, -268 to +42 bp of human $\alpha 1(I)$ procollagen gene have higher promoter activities. Binding sites for Ap-1, Sp-1 may be among the cis-regulatory elements recognizing consensus transcription factors responsible for basal promoter activity of sequence -268 to +42 bp. The anti-fibrotic capacities of TNF α and IFNs are associated with their transcriptional regulation of type I collagen. Transfection of the promoter competitors can partially reverse the promoter activity, suggesting that promoter competitors for highly active promoters may be a novel antifibrotic tool.

MATERIALS AND METHODS

Cell culture

Human dermal fibroblast culture was established by explanting tissue specimens obtained from the abdominal skin of a 3-year old male patient because of burn of his left arm and requiring skin transplantation. The cells were maintained under standard conditions in Dulbecco's modified Eagle's medium (DMEM, Gibco, USA) supplemented with 100 mL/L fetal calf serum (FCS, Gibco, USA). The cells in passages 3-8 were used for study.

Construction of plasmids

Plasmid pCAT3-enhancer (Promega, USA), a promoterless vector which contains SV40 enhancer and chloramphenicol

acetyltransferase (CAT) as reporter gene, was used as the recombinant plasmid backbone. The putative promoters in 6 constructions named pCOLH_{0.1}, pCOLH_{0.27}, COLH_{0.5}, pCOLH_{0.9}, pCOLH_{1.5} and pCOLH_{2.5} corresponded to sequences -105 to +42 bp, -268 to +42 bp, -496 to +42 bp, -829 to +42 bp, -1 448 to +42 bp, -2 483 to +42 bp, respectively in human $\alpha 1$ (I) procollagen gene with the same 3' ends. They were obtained by PCR with p5.3K $\alpha 1$ containing 5' flanking region -5 300 to +42 bp of human $\alpha 1$ (I) procollagen gene (gift from Dr. Sergio A. Jimenez) as template^[14]. Sense primers for PCR were as follows: pCOLH_{0.1}: 5' -ATGTCTACGCGTCTGATTGGCTGGGGCACGG-3', pCOLH_{0.27}: 5' -ATGTCTACGCGTCTGAGGACCCAGCTGCAC-3', pCOLH_{0.5}: 5' -ATGTCTACGCGTGGAGAGGTCCTCAGC ATGC-3', pCOLH_{0.9}: 5' -ATGTCTACGCGTGGCTGCTCCATCACCAAC-3', pCOLH_{1.5}: 5' -ATGTCTACGCGTCTCAGGACGAGGTA GATTG-3', pCOLH_{2.5}: 5' -ATGTCTACGCGTACATCTT CAGCCTGGGCAC-3'. Antisense primers for the 6 putative promoters were the same: 5' -ATAGTACTCGAGCGTGC CTCCTGCTCCGAC-3'. The sense and antisense primers contained *Mlu*I and *Xho*I adaptors (underlined part) which were 6 bases away from the 5' end of the primers. PCR was performed as routine with high-fidelity PCR kit (Roche) and PE-9600 PCR amplifier. The PCR products were digested with *Mlu*I and *Xho*I and then ligated to *Mlu*I-*Xho*I linearized pCAT3 vector with T4 DNA ligase (Promega). The ligation mixtures were transformed to competent *E. coli* (JM109), and the ampicillin resistant positive clones were further identified by small-scale restriction enzyme digestion and DNA sequencing (ABI 377). The correct clones were amplified and recombinant plasmids were extracted and purified with plasmid isolation kit (Qiagen). The purity and yield rate were determined in UV spectrophotometer (Du 600, Beckman).

Synthesis of oligonucleotide for binding sites of Ap-1, Sp-1 and NF-1

Consensus binding sites for Ap-1, Sp-1, and NF-1 were first synthesized as single stranded DNA (Sangon, Shanghai) and sequences were: Ap-1, 5' CGCTTGATGACTCAGCCGGAA 3'; Sp-1, 5' ATCGATCGGGGCGGGGCGCGC3'; NF-1, 5' TTTTGGATTGAAGCCAATATGATA3'. The synthesized sense and antisense single stranded DNAs were matched and mixed at a molar ratio of 1:1. After incubation of the mixtures at 95 °C for 10 min and then cooling slowly down to room temperature, the double stranded DNAs were stored at -20 °C.

DNA transfection

DNA transfection was performed with Dospere liposomal transfecting reagent (Roche, Germany) according to manufacturer's instruction. Briefly, the day before transfection, dermal fibroblasts were seeded at 5×10^5 /well in a 6-well plate (Nunc, USA) in 2 mL DMEM. The cells were incubated until 60-80% confluence. Then the medium was replaced with fresh culture medium without FCS shortly before adding transfection reagent. Two micrograms of construct plasmid together with 1 μ g of pSV β -gal (Promega, USA) as internal standard were cotransfected. CAT expression plasmid pCAT6.2 (Invitrogen, USA) was also transfected as CAT expression positive control. One milliliter medium containing 20 mL/L FCS was added to each well 6 h later. The medium was then replaced with fresh normal culture medium 24 h later. Two days after transfection, the cells were ready for reporter gene (CAT) expression measurement. For the cells transfected with pCOLH_{0.27}, 10 μ g of DNA for binding sites of Ap-1, Sp-1 or NF-1 was transfected to the cells 24 h after pCOLH_{0.27} transfection. Mock DNA transfection was included. The transfection was terminated 24 h later and ready for reporter gene detection.

To study the regulatory effect of cytokines, cells were starved for 4 h after being transfected with pCOLH_{2.5} for 24 h, then culture medium was replaced by fresh medium containing TNF α 10 μ g/L (R&D, USA), IFN α 1×10^5 U/L (PBL, England), IFN γ 1×10^5 U/L (Roche, USA) respectively. Another 24 h later, the transfection was terminated and ready for reporter gene detection.

Determination of CAT and β -galactosidase

Forty-eight hours after initial transfection, cells were washed with precooled phosphate buffered solution (PBS, 0.1 mol/L, pH7.4) and lysed with lysis buffer (Roche, USA). Aliquots of cell extracts were made for protein determination as described previously^[15]. CAT was measured by ELISA (Roche, USA) and β -galactosidase with enzyme activity analysis method (Promega, USA).

Electrophoretic mobility shift assay (EMSA)

EMSA was performed as described previously^[16]. Briefly, a fragment spanning -268 to +42 bp of the human $\alpha 1$ (I) procollagen gene was obtained by PCR with p5.3K $\alpha 1$ as template. The fragment obtained from PCR was purified, digested with *Eco*RII and 3' end-labeled with digoxigenin (Roche). Crude nuclear extracts from early passage confluent human fibroblasts were prepared according to the method described by Erdos *et al*^[17]. The protein concentration in nuclear extract was determined by Bradford method^[15]. DNA-protein binding reactions (20 μ L) were performed in a buffer containing 1 μ g of poly[d(A-T)], 1 μ g of poly L-lysine, 15 μ g of crude nuclear extract, 50 fmol of dig-labeled probes. Unlabeled probes and synthetic binding sites of Ap-1, Sp-1 and NF-1 were applied with 100-fold molar excess for competition tests. Following 20-min incubation at room temperature, DNA-protein complexes were resolved from free DNA probes by electrophoresis on 60 g/L non-denatured polyacrylamide gels. Transfer of DNA was finished by electroblotting. Signals were captured by chemiluminescent detection with alkaline phosphatase labeled anti-dig antibody and CSPD (Roche) as substrate.

RESULTS

Construction and transfection of 5'-deleted recombinant plasmids

Constructions of the 6 recombinant plasmids were verified by small-scale restriction enzyme digestion and DNA sequencing. Figure 1 shows the correct digestion of the constructs. The putative promoters in the constructions were 0.1 kb, 0.27 kb, 0.5 kb, 0.9 kb, 1.5 kb, and 2.5 kb, corresponding to -105 to +42 bp, -268 to +42 bp, -496 to +42 bp, -829 to +42 bp, -1 448 to +42 bp, -2 483 to +42 bp of human $\alpha 1$ (I) procollagen gene. DNA sequencing indicated that the inserted sequences of the putative promoters were the same as that published in GeneBank (accession No X98705). The 6 constructs containing serial 5'-deleted promoters were transiently transfected to early passage confluent human fibroblasts. Forty-eight hours after transfection, the expression of reporter gene CAT was determined by ELISA with the detection of β -galactosidase activity and protein for normalization. The expression of normalized CAT in the cells transfected with pCOLH_{2.5} was set as 1, the relative expression level of normalized CAT in cells transfected with other constructs is shown in Table 1 (mean \pm SD of three independent experiments), indicating that the highest CAT expressions were driven by -2 483 to +42 bp and -268 to +42 bp as promoters while the lowest by -105 to +42 bp.

Transfection of promoter competitors

For the cells transfected with pCOLH_{0.27}, 10 μ g of consensus recognition DNA for Ap-1, Sp-1 or NF-1 was transfected to

cells 24 h after pCOLH₁0.27 transfection. Reporter gene (CAT) was determined another 24 h later. Relative CAT expression values in different transfection groups were calculated relative to that of mock DNA transfection. The result shown in Figure 2 indicated that transfection of Ap-1 or Sp-1 DNA inhibited CAT expression approximately by 25% and 20% respectively compared to mock DNA transfection ($P < 0.05$). Transfection of NF-1 DNA did not show definite effect on reporter gene expression.

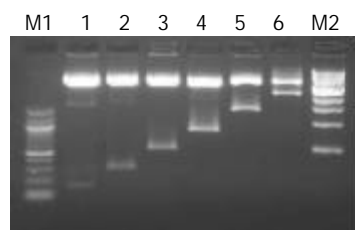


Figure 1 Electrophoresis of six constructs digested with *MluI* and *XhoI*. M1: 100 bp DNA ladder marker, M2: 1 kb DNA ladder marker, Lane1: pCOLH₁0.1, lane2: pCOLH₁0.27, lane3: pCOLH₁0.5, Lane4: pCOLH₁0.9, Lane5: pCOLH₁1.5, Lane6: pCOLH₁2.5. Six recombinant plasmids containing serial 5' -deleted flanking sequences of human $\alpha 1$ (I) procollagen gene as putative promoter were digested with *MluI* and *XhoI* at 37 °C for 1 h. The digested DNAs were fractionated on 15 g/L agarose gel showing vector DNA (4.3 kb) and insertion promoters with different sizes.

Table 1 Summary of CAT expression driven by various lengths of the 5' flanking sequence from human $\alpha 1$ (I) procollagen gene

Name of transfected constructions	Putative promoters' length (bp)	Relative activities of reporter gene (CAT, mean \pm SD) ¹
pCOLH ₁ 0.1	-105 to 42	0.10 \pm 0.02
pCOLH ₁ 0.27	-268 to 42	0.97 \pm 0.04
pCOLH ₁ 0.5	-496 to 42	0.20 \pm 0.05
pCOLH ₁ 0.9	-829 to 42	0.36 \pm 0.09
pCOLH ₁ 1.5	-1 448 to 42	0.73 \pm 0.11
pCOLH ₁ 2.5	-2 483 to 42	1.0

¹The expression of normalized CAT in the cells transfected with pCOLH₁2.5 was set as 1, the relative expression level of normalized CAT in the cells transfected with other constructs is shown in Table 1 (mean \pm SD of three independent experiments).

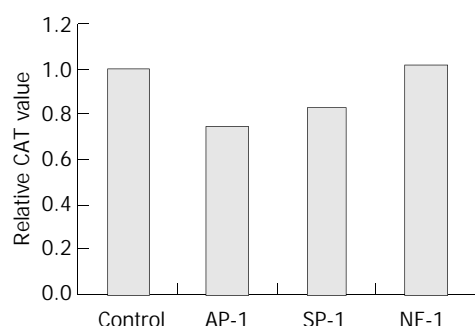


Figure 2 Effects of consensus DNA on CAT expression in pCOLH₁0.27 transfected cells. Control: mock DNA transfection, Ap-1: transfection of Ap-1 consensus DNA (10 μ g), Sp-1: transfection of Sp-1 consensus DNA (10 μ g), NF-1: transfection of NF-1 consensus DNA (10 μ g). For the cells transfected with pCOLH₁0.27, transfection of consensus recognition DNA for Ap-1, Sp-1 or NF-1 was performed 24 h after initial transfection. Reporter gene CAT was determined with ELISA after another 24 h. Relative CAT values in different transfection groups were calculated relative to that in mock DNA transfection. The

result represented three independent experiments. ^a $P < 0.05$ compared to control.

EMSA

The fragment spanning -268 to +42 bp in human $\alpha 1$ (I) procollagen gene was digested into three smaller ones (42 bp, 113 bp, 155 bp) with *EcoRII* (Figure 3). EMSA with these three labeled oligonucleotides mixture as probes showed that DNA-protein complexes were generated and detected in form of retardation bands. Competition with molar excesses of the same unlabeled probe prevented the formation of DNA-protein complexes, suggesting the specificity of the binding between DNA and protein. Excess consensus DNA for Sp-1, Ap-1 or NF-1 partially inhibited the occurrence of retardation differently, indicating the potential binding sites for Sp-1, Ap-1 and NF-1 in -268 to +42 bp of human $\alpha 1$ (I) procollagen gene (Figure 4).

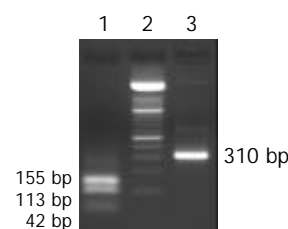


Figure 3 Electrophoresis (20 g/L agarose gel) of the fragment -268 to +42 bp digested with *EcoRII*. Lane1: *EcoRII*-digested fragment, Lane2: 100 bp DNA ladder, Lane3: 310 bp length of fragment spanning from -268 to +42bp. The 310 bp fragment spanning -268 to +42 bp of the human $\alpha 1$ (I) procollagen gene was obtained by PCR with p5.3K α 1 as template. The fragment was digested with *EcoRII*. Electrophoresis (20 g/L agarose gel) of the digested mixture showed 3 bands with different sizes (42 bp, 113 bp, 155 bp) which were labeled and used as probes in EMSA.

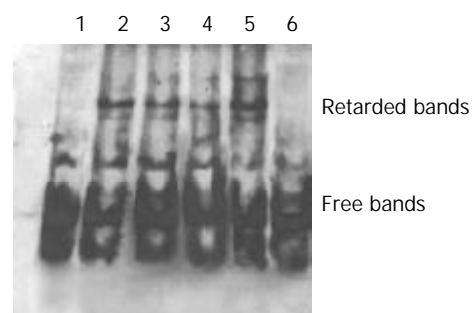


Figure 4 Result of EMSA with *EcoRII*-digested -268 to +42 bp as probe. Lane1: Labeled DNA, Lane2: Labeled DNA+ nuclear protein +NF-1 consensus DNA, Lane3: Labeled DNA + nuclear protein + Sp-1 consensus DNA, Lane4: Labeled DNA + nuclear protein + Ap-1 consensus DNA, Lane 5: Labeled DNA + nuclear protein, Lane 6: Labeled DNA + excess unlabeled DNA + nuclear protein. The existence of several retarded bands in EMSA indicated that there were several nuclear protein binding sites in sequence -268 to +42 bp (lane 5). No retardation occurred when excess unlabeled DNA probe was added to the DNA-protein reaction, confirming the specificity of the retardation (lane 6). Consensus DNAs for Sp1, Ap-1 and NF-1 were among the possible regulatory elements since the molar excess of the consensus unlabeled probe (Sp1, Ap-1, NF-1) inhibited partially the formation of retardation bands differently (lanes 2,3 and 4).

Effect of cytokines on reporter gene activity

TNF α , IFN α and IFN γ inhibited the reporter gene activity by 40-60% in the cells transfected with pCOLH₁2.5 ($P < 0.05$) compared to the control. The strongest inhibitory effect appeared in TNF α group (Table 2).

Table 2 Effect of cytokines on reporter gene activity in cells transfected with pCOLH_{2.5}

Cytokines	Relative value of reporter gene activity ¹	P Value (compared to control)
Control	1.00±0.15	
TNFα 10 μg/L	0.43±0.17	<0.05
IFNα 1×10 ⁵ U/L	0.62±0.15	<0.05
IFNγ 1×10 ⁵ U/L	0.60±0.16	<0.05

¹The reporter gene activity of the cells transfected with pCOLH_{2.5} was set as 1, the relative expression level of normalized CAT in transfected cells treated with cytokines was expressed as mean±SD of three independent experiments.

DISCUSSION

The mechanisms involved in the regulation of collagen production under fibrotic conditions are not yet completely understood. The synthesis of collagen might be modulated transcriptionally and post-transcriptionally, similar to the regulation of most of the other proteins in eukaryotic cells. Evidence suggests that the stability of newly synthesized mRNA as well as some enzymes devoted to collagen synthesis and degradation may play important roles in excessive accumulation of collagen in tissues^[18]. Recently, studies focused on transcriptional regulation revealed that there existed several important cis-acting elements in the upstream region of human or rodent type I procollagen genes^[8-11,19]. Activation of type I collagen gene was regarded to be related to the MAP kinase cascade pathway^[6,20]. Newly identified tissue specific transcription factors for transcription of collagen genes have been increasing^[21-26]. Some responsive elements of cytokines, including TGFβ1, TNFα and IFNγ have been reported to be located in procollagen genes^[7,27-29]. In previous work, we analyzed the promoter activity from mouse α2(I) procollagen gene as well as its modulation by cytokines and retinoic acid^[12,13,30]. Sequence spanning from -348 bp to +54 bp in mouse α2(I) procollagen was found to be of the highest promoter activity and partial cell specificity. The activity was influenced by TGFβ, TNFα and IFNs. In order to elucidate the transcriptional regulation of type I collagen in humans, especially the cis-acting elements and consensus transcription factors involved, six recombinant plasmids containing serial 5'-deleted flanking sequences of α1(I) procollagen gene as putative promoter were constructed here. Transient transfection of these constructions into human dermal fibroblasts showed that the sequences spanning from -2 483 bp to +42 bp and from -268 to +42 bp could drive the reporter gene with higher activity, while -105 to +42 bp had lower activity, indicating that there might be some positive and negative elements in the 2.5 kb flanking region. Our result was in agreement partially with that of Jimenez *et al.* though the fine mapping was different because of different constructs and host cells used^[14]. Further deduction from the ranked driving activity of the putative promoter suggests that positive elements may be localized at -2 483 to 1 448 bp, -1 448 to 829 bp, -829 to -498 bp, -268 to -105 bp and negative ones at -498 to 268 bp, -105 to +42 bp. Computer-based prediction (DNAssist 1.0) of this 2.5 kb flanking sequence revealed that there might be 5 binding sites for *Sp-1* (-123 bp, -1 615 bp, -1 628 bp, -2 170 bp, -2 176 bp), 1 for *NFκB* (-1 571 bp), 2 for *c-myc* (-1 118 bp, -2 406 bp), 2 for *Ap-1* (-103 bp, -1 985 bp), 1 for *NF-1* (-101 bp). Obviously, one site for *NF-1* (-101 bp), *Ap-1* (-103 bp) and *Sp-1* (-123 bp) might be located in -268+42 bp.

To further characterize the existence of Ap-1, Sp-1, and NF-1 as potential transcription factors transactivating α1(I) procollagen gene, we studied the DNA-binding capacity of sequence -268+42 bp, which showed a higher promoter activity

in transfection experiment with modified EMSA. Restriction enzyme *EcoR* II cut the target sequence into 3 smaller fragments with different sizes, *i.e.* -268 to -227 bp (42 bp), -226 to 114 bp (113 bp), and -113 to +42 bp (155 bp). The digested fragments were end-labeled with digoxigenin and used as probes in DNA-protein binding reaction (see details in MATERIALS AND METHODS). DNA-protein complexes were shown in form of DNA bands with low mobility. The existence of several retarded bands in EMSA indicates there are several nuclear protein binding sites in sequence -268 to +42 bp. No retardation could be found if excess unlabeled DNA probe was added to the DNA-protein reaction, confirming the specificity of the retardation. Consensus DNAs for Sp1, Ap-1 and NF-1 were among the possible regulatory elements since the molar excess of the consensus unlabeled probe (*Sp1*, *Ap-1*, *NF-1*) partially inhibited the formation of retardation bands differently (Figure 4).

In order to confirm the potential binding sites and their transcriptional regulatory effects on -268 to +42 bp flanking sequence, a set of competitors in forms of double stranded DNA consensus to Ap-1, Sp-1 and NF-1 were transfected to cells 24 h after pCOLH_{2.5} transfection. The competitive inhibitory effects were found in *Ap-1* (25%) and *Sp-1* (20%), indicating the positive effects of the sequences on *Ap-1* and *Sp-1* in -268 to +42 bp. The transfected sequence for *Ap-1* or *Sp-1* thus decreased -268 to +42 bp activity as promoter due to competition for binding of nuclear protein. The results were similar to those reported by Sugiura and Inagaki *et al.* who showed that some cytokines or calcium channel blockers could modulate the expression of collagen via Ap-1 and Sp-1^[9,31]. The anticipated inhibitory effect of *NF-1* competitor has not been found due to unknown reasons. No effect of *NF-1* on basal transcription or the weak effect of *NF-1* beyond detection limit might be the explanation.

The Sp1 is a ubiquitously expressed zinc-finger transcription factor recognizing GC rich sequence that is widely distributed in the promoters of various genes and is thought to be a target of intracellular signaling^[32]. It is regarded that Sp1 plays an important role in both basal and inducible regulation of type I collagen expression, and may be implicated in the increased production of collagen during the development of pathological fibrosis^[9]. Ap-1 consists of either Jun homodimers or Fos/Jun heterodimeric complexes which bind the palindromic TRE sequence TGA(C/G)TGA. Ap-1 is subjected to regulation by both phosphorylation and chemical oxidation of specific cysteine residues mapping within the DNA binding domains^[33]. In this study transfection of Ap-1 and Sp-1 oligonucleotides to pCOLH_{2.5} 0.27 transfected cells inhibited the promoter activity of -268 to +42 bp, suggesting that Ap-1 and Sp-1 sites are important for the basal promoter activity of the α1(I) procollagen gene besides mediating the response of cytokines and chemicals^[31-34]. Increased promoter activity of procollagen α2(I) induced by TGFβ1 or acetaldehyde is mediated through NF-1. The existence of NF-1 in -268 to +42 bp of human α1(I) gene has been shown by our competitive EMSA. Transfection of consensus DNA for NF-1 failed to inhibit the promoter activity of -268 bp to +42 bp in our experiment. The possible reason might be due to no or weak effect of NF-1 and thus its weak competition for the basal promoter activity.

The antifibrotic capacity of TNFα and IFNs has been reconfirmed in our study and their transcriptional regulation on collagen promoter definitely play a role in their anti-collagen production effect.

In conclusion, we find that sequences spanning from -2 483 bp to +42 bp and -268 to +42 bp in 5'-flanking region from α1(I) procollagen gene are highly active as promoters. The inhibitory cytokines including TNFα and IFNs downregulate collagen production via at least partially transcriptional regulation. The promoter activity of -268 bp to +42 bp shows

that binding sites for Sp-1, Ap-1 and NF-1 are existing candidate cis-element for transcriptional regulation in sequence -268 to +42 bp. Binding sites for Sp-1, Ap-1 are positive for basal transcription since transfections of their competitor oligo DNAs decrease the promoter activity of sequence -268 to +42 bp. Thus, transfection of competitor DNAs is applied for the first time to confirm that the sites for Sp-1 and Ap-1 are important for basal highly promoter activity. Competitors for the high active binding sites for transcription factors may be novel and promising tools for fibrotic blockade.

ACKNOWLEDGMENTS

We are especially grateful for the critical reading of the manuscript by Professor A.M. Gressner and Dr. Weiskirchen. We thank Dr. Sergio A. Jimenez for generously providing plasmid p5.3K $\alpha 1$.

REFERENCES

- Friedman SL.** Seminars in medicine of the Beth Israel Hospital, Boston. The cellular basis of hepatic fibrosis. Mechanisms and treatment strategies. *N Engl J Med* 1993; **328**: 1828-1835
- Slack JL, Liska DJ, Bornstein P.** Regulation of expression of the type I collagen genes. *Am J Med Genet* 1993; **45**: 140-151
- Rockey DC, Chung JJ.** Interferon gamma inhibits lipocyte activation and extracellular matrix mRNA expression during experimental liver injury: implications for treatment of hepatic fibrosis. *J Investig Med* 1994; **42**: 660-670
- Inagaki Y, Nemoto T, Kushida M, Sheng Y, Higashi K, Ikeda K, Kawada N, Shirasaki F, Takehara K, Sugiyama K, Fujii M, Yamauchi H, Nakao A, de Crombrughe B, Watanabe T, Okazaki I.** Interferon alfa down-regulates collagen gene transcription and suppresses experimental hepatic fibrosis in mice. *Hepatology* 2003; **38**: 890-899
- Buttner C, Skupin A, Rieber EP.** Transcriptional activation of the type I collagen genes COL1A1 and COL1A2 in fibroblasts by interleukin-4: analysis of the functional collagen promoter sequences. *J Cell Physiol* 2004; **198**: 248-258
- Papakrivopoulou J, Lindahl GE, Bishop JE, Laurent GJ.** Differential roles of extracellular signal-regulated kinase 1/2 and p38 (MAPK) in mechanical load-induced procollagen alpha(1)(I) gene expression in cardiac fibroblasts. *Cardiovasc Res* 2004; **61**: 736-744
- Kubota K, Okazaki J, Louie O, Kent KC, Liu B.** TGF-beta stimulates collagen (I) in vascular smooth muscle cells via a short element in the proximal collagen promoter. *J Surg Res* 2003; **109**: 43-50
- Ratzliff V, Lalazar A, Wong L, Dang Q, Collins C, Shaulian E, Jensen S, Friedman SL.** Zf9, a Kruppel-like transcription factor up-regulated *in vivo* during early hepatic fibrosis. *Proc Natl Acad Sci U S A* 1998; **95**: 9500-9505
- Chen SJ, Artlett CM, Jimenez SA, Varga J.** Modulation of human alpha1(I) procollagen gene activity by interaction with Sp1 and Sp3 transcription factors *in vitro*. *Gene* 1998; **215**: 101-110
- Rippe RA, Schrum LW, Stefanovic B, Solis-Herruzo JA, Brenner DA.** NF-kappaB inhibits expression of the alpha1(I) collagen gene. *DNA Cell Biol* 1999; **18**: 751-761
- Bergeron C, Page N, Joubert P, Barbeau B, Hamid Q, Chakir J.** Regulation of procollagen I (alpha1) by interleukin-4 in human bronchial fibroblasts: a possible role in airway remodelling in asthma. *Clin Exp Allergy* 2003; **33**: 1389-1397
- Gao CF, Wang H, Huang C, Kong XT.** Study of activity of promoter from mouse $\alpha 2(I)$ procollagen gene. *Chin Med J* 1999; **112**: 316-320
- Gao CF, Wang H, Wu YA, Kong XT.** The effect of cytokines on promoter activity in mouse $\alpha 2(I)$ procollagen gene. *J Med Coll PLA* 1999; **14**: 12-16
- Jimenez SA, Varga J, Olsen A, Li L, Diaz A, Herhal J, Koch J.** Functional analysis of human alpha 1(I) procollagen gene promoter. Differential activity in collagen-producing and -nonproducing cells and response to transforming growth factor beta 1. *J Biol Chem* 1994; **269**: 12684-12691
- Bradford MM.** A rapid and sensitive method for the quantitation of microgram quantities of protein utilizing the principle of protein-dye binding. *Anal Biochem* 1976; **72**: 248-254
- Gao CF, Wang H, Gao GH, Mi QM, Kong XT.** Nonisotopic analysis of sequence specific DNA-binding proteins. *Shijie Huaren Xiaohua Zazhi* 2001; **9**: 499-503
- Erdos G, Lee YJ, Cho JM, Corry PM.** Heat-induced bFGF gene expression in the absence of heat shock element correlates with enhanced AP-1 binding activity. *J Cell Physiol* 1995; **164**: 404-413
- Yata Y, Takahara T, Furui K, Zhang LP, Jin B, Watanabe A.** Spatial distribution of tissue inhibitor of metalloproteinase-1 mRNA in chronic liver disease. *J Hepatol* 1999; **30**: 425-432
- Lindahl GE, Chambers RC, Papakrivopoulou J, Dawson SJ, Jacobsen MC, Bishop JE, Laurent GJ.** Activation of fibroblast procollagen alpha 1(I) transcription by mechanical strain is transforming growth factor-beta-dependent and involves increased binding of CCAAT-binding factor (CBF/NF-Y) at the proximal promoter. *J Biol Chem* 2002; **277**: 6153-6161
- Tharaux PL, Chatziantoniou C, Fakhouri F, Dussault JC.** Angiotensin II activates collagen I gene through a mechanism involving the MAP/ER kinase pathway. *Hypertension* 2000; **36**: 330-336
- Tanaka K, Matsumoto Y, Nakatani F, Iwamoto Y, Yamada Y.** A zinc finger transcription factor, alphaA-crystallin binding protein 1, is a negative regulator of the chondrocyte-specific enhancer of the alpha1(II) collagen gene. *Mol Cell Biol* 2000; **20**: 4428-4435
- Hasegawa T, Takeuchi A, Miyaishi O, Xiao H, Mao J, Isobe K.** PTRF (polymerase I and transcript-release factor) is tissue-specific and interacts with the BFCOL1 (binding factor of a type-I collagen promoter) zinc-finger transcription factor which binds to the two mouse type-I collagen gene promoters. *Biochem J* 2000; **347**(Pt 1): 55-59
- Zhao MK, Pretorius PJ, de Vries WN.** Characterization of a novel transcription factor binding to the regulatory regions of the human pro-alpha1(I) collagen gene. *Arch Biochem Biophys* 2000; **376**: 281-287
- Kanamaru Y, Nakao A, Tanaka Y, Inagaki Y, Ushio H, Shirato I, Horikoshi S, Okumura K, Ogawa H, Tomino Y.** Involvement of p300 in TGF-beta/Smad-pathway-mediated alpha2(I) collagen expression in mouse mesangial cells. *Nephron Exp Nephrol* 2003; **95**: e36-42
- Chen A, Davis BH.** The DNA binding protein BTEB mediates acetaldehyde-induced, jun N-terminal kinase-dependent alpha1(I) collagen gene expression in rat hepatic stellate cells. *Mol Cell Biol* 2000; **20**: 2818-2826
- Drissi MH, Li X, Sheu TJ, Zuscik MJ, Schwarz EM, Puzas JE, Rosier RN, O'Keefe RJ.** Runx2/Cbfa1 stimulation by retinoic acid is potentiated by BMP2 signaling through interaction with Smad1 on the collagen X promoter in chondrocytes. *J Cell Biochem* 2003; **90**: 1287-1298
- Falanga V, Zhou L, Yufit T.** Low oxygen tension stimulates collagen synthesis and COL1A1 transcription through the action of TGF-beta1. *J Cell Physiol* 2002; **191**: 42-50
- Kinbara T, Shirasaki F, Kawara S, Inagaki Y, de Crombrughe B, Takehara K.** Transforming growth factor-beta isoforms differently stimulate proalpha2(I) collagen gene expression during wound healing process in transgenic mice. *J Cell Physiol* 2002; **190**: 375-381
- Inagaki Y, Truter S, Tanaka S, Di Liberto M, Ramirez F.** Overlapping pathways mediate the opposing actions of tumor necrosis factor-alpha and transforming growth factor-beta on alpha 2(I) collagen gene transcription. *J Biol Chem* 1995; **270**: 3353-3358
- Gao CF, Wang H, Kong XT.** IFN effect on promoter activity in mouse $\alpha 2(I)$ procollagen gene. *Shijie Huaren Xiaohua Zazhi* 1998; **6**: 201-203
- Sugiura T, Imai E, Moriyama T, Horio M, Hori M.** Calcium channel blockers inhibit proliferation and matrix production in rat mesangial cells: possible mechanism of suppression of AP-1 and CREB activities. *Nephron* 2000; **85**: 71-80
- Ghayor C, Chadichristos C, Herrouin JF, Ala-Kokko L, Suske G, Pujol JP, Galera P.** Sp3 represses the Sp1-mediated transactivation of the human COL2A1 gene in primary and de-differentiated chondrocytes. *J Biol Chem* 2001; **276**: 36881-36895
- Chung KY, Agarwal A, Uitto J, Mauviel A.** An AP-1 binding sequence is essential for regulation of the human alpha2(I) collagen (COL1A2) promoter activity by transforming growth factor-beta. *J Biol Chem* 1996; **271**: 3272-3278
- Greenwel P, Inagaki Y, Hu W, Walsh M, Ramirez F.** Sp1 is required for the early response of alpha2(I) collagen to transforming growth factor-beta1. *J Biol Chem* 1997; **272**: 19738-19745

***In vitro* cultivation of human fetal pancreatic ductal stem cells and their differentiation into insulin-producing cells**

Zhong-Xiang Yao, Mao-Lin Qin, Jian-Jun Liu, Xing-Shu Chen, De-Shan Zhou

Zhong-Xiang Yao, Mao-Lin Qin, Jian-Jun Liu, Xing-Shu Chen, De-Shan Zhou, Department of Histology and Embryology, The Third Military Medical University, Chongqing 400038, China

Supported by the National Natural Science Foundation of China, No. 30370164 and Tenth-five-year Foundation of PLA, No.01J013

Correspondence to: Dr. De-Shan Zhou and Dr. Zhong-Xiang Yao, Department of Histology and Embryology, The Third Military Medical University, Chongqing 400038, China. yaozhx@mail.tmmu.com.cn
Telephone: +86-23-68752231

Received: 2003-12-23 **Accepted:** 2004-01-08

Abstract

AIM: To isolate, culture and identify the human fetal pancreatic ductal stem cells *in vitro*, and to observe the potency of these multipotential cells differentiation into insulin-producing cells.

METHODS: The human fetal pancreas was digested by 1 g/L collagenase type IV and then 2.5 g/L trypsin was used to isolate the pancreatic ductal stem cells, followed by culture in serum-free, glucose-free DMEM media with some additional chemical substrates *in vitro* (according to the different stage). The cells were induced by glucose-free (control), 5 mmol/L, 17.8 mmol/L and 25 mmol/L glucose, respectively. The cell types of differentiated cells were identified using immunocytochemical staining.

RESULTS: The shape of human fetal pancreatic ductal stem cells cultured *in vitro* was firstly fusiform in the first 2 wk, and became monolayer and cobblestone pattern after another 3 to 4 wk. After induced and differentiated by the glucose of different concentrations for another 1 to 2 wk, the cells formed the pancreatic islet-like structures. The identification and potency of these cells were then identified by using the pancreatic ductal stem cell marker, cytokeratin-19 (CK-19), pancreatic β cell marker, insulin and pancreatic α cell marker, glucagons with immunocytochemical staining. At the end of the second week, 95.2% of the cells were positive for CK-19 immunoreactivity. Up to 22.7% of the cells induced by glucose were positive for insulin immunoreactivity, and less than 3.8% of the cells were positive for glucagon immunoreactivity in pancreatic islet-like structures. The positive ratio of immunoreactive staining was dependent on the concentration of glucose, and it was observed that the 17.8 mmol/L glucose stimulated effectively to produce insulin- and glucagons-producing cells.

CONCLUSION: The human fetal pancreatic ductal stem cells are capable of proliferation *in vitro*. These cells have multidifferentiation potential and can be induced by glucose and differentiated into insulin-producing cells *in vitro*.

Yao ZX, Qin ML, Liu JJ, Chen XS, Zhou DS. *In vitro* cultivation of human fetal pancreatic ductal stem cells and their differentiation into insulin-producing cells. *World J Gastroenterol* 2004; 10(10): 1452-1456

<http://www.wjgnet.com/1007-9327/10/1452.asp>

INTRODUCTION

Even 20 years ago, the accepted concept was that one was born with all the pancreatic β cells one ever had^[1]. However, now the concept that the pancreatic ductal stem cells exist and can differentiate into pancreatic endocrine cells are generally accepted^[2-7]. When the inability of the β cells to match the increased demand for insulin can be seen, diabetes occurs. One of the main obstacles to successful islet transplantation for diabetes is the limitation of available insulin-producing tissue^[8]. The lack of pancreatic insulin-producing tissue has given a high priority to efforts to stimulate the growth of pancreatic insulin-producing cells^[9-10].

It has been reported that the embryonic stem (ES) cells induce to generate cells expressing insulin and other pancreatic endocrine hormones^[11-15]. The cells self-assembled to form three-dimensional clusters similar in topology to normal pancreatic islets where pancreatic cell types were in close association with neurons. Glucose triggered insulin release from these cell clusters by mechanisms similar to those employed *in vivo*. When injected into diabetic mice, the insulin-producing cells underwent rapid vascularization and maintained a clustered, islet-like organization. Their use might lead to many clinical benefits but it was difficult that the differentiated cells derived from the ES cells were used to assemble functional organs^[10,16-21]. It was also shown that the duct tissue from adult human pancreas could be expanded in culture and then was directed to differentiate into glucose responsive islet-like tissue *in vitro*, but the quantities were limited, the amount would be expected to have little clinical impact^[22].

Herein we show it is easier to cultivate human fetal pancreatic ductal stem cells than adult human pancreatic ductal stem cells *in vitro* and the ductal stem cells can be induced by glucose and differentiate to insulin-producing cells.

MATERIALS AND METHODS

Specimens

The specimens ($n=5$) were collected from the Southwest Hospital of the Third Military Medical University. The samples were taken from the spontaneous abortion fetus of the embryonic age 8 stage (about 16-20 wk) of fetus according to the methods of Jirasek^[23].

Cell culture

Human fetal pancreas was digested in 1 g/L type IV collagenase for 40 min at 37 °C, naturally deposited for 10 min, the supernatant was removed. The cells were then digested in 2.5 g/L trypsin for 30 min at 37 °C, followed by centrifugation for 10 min at 1 000 r/min. The deposited cells were put into glucose-free DMEM culture medium containing 2 \times non-essential amino acid (NEAA), 1 \times B27, 100 U/mL penicillin, and 100 μ g/mL streptomycin. The cell suspensions were put into non-treated T-75 flasks having non-sticky glass coverslips inside and incubated at 37 °C in a humidified atmosphere containing 50 mL/L CO₂ in air. After 24 h the nonadherent tissue (both viable and dead) was removed, followed by the media change with additional keratinocyte growth factor (KGF, 10 ng/mL, F. Hoffmann-La

Roche Ltd, Basel, Switzerland), insulin-transferrin-selenium (ITS, 1 g/L, Sigma-Aldrich China Inc. Shanghai, China), and 2 g/mL BSA, 10 mmol/L nicotinamide (F. Hoffmann-La Roche Ltd, Basel, Switzerland). The adherent or residual cells were continuously cultured and expanded for 5-7 wk by changing the medium every 3 d. The cells were used for identification by immunostaining and further differentiation.

Cell induction and differentiation

For inducing the cells differentiation, the media with or without glucose were subdivided into 4 groups: glucose-free (control), 5 mmol/L, 17.8 mmol/L and 25 mmol/L glucose. Other elements of the media were the same as mentioned above.

Tissue fixation and immunocytochemical staining

Monolayer cells were fixed for 30 min in 40 g/L polyformaldehyde (PFA, in 0.1 mol/L phosphate buffer, pH 7.2), and then rinsed in 0.01 mol/L phosphate buffer saline (PBS, pH 7.2). The specimens were incubated with 30 mL/L H_2O_2 in pure methanol for 30 min at room temperature, followed by retrieval 3 times (1 min each time) on a microwave (750 W) in 0.1 mol/L pH 6.0 citrate buffer, and incubation with 10 g/L BSA plus 4 g/L Triton X-100 at 37 °C for 30 min. Then immunocytochemical staining was carried out by using primary antibodies of different species: monoclonal mouse anti-human cytokeratin 19 IgG1 antibody (1:100, Santa Cruz Biotechnology, Inc. California, United States of American), polyclonal rabbit anti-human insulin antibody (H-86, 1:200, Santa Cruz Biotechnology, Inc. California, United States of American), polyclonal goat anti-human glucagons IgG antibody (C-18, 1:100, Santa Cruz Biotechnology, Inc. California, United States of American). Horseradish peroxidase-labeled secondary antibody (Sigma-Aldrich China Inc. Shanghai, China) was detected by reaction with 30 mL/L H_2O_2 and 1 g/L 3, 3'-diaminobenzidine (DAB, Sigma) in solution at room temperature for 5 min, then the specimens were washed and dehydrated in a graded series by ethanol. Finally, the coverslips were mounted cell-side down on glass slides with a drop of DPX and then examined using an Olympus light microscope. Photographs were taken on Lekai-135 film. Positive cells were randomly counted on the montage of photographs generated.

RESULTS

Isolation, cultures and identification of human fetus pancreatic ductal stem cells

To promote the attachment of duct cells rather than islet cells, nonsticky culture flasks were used; these flasks had been used to maintain islets in suspension. The clumps of nonislet tissue could adhere to this nonsticky surface starting about 24 h after culture (Figure 1). Although there was considerable loss of floating tissue of pancreatic acinar tissue in culture, the quantity of cell clumps adhered increased with time. The nonadherent clumps were removed by changing the culture media. In the beginning, the adherent cells were seldom and fusiform. After the nonadherent clumps were removed, the media was changed by serum-free media with additional keratinocyte growth factor to stimulate the growth of only pancreatic ductal stem cells but not the growth of fibroblasts. The cells grew very slowly in the first 2 wk (Figure 2) and 95.2% (975/1024) of the cells were positive for CK-19 immunoreactivity (Figure 3). With additional time of 3 to 4 wk, the cells grew from the adherent clumps and formed monolayer with clear epithelial morphology. The cells were large, cobblestone patterns (Figures 4 and 5). There was a significant increase of the cultured tissue during the 5-6 wk of culture.

Differentiation of pancreatic ductal stem cells into insulin-producing cells

Once the clumps were attached and formed monolayers, the

media were changed by adding glucose in different concentration of 0, 5, 17.8 and 25 mmol/L, respectively. Over next 1-2 wk the plaques of epithelial cells became crowded, and formed a few pancreatic islet-like structures (Figure 6). Some of the cells in pancreatic islet-like structures were positive for insulin immunoreactivity (Figure 7), and a few cells were positive for glucagon immunoreactivity (Figure 8).

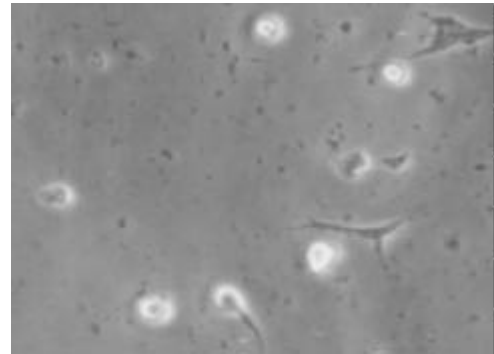


Figure 1 After being cultured for 24 h, a few cells were adhered on the bottom of non-sticky flasks, some of the cells processed protrusions ($\times 100$).

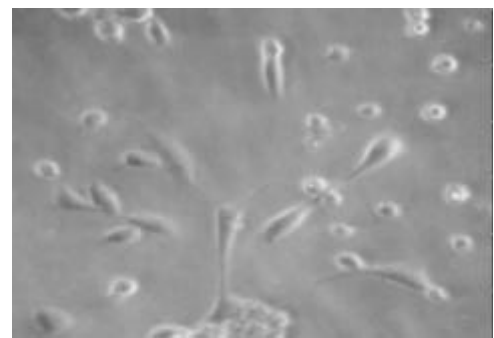


Figure 2 After being cultured for 2 wk in the media added the keratinocyte growth factor, the number of cells increased, the cells became fusiform with a few processes ($\times 100$).

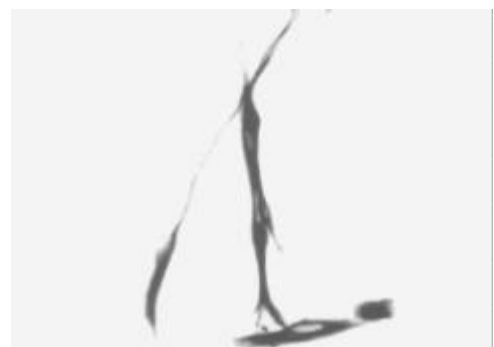


Figure 3 Most cells of culture were positive for CK-19 immunoreactivity after being cultured for 2 wk ($\times 100$).

The stainings in immunopositive cells were located in the cytoplasm, but the immunonegative cells also revealed light stainings in the perinuclear region similar to those in control group. The intensity of the immunostaining varied from one cell to another. The shape of the positive cells also varied; most of the cells were polygonal in shape, but spherical or fusiform cells were also observed. The nucleus was unstained, and some cells seemed to have 2 nuclei. Analysis of the cells from randomly generated micrographs of 25 cultured coverslips revealed different percentages of the cells immunoreactivity

for CK-19, insulin and glucagons after the cells were induced by different concentration of glucose for 1-2 wk.

After induction for 2 wk with different concentrations of glucose, the numbers of positive cells for insulin and glucagon were different. The cells were CK-19 immunonegative, while the insulin immunopositive cells were obviously increased. When the concentration of glucose was 17.8 mmol/L, the ratio of insulin positive cells reached a very high level. In the media without glucose, 108 cells of total counting 1 325 (8.2%) were positive for insulin immunostaining, and 15 cells of total counting 1 187 (1.3%) were positive for glucagons immunostaining. When the concentration of glucose reached 5 mmol/L, the number of insulin-positive cells was 153 of total counting 1 142 (13.4%), while the number of glucagons-positive cells was 19 of total counting 1 092 (1.7%). In the medium containing 17.8 mmol/L glucose, 230 insulin-positive cells of total counting 1 079 (21.3%) and 40 glucagon-positive cells of total counting 1 046 (3.8%) were observed. When the concentration of glucose was 25 mmol/L, the insulin-positive cells were 255 of total counting 1 125 (22.7%) and the glucagons-positive cells were 39 of total counting 1 127 (3.5%) (Figure 9).

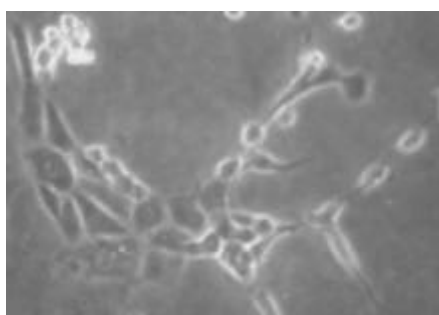


Figure 4 The cells were cobblestone pattern after being cultured for 4 wk ($\times 150$).

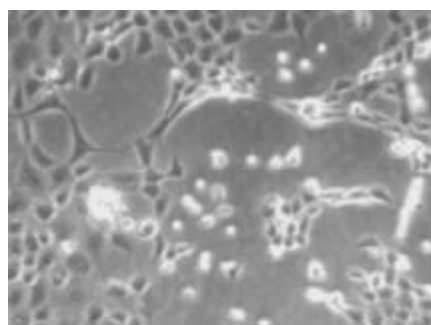


Figure 5 The cells were cobblestone pattern and formed monolayer after being cultured for 6 wk ($\times 100$).

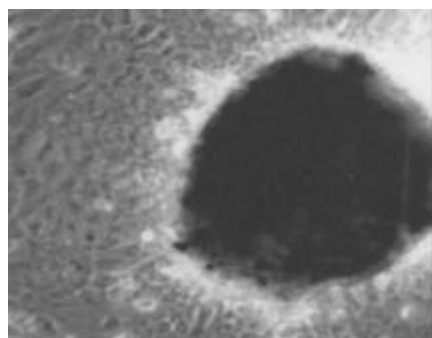


Figure 6 The cells were induced to form pancreatic islet-like structures after being cultured in the media containing 17.8 mmol/L glucose for 1 wk ($\times 100$).

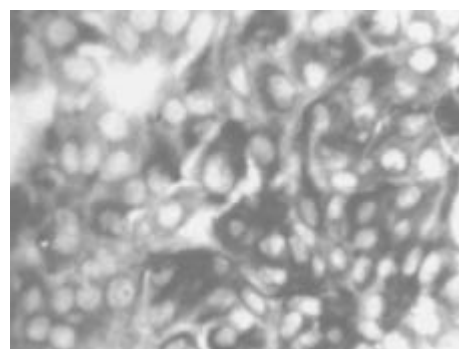


Figure 7 After being cultured in the medium containing 17.8 mmol/L glucose for 1 wk, many cells in islet-like structures were positive for insulin immunoreactivity ($\times 150$).

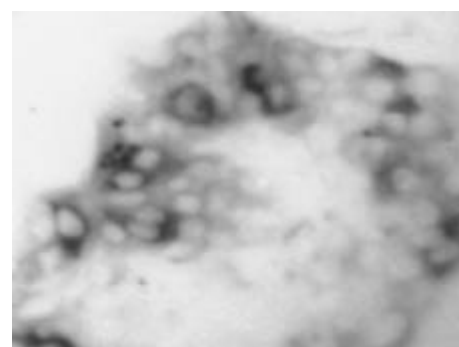


Figure 8 After being cultured in the medium containing 17 mmol/L glucose for 1 wk, a few cells in islet-like structures were positive for glucagon immunoreactivity ($\times 150$).

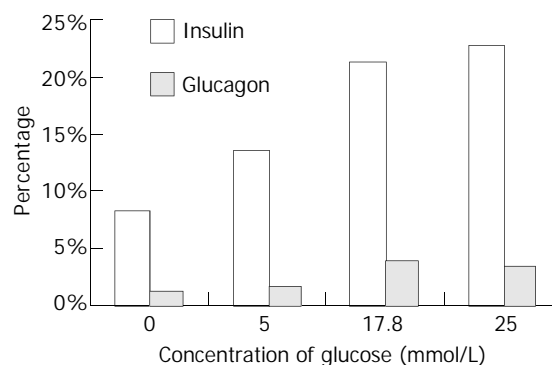


Figure 9 Percentage of immunopositive cells induced by glucose.

DISCUSSION

In pancreas, insulin is produced and secreted by specialized structures, islets of Langerhans. Diabetes, which affects thousands of million people in the world, results from abnormal function of pancreatic islets. The main obstacle to successful islet transplantation for diabetes is the limitation of available insulin-producing tissue^[24]. Herein, we introduced to generate cells expressing insulin from human fetal pancreas duct tissue. This approach may provide a potential new source of pancreatic islet cells for transplantation.

Most studies have shown there is limited *in vitro* growth of adult islet cells of any species^[25]. From the studies on rat pancreatic regeneration, it inferred that the capacity of adult pancreatic duct cells were strongly to both expand and differentiate^[26]. Bonner-Weir *et al.* showed the expansion of adult human pancreatic ductal tissue *in vitro* and its subsequent differentiation to islet cells after being overlaid with Matrigel, and over 3-4 wk culture there was a significant increase in

insulin as well as formation of islet-like structures called cultivated human islet buds^[27]. These data further provided proofs for the hypothesis that pancreatic ductal cells have the potential to lose their specific ductal epithelial cell phenotype with rapid proliferation *in vitro*, reverting to multipotent stem cells that then can differentiate into islet cells with the appropriate external stimuli^[28]. But the report showed the amount limitation and associated with loss of insulin production^[27]. In order to avoid these problems, we made use of human fetal pancreas from the spontaneous abortion human fetus, combined 2-enzyme digestion with mechanical dissection of the pancreas. The duct tissue could be dissected effectively and the single cells were rich in stem cells. The cell proliferation could be extended for at least 6 wk. The glucose can stimulate the pancreatic ductal stem cells to differentiate into insulin-producing cells.

Now, human islet isolations can yield maximum 400 000-600 000 islets per donor, which means that more than one donor may be requested for a successful transplant. In our study reported here that the pancreatic ductal stem cells, after *in vitro* expansion and glucose-induced differentiation, became organized into islet-like structures consisting of insulin- and glucagons-producing cells. Their use may lead to many clinical benefits. Because the pancreatic islets rarely adhered directly to the nonsticky flasks, and the culture medium was changed at time, the culture conditions did not favor the islets inclusion. These data provide evidence of the potential to expand and differentiate human pancreatic ductal stem cells to islet cells *in vitro*, but further optimization of conditions is needed to generate yields of islet tissue that will make an impact on islet transplantation. We have been able to expand human pancreatic ductal stem cells and then to direct its differentiation into insulin- and glucagons-producing cells, respectively. The ability to cultivate human islets from digested pancreatic ductal stem cells opens a new approach for β cell replacement therapy.

The culture condition's optimization could include further expansion of the ductal tissue or higher efficiency in differentiating cells. Of the cells adhered in the beginning, the most cells were ductal stem cells, some were fibroblasts. But the culture medium without serum and with keratinocyte growth factor favored the growth of ductal stem cells. The data from rodents suggested that *in vitro* culture of exocrine tissue (the ducts and acini) would result in ductal epithelial cells. Moreover, mouse pancreatic exocrine (acinar and ductular) tissue gave rise to epithelial cultures that were indistinguishable from cultures of isolated duct, raising the possibility that acinar cells could dedifferentiate to form duct cells^[29,30]. It is entirely possible that the cells from the smaller ducts/acini have a little capacity to differentiate into endocrine cells^[27]. Other studies suggested that between 50-95% of the rodent exocrine cells died in the initial culture condition with mainly the ductal stem cells left to replenish the cultures^[31].

In our study, the adherent cells during the early culture period seemed to be pancreatic ductal stem cells. The culture conditions were serum-free, glucose-free but including keratinocyte growth factor, and these media stimulated the proliferation of ductal stem cells but not fibroblasts. The CK-19 positive cells that formed in fusiform and cobblestone pattern were characteristic of pancreatic ductal stem cells. In contrast, the insulin-producing cells were CK-19 immunonegative and insulin immunopositive. The glucose could induce the ductal stem cells differentiation into insulin-producing cells, and the ratio of positive cells is dependent on the concentration of glucose.

Our study differs from previous work in several ways. In most other study, the human islets were isolated and expanded on an extracellular matrix substrate, in which islets were easily mixed with the ductal stem cells^[27,32,33]. With expansion as monolayers and culture in three-dimensional collagen gels,

human islets gradually lost endocrine phenotype^[27]. In the study of Bonner-Weir, mainly ductal tissue remaining after islet isolation was expanded and then coated with extracellular matrix to induce differentiation into islet cells^[27]. The potential of extracellular matrix to induce differentiation has been shown for other epithelial cell types. In the present study, we selected different concentration of glucose as the inducing element, which effectively induced the fetal ductal stem cells differentiation.

The expansion of duct tissue is effective and extensive, probably because of the removal of normal intercellular restraints found. Because the default pathway of differentiation of embryonic pancreas is thought to be that of islet formation, such restraint might be protective and necessary to prevent excessive islet formation that could produce too much insulin and even hypoglycemia^[29,30]. In the present experiment, we are able to generate new islet cells from duct stem cells, but the quantities are limited. Despite the limitations at this early stage, these findings raise the tantalizing possibility that this approach, once optimized, may generate meaningful amounts of new human insulin-producing cells from duct stem cells. This possibility has important implications for making β cell replacement therapy available to a larger number of patients with type 1 and 2 diabetes mellitus.

REFERENCES

- 1 **Bonner-Weir S.** Perspective: Postnatal pancreatic beta cell growth. *Endocrinology* 2000; **141**: 1926-1929
- 2 **Bonner-Weir S, Sharma A.** Pancreatic stem cells. *J Pathol* 2002; **197**: 519-526
- 3 **Lechner A, Habener JF.** Stem/progenitor cells derived from adult tissues: potential for the treatment of diabetes mellitus. *Am J Physiol Endocrinol Metab* 2003; **284**: E259-266
- 4 **Peshavaria M, Pang K.** Manipulation of pancreatic stem cells for cell replacement therapy. *Diabetes Technol Ther* 2000; **2**: 453-460
- 5 **Ramiya VK, Maraist M, Arfors KE, Schatz DA, Peck AB, Cornelius JG.** Reversal of insulin-dependent diabetes using islets generated *in vitro* from pancreatic stem cells. *Nat Med* 2000; **6**: 278-282
- 6 **Berna G, Leon-Quinto T, Ensenat-Waser R, Montanya E, Martin F, Soria B.** Stem cells and diabetes. *Biomed Pharmacother* 2001; **55**: 206-212
- 7 **Pattou F, Kerr-Conte J, Gmyr V, Vandewalle B, Vantyghem MC, Lecomte-Houcke M, Proye C, Lefebvre J.** Human pancreatic stem cell and diabetes cell therapy. *Bull Acad Natl Med* 2000; **184**: 1887-1899
- 8 **Miyamoto M.** Current progress and perspectives in cell therapy for diabetes mellitus. *Hum Cell* 2001; **14**: 293-300
- 9 **Halvorsen T, Levine F.** Diabetes mellitus-cell transplantation and gene therapy approaches. *Curr Mol Med* 2001; **1**: 273-286
- 10 **Lumelsky N, Blondel O, Laeng P, Velasco I, Ravin R, McKay R.** Differentiation of embryonic stem cells to insulin-secreting structures similar to pancreatic islets. *Science* 2001; **292**: 1389-1394
- 11 **Kania G, Blyszczuk P, Czyz J, Navarrete-Santos A, Wobus AM.** Differentiation of mouse embryonic stem cells into pancreatic and hepatic cells. *Methods Enzymol* 2003; **365**: 287-303
- 12 **Kim D, Gu Y, Ishii M, Fujimiya M, Qi M, Nakamura N, Yoshikawa T, Sumi S, Inoue K.** *In vivo* functioning and transplantable mature pancreatic islet-like cell clusters differentiated from embryonic stem cell. *Pancreas* 2003; **27**: E34-41
- 13 **Kahan BW, Jacobson LM, Hullett DA, Ochoada JM, Oberley TD, Lang KM, Odorico JS.** Pancreatic precursors and differentiated islet cell types from murine embryonic stem cells: an *in vitro* model to study islet differentiation. *Diabetes* 2003; **52**: 2016-2024
- 14 **Blyszczuk P, Czyz J, Kania G, Wagner M, Roll U, St-Onge L, Wobus AM.** Expression of Pax4 in embryonic stem cells promotes differentiation of nestin-positive progenitor and insulin-producing cells. *Proc Natl Acad Sci U S A* 2003; **100**: 998-1003

- 15 **Shiroy A**, Yoshikawa M, Yokota H, Fukui H, Ishizaka S, Tatsumi K, Takahashi Y. Identification of insulin-producing cells derived from embryonic stem cells by zinc-chelating dithizone. *Stem Cells* 2002; **20**: 284-292
- 16 **Docherty K**. Growth and development of the islets of Langerhans: implications for the treatment of diabetes mellitus. *Curr Opin Pharmacol* 2001; **1**: 641-650
- 17 **Peck AB**, Cornelius JG, Chaudhari M, Shatz D, Ramiya VK. Use of *in vitro*-generated, stem cell-derived islets to cure type 1 diabetes: how close are we? *Ann N Y Acad Sci* 2002; **958**: 59-68
- 18 **Kaczorowski DJ**, Patterson ES, Jastromb WE, Shambloott MJ. Glucose-responsive insulin-producing cells from stem cells. *Diabetes Metab Res Rev* 2002; **18**: 442-450
- 19 **Soria B**. *In-vitro* differentiation of pancreatic beta-cells. *Differentiation* 2001; **68**: 205-219
- 20 **Assady S**, Maor G, Amit M, Itskovitz-Eldor J, Skorecki KL, Tzukerman M. Insulin production by human embryonic stem cells. *Diabetes* 2001; **50**: 1691-1697
- 21 **Soria B**, Skoudy A, Martin F. From stem cells to beta cells: new strategies in cell therapy of diabetes mellitus. *Diabetologia* 2001; **44**: 407-415
- 22 **Peck AB**, Chaudhari M, Cornelius JG, Ramiya VK. Pancreatic stem cells: building blocks for a better surrogate islet to treat type 1 diabetes. *Ann Med* 2001; **33**: 186-192
- 23 **Jirasek JE**. Developmental stages of human embryos. *Czech Med* 1978; **1**: 156-161
- 24 **Path G**, Seufert J. Current status and perspectives of stem cell therapy for the treatment of diabetes mellitus. *Med Klin* 2003; **98**: 277-282
- 25 **Hayek A**, Beattie GM. Alternatives to unmodified human islets for transplantation. *Curr Diab Rep* 2002; **2**: 371-376
- 26 **Yamaoka T**. Regeneration therapy of pancreatic beta cells: towards a cure for diabetes? *Biochem Biophys Res Commun* 2002; **296**: 1039-1043
- 27 **Bonner-Weir S**, Taneja M, Weir GC, Tatarkiewicz K, Song KH, Sharma A, O'Neil JJ. *In vitro* cultivation of human islets from expanded ductal tissue. *Proc Natl Acad Sci U S A* 2000; **97**: 7999-8004
- 28 **Bonner-Weir S**. Stem cells in diabetes: what has been achieved. *Horm Res* 2003; **60**(Suppl 3): 10-12
- 29 **Means AL**, Leach SD. Lineage commitment and cellular differentiation in exocrine pancreas. *Pancreatolgy* 2001; **1**: 587-596
- 30 **Humphrey RK**, Smith MS, Kwok J, Si Z, Tuch BE, Simpson AM. *In vitro* dedifferentiation of fetal porcine pancreatic tissue prior to transplantation as islet-like cell clusters. *Cells Tissues Organs* 2001; **168**: 158-169
- 31 **Logsdon CD**, Williams JA. Pancreatic acinar cells in monolayer culture: direct trophic effects of caerulein *in vitro*. *Am J Physiol* 1986; **250**(4 Pt 1): G440-447
- 32 **Beattie GM**, Itkin-Ansari P, Cirulli V, Leibowitz G, Lopez AD, Bossie S, Mally MI, Levine F, Hayek A. Sustained proliferation of PDX-1⁺ cells derived from human islets. *Diabetes* 1999; **48**: 1013-1019
- 33 **Yuan S**, Rosenberg L, Paraskevas S, Agapitos D, Duguid WP. Transdifferentiation of human islets to pancreatic ductal cells in collagen matrix culture. *Differentiation* 1996; **61**: 67-75

Edited by Kumar M and Xu FM

Immune tolerance in pancreatic islet xenotransplantation

Tian-Hua Tang, Chun-Lin Li, Xin Li, Feng-Qin Jiang, Yu-Kun Zhang, Hai-Quan Ren, Shan-Shan Su, Guo-Sheng Jiang

Tian-Hua Tang, Feng-Qin Jiang, Yu-Kun Zhang, Hai-Quan Ren, Guo-Sheng Jiang, Department of Hemato-oncology, Institute of Basic Medicine, Shandong Academy of Medical Sciences, Jinan 250062, Shandong Province, China

Chun-Lin Li, Xin Li, Shan-Shan Su, Shandong Chinese Traditional Medical University, Jinan 250014, Shandong Province, China

Supported by Natural Science Foundation of Shandong Province, No. Y99C07

Correspondence to: Dr. Guo-Sheng Jiang, Department of Hemato-oncology, Institute of Basic Medicine, Shandong Academy of Medical Sciences, Jingshi Road 89, Jinan 250062, Shandong Province, China. jianggsh@hotmail.com

Telephone: +86-531-2919505 **Fax:** +86-531-2919978

Received: 2003-06-04 **Accepted:** 2003-09-18

Abstract

AIM: To observe the effect of tail vein injection with donor hepatocytes and/or splenocytes on the islet xenotransplantation rejection.

METHODS: New-born male pigs and BALB/C mice were selected as donors and recipients respectively. Islet xenotransplantation was performed in recipients just after the third time of tail vein injection with donor hepatocytes and/or splenocytes. Macrophage phagocytosis, NK(natural killing cell) killing activity, T lymphocyte transforming function of spleen cells, antibody forming function of B lymphocytes, and T lymphocyte subsets were taken to monitor transplantation rejection. The effects of this kind of transplantation were indicated as variation of blood glucose and survival days of recipients.

RESULTS: The results showed that streptozotocin (STZ) could induce diabetes mellitus models of mice. The pre-injection of donor hepatocytes, splenocytes or their mixture by tail vein injection was effective in preventing donor islet transplantation from rejection, which was demonstrated by the above-mentioned immunological marks. Each group of transplantation could decrease blood glucose in recipients and increase survival days. Pre-injection of mixture of donor hepatocytes and splenocytes was more effective in preventing rejection as compared with that of donor hepatocyte or splenocyte pre-injection respectively.

CONCLUSION: Pre-injection of donor hepatocytes, splenocytes or their mixture before donor islet transplantation is a good way in preventing rejection.

Tang TH, Li CL, Li X, Jiang FQ, Zhang YK, Ren HQ, Su SS, Jiang GS. Immune tolerance in pancreatic islet xenotransplantation. *World J Gastroenterol* 2004; 10(10): 1457-1461
<http://www.wjgnet.com/1007-9327/10/1457.asp>

INTRODUCTION

Insulin dependent diabetes mellitus (IDDM) so far is treated with a constant low dose insulin injection and immunosuppressive agents. But a large quantity of clinical data indicated that long-term insulin injection could induce insulin resistance and was

not favorable to prevent some serious complications^[1]. Long-term application of immunosuppressive drugs, for example, high-dose cyclosporine and tacrolimus, could bring about toxic effects on islets and normal liver and kidney^[2,3]. So in some cases, it is limited to use immunosuppressive drugs for a long period at high dose. However, islet transplantation has the potential to cure diabetes mellitus^[4], especially insulin-dependent diabetes mellitus^[5]. Islet transplantation could make insulin maintain normal level of blood glucose and prevent serious complications. In general, islet allotransplantation is safe and efficient to reduce hyperglycemia, and leads to insulin independence in patients with insulin dependent diabetes^[6,7]. But this kind of islets source is limited, which becomes the chief obstacle for treating patients. So it is necessary to find alternative islet sources, such as xenotransplantation of islets of new-born pigs. However, the rejection for xenotransplantation should be monitored efficiently. Usually, the way of preventing rejection lies in using high dose of immunosuppressive drugs, which gives rise to serious side effects. On the other hand, pre-injection of a suitable number of the same donor lymphocytes or blood cells could induce immune tolerance in different kinds of organ transplantations^[8-14]. Some other laboratories also reported that immunologic isolation, or transplantation of microencapsulated islets, could reduce rejection of islet xenotransplantation^[15,16]. In the present study, pig islet xenotransplantation in mice was performed after injection of donor hepatocytes, splenocytes or their mixture.

MATERIALS AND METHODS

Animals and induction of diabetes mellitus model

Eighty-four BALB/C female mice (22-24 g) and 6 new born male pigs were used as recipients and donors respectively. Each BALB/C mouse was injected 0.18-0.2 mL streptozotocin (STZ) (220 mg/kg) via tail vein. When blood glucose was increased to 11.1 mmol/L, the diabetes mellitus model of mice was used in the present experiments.

Isolation of islets, hepatocytes and splenocytes

Under sterile condition, Pig pancreases were washed three times with Hanks' solution. Trypsin digestion method was used to isolate single β cells or islets, referring to the method reported by Heiser^[17]. Activity of β cells was evaluated by dithiozon (DTZ) staining and the activity should be equal or over 90%. Under bacteria-free condition, pig livers or spleens were washed three times with serum-free RPMI1640, then ground on a 200 μ stainless steel net to make single cell suspension, washing two times (2 000 rpm/min, 5 min) with normal saline (N.S). The number of cells was adjusted to 2×10^7 /mL. The cell viability was detected by Hoechst/propidium iodine (Ho/PI), both hepatocytes and splenocytes were used as donor cells with viability of more than 95%.

Islet transplantation

For hepatocyte injection group, 0.2 mL liver single cell suspension was injected into diabetic mice via tail vein every 24 h for 3 times. After the last injection of donor hepatocytes, 0.5 mL pig islets (the number of islets was 980) was transplanted into peritoneal of mouse recipient.

For splenocyte injection group, 0.2 mL spleen single cell suspension was injected into diabetes mellitus mice via tail vein every 24 h for 3 times. After the last time of injection, 0.5 mL pig islets (the number of islets was 980) was transplanted into peritoneal mouse recipient.

For mixture injection group, 0.1 mL single hepatocyte cell suspension and 0.1 mL splenocyte single cell suspension were injected into model mice via tail vein every 24 h for 3 times. After the last time of injection, 0.5 mL pig islets (the number of islets was 980) was transplanted into their peritoneal.

For islets group, 0.2 mL serum-free RPMI1640 was injected into model mice via tail vein every 24 h for 3 times. After the last time of injection, 0.5 mL pig islets (the number of islets was 980) was transplanted into recipient peritoneal. Three mice in parallel were measured for each mark and the result was indicated as an average. Twelve mice in each group were observed in terms of their living days and survival rate.

Blood glucose measurement

The level of blood glucose in mice was measured every three days by a Glucose monitoring system before and after islet transplantation. The level of blood glucose in model mice before transplantation should be over 11.1 mmol/L. The survival of transplanted-islets was indicated as at least decreasing 2-fold as compared with that before transplantation, which was indicated as functional surviving. Rejection was monitored by the level of blood glucose in mice after islet transplantation with more than 16.5 mmol/L for a continuation of 2 times.

Macrophage phagocytosis assay

Candida albicans were used as targets, constant method in our laboratory was taken to detect phagocytosis of macrophages in abdominal cavity of mice.

Phagocytosis percent=(phagocytosis of macrophages/total macrophages)×100%,

Phagocytosis index=(number of phagocytotic *Candida albicans* in 100 macrophages /total macrophages)×100%.

Lymphocyte transformation assay

Pig spleens were washed three times with serum-free RPMI1640. The spleens were ground on a 200[#] stainless steel net. The number of cells was adjusted to 1×10⁶/mL with RPMI1640. Each well of the culture plate was added 100 μL cell suspension, 6 wells in parallel, 3 wells were added conA solution 50 μL, the other 3 wells were added RPMI1640 50 μL as control. The cells were incubated in 50 mL/L CO₂, at 37 °C for 56 h, then ³H-TdR 1 μCi/well was added and cultured cells for 72 h. Cpm value was detected with a β-liquid scintillation counter. Transformation function was evaluated as average Cpm value.

Assay of NK killing activity

For effector cells, mice spleens were made into single cell suspension as the same as above-mentioned method, and the cell density was adjusted to 1×10⁷/mL in 100 mL/L fetal calf serum(FCS) RPMI1640 medium. For target cells, exponentially growing YAC-1 cells were adjusted to 2×10⁵/mL cell suspension with 100 mL/L FCS RPMI1640. A 100 μL effector cell suspension and 100 μL target cell suspension were added into each well respectively in a 40-well plate as experimental group, 3 wells in parallel. On the other hand, 100 μL/well effector cells and 100 μL/well RPMI1640 were used as effector group, 100 μL 100 mL/L FCS RPMI1640 and 100 uL target cells as target group. They were cultured them in 50 mL/L CO₂, at 37 °C for 24 h. Then 3-(4,5-dimethylthiazol-2-yl)-2,5-diphenyl tetrazolium bromide(MTT) 20 μL/well, continually cultured

for another 4 h, centrifuged at 2 000 rpm/min 10 min, the supernatant was discarded, add 1 000 g/L dimethyl sulfoxide (MDS) 100 μL was added into each well, cells were lysed with vibration. After 10 min, A value was measured at 570 nm with an ELISA reader. NK killing activity=[1-(Experimental A-Effector A)/Target A]×100%.

T lymphocytes and subpopulations

The total number of lymphocytes was calculated directly under microscopy. T lymphocytes and its subpopulations were measured by constant strept avidin-biotin complex (SABC) staining. SABC kit was supplied by Wuhan Boshide Company.

Antibody-forming assay in vitro

Quantitative hemolytic spectrometry (QHS) was used to run antibody-forming assay. Mice spleens were washed three times with normal saline. A 200[#] stainless steel net was used to grind spleen tissues into single cell suspension. The cells were re-suspended and adjusted to a final concentration of 2×10⁷/mL Hanks buffer (pH 7.2). A 1 mL cell suspension and 1 mL 2 mL/L sheep red blood cell (SRBC) (1.5×10⁸/mL cells), then 1:10 complement 1 mL was added at 37 °C for 1 h, centrifuged at 3 000 rpm/min for 5 min, the A value of supernatant at 413 nm detected by 721 spectrophotometer. A value was indicated as the ability of antibody formation of B lymphocytes *in vitro*.

Pathological examination

Pathologic changes including inflammatory infiltration of local site of islet transplantation in different experimental groups were examined.

Statistical analysis

The experiments were repeated 3 times and the data were expressed as mean±SE, and significant difference was assessed by Student's *t* test.

RESULTS

The Variations of blood glucose level after islet transplantation is shown in Figure 1.

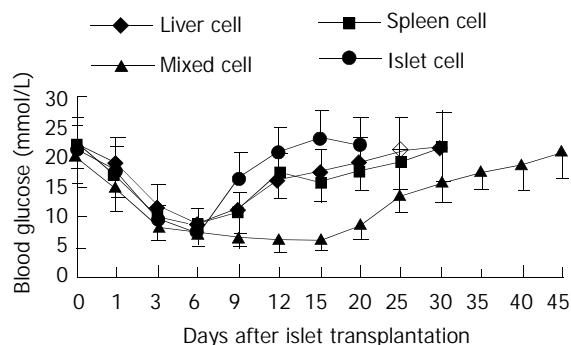


Figure 1 Variations of blood glucose after islet transplantation.

The survival time of hepatocyte injection group, splenocyte injection group, mixture group and islet group was 26.42±5.87 d, 29.56±4.52 d, 43.00±4.55 d and 16.92±2.47 d respectively (survival time of diabetic model mice was 3.86±0.85 d). The survival time of islet transplantation group was shorter than any other experimental group (*P*<0.05). So pre-injection of hepatocytes, splenocytes or their mixture from the same donor was effective in preventing rejection and delaying the time of death.

Macrophage phagocytosis in diabetic mice after pig islet xenotransplantation

Phagocytosis of macrophages in diabetic mice after pig islet xenotransplantation is summarized in Table 1.

Table 1 shows that phagocytosis percentage of islet group was increased, and the phagocytosis index of islet or hepatocyte group was obviously increased ($P<0.05$). There was no significant variation of phagocytosis percentage or index in other transplantation groups that received pre-injection of hepatocytes or mixture of hepatocytes and splenocytes 7 d after islet transplantation ($P<0.05$). After 14 d, phagocytosis percentage in hepatocyte, splenocyte and islet groups was significantly increased ($P<0.05$), phagocytosis index of islet or hepatocyte group was significantly increased ($P<0.05$).

Effect of pig islet xenotransplantation on splenic lymphocyte transforming function in mice

Seven days after transplantation, the cpm value of spleen lymphocytes in recipients of hepatocyte group, splenocyte group, mixture group or islet group was higher after pig islet

xenotransplantation than before transplantation ($P<0.05$). After 14 d, the value of hepatocyte group or islet group was still higher than that before transplantation ($P<0.05$). But there was no significant difference between splenocyte group and mixture group ($P>0.05$) (Table 2).

Effect of pig islet transplantation on NK activity of diabetic mice

NK activity of each experimental group, as compared with that before transplantation, was increased 7 d after islet transplantation ($P<0.05$), and their NK activity was continually higher than that before transplantation even 14 d after transplantation ($P<0.05$). As to the mixture group, there was no significant increase of NK activity 7 or 14 d after islet transplantation as compared with that before islet transplantation ($P>0.05$) (Table 3).

Variations of T lymphocytes in diabetic mice after pig islet xenotransplantation (Table 4)

CD₃ and CD₄ counts in hepatocyte, splenocyte or islet group

Table 1 Macrophage phagocytosis in diabetic mice after pig islet xenotransplantation

Group	Pre-treatment		7 d post-treatment		14 d post-treatment	
	Percent (%)	Index	Percent (%)	Index	Percent (%)	Index
Hepatocytes group	59.3±4.5	1.05±0.04	62.8±4.37	1.28±0.13	70.6±3.82	1.25±0.07
Splenocytes group	62.5±3.0	1.04±0.07	63.1±6.45	1.18±0.14	69.5±3.62	1.21±0.09
Mixture group	63.1±3.8	1.07±0.06	61.6±3.54	1.12±0.09	62.8±4.70	1.09±0.08
Islet group	62.0±3.3	1.06±0.08	73.5±5.51	1.41±0.18	72.7±5.71	1.47±0.10

Table 2 Effect of transplantation with pig islets on splenic lymphocyte transforming function in mice

Group	Pre-transplantation (cpm)	7 d post-transplantation (cpm)	14 d post-transplantation (cpm)
Hepatocytes group	11 437.56±1 137.55	23 453.74±4 157.28	20 178.56±4 159.74
Splenocytes group	11 437.56±1 137.55	25 834.66±3 763.37	15 336.25±3 782.38
Mixture group	11 437.56±1 137.55	21 920.05±600.08	14 345.53±2 653.28
Islets group	11 437.56±1 137.55	32 339.13±5 071.67	22 182.16±750.28

Table 3 Effect of pig islet xenotransplantation on NK activity (%) in diabetic mice

Group	Pre-treatment	7 d post-treatment	14 d post-treatment
Hepatocytes group	31.56±4.23	63.17±3.47	60.26±7.65
Splenocytes group	31.76±3.48	62.50±4.86	56.19±8.13
Mixture group	31.37±8.09	48.00±12.0	34.33±14.57
Islet group	35.67±3.51	76.23±12.50	71.00±3.0

Table 4 Variations of T lymphocytes in diabetic mice after pig islet xenotransplantation

Group	Pretreatment(%)			7 d post-treatment (%)			14 d post-treatment (%)		
	CD3	CD4	CD8	CD3	CD4	CD8	CD3	CD4	CD8
Hepatocyte group	61.6±4.5	42.0±4.6	24.3±1.5	72.7±5.5	51.6±4.5	28.0±3.6	70.0±2.0	52.7±4.9	26.7±4.2
Splenocyte group	66.0±3.6	46.3±4.0	24.6±2.5	73.0±4.4	53.3±4.5	31.3±4.1	68.7±5.7	45.3±4.1	33.0±3.6
Mixture group	64.7±2.5	44.3±6.7	25.3±4.9	65.0±5.3	47.6±3.8	28.3±2.5	61.6±3.5	47.0±4.4	27.7±2.1
Islet group	65.0±7.0	43.3±3.0	24.3±3.2	80.0±2.0	60.6±3.2	32.3±3.1	72.3±6.7	58.7±9.1	32.0±4.0

Table 5 B lymphocyte antibody-forming function (A value) in mice after transplantation (A)

Group	Pretransplantation	7 d post-transplantation	14 d post-transplantation
Hepatocyte group	0.34±0.06	0.44±0.02	0.63±0.07
Splenocyte group	0.34±0.06	0.55±0.02	0.63±0.08
Mixture group	0.34±0.06	0.55±0.01	0.50±0.06
Islet group	0.34±0.06	0.74±0.11	0.81±0.13

were up-regulated 7 days after islet transplantation. CD₈ counts in splenocyte or islet group was higher than that before islet transplantation ($P<0.05$). Fourteen days after transplantation, CD₃ and CD₄ in hepatocyte and islet groups increased ($P<0.05$), and CD₈ in splenocyte and islet groups became higher than that before transplantation ($P<0.05$).

Antibody forming assay of B lymphocytes in mice after transplantation (Table 5)

Table 5 shows that antibody forming function of all four kinds of islet transplantation group was significantly increased as compared with that before islets transplantation 7 or 14 d after transplantation ($P<0.05$).

Pathological examination

In islet transplantation group, there were a lot of lymphocyte infiltration, disruption of islets structure, or denaturation and necrosis of islet cells. Hepatocyte group with moderate lymphocyte infiltration. The mixture group had light lymphocytes infiltration.

DISCUSSION

Insulin dependent diabetes mellitus was considered as an autoimmune disease against beta cells^[18], which is usually treated with a low dose insulin injection and immunosuppressive agents. But a large quantity of clinical data indicated that long-term insulin injection could induce insulin resistance and could not prevent some serious complications^[1]. Recent studies focused on islet transplantation as a primary therapy for insulin dependent mellitus diabetes, accompanied by induction of immune tolerance to immunosuppressive agents^[19,20]. Islet allotransplantation could correct glucose imbalance and related complications, because successful islet transplantation could not only supplies the natural insulins but also other necessary biological factors. But most patients with insulin dependent diabetes mellitus could not be treated by this kind of islet transplantation because the source of allo-islets was limited. However, xenotransplantation, for example pig islet, could resolve the above-mentioned problems. Although xenotransplantation could renew the balance of glucose, rejection usually occurs, thus reducing the effect of transplantation. Islet transplantation combined with other organs or cells from the same donor could reduce rejection. Some laboratories have tried pancreas allotransplantation in combination with the same donor spleen transplantation. The results showed that the survival time of pancreas was significantly prolonged, which was attributed to the induced immunotolerance. It has been reported that bone marrow transplantation could induce the formation of hematopoiesis chimera, which could prevent acute or chronic rejection^[13-15,21,22]. So it is possible to use hematopoiesis chimera to treat insulin dependent diabetes mellitus.

T lymphocyte vaccine (TCV) could induce immunotolerance for transplantation^[23]. For example, TCV with recipient spleen cells pre-sensitized by donor antigen was used in rat heart transplantation, to observe the survival time of rat heart graft. The results showed that TCV could prolong the survival time of rat heart graft^[24]. As to the immune response, T lymphocyte proliferation reaction increased, B lymphocyte proliferation reaction was not affected, but mixed lymphocyte reaction (MLR) declined. The analysis of phenotype showed that CD₈ subpopulation increased, however there was no obvious change of antibody-dependent cell-mediated cytotoxicity (ADCC) reaction. Many other studies demonstrated that liver cells (or hepatocytes) and/or spleen cells (or splenocytes) could induce specific immune tolerance in different organ transplantations, such as kidney, marrow, heart, skin^[25-28]. In the aspect of islet transplantation, some scholars administrated pre-injection of

donor hepatocytes and/or splenocytes to induce the immune tolerance and got the positive result^[29-31].

In the present study, islet xenotransplantation was performed after pre-injection of donor hepatocytes, splenocytes, or their mixture. The results showed that the survival time of hepatocyte group, splenocyte group, mixture group was longer than islet group ($P<0.05$). Pre-injection of hepatocytes, splenocytes or their mixture from the same donor was effective in preventing rejection and prolonging survival time. In the aspect of macrophage function, macrophage phagocytosis percent in islet transplantation group was increased, and the phagocytosis index in islet or hepatocyte group was increased ($P<0.05$). There was no significant variation of phagocytosis percent or index in other transplantation groups 7 d after transplantation. After 14 d, phagocytosis in hepatocyte, splenocyte and islet group was significantly increased, phagocytosis index in islet or hepatocyte group was increased. The antibody-forming function of spleen B lymphocytes of recipients in hepatocyte group, splenocyte group, mixture group or islet group was increased 7 d after pig islet xenotransplantation. After 14 d, the B lymphocyte function in hepatocyte group or islet group was still higher than that before transplantation ($P<0.05$). As to NK cells, NK killing activity of each experimental group, as compared with before transplantation, was increased 7 d after islet transplantation, and their NK activity maintained higher than that before transplantation 14 d after transplantation. As to the mixture group, there was no significant increase in NK activity 7 or 14 d after islet transplantation as compared with that before islet transplantation ($P>0.05$). T lymphocyte subpopulation was also analyzed, the results showed that CD₃ and CD₄ percent of hepatocyte, splenocyte or islet group increased 7 d after islet transplantation. CD₈ percent of splenocyte or islet group was higher than that before islet transplantation. Fourteen days after transplantation, CD₃ and CD₄ percent of hepatocyte and islet group was still higher, and CD₈ percent of splenocyte and islet groups was higher than that before transplantation. To further examine immune tolerance in different experimental groups, pathological examination was performed. In islet transplantation group, lymphocyte infiltration was extensive, disruption of islet structure and necrosis of islet cells were also obvious. Hepatocyte group had moderate lymphocyte infiltration. The mixture group has slight lymphocyte infiltration. The results indicate that pre-injection of hepatocytes, splenocytes or mixture of them could reduce rejection by inducing immunotolerance. Although the concrete mechanism is not completely clear, pre-injection of hepatocytes and splenocytes from the same donor could induce immunotolerance of islet xenotransplantation, and prolong the survival time of islets.

REFERENCES

- 1 **Oluwale OO**, Depaz HA, Gopinathan R, Ali A, Garrovillo M, Jin MX, Hardy MA, Oluwale SF. Indirect allorecognition in acquired thymic tolerance: induction of donor-specific permanent acceptance of rat islets by adoptive transfer of alloptide-pulsed host myeloid and thymic dendritic cells. *Diabetes* 2001; **50**: 1546-1552
- 2 **Contreras JL**, Eckhoff DE, Cartner S, Bilbao G, Ricordi C, Neville DM Jr, Thomas FT, Thomas JM. Long-term functional islet mass and metabolic function after xenotransplantation in primates. *Transplantation* 2000; **69**: 195-201
- 3 **Montori VM**, Basu A, Erwin PJ, Velosa JA, Gabriel SE, Kudva YC. Posttransplantation diabetes: a systematic review of the literature. *Diabetes Care* 2002; **25**: 583-592
- 4 **White SA**, James RF, Swift SM, Kimber RM, Nicholson ML. Human islet cell transplantation—future prospects. *Diabet Med* 2001; **18**: 78-103
- 5 **Pileggi A**, Ricordi C, Alessiani M, Inverardi L. Factors influenc-

- ing Islet of Langerhans graft function and monitoring. *Clin Chim Acta* 2001; **310**: 3-16
- 6 **Horton PJ**, Hawthorne WJ, Walters SN, Patel AT, O'Connell PJ, Chapman JR, Allen RD. Induction of allogeneic islet tolerance in a large-animal model. *Cell Transplant* 2000; **9**: 877-887
 - 7 **Kahl A**, Bechstein WO, Frei U. Trends and perspectives in pancreas and simultaneous pancreas and kidney transplantation. *Curr Opin Urol* 2001; **11**: 165-174
 - 8 **Deng YM**, Tuch BE, Rawlinson WD. Transmission of porcine endogenous retroviruses in severe combined immunodeficient mice xenotransplanted with fetal porcine pancreatic cells. *Transplantation* 2000; **70**: 1010-1016
 - 9 **Wennberg L**, Song Z, Bennet W, Zhang J, Nava S, Sundberg B, Bari S, Groth CG, Korsgren O. Diabetic rats transplanted with adult porcine islets and immunosuppressed with cyclosporine A, mycophenolate mofetil, and leflunomide remain normoglycemic for up to 100 days. *Transplantation* 2001; **71**: 1024-1033
 - 10 **Li H**, Ricordi C, Inverardi L. Effects of graft-versus-host reaction on intrahepatic islet transplants. *Diabetes* 1999; **48**: 2292-2299
 - 11 **Ikebukuro K**, Adachi Y, Yamada Y, Fujimoto S, Seino Y, Oyaizu H, Hioki K, Ikehara S. Treatment of streptozotocin-induced diabetes mellitus by transplantation of islet cells plus bone marrow cells via portal vein in rats. *Transplantation* 2002; **73**: 512-518
 - 12 **Kawai T**, Sogawa H, Koulmanda M, Smith RN, O'Neil JJ, Wee SL, Boskovic S, Sykes M, Colvin RB, Sachs DH, Auchincloss H Jr, Cosimi AB, C-Ko DS. Long-term islet allograft function in the absence of chronic immunosuppression: a case report of a non-human primate previously made tolerant to a renal allograft from the same donor. *Transplantation* 2001; **72**: 351-354
 - 13 **Wu T**, Levay YB, Heuss N, Sozen H, Kirchhof N, Sutherland DER, Hering B, Guo Z. Inducing tolerance to MHC-matched allogeneic islet grafts in diabetic NOD mice by simultaneous islet and bone marrow transplantation under nonirradiative and nonmyeloablative conditioning therapy. *Transplantation* 2002; **74**: 22-27
 - 14 **Girman P**, Kriz J, Dovolilova E, Cihalova E, Saudek F. The effect of bone marrow transplantation on survival of allogeneic pancreatic islets with short-term tacrolimus conditioning in rats. *Ann Transplant* 2001; **6**: 43-45
 - 15 **Maria-Engler SS**, Mares-Guia M, Correa ML, Oliveira EM, Aita CA, Krogh K, Genzini T, Miranda MP, Ribeiro M, Vilela L, Noronha IL, Eliaschewitz FG, Sogayar MC. Microencapsulation and tissue engineering as an alternative treatment of diabetes. *Braz J Med Biol Res* 2001; **34**: 691-697
 - 16 **Gamian E**, Kochman A, Rabczynski J, Burczak K. Biocompatibility testing and function of a pancreatic prosthesis consisting of viable pancreatic islets encapsulated in PVA macrocapsules. *Polim Med* 1999; **29**: 3-20
 - 17 **Heiser A**, Ulrichs K, Muller-Ruchholtz W. Isolation of porcine pancreatic islets: low trypsin activity during the isolation procedure guarantees reproducible high islet yields. *J Clin Lab Anal* 1994; **8**: 407-411
 - 18 **Petruzzio P**, Andreelli F, McGregor B, Lefrancois N, Dawahra M, Feitosa LC, Dubernard JM, Thivolet C, Martin X. Evidence of recurrent type I diabetes following HLA-mismatched pancreas transplantation. *Diabetes Metab* 2000; **26**: 215-218
 - 19 **Thomas JM**, Contreras JL, Smyth CA, Lobashevsky A, Jenkins S, Hubbard WJ, Eckhoff DE, Stavrou S, Neville DM Jr, Thomas FT. Successful reversal of streptozotocin-induced diabetes with stable allogeneic islet function in a preclinical model of type 1 diabetes. *Diabetes* 2001; **50**: 1227-1236
 - 20 **Sutherland DE**, Gruessner RW, Dunn DL, Matas AJ, Humar A, Kandaswamy R, Mauer SM, Kennedy WR, Goetz FC, Robertson RP, Gruessner AC, Najarian JS. Lessons learned from more than 1,000 pancreas transplants at a single institution. *Ann Surg* 2001; **233**: 463-501
 - 21 **Good RA**, Verjee T. Historical and current perspectives on bone marrow transplantation for prevention and treatment of immunodeficiencies and autoimmunities. *Biol Blood Marrow Transplant* 2001; **7**: 123-135
 - 22 **Ciancio G**, Miller J, Garcia-Morales RO, Carreno M, Burke GW, Roth D, Kupin W, Tzakis AG, Ricordi C, Rosen A, Fuller L, Esquenazi V. Six-year clinical effect of donor bone marrow infusions in renal transplant patients. *Transplantation* 2001; **71**: 827-835
 - 23 **Lakey JR**, Singh B, Wamock GL, Elliott JF, Rajotte RV. Long-term survival of syngeneic islet grafts in BCG-treated diabetic NOD mice can be reversed by cyclophosphamide. *Transplantation* 1995; **59**: 1751-1753
 - 24 **Shanqi Y**, Suisheng X. Study on the mechanisms of T cell vaccination-induced survival prolongation of cardiac allograft in rats. *Zhonghua Qiguan Yizhi Zazhi* 2000; **21**: 303-305
 - 25 **Motoyama K**, Arima T, Yu S, Lehmann M, Flye MW. The kinetics of tolerance induction by nondepleting anti-CD4 monoclonal antibody (RIB 5/2) plus intravenous donor alloantigen administration. *Transplantation* 2000; **69**: 285-293
 - 26 **Smyk-Pearson SK**, Bakke AC, Held PK, Wildin RS. Rescue of the autoimmune scurfy mouse by partial bone marrow transplantation or by injection with T-enriched splenocytes. *Clin Exp Immunol* 2003; **133**: 193-199
 - 27 **Nakafusa Y**, Goss JA, Mohanakumar T, Flye MW. Induction of donor-specific tolerance to cardiac but not skin or renal allografts by intrathymic injection of splenocyte alloantigen. *Transplantation* 1993; **55**: 877-882
 - 28 **Dono K**, Maki T, Wood ML, Monaco AP. Induction of tolerance to skin allografts by intrathymic injection of donor splenocytes. Effect of donor-recipient strain combination and supplemental rapamycin. *Transplantation* 1995; **60**: 1268-1273
 - 29 **Sun J**, Wang X, Wang C, Sheil AG. Sequential transplantation induces islet allograft tolerance. *Microsurgery* 2001; **21**: 148-152
 - 30 **Sutherland DE**, Gruessner RW, Gruessner AC. Pancreas transplantation for treatment of diabetes mellitus. *World J Surg* 2001; **25**: 487-496
 - 31 **Sakuma Y**, Uchida H, Nagai H, Kobayashi E. High-dose tacrolimus and lengthy survival of the combined rat pancreas/spleen graft in a high-responder combination. *Transpl Immunol* 2001; **9**: 37-42

Edited by Wang XL Proofread by Xu FM

Establishment and characterization of human hepatocellular carcinoma cell line FHCC-98

Chao-Yang Lou, Ying-Ming Feng, Ai-Rong Qian, Yu Li, Hao Tang, Peng Shang, Zhi-Nan Chen

Chao-Yang Lou, Ying-Ming Feng, Department of Oncology, Tangdu Hospital, Fourth Military Medical University, Xi'an 710038, Shaanxi Province, China

Peng Shang, Ai-Rong Qian, Yu Li, Hao Tang, Zhi-Nan Chen, Department of Cell Biology, Fourth Military Medical University, Xi'an 710032, Shaanxi Province, China

Supported by the National High-Tech Research and Development Program of China, NO. 2001AA215061

Co-correspondents: Zhi-Nan Chen

Correspondence to: Dr. Peng Shang, Department of Cell Biology, Fourth Military Medical University, Xi'an 710032, Shaanxi Province, China. chcerc7@fmmu.edu.cn

Telephone: +86-29-83374547

Received: 2004-03-15 **Accepted:** 2004-04-10

Abstract

AIM: To establish a novel human hepatocellular carcinoma (HCC) cell line FHCC-98 from HCC tissue and to provide a suitable model for studying HCC occurrence, progress and metastasis.

METHODS: Serially passaged cells were cultured and their morphologies were observed under light and electron microscope. Cytogenetic study was conducted by using flow cytometry and chromosome analysis. Expressions of tumor markers such as α -fetoprotein (AFP), cytokeratin (CK) and hepatoma metastasis-associated factor HAb18G/CD147 on the FHCC-98 cells were detected by immunocytochemistry or Western blotting. Lactic dehydrogenase (LDH) isoenzymes were detected by polyacrylamide gel electrophoresis (PAGE). Xenograft was performed by inoculating FHCC-98 cells into the flanks of nude mice.

RESULTS: Morphology of FHCC-98 cells was the same as that of other malignant cells. The expressions of the cells were positive for HAb18G/CD147 and CK, and negative for AFP. Its population doubling time was 21.4 h. The cell DNA was tetraploid and the major chromosomes were triploid by cytogenetics analysis. The tumorigenicity in nude mice was 100%. PAGE showed four bands representing LDH₂, LDH₃, LDH₄ and LDH₅.

CONCLUSION: FHCC-98 is a novel HCC cell line and an ideal cell model for further exploring the mechanism of hepatocellular carcinoma invasion and metastasis.

Lou CY, Feng YM, Qian AR, Li Y, Tang H, Shang P, Chen ZN. Establishment and characterization of human hepatocellular carcinoma cell line FHCC-98. *World J Gastroenterol* 2004; 10 (10): 1462-1465

<http://www.wjgnet.com/1007-9327/10/1462.asp>

INTRODUCTION

Hepatocellular carcinoma (HCC) is one of the most common malignant tumors. It ranks fifth in frequency worldwide among

all malignancies and causes 1 million deaths annually^[1], yet its incidence is increasing steadily in various countries^[2-4]. Epidemiology studies showed that primary liver cancer is the second mortality in China^[5] and it accounts for 53% of all liver cancer death worldwide^[6]. Though with great development in diagnosis and therapy, the prognosis of patients with HCC remains dismal for its high rate of metastasis and recurrence. For patients in advanced stages, the median survival is less than 6 mo, no matter what kinds of therapy were managed^[7-11]. So it is urgent to further explore the mechanism of HCC occurrence, progress and metastasis. HCC cell lines are powerful tools. Until now, ten of human HCC cell lines^[12-27] have been established, and every cell line has its own characteristics and offers convenience for various experiments. Stability, homogeneity and easy to culture are important parameters for good cell lines. Here we report a new HCC cell line, which has been maintained for five years through 500 passages.

MATERIALS AND METHODS

Patient

Tumor tissue obtained from a 39-year-old male HCC patient who lived in northwest China was used to establish a cell line. His family history of oncology was unknown, but there was no history of hepatitis or blood transfusions. There was no operation history. Investigations showed AST of 86 U/L, α -fetoprotein 8 ng/mL, carcinoembryonic antigen (CEA) 2.8 ng/mL and HBsAg(-). In 1998, the patient complained of upper right abdominal tender pain. A computerized-tomography demonstrated a 10 cm×11 cm space-occupying lesion in the right lobe of liver. A partial liver resection was performed. Pathologic diagnosis confirmed HCC with middle differentiation. The patient died of lung metastasis after 3 mo.

Primary culture

A slice portion of sample was obtained under sterile conditions and washed by RPMI 1640 (Life Technology) 3 times and minced with surgical blades into pieces smaller than 1 mm³, then these pieces were put into tissue-culture flasks and incubated at 37 °C and 50 mL/L CO₂ (Heraeus, Germany) with RPMI 1640 medium supplemented with 100 U/mL penicillin, 100 μ g/mL streptomycin and 200 mL/L FBS. One week later, cells migration was observed and some colonies were formed. Those colonies were detached with 2.5 g/L trypsin and pulled into 25 cm² flasks in RPMI 1640 medium with 200 mL/L FBS. The medium was renewed two or three times a week. After stable growth, the same medium with 100 mL/L FBS was used as maintenance medium. When cells were confluent, they were detached with 2.5 g/L trypsin and passaged at the ratio of 1:2 or 1:3. At the 80th passage (about 30 mo after the sample was got), a stable cell line was considered to be established.

Morphological observations

Cells were observed daily under an invert microscope (Olympus). Cells coated on tissue-culture slides were washed with PBS (pH 7.4) 3 times, then fixed with cool pure acetone for 10 min and stained with hematoxylin and eosin (HE

staining). For electron microscope observation, 4×10^6 cells were centrifuged at 1 000 r/min for 10 min, then fixed in 30 g/L glutaraldehyde for 30 min and embedded in paraffin and ultra-thin sectioned. The section was observed with a JEM 2000 transmission electron microscope (JEOL)^[22].

Growth properties

Growth curve was analyzed by modified MTT assay^[24]. Cells in exponential growth phase at 16th passage were collected. Single-cell suspension (5×10^4 /mL) was added to (200 μ L/well) a 24-well plate, incubated at 37 °C with 50 mL/L CO₂, then MTT (5 mg/mL) was added to the wells (20 μ L/well) every 24 h for 7 consecutive days. The plate was incubated in cell incubator for 4 h, and then the supernatants were removed and 150 μ L DMSO was added into each well. After incubation for 30 min, the dye-stained liquid was removed to a 96-well plate. Absorbency at 490 nm ($A_{490\text{nm}}$) was determined by M450 (Bio-Rad) enzyme-linked reader. The growth curve was plotted by half-height method.

FHCC-98 cells were incubated in another 24-well plate (1.2×10^4 /mL). Attachment efficiency was measured by counting the cell number every 2 h.

Attachment efficiency = (number of cells/120 000) \times 100%.

To determine the cloning rate, 1.5×10^2 cells in suspension in a culture medium containing 8 g/L agar were applied to a base layer of a culture medium containing 1.7% agar. The Petri dish was incubated for 12 d at 37 °C in a humidified atmosphere containing 50 mL/L CO₂, and colonies containing more than 5 cells were counted.

$$\text{Cloningrate} = \frac{\text{Number of clones}}{150} \times 100\%$$

Flow cytometry

Single-cell suspensions containing 2×10^6 cells were treated following the standardized protocol and cell cycle analysis was performed by flow-cytometry (ELITE ESP Coulter)^[22].

Chromosome analysis

Cells were cultured for 2 h in the culture medium containing 0.05 μ g/mL of colcemid and trypsinized, swollen with 0.075 mol/L KCl solution for 15 min and fixed with methanol: acetic acid (3:1) 3 times. Following air-drying, metaphase smears were stained with Giemsa. Samples were observed with oil immersion objective and photographed^[18].

Immunocytochemistry

Cells cultured on slides for 24 h were washed 3 times with PBS and then fixed in acetone for 10 min at room temperature. AFP and cytokeratin were detected by immunocytochemistry using SP method. The slides were viewed under light microscope and the degree of staining was assessed.

Western blotting

Tumor metastasis-associated factor HAb18G/CD147^[28,29] was detected by western blotting. Single-cell suspension (1.0×10^5 /mL) was collected, and centrifuged at 800 r/min. The cell pellets were collected and resuspended in lysis buffer of 50 mmol/L Tris-HCl (pH 8.0), 150 mmol/L NaCl, 0.2 g/L azido sodium, 1 g/L SDS, 100 μ g/mL PMSF, 10 g/L Triton X-100, 5 g/L deoxycholic acid and protease inhibitor for 10 min on the ice. The lysis solution was centrifuged at 16 000 g for 10 min at 4 °C and the supernatants were collected, and the protein concentration was detected with Lowery's method. SDS-PAGE was carried out. Western blotting was performed with secondary antibodies coupled to horseradish peroxidases and detected using ECL reagents (Amersham, Freiburg, German).

ConA coagulation test

Single-cell suspension (5.0×10^5 /mL) was mixed with the same volume of ConA and the mixture were diluted and incubated at 37 °C in 50 mL/L CO₂ for 20 min. Human embryonic lung cell was used as contrast. Assembling reaction was observed.

Isoenzyme analysis

LDH isoenzymes were detected by PAGE. FHCC-98 cells were trypsinized and 8.0×10^6 cells were re-suspended in sterile saline. The cell suspension was centrifuged at 1 000 r/min for 10 min twice and then re-suspended in 0.5 mL Tris-HCl (150 mmol/L, pH 7.6). The sample was repeatedly frozen and thawed at -40 °C and 37 °C for 6 times, then centrifuged at 3 000 r/min 4 °C for 20 min. The supernatant was stored under -20 °C for using. The SDS-PAGE sample buffer was 100 mmol/L Tris-HCl (pH 6.8) supplemented with 200 mL/L glycerite and 2 g/L bromphenol blue. The sample was mixed with an equal volume of buffer and used for PAGE. The stacking gel was 50 g/L while separation gel 60 g/L. The staining solution was composed of oxidized NAD⁺ (5 mg/mL), NBT (2 mg/mL), PMS (1 mg/mL) and sodium lactate (60 g/L). The minigels were run at a constant voltage (100 V) for 2 h and then stained for 1 h. The gel was fixed in 70 mL/L acetic acid over 16 h and photographed.

Xenograft

Ten 4-6-week-old nude mice (supplied by the animal center of Fourth Military Medical University) of both sexes bred under specific pathogen-free (SPF) conditions were used in the heterotransplantation experiments. Cells (2.0×10^6) suspended in medium (0.2 mL) were injected subcutaneously into flanks of each mouse.

Mycoplasma detection

Mycoplasma was detected by transmission electron microscopy.

RESULTS

Morphology

Polygonal epithelial-like cells in culture were identified to have large nuclei and the ratio of nuclear/cytoplasmic increased. Cells grew well at a high density ($>1 \times 10^6$ /mL). Electron microscopy revealed that abundant microvilli distributed on the cell surface (Figure 1). Desmosomes and gap junction could be seen between cells (Figure 2). Glycogen granules were rich in cytoplasm and mitochondria were in a round shape. Ribosome and rough endoplasmic reticulum were moderate. Atypical nuclei were conspicuous and euchromatin was rich. Karyokinesis and pathologic mitosis were frequently uncoupled.

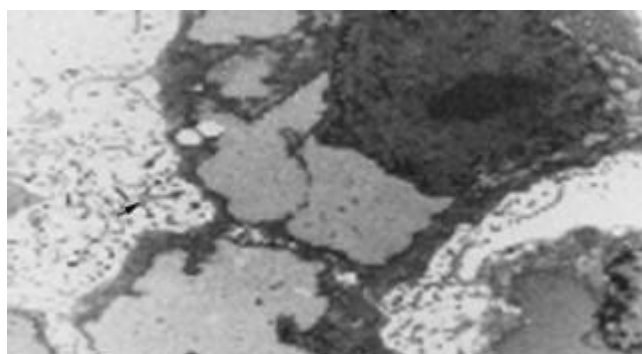


Figure 1 Ultrastructure of FHCC-98 illustrating the clear and abundant microvilli (Original magnification: $\times 4\,000$).

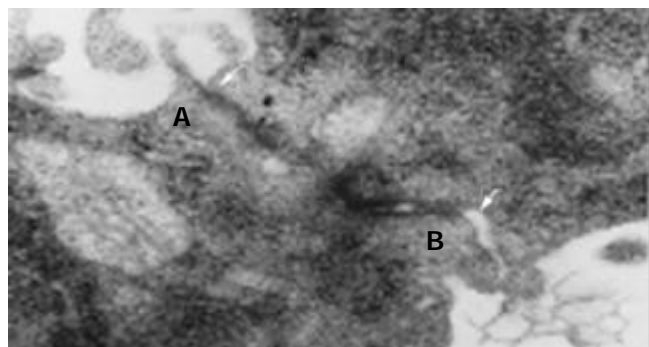


Figure 2 Desmosomes (A) and gap junction (B) between cells (Original magnification: $\times 30\,000$).

Growth kinetics

The growth curve at the sixteenth passage (Figure 3) showed a stationary-phase at the beginning and at the end of the experiment, the exponential growth lasted about 3 d. The population doubling time of FHCC-98 was 21.4 h. At the time points of 2, 4, 6 and 8 h, the attachment efficiencies were 54.2%, 83.3%, 89.2% and 93.7%, respectively. The percentage of colony-forming cells in soft agar was an average of 32.6%.

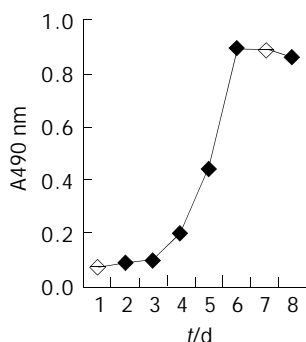


Figure 3 Growth curve of FHCC-98 cells in RPMI 1640+100 mL/LFBS at the 16th passage.

Cytogenetics studies

Chromosome analysis revealed the number of chromosomes per cell varied from 58 to 80 with a number in the triploid of 91%. FHCC-98 cell DNA became tetraploid. 75.0% cells were in G₁ phase, while 7.0% cells were in G₂ phase and 18.0% in S phase. The DNA index was 1.857.

Immunological characteristics

The FHCC-98 cell line was positive for CK and negative for AFP.

Western blotting

Western blotting showed that FHCC-98 was positive for HAb18G/CD147 and the band showed a single one with M_r 61 000 (Figure 4).

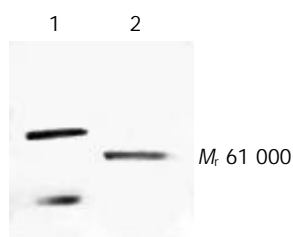


Figure 4 Western blotting of HAb18G/CD147 on FHCC-98 cell line. Lane 1: HAb18 mAb; Lane 2: HAb18G.

ConA test

The FHCC-98 cells were coagulated in 3.91 $\mu\text{g/mL}$ of ConA while human embryonic lung cells had no response to 250 $\mu\text{g/mL}$ of ConA.

Isoenzyme analysis

PAGE analysis revealed that FHCC-98 had tumor typical isoenzymes of LDH without LDH₁ (Figure 5). LDH₂, LDH₃, LDH₄ and LDH₅ isoenzymes were separated to relative activities (percentage of total LDH) of 3%, 19%, 49% and 29%, respectively.

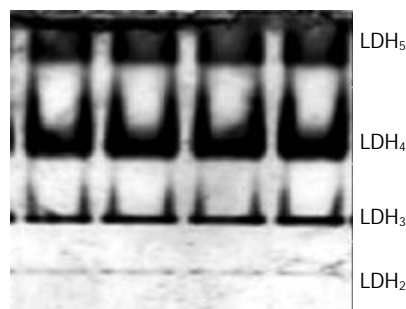


Figure 5 LDH isoenzyme analysis of FHCC-98.

Xenograft

Ten days after heterotransplantation of FHCC-98 cells into nude mice, subcutaneous tumors appeared at the sites of inoculation and grew rapidly in size during the next 20 d. Average tumor volumes on d 10, 14 and 30 were 42.4 ± 17.8 , 76.6 ± 43.4 , and 471.4 ± 187.5 mm³, respectively.

Mycoplasma detection

No mycoplasma contamination was detected in FHCC-98 cells from passages 16 and 28.

DISCUSSION

It is well known that heterogeneous tumors have diverse biologic behaviors, outcomes, and responses to therapy whether *in vivo* or *in vitro*. Malignant tumors show their genetic heterogeneities, differentiation and metastasis, which have been demonstrated in various kinds of tumors^[30-34], and even in permanent cell lines with different biological characteristics^[22,23,34]. Since the establishment of the first human HCC cell line in 1963 (Chen *et al.* *Chin Med J*, 1963; 82: 228), more than ten human HCC cell lines have been established, most of which are positive for either HBV, HCV or AFP, yet they differed in biological properties. HBV is the main viral cause of HCC in China. Unfortunately, there are about 30% HCC patients are AFP or HBV negative, partially due to the extensive necrosis of tumor mass. As a tumor marker, AFP's sensitivity and specificity for HCC detection depend on the diagnostic level and the cutoff level^[35]. Different detection approaches may have different results. In this study, immunocytochemical method was applied to detect AFP and the result was consistent with that by RIA. Up to now, human HCC cell lines with both AFP negative and HBV negative have been rarely reported. Fortunately, we established a HCC cell line, which was negative for both AFP and HBV.

FHCC-98 demonstrated the same epithelial-type morphology as other HCC cell lines. FHCC-98 showed no contact inhibition when the cell density was high. As important metabolic parameters of HCC, LDH₄ and LDH₅ had high activities, and LDH₁ had no, suggesting the existence of anaerobic respiration in HCC. Hypoxia and overgrowth of

cancerous tissue specifically repressed the activity of AFP, and the target was c-Myc, suggesting that c-Myc regulated AFP gene expression^[36]. Such changes in LDH₅ might be a factor hindering the synthesis of AFP and resulting in AFP-negative patients. FHCC-98 may be used as a model for anti-oxidant therapy of tumors. FHCC-98 has its own characteristics. The first prominent characteristic of the cell line is its biological properties of high concordance and little variation among different passages including its morphology, growth kinetics, chromosome, AFP and LDH isoenzyme; The second one is that its population doubling time was relatively shorter and it grew more rapidly compared with other human HCC cell lines^[12,14,18,20,23,25]. High coagulation of the cells showed that it could proliferate rapidly without contact inhibition. The third one is its high tumorigenicity in nude mice. And the last one of the cell line is that it can grow in various medium cultures, such as RPMI 1640 and DMEM with different concentrations of FBS.

In conclusion, we believe that FHCC-98 is a novel HCC cell line and a valuable cell model for studying HCC *in vitro* and *in vivo*, especially for AFP- and HBV-negative HCC.

REFERENCES

- 1 **Yu AS**, Keffe EB. Management of hepatocellular carcinoma. *Rev Gastroenterol Disord* 2003; **3**: 8-24
- 2 **El Serag HB**, Mason AC. Rising incidence of hepatocellular carcinoma in the United States. *N Engl J Med* 1999; **340**: 745-750
- 3 **Kiyosawa K**, Tanaka E. Characteristics of hepatocellular carcinoma in Japan. *Oncology* 2002; **62**(Suppl 1): 5-7
- 4 **Tang ZY**. Hepatocellular carcinoma-cause, treatment and metastasis. *World J Gastroenterol* 2001; **7**: 445-454
- 5 **Zhang S**, Li L, Lu F. Mortality of primary liver cancer in China from 1990 through 1992. *Zhonghua Zhongliu Zazhi* 1999; **21**: 245-249
- 6 **Pisani P**, Parkin DM, Bray F, Ferlay J. Estimates of the worldwide mortality from 25 cancers in 1990. *Int J Cancer* 1999; **83**: 18-29
- 7 **Johnson PJ**. Hepatocellular carcinoma: is current therapy really altering outcome? *Gut* 2002; **51**: 459-462
- 8 **Watanabe T**, Omori M, Fukuda H, Takada H, Miyao M, Mizuno Y, Ohsawa I, Sato Y, Hasegawa T. Analysis of sex, age and disease factors contributing to prolonged life expectancy at birth, in cases of malignant neoplasms in Japan. *J Epidemiol* 2003; **13**: 169-175
- 9 **Ziparo V**, Balducci G, Lucandri G, Mercantini P, Di Giacomo G, Fernandes E. Indications and results of resection for hepatocellular carcinoma. *Eur J Surg Oncol* 2002; **28**: 723-728
- 10 **Kanematsu T**, Furui J, Yanaga K, Okudaira S, Shimada M, Shirabe K. A 16-year experience in performing hepatic resection in 303 patients with hepatocellular carcinoma: 1985-2000. *Surgery* 2002; **131**(1 Suppl): S153-S158
- 11 **Aguayo A**, Patt YZ. Liver cancer. *Clin Liver Dis* 2001; **5**: 479-507
- 12 **Yano H**, Maruiwa M, Murakami T, Fukuda K, Ito Y, Sugihara S, Kojiro M. A new human pleomorphic hepatocellular carcinoma cell line, KYN-2. *Acta Pathol Jpn* 1988; **38**: 953-966
- 13 **Dor I**, Namba M, Sato J. Establishment and some biological characteristics of human hepatoma cell lines. *Gann* 1975; **66**: 385-392
- 14 **Alexander JJ**, Bey EM, Geddes EW, Lecatsas G. Establishment of a continuously growing cell line from primary carcinoma of the liver. *S Afr Med J* 1976; **50**: 2124-2128
- 15 **Tang ZY**, Sun FX, Tian J, Ye SL, Liu YK, Liu KD, Xue Q, Chen J, Xia JL, Qin LX, Sun HC, Wang L, Zhou J, Li Y, Ma ZC, Zhou XD, Wu ZQ, Lin ZY, Yang BH. Metastatic human hepatocellular carcinoma models in nude mice and cell line with metastatic potential. *World J Gastroenterol* 2001; **7**: 597-601
- 16 **Murakami T**, Yano H, Maruiwa M, Sugihara S, Kojiro M. Establishment and characterization of a human combined hepatocarcinoma cell line and its heterologous transplantation in nude mice. *Hepatology* 1987; **7**: 551-556
- 17 **Saito H**, Morizane T, Watanabe T, Kagawa T, Iwabuchi MN, Kumagai N, Inagaki Y, Tsuchimoto K, Tsuchiya M. Establishment of a human cell line (HCC-T) from a patient with hepatoma bearing no evidence of hepatitis B or A virus infection. *Cancer* 1989; **64**: 1054-1060
- 18 **Sing GK**, Pace R, Prior S, Scott JS, Shield P, Martin N, Searle J, Battersby C, Powell LW, Cooksley WG. Establishment of a cell line from a hepatocellular carcinoma from a patient with hemochromatosis. *Hepatology* 1994; **20**(1 Pt 1): 74-81
- 19 **Le Jossic C**, Glaize D, Corcos L, Diot C, Dezier JF, Fautrel A, Guguen-Guillouzo C. Trans-Acting factors, detoxication enzymes and hepatitis B virus replication in a novel set of human hepatoma cell lines. *Eur J Biochem* 1996; **238**: 400-409
- 20 **Lee JH**, Ku JL, Park YJ, Lee KU, Kim WH, Park JG. Establishment and characterization of four human hepatocellular carcinoma cell lines containing hepatitis B virus DNA. *World J Gastroenterol* 1999; **5**: 289-295
- 21 **Seki S**, Kitada T, Kawada N, Sakaguchi H, Kadoya H, Nakatani K, Satake K, Kuroki T. Establishment and characteristics of human hepatocellular carcinoma cells with metastasis to lymph nodes. *Hepatogastroenterology* 1999; **46**: 2812-2817
- 22 **Tian J**, Tang ZY, Ye SL, Liu YK, Lin ZY, Chen J, Xue Q. New human hepatocellular carcinoma (HCC) cell line with highly metastatic potential (MHCC97) and its expressions of the factors associated with metastasis. *Br J Cancer* 1999; **81**: 814-821
- 23 **Li Y**, Tang ZY, Ye SL, Liu YK, Chen J, Xue Q, Chen J, Gao DM, Bao WH. Establishment of cell clones with different metastatic potential from the metastatic hepatocellular carcinoma cell line MHCC97. *World J Gastroenterol* 2001; **7**: 630-636
- 24 **Yang JX**, Tang WX. Establishment of a cisplatin-induced human hepatocellular carcinoma drug-resistant cell line and its biological characteristics. *Aizheng* 2002; **21**: 872-876
- 25 **Wu X**, Wang Z, Liu B, Liu J, Gao Y, Li Z, Liu C. Establishment and characterization of human extrahepatic growing hepatocellular carcinoma cell line EGHC-9901. *Zhonghua Waike Zazhi* 2002; **40**: 616-617
- 26 **Li Y**, Tang Z, Ye S, Liu Y, Chen J, Xue Q, Huang X, Chen J, Bao W, Yang J, Gao D. Establishment of human hepatocellular carcinoma cell line with spontaneous pulmonary metastasis through *in vivo* selection. *Zhonghua Yixue Zazhi* 2002; **82**: 601-605
- 27 **Wen JM**, Huang JF, Hu L, Wang WS, Zhang M, Sham JS, Xu JM, Zeng WF, Xie D, Liang LJ, Guan XY. Establishment and characterization of human metastatic hepatocellular carcinoma cell line. *Cancer Genet Cytogenet* 2002; **135**: 91-95
- 28 **Jiang JL**, Zhou Q, Yu MK, Ho LS, Chen ZN, Chan HC. The involvement of HAb18G/CD147 in regulation of store-operated calcium entry and metastasis of human hepatoma cells. *J Biol Chem* 2001; **276**: 46870-46877
- 29 **Li Y**, Shang P, Qian AR, Wang L, Yang Y, Chen ZN. Inhibitory effects of antisense RNA of HAb18G/CD147 on invasion of hepatocellular carcinoma cells *in vitro*. *World J Gastroenterol* 2003; **9**: 2174-2177
- 30 **Kim GJ**, Cho SJ, Won NH, Sung JM, Kim H, Chun YH, Park SH. Genomic imbalances in Korean hepatocellular carcinoma. *Cancer Genet Cytogenet* 2003; **142**: 129-133
- 31 **Shindo-Okada N**, Takeuchi K, Nagamachi Y. Establishment of cell lines with high- and low-metastatic potential from PC-14 human lung adenocarcinoma. *Jpn J Cancer Res* 2001; **92**: 174-183
- 32 **Tammen H**, Kreipe H, Hess R, Kellmann M, Lehmann U, Pich A, Lamping N, Schulz-Knappe P, Zucht HD, Lilischkis R. Expression profiling of breast cancer cells by differential peptide display. *Breast Cancer Res Treat* 2003; **79**: 83-93
- 33 **Nelson SJ**, Cha S. Imaging glioblastoma multiforme. *Cancer J* 2003; **9**: 134-145
- 34 **Yang J**, Qin LX, Ye SL, Liu YK, Li Y, Gao DM, Chen J, Tang ZY. The abnormalities of chromosome 8 in two hepatocellular carcinoma cell clones with the same genetic background and different metastatic potential. *J Cancer Res Clin Oncol* 2003; **129**: 303-308
- 35 **Mazure NM**, Chauvet C, Bois-Joyeux B, Bernard MA, Nacer-Cherif H, Danan JL. Repression of alpha-fetoprotein gene expression under hypoxic conditions in human hepatoma cells: characterization of a negative hypoxia response element that mediates opposite effects of hypoxia inducible factor-1 and c-Myc. *Cancer Res* 2002; **62**: 1158-1165
- 36 **Taketa K**, Okada S, Win N, Hlaing NK, Wind KM. Evaluation of tumor markers for the detection of hepatocellular carcinoma in Yangon General Hospital, Myanmar. *Acta Med Okayama* 2002; **56**: 317-330

Overexpression of annexin 1 in pancreatic cancer and its clinical significance

Xiao-Feng Bai, Xiao-Guang Ni, Ping Zhao, Shang-Mei Liu, Hui-Xin Wang, Bing Guo, Lan-Ping Zhou, Fang Liu, Jin-Sheng Zhang, Kun Wang, Yong-Qiang Xie, Yong-Fu Shao, Xiao-Hang Zhao

Xiao-Feng Bai, Xiao-Guang Ni, Ping Zhao, Shang-Mei Liu, Hui-Xin Wang, Lan-Ping Zhou, Fang Liu, Jin-Sheng Zhang, Yong-Qiang Xie, Yong-Fu Shao, Xiao-Hang Zhao, National Laboratory of Molecular Oncology, Department of Abdominal Surgery, Department of Pathology, Cancer Institute and Hospital, Chinese Academy of Medical Sciences and Peking Union Medical College, Beijing 100021, China

Kun Wang, Xiao-Hang Zhao, Beijing Yanjing Hospital, Beijing 100037, China

Bing Guo, Department of Head, Neck and Breast, Mudanjiang Tumor Hospital, Mudanjiang 157009, Heilongjiang Province, China

Supported by National Natural Science Foundation of China NO. 30240050, 30225045, 39990570, 30171049, and 30370713 and National High Tech R & D Program of China, 2001AA227091

Co-first-authors: Xiao-Guang Ni

Correspondence to: Xiao-Hang Zhao, M.D., Ph.D. National Laboratory of Molecular Oncology, Cancer Institute and Hospital, Chinese Academy of Medical Sciences and Peking Union Medical College, Beijing 100021, China. zhaoxh@pubem.cicams.ac.cn

Telephone: +86-10-67709015 **Fax:** +86-10-67709015

Received: 2004-01-15 **Accepted:** 2004-02-24

Abstract

AIM: To investigate the expression of annexin I in pancreatic cancer and its relationship with the clinicopathologic factors, and to evaluate its potential clinical significance.

METHODS: Annexin I expression was analyzed by Western blot and immunohistochemical staining in pancreatic adenocarcinoma and multi-tissue microarrays (MTAs).

RESULTS: Western blot analysis showed that annexin I was overexpressed in 84.6% (11/13) pancreatic ductal adenocarcinomas. Immunohistochemistry analysis of pancreatic cancer in MTAs showed that annexin I protein was 71.4%(30/42) positive which was markedly increased compared with that in the tumor matched normal pancreas tissues 18.4%(7/38) ($P<0.01$). In the meantime, the high expression of annexin 1 was correlated with the poor differentiation of pancreatic adenocarcinoma.

CONCLUSION: Annexin 1 overexpression is a frequent biological marker and correlates with the differentiation of pancreatic cancer during tumorigenesis.

Bai XF, Ni XG, Zhao P, Liu SM, Wang HX, Guo B, Zhou LP, Liu F, Zhang JS, Wang K, Xie YQ, Shao YF, Zhao XH. Overexpression of annexin 1 in pancreatic cancer and its clinical significance. *World J Gastroenterol* 2004; 10(10): 1466-1470
<http://www.wjgnet.com/1007-9327/10/1466.asp>

INTRODUCTION

Pancreatic cancer is one of the most lethal malignancies with less than 3-5% of the overall five-year survival rate, and the patients normally die within six months after diagnosis^[1]. There

are some indications that the incidence of pancreatic cancer following an upward increase, in recent years it has reached a plateau and in some countries there is even a slight decrease. But in China the incidence and mortality rates of this disease have taken an upward trend countrywide. Based on the data of demography and death collected through Chinese Disease Surveillance Point System (DSPS) over the period of 1991-2000, the age-standardized mortality rate due to pancreatic cancer increased from 2.18 in 1991 to 3.26 in 2000 per 1000 000 populations and the peak mortality of pancreatic cancer might arrive in China in the next few decades^[2]. In the United States, more than >30 000 people were diagnosed and died of pancreatic cancer in 2003, representing the fourth leading cause of cancer death^[1]. The significant factor for the poor prognosis of pancreatic cancer may be attributed to its biological aggressiveness, the difficulty of early diagnosis, and poor response to conventional therapeutics, those reflect a fact that pancreatic cancer is a poorly understood disease and the etiologic factors and the molecular basis for these characteristics are unknown. Comparisons of global gene and protein expression profiles between pancreatic cancer and normal pancreas using high-throughput methods could provide important information about the molecular characteristics and reveal some new specific or associated biomarkers of pancreatic cancer with promise for development into novel diagnostic or therapeutic targets^[3-7].

Annexin 1, a member of annexin family, was found with expression alterations in different kinds of malignant tumors. The molecular mechanisms and the clinical significance of annexin I altered expression still remain a debate. In this study, we investigated annexin I expression and distributions in a large number of pancreatic cancer specimens via Western blot and immunohistochemistry analysis based on multi-tissue microarrays (MTAs).

MATERIALS AND METHODS

Patients and specimens

Fresh tissue samples of 13 pancreatic cancers and their corresponding normal counterparts were obtained at the time of resection with informed consent from Cancer Institute and Hospital (CIH), Chinese Academy of Medical Sciences (CAMS) and Peking Union Medical College (PUMC) during November 2001 and November 2003. The samples were cut into two parts, one was snap-frozen in liquid nitrogen before storage at -80 °C, and the other was fixed with 10% formalin for histopathological diagnosis. Histological diagnosis of these samples was all pancreatic ductal adenocarcinomas. This group consisted of 8 males and 5 females with a median age of 64 years (range, 39-75 years). None of them received preoperative radiotherapy or chemotherapy.

Formalin-fixed paraffin-embedded tissue blocks of pancreatic cancer and normal pancreatic tissue were collected from the archives of the Department of Surgery at CIH, CAMS and Mudanjiang Tumor Hospital between January 1991 and August 2002 and subjected to tissue microarray construction. There were 32 pancreatic ductal adenocarcinomas, 6 mucinous

adenocarcinomas, 4 acinar cell carcinomas, 7 islet cell carcinomas, 8 ampulla of Vater carcinomas. The median age of these patients (37 males and 20 females) at the diagnosis was 60 years (range, 19-71 years).

Human pancreatic cancer cell lines BxPC-3 and PANC-1 were purchased from American Type Culture Collection (Manassas, VA). BxPC-3 and PANC-1 cells were cultured in RPMI 1640 and Dulbecco's modified Eagle's medium, respectively, and supplemented with 100 g/L heat-inactivated fetal bovine serum, 100 U/mL penicillin, and 100 µg/mL streptomycin.

Western blot analysis

Total tissue and cell lysate were prepared in extraction buffer containing 50 mmol/L Tris-HCl (pH 7.4), 150 mmol/L NaCl, 10 g/L Triton-100, 1 g/L SDS, 1 mmol/L EDTA, 1 mmol/L AEBSF, 20 µg/mL aprotinin, and 20 µg/mL leupeptin. After centrifugation at 12 000 g for 15 min at 4 °C, the supernatant was collected, and protein concentration was determined by Bradford method^[8]. Equal amounts of total protein (10 µg) from each sample were loaded and separated by 120 g/L SDS-polyacrylamide gel electrophoresis, and then transferred to Hybond-P polyvinylidene difluoride (PVDF) membrane (Amersham Pharmacia Biotech, Piscataway, NJ). After blocked with 50 g/L nonfat dry milk in PBS (pH 7.4) with 1 g/L Tween-20, membranes were probed with a mouse anti-annexin I monoclonal antibody (1:1 000 dilution, BD Biosciences Pharmingen, Chicago, IL), followed by subsequent incubation with horseradish peroxidase-conjugated goat anti-mouse secondary antibody (1:3 000 dilution, Santa Cruz Biotechnology, Santa Cruz, CA). Visualization of the protein bands was performed by the enhanced chemiluminescence kit (Santa Cruz Biotechnology). Parallel Western blot was probed with an anti- α -tubulin monoclonal antibody (Santa Cruz Biotechnology) as a loading control.

MTAs construction and immunohistochemistry analysis

Formalin-fixed paraffin-embedded tissue blocks containing pancreatic adenocarcinoma and normal pancreatic tissues were identified on the hematoxylin and eosin stained slide and marked. The marked areas in the corresponding paraffin block (donor block) were used for tissue microarray construction. From these defined areas of each specimen, triplicate tissue cores with a diameter of 0.6 mm were taken from donor block and arrayed into a recipient paraffin block using a tissue puncher/arrayer (Beecher Instruments, Silver Spring, MD) as previously described^[9]. Five micrometer sections of the tissue array block were cut and placed on Fisherbrand Colorfrost/Plus microscope slides (Fisher scientific, Pittsburgh, PA) for immunohistochemical staining.

The streptavidin-peroxidase method was used for the immunostaining of annexin I. Briefly, after deparaffinization in xylene and rehydration in grade ethanol, endogenous peroxidase activity was blocked by incubation with 3% hydrogen peroxide for 10 min. Tissue sections were then heated at 100 °C in 10 mmol/L citrate buffer (pH 6.0) for 10 min to retrieve antigens and pre-incubated with normal horse serum for 20 min at room temperature. Mouse anti-annexin I monoclonal antibody (BD Biosciences Pharmingen) diluted 1:100 was used as the primary antibody, and the specimens were incubated with it overnight at 4 °C, followed by addition of biotinylated anti-mouse secondary antibody and streptavidin-horseradish peroxidase (Zymed Laboratories, South San Francisco, CA). 3,3'-diaminobenzidine was used as a chromogen, and hematoxylin was used for counterstaining. For negative control purposes, the same procedure was followed except that the primary antibody was replaced by PBS. Known immunostaining-positive slides were used as positive controls.

The level of annexin I expression was calculated by combining an estimate of the percentage of immunoreactive cells (quantity score) with an estimate of the staining intensity (staining intensity score) as follows. No staining was scored as 0, 1-10% of cells with positive staining were scored as 1, 10-50% as 2, 50-70% as 3, and 70-100% as 4. Staining intensity was rated on a scale of 0 to 3 as follows: 0=negative (no color); 1=weak (weak yellow), 2=moderate (yellow), and 3=strong (brown). The raw data were converted to the immunohistochemical score (IHS) by multiplying the quantity and staining intensity scores. Therefore, the score could range from 0 to 12. The IHS score >3 was considered as positive expression^[10].

Statistical analysis

Statistical analysis was performed using the SPSS 10.0 software package (SPSS, Chicago, IL). The annexin I expression in different groups was analyzed using Mann-Whitney *U* test. The correlation between annexin I and each clinicopathologic factor was assessed with the Spearman rank correlation test. *P* value of less than 0.05 was considered statistically significant.

RESULTS

Western blot analysis of annexin I expression

Ten micrograms of protein extracts of pancreatic ductal adenocarcinoma tissues and their corresponding normal pancreas tissues from 13 different patients was prepared for Western blot analysis using monoclonal anti-annexin I antibody. This antibody could detect specific bands migrating at 37 ku (Figure 1). Western blot revealed that the expression of annexin I was low or undetectable in normal pancreas tissues. The level of annexin I expression was markedly increased in pancreatic ductal adenocarcinoma. Annexin I overexpression was found in 84.6% (11/13) pancreatic ductal adenocarcinoma tissues. There was also a strong expression of annexin I in pancreatic cancer cell lines.

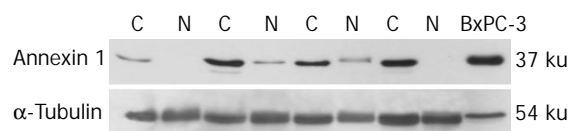


Figure 1 Western blot analysis of annexin I in pancreatic ductal adenocarcinoma. Ten micrograms of total protein extracts from pancreatic tissues and cell lines were run on 120 g/L SDS-PAGE, and annexin I protein expression was probed with mouse anti-annexin I monoclonal antibody and visualized by chemiluminescence (*top panel*). C: pancreatic ductal adenocarcinoma tissues; N: normal pancreas tissues; BxPC-3: human pancreatic adenocarcinoma cell line. α -Tubulin was used as an internal control (*bottom panel*).

Immunohistochemistry analysis of annexin I using pancreatic cancer MTAs

We carried out immunohistochemical studies for annexin I on the paraffin-embedded pancreatic cancer tissue microarray (Figure 2. A, B). This tissue microarray contained a total of 256 tissue spots consisting of 32 pancreatic ductal adenocarcinomas, 6 mucinous adenocarcinomas, 4 acinar cell carcinomas, 7 islet cell carcinomas, 8 ampulla of Vater carcinomas, and 38 normal pancreas tissues. In the normal pancreas, the positive rate of annexin I expression was 18.4% (7/38). It was found that most of normal pancreatic acinar and ductal cells did not express annexin I. There were only a small number of acinar cells that were observed. Annexin I cytoplasmic positive and the scattered positive cells were mainly located on the outside of acinar lumen (Figure 2. C, D). In contrast, positive expression of annexin I in

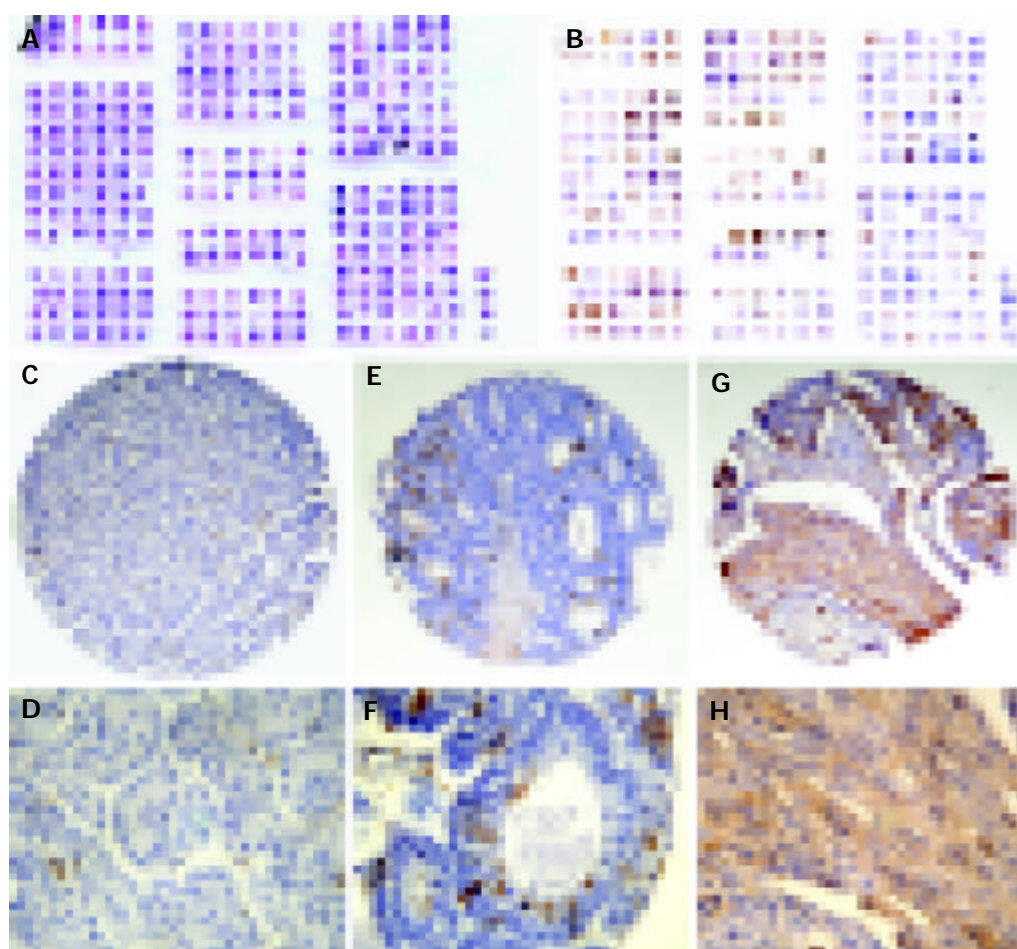


Figure 2 Immunohistochemical analysis of annexin I expression on pancreatic cancer MTAs. A and B: Overview of the H & E staining and immunohistochemical staining of annexin I on pancreatic cancer MTAs; C ($\times 200$) and D ($\times 400$): normal pancreas; E ($\times 200$) and F ($\times 400$): well differentiated ductal adenocarcinoma; G ($\times 200$) and H ($\times 400$): poorly differentiated ductal adenocarcinoma.

pancreatic cancer (71.4%, 30/42) was up-regulated significantly ($P < 0.01$). The different subtypes of the tumor were observed partially positive (Table 1). The possible relationships between annexin I expression with some clinicopathologic factors were additionally analyzed. It was found that the positive expression rate of annexin I in poorly differentiated pancreatic ductal adenocarcinomas (81.8%, 9/11) increased markedly compared with the well and moderately differentiated types (71.4%, 15/21) ($P < 0.05$). According to the progress of tumorigenesis, the distributions of annexin I were found altered from the outside of normal acinar lumen to the inside cancerous acinar lumen in the well differentiated ductal adenocarcinomas, and then to the most of poorly differentiated ductal adenocarcinomas separately (Figure 2. C, D, E, F, G, H). There were no statistically significant correlations between annexin I expression and lymph node metastasis and TNM stages (Table 2).

Table 1 Annexin I expression in normal pancreas and cancer tissues

Group	<i>n</i>	Positive rate of annexin I expression (%)	<i>P</i> value
Normal pancreas	38	18.4(7/38)	<0.0001
Pancreatic cancer	42	71.4(30/42)	
Ductal adenocarcinoma	32	75(24/32)	
Mucinous adenocarcinoma	6	83.3(5/6)	
Acinar cell carcinoma	4	25(1/4)	
Islet cell carcinoma	7	57.1(4/7)	
Ampulla of Vater carcinoma	7	57.1(4/7)	

Table 2 Correlation of annexin I expression with clinicopathologic factors of pancreatic adenocarcinoma on tissue microarray

Clinicopathologic factors	<i>n</i>	Positive expression rate of annexin I (%)	<i>P</i> value
Histological differentiation			0.012
High and moderate	21	71.4(15/21)	
Poor	11	81.8(9/11)	
Lymph node metastasis			0.810
Yes	8	75(6/8)	
No	34	73.5(25/3)	
TNM stage			0.551
I	15	66.7(10/15)	
II	21	81(17/21)	
III	5	60(3/5)	

DISCUSSION

Annexin I belongs to the family of the calcium and phospholipid-binding proteins, called annexins. Annexins are cytosolic or associated with the membrane or the cytoskeleton in a calcium-dependent manner. Annexin I is one of the more extensively studied annexins, which was initially cloned as phospholipase A2 (PLA2) inhibitor^[11]. Annexin I is a steroid-regulated protein and thus implicated in some actions of glucocorticoids, including inhibition of cell proliferation, anti-inflammatory effects, the regulation of cell migration, differentiation, death and the hypothalamic-pituitary axis^[12-16]. To date, there are some contradictory descriptions on annexin I expression in human

cancers. It has been reported that annexin I is up-regulated in human breast cancer^[17], hepatocellular carcinoma^[18], and pituitary adenoma^[19] and down-regulated in human esophageal squamous cell carcinoma^[20], prostate cancer^[21], and endometrial carcinoma^[22]. In this study, we found that annexin I was significantly overexpressed in pancreatic cancer by Western blot and immunohistochemistry, which was consistent with the results of gene expression profile analysis.

Annexin I is expressed in a tissue-specific manner in rodents. The highest annexin 1 expression level was found in lung and placenta; moderate in spleen, thymus, prostate, and submaxillary gland; and low (or absent) in muscle, brain, and liver^[23]. However, it was found that annexin I expression and phosphorylation were not only up-regulated during liver regeneration and transformation in antithrombin III SV40 T large antigen transgenic mice, but also overexpressed at both the transcriptional and translational levels in tumorous and nontumorous regions of hepatocellular carcinoma (HCC)^[18,24]. Annexin I up-regulation has been found to be correlated with increased synthesis of epidermal growth factor (EGF) and consequently with increased phosphorylation of EGF receptor (EGFR). Annexin I is a substrate for tyrosine kinases such as EGFR^[23,25] and for serine/threonine kinases such as protein kinase C^[26]. Annexin I can specifically modulate the extracellular signal-regulated kinase (ERK) signal cascade at an upstream site probably by associating with key signal components including the adaptor protein Grb2. Increased expression of annexin I could lead to constitutive activation of ERK1/2 kinase in macrophages^[27]. These findings implicated that annexin I might involve in mitogenic signal transduction and regulate cell growth. It was found that the level of annexin I expression increased three to four fold when quiescent human diploid foreskin fibroblasts (HFF) cells were stimulated to proliferate^[28]. This observation suggested that annexin I might be directly or indirectly involved in cellular proliferation. Pancreatic cancer demonstrated abnormally high expression of a number of important tyrosine kinase growth factors and receptors, particularly of the EGF family, which may contribute to the neoplasm's growth by autocrine and paracrine effects^[29]. Because annexin I is a substrate protein of EGFR, we can postulate that activated EGFR pathway promotes the annexin I up-regulation and then might associate with pancreas malignant transformation. We evaluated the relationship between annexin I and the clinicopathological factors of pancreatic cancer, and found that higher annexin I expression was correlated with the poorly differentiated type of pancreatic cancer, which was similar to the finding in HCC^[18]. These results suggest that annexin I is also involved in histological differentiation. It is interesting that the location of annexin I expression in different histologically differentiated types was changed, the reason for this change is not clear, which might be due to the role of annexin I in different places^[30].

On the other hand, enhanced expression of annexin I could reduce *in vitro* peripheral blood lymphocyte response to mitogens and might involve in the immunosuppressive mechanism of tumor-bearing hosts^[31]. Annexin I-derived peptides could inhibit antigen-driven human T cell proliferation and cytokine production^[32]. High constitutive levels of annexin I in leukaemic cells might protect them against immune-mediated killing^[33]. These evidences suggested that elevated annexin I might influence the immune defence system of body and might serve as a poor prognostic marker.

In conclusion, the present results show that overexpression of annexin I is a frequent event in pancreatic cancer, which may be one of the factors that link with the malignant transformation, lower differentiation and poor prognosis of pancreatic cancer. Detection of annexin I expression may be assistant to clinical diagnosis and can assess the prognosis of

pancreatic cancer. However, more efforts need to address the molecular mechanisms.

ACKNOWLEDGMENTS

We thank professor You-Yong Lu, Ms. Min Zhao and Dr. Zhuo-Bin Tang, Beijing Laboratory of Molecular Oncology, Beijing Institute for Cancer Research of Peking University for their help with tissue microarray construction.

REFERENCES

- 1 **Jemal A**, Murray T, Samuels A, Ghafoor A, Ward E, Thun MJ. Cancer statistics, 2003. *CA Cancer J Clin* 2003; **53**: 5-26
- 2 **Wang L**, Yang GH, Lu XH, Huang ZJ, Li H. Pancreatic cancer mortality in China (1991-2000). *World J Gastroenterol* 2003; **9**: 1819-1823
- 3 **Tan ZJ**, Hu XG, Cao GS, Tang Y. Analysis of gene expression profile of pancreatic carcinoma using cDNA microarray. *World J Gastroenterol* 2003; **9**: 818-823
- 4 **Rosty C**, Christa L, Kuzdzal S, Baldwin WM, Zahurak ML, Carnot F, Chan DW, Canto M, Lillemoe KD, Cameron JL, Yeo CJ, Hruban RH, Goggins M. Identification of hepatocarcinoma-intestine-pancreas/pancreatitis-associated protein I as a biomarker for pancreatic ductal adenocarcinoma by protein biochip technology. *Cancer Res* 2002; **62**: 1868-1875
- 5 **Iacobuzio-Donahue CA**, Maitra A, Shen-Ong GL, van Heek T, Ashfaq R, Meyer R, Walter K, Berg K, Hollingsworth MA, Cameron JL, Yeo CJ, Kern SE, Goggins M, Hruban RH. Discovery of novel tumor markers of pancreatic cancer using global gene expression technology. *Am J Pathol* 2002; **160**: 1239-1249
- 6 **Han H**, Bearss DJ, Browne LW, Calaluze R, Nagle RB, Von Hoff DD. Identification of differentially expressed genes in pancreatic cancer cells using cDNA microarray. *Cancer Res* 2002; **62**: 2890-2896
- 7 **Iacobuzio-Donahue CA**, Maitra A, Olsen M, Lowe AW, van Heek NT, Rosty C, Walter K, Sato N, Parker A, Ashfaq R, Jaffee E, Ryu B, Jones J, Eshleman JR, Yeo CJ, Cameron JL, Kern SE, Hruban RH, Brown PO, Goggins M. Exploration of global gene expression patterns in pancreatic adenocarcinoma using cDNA microarrays. *Am J Pathol* 2003; **162**: 1151-1162
- 8 **Bradford MM**. A rapid and sensitive method for the quantitation of microgram quantities of protein utilizing the principle of protein-dye binding. *Anal Biochem* 1976; **72**: 248-254
- 9 **Kononen J**, Bubendorf L, Kallioniemi A, Barlund M, Schraml P, Leighton S, Torhorst J, Mihatsch MJ, Sauter G, Kallioniemi OP. Tissue microarrays for high-throughput molecular profiling of tumor specimens. *Nat Med* 1998; **4**: 844-847
- 10 **Friedrichs K**, Gluba S, Eidtmann H, Jonat W. Overexpression of p53 and prognosis in breast cancer. *Cancer* 1993; **72**: 3641-3647
- 11 **Wallner BP**, Mattaliano RJ, Hession C, Cate RL, Tizard R, Sinclair LK, Foeller C, Chow EP, Browning JL, Ramachandran KL, Pepinsky RB. Cloning and expression of human lipocortin, a phospholipase A2 inhibitor with potential anti-inflammatory activity. *Nature* 1986; **320**: 77-81
- 12 **Flower RJ**, Rothwell NJ. Lipocortin-1: cellular mechanisms and clinical relevance. *Trends Pharmacol Sci* 1994; **15**: 71-76
- 13 **Parente L**, Solito E. Annexin I: more than an anti-phospholipase protein. *Inflamm Res* 2004; **53**: 125-132
- 14 **Perretti M**, Gavins FN. Annexin 1: an endogenous anti-inflammatory protein. *News Physiol Sci* 2003; **18**: 60-64
- 15 **de Coupade C**, Solito E, Levine JD. Dexamethasone enhances interaction of endogenous Annexin 1 with L-selectin and triggers shedding of L-selectin in the monocytic cell line U-937. *Br J Pharmacol* 2003; **140**: 133-145
- 16 **Buckingham JC**, Flower RJ. Lipocortin 1: a second messenger of glucocorticoid action in the hypothalamo-pituitary-adrenocortical axis. *Mol Med Today* 1997; **3**: 296-302
- 17 **Ahn SH**, Sawada H, Ro JY, Nicolson GL. Differential expression of annexin I in human mammary ductal epithelial cells in normal and benign and malignant breast tissues. *Clin Exp Metastasis* 1997; **15**: 151-156
- 18 **Masaki T**, Tokuda M, Ohnishi M, Watanabe S, Fujimura T, Miyamoto K, Itano T, Matsui H, Arima K, Shirai M, Maeba T,

- Sogawa K, Konishi R, Taniguchi K, Hatanaka Y, Hatase O, Nishioka M. Enhanced expression of the protein kinase substrate annexin in human hepatocellular carcinoma. *Hepatology* 1996; **24**: 72-81
- 19 **Mulla A**, Christian HC, Solito E, Mendoza N, Morris JF, Buckingham JC. Expression, subcellular localization and phosphorylation status of annexins 1 and 5 in human pituitary adenomas and a growth hormone-secreting carcinoma. *Clin Endocrinol* 2004; **60**: 107-119
- 20 **Paweletz CP**, Ornstein DK, Roth MJ, Bichsel VE, Gillespie JW, Calvert VS, Vocke CD, Hewitt SM, Duray PH, Herring J, Wang QH, Hu N, Linehan WM, Taylor PR, Liotta LA, Emmert-Buck MR, Petricoin EF 3rd. Loss of annexin I correlates with early onset of tumorigenesis in esophageal and prostate carcinoma. *Cancer Res* 2000; **60**: 6293-6297
- 21 **Xin W**, Rhodes DR, Ingold C, Chinnaiyan AM, Rubin MA. Dysregulation of the annexin family protein family is associated with prostate cancer progression. *Am J Pathol* 2003; **162**: 255-261
- 22 **Da J**, Meng X, Wang P, Yang Z, Zhu Y. Significance on expressions of Annexin-I and its correlative gene proteins in endometrial hyperplasia, atypical hyperplasia and endometrial carcinoma. *Zhonghua Binglixue Zazhi* 2001; **30**: 256-259
- 23 **De BK**, Misono KS, Lukas TJ, Mroczkowski B, Cohen S. A calcium-dependent 35-kilodalton substrate for epidermal growth factor receptor/kinase isolated from normal tissue. *J Biol Chem* 1986; **261**: 13784-13792
- 24 **de Coupade C**, Gillet R, Bennoun M, Briand P, Russo-Marie F, Solito E. Annexin I expression and phosphorylation are upregulated during liver regeneration and transformation in antithrombin III SV40 T large antigen transgenic mice. *Hepatology* 2000; **31**: 371-380
- 25 **Fava RA**, Cohen S. Isolation of a calcium-dependent 35-kilodalton substrate for the epidermal growth factor receptor/kinase from A-431 cells. *J Biol Chem* 1984; **259**: 2636-2645
- 26 **Khanna NC**, Tokuda M, Chong SM, Waisman DM. Phosphorylation of p36 *in vitro* by protein kinase C. *Biochem Biophys Res Commun* 1986; **137**: 397-403
- 27 **Aldridge LC**, Harris HJ, Plevin R, Hannon R, Bryant CE. The annexin protein lipocortin 1 regulates the MAPK/ERK pathway. *J Biol Chem* 1999; **274**: 37620-37628
- 28 **Schlaepfer DD**, Haigler HT. Expression of annexins as a function of cellular growth state. *J Cell Biol* 1990; **111**: 229-238
- 29 **Coppola D**. Molecular prognostic markers in pancreatic cancer. *Cancer Control* 2000; **7**: 421-427
- 30 **Liu Y**, Wang HX, Lu N, Mao YS, Liu F, Wang Y, Zhang HR, Wang K, Wu M, Zhao XH. Translocation of annexin I from cellular membrane to the nuclear membrane in human esophageal squamous cell carcinoma. *World J Gastroenterol* 2003; **9**: 645-649
- 31 **Koseki H**, Shiiba K, Suzuki Y, Asanuma T, Matsuno S. Enhanced expression of lipocortin-1 as a new immunosuppressive protein in cancer patients and its influence on reduced *in vitro* peripheral blood lymphocyte response to mitogens. *Surg Today* 1997; **27**: 30-39
- 32 **Kamal AM**, Smith SF, De Silva Wijayasinghe M, Solito E, Corrigan CJ. An annexin I (ANXA1)-derived peptide inhibits prototype antigen-driven human T cell Th1 and Th2 responses *in vitro*. *Clin Exp Allergy* 2001; **31**: 1116-1125
- 33 **Wu YL**, Jiang XR, Lillington DM, Newland AC, Kelsey SM. Upregulation of lipocortin 1 inhibits tumour necrosis factor-induced apoptosis in human leukaemic cells: a possible mechanism of resistance to immune surveillance. *Br J Haematol* 2000; **111**: 807-816

Edited by Kumar M and Wang XL Proofread by Xu FM

Mesenteric artery remodeling and effects of imidapril and irbesartan on it in spontaneously hypertensive rats

Zhong-Sheng Zhu, Jin-Ming Wang, Shao-Liang Chen

Zhong-Sheng Zhu, Jin-Ming Wang, Department of Cardiovascular Medicine, People's Hospital of Wuhan University, Wuhan 430060, Hubei Province, China

Shao-Liang Chen, Department of Cardiovascular Medicine, Third Affiliated Hospital of Nanjing Medical University, Nanjing 210006, Jiangsu Province, China

Supported by the Natural Science Foundation of Education Office of Hubei Province, No. 2000B03023/3011400802

Correspondence to: Dr. Zhong-Sheng Zhu, Department of Cardiovascular Medicine, Third Affiliated Hospital of Nanjing Medical University, Nanjing 210006, Jiangsu Province, China. zhuzhongsheng6966@hotmail.com

Telephone: +86-13016973706

Received: 2003-10-24 **Accepted:** 2003-12-08

Abstract

AIM: To investigate the remodeling of mesenteric artery and the expression of TGF- β_1 , c-Jun in mesenteric artery and effects of imidapril and irbesartan on the remodeling in spontaneously hypertensive rats (SHR).

METHODS: Thirty SHR (male/female, 21/9), aged 13 wk, were randomly divided into 3 groups (7 male rats and 3 female rats each group): SHR group, imidapril group (imidapril 3 mg/kg·d was given in drinking water for 14 wk), and irbesartan group (irbesartan 50 mg/kg·d was given in drinking water for 14 wk). Ten homogenous Wistar Kyoto rats, 5 males and 5 females, weighing 206±49 g, were selected as normal control group (WKY group). Systolic pressure was measured on d 1, 2, 4, 6, 8, 10, 12 and 14 during the experiment and the rats were killed at the end of the experiment. Angiotensin II (Ang II) level in plasma and mesenteric arteries was measured by radioimmunoassay. The morphology of the secondary branches of mesenteric artery were examined by light microscopy and electron microscopy. Reverse transcription polymerase chain reaction (RT-PCR) was used to detect the expression of transforming growth factor TGF- β_1 and c-Jun mRNA.

RESULTS: Compared with imidapril group and irbesartan group, the blood pressure was remarkably increased in SHR group. Ang II level in plasma and mesenteric arteries in SHR group was the same or lower than that in WKY group, and was higher in irbesartan group and lower in imidapril group. The remodeling of mesenteric arteries in SHR group was mostly obvious among the 4 groups. The ratio of TGF- β_1 absorbed light value to GAPDH absorbed light value in the SHR group was 0.887±0.019, which was significantly higher than that in WKY group, imidapril group, and irbesartan group with the ratios of 0.780±0.018, 0.803±0.005, and 0.847±0.017, respectively ($P<0.01$). Ang II level in plasma and mesenteric arteries in imidapril group was significantly lower than that in irbesartan group ($P<0.05$). The c-Jun absorbed light value/GAPDH absorbed light value of mesenteric arteries in the SHR group was 0.850±0.015, which was significantly higher than that in the WKY, imidapril, and irbesartan groups (0.582±0.013,

0.743±0.012, and 0.789±0.013, respectively, $P<0.01$), and was significantly lower in imidapril group than in irbesartan group ($P<0.05$).

CONCLUSION: Imidapril and irbesartan can not only control blood pressure but also inhibit mesenteric arteries remodeling and mRNA expression of TGF- β_1 , c-Jun in SHR. Imidapril is more effective than irbesartan.

Zhu ZS, Wang JM, Chen SL. Mesenteric artery remodeling and effects of imidapril and irbesartan on it in spontaneously hypertensive rats. *World J Gastroenterol* 2004; 10(10): 1471-1475

<http://www.wjgnet.com/1007-9327/10/1471.asp>

INTRODUCTION

It has been reported^[1-3] that angiotensin-converting enzyme inhibitor (ACEI) and angiotensin II type 1 (AT1) receptor antagonist can inhibit resistance blood vessel remodeling, but their action mechanism is still unknown. We selected irbesartan and imidapril to interfere mesenteric artery remodeling in spontaneously hypertensive rats (SHR) to investigate the expression of c-Jun and TGF- β_1 mRNA in resistance blood vessel of each group rats with reverse transcription polymerase chain reaction (RT-PCR) and to illustrate the mechanism of resistance blood vessel remodeling in hypertension and possible mechanism of these two drugs inhibiting mesenteric artery remodeling and possible effect on the inhibition of mesenteric artery remodeling.

MATERIALS AND METHODS

Materials

Thirty 13-wk old SHR (male/female, 21/9, provided by Fuwai Hospital in Beijing) with an average body mass of 228±39 g were randomly divided into 3 groups: SHR positive control group, imidapril treatment group (3 mg/kg·d), irbesartan treatment group (50 mg/kg·d). Ten homogenous Wistar-Kyoto rats [provided by Fuwai Hospital in Beijing, in which female rats were 5, male rats were 5, their average body mass was 206±49 g.] were selected as normal control group. During the 14-wk trial, all rats were in the breeding conditions: temperature 18-25 °C, humidity 40-60%, protein feed concentration 22-25%.

Methods

Irbesartan (presented by Hengrui Pharmacy Factory of Jiangsu Province) 50 mg/kg·d^[4] and imidapril (presented by Tianbian Pharmacy Factory of Tianjin) 3 mg/kg·d^[5] were dissolved in drinking water for 14 successive wk, respectively. Index observed included tail artery systolic blood pressure, angiotensin II (Ang II), histology of mesenteric artery. Fourteen weeks after irbesartan and imidapril interfering, all rats were killed and the second grade embranchment of mesenteric artery (about 2 mm) was taken and put into 25/L of glutaral for fixing, then transmission electron microscope (H-600, Hitachi in Japan) was used. About 1 mm of the artery was put into 100 g/L of neutral

formaldehyde and stained with HE, then observed by light microscope. Morphology of mesenteric artery was by a computer-assisted image analysis system. RT-PCR analysis was performed for TGF- β_1 ^[6] and c-Jun^[7] mRNA level in mesenteric artery.

SPSS 10.0 statistically analyzed the data and results were expressed as mean \pm SD.

RESULTS

Blood pressure from 4 groups was recorded in Table 1

Concentration of Ang II in plasma is shown in Table 2

Morphology of mesenteric artery (Figure 1)

Intima, vessel media, vessel wall were not increased in WKY group. Vessel lumen was relatively wider (A). Intima, vessel media and vessel wall were increased. Vessel lumen was relatively narrow in SHR (B), imidapril (C) and irbesartan (D) groups. The ratios of intima-media thickness / lumen radius, media / lumen area, lumen / vessel radius in 4 groups are shown in Table 3.

Microstructure of mesenteric arteries (transmission electron microscope, Figure 2)

As shown in A for WKY group, endothelial cells of intima were

abundant and normal, media had more smooth muscle cells. As shown in B for SHR group, endothelial cells of intima had vacuoles and fibrous tissues with adventitial hyperplasia, the thickness of adventitia was increased, media was severely fibrous and the fibrous tissue extended to smooth muscle layer and invaded internal elastic lamina, internal elastic lamina was tortuous and atrophic, some of smooth muscle cells were replaced by fibrous tissue. As shown in C for irbesartan group, endothelial cells of intima had vacuoles and marrow type corpses, internal elastic lamina was tortuous and atrophic and infiltrated by collagen fibers, but fibrosis in whole blood vessel wall relieved as compared with SHR group. The number of smooth muscle cells in media was slightly more than that in SHR group. As shown in D for imidapril group, endothelial cells of intima had marrow type corpses but no vacuole, the number of smooth muscle cells in media was more than that in irbesartan group, internal elastic lamina had a close-to-normal distribution, local internal elastic lamina was narrowed, fibrosis did not occur on blood vessel walls.

RT-PCR analysis of TGF- β_1 and c-Jun mRNA level in mesenteric artery (Figure 3)

mRNA expression levels of TGF- β_1 and c-Jun were analyzed by RT-PCR. Agarose gel electrophoresis of the PCR products was carried out to measure the relative intensity of the expression (A and B, Table 4).

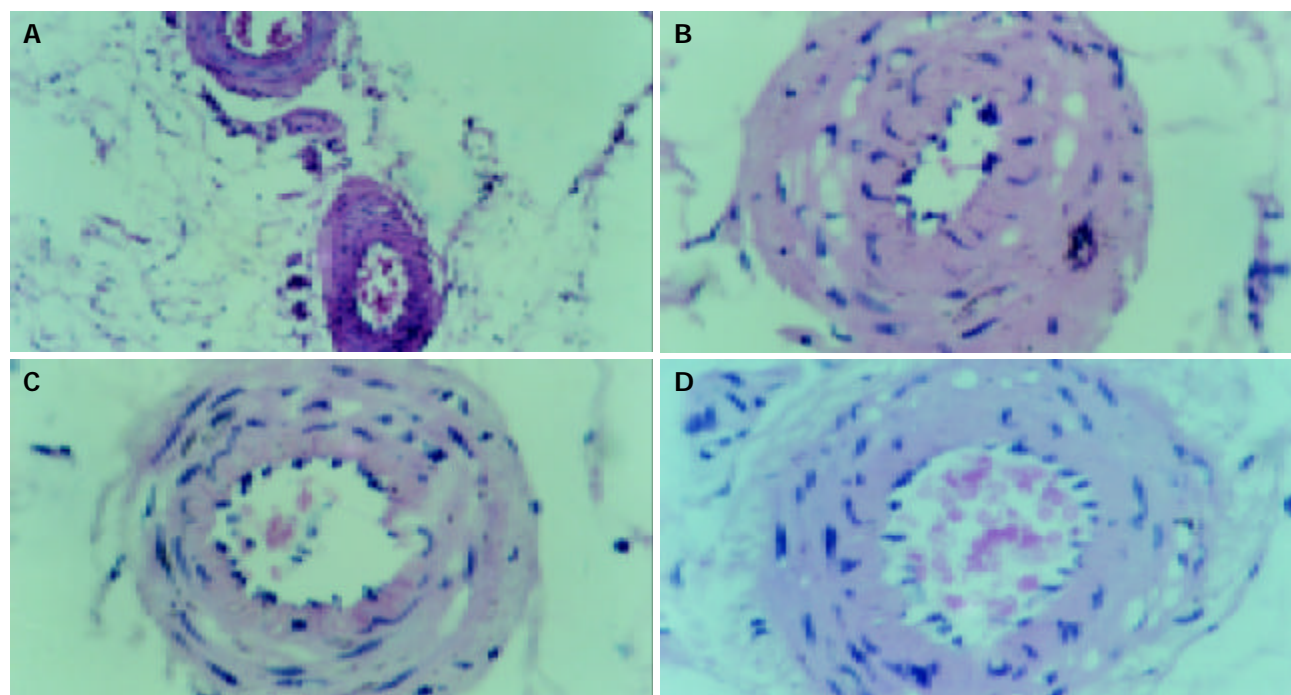


Figure 1 Morphology of mesenteric artery, A: Intima, media of vessel wall are not increased in WKY group and vessel lumen is relatively wider (HE, $\times 100$). B: Intima, media of vessel wall are increased in SHR group and vessel lumen is relatively narrow (HE, $\times 400$). C: Intima, media of vessel wall are increased in imidapril group and lumen of vessel is relatively narrow (HE, $\times 400$). D: Intima, media of vessel wall are increased in irbesartan group and lumen of vessel is relatively narrow (HE, $\times 400$).

Table 1 Blood pressure measured in WKY, SHR, imidapril and irbesartan groups (mean \pm SD, $n=10$)

Group	Blood pressure (mmHg)							
	13-wk-old	14-wk-old	15-wk-old	17-wk-old	19-wk-old	21-wk-old	24-wk-old	26-wk-old
WKY	105.90 \pm 16.10 ^d	115.70 \pm 9.19	112.00 \pm 7.53	90.00 \pm 9.13	125.50 \pm 7.62	116.00 \pm 6.99	116.00 \pm 11.25	121.50 \pm 4.74
SHR	134.40 \pm 7.72	140.00 \pm 17.48	151.00 \pm 24.59 ^b	160.00 \pm 14.90 ^f	177.00 \pm 16.19 ^f	177.50 \pm 14.39 ^f	190.00 \pm 19.00 ^f	198.10 \pm 14.04 ^f
Imidapril	131.50 \pm 6.68	124.30 \pm 7.02	127.50 \pm 8.58	125.00 \pm 7.45	130.80 \pm 15.16	138.00 \pm 12.52	127.00 \pm 11.10	142.00 \pm 6.32
Irbesartan	140.10 \pm 5.90	132.50 \pm 15.14	124.00 \pm 18.83	122.50 \pm 20.17	128.00 \pm 12.06	138.00 \pm 6.32	126.00 \pm 6.15	141.00 \pm 14.87

^b $P<0.01$ vs WKY, imidapril, irbesartan groups; ^d $P<0.01$ vs SHR, imidapril, irbesartan groups; ^f $P<0.01$ vs WKY, imidapril, irbesartan groups.

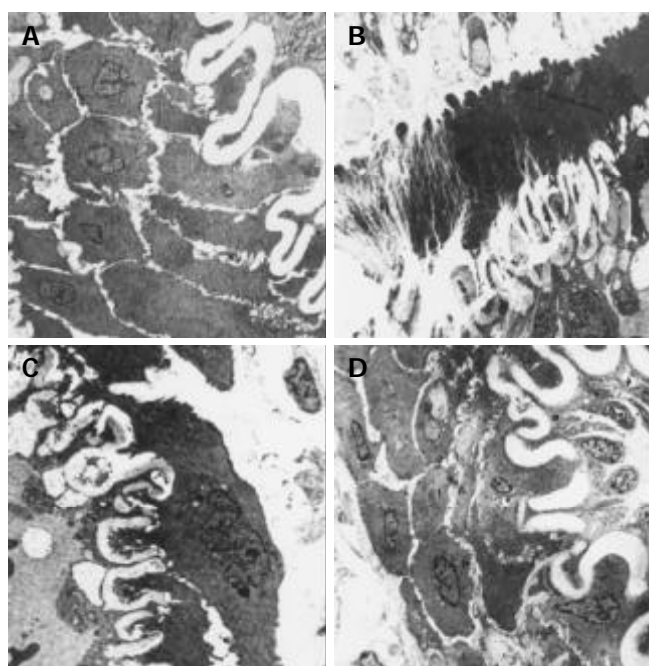


Figure 2 Microstructure of mesenteric arteries (transmission electron microscope). A: WKY group, endothelial cells of intima were abundant and normal, Media has more smooth muscle cells, internal elastic lamina is normal ($\times 2\,000$). B: SHR group, endothelial cells of intima had vacuole and fibrous tissue with adventitial hyperplasia; thickness of the adventitia was increased; media was severely fibrous and the fibrous tissue extended to smooth muscle layer and invaded internal elastic lamina; internal elastic lamina was tortuous and atrophic; some of smooth muscle cells were replaced by fibrous tissue ($\times 2\,500$). C: Irbesartan group, endothelial cells of intima have vacuole and marrow type corpses, internal elastic lamina was tortuous and atrophic and infiltrated by collagen fibers ($\times 2\,500$). D: Imidapril group, endothelial cells of intima have marrow type corpses but no vacuole, numbers of smooth muscle cells in media were more than those in irbesartan group; internal elastic lamina got a close-to-normal distribution; local internal elastic lamina got narrow, fibrosis did not occur on blood vessel wall ($\times 2\,000$).

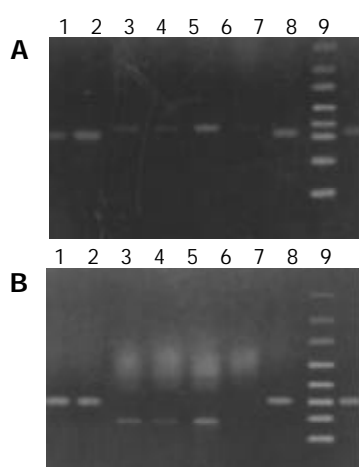


Figure 3 Agarose gel electrophoresis of TGF- β_1 and c-Jun mRNA RT-PCR product of mesenteric arteries. A: Agarose gel (2%) electrophoresis of TGF- β_1 mRNA RT-PCR product of mesenteric arteries of 4 groups. 1: WKY group GAPDH, 2: SHR group GAPDH, 3: irbesartan group, 4: imidapril group, 5: SHR group, 6: WKY group, 7: irbesartan group GAPDH, 8: pGEM-7Zf(+)/Hae III markers (from top to bottom: 102, 142, 174, 267, 289, 328, 434, 657 bp), 9: imidapril group GAPDH. B: Agarose gel (2%) electrophoresis of c-Jun mRNA RT-PCR product of

mesenteric arteries of 4 groups. 1: SHR group GAPDH, 2: WKY group GAPDH, 3: irbesartan group, 4: imidapril group, 5: SHR group, 6: WKY group, 7: irbesartan group GAPDH, 8: pGEM-3Zf(+)/Hae III markers (from top to bottom: 18, 80, 102, 174, 267, 314, 434, 587 bp), 9: imidapril group GAPDH.

Table 2 Concentration of Ang II in plasma (mean \pm SD, $n=7$)

Group	Plasma (pg/mL)	Mesenteric artery (pg/100 mg)
WKY	303.15 \pm 16.99	2 218.63 \pm 242.37
SHR	318.77 \pm 16.83	2 138.48 \pm 110.56 ^a
Imidapril	307.43 \pm 25.20	1 888.92 \pm 147.46 ^{ce}
Irbesartan	571.38 \pm 57.89 ^b	3 509.18 \pm 168.44 ^{bfg}

^a $P<0.05$ vs WKY, ^b $P<0.01$ vs WKY, SHR, imidapril group, ^c $P<0.05$ vs WKY, ^e $P<0.05$ vs SHR, ^f $P<0.01$ vs SHR, ^g $P<0.01$ vs WKY, ^g $P<0.05$ vs imidapril.

Table 3 Comparisons of ratios of intima-media thickness / lumen radius, media / lumen area, lumen / vessel radius in four groups (mean \pm SD, $n=7$)

Group	Media thickness (mm)/lumen radius (mm)	Media area (mm ²)/lumen area (mm ²)	Lumen radius (mm)/vessel radius (mm)
WKY	0.75 \pm 0.09	0.35 \pm 0.04	0.65 \pm 0.01
SHR	2.67 \pm 0.20 ^a	1.21 \pm 0.14 ^a	0.46 \pm 0.01 ^a
Imidapril	1.67 \pm 0.13 ^{ec}	0.71 \pm 0.05 ^{ec}	0.51 \pm 0.01 ^{ec}
Irbesartan	1.47 \pm 0.27 ^{ge}	0.65 \pm 0.14 ^{ge}	0.53 \pm 0.01 ^{ge}

^a $P<0.05$ vs WKY; ^c $P<0.05$ vs SHR; ^e $P<0.05$ vs WKY; ^e $P<0.05$ vs SHR; ^g $P<0.05$ vs WKY.

Table 4 Absorbance of c-Jun/absorbance of GAPDH, absorbance of TGF- β_1 /absorbance of GAPDH (mean \pm SD, $n=5$)

Group	Absorbance of c-Jun /absorbance of GAPDH	Absorbance of TGF- β_1 /absorbance of GAPDH
WKY group	0.582 \pm 0.013	0.780 \pm 0.018
SHR group	0.850 \pm 0.015 ^b	0.887 \pm 0.019 ^d
Imidapril group	0.743 \pm 0.012 ^a	0.803 \pm 0.005 ^c
Irbesartan group	0.789 \pm 0.013	0.847 \pm 0.017

$F=1\,340$ in the ratio of absorbance of c-Jun/absorbance of GAPDH. ^a $P<0.05$ vs irbesartan group, ^b $P<0.01$ vs WKY, imidapril, irbesartan group. $F=198$ in the ratio of Absorbance of TGF- β_1 /absorbance of GAPDH. ^c $P<0.05$ vs irbesartan group, ^d $P<0.01$ vs WKY, imidapril, irbesartan group.

DISCUSSION

It is known that elevated blood pressure in essential hypertension patients and spontaneously hypertensive rats (SHR) related to the renin-angiotensin system (RAS)^[8-10]. The main effector peptide of RAS was Ang II^[11], which played an essential role in the pathogenesis of hypertension through the regulation of cell growth, inflammation, and fibrosis^[12]. The main biological effects of Ang II has been found to be the enhancement of smooth muscle contraction, aldosterone release^[13], arginine vasopressin release, cell proliferation, adjustment of body fluid balance. It had a close relation to blood vessel remodeling^[14]. There were 2 main angiotensin II receptors, AT1 and AT2^[15,16]. The AT1 receptor was responsible for most of the pathophysiologic actions of angiotensin II^[17], including cell proliferation, production of growth factors and cytokines, and fibrosis. AT2 could cause antiproliferation and counteract the cell growth induced by AT1 activation^[18]. In addition, pressure-lowering agent also had actions on blood vessel remodeling^[19]. Both

ACEI and AT1 acceptor antagonists have been shown to act selectively on different cycles and they not only had satisfactory decompression effect, but also might inhibit blood vessel remodeling^[20,21].

These results suggest that imidapril and irbesartan have ideal decompression effects and inhibiting action upon angiotensin-converting enzymes and AT1 acceptors. Blood pressure gradually rose and arrived to 200 mmHg in 26 wk-old SHR, but blood pressure in imidapril and irbesartan groups fluctuated within normal ranges and no obvious difference was observed between the 2 groups. Ang II level in plasma gradually increased in SHR group and slowly decreased in imidapril group compared with that in WKY group performed with radioimmunoassay, but there was no statistical significance between them. Ang II level in plasma increased in irbesartan group and it had a significant difference when compared with that in WKY group. Ang II level decreased in mesenteric artery in SHR group and it was obvious in imidapril group. Ang II level increased in mesenteric artery in irbesartan group and it had a significant difference. Campbell *et al.*^[22] made clear with experiment that Ang II levels in SHR plasma, lung, kidney, heart, adrenal, aorta, brown adipose tissue were lower than the levels in Donryu rats. In this experiment, Ang II levels in plasma of SHR group and WKY group and mesenteric artery were consistent with Duncan's experiment. Moreover, imidapril decreased Ang II levels and irbesartan increased Ang II levels^[23] in SHR plasma and mesenteric artery in this experiment.

Light microscopy and electron microscopy displayed that imidapril and irbesartan might inhibit structure alterations especially interstitial fibrosis. Furthermore, the effect of imidapril was better than that of irbesartan. It should be pointed out that electron microscopy of mesenteric artery displayed that the pathology of mesenteric artery remodeling in SHR possibly involved in fibrous tissue hyperplasia in adventitia, fibrosis in media, structure and function damage in endothelial cells. Castro *et al.*^[24] believed that extracellular matrix (ECM) accumulation in blood vessel walls could be attributable to constriction of artery lumen in hypertension. The pathological changes of resistance vessels could relate to the synthesis and excretion reduction of proteoglycan in blood vessel smooth muscle cells.

Several experiments have shown that Ang II could induce vascular smooth muscle cell proliferation *in vivo*. Griffin suggested that Ang II infusion in rats increased mesenteric vascular media width, media cross-sectional area and media/lumen ratio, and these changes were not inhibited by hydralazine despite normalization of blood pressure. Kim *et al.*^[25] also revealed that aortic ERK and JNK activities were significantly increased with the development of hypertension, and in particular, these activities were gradually and chronically enhanced in the development of hypertension and associated with an increase in aortic weight. *In vitro* experiments have also shown that Ang II stimulated protein synthesis and induced cellular hypertrophy in cultured vascular smooth muscle cells via AT1 receptors. More and more evidences have shown that AT1 receptors couple to a heterotrimeric G protein Gq. The activation of AT1 receptors could not only lead to the activation of PLC- β and increases of diacylglycerol and Ca²⁺ in cells but also activate intracellular signal transduction in cultured vascular smooth muscle cells. Schmitz *et al.*^[26] reported that Ang II could also activate JNK of vascular smooth muscle cells. JNK is well known to increase c-Jun transactivation by phosphorylating c-Jun on 2 critical N-terminal serine residues and inducing *c-fos* gene expression. Therefore, it has been well known that JNK is involved in the activation of transcription factor, AP-1^[27]. AP-1 is bound to TPA response component (TRE) of nucleus DNA to accelerate transcription and to increase proliferation and protein synthesis of vascular smooth

muscle cells. In vascular smooth muscle cells, activation of ERK and AP-1 could increase expression of TGF- β_1 mRNA^[28]. Both vascular endothelial cells and vascular smooth muscle cells could synthesis TGF- β_1 ^[29]. TGF- β_1 has been found to be one kind of multi-function proteins^[30] and to adjust hypertrophy and polyploidy of many kinds of cells and to stimulate and inhibit hyperplasia. In a word, it relates to vessel remodeling. TGF- β_1 is bound to specific receptors in cell surface to initiate the intracellular p53-dependent signaling cascade, resulting in down regulation or inhibition of cyclin-dependent kinases 2 and 4, and inducing cell cycle arrest in G₁. Ang II can mediate intracellular signal transduction of vascular smooth muscle cells. Remodeling of mesenteric artery in SHR would be inhibited if the expression of c-Jun and/or TGF- β_1 could be inhibited. Therefore, this experiment used AT1 receptor antagonist irbesartan and ACE inhibitor imidapril to interfere mesenteric artery remodeling in SHR in order to investigate the expression difference of c-Jun and TGF- β_1 mRNA in mesenteric artery with RT-PCR and to illustrate the intervention action and effect difference of these two kinds of drugs on inhibiting mesenteric artery remodeling.

Compared with WKY group, the mRNA level of TGF- β_1 and c-Jun in mesenteric arteries of SHR group was obviously increased. Imidapril and irbesartan might inhibit the expression of c-Jun and TGF- β_1 mRNA in mesenteric artery of SHR. Imidapril was better than irbesartan in preventing mesenteric arteries from structure modulation especially fibrosis and expression of TGF- β_1 , -Jun mRNA. Ohta *et al* proved that aortic TGF- β_1 , fibronectin, and collagen type IV WmRNA levels were higher in SHR than in WKY, and all of these elevated mRNAs in the aorta of SHR were significantly reduced by an ACE inhibitor, alacepril (50 mg/kg·d), or an AT1 receptor antagonist, SC-52458 (50 mg/kg·d). Kim *et al.*^[31] also showed that treatment with AT1 receptor antagonist (E4177, 20 mg/kg·d) significantly inhibited the activation of JNK and ERK in injured arteries. These experiments illuminate that the results in our investigation are acceptable. Further study should be done for the combined action of imidapril and irbesartan.

REFERENCES

- 1 **Kawano H**, Cody RJ, Graf K, Goetze S, Kawano Y, Schnee J, Law RE, Hsueh WA. Angiotensin II enhances integrin and alpha-actinin expression in adult rat cardiac fibroblasts. *Hypertension* 2000; **35**(1 Pt 2): 273-279
- 2 **Touyz RM**, He G, El Mabrouk M, Diep Q, Mardigyan V, Schiffrin EL. Differential activation of extracellular signal-regulated protein kinase 1/2 and p38 mitogen activated-protein kinase by AT1 receptors in vascular smooth muscle cells from Wistar-Kyoto rats and spontaneously hypertensive rats. *J Hypertens* 2001; **19**(3 Pt 2): 553-559
- 3 **Ledingham JM**, Phelan EL, Cross MA, Lavery R. Prevention of increases in blood pressure and left ventricular mass and remodeling of resistance arteries in young New Zealand genetically hypertensive rats: the effects of chronic treatment with valsartan, enalapril and felodipine. *J Vasc Res* 2000; **37**: 134-145
- 4 **Intengan HD**, Thibault G, Li JS, Schiffrin EL. Resistance artery mechanics, structure, and extracellular components in spontaneously hypertensive rats: effects of angiotensin receptor antagonism and converting enzyme inhibition. *Circulation* 1999; **100**: 2267-2275
- 5 **Yokota S**, Naito Y, Yoshida H, Ohara N, Adachi T, Narita H. Cardioprotective effects of an angiotensin-converting-enzyme inhibitor, imidapril, and Ca²⁺ channel antagonist, amlodipine, in spontaneously hypertensive rats at established stage of hypertension. *Jpn J Pharmacol* 1998; **77**: 79-87
- 6 **Ando T**, Okuda S, Tamaki K, Yoshitomi K, Fujishima M. Localization of transforming growth factor-beta and latent transforming growth factor-beta binding protein in rat kidney. *Kidney Int* 1995; **47**: 733-739

- 7 **Kreisberg JJ**, Radnik RA, Ayo SH, Garoni J, Saikumar P. High glucose elevates c-fos and c-jun transcripts and proteins in mesangial cell cultures. *Kidney Int* 1994; **46**: 105-112
- 8 **Umemura S**. Genetic aspect of essential hypertension. Article in Japanese. *Rinsho Byori* 2003; **51**: 813-817
- 9 **Petrovic D**, Bidovec M, Peterlin B. Gene polymorphisms of the renin-angiotensin-aldosterone system and essential arterial hypertension in childhood. *Folia Biol* 2002; **50**: 53-56
- 10 **Lijnen PJ**, Petrov VV. Role of intracardiac renin-angiotensin-aldosterone system in extracellular matrix remodeling. *Methods Find Exp Clin Pharmacol* 2003; **25**: 541-564
- 11 **Unger T**. Blood pressure lowering and renin-angiotensin system blockade. *J Hypertens Suppl* 2003; **21**(Suppl 6): S3-7
- 12 **Ruiz-Ortega M**, Ruperez M, Esteban V, Egido J. Molecular mechanisms of angiotensin II-induced vascular injury. *Curr Hypertens Rep* 2003; **5**: 73-79
- 13 **Fritsch Neves M**, Schiffrin EL. Aldosterone: a risk factor for vascular disease. *Curr Hypertens Rep* 2003; **5**: 59-65
- 14 **Williams B**. Angiotensin II and the pathophysiology of cardiovascular remodeling. *Am J Cardiol* 2001; **87**(8A): 10C-17C
- 15 **Rizkalla B**, Forbes JM, Cooper ME, Cao Z. Increased renal vascular endothelial growth factor and angiopoietins by angiotensin II infusion is mediated by both AT1 and AT2 receptors. *J Am Soc Nephrol* 2003; **14**: 3061-3071
- 16 **Zhou Y**, Dirksen WP, Babu GJ, Periasamy M. Differential vasoconstrictions induced by angiotensin II: role of AT1 and AT2 receptors in isolated C57BL/6J mouse blood vessels. *Am J Physiol Heart Circ Physiol* 2003; **285**: H2797-2803
- 17 **Touyz RM**, Tabet F, Schiffrin EL. Redox-dependent signalling by angiotensin II and vascular remodeling in hypertension. *Clin Exp Pharmacol Physiol* 2003; **30**: 860-866
- 18 **Hannan RE**, Davis EA, Widdop RE. Functional role of angiotensin II AT2 receptor in modulation of AT1 receptor-mediated contraction in rat uterine artery: involvement of bradykinin and nitric oxide. *Br J Pharmacol* 2003; **140**: 987-995
- 19 **Iizuka K**, Murakami T, Kawaguchi H. Pure atmospheric pressure promotes an expression of osteopontin in human aortic smooth muscle cells. *Biochem Biophys Res Commun* 2001; **283**: 493-498
- 20 **Contreras F**, de la Parte MA, Cabrera J, Ospino N, Israili ZH, Velasco M. Role of angiotensin II AT1 receptor blockers in the treatment of arterial hypertension. *Am J Ther* 2003; **10**: 401-408
- 21 **Yavuz D**, Koc M, Toprak A, Akpınar I, Velioglu A, Deyneli O, Haklar G, Akalin S. Effects of ACE inhibition and AT1-receptor antagonism on endothelial function and insulin sensitivity in essential hypertensive patients. *J Renin Angiotensin Aldosterone Syst* 2003; **4**: 197-203
- 22 **Campbell DJ**, Duncan AM, Kladis A, Harrap SB. Angiotensin Peptides in spontaneously Hypertensive and Normotensive Donryu rats. *Hypertension* 1995; **25**: 928-934
- 23 **Duke LM**, Paull JR, Widdop RE. Cardiovascular status following combined angiotensin-converting enzyme and AT1 receptor inhibition in conscious spontaneously hypertensive rats. *Clin Exp Pharmacol Physiol* 2003; **30**: 317-323
- 24 **Castro CM**, Cruzado MC, Miatello RM, Risler NR. Proteoglycan production by vascular smooth muscle cells from resistance arteries of hypertensive rats. *Hypertension* 1999; **34**(4 Pt 2): 893-896
- 25 **Kim S**, Murakami T, Izumi Y, Yano M, Miura K, Yamanaka S, Iowa H. Extracellular signal-regulated kinase and c-Jun NH2-terminal kinase activities are continuously and differentially increased in aorta of hypertensive rats. *Biochem Biophys Res Commun* 1997; **236**: 199-204
- 26 **Schmitz U**, Ishida T, Ishida M, Surapichat J, Hasham MI, Pelech S, Berk BC. Angiotensin II stimulates p21-activated kinase in vascular smooth muscle cells: role in activation of JNK. *Circ Res* 1998; **82**: 1272-1278
- 27 **Yano M**, Kim S, Izumi Y, Yamanaka S, Iwao H. Differential activation of cardiac c-jun amino-terminal kinase and extracellular signal-regulated kinase in angiotensin II-mediated hypertension. *Circ Res* 1998; **83**: 752-760
- 28 **Hamaguchi A**, Kim S, Izumi Y, Zhan Y, Yamanaka S, Iwao H. Contribution of extracellular signal-regulated kinase to angiotensin II-induced transforming growth factor- β_1 expression in vascular smooth muscle cells. *Hypertension* 1999; **34**: 126-131
- 29 **Ebisui O**, Dilley RJ, Li H, Funder JW, Liu JP. Growth factors and extracellular signal-regulated kinase in vascular smooth muscle cells of normotensive and spontaneously hypertensive rats. *J Hypertens* 1999; **17**: 1535-1541
- 30 **Gekle M**, Knaus P, Nielsen R, Mildenerberger S, Freudinger R, Wohlfarth V, Sauvage C, Christensen EL. Transforming growth factor-beta1 reduces megalin- and cubilin-mediated endocytosis of albumin in proximal-tubule-derived opossum kidney-cells. *J Physiol* 2003; **552**(Pt 2): 471-481
- 31 **Kim S**, Izumi Y, Yano M, Hamaguchi A, Miura K, Yamanaka S, Miyazaki H, Iwao H. Angiotensin blockade inhibits activation of mitogen-activated protein kinases in rat balloon-injured artery. *Circulation* 1998; **97**: 1731-1737

Edited by Wang XL and Xu FM

Signal pathways involved in emodin-induced contraction of smooth muscle cells from rat colon

Tao Ma, Qing-Hui Qi, Jian Xu, Zuo-Liang Dong, Wen-Xiu Yang

Tao Ma, Qing-Hui Qi, Jian Xu, Zuo-Liang Dong, Department of Surgery, General Hospital of Tianjin Medical University, 300052, Tianjin, China

Wen-Xiu Yang, Division of Biophysics, Department of Physics, Nankai University, Tianjin 300071, China

Supported by the National Natural Science Foundation of China, No.30171198

Correspondence to: Dr. Qing-Hui Qi, Department of Surgery, General Hospital of Tianjin Medical University, Tianjin 300052, China. mataoemail@yahoo.com.cn

Telephone: +86-22-84283767

Received: 2003-06-04 **Accepted:** 2003-11-19

Abstract

AIM: To investigate the effects induced by emodin on single smooth muscle cells from rat colon *in vitro*, and to determine the signal pathways involved.

METHODS: Cells were isolated from the muscle layers of Wistar rat colon by enzymatic digestion. Cell length was measured by computerized image micrometry. Intracellular Ca^{2+} ($[\text{Ca}^{2+}]_i$) signals were studied using the fluorescent Ca^{2+} indicator fluo-3 and confocal microscopy. PKC α distribution at rest state or after stimulation was measured with immunofluorescence confocal microscopy.

RESULTS: (1) Emodin dose-dependently caused colonic smooth muscle cells contraction; (2) emodin induced an increase in intracellular Ca^{2+} concentration; (3) the contractile responses induced by emodin were respectively inhibited by preincubation of the cells with ML-7 (an inhibitor of MLCK) and calphostin C (an inhibitor of PKC); (4) Incubation of cells with emodin caused translocation of PKC α from cytosolic area to the membrane.

CONCLUSION: Emodin has a direct contractile effect on colonic smooth muscle cell. This signal cascade induced by emodin is initiated by increased $[\text{Ca}^{2+}]_i$ and PKC α translocation, which in turn lead to the activation of MLCK and the suppression of MLCP. Both of them contribute to the emodin-induced contraction.

Ma T, Qi QH, Xu J, Dong ZL, Yang WX. Signal pathways involved in emodin-induced contraction of smooth muscle cells from rat colon. *World J Gastroenterol* 2004; 10(10): 1476-1479
<http://www.wjgnet.com/1007-9327/10/1476.asp>

INTRODUCTION

Gastrointestinal dysmotility underlies frequent clinical entities such as diabetes mellitus, chronic constipation, irritable bowel syndrome, postoperative ileus *etc.* Currently few drugs have been proven to be efficient at improving motility. Emodin is a naturally occurring anthraquinone present in the roots and bark of numerous plants of the genus *Rhamnus*^[1]. Extracts from the roots, bark, and/or dried leaves of buckthorn, senna, cascara,

aloe, frangula, and rhubarb have been used as laxatives since ancient times and currently are widely used in the preparation of herbal laxative preparations in China^[2-5]. Anthraquinone glycosides are poorly absorbed from the gastrointestinal tract but are cleaved by gut bacteria to produce aglycones, including emodin which are more readily absorbed and thought to be responsible for the purgative properties of these preparations^[1]. The reported biological effects of emodin include antitumor, antibacterial and anti-inflammatory actions^[6-9]. Emodin also possesses prokinetic effect on gastrointestinal tract. Stimulatory actions of emodin on gastrointestinal smooth muscle have been described in several studies^[10-12]. However, its mechanism in accelerating gastrointestinal motion is not yet clarified.

It is now understood that the contraction of smooth muscle cells involves two processes^[13-16]: (a) The concentration of intracellular Ca^{2+} increases; this Ca^{2+} increase results in phosphorylation of myosin and consequently an increased contractility. (b) The sensitivity of the myofilaments to Ca^{2+} increases. Pharmacological agents can stimulate smooth muscle cell contractions by mobilizing intracellular Ca^{2+} and/or enhancing Ca^{2+} sensitivity.

Because of the potential therapeutic implications of emodin in gastrointestinal hypomotility disorders, this study was then designed to further characterize the effects of emodin on smooth muscle cells from rat colon *in vitro* and to investigate the signal transduction cascade leading to cell contraction induced by emodin.

MATERIALS AND METHODS

Materials

Fluo-3 AM and Pluronic F-127 were from Molecular Probes (USA). Rabbit anti-PKC α IgG and goat anti-rabbit IgG FITC were from Santa Cruz Biotechnology (USA). Collagenase type II, emodin, trypsin inhibitor and HEPES were all purchased from Sigma Co (USA). DMEM was purchased from GIBCO Co., USA. FBS was from Hyclone (USA). All other reagents were from LianXing Co., Ltd (China). Emodin was dissolved in dimethyl sulfoxide and ethanol mixture (2:8) to make stock solution and the final concentration of the vehicle in the solution did not exceed 0.1%.

Methods

Isolation of smooth muscle cells Smooth muscle cells from rat distal colon were isolated as described previously^[13]. Briefly, a segment of 5-cm long distal colon was dissected and digested to yield isolated smooth muscle cells. The tissue was incubated for 2 successive 30-min periods at 31 °C in 10 mL of HEPES (pH7.4) containing 1 g/L collagenase type II and 0.1 g/L soybean trypsin inhibitor. After the second enzymatic incubation, the medium was filtered through 500 μm Nitex mesh. The partially digested tissue left on the filter was washed with collagenase-free buffer solution, and muscle cells were allowed to disperse spontaneously for 30 min. The cells were harvested by centrifugation at 350 r/min for 10 min. After a hemocytometric cell count, the harvested cells were resuspended in collagenase-free buffer solution and diluted as needed.

Measurement of smooth muscle cell contraction Individual cell length was measured by scanning micrometry as described previously^[13]. Aliquots consisting of 1×10^4 cells in 0.25 mL of medium were added to 50 μ L of a solution containing emodin with or without prior incubation with ML-7 (10^{-5} mol/L) or Calphostin C (10^{-6} mol/L). The reaction was allowed to proceed for 1 min and terminated by the addition of acrolein at a final concentration of 10 mL/L. The lengths of 30 consecutive intact healthy cells were measured through a phase-contrast microscope fitted with a video camera and connected to a Legend computer. The CIMAS program was used to measure the length. The contractile response was defined as the decrease in the average length of the 30 cells and was expressed as the percent change relative to control length.

Single cell intracellular Ca^{2+} measurements Changes in $[\text{Ca}^{2+}]_i$ were estimated as described elsewhere by using laser scanning confocal microscopy (Radiance 2000; Bio-rad, Hertfordshire, UK)^[17] linked to an inverted epifluorescence microscope (Olympus, Japan). The scanning box was set at a resolution of 256×256 . Only one fixed combination of laser intensity (20% maximum) and photomultiplier gain (1 800 of a maximum of 4 096) was used during scanning.

To load the cells with fluorescent Ca^{2+} indicator fluo-3, smooth muscle cells on the coverslips were incubated with 5 μ mol/L of the membrane permeant acetoxymethyl ester of the dye (fluo-3 AM; Molecular Probes, USA) and Pluronic F-127 (0.4 g/L; Molecular Probes, USA) dissolved in HEPES-ringer buffer [containing (mmol/L): NaCl 135, KCl 5.9, CaCl_2 1.5, MgCl_2 1.2, HEPES 11.6 and glucose 11.5, at pH 7.3] for 30 min at 37 °C. Cells were subsequently washed twice with HEPES-ringer buffer and further incubated for 20 min to allow de-esterification of the dye.

Coverglass chambers were then mounted on the microscope stage and continuously superfused with HEPES-ringer buffer. The cells loaded with fluo-3 were illuminated at 488 nm, and fluorescent emissions of 525/30 nm were recorded at an intensity of fluo-3. Digital Ca^{2+} images were collected at 10 s intervals. Because fluo-3 is a single wavelength indicator, it is not possible to apply the ratiometric method to quantitative determination of $[\text{Ca}^{2+}]_i$. Therefore, the intensity of fluo-3 fluorescence was normalized in the temporal analysis. The relative values of fluorescence intensity of the dye (Ft) were used to represent the $[\text{Ca}^{2+}]_i$.

Cell culture and confocal imaging of PKC α cell culture After enzymatic incubation, the dispersed cells were collected in DMEM with 100 mL/L FBS-medium, then transferred to coverslips coated with poly-L-lysine, and allowed to settle overnight in a humidified 50 mL/L CO_2 environment.

Cell fixation and permeabilization Cells were either untreated or treated with emodin (50 μ mol/L), and the reaction was stopped by removing the medium and adding 40 g/L formaldehyde to PBS. Cells were fixed in PBS for 10 min. Then the fixative was removed, and the cells were washed with PBS. Thereafter the cells were permeabilized by adding the permeabilization solution [(0.1 mL TritonX-100, 90 mL distilled water, and 10 mL PBS (10 \times)] for 10 min. After permeabilization, the cells were rinsed 3 times with PBS.

Labeling with PKC α antibody and confocal microscopy Cells were incubated for 1 h with normal goat serum, followed by 3 washes in PBS with gentle agitation. Subsequently, the cells were incubated for 1 h with the primary antibody, a rabbit anti-PKC α IgG followed by 3 washes with PBS with gentle agitation. This step was followed by incubation of the cells for 1 h with secondary antibody (goat anti-rabbit IgG FITC). Then the cells were washed 3 times with PBS with gentle agitation. Finally, the cells on the coverslip were mounted onto a slide. Control slides were made by incubating cells with the secondary antibody only. The excitation parameter for fluorescent probes

was as follows: FITC excitation at 488 nm and emission at 520 nm. Immunostained cells were visualized with an Olympus $\times 40$ objective by confocal laser scanning microscopy (Bio-Rad radiance 2000). Image restoration and analysis were performed in Lasershar2000 and Laserpix.

Statistical analysis

The data are presented as mean \pm SD, and n represents the number of experiments. Statistical analysis was made by Student's unpaired *t* test when applicable. *P* values less than 0.05 were considered to be significant.

RESULTS

Effect of emodin on colonic smooth muscle cell length

Freshly isolated colonic smooth muscle cells appeared in spindle shape with diverse length (range from 44–121 μ m). Some of them were relaxed while others were at different phases of contraction (Figure 1). In resting state, the average cell length was 84.26 μ m. The application of emodin to freshly isolated smooth muscle cells induced a reduction in cell length. This reduction in cell length reflected contraction of the smooth muscle cells. Emodin at concentrations of 5 to 100 μ mol/L induced a concentration-dependent contraction (Figure 2). Maximal contraction of $19.17 \pm 2.59\%$ was observed with 50 μ mol/L of emodin.



Figure 1 Freshly isolated colonic smooth muscle cells appeared in spindle shape with diverse length. Some of them were relaxed while others were at different phases of contraction.

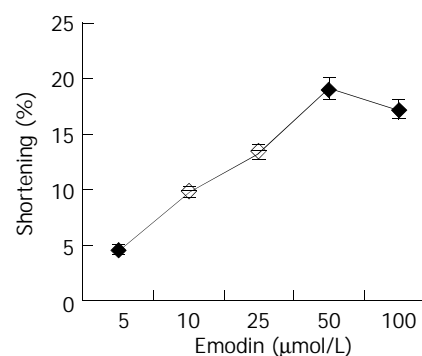


Figure 2 Dose-response curve representing the effects of emodin on the length of isolated colonic smooth muscle cell. Values are mean \pm SD of 3 experiments.

Effect of emodin on $[\text{Ca}^{2+}]_i$

Basal $[\text{Ca}^{2+}]_i$ levels were not significantly different between cells and the relative fluorescence intensity ranged from 38.46 to 52.59 (46.56 ± 3.79). At each concentration of emodin, the $[\text{Ca}^{2+}]_i$ response of 20 cells was determined. The application of emodin at concentrations from 5 to 100 μ mol/L could trigger

an increase in $[Ca^{2+}]_i$. The $[Ca^{2+}]_i$ responses to varying emodin concentrations are shown in Figure 3.

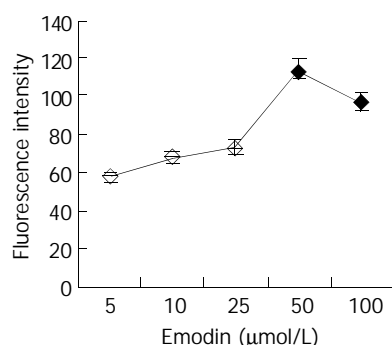


Figure 3 $[Ca^{2+}]_i$ response of colonic smooth muscle cells to emodin.

Effect of ML-7 and Calphostin C on emodin-induced contraction of colonic smooth muscle cells

Freshly isolated smooth muscle cells were treated with emodin (50 μmol/L) for 1 min with or without prior incubation with ML-7 (an inhibitor of MLCK, 10^{-5} mol/L) or Calphostin C (an inhibitor of PKC, 10^{-6} mol/L). The application of 50 μmol/L emodin to freshly isolated colonic smooth muscle cells induced a reduction in cell length ($19.17 \pm 2.59\%$). And $42.93 \pm 6.16\%$ of the contractile response induced by emodin was inhibited by preincubation of the cells with ML-7 ($P < 0.05$). Similarly, $51.12 \pm 3.87\%$ of the contractile response induced by emodin was inhibited by Calphostin C ($P < 0.05$). (Figure 4).

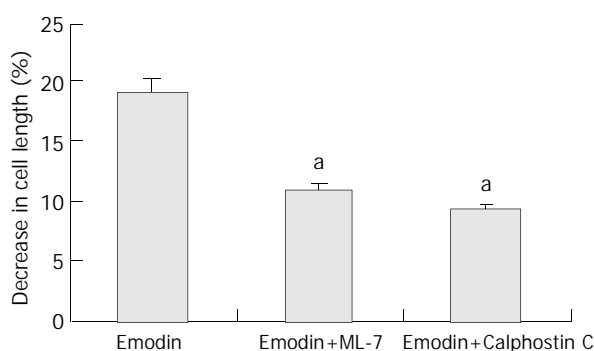


Figure 4 Effect of ML-7 and calphostin C on emodin-induced contraction of colonic smooth muscle cells. Emodin-induced cell shortening was $19.17 \pm 2.59\%$. Preincubation of the cells with ML-7 and calphostin C resulted in a decrease in cell contraction. ^a $P < 0.05$ vs Emodin group.

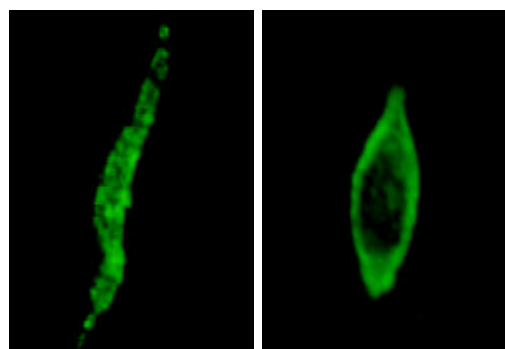


Figure 5 Membrane translocation of PKCα in response to emodin stimulation in smooth muscle cells of rat colon. Confocal microscopy showed PKCα distributed throughout the cell at rest state (left). When cells were stimulated with emodin (50 μmol/L), PKCα translocated to the membrane (right).

Emodin-induced translocation of PKCα in colonic smooth muscle cell

PKCα is thought to be inactive in the cytoplasm and therefore must translocate to the plasma membrane to be activated. Recent studies have demonstrated that PKCα can translocate from the cytoplasm to membrane on stimulation by contractile agonists during smooth muscle cell contraction^[18-21]. To determine whether activation of PKCα is involved in contraction of smooth muscle cells induced by emodin, we performed immunofluorescent labeling of PKCα in isolated smooth muscle cells, followed by confocal microscopy. Our data indicate that, at resting state, PKCα is mainly distributed throughout the cytoplasm. This is in contrast to the distribution of PKCα following emodin stimulation, as shown in Figure 5, PKCα translocated from the cytosolic part and aligned itself along the membranes of contracted cells.

DISCUSSION

Previous studies have indicated that emodin possesses prokinetic effect on gastrointestinal tract^[10-12]. Using confocal microscopy and cell isolation technique, the present study focused on emodin's cellular effect on smooth muscle cells from rat colon *in vitro* and investigated the signal mechanisms underlying its effect.

Our study showed that some of the action of emodin on gastrointestinal tract is exerted on the smooth muscle cells, as application of emodin to colonic smooth muscle cells resulted in a decrease in cell length. To our knowledge, this is the first study to show a direct contractile effect of emodin on gastrointestinal smooth muscle cells.

It is well established that Ca^{2+} /calmodulin-mediated phosphorylation of the light chain of smooth muscle myosin is a major regulatory mechanism for smooth muscle contraction^[22-26]. Stimulation of smooth muscle cells by specific agonists induces Ca^{2+} mobilization and activation of myosin light chain (MLC) kinase, which subsequently phosphorylates MLC and activates the myosin ATPase. The cascade of events described above leads to contraction of smooth muscle. Yang *et al.* have demonstrated that emodin could evoke increases in $[Ca^{2+}]_i$ in guinea-pigs taenia coli cells^[12]. In the present study, we observed the changes in $[Ca^{2+}]_i$ induced by emodin in single smooth muscle cell by using confocal microscopy and fluo-3 loading technique. Our data showed that, when applied to isolated smooth muscle cells, emodin induced a significant increase in $[Ca^{2+}]_i$. The effect of emodin on $[Ca^{2+}]_i$ indicated that emodin-mediated contractions were Ca^{2+} -dependent and MLCK pathways might be involved in emodin-induced contractions. We then carried out contraction studies in which we tested the effect of ML-7, a MLCK inhibitor, on emodin-induced contraction. As shown in Figure 4, the emodin-mediated contraction was significantly attenuated by ML-7. Taken together, these observations suggested that incubation of smooth muscle cells with emodin seemed to trigger a cascade of events including increase in $[Ca^{2+}]_i$, activation of MLCK and then cell contraction.

However, only $(42.93 \pm 6.16)\%$ of the contractile effect elicited by emodin was inhibited by ML-7. Therefore, it is possible that the rest of the emodin-induced contraction is mediated through an alternative pathway different from myosin light chain phosphorylation. Indeed, the rising of $[Ca^{2+}]_i$ has been found to be insufficient to explain excitation-contraction of smooth muscle cell, because the cytosolic concentration of Ca^{2+} is not always proportional to the extent of MLC phosphorylation and the force of contraction in smooth muscle cells. Other regulatory mechanisms have been proposed^[22,2-30]. Evidence accumulated that PKCα activation may contribute to the contraction of smooth muscle cells through a kinase cascade involving suppressing the activity of myosin light

chain phosphatase (MLCP) and increasing the sensitivity of contractile apparatus to Ca^{2+} . Therefore, we attempted to study the role of PKC α in emodin-induced contraction. The results of our contractile experiments showed that calphostin C, a PKC inhibitor, significantly suppressed the contraction induced by emodin, which suggested that PKC α might play a role in emodin-induced cell contraction. Lee has demonstrated that PKC α plays a critical role in emodin-induced apoptosis in CH27 and H460 cells^[7]. In order to verify the role of PKC α in emodin-induced contraction, we next examined the effect of emodin on the activity of PKC α . Previous studies have demonstrated that PKC α is activated by agonist and translocated from the cytoplasm to the plasma membrane through a complex mechanism during smooth muscle cell contraction. Although the exact nature of the translocation is still unclear, it has been suggested that the recruitment of cytosolic PKC α to the membrane is a pivotal component of signal mechanism which mediates the contraction of smooth muscle cell^[31-33]. In our study, it was shown that PKC α distribution at rest appeared homogeneous throughout the cell, which is in agreement with previous studies. After stimulation of colonic smooth muscle cells with emodin, PKC α underwent a distinct translocation to the membrane. These data above strongly suggest that emodin may exert its contractile effects on smooth muscle cells via PKC α activation.

On the basis of our findings, we propose the existence of an intracellular signaling cascade leading to cell contraction in colonic smooth muscle induced by emodin. This cascade is initiated by increased $[\text{Ca}^{2+}]_i$ and PKC α translocation, which in turn lead to the activation of MLCK and the suppression of MLCP, both of which contribute to the emodin-induced contraction. And these results provide evidence for an excitatory role of emodin in colonic smooth muscle cells contraction and indicate that emodin may be a promising prokinetic agent in ameliorating colonic hypomotility.

REFERENCES

- Liang JW, Hsiu SL, Wu PP, Chao PD. Emodin pharmacokinetics in rabbits. *Planta Med* 1995; **61**: 406-408
- Xie WL, Lin XZ, Ma DL, Li H. Effect of DACHENGQITANG* on phosphodiesterase in enteral smooth muscle cell in rats. *Chin Traditional Herbal Drug* 2001; **4**: 339-341
- Chen H, Wu X, Guan F. Protective effects of tongli gongxia herbs on gut barrier in rat with multiple organ dysfunction syndrome. *Chin J Int Traditional Western Med* 2000; **2**: 120-122
- You SY, Wu XZ, Liu ML. Effects of dachengqi decoction on gut hormones and intestinal movement after cholecystectomy. *Chin J Int Traditional Western Med* 1994; **9**: 522-524
- Xia Q, Jiang JM, Gong X, Chen GY, Li L, Huang ZW. Experimental study of Tong Xia purgative method in ameliorating lung injury in acute necrotizing pancreatitis. *World J Gastroenterol* 2000; **6**: 115-118
- Lee HZ. Effects and mechanisms of emodin on cell death in human lung squamous cell carcinoma. *Br J Pharmacol* 2001; **1**: 11-20
- Lee HZ. Protein kinase C involvement in aloe-emodin- and emodin-induced apoptosis in lung carcinoma cell. *Br J Pharmacol* 2001; **5**: 1093-1103
- Srinivas G, Anto RJ, Srinivas P, Vidhyalakshmi S, Senan VP, Karunakaran D. Emodin induces apoptosis of human cervical cancer cells through poly(ADP-ribose) polymerase cleavage and activation of caspase-9. *Eur J Pharmacol* 2003; **473**: 117-125
- Kuo YC, Meng HC, Tsai WJ. Regulation of cell proliferation, inflammatory cytokine production and calcium mobilization in primary human T lymphocytes by emodin from *Polygonum hypoleucum* Ohwi. *Inflamm Res* 2001; **2**: 73-82
- Jin ZH, Ma DL, Lin XZ. Study on effect of emodin on the isolated intestinal smooth muscle of guinea-pigs. *Zhongguo Chin J Int Traditional Western Med* 1994; **14**: 429-431
- Li J, Yang W, Hu W, Wang J, Jin Z, Wang X, Xu W. Effects of emodin on the activity of K channel in guinea pig taenia coli smooth muscle cells. *Acta Pharmaceutica Sinica* 1998; **5**: 321-325
- Yang WX, Wang J, Li JY. Characteristics of emodin evoked $[\text{Ca}^{2+}]_i$ and inhibition of GDP in guinea pig taenia coli cells. *Acta Biophysica Sinica* 2001; **1**: 165-169
- Wang P, Bitar KN. RhoA regulates sustained smooth muscle contraction through cytoskeletal reorganization of HSP27. *Am J Physiol* 1998; **274**(6 Pt 1): G1454-1462
- Fan J, Byron KL. Ca^{2+} signalling in rat vascular smooth muscle cells: a role for protein kinase C at physiological vasoconstrictor concentrations of vasopressin. *J Physiol* 2000; **524**(Pt 3): 821-831
- Taggart MJ, Lee YH, Morgan KG. Cellular redistribution of PKC α , rhoA and ROK α following smooth muscle agonist stimulation. *Exp Cell Res* 1999; **251**: 92-101
- Ibitayo AI, Sladick J, Tuteja S, Louis-Jacques O, Yamada H, Groblewski G, Welsh M, Bitar KN. HSP27 in signal transduction and association with contractile proteins in smooth muscle cells. *Am J Physiol* 1999; **277**(2 Pt 1): G445-454
- Claing A, Shbaklo H, Plante M, Bkaily G, D'Orleans-Juste P. Comparison of the contractile and calcium-increasing properties of platelet-activating factor and endothelin-1 in the rat mesenteric artery and vein. *Br J Pharmacol* 2002; **135**: 433-443
- Li L, Eto M, Lee MR, Morita F, Yazawa W, Kitazawa T. Possible involvement of the novel CPI-17 protein in protein kinase C signal transduction of rabbit arterial smooth muscle. *J Physiol* 1998; **508**(Pt 3): 871-881
- Sanders KM. Invited review: Mechanisms of calcium handling in smooth muscles. *J Appl Physiol* 2001; **3**: 1438-1449
- Cao W, Sohn UD, Bitar KN, Behar J, Biancani P, Harnett KM. MAPK mediates PKC-dependent contraction of cat esophageal and lower esophageal sphincter circular smooth muscle. *Am J Physiol Gastrointest Liver Physiol* 2003; **285**: G86-95
- Ratz PH, Meehl JT, Eddinger TJ. RhoA kinase and protein kinase C participate in regulation of rabbit stomach fundus smooth muscle contraction. *Br J Pharmacol* 2002; **137**: 983-992
- Somlyo AP, Somlyo AV. Signal transduction and regulation in smooth muscle. *Nature* 1994; **372**: 231-236
- Vorotnikov AV, Krymsky MA, Shirinsky VP. Signal transduction and protein phosphorylation in smooth muscle contraction. *Biochemistry* 2002; **67**: 1309-1328
- Makhlof GM, Murthy KS. Signal transduction in gastrointestinal smooth muscle. *Cell Signal* 1997; **9**: 269-276
- Bolton TB, Prestwich SA, Zholos AV, Gordienko DV. Excitation-contraction coupling in gastrointestinal and other smooth muscles. *Annu Rev Physiol* 1999; **61**: 85-115
- Harnett KM, Biancani P. Calcium-dependent and calcium-independent contractions in smooth muscles. *Am J Med* 2003; **115** (Suppl): 24S-30S
- Kitazawa T, Eto M, Woodsome TP, Brautigan DL. Agonists trigger G protein-mediated activation of the CPI-17 inhibitor phosphoprotein of myosin light chain phosphatase to enhance vascular smooth muscle contractility. *J Biol Chem* 2000; **275**: 9897-9900
- Sato A, Hattori Y, Sasaki M, Tomita F, Kohya T, Kitabatake A, Kanno M. Agonist-dependent difference in the mechanisms involved in Ca^{2+} sensitization of smooth muscle of porcine coronary artery. *J Cardiovasc Pharmacol* 2000; **5**: 814-821
- Yamada A, Ohya S, Hirano M, Watanabe M, Walsh MP, Imaizumi Y. Ca^{2+} sensitization of smooth muscle contractility induced by ruthenium red. *Am J Physiol* 1999; **276**(3 Pt 1): C566-575
- Gokina NI, Osol G. Temperature and protein kinase C modulate myofilament Ca^{2+} sensitivity in pressurized rat cerebral arteries. *Am J Physiol* 1998; **274**(6 Pt 2): H1920-1927
- Bitar KN. HSP27 phosphorylation and interaction with actin-myosin in smooth muscle contraction. *Am J Physiol Gastrointest Liver Physiol* 2002; **282**: G894-903
- Li C, Fultz ME, Wright GL. PKC- α shows variable patterns of translocation in response to different stimulatory agents. *Acta Physiol Scand* 2002; **174**: 237-246
- Taggart MJ, Leavis P, Feron O, Morgan KG. Inhibition of PKC α and rhoA translocation in differentiated smooth muscle by a caveolin scaffolding domain peptide. *Exp Cell Res* 2000; **258**: 72-81

Characterization and enrichment of hepatic progenitor cells in adult rat liver

Ai-Lan Qin, Xia-Qiu Zhou, Wei Zhang, Hong Yu, Qin Xie

Ai-Lan Qin, Xia-Qiu Zhou, Wei Zhang, Hong Yu, Qin Xie,
Department of Infectious Diseases, Ruijin Hospital, Shanghai Second
Medical University, Shanghai 200025, China

Supported by Shanghai Science Development Foundation, No.
004119044

Correspondence to: Dr. Ai-Lan Qin, Department of Infectious Diseases,
Ruijin Hospital, Shanghai 200025, China. ellen2111@sina.com.cn

Telephone: +86-21-64311242

Received: 2003-08-26 **Accepted:** 2003-10-27

Abstract

AIM: To detect the markers of oval cells in adult rat liver and to enrich them for further analysis of characterization *in vitro*.

METHODS: Rat model for hepatic oval cell proliferation was established with 2-acetylaminofluorene and two third partial hepatectomy (2-AAF/PH). Paraffin embedded rat liver sections from model (11 d after hepatectomy) and control groups were stained with HE and OV6, cytokeratin19 (CK19), albumin, alpha fetoprotein (AFP), connexin43, and c-kit antibodies by immunohistochemistry. Oval cell proliferation was measured with BrdU incorporation test. C-kit positive oval cells were enriched by using magnetic activated cell sorting (MACS). The sorted oval cells were cultured in a low density to observe colony formation and to examine their characterization *in vitro* by immunocytochemistry and RT-PCR.

RESULTS: A 2-AAF/PH model was successfully established to activate the oval cell compartment in rat liver. BrdU incorporation test of oval cell was positive. The hepatic oval cells coexpressed oval cell specific marker OV6, hepatocyte-marker albumin and cholangiocyte-marker CK19. They also expressed AFP and connexin 43. C-kit, one hematopoietic stem cell receptor, was expressed in hepatic oval cells at high levels. By using c-kit antibody in conjunction with MACS, we developed a rapid oval cell isolation protocol. The sorted cells formed colony when cultured *in vitro*. Cells in the colony expressed albumin or CK19 or coexpressed both and BrdU incorporation test was positive. RT-PCR on colony showed expression of albumin and CK19 gene.

CONCLUSION: Hepatic oval cells in the 2-AAF/PH model had the properties of hepatic stem/progenitor cells. Using MACS, we established a method to isolate oval cells. The sorted hepatic oval cells can form colony *in vitro* which expresses different combinations of phenotypic markers and genes from both hepatocytes and cholangiocyte lineage.

Qin AL, Zhou XQ, Zhang W, Yu H, Xie Q. Characterization and enrichment of hepatic progenitor cells in adult rat liver. *World J Gastroenterol* 2004; 10(10): 1480-1486

<http://www.wjgnet.com/1007-9327/10/1480.asp>

INTRODUCTION

It has ever been disputed whether there are stem/progenitor

cells in liver, because the liver is a quiescent organ and the adult liver can regenerate by hepatocytes reentering into cell cycle after surgical resection or injury^[1-3]. But it is now generally accepted that the liver contains hepatic stem cells/progenitor cells. When the ability of hepatocytes to divide and replace damaged tissues is compromised under the condition of severe and chronic liver injury caused by drugs, viruses and toxins, a subpopulation of liver cells termed oval cells, is induced to proliferate. Extensive studies in rodent models of hepatocarcinogenesis and other non-carcinogenic injury models suggest that oval cells may represent a facultative hepatic progenitor/stem cell compartment. These cells not only can be activated to proliferate but also differentiate both into mature hepatocytes and biliary epithelial cells under certain conditions^[4-7]. So these hepatic stem/progenitor cells (HSCs/HPCs) are ideal sources for cell therapy such as cell transplantation or tissue engineered bioartificial organs and identification of HSCs/HPCs has become increasingly important.

Hematopoiesis and hepatic development share common stages. During fetal development, hematopoietic stem cells move out of the yolk sac and into the developing liver. Simultaneous with the appearance of hematopoiesis, hematopoietic stem cells can be detected in the fetal liver (data not shown). It is increasingly apparent that HSCs/HPCs share common characteristics with stem cells of the hematopoietic system^[8,9]. C-kit is a hematopoietic stem cell receptor, and it is also expressed in hepatic oval cells^[10,11]. 2-Acetylaminofluorene and partial hepatectomy (2-AAF/PH) are a traditional model to activate oval cells in rat liver^[12]. We were also successful in establishment of an oval cell proliferation model treated with 2-AAF/PH. The current studies were performed to detect the markers expressed in rat oval cells and used c-kit antibody as well as magnetic activated cell sorting (MACS) to highly enrich the population of hepatic oval cells for further analysis of colony formation and characterization *in vitro*.

MATERIALS AND METHODS

Oval cell compartment proliferation/activation

Male SD rats (about 150 g) were supplied by Laboratory Animal Center of Chinese Academy of Sciences. They were fed 5, 10, 15 and 20 mg/kg body mass 2-AAF (dissolved in polyethylene glycol, Sigma) daily by oral gavage for 6 d and up to 7 d after operation and the control rats were fed saline. On the 7th d, rats were partially hepatectomized under general ether anesthesia and were not fed 2-AAF on the same day. The time points of this study were counted when partial hepatectomy was performed. One hour before the animals were killed, they received an intraperitoneal injection of BrdU (100 mg/kg body weight) (Sigma) to detect proliferation of oval cells (BrdU incorporation test). Liver tissue obtained was processed in the same manner described in immunohistochemistry methods.

Immunohistochemistry

Liver tissue was divided and fixed in 40 g/L buffered formaldehyde. All staining procedures for light microscopy

Table 1 First and second antibodies for immunohistochemistry

First antibody	Dilution	Second antibody	Dilution	Chromogen
OV6 (mouse IgG) ¹	1:100	Goat anti-mouse IgG (HRP or FITC)	1:150 1:200	DAB(brown) green fluorescence
CK19(mouse IgG) ²	1:150	Goat anti-mouse IgG (HRP)	1:150	DAB (brown)
Albumin (rabbit IgG)	1:400	Goat anti-rabbit IgG (AP)	1:50	Fuchsin (red) or NBT/BCIP(blue)
AFP (mouse IgG)	1:400	Goat anti-mouse IgG (HRP)	1:200	DAB(brown)
Connexin 43(mouse IgM) ²	1:400	Goat anti-mouse IgM (HRP)	1:200	DAB (brown)
C-kit (rabbit IgG) ³	1:50	Goat anti-rabbit IgG (AP)	1:50	Fuchsin(red) or NBT/BCIP(blue)
BrdU (mouse IgG)	1:50	Goat anti-mouse IgG (HRP)	1:150	DAB(brown)

Note:1=a gift from professor Sell S, 2=from Sigma, 3=from Santa Cruz, others were from DAKO Company.

were performed on paraffin-embedded 4 μ m sections. The sections were deparaffinized in xylene and rehydrated through graded alcohol. Routine histological examinations were made for liver sections stained with hematoxylin-eosin. Antigen retrieval was made by microwave - citrate buffer method, and then they were digested with trypsin (1 g/L trypsin, 1 g/L calcium chloride) at 37 °C for 30 min. For BrdU staining, the sections were immersed in 4N HCl for 15 min for DNA degeneration and neutralized with TBS. Single cells from suspensions were collected on glass slides by cytocentrifugation and air dried. All cells were fixed in methanol at 4 °C for 20 min. Endogenous peroxidase was inactivated by DAKO peroxidase blocking reagent for 10 min. The sections were incubated with 100 mL/L normal goat serum in TBS at room temperature for 20 min to block non-specific binding. For immunostaining, the primary antibody and second antibody are shown in Table 1. Double immunostaining for studies of antigen colocalization was performed with selected antibodies (OV6 vs albumin, CK19 vs albumin) using different chromogens (DAB and Fuchsin or NTB/BCIP). All antibodies were diluted with DAKO antibody diluent. Specimens were incubated with first antibody at 4 °C overnight, and then incubated with second antibody at room temperature for 1 h. For each antibody negative controls were performed by either blocking with appropriate nonimmune serum or by omitting the primary antibody from the protocol.

Cell sorting and culture

Rat liver cells were isolated by a two-step collagenase IV digestion method according to the protocol established by Seglen^[13]. The nonparenchymal cell fraction was determined to contain the hepatic oval cell population as described by Yaswen *et al*^[14]. Hepatocytes were separated from the nonparenchymal cell portion by low-speed centrifugation (50 r/min \times 1 min). About one third of the total liver cells were nonparenchymal cells.

Immunohistochemistry was performed on the parenchymal and nonparenchymal fractions to ensure that the cells of interest were in the nonparenchymal cell fraction. The portion of nonparenchymal cells was further purified using magnetic activated cell sorting (MACS). Cells were incubated with CD45 antibody (1:50) and rat erythroid cell antibody (1:200) (BD Pharmingen) at 4 °C for 10 min and incubated with magnetic goat anti-mouse IgG (1:5) at 4 °C for 15 min. MACS was performed according to the manufacturer's recommendations (Miltenyi Biotec). The depleted fraction was incubated with c-kit antibody (1:50) and then incubated with magnetic goat anti-rabbit IgG (1:50). The c-kit+ fraction was collected for immunohistochemistry and culture *in vitro*.

The sorted c-kit+ cells were resuspended in DMEM/F-12

medium supplemented with 100 g/L fetal bovine serum, insulin-transferrin-sodium selenite, dexamethasone (1×10^{-7} mol/L), nicotinamide (10 mmol/L), L-glutamine (2 mmol/L), β -mercaptoethanol (0.1 mmol/L), HEPES (10 mmol/L) and penicillin/streptomycin. They were placed in 96-well plates, the same volume of supernatant from cultured ED13 fetal liver cells was added and incubated at 37 °C with 50 mL/L CO₂. Human recombinant hepatocyte growth factor (HGF, 50 ng/mL), epidermal growth factor (EGF, 20 ng/mL) and α -transforming growth factor (TGF- α , 20 ng/mL) were added 24-48 h after initiation of culture.

Phenotypic characterization of cultured cells

After 7 days, BrdU with a final concentration of 10 μ M/L was added to the medium and incubated for 3 h. The cells were fixed with methanol at 4 °C for 20 min, and washed with PBS containing 0.5 g/L polyoxyethylene sorbitan monolaurate (Tween 20). Cytochemical staining was performed with BrdU, c-kit, albumin, and CK19 antibodies. The staining method was the same as immunohistochemistry.

Reverse-transcription polymerase chain reaction analysis

Characteristics of cultured cells were evaluated by reverse-transcription polymerase chain reaction (RT-PCR). mRNA was extracted from the cell colonies using a QuickPrep micro mRNA purification kit (Qiagen) according to the supplier's recommended protocol. cDNA was synthesized using oligo-d (T)15 and Omniscript RT kit. A 20 μ L of reaction mixture containing 1 \times Buffer RT, 0.5 mmol/L dNTP, 10 unit RNasin, 4 unit Omniscript reverse transcriptase and 1-2 μ g RNA template was incubated at 37 °C for 1 h. PCR was done using HotStarTaq DNA polymerase in 25 μ L of the reaction mixture (1 \times PCR buffer, 0.5 unit HotStar Taq DNA polymerase, 200 μ mol/L dNTP) with hepatocyte-specific primers for albumin (5' -GAG AAG TGC TGT GCT GAA GG-3' and 5' -TCA GAG TGG AAG GTG AAG GT-3'), α -fetoprotein (5' -AAC ACA TCC AGG AGA GCC AG-3' and 5' -TTC TCC AAG AGG CCA GAG AA-3'), cholangiocyte-specific primers for CK19 (5' -CTG TCT TGG TCC GGT CAC TG-3' and 5' -GGC ATC TTG GTC TGT GTC AT-3'). PCR cycles were as follows: initial denaturation at 95 °C for 15 min, followed by 35 cycles at 94 °C for 45 s, at 55 °C for 1 min, at 72 °C for 45 s, and final extension at 72 °C for 10 min. PCR products were separated in 20 g/L agarose gel.

RESULTS

Activation of oval cell proliferation

Oval cells could be seen in 2-AAF treated rat liver at the dosage from 10 mg/kg to 20 mg/kg weight mass 7 to 13 d after partial

hepatectomy. The peak of oval cell proliferation occurred 11 d after hepatectomy. The histologic changes in liver sections from rats exposed to 2-AAF at the dosage of 10 mg/kg body mass for 6 d, followed by partial hepatectomy and sacrifice 11 d posthepatic injury are shown in Figure 1. The proliferated oval cells were small in size (approximately 10 μ m) with a large nuclei to cytoplasm ratio, radiating from the periportal region forming primitive ductular structures with poorly defined lumen. The control rat liver showed complete lobular structure without oval cell proliferation (Figures 1C and D). DNA synthesis in the oval cells was examined by BrdU incorporation test, and many of the oval cells were in S-phase with their nuclei stained positive by nuclear immunohistochemical staining for BrdU. DNA synthesis in epithelial cells of the portal bile ductules was also examined by BrdU incorporation (Figure 2).

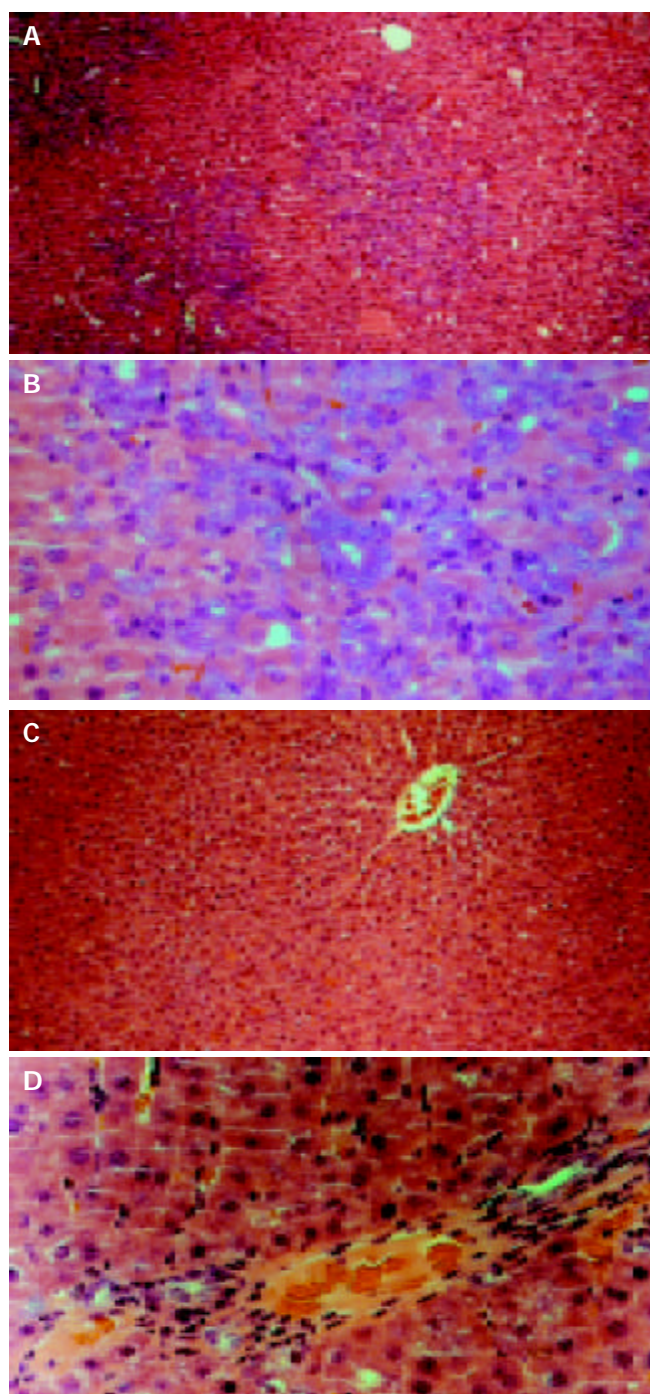


Figure 1 Rat liver sections obtained from 2-AAF/PH (11 d after operation) and control. Sections were stained with hematoxylin-eosin. (A and B) show liver sections obtained from

2-AAF/PH-treated rats at low ($\times 100$) and high ($\times 400$) magnification. Small oval cells (arrows) can be seen close proximity to proliferating bile ducts and in areas of ductular proliferation or in acinar arrangements around hepatocytes. The oval cells radiate from the periportal region, forming primitive ductular structures with poorly defined lumen. (C and D) show liver tissue from control rats at low and high magnification. Hepatocyte proliferation can be seen in the typical liver architecture. Central vein (CV) and portal triad region can be seen.

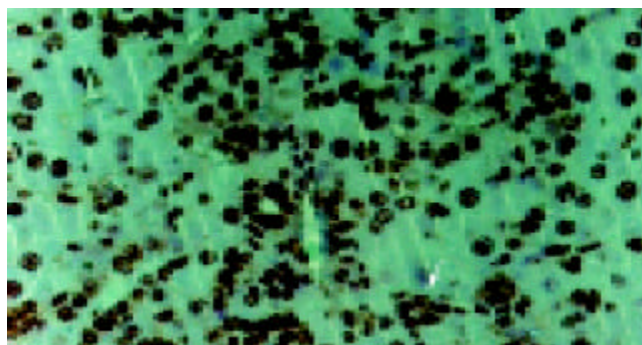
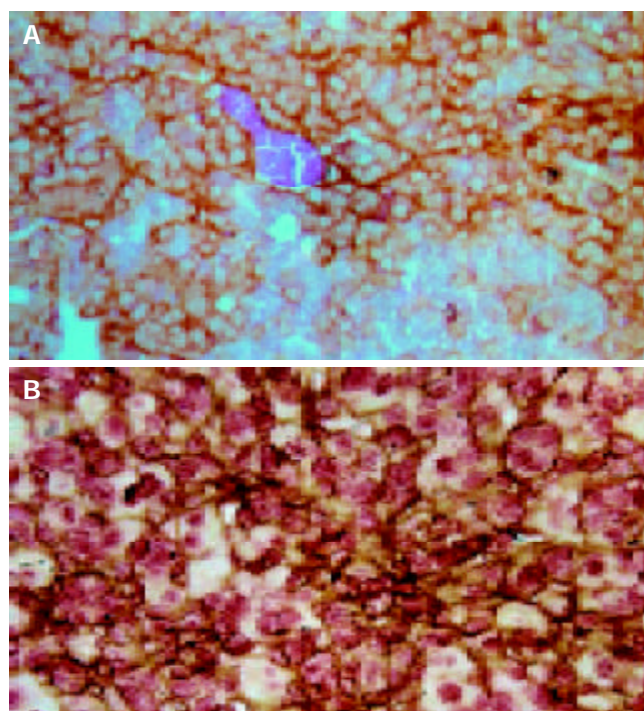


Figure 2 Immunohistochemistry of liver sections obtained from 11 2-AAF/PH rats. BrdU staining of oval cells in proliferative state. Arrows indicate oval cells.

Immunohistochemistry for marker on activated hepatic oval cells

The sections were stained with antibodies for oval specific marker, biliary lineage marker and hepatocyte lineage markers (OV6, CK19, albumin and AFP). The oval cells generated from 2-AAF/PH treated rat liver were positive for OV6 (Figure 3A), CK19 (Figure 3C), albumin (Figures 3B and D) and AFP (Figure 3E). Double immunohistochemistry showed that oval cells coexpressed OV6 and albumin or CK19 and albumin (Figures 3B and D). The oval cells were stained positive for connexin 43, but the sections from control rats were negative for connexin 43 (Figure 3F). In Figure 3G, oval cells expressed c-kit antigen, the ductular cells appeared to be positive with little to no staining for c-kit. No liver sections from control rat were stained positive for c-kit (Figure 3H).



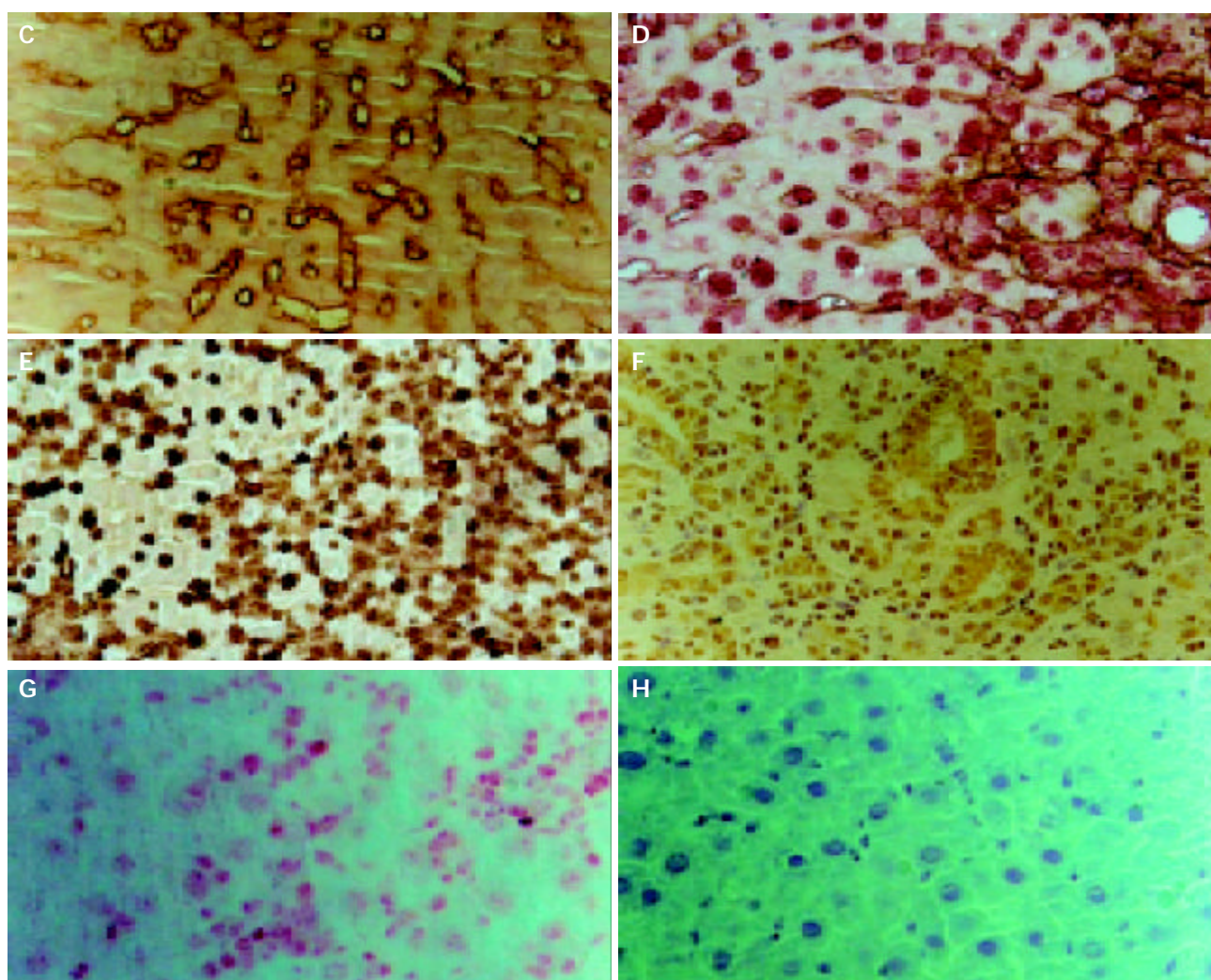


Figure 3 Immunohistochemical staining of liver sections from rat liver exposed to 2-AAF/PH (d 11) at high magnification. A: Staining for OV6, Arrows point to OV6-positive oval cells. B: Double immunohistochemical staining for OV6 (brown) and albumin (red). C: Staining for cytokeratin19(CK19). Ductular lumen face and oval cells were positive. Arrows point of CK19-positive cells. D: Double immunohistochemical staining for CK19 (brown) and albumin (red). Arrows point to oval cells with tow markers. E: Staining for AFP. F: Staining for connexin43, Arrows point to connexin43 positive oval cells. G: Staining for C-kit, Oval cells were stained with red. H: Negative control.

Purification and proliferation of *c-kit*⁺ oval cells

In order to define the phenotype, growth, and differentiation potential of individual *c-kit*⁺ cells, we used an immunoselection and cell culture strategy. After parenchymal cells were separated from nonparenchymal cells, antibody against *c-kit* was used to purify *c-kit*⁺ cells from nonparenchymal fraction by MACS. Immunohistochemical staining for OV6 showed that more than 90% sorted cells were positive (Figure 4).

After incubated for 24 h, most sorted *c-kit*⁺ cells adhered to collagen IV coated plate. By day 3 single cells proliferated to form colonies which expanded up to several hundred cells at 2 wk (Figures 5A, B). Figure 6 shows BrdU incorporation of a cultured *c-kit*⁺ oval cell colony, most cells were positive with their nuclei stained brown.

Characterization of *c-kit*⁺ oval cells

To determine the characterization of the colonies, we studied constituent cells by immunohistochemistry using albumin and CK19 as lineage markers as well as *c-kit*. After 1 wk, some progeny of *c-kit*⁺ oval cells in the colony lost the *c-kit* marker of parental generation (Figure 6). Most colonies at 2 wk contained 3 types of cells, namely albumin positive cells, CK19 positive cells, both albumin and CK19 positive cells (Figure 7). RT-PCR was performed to identify the expression

of genes encoding markers in both hepatocyte and cholangiocyte lineages (hepatocytes: albumin, α -fetoprotein; cholangiocytes: CK19). Almost all colonies contained mRNA of both hepatocyte-specific and cholangiocyte-specific genes at 2 wk (Figure 8). These results of RT-PCR and immunocytochemistry showed the bipotent differentiation ability of the sorted *c-kit*⁺ oval cells.

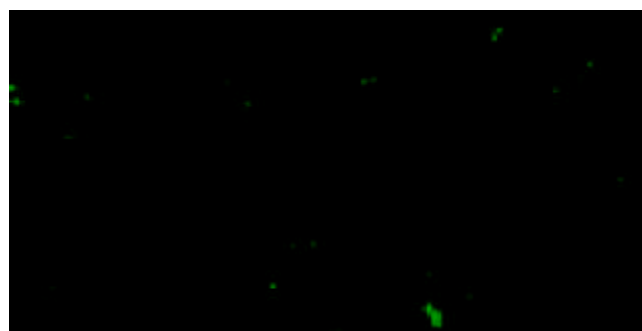


Figure 4 Immunocytochemistry for OV6 on cytocentrifuged preparations of *C-kit*⁺ MACS sorted cells from 2-AAF/PH treated rats. The sorted *C-kit*⁺ cells were stained with oval cell-specific antibody OV6 (green).

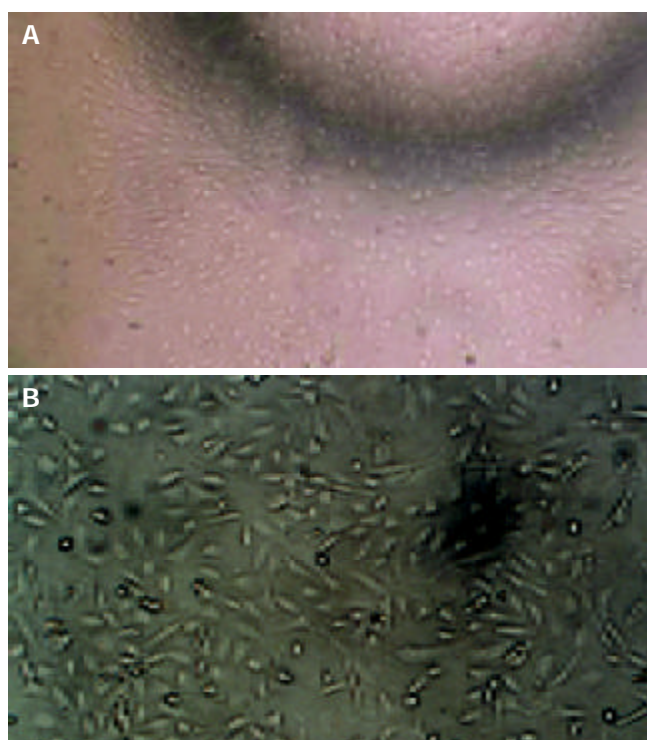


Figure 5 Phase contrast photomicrographs showing formation of a colony by a sorted C-kit⁺ oval cell after cultured *in vitro* for 2 wk. (A: ×100; B: ×200).

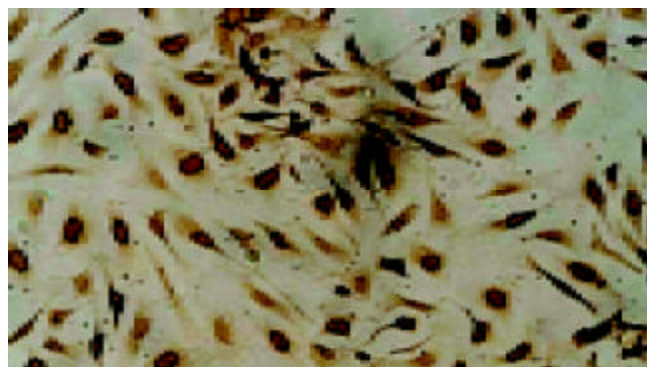


Figure 6 Double immunocytochemistry for BrdU incorporation and C-kit staining on sorted c-kit⁺ oval cell colony on d 7. Most cells had their nuclei stained with BrdU (arrow). Though they came from one precursor, many cells lost c-kit marker, just some of them were still c-kit positive stained blue (arrowheads). (×400).

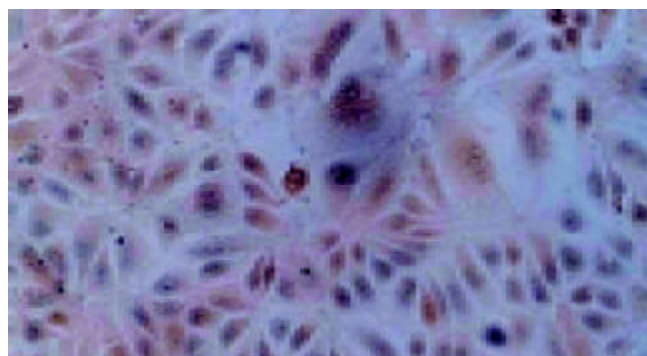


Figure 7 Dual staining of cultured sorted oval cell colony with albumin (dark blue) and CK19 (brown). Some cells were stained with both markers (Arrows) and the others were stained only one marker. (×400).

750 bp
500 bp

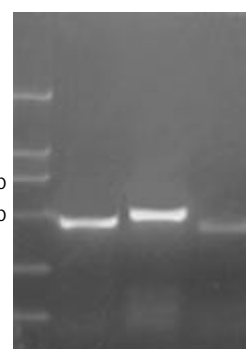


Figure 8 RT-PCR analysis of gene expression. RNA was isolated from sorted cell colony.

DISCUSSION

Since liver transplantation is the only available current therapy for end-stage liver failure and there is an ever-increasing shortage of donor livers, cell therapy from alternative cell source might offer a new therapeutic approach against liver disease^[15]. In recent years, such studies have been conducted successfully using primary hepatocytes in rodent models, and current research is being conducted to isolate progenitor or stem cells that should have the highest potential for effective liver repopulation. Therefore, identification of hepatic/progenitor cells has become increasingly important. Stem cells are defined as the cells with the self-renewing activity and capability of generating multiple types of lineage committed cells. As for the hepatocytic lineage, stem cells had to possess the ability to generate both parenchymal hepatocytes and bile duct epithelial cells^[16]. After debated for many years, it has been generally accepted that the liver contains cells with stem-like properties and that these cells can be activated to proliferate and differentiate into mature hepatocytes and cholangiocytes under certain pathophysiologic circumstances^[17,18]. These cells might be related to the so-called “oval cells”, originally identified by Farber as immature epithelial cells with oval shaped nuclei and scant cytoplasm^[19].

Activation of the oval cell proliferation could be induced by many rodent models^[20-22], we chose modified Solt-Farber model to activate oval cells^[12]. The model could be successfully established by 2-AAF at the dosage from 10 mg to 20 mg and the peak of oval cell proliferation was on d11 after partial hepatectomy. Immunohistochemical staining showed that the oval cells expressed oval cell-specific marker OV6, cholangiocyte lineage marker CK19 and hepatocyte lineage marker albumin and AFP. OV6 and albumin or CK19. Albumin was coexpressed in the same oval cells by double immunohistochemistry. These data suggest that the oval cells may represent a facultative hepatic progenitor/stem cell compartment. The oval cells also expressed connexin 43, but the liver cells in the control rat liver expressed connexin 32 instead of connexin 43 (data not shown). Gap junctional intercellular communication (GJIC) was considered to play a key role in the maintenance of tissue independence and homeostasis in multicellular organisms by controlling the growth of GJIC-connected cells. Gap junction channels are composed of connexin molecules, connexin 43 is expressed on immature liver cells or cholangiocytes, connexin 26 and connexin 32 are expressed on hepatocytes. As hepatocytes differentiate, the proportions of connexin 43 then 26 mRNAs decrease while that of connexin 32 mRNA increases. Connexin 43 was also expressed in fetal liver cells and the expression of connexin 43 declined after birth^[23]. Neveu reported that proliferating oval cells expressed diffuse connexin 43 immunoreactivity. Differentiation of oval cells into basophilic hepatocytes resulted in their alterations in Cx32 and

Cx26 expression^[24]. Since the oval cells were generated by the proliferation of terminal bile ducts, they formed structures representing an extension of the canals of Hering^[25], and there are many common features between immature embryonic hepatic cells and oval cells such as expression of AFP and connexin 43. It is reasonable to assume that oval cells may be a direct progeny of resident undifferentiated liver stem cells. Suzuki *et al.* have identified a population of hepatic stem cells that exist in developing mouse liver, and these cells may represent the resident hepatic stem cells which possess multilineage differentiation potential and self-renewing capability^[26,27]. Chen also^[28] reported that transfused oval cells through caudal vein can migrate into the parenchyma of the liver and are settled there.

Hepatic progenitor cells share common characteristics with stem cells of the hematopoietic system. Classical hematopoietic markers, including Thy-1, CD34, c-kit were expressed on the surface of oval cells^[8-11]. After bone marrow transplantation, a proportion of the regenerated hepatic cells was shown to be donor-derived^[29]. Intravenous injection of adult bone marrow cells (c-kit^{high}Thy^{low}Lin^{low}Sca-1⁺) in the FAH^{-/-} mouse, an animal model of tyrosinemia type I, rescued the mouse and restored the biochemical function of its liver^[30]. Crosby *et al.*^[11] reported that there were c-kit⁺ cells in the periportal tract surrounding bile ducts, which coexpressed CK19. After cultured in biliary cell growth media, the isolated c-kit positive cells could form colony with the properties of cholangiocytes^[11]. We also found that oval cells in the periportal area in 2-AAF/PH expressed c-kit, but hepatocytes and liver in control animal were stained negative. The evidence of a cell lineage relationship between the hematopoietic system and the liver supports the extrahepatic origin of hepatic progenitors.

Suzuki *et al.* recently reported that CD49f^{low}c-Kit⁺ CD45^{TER119} cell subpopulation in ED13.5 mouse fetal liver could form large colonies designated as 'hepatic colony-forming-unit in culture' (H-CFU-C), and expression of *c-kit*, *CD34* and *thy-1* became detectable in some of these colonies on d 21^[26]. These data may suggest that not only exogenous hepatic stem/progenitor cells derived from circulating bone marrow express hematopoietic stem cell markers, but endogenous tissue-determined stem/progenitor cells express such markers.

C-kit stem cell receptor tyrosine kinase (KIT) and its ligand, stem cell factor (SCF) system play a crucial role in the development of oval cells. If the c-kit kinase activity was severely impaired, the number of oval cells on d 7, 9, and 13 after PH was significantly reduced to 15%, 18%, and 27% of those in control normal rats in the AAF/PH model, respectively^[10]. So we chose c-kit as a surface marker to purify oval cells. After depletion of CD45⁺ cells and rat erythroid cells from nonparenchymal fractions, oval cells were further enriched by MACS using c-kit antibody. The result showed that more than 90% sorted cells were OV6 positive. After cultured in our special medium the sorted oval cells could form large colonies. BrdU incorporation test was positive in most progenies of oval cells on d 7, indicating that the sorted oval cells have high growth potential. At wk 2, some of the progenies lost the c-kit marker of the sorted cells. Immunohistochemical staining showed that there were 3 types of cells in the colony after cultured for 2 wk *in vitro*, that marked albumine, only CK19, and both albumin and CK19. RT-PCR on the colony showed that expression of albumin, AFP and CK19 genes was detectable. All these data suggest that the sorted oval cells are facultative hepatic stem/progenitor cells with self-renewing capacity and can differentiate along hepatocyte and cholangiocyte lineages *in vitro*, and the progeny lost stem cell marker during differentiation. Crosby *et al.* purified c-kit positive cells from

cirrhotic tissue by MACS and the sorted cells could form colonies with 2 types of cells in morphology cultured *in vitro* on d 7. But the sorted c-kit⁺ or CD34⁺ cells by Crosby *et al.* could only differentiate along cholangiocyte lineage^[11]. The difference might be due to the fact that they used just biliary cell growth medium.

In conclusion, we successfully isolated and purified viable c-kit positive oval cells which had high growth potential and multilineage differentiation activity from the 2-AAF/PH rat liver. The properties of proliferation and differentiation *in vivo* are still to be studied by cell transplantation.

REFERENCES

- 1 **Fausto N.** Liver regeneration: from laboratory to clinic. *Liver Transpl* 2001; **7**: 835-844
- 2 **Michalopoulos GK, DeFrances MC.** Liver regeneration. *Science* 1997; **276**: 60-66
- 3 **Overturf K, Al-Dhalimy M, Ou CN, Finegold M, Grompe M.** Serial transplantation reveals the stem-cell-like regenerative potential of adult mouse hepatocytes. *Am J Pathol* 1997; **151**: 1273-1280
- 4 **Alison MR, Poulson R, Forbes SJ.** Update on hepatic stem cells. *Liver* 2001; **21**: 367-373
- 5 **Lowes KN, Croager EJ, Olynyk JK, Abraham LJ, Yeoh GC.** Oval cell-mediated liver regeneration: Role of cytokines and growth factors. *J Gastroenterol Hepatol* 2003; **18**: 4-12
- 6 **Fujikawa T, Hirose T, Fujii H, Oe S, Yasuchika K, Azuma H, Yamaoka Y.** Purification of adult hepatic progenitor cells using green fluorescent protein (GFP) - transgenic mice and fluorescence-activated cell sorting. *J Hepatol* 2003; **39**: 162-170
- 7 **Alison M, Golding M, El-Lalani N, Sarraf C.** Wound healing in the liver with particular reference to stem cells. *Philos Trans R Soc Lond B Biol Sci* 1998; **353**: 877-894
- 8 **Petersen BE, Goff JP, Greenberger JS, Michalopoulos GK.** Hepatic oval cells express the hematopoietic stem cell marker Thy-1 in the rat. *Hepatology* 1998; **27**: 433-445
- 9 **Omori N, Omori M, Evarts RP, Teramoto T, Miller MJ, Hoang TN, Thorgerirsson SS.** Partial cloning of rat CD34 cDNA and expression during stem cell-dependent liver regeneration in the adult rat. *Hepatology* 1997; **26**: 720-727
- 10 **Matsusaka S, Tsujimura T, Toyosaka A, Nakasho K, Sugihara A, Okamoto E, Uematsu K, Terada N.** Role of c-kit receptor tyrosine kinase in development of oval cells in the rat 2-acetylaminofluorene/partial hepatectomy model. *Hepatology* 1999; **29**: 670-676
- 11 **Crosby HA, Kelly DA, Strain AJ.** Human hepatic stem-like cells isolated using c-kit or CD34 can differentiate into biliary epithelium. *Gastroenterology* 2001; **120**: 534-544
- 12 **Tatematsu M, Kaku T, Medline A, Farber E.** Intestinal metaplasia is a common option of oval cells in relation to cholangiofibrosis in liver of rats exposed to 2-acetylaminofluorene. *Lab Invest* 1985; **52**: 354-362
- 13 **Seglen PO.** Hepatocyte suspensions and cultures as tools in experimental carcinogenesis. *J Toxicol Environ Health* 1979; **5**: 551-560
- 14 **Yaswen P, Hayner NT, Fausto N.** Isolation of oval cells by centrifugal elutriation and comparison with other cell types purified from normal and preneoplastic livers. *Cancer Res* 1984; **44**: 324-331
- 15 **Strom SC, Chowdhury JR, Fox JJ.** Hepatocyte transplantation for the treatment of human disease. *Semin Liver Dis* 1999; **19**: 39-48
- 16 **Kinoshita T, Miyajima A.** Cytokine regulation of liver development. *Biochim Biophys Acta* 2002; **1592**: 303-312
- 17 **Sell S.** Liver stem cells. *Mod Pathol* 1994; **7**: 105-112
- 18 **Sell S.** Heterogeneity and plasticity of hepatocyte lineage cells. *Hepatology* 2001; **33**: 738-750
- 19 **Farber E.** Similarities in the sequence of early histologic changes induced in the liver of rat by ethionine, 2-acetylaminofluorene, and 3-methyl-4-dimethylaminobenzene. *Cancer Res* 1956; **16**: 142-148
- 20 **Akhurst B, Croager EJ, Farley-Roche CA, Ong JK, Dumble ML,**

- Knight B, Yeoh GC. A modified choline-deficient, ethionine-supplemented diet protocol effectively induces oval cells in mouse liver. *Hepatology* 2001; **34**: 519-522
- 21 **Dabeva MD**, Shafritz DA. Activation, proliferation and differentiation of progenitor cells into hepatocytes in the D-galactosamine model of liver regeneration. *Am J Pathol* 1993; **143**: 1606-1620
- 22 **Factor VM**, Radaeva SA, Thorgeirsson SS. Origin and fate of oval cells in dipin-induced hepatocarcinogenesis in the mouse. *Am J Pathol* 1994; **145**: 409-422
- 23 **Rosenberg E**, Faris RA, Spray DC, Monfils B, Abreu S, Danishefsky I, Reid LM. Correlation of expression of connexin mRNA isoforms with degree of cellular differentiation. *Cell Adhes Commun* 1996; **4**: 223-235
- 24 **Neveu MJ**, Hully JR, Babcock KL, Vaughan J, Hertzberg EL, Nicholson BJ, Paul DL, Pitot HC. Proliferation-associated differences in the spatial and temporal expression of gap junction genes in rat liver. *Hepatology* 1995; **22**: 202-212
- 25 **Paku S**, Schnur J, Nagy P, Thorgeirsson SS. Origin and structural evolution of the early proliferating oval cells in rat liver. *Am J Pathol* 2001; **158**: 1313-1323
- 26 **Suzuki A**, Zheng Yw YW, Kaneko S, Onodera M, Fukao K, Nakauchi H, Taniguchi H. Clonal identification and characterization of self-renewing pluripotent stem cells in the developing liver. *J Cell Biol* 2002; **156**: 173-184
- 27 **Suzuki A**, Zheng Y, Kondo R, Kusakabe M, Takada Y, Fukao K, Nakauchi H, Taniguchi H. Flow-cytometric separation and enrichment of hepatic progenitor cells in the developing mouse liver. *Hepatology* 2000; **32**: 1230-1239
- 28 **Chen JZ**, Hong H, Xiang J, Xue L, Zhao GQ. A selective tropism of transfused oval cells for liver. *World J Gastroenterol* 2003; **9**: 544-546
- 29 **Petersen BE**, Bowen WC, Patrene KD, Mars WM, Sullivan AK, Murase N, Boggs SS, Greenberger JS, Goff JP. Bone marrow as a potential source of hepatic oval cells. *Science* 1999; **284**: 1168-1170
- 30 **Lagasse E**, Connors H, Al-Dhalimy M, Reitsma M, Dohse M, Osborne L, Wang X, Finegold M, Weissman IL, Grompe M. Purified hematopoietic stem cells can differentiate into hepatocytes *in vivo*. *Nat Med* 2000; **6**: 1229-1234

Edited by Zhang JZ and Wang XL **Proofread by** Xu FM

• BASIC RESEARCH •

Influence of serum collected from rat perfused with compound *Biejiaaruangan* drug on hepatic stellate cells

Shun-Gen Guo, Wei Zhang, Tao Jiang, Min Dai, Lu-Fen Zhang, Yi-Chun Meng, Li-Yun Zhao, Jian-Zhao Niu

Shun-Gen Guo, Wei Zhang, Min Dai, Li-Yun Zhao, Jian-Zhao Niu, Laboratory of Cell and Biochemistry, Beijing University of Traditional Chinese Medicine, Beijing 100029, China

Tao Jiang, Department of Histology and Embryology, Medical College of Chinese People's Armed Police Forces, Tianjin 300162, China

Lu-Fen Zhang, College of Acupuncture and Moxibustion, Beijing University of Traditional Chinese Medicine, Beijing 100029, China

Yi-Chun Meng, Central Experimental Laboratory, Beijing Military Medicine College, Beijing 100071, China

Supported by the National Natural Science Foundation of China for Key Project, No. 30130220

Correspondence to: Shun-Gen Guo, Laboratory of Cell and Biochemistry, Beijing University of Traditional Chinese Medicine, Beijing 100029, China. guoshungen@sina.com

Telephone: +86-10-64286926 **Fax:** +86-10-64286871

Received: 2003-08-05 **Accepted:** 2003-10-27

Abstract

AIM: To observe the effect of compound *Biejiaaruangan* decoction (CJRG) (composite prescription of Carapax trionycis for softening the liver) on proliferation, activation, excretion of collagen and cytokine of hepatic stellate cells (HSCs) and to find the mechanism of prevention and treatment of hepatic fibrosis by CJRG.

METHODS: Using MTT, immunohistochemistry and image analysis technology, the related indexes for proliferation, activation, excretion of collagen and cytokine of hepatic stellate cells were detected in 24 h, 48 h, and 72 h after administration of different dosages of CJRG.

RESULTS: Statistical analysis showed that serum collected from rat perfused with CJRG could restrain the proliferation of HSC in 48 h and 72 h especially in high and medium dosage groups, markedly decrease the expression of desmin, synapsin and platelet derived growth factor (PDGF) in HSC in 24 h, 48 h and 72 h, as well as the expression of α -SMA, collagen III, TIMP and TGF β 1 in 48 h and 72 h, decrease the excretion of collagen I in 72 h. CJRG serum had no significant effect on collagens I, III and TIMP in 24 h.

CONCLUSION: CJRG serum has a good curative effect on hepatic fibrosis. Its main mechanism may be related to the following factors. The drug serum can restrain the proliferation and activation of HSC, decrease the number of activated HSC and the total number of HSC, the excretion of collagens I, III, enhance the degradation of collagen and restore the balance of synthesis and degradation of collagen, inhibit the expression of transforming growth factor β 1 (TGF β 1) and platelet derived growth factor (PDGF) in HSC, block and delay the process of hepatic fibrosis. Synapsin is a new marker of activation of HSC, which provides a theoretical and testing basis for neural regulation in the developing process of hepatic fibrosis.

Guo SG, Zhang W, Jiang T, Dai M, Zhang LF, Meng YC, Zhao

LY, Niu JZ. Influence of serum collected from rat perfused with compound *Biejiaaruangan* drug on hepatic stellate cells. *World J Gastroenterol* 2004; 10(10): 1487-1494

<http://www.wjgnet.com/1007-9327/10/1487.asp>

INTRODUCTION

Hepatic fibrosis is an inevitable pathological process of chronic liver disease to hepatic cirrhosis. Hepatic fibrosis is caused by excessive deposition of extracellular matrix (ECM), which is the result of more synthesis and less degradation of ECM. A clinical and experimental study has found that liver cells, hepatic stellate cells (HSC), kupffer cells and sinus endothelial cells all take part in the formation of hepatic fibrosis, in which HSC plays a very important role^[1]. Activation of HSC is commonly regarded as the major link of hepatic fibrosis and the main resource of synthesis of ECM^[2]. The main characteristic of activation of HSC is excessive proliferation of HSC^[3]. In addition, desmin is regarded as a marking protein of HSC and α -SMA is regarded as a marker of activation of HSC^[4]. A foreign study has reported that in process of activation of HSC, the expression of synapsin can increase^[5]. Activation of HSC can lead to excessive synthesis of collagen. MMP and TIMP also jointly take part in the synthesis and degradation of collagen^[6]. Multiple cytokines including TGF β 1 and PDGF play a very important role in proliferation, activation of HSC and synthesis of ECM^[7]. Therefore, it may be a good strategy to restrain the amount of activated HSC, decrease the synthesis and excretion of collagens I, III and TIMPs, and promote the synthesis and excretion of MMPs. Aiming at HSC, it has become a control issue in anti-hepatic fibrosis to restrain its proliferation, decrease the synthesis of ECM and accelerate the degradation of ECM, and even inverse activated HSC to silent HSC. Traditional Chinese medicine has shown its own advantage in treating some difficult diseases. Approved by the government, compound *Biejiaaruangan* decoction (CJRG) has been used as the first traditional Chinese medicine for treating hepatic fibrosis (approval document number: 1999 2-102). Clinical observations in Beijing, Shanghai and Hubei Province proved that its effective rate was 78.9% in 121 patients by the first hepatic puncture and in 52 patients by the second hepatic puncture. However, further study of its detailed anti-hepatic fibrosis mechanism is still needed. On the basis of the above-mentioned theory and research developments, our study with the cell culture as technical platform, was to observe the influence of serum collected from rats perfused with CJRG on activation and proliferation of HSC *in vitro*, and using immunohistochemistry and image analysis technology to observe its influence on the expressions of desmin, α -SMA, synapsin, collagens I, III, TIMP, TGF β 1 and PDGF of HSC *in vitro*.

MATERIALS AND METHODS

Main reagents

RPMI1640 was produced by Gibco, fetal bovine serum was produced by Hyclone, and 96-well plates by Costa. Dimethyl sulfoxide (DMSO), ethylenediaminetetra-acetic acid (EDTA), 3-

(4,5-dimethyl-1-thiazol-2-yl), 2,5-diphenyl tetrazolium bromide (MTT), N-2-Hydroxyethylpiperazine-N'-2-ethane sulfonine acid (HEPES), and trypsin were all products of Sigma. Rat desmin monoclonal antibody and rat α -SMA monoclonal antibody were bought from DAKO, rat synapsin monoclonal antibody was bought from Santa Cruz. Rat collagen I and III monoclonal antibodies, rat TIMP and PDGF as well as TGF- β 1 monoclonal antibodies, ABC and DAB test kits were all bought from Beijing Zhongshan Biotechnology Inc.

SD rat HSC line

The HSC line was established in our laboratory and prepared after long-term generation.

Preparation of SD rat serum^[8]

Normal SD rat serum A normal rat weighting 350 g fasted for 12 h was injected with diethylether for anesthesia. Under the sterile condition, 10 mL blood was obtained from abdominal aorta, then held for 2 h at room temperature. Blood serum was made by centrifugation at 427 g for 10 min, inactivated at 56 °C for 60 min, and frozen at -60 °C.

Hepatic fibrosis model SD rat serum Adapted Hernandez-Munoz method was used to establish animal model of hepatic fibrosis^[9], 0.2 mL CCl₄ (Olive oil, 1:6 dilution) was injected into abdominal cavity, three times each week for 7 wk. Serum preparation and preservation were the same as those of the normal SD rat serum.

Drug serum With 3.5, 7 and 14 times of human body dosage as low, medium and high dosage groups respectively, CBJRG was perfused into rat stomach 3 times at 12 h intervals. Rats were fasted for 12 h before the third perfusion and blood sampling was conducted from abdominal aorta 2 h after the third perfusion. Serum preparation and preservation were the same as those of the normal SD rat serum.

Cell culture and grouping

Rat HSCs were inoculated in RPMI1640 with 100 g/L fetal bovine serum, and cultivated at 37 °C in an incubator containing 50 mL/L CO₂ to logarithm growth time. After treatment with digestive fluid, HSCs were suspended by adding D-Hank's fluid, deposited by centrifugation at 190 g with 5 min, and then counted. Using RPMI1640 containing 100 g/L fetal bovine serum, HSCs were adjusted to a density of 5×10^4 /mL and added to a 24-well plate containing flying sheet, 0.2 mL each well. According to intervening factors, HSCs were divided into 5 groups, i.e. control group, model group, high dosage serum group, medium dosage serum group and low dosage serum group. Each group had 4 wells. Upper culture medium was removed after cultivated for 12 h. Control group serum, model group serum, high dosage group serum, medium dosage group serum and low dosage group serum were accordingly added. Flying sheets were taken out respectively at 24 h, 48 h and 72 h, fixed with cold acetone for 10 min, dried and preserved at -60 °C.

Using MTT method to detect effect of drug serum on proliferation of HSC

HSCs with a density of 5×10^4 /mL were added to a 96-well plate, 0.2 mL each well. Each group contained 8 wells. Upper medium was removed after cultivated for 12 h. Control group serum, model group serum, high dosage group, medium dosage group serum and low dosage group serum were accordingly added. 50 μ L cultivating fluid was taken out respectively at 24 h, 48 h and 72 h. A 50 μ L of MTT (50 μ g MTT) was then added and the culture continued for 4 h at 37 °C. After upper fluid was removed, 150 μ L DMSO was added to each well. After concussed and dissolved, Absorbency value with wave-length of 450 nm was detected by enzyme labeled instrument (BioRad 2250, Japan).

The test was repeated 5 times.

Immunohistochemical staining

α -SMA staining Preserved cell flying sheets were immersed with PBC for 5 min, blocked with 10 mL/L H₂O₂ for 10 min, washed 3 times with PBC, 5 min each time, and then incubated with 10% goat serum for 30 min. Rat α -SMA, desmin, synapsin collagens I and II, TIMP, TGF β 1 and PDGF antibodies were diluted at a concentration of 1:100 and added as the first antibodies, staying overnight at 4 °C. After washed 3 times with PBC, 5 min each time, biotin goat anti-rat IgM was added, staying overnight at 4 °C, washed with PBC 3 times, 5 min each time. Streptavidin was added for 30 min, stained with DAB. The first antibody was replaced with fetal bovine serum as negative control, α -SMA male staining Absorbency value and relative area occupied by α -SMA male cells in the reference system were detected with TN-8502 image analysis system (Tractor Northern Co, USA). Data were treated with SPSS for ANOVA test. Results were presented mean \pm SD. $P < 0.05$ was considered statistically significant.

RESULTS

Influence of each group serum on proliferation of HSC at different time points

HSC just after digesting phase showed a global form under contrast microscope. After cultivated for 12 h, HSCs were pasted to the wall, changing into the oblate form. There were obvious lipid droplets in cytoplasm. Few cells started to show the extension of cytoplasm. After cultivated for 24 h, most cells showed the extension of cytoplasm, and some cells showed multi-angle pseudopodium and typical star-like form. The influence on proliferation of HSC detected by MTT method is presented in Table 1.

Influence of each group serum on α -SMA, desmin, synapsin of HSC at different time points

Tables 2, 3, 4 and Figures 1, 2 show the influence of each group serum on α -SMA, desmin, synapsin of HSC at different time points, which were detected with TN-8502 image analysis system.

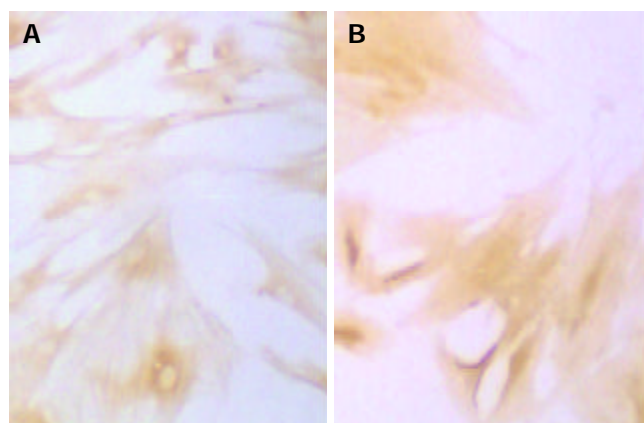


Figure 1 Immunohistochemical staining of α -SMA of SD rat HSC line in model group and medium dosage group ($\times 66$). A: Immunohistochemical staining of α -SMA of SD rat HSC line in model group. B: Immunohistochemical staining of α -SMA of SD rat HSC line in medium dosage group.

Influence of each group serum on collagen I, III and TIMP of HSC at different time points

The influence of each group serum detected with TN-8502 image analysis system on collagens I, III and TIMP of HSC at different time points is shown in Tables 5, 6, 7 and Figures 3, 4.

Table 1 Influence of each group serum on proliferation of HSC at different time points (A value: mean±SD)

	N	M	G	Z	D
24 h	0.40±0.06	0.40±0.03	0.38±0.03	0.391±0.02	0.38±0.03
48 h	0.52±0.03 ^c	0.66±0.05 ^a	0.47±0.02 ^{ac}	0.460±0.02 ^{ac}	0.51±0.03 ^c
72 h	0.75±0.09 ^c	0.96±0.05 ^a	0.55±0.07 ^{ac}	0.580±0.08 ^{ac}	0.69±0.07 ^c

N: control group; M: model group; G: high dosage group; Z: medium dosage group; D: low dosage group, ^a*P*<0.05 vs normal group; ^c*P*<0.05 vs model group.

Table 2 Influence of each group serum on α-SMA of HSC at different time points (A value: mean±SD)

	N		M		G		Z		D	
	A	Male cell area (%)	A	Male cell area (%)	A	Male cell area (%)	A	Male cell area (%)	A	Male cell area (%)
24 h	619.89±163.84 ^c	7.49±2.06 ^c	778.93±190.26 ^a	9.64±0.26 ^a	110.95±45.21 ^{ac}	0.90±0.22 ^{ac}	243.83±62.97 ^{ac}	2.72±1.48 ^{ac}	417.46±126.72 ^c	3.56±0.91 ^c
48 h	812.51±123.39 ^c	8.28±4.58 ^c	1 032.69±106.64 ^a	10.56±1.83 ^a	333.71±57.9 ^{ac}	1.55±0.29 ^{ac}	345.08±51.85 ^{ac}	3.66±1.67 ^{ac}	675.35±202.20 ^c	5.45±2.50 ^c
72 h	989.77±166.32 ^c	9.36±2.39 ^c	1 255.30±150.39 ^a	15.66±2.34 ^a	448.36±55.80 ^{ac}	3.25±0.56 ^{ac}	556.27±80.32 ^{ac}	4.66±1.24 ^{ac}	759.38±109.32 ^{ac}	6.99±1.58 ^{ac}

N: control group; M: model group; G: high dosage group; Z: medium dosage group; D: low dosage group, ^a*P*<0.05 vs normal group; ^c*P*<0.05 vs model group.

Table 3 Influence of each group serum on desmin of HSC at different time points (A value: mean±SD)

	N		M		G		Z		D	
	A	Male cell area (%)	A	Male cell area (%)	A	Male cell area (%)	A	Male cell area (%)	A	Male cell area (%)
24 h	78.93±18.56 ^c	17.49±2.06 ^c	119.69±23.84 ^a	20.64±2.26 ^a	58.95±5.21 ^{ac}	12.90±3.22 ^{ac}	63.83±12.97 ^{ac}	12.72±1.48 ^{ac}	75.46±26.72 ^c	13.56±0.91 ^c
48 h	103.78±36.64 ^c	10.28±4.58 ^c	182.51±28.43 ^a	14.56±1.83 ^a	63.71±7.94 ^{ac}	8.55±0.29 ^{ac}	65.08±18.85 ^{ac}	7.66±1.67 ^{ac}	79.35±22.28 ^c	9.35±2.50 ^c
72 h	125.30±40.39 ^c	9.36±2.39 ^c	1 255.30±150.39 ^a	15.66±2.34 ^a	448.36±55.80 ^{ac}	3.25±0.56 ^{ac}	556.27±80.32 ^{ac}	4.66±1.24 ^{ac}	759.38±109.32 ^{ac}	6.99±1.58 ^{ac}

N: control group; M: model group; G: high dosage group; Z: medium dosage group; D: low dosage group, ^a*P*<0.05 vs normal group; ^c*P*<0.05 vs model group.

Table 4 Influence of each group serum on synapsin of HSC at different time points (A value: mean±SD)

	N		M		G		Z		D	
	A	Male cell area (%)	A	Male cell area (%)	A	Male cell area (%)	A	Male cell area (%)	A	Male cell area (%)
24 h	396.29±78.56 ^c	5.49±2.06 ^c	528.79±26.84 ^c	12.93±2.33 ^c	138.92±20.21 ^{ac}	2.64±0.22 ^{ac}	190.87±52.97 ^{ac}	3.69±1.24 ^{ac}	284.54±66.72 ^c	4.05±0.91 ^c
48 h	577.78±86.84 ^c	8.28±4.58 ^c	748.57±29.73 ^c	10.56±1.83 ^c	228.71±71.94 ^{ac}	1.55±0.29 ^{ac}	338.08±108.66 ^{ac}	3.66±1.67 ^{ac}	675.35±202.20 ^c	5.45±2.50 ^c
72 h	989.77±166.32 ^c	9.36±2.39 ^c	1 255.30±150.39 ^c	15.66±2.34 ^c	448.36±55.80 ^{ac}	3.25±0.56 ^{ac}	556.27±80.32 ^{ac}	4.66±1.24 ^{ac}	759.38±109.32 ^{ac}	6.99±1.58 ^{ac}

N: control group; M: model group; G: high dosage group; Z: medium dosage group; D: low dosage group, ^a*P*<0.05 vs normal group; ^c*P*<0.05 vs model group.

Table 5 Influence of each group serum on collagen I of HSC at different time points (A value: mean±SD)

	N		M		G		Z		D	
	A	Male cell area (%)	A	Male cell area (%)	A	Male cell area (%)	A	Male cell area (%)	A	Male cell area (%)
24 h	50.87±9.84	5.49±2.06 ^c	60.63±9.26	4.64±0.26	46.95±5.21	2.90±0.22	44.83±6.97	3.72±0.48	49.46±7.36	3.89±0.79
48 h	270.51±13.56	5.28±0.58	456.78±106.64	5.56±1.83	107.79±17.9	4.45±0.29	115.28±51.85	4.66±1.67	129.35±22.20	4.45±0.50
72 h	507.77±66.38 ^c	11.36±2.39 ^c	800.30±150.39 ^a	15.66±2.34 ^a	300.23±25.80 ^{ac}	5.25±0.56 ^{ac}	329.37±45.98 ^{ac}	6.62±1.33 ^{ac}	425.38±19.32 ^c	7.99±1.25 ^c

N: control group; M: model group; G: high dosage group; Z: mdium dosage group; D: low dosage group, ^a*P*<0.05 vs normal group; ^c*P*<0.05 vs model group.

Table 6 Influence of each group serum on collagen III of HSC at different time points (A value: mean±SD)

	N		M		G		Z		D	
	A	Male cell area (%)	A	Male cell area (%)	A	Male cell area (%)	A	Male cell area (%)	A	Male cell area (%)
24 h	60.93±18.56	12.49±3.16	65.69±23.84	13.64±2.36	40.95±5.21	8.90±3.82	45.83±12.97	9.72±1.47	52.46±26.72	10.56±0.56
48 h	203.78±36.64 ^c	25.28±4.27 ^c	282.51±28.43 ^a	31.56±3.69 ^a	63.71±7.94 ^{ac}	15.55±3.59 ^{ac}	65.08±18.85 ^{ac}	17.66±1.65 ^{ac}	79.35±22.28 ^{ac}	21.35±2.36 ^{ac}
72 h	325.30±40.39 ^c	30.36±2.50 ^c	501.77±56.42 ^a	40.66±4.82 ^a	178.36±5.82 ^{ac}	23.25±4.26 ^{ac}	182.27±20.32 ^{ac}	25.66±1.29 ^{ac}	220.38±19.32 ^c	29.70±1.72 ^c

N: control group; M: model group; G: high dosage group; Z: medium dosage group; D: low dosage group, ^a*P*<0.05 vs normal group; ^c*P*<0.05 vs model group.

Table 7 Influence of each group serum on TIMP of HSC at different time points (A value: mean±SD)

	N		M		G		Z		D	
	A	Male cell area (%)	A	Male cell area (%)	A	Male cell area (%)	A	Male cell area (%)	A	Male cell area (%)
24 h	60.93±18.56	12.49±3.16	65.69±23.84	13.64±2.36	40.95±5.21	8.90±3.82	45.83±12.97	9.72±1.47	52.46±26.72	10.56±0.56
48 h	203.78±36.64 ^c	25.28±4.27 ^c	282.51±28.43 ^a	31.56±3.69 ^a	63.71±7.94 ^{ac}	15.55±3.59 ^{ac}	65.08±18.85 ^{ac}	17.66±1.65 ^{ac}	79.35±22.28 ^{ac}	21.35±2.36 ^{ac}
72 h	325.30±40.39 ^c	30.36±2.50 ^c	501.77±56.42 ^a	40.66±4.82 ^a	178.36±5.82 ^{ac}	23.25±4.26 ^{ac}	182.27±20.32 ^{ac}	25.66±1.29 ^{ac}	220.38±19.32 ^c	29.70±1.72 ^c

N: control group; M: model group; G: high dosage group; Z: medium dosage group; D: low dosage group, ^a*P*<0.05 vs normal group; ^c*P*<0.05 vs model group.

Table 8 Influence of each group serum on TGFβ1 of HSC at different time points (A value: mean±SD)

	N		M		G		Z		D	
	A	Male cell area (%)	A	Male cell area (%)	A	Male cell area (%)	A	Male cell area (%)	A	Male cell area (%)
24 h	126.56±21.69	5.14±0.69	158.79±27.63	9.67±2.59	98.92±29.25	5.48±0.49	105.69±27.96	6.72±1.74	122.56±67.84	6.21±0.98
48 h	570.78±57.61 ^c	15.78±0.78 ^c	733.58±189.73 ^a	19.39±3.76 ^a	428.71±51.30 ^{ac}	7.36±0.87 ^{ac}	458.08±37.98 ^{ac}	9.87±1.98 ^{ac}	549.35±124.29 ^c	13.27±2.77 ^a
72 h	1 279.30±147.78 ^c	21.98±2.38 ^c	1 509.87±77.50 ^a	27.58±5.65 ^a	609.37±72.85 ^{ac}	9.25±0.67 ^{ac}	823.75±158.49 ^{ac}	12.35±1.75 ^{ac}	971.57±127.83 ^c	19.30±1.36 ^c

N: control group; M: model group; G: high dosage group; Z: medium dosage group; D: low dosage group, ^a*P*<0.05 vs normal group; ^c*P*<0.05 vs model group.

Table 9 Influence of each group serum on PDGF of HSC at different time points (A value: mean±SD)

	N		M		G		Z		D	
	A	Male cell area (%)	A	Male cell area (%)	A	Male cell area (%)	A	Male cell area (%)	A	Male cell area (%)
24 h	326.47±15.31 ^c	7.14±0.69	447.69±25.47 ^a	12.05±3.87	128.87±35.14 ^{ac}	4.21±0.29	187.39±36.67 ^{ac}	7.83±0.67	227.87±54.39 ^c	9.64±0.87
48 h	479.65±38.49 ^c	24.78±5.90 ^c	659.45±76.56 ^a	37.25±4.89 ^c	214.17±54.67 ^{ac}	9.28±0.70 ^{ac}	264.58±49.57 ^{ac}	14.02±2.06 ^{ac}	379.27±75.02 ^c	18.56±3.27 ^{ac}
72 h	805.30±121.04 ^c	32.98±5.49 ^c	1 208.02±132.21 ^a	45.94±5.37 ^c	427.21±39.72 ^{ac}	15.07±2.78 ^{ac}	560.41±132.02 ^{ac}	19.28±2.09 ^{ac}	720.34±102.07 ^c	27.19±3.29 ^{ac}

N: control group; M: model group; G: high dosage group; Z: medium dosage group; D: low dosage group, ^a*P*<0.05 vs normal group; ^c*P*<0.05 vs model group.

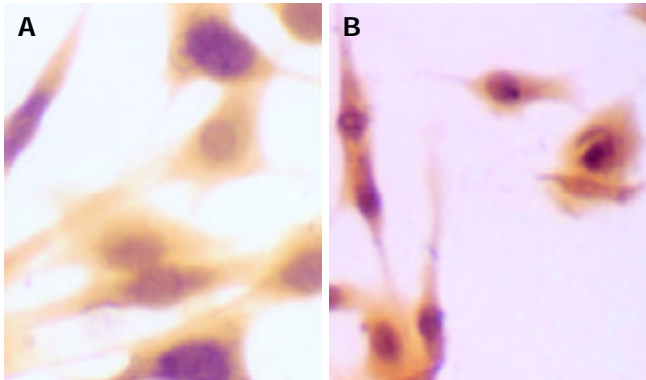


Figure 2 Immunohistochemical staining of synapsin of SD rat HSC line in model group and medium dosage group (×66). A: Immunohistochemical staining of synapsin of SD rat HSC line in model group, B: Immunohistochemical staining of synapsin of SD rat HSC line in medium dosage group.

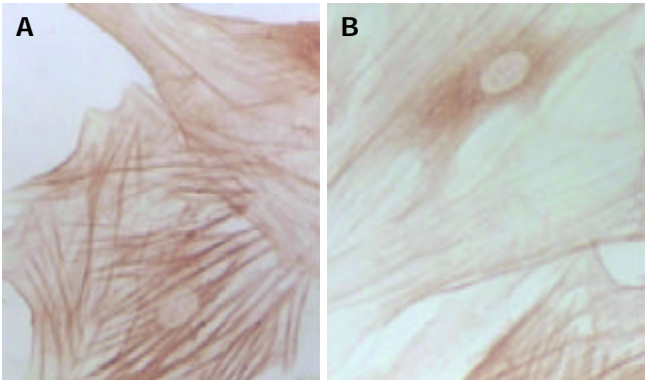


Figure 3 Immunohistochemical staining of type I collagen of SD rat HSC line in model group and medium dosage group (×132). A: Immunohistochemical staining of type I collagen of SD rat HSC line in model group, B: Immunohistochemical staining of type I collagen of SD rat HSC line in medium dosage group.

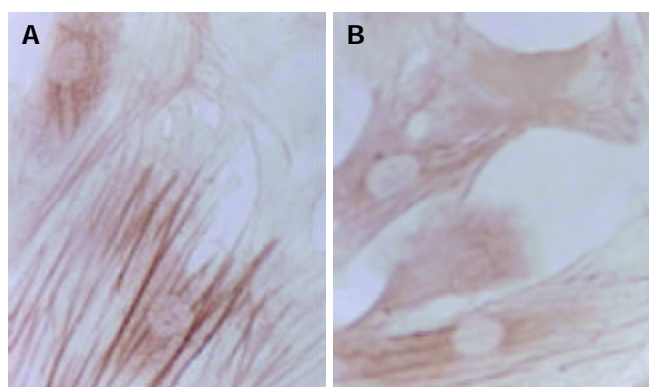


Figure 4 Immunohistochemical staining of type III collagen of SD rat HSC line in model group and medium dosage group ($\times 132$). A: Immunohistochemical staining of type III collagen of SD rat HSC line in model group, B: Immunohistochemical staining of type III collagen of SD rat HSC line in medium dosage group.

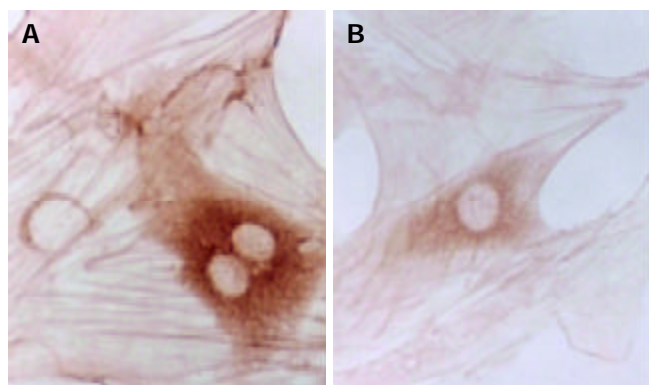


Figure 5 Immunohistochemical staining of TGF- $\beta 1$ of SD rat HSC line in model group and medium dosage group ($\times 132$). A: Immunohistochemical staining of TGF- $\beta 1$ of SD rat HSC line in model group, B: Immunohistochemical staining of TGF- $\beta 1$ of SD rat HSC line in medium dosage group.

Influence of each group serum on TGF β 1 and PDGF of HSC at different time points

The influence of each group serum detected with TN-8502 image analysis system on TGF β 1 and PDGF of HSC at different time points is shown in Tables 8, 9 and Figures 5, 6.

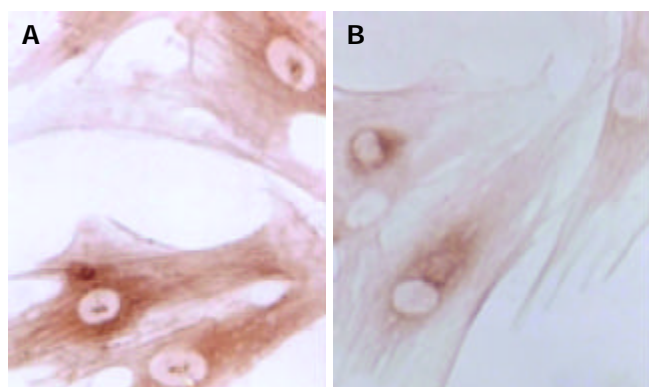


Figure 6 Immunohistochemical staining of PDGF of SD rat HSC line in model group and medium dosage group ($\times 132$). A: Immunohistochemical staining of PDGF of SD rat HSC line in model group, B: Immunohistochemical staining of PDGF of SD rat HSC line in medium dosage group.

DISCUSSION

In past studies about traditional Chinese medicine, the method of adding directly coarse extract of the medicine to environment of cells was adopted in most experiments *in vitro*. Because of the complicated components of traditional Chinese medicine, it could not effectively reflect its pharmacological role. Therefore, we adopted the blood serum pharmacological method in our experiment^[8]. After giving the drug to the animal orally, we took the drug serum as the drug source to add to the response system *in vitro*. This method could not only present the biotransformation *in vivo*, but also overcome confusion of other substances, aiding to make a pharmacokinetic study by finding the effective locus and the activity of components of traditional Chinese medicine. To avoid influence of different species animal sera on cells, animals were adopted in our experiment which were the same species with cultivated HSCs. Considering that the tested object of the drug was cells and the drug with biological reactivity in organism, we gave the drug to the animal orally with an equivalent dosage, to assure the maximum homeostasis concentration of the drug after bioconversion *in vivo*. The results of our experiment indicated that our experiment method was effective, stable and reliable.

A recent investigation has shown that proliferation and activation of HSCs are not only the central link of hepatic fibrosis, but also the cytological background of hepatic fibrosis^[10,11]. Therefore, inhibiting the proliferation and activation of HSC has important significance in prevention and treatment of chronic liver disease and anti-hepatic fibrosis. Cultivated in a non-coating plastic Petri dish, HSC could be automatically activated, thus possessing the biological characteristics of activation *in vivo*, and becoming an ideal anti-hepatic fibrosis cell model^[12]. Just as shown by the results of our experiment, with elongation of cultivating time, HSC showed multi-angle pseudopodium and typical star form. Cell proliferation and collagen synthesis were two important behaviors in activation of HSC. MTT chromatometry methods could be employed to detect cell ability of proliferation, which was based on the principle that succinic dehydrogenase in mitochondria of living cells could make ectogenous MTT recover to non-dissolvable blue and purple crystals and deposit in cells. DMSO could dissolve blue and purple crystals in cells. Adopting enzyme labeled instruments to detect the Absorbency value at some wave-length, the quantity of cells could be reflected indirectly.

The results of our experiment showed that there was no significant difference ($P > 0.05$) between all the groups 24 h after serum was added. It means that adding serum to cultivate for 24 h did not exert any effective influence and HSCs still proliferated at its original rate, suggesting that intervention in proliferation of HSCs needs a time process, which from accepting excitation of cell signal to changing proliferation quantity of HSC, is undoubtedly longer than 24 h. Thus, how to restrain the activation of HSC at earlier time to hold back quick proliferation of HSC, has undoubtedly important significance in prevention and cure of hepatic fibrosis. Our results showed that proliferation of HSC in model group in 48 h and 72 h had a significant difference compared with other groups, indicating that the model group might contain substances which could promote quick proliferation of HSC. The reason may be that after cultivated for 48 h and 72 h, the PDGF of HSC in the model group increased to the effective content, leading to excessive proliferation of HSC. But a 24 h cultivation was not enough for PDGF to increase to the effective content. This could explain our results that there was no significant proliferation of HSC in the model group after 24 h serum culture. The results of our experiment also showed that after cultivated for 48 h and 72 h, there were significant differences among the high, medium and low dosage drug serum groups and the model group ($P < 0.05$),

and between the high and medium dosage drug serum groups and the control group ($P < 0.05$), indicating that different dosage drug sera could inhibit the proliferation of HSC, and had an especially significant effect on the high and medium dosage groups. CBJRGC serum could significantly decrease and inhibit the proliferation of HSC. Its mechanism may be related to the inhibition of self-excretion or para-excretion of PDGF and TGF- β_1 ^[13], thus inhibiting the proliferation of HSC by decreasing the conversion from HSC to α -SMA.

Changes in form and function after HSC is activated could lead to production increase and degradation decrease of ECM, eventually resulting in deposition of hepatic collagens and hepatic fibrosis. Desmin could be regarded as a marker of HSC^[14], and α -SMA as the marker of activation of HSC^[15]. α -SMA is a kind of filament protein which is about 7 nm in diameter and mainly exists in smooth muscle cells as a portion of cytoplasm framework and a functional unit of cell contraction. Under normal conditions, this protein mainly exists in smooth muscle cells and myofibroblasts. There is a very small amount of this protein in HSCs of rats. In the animal model of liver diseases, HSC lost desmin expression and was changed to the expression of α -SMA in its activation process. So, α -SMA could be regarded as the marker of activation of HSC^[16]. In the process of inducing rat hepatic fibrosis by CCl₄^[17], the dynamic change of desmin male cells was a mono-cusp curve, increasing in number in the earlier period, reaching the peak in 12 wk and then gradually decreasing. A foreign study has found that increase of expression of synapsin could be regarded as another marker of activation of HSC^[18]. Our results showed that the dynamic changes in A value of male staining of α -SMA, desmin and synapsin and in the area occupied by α -SMA and synapsin male cells were almost synchronous. The area occupied by desmin male cells showed a tendency to decrease with elongation of cultivating time. This result was consistent with that reported by Li *et al.* that HSC lost the expression of desmin in its activation process^[19], suggesting that in the process of hepatic fibrosis, α -SMA, desmin and synapsin all can be regarded as the markers of activation of HSC, but each has its own characteristics. The expression of desmin in the earlier period of activation was significant, but weakened with elongation of activating time, while the expression of α -SMA and synapsin developed with elongation of activating time. It is estimated that activation and proliferation of HSC can synchronically occur. Our results also showed that after cultivated for 24 h, the expression of α -SMA had no significant difference among all groups, and after cultivated for 48 h, α -SMA male cell area was smaller than that of desmin, indicating that in the period of cultivation for 24 h and 48 h, proliferation was the main form of HSC growth, but with elongation of cultivating time, HSC began to be partly activated and changed to expression of α -SMA. Seventy-two h after cultivation, α -SMA male cell area was bigger than desmin male cell area, the amount of activated HSCs was more than that of silent HSCs and lots of HSCs altered in phenotype, further indicating that the activation of HSC could be synchronically expressed as proliferation and transformation of HSC. The results of our experiment showed that CBJRGC serum could inhibit the expressions of α -SMA, desmin and synapsin in HSC and inhibit the activation of HSC, whose drug effect was closely related to the concentration of drug serum.

Synapsin can be regarded as a new marker of activation of HSC. Its significance is to provide an important theoretic and testing basis for neuroregulation in the process of hepatic fibrosis. So far, no such study has been found in China. Our experiment firstly showed that after cultivated for 24 h, synapsin could express in HSC, and after cultivated for 48 h and 72 h, synapsin could continue to express. Expression of synapsin occurred before it was cultivated for 24 h and continued to

maintain a high level. CBJRGC serum could significantly inhibit expression of synapsin in HSC. Nevertheless, further studies such as the precise time of synapsin expression, the essential significance of the increase in its lasting expression, whether the nervous system involves regulation of stress condition of liver, and whether CBJRGC serum takes part in nervous regulation in hepatic fibrosis, are still needed.

Under normal conditions, liver contains collagen of types I, III, IV, V, and VI. Collagens I and III take the most proportion of collagen, accounting for about 60% of total collagen in liver. When hepatic fibrosis occurred, the proportion of collagens I and III might reach 95% of total collagen in liver^[20]. Thus, in hepatic fibrosis, deposited ECM mainly consists of collagens I and III.

Synthesis of collagen could reflect alternative ability of individual fiber hyperplasia of cells^[21]. Our experiment showed that after cultivated for 24 h, there was no significant difference of collagens I and III among all groups, indicating that within 24 h after acceptance of activating signal, HSC did not yet achieve enough time to excrete collagen. The outcome of our experiment showed that activated time should be longer than 24 h, so that activated HSC and transcription of collagen and cytokine could be altered. In further investigations we should observe and analyze changes in collagen-mRNA in this time process to test whether CBJRGC serum can influence collagen-mRNA. The results also suggested that to inhibit collagen in its transcriptional stage might have important significance in clinical treatment. In our experiment, collagen III began to markedly express after cultivated for 48 h, but collagen I started to markedly express after cultivated for 72 h, showing that expression of collagen III was earlier than that of collagen I, and that in the early time of hepatic fibrosis, collagen III expression took the most part of expression of collagen. Therefore collagen III can be the testing index of earlier hepatic fibrosis. The outcome of our experiment also showed that high and medium dosage groups could significantly inhibit the expression of collagen III in 48 h and 72 h and the expression of collagen I in 72 h. It means CBJRGC serum could play a role in anti-hepatic fibrosis at the earlier time when collagen was significantly expressed. It further suggested that CBJRGC serum could help quickly recover equilibration of synthesis and degradation of ECM in hepatic fibrosis, thus helping to cure hepatic fibrosis. Besides, low dosage group could only significantly inhibit the expression of collagen III in 48 h, but there was no significant difference compared with control group in 72 h. It is estimated that the effect of CBJRGC serum in inhibiting collagen III expression is related to the serum concentration of the drug.

MMP and TIMP mainly take part in regulation of equilibration in synthesis and degradation of collagen^[22]. Among numerous MMPs, MMP1 is the chief MMP, decomposing collagens I and III in liver^[23]. TIMP1 is an inhibiting factor of MMP, which plays its role by irreversibly binding to activated MMP1. Therefore, the imbalance of ratio of MMP/TIMP 1 plays a very important role in hepatic fibrosis. MMP can be inhibited by many specific or non-specific inhibitors, which at present, mainly include TIMP and α_2 -macroglobulin. TIMP 1 is the most important inhibitor of MMP and is negatively correlated to the activity of MMP.

TIMP is a kind of coding protein of multigene family^[24]. It could irreversibly bind to activated MMP and inhibit the degradation of ECM^[25]. So far, there are four kinds of TIMP isolated from tissues and cloned^[26]. TIMP-1 is a kind of 28.5 ku glycoprotein, mainly inhibiting the activity of MMPs-1 and MMP-9. As the specific inhibitor of MMP, TIMP plays a very important role in hepatic fibrosis. TIMP could inhibit MMP, which is the important reason for specific descent of degradation of ECM^[27]. HSC is the main source cell of TIMP and MMP.

The results of our experiment showed that after cultivated for 24 h, there was no significant expression of TIMP in all groups, indicating that HSC did not have enough time to excrete excessive TIMP. The activated time should be longer than 24 h, and within this time, transcription of TIMP of activated HSC might be altered. In further studies, we should observe and analyze the change of TIMP-mRNA within this time, so as to find whether CBJRGC serum can influence TIMP-mRNA. It is also suggested that to inhibit TIMP in transcriptional stage might have important significance in clinical treatment. In this experiment, TIMP of the model group maintained high expression in 48 h and 72 h, indicating that there was some substance to promote high expression of TIMP in the model group. Further study on the precise characteristics of the substance is suggested.

Researches have found that HSC is the key cell in hepatic fibrosis. Under the stimulation of chronic injury and inflammation, HSC can be activated from normal silent behavior to MFB, and meanwhile can secrete and synthesize excessive ECM, forming the foundation of hepatic fibrosis. Previous studies have indicated that activation and phenotype conversion of HSC are closely related to TGF- β 1. TGF- β is a kind of polypeptide molecule of hormone activity, which is produced from kupffer cells by self-excretion and para-excretion and could take part in many pathological and physiological processes^[28]. TGF- β has at least 5 sub-types, but there are only TGF- β 1, TGF- β 2 and TGF- β 3 in human tissue cells. After binding to the recipient on the membrane, TGF- β could phosphorylate and activate its signal transduction molecule (SMAD protein) of intracytoplasmic downstream, which could subsequently enter the nucleus, regulating the transcription of related target gene^[29]. TGF- β 1 exhibits the significant biological activity of TGF- β and is the main cytokine inducing the production of collagen. Through the mechanism of para-excretion and self-excretion, TGF- β 1 could start and maintain the activation of HSC, regulating cell proliferation, accelerating transcription of collagen and proliferation of ECM^[30].

The results of our experiment showed that after cultivated for 24 h, there was no significant expression of TGF- β 1 among all groups. It showed that it was not enough for HSC to secrete TGF- β 1 24 h after it received the activated signal. It is suggested that in further studies we should observe and analyze the change in TGF- β 1-mRNA within this time, so as to find whether CBJRGC serum can influence TGF- β 1-mRNA. Our results also showed that after cultivated for 48 h and 72 h, TGF- β 1 in the model group maintained high expression, suggesting that it could continuously stimulate activated HSC to produce collagen and accelerate hepatic fibrosis. There might be some substance in the model group which could promote high expression of TGF- β 1. Study on the precise characteristics of this substance is still needed. The results also showed that the high and medium dosage groups could markedly inhibit the expression of TGF- β 1 in 48 h and 72 h, but the low dosage group did not obviously inhibit the expression of TGF- β 1 in 48 h and 72 h, suggesting that CBJRGC serum can inhibit the expression of TGF- β 1 and its effectiveness is related to the concentration of the drug serum.

PDGF is a kind of splitting agent and can promote activation and proliferation of HSC. It has been found PI3-K is the important pathway of intramembrane signal transduction^[31]. The outcome of our experiment showed that after cultivated for 24 h, the A value and male cell area of PDGF were not completely consistent. In 24 h, the A value of PDGF in the model group was significantly higher than that in the other groups, but the male cell area did not show any significant difference compared with the other groups. Although PDGF in the model group achieved significant expression, the PDGF might not entirely come from the excretion of HSC and might

include original PDGF existing in the model group. While PDGF bound to PDGF recipient of HSC and accelerated the proliferation of HSC, the absolute proportion of HSC in the situation of excretion of PDGF did not significantly increase. The outcome of our experiment showed that the high, medium and low dosage groups all could obviously inhibit the excretion of PDGF by HSC.

In summary, we suggest that further studies on the mechanism of anti-hepatic fibrosis of CBJRGC serum should focus on mRNA expression of TIMP1, collagens I, III and TGF- β 1 and signal transduction within the cell.

REFERENCES

- 1 **Burt AD.** Pathobiology of hepatic stellate cells. *J Gastroenterol* 1999; **34**: 299-304
- 2 **Cales P.** Apoptosis and liver fibrosis: antifibrotic strategies. *Biomed Pharmacother* 1998; **52**: 259-263
- 3 **Desmouliere A,** Xu G, Costa AM, Yousef IM, Gabbiani G, Tuchweber B. Effect of pentoxifylline on early proliferation and phenotypic modulation of fibrogenic cells in two rat models of liver fibrosis and on cultured hepatic stellate cells. *J Hepatol* 1999; **30**: 621-631
- 4 **Liu X,** Zhang Z, Yang L, Chen D, Wang Y. Inhibition of the activation and collagen production of cultured rat hepatic stellate cells by antisense oligonucleotides against transforming growth factor-beta 1 is enhanced by cationic liposome delivery. *Huaxi Yikedaxue Xuebao* 2000; **31**: 133-135
- 5 **Yu WP,** Brenner S, Venkatesh B. Duplication, degeneration and subfunctionalization of the nested synapsin-Timp genes in Fugu. *Trends Genet* 2003; **19**: 180-183
- 6 **Yoshiji H,** Kuriyama S, Yoshii J, Ikenaka Y, Noguchi R, Nakatani T, Tsujinoue H, Yanase K, Namisaki T, Imazu H, Fukui H. Tissue inhibitor of metalloproteinases-1 attenuates spontaneous liver fibrosis resolution in the transgenic mouse. *Hepatology* 2002; **36**: 850-860
- 7 **Tsukamoto H.** Cytokine regulation of hepatic stellate cells in liver fibrosis. *Alcohol Clin Exp Res* 1999; **23**: 911-916
- 8 **Liu C,** Liu P, Liu CH, Zhu XQ, Ji G. Effects of Fuzhenghuayu decoction on collagen synthesis of cultured hepatic stellate cells, hepatocytes and fibroblasts in rats. *World J Gastroenterol* 1998; **4**: 548-549
- 9 **Hernandez-Munoz R,** Diaz-Munoz M, Suarez-Cuenca JA, Trejo-Solis C, Lopez V, Sanchez-Sevilla L, Yanez L, De Sanchez VC. Adenosine reverses a preestablished CC14-induced micronodular cirrhosis through enhancing collagenolytic activity and stimulating hepatocyte cell proliferation in rats. *Hepatology* 2001; **34**: 677-687
- 10 **Woo SW,** Nan JX, Lee SH, Park EJ, Zhao YZ, Sohn DH. Aloe emodin suppresses myofibroblastic differentiation of rat hepatic stellate cells in primary culture. *Pharmacol Toxicol* 2002; **90**: 193-198
- 11 **Suzuki C,** Kayano K, Uchida K, Sakaida I, Okita K. Characteristics of the cell proliferation profile of activated rat hepatic stellate cells *in vitro* in contrast to their fibrogenesis activity. *J Gastroenterol* 2001; **36**: 322-329
- 12 **Levy MT,** McCaughan GW, Marinos G, Gorrell MD. Intrahepatic expression of the hepatic stellate cell marker fibroblast activation protein correlates with the degree of fibrosis in hepatitis C virus infection. *Liver* 2002; **22**: 93-101
- 13 **Yuan N,** Wang P, Wang X, Wang Z. Expression and significance of platelet derived growth factor and its receptor in liver tissues of patients with liver fibrosis. *Zhonghua Ganzhangbing Zazhi* 2002; **10**: 58-60
- 14 **Nitou M,** Ishikawa K, Shiojiri N. Immunohistochemical analysis of development of desmin-positive hepatic stellate cells in mouse liver. *J Anat* 2000; **197**(Pt 4): 635-646
- 15 **Guma FCR,** Mello TG, Mermelstein CS, Fortuna VA, Wofchuk ST, Gottfried C, Guaragna RM, Costa ML, Borojevic R. Intermediate filaments modulation in an *in vitro* model of the hepatic stellate cell activation or conversion into the lipocyte phenotype. *Biochem Cell Biol* 2001; **79**: 409-417
- 16 **Buniatian GH,** Gebhardt R, Mecke D, Traub P, Wiesinger H.

- Common myofibroblastic features of newborn rat astrocytes and cirrhotic rat liver stellate cells in early cultures and *in vivo*. *Neurochem Int* 1999; **35**: 317-327
- 17 **Zhou X**, Zhang Y, Zhang J, Zhu H, Zhou X, Du W, Zhang X, Chen Q. Expression of fibronectin receptor, integrin alpha 5 beta 1 of hepatic stellate cells in rat liver fibrosis. *Chin Med J* 2000; **113**: 272-276
- 18 **Cheetham JJ**, Hilfiker S, Benfenati F, Weber T, Greengard P, Czernik AJ. Identification of synapsin I peptides that insert into lipid membranes. *Biochem J* 2001; **354**: 57-66
- 19 **Li H**, Zhang J, Huang G, Zhang N, Chen Q, Zhang X. Effect of retinoid kappa receptor alpha (RXRalpha) transfection on the proliferation and phenotype of rat hepatic stellate cells *in vitro*. *Chin Med J* 2002; **115**: 928-932
- 20 **Zhang Q**, Wang J, Hu M. Effects of interferon-alpha on the mRNA expression of procollagen type I and III of hepatic stellate cells and on the deposition of collagen type I and III in fibrotic liver of rats. *Zhonghua Yixue Zazhi* 1999; **79**: 695-698
- 21 **Liu WB**, Yang CQ, Jiang W, Wang YQ, Guo JS, He BM, Wang JY. Inhibition on the production of collagen type I, III of activated hepatic stellate cells by antisense TIMP-1 recombinant plasmid. *World J Gastroenterol* 2003; **9**: 316-319
- 22 **Murphy FR**, Issa R, Zhou X, Ratnarajah S, Nagase H, Arthur MJ, Benyon C, Iredale JP. Inhibition of apoptosis of activated hepatic stellate cells by tissue inhibitor of metalloproteinase-1 is mediated via effects on matrix metalloproteinase inhibition: implications for reversibility of liver fibrosis. *J Biol Chem* 2002; **277**: 11069-11076
- 23 **Iredale JP**. Hepatic stellate cell behavior during resolution of liver injury. *Semin Liver Dis* 2001; **21**: 427-436
- 24 **Yoshiji H**, Kuriyama S, Miyamoto Y, Thorgeirsson UP, Gomez DE, Kawata M, Yoshii J, Ikenaka Y, Noguchi R, Tsujinoue H, Nakatani T, Thorgeirsson SS, Fukui H. Tissue inhibitor of metalloproteinases-1 promotes liver fibrosis development in a transgenic mouse model. *Hepatology* 2000; **32**: 1248-1254
- 25 **Yang C**, Zeisberg M, Mosterman B, Sudhakar A, Yerramalla U, Holthaus K, Xu L, Eng F, Afdhal N, Kalluri R. Liver fibrosis: insights into migration of hepatic stellate cells in response to extracellular matrix and growth factors. *Gastroenterology* 2003; **124**: 147-159
- 26 **Bennett RG**, Kharbanda KK, Tuma DJ. Inhibition of markers of hepatic stellate cell activation by the hormone relaxin. *Biochem Pharmacol* 2003; **66**: 867-874
- 27 **Lichtinghagen R**, Michels D, Haberkorn CI, Arndt B, Bahr M, Flemming P, Manns MP, Boeker KH. Matrix metalloproteinase (MMP)-2, MMP-7, and tissue inhibitor of metalloproteinase-1 are closely related to the fibroproliferative process in the liver during chronic hepatitis C. *J Hepatol* 2001; **34**: 239-247
- 28 **Bissell DM**. Chronic liver injury, TGF-beta, and cancer. *Exp Mol Med* 2001; **33**: 179-190
- 29 **Okuno M**, Akita K, Moriwaki H, Kawada N, Ikeda K, Kaneda K, Suzuki Y, Kojima S. Prevention of rat hepatic fibrosis by the protease inhibitor, camostat mesilate, via reduced generation of active TGF-beta. *Gastroenterology* 2001; **120**: 1784-1800
- 30 **Arias M**, Lahme B, Van de Leur E, Gressner AM, Weiskirchen R. Adenoviral delivery of an antisense RNA complementary to the 3' coding sequence of transforming growth factor-beta1 inhibits fibrogenic activities of hepatic stellate cells. *Cell Growth Differ* 2002; **13**: 265-273
- 31 **Kinnman N**, Francoz C, Barbu V, Wendum D, Rey C, Hultcrantz R, Poupon R, Housset C. The myofibroblastic conversion of peribiliary fibrogenic cells distinct from hepatic stellate cells is stimulated by platelet-derived growth factor during liver fibrogenesis. *Laboratory Invest* 2003; **83**: 163-173

Edited by Wang XL and Zhang JZ Proofread by Xu FM

Synthesis of ribozyme against vascular endothelial growth factor₁₆₅ and its biological activity *in vitro*

Zhong-Ping Gu, Yun-Jie Wang, Yu Wu, Jin-Ge Li, Nong-An Chen

Zhong-Ping Gu, Yun-Jie Wang, Yu Wu, Department of Thoracic Surgery, Tangdu Hospital, Fourth Military Medical University, Xi'an 710038, Shaanxi Province, China

Jin-Ge Li, Department of Infectious Disease, Tangdu Hospital, Fourth Military Medical University, Xi'an 710038, Shaanxi Province, China

Nong-An Chen, Shanghai Institute of Biochemistry, Academia Sinica, Shanghai 20020, China

Correspondence to: Dr. Zhong-ping Gu, Department of Thoracic Surgery, Tangdu Hospital, Fourth Military Medical University, Xi'an 710038, Shaanxi Province, China. zhongpg@xaonline.com.cn

Telephone: +86-29-3541718

Received: 2003-12-10 **Accepted:** 2004-02-01

Abstract

AIM: To investigate the designation, synthesis and biological activity of against vascular endothelial growth factor₁₆₅ (VEGF₁₆₅) ribozyme.

METHODS: The ribozyme against VEGF₁₆₅ was designed with computer. The transcriptional vector was constructed which included the anti-VEGF₁₆₅ ribozyme and 5', 3' self-splicing ribozymes. The hammerhead ribozyme and substrate VEGF₁₆₅ mRNA were synthesized through transcription *in vitro*. The cleavage activity of the ribozyme on target RNA was observed in a cell-free system.

RESULTS: The anti-VEGF₁₆₅ ribozyme was released properly from the transcription of pGEMRz212 cleaved by 5' and 3' self-splicing ribozymes which retained its catalytic activity, and the cleavage efficiency of ribozyme reached 90.7%.

CONCLUSION: The anti-VEGF₁₆₅ ribozyme designed with computer can cleave VEGF₁₆₅ mRNA effectively.

Gu ZP, Wang YJ, Wu Y, Li JG, Chen NA. Synthesis of ribozyme against vascular endothelial growth factor₁₆₅ and its biological activity *in vitro*. *World J Gastroenterol* 2004; 10(10): 1495-1498

<http://www.wjgnet.com/1007-9327/10/1495.asp>

INTRODUCTION

Ribozyme (Rz) is one kind of RNA with site-specific ligation and cleavage activities. Being sequence-specific binding and cleaving specific RNA of ribozyme, the target gene expression can be destructed by an artificially designed and synthesized ribozyme^[1-5]. A great attention has been attracted into the field of gene therapy for cancers with the hammerhead ribozyme, by the virtue of its simple structure, small molecule, easy designation, site-specific mRNA cleavage activity, and catalytic potential^[6-13]. Many studies have showed that the growth, metastasis and prognosis of solid tumors critically related to the angiogenesis. Tumor angiogenesis is a complex process. Among all of the known factors of tumor angiogenesis, vascular endothelial growth factor (VEGF) is a vascular endothelial cell-specific mitogen and the most important and direct one that can stimulate

tumor angiogenesis. VEGF₁₆₅ is the most effective angiogenic factor in the VEGF family^[14-22]. Conversely, inhibition of VEGF expression and tumor angiogenesis to inhibit tumor growth and metastasis become a new hot spot of tumor treatment^[23-34]. In this study, the ribozyme against VEGF₁₆₅ site 212 was designed with computer, the transcriptional vector including the anti-VEGF₁₆₅ ribozyme and self-splicing ribozymes were synthesized and constructed, and the cleavage effect of the ribozyme on target mRNA in cell-free system was observed.

MATERIALS AND METHODS

Vectors

The vector pGEM-3zf(+)VEGF (carrying full length amino acids cDNA of VEGF₁₆₅) was kindly provided by Dr. Abraham (Columbia University, USA). Vector pGEMRzHBV and bacterium JM 109 were gift from Dr. Li (Department of Infectious Disease, Tangdu Hospital, Fourth Military Medical University, China).

Ribozyme design

The cleavage sites of ribozyme anti-VEGF₁₆₅ were designed by computer analysis of the secondary structure of VEGF₁₆₅ mRNA with a computer program (Chen Nong-an, Shanghai Institute of Biochemistry, Academia Sinica). According to Symon's hammerhead ribozyme structural model, the sequences of the cleavage active core of ribozyme and the flanking sequences around the cleavage sites were designed.

Ribozyme synthesis

The hammerhead ribozyme was synthesized by 35 amplification cycles of PCR (TakaRa Biotechnology Co. Ltd. Dalian, China) with the following primer: 5' TGAAGATGCTGATGAGTCCGT GAGGACGAAACTCGAT 3' and purified by electrophoresis on a 100 g/L denaturing polyacrylamide gel.

Plasmid construction

In the down stream of T7 promoter, plasmid pGEMRzHBV included 5' cis-self-splicing ribozyme, RzHBV and 3' cis-self-splicing ribozyme in order. The pGEMRzHBV was digested with *Xba* I and *Aat* II, then the linear vector was purified by 10 g/L agarose gel electrophoresis by using plasmid purification kit (Gibco, USA) according to the manufacturer's instruction. The two complementary strands of designed ribozyme gene cDNA ends were prepared by adding linkers to create sticky ends (*Xba* I and *Aat* II). The double-stranded DNA was then subcloned into the multicloning site (at *Xba* I and *Aat* II) of pGEM by using T4 DNA ligase (Promega, USA) to create the self-splicing transcriptional plasmid pGEMRz212 (Figure 1). After being transformed competent JM109 cells with pGEMRz212 and blue-white screening, the plasmids were extracted from the positive colonies. The sequences of the VEGF₁₆₅ ribozyme and self-splicing ribozymes were confirmed by restriction enzyme and DNA sequencing.

Ribozyme transcription and cleavage activity *in vitro*

The pGEM-3zf(+)VEGF was cut by *Eco*R I, and pGEMRz212 by *Xba* I and *Aat* II. The ribozyme and substrate RNAs were

prepared from the cDNA templates with T7 RNA polymerase (Gibco-BRL, USA) with [α - 32 P]UTP (Yahui Co., Beijing) by *in vitro* transcription. Both the ribozyme and substrate mRNA were synthesized by using T7 *in vitro* transcriptional kit (Gibco-BRL, USA). Equal amounts of ribozyme and substrate were mixed in 10 μ L of reaction buffer (10 mmol/L MgCl₂ and pH 7.6, 75 mmol/L Tris-HCl) at 95 °C for one minute and cooled in ice immediately. The mixture was then reacted at 37 °C for 2 h. The reaction was quenched with EDTA. The cleavage products were detected by autoradiography after 60 g/L denaturing polyacrylamide gel electrophoresis.

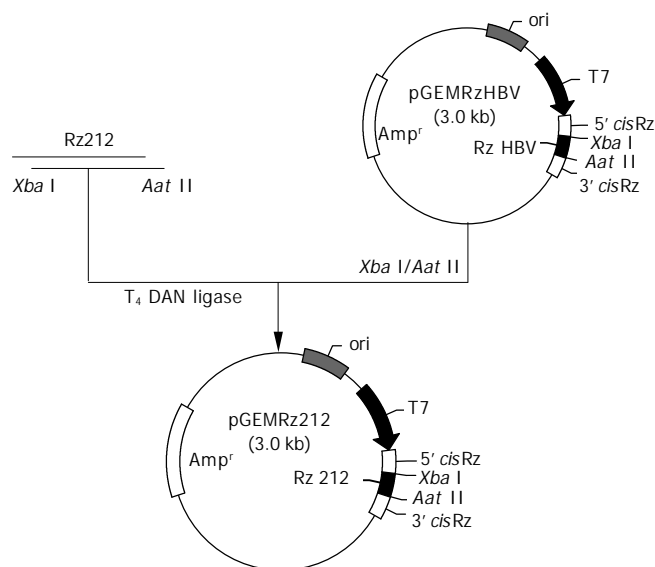


Figure 1 Diagram of construction of the vector pGEMRz212.

RESULTS

Ribozyme designation with computer

The topography of the substrate RNA could be simulated by analyzing the cleavage site and the region surrounding the cleavage site by using a RAN secondary structure folding program. In this way, it might be possible to determine whether or not the target site is buried within an obvious thermodynamically stable region of secondary structure. Among the VEGF₁₆₅ mRNA, there were four hammerhead ribozyme cleavage sites. The site 212 was selected as the optimal cleavage site due to its in single chain region of substrate RNA secondary structure and its both binding arms forming a loop structure to expose for ribozyme cleavage interaction as well as site 212 creating the ribozyme essential core (Figure 2). We called the ribozyme RZ212.

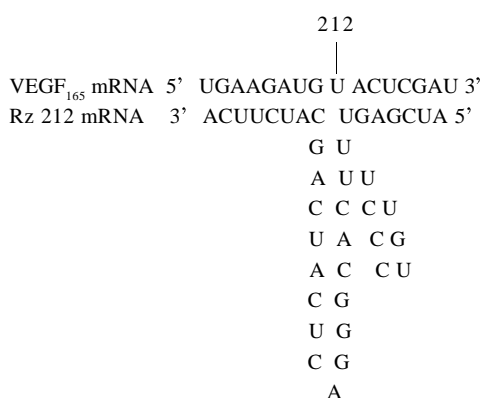


Figure 2 Sequencing of the RZ212 and the target mRNA of VEGF₁₆₅.

Synthesis and transcription RZ212

The synthesized ribozyme was confirmed by restriction enzyme and sequencing analysis. The ribozyme molecule was transcribed *in vitro*. Autoradiography showed three fragments after electrophoresis. The fragments were 5' *cis* ribozyme (64 nt), 3' *cis* ribozyme (54 nt) and RZ212 (47 nt), respectively (Figure 3). The results indicated synthesized ribozyme presenting self-cleavage and releasing the desired ribozyme.

Cleavage activity of RZ212

The cleavage reaction was carried out *in vitro* in a cell-free system. RZ212 cleaved the substrate VEGF₁₆₅ mRNA into 2 fragments (259 nt and 380 nt) (Figure 4) consistent with anticipation. After being cleaved by ribozyme, the density was analyzed by using laser density scanner and the substrate residue was just about 9.3%, indicating that the substrate was nearly cleaved completely by ribozyme.

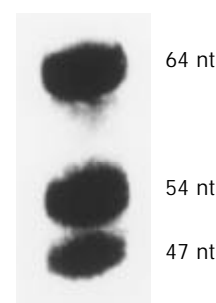


Figure 3 Transcription of pGEMRz212.

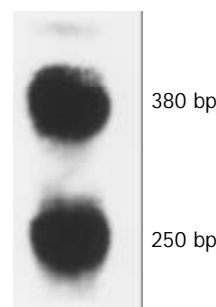


Figure 4 Cleavage activity of VEGF₁₆₅ mRNA with RZ212.

DISCUSSION

The cleavage site and both binding arms must be considered attentively while designing ribozyme. First of all, the cleavage site should be in the important functional region of the target gene assuring the corresponding protein function lost after being cleaved. In addition, the flanking sequences around the cleavage site should be as conserved as possible so that the ribozyme cleavage spectrum become broader. The ribozyme arms sequence context can also influence cleavage rate significantly. In a simple term, the longer the binding arms, the lower the turnover in cleavage of short substrate^[35]. Results from various studies have indicated that ribozyme activity is closely related to the arms length and this depends somewhat on the sequence context^[36,37]. The ribozyme design program we used was approved and improved continuously by experiments. It can resolve the cleavage site design and the sequence surrounding the cleavage site as well as the predicting of ribozyme secondary structure. In this study, we designed successfully the ribozyme target VEGF₁₆₅ mRNA site 212 using the program, synthesized RZ212 and constructed self-cleavage plasmid pGEMRz212. *In vitro* transcription and cleavage

experiment showed that the designed ribozyme was released and cut the target mRNA into two fragments.

Practically, ribozyme gene was constructed in the transcriptional and eukaryotic vector. The ribozyme molecule was transcribed in cells. But there are some long additional sequence in the both arms of ribozyme. The long additional sequence has a strong secondary structure and influenced ribozyme catalytic core, resulted in forming the incorrect secondary structure, even blocking ribozyme binding site. The long additional sequence also influenced ribozyme dissociation from the cleaved target mRNA and reduced cleavage rate^[38,39]. In order to cleave the long additional sequence, we designed and constructed the trimming plasmid pGEMRz212, which included 5' *cis*-self-splicing ribozyme, Rz212 and 3' *cis*-self-splicing ribozyme in order. The long additional sequence was cleaved while pGEMRz212 transcription *in vitro* and VEGF₁₆₅ mRNA specific ribozyme released without long additional sequence. The result showed 5' and 3' *cis* ribozyme neither cleaved the substrate and nor influenced Rz212 cleavage efficacy.

Compared with antisense RNA, ribozyme can not only block target mRNA but also cleave the target mRNA in a sequence-specific manner. Ribozyme has received much attention for their potential use due to their inherent simplicity, relatively small size, repetition use and the ability to be incorporated into a variety of flanking sequence motifs without changing site-specific cleavage capacities^[40-42]. In this experiment, the cleavage efficacy of ribozyme we designed and synthesized reached up to 90.7%. It can suppress effectively the expression of substrate. This research may facilitate the development of ribozyme anti-angiogenesis gene therapy for the treatment in the tumors. Further studies are required for therapeutic application of anti-angiogenesis in human cancer.

REFERENCES

- Doherty EA**, Doudna JA. Ribozyme structures and mechanisms. *Annu Rev Biophys Biomol Struct* 2001; **30**: 457-475
- Takagi Y**, Warashina M, Stec WJ, Yoshinari K, Taira K. Recent advances in the elucidation of the mechanisms of action of ribozymes. *Nucleic Acids Res* 2001; **29**: 1815-1834
- Aigner A**, Renneberg H, Bojunga J, Apel J, Nelson PS, Czubayko F. Ribozyme-targeting of a secreted FGF-binding protein (FGF-BP) inhibits proliferation of prostate cancer cells *in vitro* and *in vivo*. *Oncogene* 2002; **21**: 5733-5742
- Li JG**, Lian JQ, Jia ZS, Feng ZH, Nie QH, Wang JP, Huang CX, Bai XF. Effect of ribozymes on inhibiting expression of HBV mRNA in HepG2 cells. *Shijie Huaren Xiaohua Zazhi* 2003; **11**: 161-164
- Tekur S**, Ho SM. Ribozyme-mediated downregulation of human metallothionein II(a) induces apoptosis in human prostate and ovarian cancer cell lines. *Mol Carcinog* 2002; **33**: 44-55
- Lin JS**, Song YH, Kong XJ, Li B, Liu NZ, Wu XL, Jin YX. Preparation and identification of anti-transforming growth factor beta1 U1 small nuclear RNA chimeric ribozyme *in vitro*. *World J Gastroenterol* 2003; **9**: 572-577
- Zheng Y**, Zhang J, Qu L. Effects of anti-HPV16E6-ribozyme on phenotype and gene expression of a cervical cancer cell line. *Chin Med J* 2002; **115**: 1501-1506
- Jia ZS**, Chen L, Hao CQ, Feng ZH, Li JG, Wang JP, Cao YZ, Zhou YX. Intracellular immunization by hammerhead ribozyme against HCV. *Shijie Huaren Xiaohua Zazhi* 2003; **11**: 148-150
- Castanotto D**, Li JR, Michienzi A, Langlois MA, Lee NS, Puymirat J, Rossi JJ. Intracellular ribozyme applications. *Biochem Soc Trans* 2002; **30**(Pt 6): 1140-1145
- Liu XJ**, Wu QM, Liu CZ, Yu JP, Wang Q. Construction and assessment of eukaryotic expression plasmid pBBS212Rz containing ribozyme gene against hTR. *Shijie Huaren Xiaohua Zazhi* 2002; **10**: 1261-1263
- Tong Q**, Zhao J, Chen Z, Zeng F, Lu G. Effects of blocking androgen receptor expression with specific hammerhead ribozyme on *in vitro* growth of prostate cancer cell line. *Chin Med J* 2003; **116**: 1515-1518
- Goodchild J**. Hammerhead ribozymes for target validation. *Expert Opin Ther Targets* 2002; **6**: 235-247
- Goodchild J**. Hammerhead ribozymes: biochemical and chemical considerations. *Curr Opin Mol Ther* 2000; **2**: 272-281
- Carmeliet P**. Angiogenesis in health and disease. *Nat Med* 2003; **9**: 653-660
- Gu ZP**, Wang YJ, Li JG, Zhou YA. VEGF₁₆₅ antisense RNA suppresses oncogenic properties of human esophageal squamous cell carcinoma. *World J Gastroenterol* 2002; **8**: 44-48
- Hughes GC**, Biswas SS, Yin B, Coleman RE, DeGrado TR, Landolfo CK, Lowe JE, Annex BH, Landolfo KP. Therapeutic angiogenesis in chronically ischemic porcine myocardium: comparative effects of bFGF and VEGF. *Ann Thorac Surg* 2004; **77**: 812-818
- Fernandez M**, Vizzutti F, Garcia-Pagan JC, Rodes J, Bosch J. Anti-VEGF receptor-2 monoclonal antibody prevents portal-systemic collateral vessel formation in portal hypertensive mice. *Gastroenterology* 2004; **126**: 886-894
- Willett CG**, Boucher Y, di Tomaso E, Duda DG, Munn LL, Tong RT, Chung DC, Sahani DV, Kalva SP, Kozin SV, Mino M, Cohen KS, Scadden DT, Hartford AC, Fischman AJ, Clark JW, Ryan DP, Zhu AX, Blaszkowsky LS, Chen HX, Shellito PC, Lauwers GY, Jain RK. Direct evidence that the VEGF-specific antibody bevacizumab has antivascular effects in human rectal cancer. *Nat Med* 2004; **10**: 145-147
- Fondevila C**, Metges JP, Fuster J, Grau JJ, Palacin A, Castells A, Volant A, Pera M. p53 and VEGF expression are independent predictors of tumour recurrence and survival following curative resection of gastric cancer. *Br J Cancer* 2004; **90**: 206-215
- Van Trappen PO**, Steele D, Lowe DG, Baithun S, Beasley N, Thiele W, Weich H, Krishnan J, Shepherd JH, Pepper MS, Jackson DG, Sleeman JP, Jacobs IJ. Expression of vascular endothelial growth factor (VEGF)-C and VEGF-D, and their receptor VEGFR-3, during different stages of cervical carcinogenesis. *J Pathol* 2003; **201**: 544-554
- Buchler P**, Reber HA, Ullrich A, Shiroiki M, Roth M, Buchler MW, Lavey RS, Friess H, Hines OJ. Pancreatic cancer growth is inhibited by blockade of VEGF-RII. *Surgery* 2003; **134**: 772-782
- Belotti D**, Paganoni P, Manenti L, Garofalo A, Marchini S, Tarabozetti G, Giavazzi R. Matrix metalloproteinases (MMP9 and MMP2) induce the release of vascular endothelial growth factor (VEGF) by ovarian carcinoma cells: implications for ascites formation. *Cancer Res* 2003; **63**: 5224-5229
- Li Q**, Dong X, Gu W, Qiu X, Wang E. Clinical significance of co-expression of VEGF-C and VEGFR-3 in non-small cell lung cancer. *Chin Med J* 2003; **116**: 727-730
- Qi JH**, Ebrahim Q, Moore N, Murphy G, Claesson-Welsh L, Bond M, Baker A, Anand-Apte B. A novel function for tissue inhibitor of metalloproteinases-3 (TIMP3): inhibition of angiogenesis by blockage of VEGF binding to VEGF receptor-2. *Nat Med* 2003; **9**: 407-415
- LeCouter J**, Lin R, Ferrara N. Endocrine gland-derived VEGF and the emerging hypothesis of organ-specific regulation of angiogenesis. *Nat Med* 2002; **8**: 913-917
- Riedel F**, Gotte K, Li M, Hormann K, Grandis JR. Abrogation of VEGF expression in human head and neck squamous cell carcinoma decreases angiogenic activity *in vitro* and *in vivo*. *Int J Oncol* 2003; **23**: 577-583
- Ferrara N**. Role of vascular endothelial growth factor in physiologic and pathologic angiogenesis: therapeutic implications. *Semin Oncol* 2002; **29**(6 Suppl 16): 10-14
- Bikfalvi A**, Bicknell R. Recent advances in angiogenesis, anti-angiogenesis and vascular targeting. *Trends Pharmacol Sci* 2002; **23**: 576-582
- Dvorak HF**. Vascular permeability factor/vascular endothelial growth factor: a critical cytokine in tumor angiogenesis and a potential target for diagnosis and therapy. *J Clin Oncol* 2002; **20**: 4368-4380
- Ferrara N**. VEGF and the quest for tumour angiogenesis factors. *Nat Rev Cancer* 2002; **2**: 795-803
- Hasan J**, Byers R, Jayson GC. Intra-tumoural microvessel den-

- sity in human solid tumours. *Br J Cancer* 2002; **86**: 1566-1577
- 32 **Chiarug V**, Ruggiero M, Magnelli L. Angiogenesis and the unique nature of tumor matrix. *Mol Biotechnol* 2002; **21**: 85-90
- 33 **Carmeliet P**, Jain RK. Angiogenesis in cancer and other diseases. *Nature* 2000; **407**: 249-257
- 34 **Yancopoulos GD**, Davis S, Gale NW, Rudge JS, Wiegand SJ, Holash J. Vascular-specific growth factors and blood vessel formation. *Nature* 2000; **407**: 242-248
- 35 **Sun LQ**, Cairns MJ, Saravolac EG, Baker A, Gerlach WL. Catalytic nucleic acids: from lab to applications. *Pharmacol Rev* 2000; **52**: 325-347
- 36 **Takagi Y**, Suyama E, Kawasaki H, Miyagishi M, Taira K. Mechanism of action of hammerhead ribozymes and their applications *in vivo*: rapid identification of functional genes in the post-genome era by novel hybrid ribozyme libraries. *Biochem Soc Trans* 2002; **30**(Pt 6): 1145-1149
- 37 **Blount KF**, Uhlenbeck OC. The hammerhead ribozyme. *Biochem Soc Trans* 2002; **30**(Pt 6): 1119-1122
- 38 **Amarzguioui M**, Prydz H. Hammerhead ribozyme design and application. *Cell Mol Life Sci* 1998; **54**: 1175-1202
- 39 **Pennati M**, Binda M, Colella G, Zoppe' M, Folini M, Vignati S, Valentini A, Citti L, De Cesare M, Pratesi G, Giacca M, Daidone MG, Zaffaroni N. Ribozyme-mediated inhibition of survivin expression increases spontaneous and drug-induced apoptosis and decreases the tumorigenic potential of human prostate cancer cells. *Oncogene* 2004; **23**: 386-394
- 40 **Weng DE**, Usman N. Angiozyme: a novel angiogenesis inhibitor. *Curr Oncol Rep* 2001; **3**: 141-146
- 41 **Brattstrom D**, Bergqvist M, Hesselius P, Larsson A, Wagenius G, Brodin O. Serum VEGF and bFGF adds prognostic information in patients with normal platelet counts when sampled before, during and after treatment for locally advanced non-small cell lung cancer. *Lung Cancer* 2004; **43**: 55-62
- 42 **Im SA**, Kim JS, Gomez-Manzano C, Fueyo J, Liu TJ, Cho MS, Seong CM, Lee SN, Hong YK, Yung WK. Inhibition of breast cancer growth *in vivo* by antiangiogenesis gene therapy with adenovirus-mediated antisense-VEGF. *Br J Cancer* 2001; **84**: 1252-1257

Edited by Kumar M Proofread by Xu FM

Auxiliary *en-bloc* liver-small bowel transplantation with partial pancreas preservation in pigs

Zhen-Yu Yin, Xiao-Dong Ni, Feng Jiang, Ning Li, You-Sheng Li, Xiao-Ming Wang, Jie-Shou Li

Zhen-Yu Yin, Xiao-Dong Ni, Feng Jiang, Ning Li, You-Sheng Li, Jie-Shou Li, Research Institute of General Surgery, School of Medicine, Nanjing University, Nanjing 210093, Jiangsu Province, China

Zhen-Yu Yin, Xiao-Ming Wang, Department of General Surgery, Zhongshan Hospital, Xiamen 361004, Fujian Province, China

Correspondence to: Zhen-Yu Yin, Department of General Surgery, Zhongshan Hospital, Xiamen 361004, Fujian Province, China. davidmd@sohu.com

Telephone: +86-592-2292045 **Fax:** +86-592-2212328

Received: 2003-8-30 **Accepted:** 2003-10-07

Abstract

AIM: The aim of this study was to describe an auxiliary combined liver-small bowel transplantation model with the preservation of duodenum, head of pancreas and hepatic biliary system in pigs. The technique, feasibility, security and immunosuppression were commented.

METHODS: Forty outbred long-white pigs were randomized into two groups, and the auxiliary composite liver/small bowel allotransplantations were undertaken in 10 long-white pigs in each group with the recipient liver preserved. Group A was not treated with immunosuppressive drugs while group B was treated with cyclosporine A and methylprednisolone after operation. The hemodynamic changes and amylase of body fluid (including blood, urine and abdominal drain) were analyzed.

RESULTS: The average survival time of the animals was 10 ± 1.929 d (6 to 25 d) in group A while more than 30 d in group B. The pigs could tolerate the hemodynamic fluctuation during operation and the hemodynamic parameters recovered to normal 2 h after blood reperfusion. The transient high amylase level was decreased to normal one week after operation and autopsy showed no pancreatitis.

CONCLUSION: Auxiliary *en-bloc* liver-small bowel transplantation with partial pancreas preservation is a feasible and safe model with simplified surgical techniques for composite liver/small bowel transplantation. This model may be used as a preclinical training model for clinical transplantation method, clinical liver-small bowel transplantation related complication research, basic research including immunosuppressive treatment, organ preservation, acute rejection, chronic rejection, immuno-tolerance and xenotransplantation.

Yin ZY, Ni XD, Jiang F, Li N, Li YS, Wang XM, Li JS. Auxiliary *en-bloc* liver-small bowel transplantation with partial pancreas preservation in pigs. *World J Gastroenterol* 2004; 10(10): 1499-1503

<http://www.wjgnet.com/1007-9327/10/1499.asp>

INTRODUCTION

Combined liver and small bowel transplantation (LSBT) is a

life-saving procedure in patients especially in children with intestinal failure and parenteral nutrition-related end-stage liver diseases^[1]. Recently, due to success in clinical technology and improvement of the operative modality, the American Health Care Financing Administration (HCFA) has granted combined liver-intestinal transplantation as the standard therapeutic modality for patients with irreversible intestinal failure^[2]. Patients undergoing composite liver-small bowel transplantation are mostly children. As conventional LSBT requires a loop of defunctionalized (Roux) allograft small bowel for biliary drainage^[3], its posttransplant biliary complications including anastomotic leaks and obstruction in 12% of cases, were significantly related with morbidity and mortality^[4]. In addition, the conventional composite transplantation needs more vascular anastomoses which would lead not only to more complications including vascular thrombosis but also more difficulties of the surgical techniques. In the present study, we described an auxiliary transplantation technique for LSBT by preserving duodenum, partial head of pancreas and hepatobiliary system in pigs. Experience with this technique and the immunosuppressive treatment for LSBT in pig has not been reported in the literature.

MATERIALS AND METHODS

Forty outbred long-white pigs weighing 20 - 40 kg were divided into 2 groups with random sex, and 10 LSBTs were undertaken in each group. The weight of the donor was generally lower than that of the corresponding recipient. Group A was not treated with immunosuppressive drugs while group B was treated by immunosuppressive therapy consisting of cyclosporine A and methylprednisolone after operation.

The animals were not allowed to eat for 24 h and to drink for 4 h before operation respectively. Gut decontamination was attempted in all donors with an oral antibiotic preparation 3 d before surgery.

After anesthesia with 25 mg/kg of intravenous pentobarbital sodium, the animals were intubated and mechanically ventilated with a mixture of oxygen, nitrous oxide and isoflurane. In addition, standard intravenous antibiotic prophylaxis was instituted with cefotaxime at the time of surgery.

Initial exposure and isolation of abdominal organs

The procurement varied in details but followed the standard techniques for human multiorgan retrieval and our previous report^[5-8].

Briefly, the proximal 3 to 4 m of jejunum (the total length of porcine small bowel is about 15 m) together with the liver was procured as the graft. After the redundant small bowel and the dissociative colon were removed from the operative field, the duodenum, proximal jejunum and aorta could be well exposed. An extensive Kocher maneuver allowed visualization of the inferior vena cava and its branch. The subhepatic vena cava was dissected and encircled. The left and right renal veins were ligated respectively. The superior mesenteric and celiac arteries were identified after extending dissection of the aorta. The right and left renal arteries were then isolated and ligated. The subrenal aorta was isolated and encircled distally for the

eventual insertion of an infusion cannula. The abdominal aorta was also encircled above the celiac axis for later crossclamping when cold fluid was infused through the distal aortic cannula^[9]. The splenic vein was then freed and prepared for portal perfusion cannulation after division of the splenic artery. The splenic vein should be well protected when dividing the splenic artery^[10].

In situ cooling and removal of organs

After completion of the preliminary dissection and collection of the donor's blood, the liver and small bowel connected by the portal vein and aortic segment were lavaged *in situ* with UW solution (Figure 1). The donor was fully heparinized and the previously encircled proximal aorta was crossclamped, and the distal donor aorta was cannulated with infusion of cold UW solution. For simultaneous portal venous infusion, a venous cannula was placed into the splenic vein and infused with the UW solution. The intrapericardial inferior vena cava and subhepatic vena cava were transected to decompress the infused solution as in other reports^[11,12]. The amount of infusion was variable (50-100 mL/kg). After infusion, the graft containing liver, hepatic hilus, pancreatic-duodeno complex, spleen together with splenic vein, and small bowel was achieved with preservation of a segment of aorta containing the superior mesenteric artery and celiac trunk in continuity. The intestine was entrapped by stapling its two ends and carried with the specimen throughout the preservation. Thus the graft was *en bloc* removed and stored in UW solution at 0 to 4 °C.

Back table procedure was performed in the cold UW solution. It included suturing the orifice of suprahepatic vena cava and the proximal end of the aorta. The spleen was removed. The body and tail of the pancreas along the portal vein were isolated and transected, leaving partial pancreatic head attached to the allograft duodenum. This preserved the superior and inferior pancreaticoduodenal arcades. The stump of the pancreas was stapled and then oversewn with a running suture using 4-0 polypropylene.

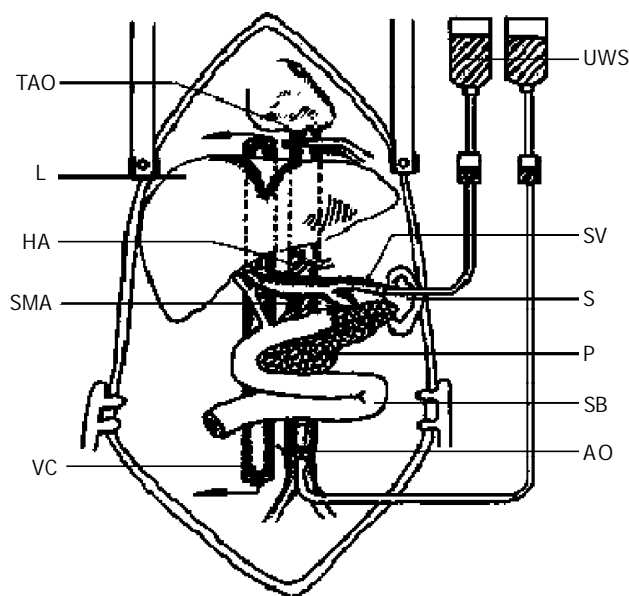


Figure 1 Infusion of grafts, (UWS=UW solution, SV=splenic vein, S=spleen, P=pancreas, SB=small bowel, AO=abdominal aorta, TAO=thoracic aorta, L=liver, HA=hepatic artery, SMA=supermesenteric artery, VC=vena cava).

Recipient operation

After anesthesia, a monitor was placed on the recipient. Two venous catheters (with one Swan-Ganz catheter) were inserted

for transfusion and hemodynamic parameters including central venous pressure (CVP), right ventricle pressure (VP), cardiac output (CO), pulmonary artery wedge pressure (PAWP) at the time of preoperation, the time just before blood reperfusion, 5 min, 30 min, 1 h and 2 h after blood reperfusion. The arterial blood pressure was monitored through a femoral artery catheter. The amylase levels of the blood, urine and abdominal drainage postoperative d 1, 3, 5, 7 were collected (determined by Somogyi method).

When the recipient's abdomen was opened, the dissociative colon and its mesentery were dissected and removed to ensure enough celiac space for the composite graft. Then, the end of the ascending colon and the end of the ileum were anastomosed directly to maintain the gastroenterologic continuity of the recipient.

The subrenal aorta was exposed and encircled 2 cm under the renal artery. Small arterial and lymphatic vessels along the aorta were ligated to avoid later bleeding or lymphorrhea. Subhepatic vena cava was also dissected and encircled. The subrenal vena cava was used for the donor out-flow anastomosis.

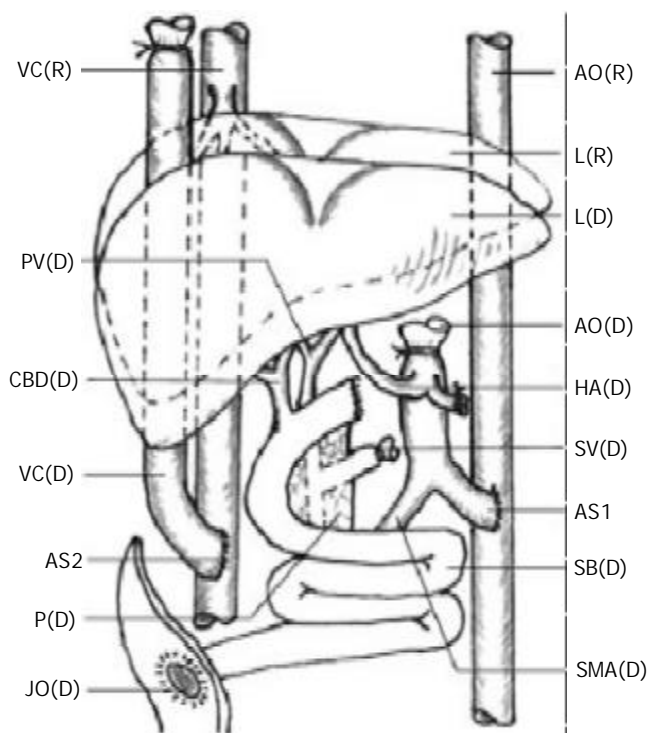


Figure 2 Auxiliary en-bloc liver-small bowel transplantation, (D=donor, R=recipient, AO=aorta, L=liver, HA=hepatic artery, SV= splenic vein, SB=small bowel, SMA=supermesenteric artery, VC= vena cava, PV=portal vein, CBD=common bile duct, P=pancreas, JO=jejunum ostomy, AS1=aorta-aorta anastomosis, AS2=vena cava- vena cava anastomosis).

Graft implantation and revascularization

The transplantation methods varied in details but followed the principles as described previously^[6,8] (Figure 2).

The arterial inflow was created via an end-to-side anastomosis of the graft aorta to the subrenal native aorta with a running polypropylene suture. Donor and recipient vena cava were anastomosed end to side. The venous outflow was the anastomosis of the end of the graft subhepatic vena cava to the side of the native subhepatic vena cava.

Before reperfusion, unclamping and perfusion of the allograft liver were achieved after a lavage of 300 to 500 mL donor blood or Ringer's solution through the splenic vein. The end of the spleen vein was ligated after the lavage.

The proximal duodenum was closed. A jejunostomy was

made at the end of donor distal intestine for early decompression and surveillance endoscopy as described in some clinical reports^[13,14].

After operation, the animals were returned to the monitor room, where hemodynamic monitoring and mechanical ventilation were performed as needed 24 h after operation. Due to the high rate of inflammatory complications, broad-spectrum antibacterial prophylaxis was administered for 5 d. Lactated Ringer's solution and parenteral nutrition were given daily for 2 d after operation.

Immunosuppressive drugs were used in the pigs of group B. Cyclosporine A was started at 15 mg/kg·d by venous injection in the first week, then reduced to 5 mg/kg·d from the second week as maintenance treatment. Methylprednisolone, used for induction and maintenance, was started with 500 mg at the first 24 h postoperation, reduced by 50% to about 2 mg/kg·d for the first week, then reduced by 50% on d 8 and again on day 15.

The survived animals were sacrificed for autopsy 30 d after operation.

RESULTS

After reperfusion, the liver was soft and pink with bile production, evidenced by jejunostomy drainage. If the liver was harder than normal, the outflow of the liver might be obstructed and the vena cava anastomosis needed to be checked. The small bowel should be perfused well, with good mesenteric arterial inflow and venous outflow. The peristalsis and intraluminal mucus production were evident within 15 min after reperfusion.

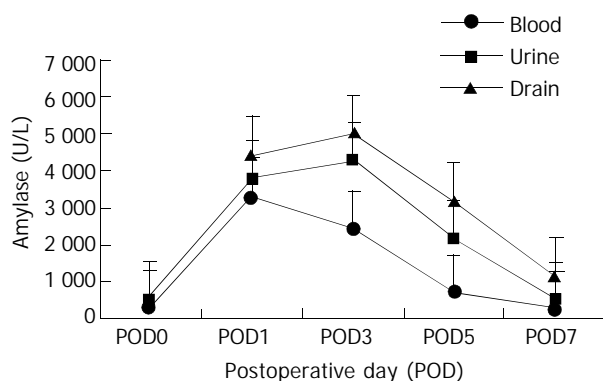


Figure 3 Postoperative amylase changes.

Table 1 Postoperative amylase in body fluid (U/L)

POD	0	1	3	5	7
Blood	329.60±28.31	3 314.70±415.29	2 448.60±413.53	718.70±103.61	327.70±27.58
Urine	514.80±55.67	3 404.80±335.96	4 307.40±429.16	2 187.00±148.43	491.40±48.80
Drain	---	4 444.80±545.67	5 023.80±472.64	3 217.20±213.91	1 177.10±98.12

POD=postoperative day.

Table 2 Hemodynamics changes

Time	N	preRP	RP5	RP30	RP60	RP120
CVP (cmH ₂ O)	14.80±0.42	13.00±0.49	10.20±1.07	9.50±0.27	9.90±0.37	14.00±0.36
VP (cmH ₂ O)	33.70±2.09	31.70±2.64	27.70±1.93	24.60±1.65	27.30±1.71	32.60±1.92
PAWP (cmH ₂ O)	16.70±0.59	13.40±0.40	16.30±0.52	14.10±0.41	15.90±0.46	17.20±0.44
CO (L/min)	4.48±0.15	3.36±0.22	4.27±0.15	3.98±0.15	4.23±0.15	4.59±0.16

CVP=central venous pressure, VP=ventricle pressure, PAWP=pulmonary artery wedge pressure, CO=cardiac output, N=normal, preRP=pre-reperfusion, RP5=5 min after reperfusion, RP30=30 min after reperfusion, RP60=60 min after reperfusion, RP120=120 min after reperfusion.

During the first three days, the intestinal graft stoma appeared healthy, and the mucosa was pink, moist, and well vascularized. No intestinal edema was found in most cases with output of bile-stained stool.

Histopathologic studies of the grafts showed no significant preservation injury. None of the biopsies obtained in the first postoperative week had histological evidence of submucosal bacterial invasion. The frequent cause of death of the pigs in group A was postoperative rejection evidenced by graft pathological examinations when the animal was dead.

Animals died 24 h after reperfusion were ruled out from the statistic series. One pig died because of operative techniques in group A, and all other animals in groups A and B lived for more than 24 h. The average survival time was 10.33±1.929 d (6 to 25 d) in group A while more than 30 d in group B. The difference was significant by Student's *t* test ($P<0.01$).

The hemodynamic changes are shown in Table 1. The results suggested that all hemodynamic parameters including CVP, CO, VP and PAWP were decreased during operation, but recovered very quickly after blood reperfusion, and returned to normal 2 h after blood reperfusion as shown in Figure 3.

Neither the duodenal allografts had signs of ischemia or stump leakage, nor any biliary complication. Blood, urine and abdominal drains were monitored serially for amylase level. Chemical pancreatitis was observed during the early postoperative period with amylase-rich fluid drainage.

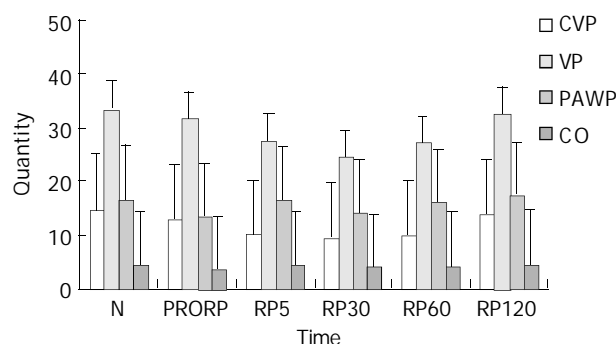


Figure 4 Hemodynamic changes.

The amylases in the body fluid are shown in Table 2. Amylases in blood, urine and abdominal drainage increased promptly after operation and reached their peak in the first three postoperative days. The levels then decreased with time.

and returned to preoperative level after one week as shown in Figure 4. Postoperative biopsy showed no sign of pancreatitis and also autopsy did not show any evidence of severe pancreatitis or calcification. Autopsy of the pigs in group B showed no evidence of graft rejection.

DISCUSSION

Total parenteral nutrition (TPN) for short bowel syndrome would induce end-stage liver diseases. In considering intestinal transplantation for treatment, 60% to 70% them required simultaneous liver allografts^[4,7]. Although many clinical liver/small bowel transplantations (LSBT) were reported from different medical centers^[15-17], it remains an experimental procedure^[18]. Although large animals that share physiological and anatomical similarities with humans, comparing to the widely used rat LSBT model^[19,20], large animal models such as LSBT in pigs and its related research were rarely reported.

Feasibility and benefits of auxiliary composite liver-small bowel transplantation model

As compared to the five anastomoses in conventional composite liver-small bowel transplantation including suprahepatic vena cava anastomosis, subhepatic vena cava anastomosis, hepatic artery anastomosis, portal vein anastomosis and bile duct anastomosis, only two anastomoses including aorta-aorta anastomosis and subhepatic vena cava anastomosis were needed in the auxiliary composite liver-small bowel transplantation model. This model could not only decrease possible complications related to the anastomoses such as bleeding, vascular obstruction, postoperative thromboses and bile leakage, but also simplify the surgical techniques. In this model, the vena cava anastomosis was modified by replacing the major hepatic vein (or suprahepatic vena cava) anastomosis in classical Piggy-back transplantation by the subhepatic vena cava anastomosis. This modification has at least two advantages in porcine LSBT. One is that subhepatic vena cava anastomosis can be easily performed, the other is that subhepatic vena cava anastomosis can adjust a flexible anastomotic interval to ensure the aorta-aorta anastomosis easier.

In clinical practice, Abu-Elmagd suggested that LSBT with preservation of pancreatic head and duodenum had some advantages including avoidance of biliary complications and simplification of the operative procedure^[20]. These possible advantages were also shown in animal LSBT.

The LSBT transplant procedure is a much more arduous surgical endeavor. The technique of retaining duodenum and the head of pancreas would simplify the back table preparation and avoid risks associated with dissection of the donor hepatic hilus.

Retrieval for composite grafts using the standard technique involved an obligatory reconstruction of the biliary system with a defunctionalized loop of proximal allograft jejunum^[3]. In this porcine LSBT model, no biliary reconstruction was required, so that the source of complications such as bile leakage, biliary tract stricture or even death of recipient could be avoided. Liver transplantation related biliary complication rate was about 12%, which would result in about 19% of mortality^[21,22]. LSBT with preservation of partial pancreas and duodenum would remarkably decrease such complications.

The potential benefits of any intestinal segment which was kept in direct continuity with alimentary tract freeing the pig for TPN would be enhanced without donor or recipient bowel for Roux-en-Y biliary reconstruction. The advantage of the composite technique was to maintain the hepatic hilus. The use of liver artery and superior mesenteric artery with a large arterial conduit would minimize the risk of hepatic artery thrombosis compared to isolated graft^[13,23].

Safety of porcine auxiliary LSBT with pancreatic head and duodenum

The porcine retrohepatic vena cava is passing through the liver parenchyma with numerous small hepatic veins in this segment besides the major hepatic veins. It is dangerous to remove the liver parenchyma by dissecting the retrohepatic vena cava with high risk of fetal blood loss. This is the reason why the classic piggyback liver transplantation is not suitable in pig. Typical orthotopic liver transplantation in combined LSBT needs not only blood shunt during operation but also a segment of additional artery to prolong the aorta to ensure the arterial anastomosis in pigs. Auxiliary LSBT could avoid the disadvantages of these transplantations.

In conventional composite liver-small bowel transplantation, blood shunt was always needed in the process of vascular exclusion. In pigs, this was much more important because the blood passing through portal vein was accounted for more than 60% of the total porcine blood. The vascular exclusion would lead to sudden cardiac failure and death of the pigs. Auxiliary composite liver-small bowel transplantation model with partial vascular exclusion during the vascular anastomosis did not lead to irreversible hemodynamic changes that would occur without blood shunt. This method would also avoid other possible hemodynamic damages such as kidney injuries, postoperative thrombosis and ischemia of the lower limb.

Inclusion of duodenum and pancreatic head to maintain continuity of the biliary system was associated with early postoperative allograft pancreatitis, but no significant mortality was reported^[24]. This complication was also found in our study. It could be detected by measuring amylase and lipase in peritoneal fluid from abdominal drains, blood and urine^[25]. In our study, chemical pancreatitis as shown in the experiment was always transient. The elevated amylase level would return to normal within one week and autopsy showed no signs of severe pancreatitis. At present, the following measures could be considered to protect the allografted pancreas from postoperative pancreatitis, namely to limit the amount and pressure of the cold solution used in perfusion^[3], to procure the pancreas *en-bloc* with the graft and avoid over-dissection of the tissue and vessels around duodenum and pancreas^[26], to ligate the pancreatic duct and suture the pancreatic interface efficiently and definitely.

Immunosuppressive treatment of auxiliary LSBT pigs

The optimal immunosuppressive treatment was not determined in big organ transplantations. Triple drugs (cyclosporine or FK506, azathioprine and prednisolone) and quadruple drugs (ATG, cyclosporine or FK506, azathioprine and prednisolone) treatment in pig transplantation were reported in the literature^[27-29]. But the optimal dose of immunosuppressive drugs was ascertained in previous reports. The suggested dose of cyclosporine was from 3 mg/kg·d to 25 mg/kg·d by IV or SB injection^[27,28,30,31]. Some reports indicated that pigs required a higher dose of cyclosporine than humans to prevent allograft rejection in thymus transplantation^[32]. Other authors suggested that immunosuppressive protocols that were successful in preventing allograft rejection in humans had no long-term effect on allografted pigs and the dose of most immunosuppressive agents administered to control rejection in pigs should be higher than that used in humans^[33]. This might be due to differences of absorption, binding, metabolism and excretion of the drugs in pigs. So we used the maintenance dose of CsA 5 mg/kg·d after a loading dose of 15 mg/kg·d, and the composite transplanted liver small bowel graft with preservation of pancreas head could be protected by CsA and methylprednisolone against acute rejection.

Some reports suggested that LSBT with preservation of duodenum and pancreatic head would neither increase the possibility of rejection nor require more immunosuppressive

treatment than standard LSBT without preservation of pancreas and duodenum^[13,23]. The presence of allograft pancreas in multivisceral allografts was not an important risk factor for mortality, and the incidence of rejection of pancreatic was only 12% in some report^[13]. So the technique with preservation of the pancreas should be considered safe in composite LSBT.

In summary, auxiliary en-bloc liver-small bowel transplantation with partial pancreas preservation is a feasible and safe model with simplified surgical techniques for composite liver/small bowel transplantation in pigs. This model might be used as a preclinical training model for clinical transplantation method, clinical liver-small bowel transplantation related complication research, basic research including immunosuppressive treatment, organ preservation, acute rejection, chronic rejection, immuno-tolerance and xenotransplantation research.

REFERENCES

- 1 **Lacaille F**, Canioni D, Fournet JC, Revillon Y, Cezard JP, Goulet O. Centrilobular necrosis in children after combined liver and small bowel transplantation. *Transplantation* 2002; **73**: 252-257
- 2 **Abu-Elmagd K**, Bond G. The current status and future outlook of intestinal transplantation. *Minerva Chir* 2002; **57**: 543-560
- 3 **Furukawa H**, K Abu-Elmagd K, Reyes JL. Technical aspects of intestinal transplantation, in: Braverman MH, Tawas RL, (eds): Surgical Technology International II, San Francisco CA. *TF Laszlo* 1994: 165-170
- 4 **Reyes J**, Bueno J, Kocoshis S, Green M, Abu-Elmagd K, Furukawa H, Barksdale EM, Strom S, Fung JJ, Todo S, Irish W, Starzl TE. Current status of intestinal transplantation in children. *J Pediatr Surg* 1998; **33**: 243-254
- 5 **Starzl TE**, Todo S, Tzakis A, Alessiani M, Casavilla A, Abu-Elmagd K, Fung JJ. The many faces of multivisceral transplantation. *Surg Gynecol Obstet* 1991; **172**: 335-344
- 6 **Casavilla A**, Selby R, Abu-Elmagd K, Tzakis A, Todo S, Reyes J, Fung J, Starzl TE. Logistics and technique for combined hepatic-intestinal retrieval. *Ann Surg* 1992; **216**: 605-609
- 7 **Williams JW**, Sankary HN, Foster PF. Technique for splanchnic transplantation. *J Pediatr Surg* 1991; **26**: 79-81
- 8 **Yin ZY**, Ni XD, Jiang F, Li N, Li YS, Li JS. Modified technique for combined liver-small bowel transplantation in pigs. *World J Gastroenterol* 2003; **9**: 1625-1628
- 9 **Abu-Elmagd K**, Fung J, Bueno J, Martin D, Madariaga JR, Mazariegos G, Bond G, Molmenti E, Corry RJ, Starzl TE, Reyes J. Logistics and technique for procurement of intestinal, pancreatic, and hepatic grafts from the same donor. *Ann Surg* 2000; **232**: 680-687
- 10 **de Ville de Goyet J**, Mitchell A, Mayer AD, Beath SV, McKiernan PJ, Kelly DA, Mirza D, Buckles JA. En block combined reduced-liver and small bowel transplants: from large donors to small children. *Transplantation* 2000; **69**: 555-559
- 11 **Starzl TE**, Hakala TR, Shaw BW Jr, Hardesty RL, Rosenthal TJ, Griffith BP, Iwatsuki S, Bahnson HT. A flexible procedure for multiple cadaveric organ procurement. *Surg Gybecol Obstet* 1984; **158**: 223-230
- 12 **Starzl TE**, Miller C, Bronznick B, Makowka L. An improved technique for multiple organ harvesting. *Surg Gybecol Obstet* 1987; **165**: 343-348
- 13 **Reyes J**, Fishbein J, Bueno J, Mazariegos G, Abu-Elmagd K. Reduced-size orthotopic composite liver-intestinal allograft. *Transplantation* 1998; **66**: 489-492
- 14 **Todo S**, Tzakis AG, Abu-Elmagd K, Reyes J, Fung JJ, Casavilla A, Nakamura K, Yagihashi A, Jain A, Murase N. Cadaveric small bowel and small bowel-liver transplantation in humans. *Transplantation* 1992; **53**: 369-376
- 15 **Grant D**. London health sciences centre, ontario, canada. Intestinal transplantation: 1997 report of the international registry. Intestinal transplant registry. *Transplantation* 1999; **67**: 1061-1064
- 16 **Todo S**, Reyes J, Furukawa H, Abu-Elmagd K, Lee RG, Tzakis A, Rao AS, Starzl TE. Outcome analysis of 71 clinical intestinal transplantations. *Ann Surg* 1995; **222**: 270-280
- 17 **Goulet O**, Jan D, Sarnacki S, Brousse N, Colomb V, Salomon R, Cuenod B, Piloquet H, Ricour C, Revillon Y. Isolated and combined liver-small bowel transplantation in Paris: 1987-1995. *Transplant Proc* 1996; **28**: 2750
- 18 **Muiesan P**, Dhawan A, Novelli M, Mieli-Vergani G, Rela M, Heaton ND. Isolated liver transplant and sequential small bowel transplantation for intestinal failure and related liver disease in children. *Transplantation* 2000; **11**: 2323-2326
- 19 **Zhong R**, He G, Sakai Y, Zhang Z, Garcia B, Li XC, Jevnikar A, Grant D. The effect of donor-recipient strain combination on rejection and graft-versus-host disease after small bowel/liver transplantation in the rat. *Transplantation* 1993; **56**: 381-385
- 20 **Li XC**, Zhong R, He G, Sakai Y, Garcia B, Jevnikar A, Grant D. Host immune suppression after small bowel/liver transplantation in rats. *Transpl Int* 1994; **7**: 131-135
- 21 **Lopez RR**, Benner KG, Ivancev K, Keeffe EB, Deveney CW, Pinson CW. Management of biliary complications after liver transplantation. *Am J Surg* 1992; **163**: 519-524
- 22 **Greif F**, Bronsther OL, Van Thiel DH, Casavilla A, Iwatsuki S, Tzakis A, Todo S, Fung JJ, Starzl TE. The incidence, timing, and management of biliary tract complications after orthotopic liver transplantation. *Ann Surg* 1994; **219**: 40-45
- 23 **Bueno J**, Abu-Elmagd K, Mazariegos G, Madariaga J, Fung J, Reyes J. Composite liver-small bowel allografts with preservation of donor duodenum and hepatic biliary system in children. *J Pediatr Surg* 2000; **35**: 291-296
- 24 **Casavilla A**, Selby R, Abu-Elmagd K, Tzakis A, Todo S, Starzl TE. Donor selection and surgical technique for en bloc liver-small bowel graft procurement. *Transplant Proc* 1993; **25**: 2622-2623
- 25 **Abu-Elmagd K**, Reyes J, Todo S, Rao A, Lee R, Irish W, Furukawa H, Bueno J, McMichael J, Fawzy AT, Murase N, Demetris J, Rakela J, Fung JJ, Starzl TE. Clinical intestinal transplantation: new perspectives and immunologic considerations. *J Am Coll Surg* 1998; **186**: 512-527
- 26 **Kato T**, Romero R, Verzaro R, Misiakos E, Khan FA, Pinna AD, Nery JR, Ruiz P, Tzakis AG. Inclusion of entire pancreas in the composite liver and intestinal graft in pediatric intestinal transplantation. *Pediatr Transplant* 1999; **3**: 210-214
- 27 **Gruessner RW**, Fasola C, Fryer J, Nakhleh RE, Kim S, Gruessner AC, Beebe D, Moon C, Troppmann C, Najarian JS. Quadruple Immunosuppression in a pig model of small bowel transplantation. *J Surg Res* 1996; **61**: 260-266
- 28 **McCurry KR**, Parker W, Cotterell AH, Weidner BC, Lin SS, Daniels LJ, Holzknicht ZE, Byrne GW, Diamond LE, Logan JS, Platt JL. Humoral responses to pig-to-baboon cardiac transplantation: implications for the pathogenesis and treatment of acute rejection and for accommodation. *Hum Immunol* 1997; **58**: 91-105
- 29 **Wennberg L**, Groth CG, Tibell A, Zhu S, Liu J, Rafael E, Soderlund J, Biggerfeld P, Morris RE, Karlsson-Parra A, Korsgren O. Triple drug treatment with cyclosporine, leflunomide and mycophenolate mofetil prevents rejection of pig islets transplanted into rats and primates. *Transplant Proc* 1997; **29**: 2498
- 30 **Alvira LG**, Herrera N, Salas C, Pereira F, Herrera J, Sua' rez-Massa MD, Castillo-Olivares JL. Influence of cyclosporine on graft regeneration and function after liver transplantation: trial in pigs. *Trans Proc* 2002; **34**: 315-316
- 31 **Biffi R**, Privitera G, Matinato C, Pozzi S, Marzona L, De Ral P, Andreoni B, Tiberio G, Frezza E, Van Thiel DH. Parenteral antibiotics and selective intestinal decontamination do not prevent enteric bacterial overgrowth or translocation observed in a swine model of small bowel transplantation. *J Surg Res* 1995; **58**: 391-394
- 32 **Tuch BE**, Wright DC, Martin TE, Keogh GW, Deol HS, Simpson AM, Roach W, Pinto AN. Differentiation of fetal pig endocrine cells after allografting into the thymus gland. *Transplantation* 1999; **67**: 1184-1187
- 33 **Wright DC**, Deol HS, Tuch BE. A comparison of the sensitivity of pig and human peripheral blood mononuclear cells to the antiproliferative effects of traditional and newer immunosuppressive agents. *Transpl Immunol* 1999; **7**: 141-147

• CLINICAL RESEARCH •

Biochemical and radiological predictors of malignant biliary strictures

Ibrahim A. Al-Mofleh, Abdulrahman M. Aljebreen, Saleh M. Al-Amri, Rashed S. Al-Rashed, Faleh Z. Al-Faleh, Hussein M. Al-Freihi, Ayman A. Abdo, Arthur C. Isnani

Ibrahim A. Al-Mofleh, Abdulrahman M. Aljebreen, Saleh M. Al-Amri, Rashed S. Al-Rashed, Faleh Z. Al-Faleh, Hussein M. Al-Freihi, Ayman A. Abdo, Gastroenterology Division, department of Medicine (38), King Khalid University Hospital, Riyadh, Kingdom of Saudi Arabia
Arthur C. Isnani, King Khalid University Hospital, College of Medicine and Research Center (74), PO Box 2925, Riyadh 11461, Kingdom of Saudi Arabia

Correspondence to: Professor Ibrahim A. Al-Mofleh, Gastroenterology Division, Department of Medicine (38), King Khalid University Hospital, PO Box 2925, Riyadh 11461, Kingdom of Saudi Arabia
Telephone: +966-467-1215 **Fax:** +966-467-1217

Received: 2003-11-22 **Accepted:** 2004-01-09

Abstract

AIM: Differentiation of benign biliary strictures (BBS) from malignant biliary strictures (MBS) remains difficult despite improvement in imaging and endoscopic techniques. The aim of this study was to identify the clinical, biochemical and or radiological predictors of malignant biliary strictures.

METHODS: We retrospectively reviewed all charts of patients who had biliary strictures (BS) on endoscopic retrograde cholangiopancreatography (ERCP) or percutaneous cholangiography (PTC) in case of unsuccessful ERCP from March 1998 to August 2002. Patient characteristics, clinical features, biochemical, radiological and biopsy results were all recorded. Stricture etiology was determined based on cytology, biopsy or clinical follow-up. A receiver operator characteristic (ROC) curve was constructed to determine the optimal laboratory diagnostic criterion threshold in predicting MBS.

RESULTS: One hundred twenty six patients with biliary strictures were enrolled, of which 72 were malignant. The mean age for BBS was 53 years compared to 62.4 years for MBS ($P=0.0006$). Distal bile duct stricture was mainly due to a malignant process 48.6% vs 9% ($P=0.001$). Alkaline phosphates and AST levels were more significantly elevated in MBS ($P=0.0002$). ROC curve showed that a bilirubin level of 84 $\mu\text{mol/L}$ or more was the most predictive of MBS with a sensitivity of 98.6%, specificity of 59.3% and a positive likelihood ratio of 2.42 (95% CI=0.649-0.810). Proximal biliary dilatation was more frequently encountered in MBS compared to BBS, 73.8% vs 39.5% ($P=0.0001$). Majority of BBS (87%) and MBS (78%) were managed endoscopically.

CONCLUSION: A serum bilirubin level of 84 $\mu\text{mol/L}$ or greater is the best predictor of MBS. Older age, proximal biliary dilatation, higher levels of bilirubin, alkaline phosphatase, ALT and AST are all associated with MBS. ERCP is necessary to diagnose and treat benign and malignant biliary strictures.

Al-Mofleh IA, Aljebreen AM, Al-Amri SM, Al-Rashed RS, Al-Faleh FZ, Al-Freihi HM, Abdo AA, Isnani AC. Biochemical and radiological predictors of malignant biliary strictures. *World J Gastroenterol* 2004; 10(10): 1504-1507

<http://www.wjgnet.com/1007-9327/10/1504.asp>

INTRODUCTION

Biliary stricture (BS) may result from an intra or extra-luminal benign or malignant process. Although history, laboratory investigations and imaging techniques may help to differentiate benign from malignant biliary strictures, it remains a clinical challenge. Endoscopic retrograde cholangiopancreatography (ERCP) has been considered the method of choice for the diagnosis of BS as a result of its accuracy in establishing the site and cholangiographic features of stricture^[1]. Cytology specimens can be obtained, which has a sensitivity rate of only 35% but a specificity rate approaching 100% for the diagnosis of malignancy^[2].

Recently, new imaging techniques with increased diagnostic yield have emerged. For instance, magnetic resonance cholangiopancreatography (MRCP) as a non-invasive method has similar or even better diagnostic yield with the advantage of avoiding complications of ERCP^[1,3,4]. Also, with the advent of multislice CT (MS-CT), it has been possible to detect minute biliary and pancreatic tumours as well as small lymph nodes and vessels^[5]. MS-CT cholangiography has become valuable in pre-operative evaluation and determining unresectability^[6]. Therefore, CT has maintained as the method of choice for pancreatic and biliary tumours imaging^[7,8]. Furthermore, intraductal ultrasonography (IDUS) has been valuable in the differentiation of MBS from BBS. It has increased the accuracy of ERC-tissue sampling, but it has not been suitable for staging lymphadenopathy-associated MBS^[8].

The aim of this study was to identify the clinical, biochemical and or radiological predictors of malignant biliary strictures.

MATERIALS AND METHODS

All patients with biliary strictures from March 1998 to August 2002 who had ERCP or PTC in case of unsuccessful ERCP were included. Demographic characteristics, presenting features, laboratory data, imaging technique findings and management modalities were analyzed.

Definition of biliary strictures was suggested by cholangiographic features and it was supported by brush cytology, fine needle aspiration (FNA), the presence of mass or metastases by imaging and or clinical follow-up.

ERCP was performed by three experienced gastroenterologists using 4.2 mm channel duodenoscopes (Pentax or Olympus). All patients received diazepam and demerol as premedication. In addition, patients with biliary dilatation received cefuroxime prophylaxis. Endoscopic and cholangiographic findings were recorded.

Biopsy and brushing materials were obtained when feasible, strictures dilated with balloon or Soehendra dilator and large 10-12 F stent inserted.

Data collected were entered into the computer using Microsoft Excel. After all data were checked for completeness, statistical analysis was performed using Stat Pac gold analysis software and Microsoft Excel programs. Two-tailed P values of less than 0.05 were considered statistically significant. A receiver operator characteristic (ROC) curve was constructed

to determine the optimal laboratory diagnostic criterion threshold (*i.e.* total bilirubin, ALT, AST and alkaline phosphatase) in predicting a malignant biliary stricture. A ROC curve displayed the false positive rate on the x axis (specificity), and the true positive rate on the y axis (sensitivity) for varying test thresholds, thus plotting the performance of a diagnostic test^[10]. The ideal cut-off criteria for the laboratory results were chosen by determining the point lying geometrically closest to an ideal test with 100% specificity and sensitivity^[11].

RESULTS

One hundred twenty six patients were included, 54 of those had a BBS while 72 had a MBS. The main causes of BBS were related to stone disease (choledocholithiasis, Mirizzi syndrome or postcholecystectomy). In 22 patients the cause could not be identified. Cholangiocarcinoma and pancreatic head carcinoma were the most common causes of MBS. Other causes of BS are shown in Table 1.

The mean age of patients with MBS (62.4±11.7 years) was significantly higher than that of patients with BBS (53±18 years) ($P=0.0006$). Fifty percent of BBS were proximal ($P=0.01$) and approximately 50% of MBS were distal ($P<0.001$). There were no significant gender differences (Table 2). Jaundice was found in more than 80% of patients with BBS and MBS, and right upper quadrant (RUQ) pain in 50% of patients. Anorexia, weight loss and fever were less common and no significant differences were observed when both groups were compared (Table 3).

Table 1 Causes of biliary strictures ($n=126$)

Benign	n	%	Malignant	n	%
Choledocholithiasis	12	22	Cholangiocarcinoma	31	43
Mirizzi syndrome	7	13	Pancreatic head CA	23	32
Postcholecystectomy	6	11	Ampullary CA	5	7
Sclerosing cholangitis	3	5.5	Gallbladder CA	5	7
Choledochal cyst	2	3.7	Metastatic CA	4	5.5
Chronic pancreatitis	1	1.9	Hepatocellular CA	2	2.7
Juxtapapillary diverticulum	1	1.9	Lymphoma	2	2.7
Non-specified	22	40.7			
TOTAL	54		TOTAL	72	

Table 2 Demographic data of patients with biliary strictures ($n=126$)

	Benign	Malignant	P value
Number of patients	54 (%)	72 (%)	
Mean age	53±18	62.4±11.7	0.0006
Males	25 (46)	41 (56.9)	0.2255
Females	29 (54)	31 (43.1)	0.2255
Sites of biliary stricture			
Proximal	27 (50)	20 (27.7)	0.0107
Middle	22 (41)	17 (23.6)	0.0394
Distal	5 (9)	35 (48.6)	<0.001

Table 3 Presenting symptoms of patients with biliary strictures ($n=126$)

	Benign $n=54$ (%)	Malignant $n=72$ (%)	P value
Jaundice	44 (81)	61 (84.7)	0.5884
RUQ pain	27 (50)	38 (52.8)	0.7561
Weight loss	4 (7)	11 (15.3)	0.1326
Fever	3 (5)	7 (9.7)	0.3066
Anorexia	4 (7)	7 (9.7)	0.5843

Mean serum values of bilirubin, alkaline phosphatase, ALT and AST were significantly higher in patients with MBS. However GGT levels were not significantly different in both groups (Table 4).

As shown in Table 5 and Figure 1, ROC analysis identified total bilirubin of 84 $\mu\text{mol/L}$ as the best cut-off value for predicting a malignant biliary stricture with a sensitivity of 98.6%, a specificity of 59.3% and a positive likelihood ratio of 2.42 (area under the curve=0.735, SE=0.044, 95% CI=0.649-0.810). On the other hand, ROC analysis showed that other laboratory tests including ALT, AST and alkaline phosphates to have a poor sensitivity and specificity.

Proximal biliary dilatation was more frequently encountered in MBS compared to BBS, 73.8% vs 39.5% ($P=0.0001$). Majority of patients, 87% of BBS and 78% of MBS were treated endoscopically.

Table 4 Laboratory data of patients with biliary strictures ($n=126$)

	Benign $n=54$	Malignant $n=72$	P value
Total bilirubin ($\mu\text{mol/L}$)	142.6±98.4	184.61±120.8	0.0389
Direct bilirubin ($\mu\text{mol/L}$)	102.4±95.3	138.10±98.5	0.0433
Alkaline phosphatase (IU/L)	108.5±48.5	145.50±57.5	0.0002
GGT (IU/L)	397.0±496.5	436.50±325.1	0.591
ALT (IU/L)	52.7±38.3	66.94±35.6	0.0339
AST (IU/L)	76.5±43.2	107.80±45.7	0.0002

Table 5 Receiver operator characteristic (ROC) test results in predicting malignant biliary strictures

Parameter	Cut-off value	Sensitivity (%)	Specificity (%)	+LR	-LR
Total bilirubin ($\mu\text{mol/L}$)	84	98.6	59.3	2.42	0.02
Direct bilirubin ($\mu\text{mol/L}$)	63	91.7	61.1	2.36	0.14
Alkaline phosphatase (IU/L)	136	59.7	83.3	3.58	0.48
GGT (IU/L)	246	80.6	53.7	1.74	0.36
ALT (IU/L)	68	45.8	81.5	2.47	0.66
AST (IU/L)	85	76.4	74.1	2.95	0.32

+LR=positive likelihood ratio; -LR=negative likelihood ratio.

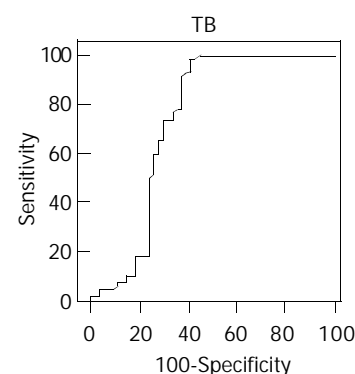


Figure 1 ROC analysis of total bilirubin.

DISCUSSION

The differentiation between benign and malignant biliary strictures can be difficult but is of obvious importance in regard to prognosis and planning optimal therapy.

In our study, majority of patients with BS presented with obstructive jaundice and half had right upper quadrant pain. Other less frequent symptoms included anorexia, weight loss and fever. In contrast to Tandon *et al*^[12], who have encountered more anorexia and weight loss in MBS, we found no significant difference between MBS and BBS. This could be due to the early stage at presentation in our patients.

In our study, although statistically significant differences were found in most biochemical parameters, bilirubin was the best predictor of malignant biliary stricture. A serum bilirubin level of 84 $\mu\text{mol/L}$ or greater was highly predictive of malignant biliary stricture with a sensitivity of 98.6%, a specificity of 59.3% and a positive likelihood ratio of 2.42. Furthermore, proximal biliary dilatation was more frequently encountered in MBS compared to BBS, 73.8% vs 39.5% ($P=0.0001$). Similarly, in a prospective study of 29 patients, Bain *et al.* have shown that a bilirubin of level of 75 $\mu\text{mol/L}$ or greater or a stricture length of greater than 14 mm was highly predictive of malignant biliary stricture. In the same study, intrahepatic duct dilatation was present in 93% of malignant strictures versus 36% of BBS ($P=0.002$)^[13].

In our study, we found that distal bile duct strictures were mainly due to a malignant process, 48.6% vs 9% in BBS ($P<0.001$), which is contrary to other studies. This is probably because we have rarely encountered BBS secondary to chronic pancreatitis which is commonly present with distal benign BS (we had only one patient).

ERCP remains to be an important imaging technique in the diagnosis and treatment of obstructive jaundice^[14]. The yield of ERCP in differentiating MBS from BBS can be further improved with tissue sampling. Sensitivity of biliary fluid and brushing cytology is unsatisfactorily low. It can be improved by combining fine needle aspiration biopsy with intraductal forceps biopsy. This method has been known as triple tissue sampling^[15,16]. Despite the triple tissue sampling, the sensitivity and negative predictive value have not exceeded 62% and 39%, respectively^[16]. Furthermore, brushing cytology yield could be improved by stricture brushing after a 10 F dilatation of malignant stricture^[17]. Similar observation on improvement of bile cytology has been reported earlier by Mohandas *et al*^[18]. Evaluation of cytology specimens for aneuploidy and tumour markers, CA 19-9 and CEA might also increase the diagnostic yield^[19].

Recently, intraductal ultrasonography (IDUS) has been evaluated in the differential diagnosis of MBS from BBS with conflicting results. While Gress *et al.* have not found reliable differentiation criteria^[20], Inui *et al.* and Tamada *et al.*, who used special biliary and pancreatic probes, have provided encouraging results^[21,22]. However, its accuracy is still not exceeding 80%. IDUS has been reported to be superior to conventional endoscopic ultrasonography in terms of diagnostic accuracy, and prediction of tumour respectability^[23].

Treatment of BS depends on the etiology, benign or malignant, magnitude of damage in post-surgical injuries and prediction of respectability of MBS. Endoscopic management of BBS has been considered the primary method before the decision of surgical intervention^[24]. Major bile duct injuries require surgical construction. After initial evaluation of anatomy by direct cholangiogram and inserting a biliary drain, surgical reconstruction with Roux-en-Y hepaticojejunostomy has been associated with an overall success rate exceeding 90%^[25]. It has been considered as the best treatment modality of BBS^[26]. On the other hand Born *et al.* have considered endoscopic or percutaneous management as an adequate short and long-term alternative to surgery^[27].

The decision of therapeutic modality for biliary or pancreatic tumours depends on the evaluation of respectability. It is important to determine preoperatively the spread of MBS. These events may help decide the appropriate treatment for

each condition. Surgery has to be considered for the management of resectable tumours. However, at the time when the diagnosis of MBS has been established, it is often late for curable resection^[28]. Therefore, endoscopic approach remains the method of choice for palliation. Majority of our patients (78%) had endoscopic palliation.

In a large series with 505 patients, Costamagna *et al.* strongly suggested ERCP in the diagnosis and palliation of all patients with suspected MBS^[29]. ERCP has been considered as the optimal technique for diagnosis and palliation of MBS^[30].

In conclusion, a serum bilirubin level of 84 $\mu\text{mol/L}$ or greater is the best predictor of MBS. Older age, proximal biliary dilatation, higher levels of bilirubin, alkaline phosphates, ALT and AST are all associated with MBS. ERCP is the best imaging technique in demonstrating stricture and biliary dilatation, and remains the method of choice in managing BBS and MBS.

REFERENCES

- 1 Hawes RH. Diagnostic and therapeutic uses of ERCP in pancreatic and biliary tract malignancies. *Gastrointest Endosc* 2002; **56**(6 Suppl): S201-205
- 2 Scudera PL, Koizumi J. Brush Cytology evaluation of lesions encountered during ERCP. *Gastrointest Endosc* 1990; **36**: 281-284
- 3 Hall-Craggs MA, Allen CM, Owens CM, Theis BA, Donald JJ, Paley M, Wilkinson ID, Chong WK, Hatfield AR, Lees WR. MR Cholangiography: Clinicalevaluation in 40 cases. *Radiology* 1993; **189**: 423-427
- 4 Soto JA, Barish MA, Yucel ED, Steinberg D, Ferucci JT, Chuttani R. Magnetic resonance cholangiography: Comparison with endoscopic retrograde cholangiography. *Gastroenterology* 1996; **110**: 589-597
- 5 Kim HJ, Kim MH, Lee SK, Yoo KS, Seo DW, Min YI. Tumour vessel: a valuable cholangioscopic clue of malignant biliary stricture. *Gastrointest Endosc* 2000; **52**: 635-638
- 6 O'Malley ME, Boland GW, Wood BJ, Fernandez-del-Castillo C, Warshaw AL, Meuller PR. Adenocarcinoma of the head of the pancreas: determination of surgical unresectability with thin section pancreatic-phase helical CT. *Am J Roentgenol* 1999; **173**: 1513-1518
- 7 Cha JH, Han JK, Kim TK, Kim AY, Park SJ, Choi BI, Suh KS, Kim SW, Han MC. Preoperative evaluation of Klatskin tumour: Accuracy of spiral CT in determining vascular invasion as a sign of unresectability. *Abdom Imaging* 2000; **25**: 500-507
- 8 Morteale KJ, Ji H, Ros PR. CT and magnetic resonance imaging in pancreatic and biliary tract malignancies. *Gastrointest Endosc* 2002; **56**(6 Suppl): S206-212
- 9 Farell RJ, Agarwal B, Brandwein SL, Underhill J, Chuttani R, Pleskow DK. Intraductal US is useful adjunct to ERCP for distinguishing malignant from benign biliary strictures. *Gastrointest Endosc* 2002; **56**: 681-687
- 10 McNeil BJ, Keller E, Adelstein SJ. Primer on certain elements of medical decision making. *N Engl J Med* 1975; **293**: 211-215
- 11 Hanley JA, McNeil BJ. A method of comparing the areas under receiver operating characteristic curves derived from the same cases. *Radiology* 1983; **148**: 839-843
- 12 Tandon RK, Mehrotra R, Arora A, Acharya SK, Vashisht S. Biliary strictures on ERCP: A study in Northern India. *J Assoc Physicians India* 1994; **42**: 865-870
- 13 Bain VG, Abraham N, Jhangri GS, Alexander TW, Henning RC, Hoskinson ME, Maguire CG, Lalor EA, Sadowski DC. Prospective study of biliary strictures to determine the predictors of malignancy. *Can J Gastroenterol* 2000; **14**: 397-402
- 14 Khurram M, Durrani AA, Hasan Z, Butt AA, Ashfaq S. Endoscopic retrograde cholangiopancreatographic evaluation of patients with obstructive jaundice. *J Coll Physicians Surg Pak* 2003; **13**: 325-328
- 15 Fogel EL, Sherman S. How to improve the accuracy of diagnosis of malignant biliary strictures. *Endoscopy* 1999; **31**: 758-760
- 16 Jailwala J, Fogel EL, Sherman S, Gottlieb K, Fluekiger J, Bucksot LG, Lehman GA. Triple tissue sampling at ERCP in malignant biliary obstruction. *Gastrointest Endosc* 2000; **51**(4 Pt 1): 383-390
- 17 Parasher VK, Huibregtse K. Endoscopic retrograde wire-guided

- cytology of malignant biliary strictures using a novel scraping brush. *Gastrointest Endosc* 1998; **48**: 288-290
- 18 **Mohandas KM**, Swaroop VS, Gullar SU, Dave UR, Jagannath P, DeSouza LJ. Diagnosis of malignant obstructive jaundice by bile cytology: results improved by dilating the bile duct strictures. *Gastrointest Endosc* 1994; **40**(2 Pt 1): 150-154
 - 19 **Ryan ME**, Baldauf MC. Comparison of flow cytometry for DNA content and brush cytology for detection of malignancy in pancreatobiliary strictures. *Gastrointest Endosc* 1994; **40**(2 Pt 1): 133-139
 - 20 **Gress F**, Chen YK, Sherman S, Savides T, Zaidi S, Jaffe P, Lehman G, Wonn MJ, Hawes R. Experience with a catheter-based ultrasound probe in the bile duct and pancreas. *Endoscopy* 1995; **27**: 178-184
 - 21 **Inui K**, Nakazawa S, Yoshino J, Wakabayashi T, Okushima K, Nakamura Y, Hattori T, Miyoshi H. Ultrasound probes of biliary lesions. *Endoscopy* 1998; **30** (Suppl 1): A 120-123
 - 22 **Tamada K**, Hagai H, Yasuda Y, Tomiyama T, Ohashi A, Wada S, Kanai N, Satoh Y, Ido K, Sugano K. Transpapillary intraductal US prior to biliary drainage in the assessment of longitudinal spread of extrahepatic bile duct carcinoma. *Gastrointest Endosc* 2001; **53**: 300-307
 - 23 **Menzel J**, Poremba C, Dietl KH, Domschke W. Preoperative diagnosis of bile duct strictures. Comparison of intraductal ultrasonography with conventional endosonography. *Scand J Gastroenterol* 2000; **35**: 77-82
 - 24 **Al-Karawi MA**, Mohamed AELS. Endoscopic management of benign biliary strictures. *Saudi Med J* 1994; **15**: 56-60
 - 25 **Lillemoe KD**, Melton GB, Cameron JL, Pitt HA, Campbell KA, Talomini MA, Sauter PA, Coleman J, Yeo CJ. Postoperative bile duct strictures: Management and outcome in the 1990s. *Ann Surg* 2000; **232**: 430-441
 - 26 **Tocchi A**, Mazzoni G, Liotta G, Costa G, Lepre L, Miccini M, DeMasi E, Lamazza MA, Fiori E. Management of benign biliary strictures: biliary enteric anastomosis vs endoscopic stenting. *Arch Surg* 2000; **135**: 153-157
 - 27 **Born P**, Rosch T, Bruhl K, Sandsch W, Allescher HD, Frimberger E, Classen M. Long-term results of endoscopic and percutaneous transhepatic treatment of benign biliary strictures. *Endoscopy* 1999; **31**: 725-731
 - 28 **Sugiyama M**, Atomi Y, Kuroda A, Muto T. Bile duct carcinoma without jaundice: Clues to early diagnosis. *Hepatogastroenterology* 1997; **44**: 1477-1483
 - 29 **Costamagna G**, Gabrielli A, Mutignani M, Perri V, Bunonato M, Crucitti F. Endoscopic diagnosis and treatment of malignant biliary strictures: review of 505 patients. *Acta Gastroenterol Belg* 1993; **56**: 201-206
 - 30 **Al-Mofleh IA**, Rashed RS, Al-Amri SM, Al-Ghamdi AS, Al-Faleh FZ, Al-Freih HM, Isnani ACL. Malignant biliary strictures: Diagnosis and management. *Saudi Med J* 2003; **24**: 1360-1363

Edited by Wang XL Proofread by Xu FM

• CLINICAL RESEARCH •

Polymorphisms at cholesterol 7 α -hydroxylase, apolipoproteins B and E and low density lipoprotein receptor genes in patients with gallbladder stone disease

Zhao-Yan Jiang, Tian-Quan Han, Guang-Jun Suo, Dian-Xu Feng, Sheng Chen, Xing-Xing Cai, Zhi-Hong Jiang, Jun Shang, Yi Zhang, Yu Jiang, Sheng-Dao Zhang

Zhao-Yan Jiang, Tian-Quan Han, Guang-Jun Suo, Dian-Xu Feng, Sheng Chen, Xing-Xing Cai, Zhi-Hong Jiang, Jun Shang, Yi Zhang, Yu Jiang, Sheng-Dao Zhang, Department of Surgery, Ruijin Hospital, Shanghai Second Medical University, Shanghai Institute of Digestive Surgery, Shanghai 200025, China
Supported by a grant from Shanghai Science and Technology Committee in China, No. 954119027

Correspondence to: Tian-Quan Han, M.D., Ph.D., Department of Surgery, Ruijin Hospital, Shanghai Second Medical University, Shanghai 200025, China. digsurgrj@yahoo.com.cn

Telephone: +86-21-64373909 **Fax:** +86-21-64373909

Received: 2003-04-08 **Accepted:** 2003-05-19

Abstract

AIM: To investigate the relationship between gallbladder stone disease (GSD) and single nucleotide polymorphisms of cholesterol 7 α -hydroxylase (*CYP7A*) gene promoter, apolipoprotein (*APO*) B gene exon 26, *APOE* gene exon 4 or microsatellite polymorphism of low density lipoprotein receptor (*LDLR*) gene exon 18.

METHODS: Genotypes of *CYP7A*, *APOB*, *APOE* and *LDLR* genes were determined in 105 patients with GSD diagnosed by B-mode ultrasonography and 274 control subjects. Serum lipids were analyzed with HITACHI 7060 automatic biochemical analyzer.

RESULTS: Body mass index (BMI) was significantly higher in patients with GSD (24.47 \pm 3.09) than in controls (23.50 \pm 2.16). Plasma total cholesterol was lower in patients with GSD (4.66 \pm 0.92 mmol/L) than in controls (4.91 \pm 0.96 mmol/L), $P < 0.01$ after adjusted for age, sex and BMI. The significantly higher frequency of A allele of *CYP7A* gene polymorphism and X+ allele of *APOB* gene polymorphism was seen in GSD patients. Percentages of A allele in patients and controls were 62.86% and 54.38% ($P < 0.05$) and those of X+ allele 8.57% and 4.01% ($P < 0.01$). Subjects with A allele had significantly lower plasma total cholesterol and LDL cholesterol than subjects with CC homozygote. In a multiple variable logistic regression model, the BMI (OR=1.13, 95% CI: 1.05-1.22), A allele (OR=1.48, 95% CI: 1.05-2.09) and X+ allele (OR=2.28, 95% CI: 1.14-4.59) were positively associated with GSD ($P < 0.05$). Plasma total cholesterol (OR=0.69, 95% CI: 0.64-0.74) was negatively related to GSD ($P < 0.05$).

CONCLUSION: With an association analysis, it was determined that A allele of *CYP7A* gene and X+ allele of *APOB* gene might be considered as risk genes for GSD. These alleles are related with differences of serum lipids among subjects. Multiple-variable logistic regression model analysis showed that besides BMI, GSD was affected by polygenetic factors. But the mechanism for these two alleles responsible for GSD requires further investigations.

Jiang ZY, Han TQ, Suo GJ, Feng DX, Chen S, Cai XX, Jiang ZH, Shang J, Zhang Y, Jiang Y, Zhang SD. Polymorphisms at cholesterol 7 α -hydroxylase, apolipoproteins B and E and low density lipoprotein receptor genes in patients with gallbladder stone disease. *World J Gastroenterol* 2004; 10(10): 1508-1512 <http://www.wjgnet.com/1007-9327/10/1508.asp>

INTRODUCTION

Gallbladder stone disease (GSD) is prevalent in China with a gradually increasing incidence. Studies on the pathogenesis of GSD have demonstrated that supersaturation of biliary cholesterol caused by excessive biliary cholesterol and/or decreased bile acid is the requisite for the formation of gallstones^[1]. Both the cholesterol secreted into bile and the bile acids converted from cholesterol in the liver are involved in regulating cholesterol homeostasis. It was shown in studies^[2-4] that genetic variations might affect gallstone formation. In 1995, Khajuana *et al.* reported a murine lithogenic gene, *Lith 1*, as a possible regulator of hepatic cholesterol synthesis^[4]. The primary *Lith* phenotype was considered to induce secondary events characterized by multiple enzyme alterations which increase available cholesterol and supply the sterol to hepatocytes for hypersecretion into bile^[5]. Additional quantitative traits linkage analysis^[6] maps other *Lith* genes on murine chromosomes 6, 7, 8, 10, 19 and X to confirm the polygenic mode of inheritance. A few studies^[7-10] have focused on the relationship between human GSD and certain genetic factors contributing to cholesterol metabolism.

Cholesterol 7 α -hydroxylase (*CYP7A*, EC 1.14.13.17), a cytochrome P-450 enzyme, is the rate limiting enzyme of hepatic bile acid synthesis, with its activity regulated by bile acids, cholesterol and hormones^[11]. Although the amino acid sequence of *CYP7A* between species is highly homologous (80-90% sequence identity), species respond differently to diet cholesterol^[12]. As compared with control subjects, the activity of *CYP7A* varied in patients with gallstones^[13-15], and diminished or elevated patterns were observed. The heterogeneity of activities of *CYP7A* in patients with GSD may be related to *CYP7A* polymorphisms. A linkage of A-204C single nucleotide polymorphism of the *CYP7A* gene promoter with plasma low density lipoprotein (*LDL*) cholesterol was found in recent studies of nuclear families^[16] and within the general population^[17]. However, the polymorphism for patients with GSD has never been studied. Apolipoprotein (*APO*) E^[18] is an extremely efficient ligand for the *LDLR* and is the determinant for receptor-mediated catabolism of all *APOE* containing lipoproteins. The polymorphism of *APOE* is controlled by three alleles in exon 4, namely $\epsilon 2$, $\epsilon 3$ and $\epsilon 4$. The physiological importance of *APOE* exhibits in disorders of lipoprotein metabolism such as atherosclerosis^[19] as well as in Alzheimer's disease which is not obviously related to lipoprotein metabolism^[20]. The role of *APOE* has also been examined in relation to GSD^[7,9]. The *APOE4* allele is associated with high cholesterol content in gallstones^[7,9], faster crystallization^[7] and frequent stone recurrence after lithotripsy^[21].

Table 1 PCR condition and restriction enzymes

Genes	Primers	Annealing temp	RE
CYP7A ^[16, 17]	5' TGGTAGGTAAATTATTAATAGATGT 3' 5' AAATTAATGGATGAATCAAAGAGC 3'	61 °C	Bsa I
apo B ^[10]	5' GGA GAC TAT TCA GAA GCT AA 3' 5' GAA GAG CCT GAA GAC TGA CT 3'	60 °C	Xba I
apo E ^[24]	5' ACAGAATTCGCCCCGGCCTGGTACAC 3' 5' TAAGCTTGGCACGGCTGTCCAAGGA 3'	60 °C	Hha I
LDL receptor ^[25]	5' CACTTTGTATATTGGTTGAAACTGT 3' 5' CACTGAACAAATACAGCAACCAGGG 3'	62 °C	

The *LDLR* on the surface of hepatocytes plays an important role in cholesterol homeostasis in humans^[22]. The receptor can recognize *APOB* or *APOE* containing lipoproteins such as LDL and high-density lipoprotein (HDL) with different affinities mediating the absorption of plasma lipoproteins. There are many polymorphic sites on this gene and some of those are related to plasma cholesterol metabolism^[23].

In the present study, we analyzed the polymorphism of A-204C of *CYP7A* gene promoter, *APOE* exon 4 and microsatellite polymorphism of *LDLR* gene exon 18. Their relationships with asymptomatic GSD on the Chinese Han population were examined. The association of Xba I polymorphism on *APOB* gene exon 26 with GSD, shown in our previous study^[10], was also evaluated using multiple regression analysis.

MATERIALS AND METHODS

Patients

A total of 379 subjects were recruited for this study from February to May 1998. Patients in this study consisted of 78 males and 27 females with stones and/or cholesterol crystals in their gallbladder. None of the patients had previous onset of cholecystitis defined as colic, fever with chills or jaundice. Two hundred and seventy-four healthy subjects (184 males and 90 females) with normal liver, kidney and endocrine function were included as controls. The mean ages of patients and controls were 47.53 and 47.94 years, respectively. After a 12-h fast, the participants received B-mode ultrasonography with Aloka 500/SSD equipped with a transducer of 3.5 MHz. A total of 10 mL venous blood was extracted and half of it was immediately mixed with ACD anti-coagulants containing citric acid, sodium citric acid and glucose for DNA extraction. The other half of this sample was prepared for biochemical analysis. Body mass index (BMI) was calculated by weight/height² (kg/m²). All subjects gave informed consent to participate in this study which was approved by the Ethical Committee of Ruijin Hospital, Shanghai Second Medical University.

Analysis of plasma lipids and lipoproteins

Plasma total cholesterol, triglyceride, HDL cholesterol, LDL cholesterol, APO AI and APO B were assayed by commercially available kits (Boehringer Mannheim GmbH, Mannheim, Germany) on an automatic analyzer (HITACHI 7060, Hitachi Koki Co. Ltd., Hitachinaka City, Japan).

Genotyping

Genomic DNA was extracted from leukocytes using a method provided by GIBCO-BRL DNA extraction kit (Cat: #28350-015, GIBCO-BRL, Gaithersburg, MD, USA). The fragments containing target polymorphic sequences of *CYP7A*, *APOB*, *APOE* and *LDLR* genes were amplified using polymerase chain reaction (PCR) on PTC-200 Peltier Thermal Cycler (MJ Research Inc, MA, USA). Primers and the conditions of PCR are listed in Table 1. For the single nucleotide polymorphisms of *CYP7A*,

APOB and *APOE*, the products of PCR were each digested by restriction enzymes (New England Biolabs Inc., Beverly, MA, USA). The enzymes are indicated in Table 1. The digested PCR products were electrophoresed in agarose gel; then stained with ethidium bromide and visualized under ultraviolet light. A 968-bp fragment containing A-204C polymorphism of *CYP7A* gene was digested with restrictive enzyme *Bsa I* (New England Biolabs Inc., Beverly, MA, USA) and electrophoresed on 10 g/L agarose gel and stained with ethidium bromide. The band with a cutting site was designated as C allele and that without as A allele. A 244-bp fragment containing *APOE* exon 4 gene was digested with *Hha I* followed by electrophoresis on 100 g/L polyacrylamide gel and then stained with silver. The genotypes were determined from the pattern of restrictive fragments on the gel as described in detail by Hixson and Vernier^[24]. The bands representing the genotype of microsatellite polymorphism of *LDLR* gene exon 18 were obtained from direct electrophoresis on 100 g/L PAGE (100 v, 2.5 h) and stained with silver. The genotype of *LDLR* gene was determined for the bands with 106-bp as A allele (7 repeats of TA), 108-bp as B allele (8 repeats of TA) or 112-bp as C allele (10 repeats of TA)^[25]. Genotyping of *APOB* gene was performed as previously described by Han *et al.*^[10].

Statistics

The results were expressed as means±SD. The differences in concentrations of lipids between patients and controls and those among genotypes were calculated using Student's *t* test. Statistical analysis was performed using the statistical software package SAS 6.12 for Windows (SAS Institute Inc., Cary, NC, USA). SAS GLM procedure was used to compare the concentrations of lipids between patients and controls after adjustment for sex, age and BMI. Frequencies of alleles between patients and controls were evaluated for statistical significance using Chi-square test. A multivariate model was used to predict the relative odds of GSD with all the variables by multiple logistic regressions. Logistic regression coefficients and standard errors were calculated to determine the estimates of odds ratio (OR) and 95% confidence intervals (CI) for significant factors.

RESULTS

Demographic and biochemical characteristics

Gallbladder stones and/or cholesterol crystals were detected in 105 cases by B-mode ultrasonography. The demographic characteristics and biochemistry are shown in Table 2. BMI was significantly higher in the patients than in the controls (24.47±3.09 vs 23.50±2.16, *P*<0.01). Concentrations of plasma total cholesterol and APO AI were significantly lower in patients than in controls. Although the concentrations of HDL cholesterol and LDL cholesterol were slightly lower in patients than in controls, the differences were not significant. Plasma lipid levels varied with sex, age and BMI. We compared the plasma lipids between patients and controls using the analysis of covariance. After

adjustment for sex, age and BMI, the plasma total cholesterol and LDL cholesterol as well as APO B were found significantly lower in patients than in controls as shown in Table 2.

Table 2 Demographic characteristics and biochemistry for patients and controls

	Patients	Controls	P value	P value ¹
No. (male/female)	105 (78/27)	274 (184/90)		
Age (yr)	47.53±10.98	47.94±12.21		
BMI (kg/m ²)	24.47±3.09	23.50±2.16	<0.01	
Triglycerine (mmol/L)	1.32±1.15	1.19±0.82		
Cholesterol (mmol/L)	4.66±0.92	4.91±0.96	<0.05	<0.01
HDL (mmol/L)	1.33±0.36	1.40±0.34		
LDL (mmol/L)	2.56±0.67	2.69±0.73		<0.05
apo A I (g/L)	1.34±0.21	1.39±0.18	<0.05	
apo B (g/L)	1.00±0.22	1.03±0.24		<0.05

¹After adjustment for sex, age and BMI.

Distribution of genotypes and association of polymorphisms with GSD

Figure 1 indicates the genotypes of *CYP7A*, *APOB*, *APOE* and *LDLR* gene polymorphisms. The distributions of genotypes for patients and controls are listed in Table 3. Using Chi-square test, there was a significantly higher frequency of A allele of *CYP7A* gene and X+ allele of *APOB* gene observed in patients compared with controls (A allele: 62.86% vs 54.38%, $P<0.05$; X+ allele: 8.57% vs 4.01%, $P<0.01$, Table 4). There were no significant differences between patients and controls in the polymorphisms of *APOE* gene and *LDLR* gene.

Association between gene polymorphism and plasma lipid concentrations

Table 5 indicates that plasma total cholesterol, LDL cholesterol and APOB were lower in subjects with A allele (AA homozygote or AC heterozygote) than in those without A allele (CC homozygote). The difference was significant only within the control group or within the group combining patients and controls, but not in the patients only group. Within each genotype, the difference of lipid concentration was incongruent between

patients and controls. In subjects with A allele, the LDL cholesterol was significantly higher in patients than in controls, while in subjects without A allele, patients had significantly lower concentrations of HDL cholesterol and APOAI.

Table 3 Distribution of genotypes for patients and controls

Genes	Genotypes	Patients (%)	Controls (%)
CYP7A	AA	44 (41.90)	79 (28.83)
	AC	44 (41.90)	140 (51.10)
	CC	17 (16.20)	55 (20.07)
Apo B	X+/+	1 (0.95)	0 (0)
	X+/-	16 (15.24)	22 (8.03)
	X-/-	88 (83.81)	252 (91.97)
Apo E	ε2/2	0 (0)	1 (0.36)
	ε2/3	15 (14.29)	45 (16.42)
	ε2/4	5 (4.76)	6 (2.19)
	ε3/3	73 (69.52)	183 (66.80)
	ε3/4	11 (10.48)	37 (13.50)
	ε4/4	1 (0.95)	2 (0.73)
	ε4/3	1 (0.95)	2 (0.73)
LDL receptor	AA	41 (39.05)	90 (32.85)
	AB	2 (1.90)	13 (4.74)
	AC	32 (30.48)	104 (37.96)
	BB	3 (2.85)	4 (1.46)
	BC	8 (7.62)	22 (8.03)
	CC	19 (18.60)	41 (14.96)

Table 4 Frequency of alleles for patients and controls (%)

Genes	Alleles	Patients	Control
CYP7A	A	62.86 ^a	54.38
	C	37.14	45.62
Apo B	X+	8.57 ^b	4.01
	X-	91.43	95.99
Apo E	ε2	9.52	9.67
	ε3	81.90	81.75
	ε4	8.57	8.57
LDL receptor	A	55.24	54.20
	B	7.62	7.84
	C	37.14	37.96

^a $\chi^2=4.44$, $P<0.05$; ^b $\chi^2=6.31$, $P<0.01$.

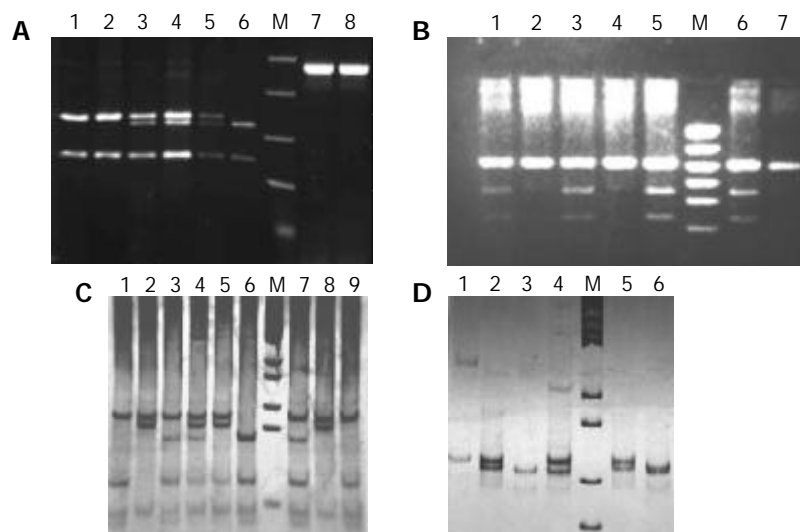


Figure 1 Genotypes of *CYP7A*, apolipoproteins B, E and *LDLR* receptor gene. A: *CYP7A* gene, M: DNA Marker: 1 000, 750, 500, 300, 150 bp (Cat. G3161, Promega, Madison, WI, USA); lanes 1, 2: AA type; lanes 3-5: AC type; lane 6: CC type; lanes 7, 8: PCR products, B: Apolipoprotein B gene, M: DNA Marker: 1 543, 994, 695, 515, 377, 237 bp (Cat. MG0781, SABC, Shanghai, China), lane 1, 3, 5, 6: X+/- type; 2, 4, 7: X-/- type. C: Apo E gene, M: pGEM 7zf(+)/Hae III DNA Marker (Cat. MG0861, SABC, Shanghai, China), from lanes 1-9: ε3/3, ε2/2, ε3/4, ε2/4, ε2/3, ε4/4, ε3/4, ε2/2, ε3/3 types. D: *LDLR* receptor gene, M: pGEM 7zf(+)/Hae III DNA Marker, from lanes 1-6: CC, BC, AA, AC, BC and AB types.

Table 5 Association of CYP7A gene polymorphism with plasma lipids

	Patients		Controls		All	
	AA/AC	CC	AA/AC	CC	AA/AC	CC
No.	88	17	219	55	307	72
Triglyceride (mmol/L)	1.25±0.99	1.70±7.77	1.15±0.82	1.36±0.81	1.18±0.87	1.44±1.11
Cholesterol (mmol/L)	4.64±0.95	4.78±0.79	4.84±0.94 ^c	5.16±0.99 ^c	4.78±0.95 ^g	5.07±0.95 ^g
HDL (mmol/L)	1.32±0.37 ^a	1.35±0.32	1.42±0.34 ^a	1.33±0.72	1.39±0.35	1.33±0.32
LDL (mmol/L)	2.56±0.70	2.59±0.45 ^c	2.63±0.72 ^c	2.91±0.72 ^{e, c}	2.61±0.71 ^g	2.83±0.67 ^g
Apo AI (g/L)	1.34±0.22 ^a	1.36±0.15	1.39±0.18 ^a	1.36±0.20	1.38±0.19	1.36±0.18
Apo B (g/L)	1.00±0.23	1.02±0.15	1.01±0.24 ^c	1.10±0.23 ^c	1.01±0.23 ^g	1.08±0.22 ^g

^a*P*<0.05, patients vs controls with AA/AC genotype, ^c*P*<0.05, AA/AC vs CC within control group, ^e*P*<0.05, patients vs controls with CC genotype, ^g*P*<0.05, AA/AC vs CC in all the subjects.

Logistic regression analysis

A multiple variable logistic regression analysis was performed to compare the effects of both genetic factors and other quantitative variables. In Table 6, only *CYP7A* (OR=1.48, *P*<0.05) and *APOB* (OR=2.28, *P*<0.05) gene polymorphism, plasma cholesterol (OR=0.69, *P*<0.01) and BMI (OR=1.13, *P*<0.05) were correlated with GSD (Table 6).

Table 6 Stepwise logistic regression of multiple variables

Variables	OR	95% CI
A allele ^a	1.48	1.05-2.09
X+ allele ^a	2.28	1.14-4.59
Cholesterol ^b	0.69	0.64-0.74
BMI ^a	1.13	1.05-1.22

^a*P*<0.05; ^b*P*<0.01.

DISCUSSION

Epidemiological studies have stressed the relationship between plasma lipid concentration and GSD. The present study indicated that patients with GSD had lower plasma cholesterol, even after adjustment for sex, age and BMI. Our results were consistent with those of Juvonen^[7], Scragg^[26] and Attili^[27], although there were unchanged results^[28] or only lowered plasma cholesterol levels in women^[29] reported by other authors. The plasma lipid concentrations varied in populations due to diet habits, genetic factors, ethnicity, etc. This explains why previous studies remain controversial. Whether changes in plasma lipid concentration are major factors inducing GSD or represent the end stage of gallstone formation is still questionable. The mechanism for the change in plasma lipid concentrations that increases the risk for GSD is also unclear. However, epidemiological studies indicate that genetic predisposition has been confirmed to have a close relation with GSD. Our present study on the Chinese Han population verified that GSD was genetically controlled by polygenic factors. A-204C polymorphism at *CYP7A* gene promoter and Xba I polymorphism at *APOB* gene may be susceptible genes linked to GSD.

Our previous study on the *APOB* gene Xba I polymorphism revealed that X+ allele was associated with a higher incidence of GSD^[10]. The relationship between GSD and the other three polymorphic sites, A-204C polymorphism of *CYP7A*, Hha I polymorphism of *APOE* and a dinucleotide repeat microsatellite polymorphism of *LDLR*, was also studied by our group. Only did *CYP7A* gene polymorphism seem to be related to GSD. We found a significantly higher frequency of A allele in patients than in controls (0.62 vs 0.54, *P*<0.05). The A-204C polymorphism located 204 bp upstream of the transcription start site of *CYP7A*^[17]. This single nucleotide polymorphism^[16],

at which site C replaced A, created a cutting site for the Bsa I restrictive enzyme. The frequency of A allele of *CYP7A* gene was 0.58^[16] in the Caucasian population and 0.60 in Framingham families^[17] which was slightly higher than that in the Chinese Han population. Analysis of plasma lipid levels revealed that plasma LDL cholesterol concentrations were associated with A-204C polymorphism, similar to the results of Wang *et al.* and Couture^[16,17]. Individuals with A allele tended to have lower LDL cholesterol concentrations. This difference was significant in controls, but not in patients in this study. No studies have assayed the activity of hepatic *CYP7A* among different genotypes up to this time. The mechanism and rationale for A allele to induce low LDL cholesterol are still unknown.

Contrary to our expectation, there was no association between *APOE* gene and GSD or between *LDLR* gene and GSD. Since *APOE* isoforms had different affinities to receptors^[22] affecting lipid metabolism, there was a demonstrated relationship between *APOE* gene polymorphism and various plasma lipids. Its polymorphism was well documented in atherosclerosis^[19] and Alzheimer's disease^[20] as well as cholesterol gallstone disease^[7,9]. Juvonen^[7] studied for the first time the relationship between *APOE* polymorphism and gallstones. Patients with ε4 allele had higher cholesterol content in stones, rapid cholesterol crystallization and shorter median nucleation time in the Finnish population^[7] while Bertomeu^[9] found significantly higher ε4 allele frequency in Spanish patients with gallstones. But other studies^[9,30,31] had contradictory results. There were reports that median nucleation time^[9] was similar in patients between the genotypes and that the cholesterol saturation index^[30] was lower in patients with ε4 allele. Our study concluded that there was no significant difference in the frequency of ε4 allele between patients and controls. A similar result on Chinese patients with GSD was reported previously in a study from Sichuan, China^[32].

LDLR was important for the absorption of APOB and APOE containing lipoproteins^[22]. Herein, we studied a dinucleotide repeat polymorphism. The frequency of these alleles did not differ between the patient and control groups. But we could not exclude the possibility of existence of other polymorphic sites to account for the differences in hepatic LDLR activities that, in turn, would lead to high absorption of plasma cholesterol for biliary secretion.

We analyzed all our variables using a logistic regression model to evaluate the role of genetic factors and quantitative variables. Higher cholesterol concentration in serum may provide a protective factor for GSD since it is negatively related with GSD (OR<1). The cause of gallstone formation might be due to hepatic overabsorption of cholesterol via receptors such as SRB1^[33] or LDLR^[22] leading to hypersaturation of biliary cholesterol. Besides BMI and cholesterol, GSD may be controlled by multiple genetic factors such as the *APOB* gene or *CYP7A* gene. The OR of the *APOB* gene polymorphism

was 2.28, and *CYP7A* was 1.48 with $P < 0.05$. This implies that subjects with A allele of *CYP7A* gene or X+ allele of *APOB* gene can easily form gallstones.

The present study determined the relationship between *CYP7A* or *APOB* gene polymorphism and GSD. However, the relationship should be investigated further in family pedigrees with GSD. Since gene polymorphisms are heterogeneous among ethnic groups, GSD may be caused by different risk genes among different population. The main cause for GSD is hypersaturation of biliary cholesterol. So all genes (known or yet to be determined) involved in hepatic cholesterol metabolism remain the focus for future studies to discover the primary risk genes for GSD. Once a human genomic map for GSD, similar to murine^[34], is completed, it can be useful for early predictive and preventive measures for subjects susceptible to GSD. The genomic map will provide the necessary link in the discovery of effective pharmaceutical agents for treatment.

REFERENCES

- 1 **Apstein MD**, Carey MC. Pathogenesis of cholesterol gallstones: a parsimonious hypothesis. *Eur J Clin Invest* 1996; **26**: 343-352
- 2 **Miquel JF**, Covarrubias C, Villaroel L, Mingrone G, Greco AV, Puglielli L, Carvallo P, Marshall G, Del Pino G, Nervi F. Genetic epidemiology of cholesterol cholelithiasis among Chilean Hispanics, Amerindians, and Maoris. *Gastroenterology* 1998; **115**: 937-946
- 3 **Duggirala R**, Mitchell BD, Blangero J, Stern MP. Genetic determinants of variation in gallbladder disease in the Mexican-American population. *Genet Epidemiol* 1999; **16**: 191-204
- 4 **Khanuja B**, Cheah YC, Hunt M, Nishina PM, Wang DQH, Chen HW, Billheimer JT, Carey MC, Paigen B. *Lith1*, a major gene affecting cholesterol gallstone formation among inbred strains of mice. *Proc Natl Acad Sci U S A* 1995; **92**: 7729-7733
- 5 **Lammert F**, Wang DQH, Paigen B, Carey MC. Phenotypic characterization of *Lith* genes that determine susceptibility to cholesterol cholelithiasis in inbred mice: integrated activities of hepatic lipid regulatory enzymes. *J Lipid Res* 1999; **40**: 2080-2090
- 6 **Paigen B**, Schork NJ, Svenson KL, Cheah YC, Mu JL, Lammert F, Wang DQH, Bouchard G, Carey MC. Quantitative trait loci mapping for cholesterol gallstones in AKR/J and C57L/J strains of mice. *Physiol Genomics* 2000; **4**: 59-65
- 7 **Juononen T**, Kervinen K, Kairaluoma MI, Lajunen LHJ, Kesäniemi YA. Gallstone cholesterol content is related to apolipoprotein E polymorphism. *Gastroenterology* 1993; **104**: 1806-1813
- 8 **Juononen T**, Savolainen MJ, Kairaluoma MI, Lajunen LHJ, Humphries SE, Kesäniemi YA. Polymorphisms at the apoB, apoA-I, and cholesteryl ester transfer protein gene loci in patients with gallbladder disease. *J Lipid Res* 1995; **36**: 804-812
- 9 **Bertomeu A**, Ros E, Zambón D, Vela M, Pérez-Ayuso RM, Targarona E, Trías M, Sanllehy C, Casals E, Ribó JM. Apolipoprotein E polymorphism and gallstones. *Gastroenterology* 1996; **111**: 1603-1610
- 10 **Han T**, Jiang Z, Suo G, Zhang S. Apolipoprotein B-100 gene *Xba* I polymorphism and cholesterol gallstone diseases. *Clin Genet* 2000; **57**: 304-308
- 11 **Einarsson C**, Ellis E, Abrahamsson A, Ericzon BG, Björkhem I, Axelsson M. Bile acid formation in primary human hepatocytes. *World J Gastroenterol* 2000; **6**: 522-525
- 12 **Xu G**, Shneider BL, Shefer S, Nguyen LB, Batta AK, Tint GS, Arrese M, Thevananthar S, Ma L, Stengelin S, Kramer W, Greenblatt D, Pcolinsky M, Salen G. Ileal bile acid transport regulates bile acid pool, synthesis, and plasma cholesterol levels differently in cholesterol-fed rats and rabbits. *J Lipid Res* 2000; **41**: 298-304
- 13 **Ito T**, Kawata S, Imai Y, Kakimoto H, Trzaskos JM, Matsuzawa Y. Hepatic cholesterol metabolism in patients with cholesterol gallstones: enhanced intracellular transport of cholesterol. *Gastroenterology* 1996; **110**: 1619-1627
- 14 **Reihner E**, Angelin B, Björkhem I, Einarsson K. Hepatic cholesterol metabolism in cholesterol gallstone disease. *J Lipid Res* 1991; **32**: 469-475
- 15 **Shoda J**, He BF, Tanaka N, Matsuzaki Y, Osuga T, Yamamori S, Miyazaki H, Sjövall J. Increase of deoxycholate in supersaturated bile of patients with cholesterol gallstone disease and its correlation with de novo syntheses of cholesterol and bile acids in liver, gallbladder emptying, and small intestinal transit. *Hepatology* 1995; **21**: 1291-1302
- 16 **Wang J**, Freeman DJ, Grundy SM, Levine DM, Guerra R, Cohen JC. Linkage between cholesterol 7 α -hydroxylase and high plasma low-density lipoprotein cholesterol concentrations. *J Clin Invest* 1998; **101**: 1283-1291
- 17 **Couture P**, Otvos JD, Cupples LA, Wilson PWF, Schaefer EJ, Ordovas JM. Association of the A-204C polymorphism in the cholesterol 7 α -hydroxylase gene with variations in plasma low density lipoprotein cholesterol levels in the Framingham offspring study. *J Lipid Res* 1999; **40**: 1883-1889
- 18 **Mahley RW**. Apolipoprotein E: cholesterol transport protein with expanding role in the cell biology. *Science* 1988; **240**: 622-630
- 19 **Curtiss LK**, Boisvert WA. Apolipoprotein E and atherosclerosis. *Curr Opin Lipidol* 2000; **11**: 243-251
- 20 **Strittmatter WJ**, Saunders AM, Schmechel D, Pericak-Vance M, Enghild J, Salvesen GS, Roses AD. Apolipoprotein E: high-avidity binding to β -amyloid and increased frequency of type 4 allele in late-onset familial Alzheimer disease. *Proc Natl Acad Sci U S A* 1993; **90**: 1977-1981
- 21 **Portincasa P**, van Erpecum KJ, van de Meeberg PC, Dallinga-Thie GM, de Bruin TWA, van Berge-Henegouwen GP. Apolipoprotein E4 genotype and gallbladder motility influence speed of gallstone clearance and risk of recurrence after extracorporeal shock-wave lithotripsy. *Hepatology* 1996; **24**: 580-587
- 22 **Brown MS**, Goldstein JL. A receptor-mediated pathway for cholesterol homeostasis. *Science* 1986; **232**: 34-47
- 23 **Pedersen JC**, Berg K. Normal DNA polymorphism at the low density lipoprotein receptor (LDLR) locus associated with serum cholesterol level. *Clin Genet* 1988; **34**: 306-312
- 24 **Hixson JE**, Vernier DT. Restriction isotyping of human apolipoprotein E by gene amplification and cleavage with Hha I. *J Lipid Res* 1990; **31**: 545-548
- 25 **Zuliani G**, Hobbs HH. Dinucleotide repeat polymorphism at the 3' end of the LDL receptor gene. *Nucleic Acid Res* 1990; **18**: 4300
- 26 **Scragg RKR**, Calvert GD, Oliver JR. Plasma lipids and insulin in gall stone disease: a case-control study. *Br Med J* 1984; **289**: 521-525
- 27 **Attili AF**, Capocaccia R, Carulli N, Festi D, Roda E, Barbara L, Capocaccia L, Menotti A, Okolicsanyi L, Ricci G, Lalloni L, Mariotti S, Sama C, Scafato E. Factors associated with gallstone disease in the MICOL experience. *Hepatology* 1997; **26**: 809-818
- 28 **Barbara L**, Sama C, Labate AMM, Taroni F, Rusticali AG, Festi D, Sapio C, Roda E, Banterle C, Puci A, Formentini F, Colasanti S, Nardin F. A population study on the prevalence of gallstone disease: the Sirmione study. *Hepatology* 1987; **7**: 913-917
- 29 **GREPCO**. The epidemiology of gallstone disease in Rome, Italy. Part II. Factors associated with the disease. *Hepatology* 1988; **8**: 907-913
- 30 **van Erpecum KJ**, van Berge-Henegouwen GP, Eckhardt ERM, Portincasa P, van de Heijning BJM, Dallinga-Thie GM, Groen AK. Cholesterol crystallization in human gallbladder bile: relation to gallstone number, bile composition, and apolipoprotein E4 isoform. *Hepatology* 1998; **27**: 1508-1516
- 31 **Ko CW**, Beresford SAA, Alderman B, Jarvik GP, Schulte SJ, Calhoun B, Tsuchida AM, Koepsell TD, Lee SP. Apolipoprotein E genotype and the risk of gallbladder disease in pregnancy. *Hepatology* 2000; **31**: 18-23
- 32 **Lin QY**, Xiao LJ, Chen NS, Li N, Fu MD, Yan LN. A prospective study on the serum lipids in different apo E genotype patients with gallstones. *Zhonghua Yixue Yichuanxue Zazhi* 1997; **14**: 223-226
- 33 **Ji Y**, Wang N, Ramakrishnan R, Sehayek E, Huszar D, Breslow JL, Tall AR. Hepatic scavenger receptor BI promotes rapid clearance of high density lipoprotein free cholesterol and its transport into bile. *J Biol Chem* 1999; **274**: 33398-33402
- 34 **Lammert F**, Carey MC, Paigen B. Chromosomal organization of candidate genes involved in cholesterol gallstone formation: a murine gallstone map. *Gastroenterology* 2001; **120**: 221-238

• CLINICAL RESEARCH •

Different therapy for different types of ulcerative colitis in China

Xue-Liang Jiang, Hui-Fei Cui

Xue-Liang Jiang, Department of Gastroenterology, Chinese PLA General Hospital of Jinan Military Command, Jinan 250031, Shandong Province, China

Hui-Fei Cui, College of Pharmaceutical Science, Shandong University, Jinan 250012, Shandong Province, China

Supported by Youth Research Foundation of the Public Health Bureau of Shandong Province, No. 2001CA2EFB2

Correspondence to: Dr. Xue-Liang Jiang, Department of Gastroenterology, Chinese PLA General Hospital of Jinan Military Command, 25 Shifanlu, Jinan 250031, Shandong Province, China. jiangxueliang678@126.com

Telephone: 13585909956

Received: 2003-08-08 **Accepted:** 2003-10-07

Abstract

AIM: To study the different therapy for different types of ulcerative colitis (UC) in China.

METHODS: Among 102 UC patients, 42 chronic relapse type UC patients were randomly divided into olsalazine sodium treatment group ($n=21$) and SASP group ($n=21$). Clinical effects and safety were observed in the 2 groups. Forty-two first episode type UC patients were randomly divided into Heartleaf houttuynia herb treatment group ($n=21$) and SASP group ($n=21$). Clinical effects were observed in the 2 groups while ultrastructure of colonic mucosa, ICAM-1 and the pressure of distant colon were studied in Heartleaf houttuynia herb group. Eighteen patients (8 males, 10 females) with refractory UC and unresponsive to high-dose prednisolone and sulfasalazine therapy more than one month were treated with Kangshuanling (7 200 U/d). Prednisolone was gradually stopped and sulfasalazine was maintained. Stool frequency, rectal bleeding, colonoscopy, general well-being, histology were observed and CD62p, CD63, CD54, Pgp-170 (flow cytometry), TXA2 (RIA), blood platelet aggregation rate and thrombosis length *in vitro* were assessed.

RESULTS: In the 42 chronic relapse type UC patients, the overall clinical effects of olsalazine sodium group (complete remission in 16, improvement in 4, inefficiency in 1) were better than those of SASP group (complete remission in 10, improvement in 4, inefficiency in 7, $P<0.05$). Symptomatic remission of olsalazine sodium group (complete remission in 15, partial remission in 5, inefficiency in 1) was better than that of SASP group (complete remission in 10, partial remission in 5, inefficiency in 6, $P<0.05$). The colonoscopic remission of olsalazine sodium group (complete remission in 11, partial remission in 9, inefficiency in 1) was better than that of SASP group (complete remission in 7, partial remission in 8, inefficiency in 6, $P<0.05$). The histologic remission of olsalazine sodium group (complete remission in 13, partial remission in 7, inefficiency in 1) was better than that of SASP group (complete remission in 6, partial remission in 10, inefficiency in 5, $P<0.05$). The side effects of gastrointestinal tract in olsalazine sodium group were less than those of SASP group except for frequency of watery diarrhea. No other side effects were observed in

olsalazine sodium group while ALT increase, WBC decrease and skin eruption were observed in SASP group. Two patients relapsed in olsalazine sodium group while 8 cases relapsed in SASP group during the flow-up period (from six months to one year). In the 42 first episode type UC patients, the clinical effect of Heartleaf houttuynia herb group (complete remission in 20, 95.2%; improvement in 1, 4.8%) was better than that of SASP group (complete remission in 15, 72.4%, improvement in 5, 23.8%; inefficiency in 1, 3.8%, $P<0.01$). The time of stool frequency recovering to normal (5.6 ± 3.3 d), and blood stool disappearance (6.7 ± 3.8 d) and abdominal pain disappearance (6.1 ± 3.5 d) in Heartleaf houttuynia herb group was all shorter than that in SASP group (9.5 ± 4.9 d, 11.7 ± 6.1 d, 10.6 ± 5.3 d, $P<0.01$). Heartleaf houttuynia herb could inhibit the epithelial cell apoptosis of colonic mucous membrane and the expression of ICAM-1 ($45.8\pm 5.7\%$ vs $30.7\pm 4.1\%$, $P<0.05$). Compared with normal persons, the mean promotive speed of contraction wave stepped up (4.6 ± 1.6 cm/min vs 3.2 ± 1.8 cm/min, $P<0.05$) and the mean amplitude of the wave decreased (14.2 ± 9.3 kPa vs 18.4 ± 8.0 kPa, $P<0.05$) in active UC patients. After treatment with Heartleaf houttuynia herb, these 2 indexes improved significantly (17.3 ± 8.3 kPa, 3.7 ± 1.7 cm/min, $P<0.05$). In normal persons, the postprandial pressure of sigmoid (2.9 ± 0.9 kPa) was higher than that of descending colon (2.0 ± 0.7 kPa) and splenic flexure (1.7 ± 0.6 kPa), while the colonic pressure (1.5 ± 0.5 kPa, 1.4 ± 0.6 kPa, 1.3 ± 0.6 kPa) decreased significantly ($P<0.05$) in active UC patients. After treatment with Heartleaf houttuynia herb, the colonic pressure (2.6 ± 0.8 kPa, 1.8 ± 0.6 kPa, 1.6 ± 0.5 kPa) recovered to normal. The pain threshold of distant colon (67.3 ± 18.9 mL) in active UC patients decreased significantly compared with that of normal persons (216.2 ± 40.8 mL, $P<0.05$) and recovered to normal after treatment with Heartleaf houttuynia herb (187.4 ± 27.2 mL, $P<0.05$). In the 18 refractory UC patients with platelet activation, after more than 4 wk of combined Kangshuanling and sulfasalazine therapy, 16 patients achieved clinical remission, with a highly significant statistical difference ($P<0.01$) between pre-and post-treatment mean scores for all disease parameters: stool frequency (8.2/d vs 1.6/d), rectal bleeding (score 2.7 vs 0.3), colonoscopy (score 2.6 vs 1.1), histology (score 12.0 vs 5.0), general well being (score 4.0 vs 0.6) and CD62p ($8.0\pm 3.1\%$ vs $4.1\pm 1.8\%$), CD63 ($6.3\pm 2.1\%$ vs $3.2\pm 1.6\%$), TXA2 (548 ± 85 ng/L vs 390 ± 67 ng/L), platelet aggregation rate ($43.2\pm 10.7\%$ vs $34.8\pm 8.1\%$), thrombosis length *in vitro* (2.3 ± 0.6 cm vs 1.8 ± 0.3 cm), CD54 in blood ($26.9\pm 6.9\%$ vs $14.4\pm 5.1\%$), CD54 in tissues ($51.1\pm 6.2\%$ vs $23.1\pm 4.1\%$), Pgp-170 in blood ($18.9\pm 3.9\%$ vs $10.4\pm 2.7\%$), Pgp-170 in tissues ($16.5\pm 3.2\%$ vs $10.2\pm 2.3\%$, $P<0.01$ or 0.05).

CONCLUSION: Based on the characteristics of UC cases in China, different therapy should be given to different types of UC with expected satisfactory results.

Jiang XL, Cui HF. Different therapy for different types of ulcerative colitis in China. *World J Gastroenterol* 2004; 10(10): 1513-1520

<http://www.wjgnet.com/1007-9327/10/1513.asp>

INTRODUCTION

Ulcerative colitis (UC) is a common digestive disease in Western countries. It was believed that the occurrence of UC was rare in China. But recent reports reveal that UC cases have increased remarkably^[1,2]. According to our study, UC cases from 1991 to 2000 have increased 2.7 times compared with those from 1981 to 1990^[3-5]. Due to the fact that the etiology and mechanism of UC are still not quite clear, and there is no specific treatment available, the disease usually becomes chronic with repeated relapses, thus seriously endangering patient's health^[6-25]. SASP and corticosteroid, despite their widespread use in the treatment of UC, do not offer an ideal cure because of its long course of treatment, various adverse reactions as well as tendency to relapse when medication stops. The emphasis laid on the study of UC, therefore, is to find an effective drug with fewer adverse reactions in accord with the characteristics of UC cases in China. The diagnosis and treatment of UC still remain a challenge to clinicians^[26-34]. Respecting treatment and improvement of curative effect in refractory cases, lower of relapse rate and reduction of side effects of aminosalicylic acid and corticosteroids are questions to be encountered. Based upon the characteristics of UC cases in China, we adopted the method of giving different therapy to different types of UC, hoping to get better therapeutic results.

MATERIALS AND METHODS

Total cases

A total of 102 UC patients (42 chronic relapse type, 42 first episode type, 18 refractory type) were studied, their diagnoses conformed to the criteria of Lennard-Jones^[28].

Chronic relapse type

Among the 42 chronic relapse type cases, 19 were males and 23 females with an average age of 32.6 years. They had a UC history of 6 mo to 5 years and bloody diarrhea, abdominal pain of varying degrees. Pathological changes above the sigmoid were found in 12 and 30 patients by colonoscopic examinations, respectively. Lesions were characterized by ulcerations, crypt abscesses, non-specific inflammation and atypical hyperplasia, *etc.* They were randomly divided into treatment group which received olsalazine sodium capsules (Tianjin Lisheng Pharmaceutical Co., Ltd. 250 mg) were used twice a day (1.0 g/d) for 8 wk, and comparison group received sulfasalazine (1.0) 4 times a day for 8 wk. There was no significant difference in the severity of symptoms between olsalazine group (11 mild, 8 moderate, 2 severe) and SASP group (13 mild, 7 moderate, 1 severe, Ridit analysis, $P > 0.05$). For patients who could not tolerate diarrhea of 2-3 times a day, 1-2 bills of imodium were given daily, but not more than 10 d. Patients were seen before and after 1, 2, 4, 6, 8 wk of treatment. Symptoms and physical signs were recorded. Colonoscopy was done 3 d before treatment and within 3 d after completion of treatment. A total of 7 items were observed and recorded. Purulent secretion and pseudopolyp were classified into 2 grades. Ulcer, erosion, mucous bleeding, hyperemic edema and vascular blurring were classified into grades 0, 1, 2, 3, 4 based upon the severity (0=nil, 1=mild, 2=moderate, 3=relative severe, 4=severe). Routine blood and stool tests were performed before and after 1, 2, 4, 6 and 8 wk of treatment. Coagulation time and erythrocyte sedimentation rate were examined before and after 4 and 8 wk of treatment. Blood serum potassium, sodium, chloride, anhydride, urea nitrogen, ALT and total bilirubin were examined before and after 8 wk of treatment. Histological examination with grading of its changes was performed on colonoscopic biopsy specimens before and after treatment (grade 0: no polymorphonuclear cell, grade 1: some polymorphonuclear cells in lamina

propria, grade 2: obvious polymorphonuclear cells infiltration in lamina propria involving more than 50% of recesses, grade 3: massive polymorphonuclear cells with recess abscess, grade 4: obvious acute inflammation with ulcer). Criteria of therapeutic efficacy were adopted that proposed by Chinese Society of Gastroenterology^[35] (complete remission: subsidence of clinical symptoms with relative normal mucous membrane in colonoscopy, effective: basically without symptoms and mild mucous inflammatory reaction or pseudopolyp formation upon colonoscopy, ineffective: no improvement in clinical symptoms, colonoscopic and pathologic examinations). Complete clinical remission: after 8 wk treatment, defecation 0-2 times a day, with no gross blood or microscopic red cells in stool; partial remission: after 8 wk of treatment, defecation 3-4 times a day, with no gross blood in stool but less than 10 RBC per high power microscopic field; no improvement: defecation 5 times or more per day with gross bloody stool. Colonoscopic remission: complete remission (among the 7 items, 5 or more lowered by a grade after treatment), partial remission (3-4 items lowered by a grade after treatment), no remission (0-2 items lowered by a grade after treatment). Histological remission: complete remission (pathological grade lowered after treatment, being grades 0-1), partial remission (pathological grade lowered after treatment, but still >1), no remission (no change before and after treatment). Adverse reactions record: nausea, diarrhea, insomnia, abdominal pain, dizziness, rash, lumbar soreness, edema, *etc.* Their time of occurrence, severity, duration and measures taken for treatment were recorded.

First episode type

Among the 42 cases of first episode type, 16 were males and 26 females with average age of 31.4 years. They had a UC history of 1 mo to a year, and all had bloody diarrhea, abdominal pain of different degrees. Lesions above the sigmoid were found in 2 patients by colonoscopic examination, while pathological changes were found below the sigmoid in 40 patients. Lesions were characterized by ulceration, crypt abscesses, non-specific inflammation and atypical hyperplasia, *etc.* They were randomly divided into treatment group that received treatment of heartleaf houttuynia (2 kg/L, pH 4.0-6.0, Nanfang pharmaceutical Co., Ltd.) enema (20 mL diluted with NS 100 mL, once every evening before sleep for 1-2 mo), and SASP group that administered 1 g of SASP four times a day for 1-2 mo. Clinical observations included frequency of defecation, bloody stool, and general condition. Therapeutic effects^[28]: complete remission (complete disappearance of symptoms with mucous membrane returned to normal in colonoscopy), partial remission (abatement of symptoms with conditions of mucous membrane improved, only a small amount of red blood cells and leucocytes found in routine stool test), no remission (no obvious changes both in symptoms and in colonoscopy). Ultrastructure^[7] Microvilli, mitochondria and apoptosis were observed under electronic microscopy. Content of CD54 (ICAM-1, Immunotech) in colonic mucous membrane was examined according to our methods^[15].

PC Polygraph HR (CTD-SYNECTICS, Sweden) was used to examine colonic motility. Distances between the 8 tracts (outer diameter 8 mm and side hole diameter 1 mm) of manometric tube were 5 cm, medication that would affect gastrointestinal motility was suspended at least for 3 d before the examination. Intestinal tract was cleaned in the afternoon prior to the examination and food intake was suspended during the day of examination. Manometric tube was inserted to colonic splenic flexure as guided by colonoscopy. Colonic motility of each patient was recorded one hour before meal and two hours after meal, the result was then analyzed by Polygram and Windows Polygram. Contractions above 6.67 kPa and spreading

to side holes 10 cm away were regarded as propulsive contractions, while contractions below 1.33 kPa were not considered so as to minimize the effect of respiration. Baseline was automatically set up by computer, which calculated the mean oscillation amplitude every 30 min before and after meals. Hand injectors were used to fill air of 20 mL each time to the self-made rubber air pocket with the maximum capacity of 120 mL at 30 s intervals. Patients' feeling of expansion of air pocket was recorded (cognitive, defecation and pain threshold values).

Refractory UC patients with platelet activation

Among the 18 refractory UC patients, there were 8 males and 10 females aged 20 to 52 years (mean 32.4 years), including 10 cases of severe UC, and 8 moderately severe UC. Duration of diseases ranged from 7 mo to 10 years (mean 4.3 years). Rectal bleeding, diarrhea, mucus stool, abdominal pain were the main symptoms. Three patients were associated with thromboembolic diseases. All patients were treated with high-dose corticosteroid and sulfasalazine for more than 4 wk without effect, sulfasalazine was maintained in combination with Kangshuanling sublingual tablet (low molecular heparin, produced by Shandong Songling Pharmaceutical Factory, 2 tablets, 3 times daily (7 200U/d) for 15 d, then 1 tablet, 3 times daily (3 600 U/d) for more than 4 wk). Prednisolone was tapered and stopped.

Pre- and post-treatment scores were calculated for the following disease parameters^[36]: (1) Stool frequency (average number per day for the past week); (2) Rectal bleeding (0: absent, 1: streak of blood on stools occasionally, 2: obvious blood on stool frequently, 3: complete bloody stools); (3) Colonoscopic appearance 0: normal vascular pattern, 1: mild lesion (loss of vascular pattern, mucosal edema, no bleeding), 2: moderate lesion (granularity and friability of the mucosa), 3: severe lesion (discrete ulceration and spontaneous bleeding); (4) Histological grading: serial biopsies from rectum and colon were taken. Five histological changes seen in UC (cellular infiltrate in lamina propria, cryptitis, crypt abscess formation, goblet cell depletion, and regenerative hyperplasia of epithelium). Each was scored from 0 (absent) to 3 (severe). A total UC score of 5 or less indicated mild disease; 5-10, moderate; and 10-15, severe disease. (5) General health status (0: excellent, 1: good, 2: poor, 3: poorer, 4: very poor, 5: poorest).

To assess platelet activation and aggregability^[22,37], we used a sensitive flow cytometric technic designed to render minimize sample handling and render fixation unnecessary to quantify platelet activation. Blood samples were incubated 10 min before venesection with fluorescein isothiocyanate (FITC) conjugated antibodies to the platelet surface antigens, P-selectin (CD62P) and CD63 (Immunotech, Marseilles, France). Analysis was made 15 min before venesection using a BD (Becton Dickinson Immunocytometry Systems) FAC scan. TXA-2 (Suzhou Medical College) was measured using RIA method, samples were taken without tourniquet into chilled tubes containing 1:9 anticoagulant/ antiaggregant solution (trisodium citrate 3.8%), centrifuged for 15-30 min, later at 4 °C for 30 min to minimize *in vitro* activation, supernatant was decanted off and stored at -20 °C for assay within 3 mo. Platelet aggregation rates (PAR) and thrombosis length (TL) *in vitro* were assessed by XSN-RII instrument according to the manufacturer's instructions. CD54 and Pgp-170 in blood and tissues were measured using flow cytometric technique according to our previous report^[15] and literature^[38,39].

Statistical analysis

T test and Ridit analysis were adopted. Student's *t* test and Friedman test were used to assess the significance of differences between mean pre- and post-treatment parameters.

RESULTS

Chronic relapse type UC

In the 42 chronic relapse type UC patients, the total clinical effect of olsalazine sodium group (complete remission in 16 cases, improvement in 4 patients, inefficiency in one case) was better than that of SASP group (complete remission in 10 cases, improvement in 4, inefficiency in 7, $P < 0.05$). The clinical symptomatic remission of olsalazine sodium group (complete remission in 15 cases, partial in 5, inefficiency in one) was better than that of SASP group (complete remission in 10 cases, partial in 5, inefficiency in 6, $P < 0.05$). The colonoscopic remission of olsalazine sodium group (complete remission in 11 cases, partial in 9, inefficiency in 1) was better than that of SASP group (complete remission in 7 cases, partial in 8, inefficiency in 6, $P < 0.05$). The colonoscopic images of pre and post treatment with olsalazine are shown in Figure 1. The histologic remission of olsalazine sodium group (complete remission in 13 cases, partial in 7, inefficiency in 1) was better than that of SASP group (complete remission in 6 cases, partial in 10, inefficiency in 5, $P < 0.05$). The side effects of gastrointestinal tract in olsalazine sodium group were less than those of SASP group (abdominal discomfort: 3 vs 15, heartburn 1 vs 7, nausea 2 vs 5) except for frequency of watery diarrhea (5 vs 1). No other side effects were observed in olsalazine sodium group while increased ALT (1 case), decreased WBC (1 case) and skin eruption (2 cases) were observed in SASP group. Two patients relapsed in olsalazine sodium group while 8 cases relapsed in SASP group during the flow-up period (from 6 mo to 1 year).

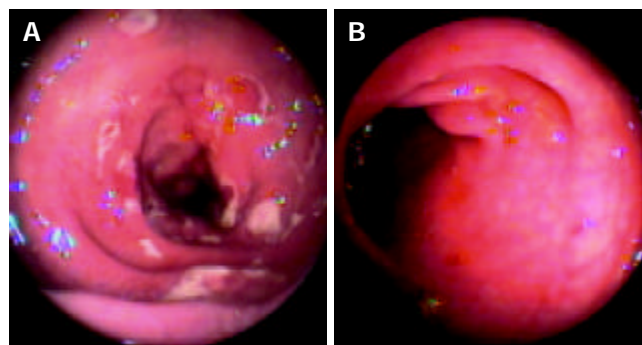


Figure 1 Colonoscopic image before and after treatment of olsalazine. A: Colonoscopic image before treatment of olsalazine; B: Colonoscopic image after treatment of olsalazine for 4 wk.

First episode type UC

In the 42 first episode type UC patients, the clinical effect of Heartleaf houttuynia herb group (complete remission in 20 cases, 95.2%; improvement in 1 case, 4.8%) was better than that of SASP group (complete remission in 15 cases, 72.4%; improvement in 5 cases, 23.8%; inefficiency in 1 case, 3.8%, $P < 0.01$). The time of stool frequency recovering to normal (5.6 ± 3.3 d), blood stool disappearance time (6.7 ± 3.8 d) and abdominal pain disappearance time (6.1 ± 3.5 d) in Heartleaf houttuynia herb group were all shorter than those in SASP group (9.5 ± 4.9 d, 11.7 ± 6.1 d, 10.6 ± 5.3 d, $P < 0.01$). Pathological changes of ultrastructure, such as swollen mitochondria with depleted ridge, shortened microvilli, maldevelopment of goblet cells and increased epithelial cell apoptosis (Figure 2) could be found on the surface of mucous membrane and recess prior to Heartleaf houttuynia herb injection treatment, which recovered to normal gradually after treatment (Figure 3).

Heartleaf houttuynia herb could inhibit the expression of CD54 (ICAM-1) of colonic mucous membrane (45.8 ± 5.7 vs $30.7 \pm 4.1\%$, $P < 0.05$, Figure 4).

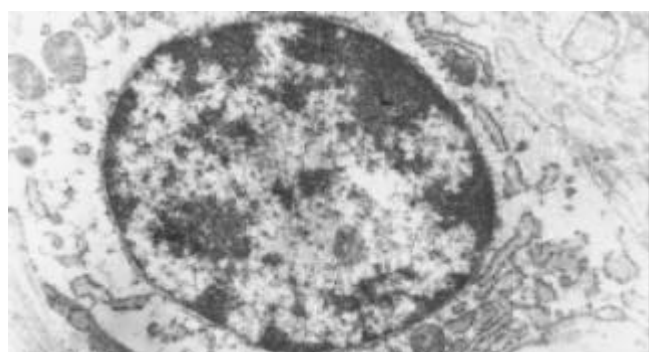


Figure 2 Epithelial cell apoptosis and swollen mitochondria with depleted ridge in UC patients.

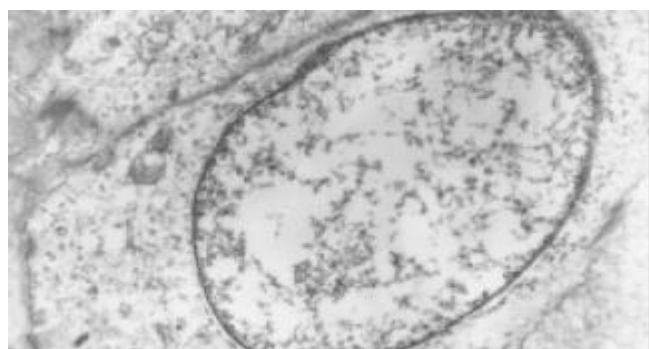


Figure 3 Gradual recovery of epithelial cells to normal after treatment with Heartleaf houttuynia herb injection.

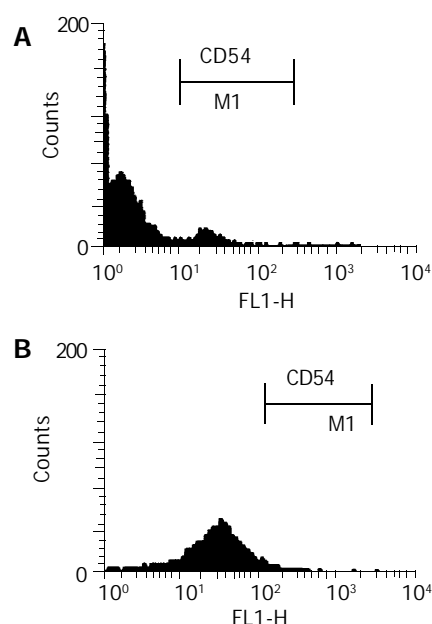


Figure 4 Expression of CD54 (ICAM-1) in colonic mucous membrane of UC patients before and after treatment of Heartleaf houttuynia herb. A: Increased expression of CD54 in colonic mucous membrane of UC patients before treatment of Heartleaf houttuynia herb; B: Decreased expression of CD54 in colonic mucous membrane of UC patients after treatment of Heartleaf houttuynia herb.

Compared with normal persons, the mean promotive speed of contraction wave stepped up (4.6 ± 1.6 cm/min vs 3.2 ± 1.8 cm/min, $P < 0.05$) and the mean amplitude of wave decreased (14.2 ± 9.3 kPa vs 18.4 ± 8.0 kPa, $P < 0.05$) in active UC patients. After treatment of Heartleaf houttuynia herb, these 2 indexes improved significantly (17.3 ± 8.3 kPa, 3.7 ± 1.7 cm/min, $P < 0.05$). In normal persons, the

post-meal pressure of sigmoid (2.9 ± 0.9 kPa) was higher than that of descending colon (2.0 ± 0.7 kPa) and splenic flexure (1.7 ± 0.6 kPa), while the respective colonic pressures (1.5 ± 0.5 kPa, 1.4 ± 0.6 kPa, 1.3 ± 0.6 kPa) were significantly decreased ($P < 0.05$) in active UC patients. After treatment of Heartleaf houttuynia herb, the colonic pressures (2.6 ± 0.8 kPa, 1.8 ± 0.6 kPa, 1.6 ± 0.5 kPa) recovered to normal.

The pain threshold of distant colon (67.3 ± 18.9 mL) in active UC patients decreased significantly compared with that in normal persons (216.2 ± 40.8 mL, $P < 0.05$) and recovered to normal after treatment of Heartleaf houttuynia herb (187.4 ± 27.2 mL, $P < 0.05$). There were no adverse reactions in Heartleaf houttuynia herb therapy, while SASP therapy had adverse reactions such as heartburn (5 cases), increased ALT (1 case), decreased WBC (1 case) and rash (2 cases).

Refractory UC patients with platelet activation

Sixteen patients achieved clinical remission (normal stool frequency and no rectal bleeding) after combined treatment of Kangshuanling sublingual tablets with sulfasalazine. Two patients had reduced rectal bleeding only. The average time of marked improvement and remission was 3 wk (1-5 wk), and 6 wk (1-12 wk), respectively. Rectal bleeding ceased in 16 patients (4 patients within 7-14 d, the others within 2-6 wk). Sixteen patients improved in general health condition earlier than bowel symptoms. There was highly significant improvement in mean scores for all disease parameters (Table 1).

Blood contents of CD62p, CD63, TXA2, platelet aggregation rate (PAR) and thrombosis length (TL) in vitro

All the indexes in refractory UC patients increased significantly as compared with the normal controls ($P < 0.01$). After treatment with Kangshuanling sublingual tablets, all the parameters of UC patients decreased ($P < 0.05$, but CD62P and CD63 remained higher than normal ($P < 0.05$, Table 2, Figure 5).

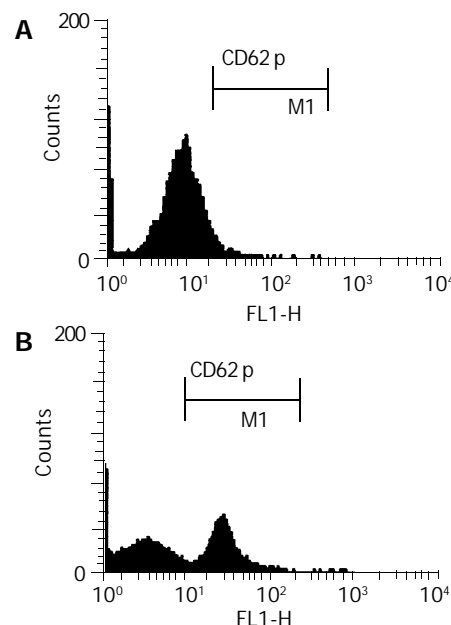


Figure 5 CD62p in blood of normal persons and active UC patients. A: CD62p in blood of normal persons; B: Significant increase of CD62p in blood of active UC patients.

CD54 and products of MDR expression (Pgp-170) in blood and tissues

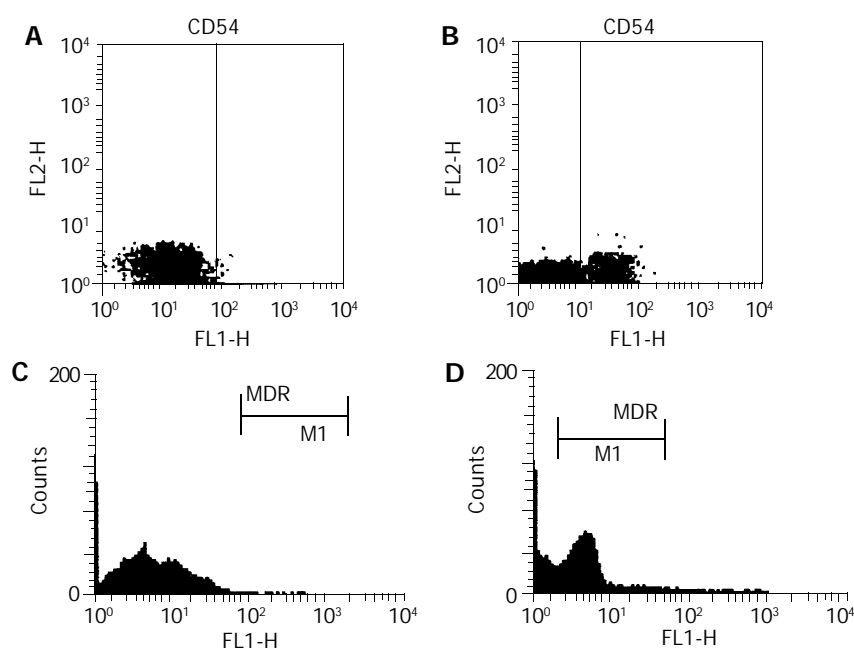
Compared with normal persons (Figure 6A), CD54 elevated in both blood and tissues in refractory UC patients ($P < 0.01$), CD54 in tissues was higher than in blood (Figure 6B). After treatment

Table 1 Therapeutic effects of Kangshuanling sublingual tablets on refractory UC patients

Group	Stool frequency (times/d)	Rectal bleeding (score)	Colonoscopy (score)	Histology (score)	Well-being (score)
Pre-treatment	8.2	2.7	2.6	12.0	3.9
Post-treatment	1.6 ^b	0.3 ^b	1.1 ^b	5.0 ^b	0.7 ^b

^b $P < 0.01$ vs pretreatment.**Table 2** Effects of Kangshuanling sublingual tablet on CD62P and CD63, TXA2, platelet aggregation rate (PAR) and thrombosis length (TL) *in vitro* in UC patients (mean \pm SD)

Group	CD62p (%)	CD63 (%)	TXA2 (ng/L)	PAR (%)	TL (cm)
UC patients					
Pre-treatment	8.0 \pm 3.1 ^b	6.3 \pm 2.1 ^b	548.2 \pm 84.9 ^b	43.2 \pm 10.1 ^b	2.3 \pm 0.6 ^b
Post-treatment	4.1 \pm 1.8 ^{a,d}	3.2 \pm 1.6 ^{a,d}	390.1 \pm 67.0 ^d	34.8 \pm 8.1 ^d	1.8 \pm 0.3 ^d
Normal controls	1.9 \pm 0.4	1.6 \pm 0.8	340.2 \pm 40.4	34.1 \pm 9.1	1.7 \pm 0.4

^a $P < 0.05$, ^b $P < 0.01$ vs normal controls; ^d $P < 0.01$ vs pretreatment.**Figure 6** CD54 and MDR in tissues of normal persons and refractory UC patients. A: CD54 in tissues of normal persons; B: Significant increase of CD54 in tissues of refractory UC patients; C: MDR in tissues of normal persons; D: Significant increase of MDR in tissues of refractory UC patients.

with Kangshuanling sublingual tablets, CD54 was significantly decreased in both blood and tissues ($P < 0.01$), but still higher than that in normal controls ($P < 0.05$), (Table 3). Compared with normal persons (Figure 6C), Pgp-170 elevated in both blood and tissues in refractory UC patients ($P < 0.01$, Figure 6D), there was no difference between Pgp-170 in tissues and blood. After treatment with Kangshuanling sublingual tablets, Pgp-170 was significantly decreased in both blood and tissues ($P < 0.05$), but still higher than that of normal controls ($P < 0.05$), (Table 3).

Table 3 Effects of Kangshuanling sublingual tablets on CD54 in UC patients (mean \pm SD, %)

Group	Blood CD54	Tissue CD54	Blood Pgp-170	Tissue Pgp-170
UC patients				
Pre-treatment	26.9 \pm 6.9 ^b	51.1 \pm 6.2 ^b	18.9 \pm 3.9 ^b	16.5 \pm 3.2 ^b
Post-treatment	14.4 \pm 5.1 ^{a,d}	23.1 \pm 4.1 ^{a,d}	10.4 \pm 2.7 ^{a,c}	10.2 \pm 2.3 ^{a,c}
Normal controls	6.2 \pm 3.7	8.8 \pm 3.2	6.2 \pm 2.2	6.8 \pm 3.1

^a $P < 0.05$, ^b $P < 0.01$ vs normal controls; ^c $P < 0.05$ vs pre-treatment,^d $P < 0.01$ vs pre-treatment.

Complications

No complications were found during the treatment with Kangshuanling sublingual tablets.

DISCUSSION

SASP is still widely used in the treatment of chronic relapse type ulcerative colitis, with advantages such as quick effect and high clinical remission rate. However, its effect is not satisfactory in some chronic cases and has various adverse reactions. In addition, UC usually relapses when medication is stopped. Therefore, we should place emphasis in the study of UC on more effective drugs with less adverse reactions^[2,27-31]. At present, the cause and pathogenesis of UC are unclear^[1-15], nonspecific anti-inflammatory drugs, in a relatively long period, will still remain as the main drugs for treating UC. While the curative effect of traditional aminosalicic acid has been affirmed, its side reactions are too many. Main approaches today centered on enhancing the curative effect and reducing side reactions by developing new preparations and changing routes of administration^[1]. SASP, when taken orally, is cleaved by bacteria in the colon into 5-ASA and Sulfapyridine. The

former is the effective component of SASP, and the latter is the carrier of 5-ASA, which may cause such side reactions as sulfanilamide allergy, gastrointestinal upset, hepatorenal impairment, thus affecting its clinical application. In the present study, the above mentioned side reactions in various degrees were also seen in the SASP group. Therefore, to achieve a satisfactory curative effect but without toxicity, the best therapy for UC is to administer 5-ASA that does not contain sulfapyridine and to make it working on diseased areas directly. 5-ASA, however, is usually absorbed rapidly, hence unable to reach inflamed mucous membrane. So, the question posed for the development of new drugs for UC, is how to make 5-ASA reaching and working on the diseased area. Olsalazine sodium gives an answer to this problem, for it is the prodrug of 5-ASA, formed by 2-molecules of 5-ASA jointed by diazo bond. When it is taken orally, only a very small amount is absorbed before reaching colon (absorbing rate <5%). It does not decompose and its biological utilization rate in the body is extremely low. When it reaches the colon, bacterial enzymes in the colon split the diazo bond, liberating the two-molecules of 5-ASA. It has no side effects of SASP, while maintaining the same curative effects. Olsalazine sodium has been on market for more than 10 years and its curative effect on UC and safety have been widely accepted. Domestic olsalazine sodium is a fourth grade new drug jointly developed by Tianjin Lisheng Pharmaceutical Co., Ltd. and Tianjing Medical Research Institute. The fourth grade new drug with the trade name "Changmei", in capsule form was put into market in 2000. This study centered on the clinical effects and safety of olsalazine sodium in patients with chronic UC. Our results indicated that olsalazine sodium was superior to SASP in overall clinical response rate, amelioration of clinical symptoms, colonoscopic examination and histology test. In addition, it has fewer side effects on digestive tract and is unharmed to liver function, WBC and skin. The cause of the increased watery stool frequencies may be related with sodium salt, which inhibits intestinal absorption of water. It mainly occurs at the beginning of medication or during increase of dosage. This side effect, however, does not affect the continuing medication. Patients' worries may be eliminated when the cause is explained. To increase medication frequencies or to take medicine after meal may ameliorate or eliminate this symptom. Imodium may also be given temporarily to some patients to maintain curative effect. In China, the chronic relapse type accounted for 52.6% of all UC cases^[3], maintenance treatment may lower relapse rate. In summary, this study shows that the curative effect and safety of domestic olsalazine sodium is superior to SASP in the treatment of chronic UC. It boosts remission rate, lowers relapse rate and causes fewer side effect, especially applicable to patients who are irresponsive or allergic to SASP therapy.

According to our statistics, the first episode type accounted for 34.8% of all ulcerative colitis cases in China^[3]. The disease mostly starts in rectum and sigmoid colon. When Heartleaf houttuynia enema is used, it can work on diseased areas directly. In this way, it not only can avoid the effects of pH and enzyme on the medicine, but also can make the herb absorbed completely and prolong the time of drug action. Then, colonic mucous membrane will recover gradually to normal with healing of the ulcers. Volatile oil extract of fresh Heartleaf houttuynia is used to produce Heartleaf houttuynia injection. Its utility components (Houttuynin, lauraldehyde, quercitrin, isoquercitrin, etc.) are higher than that of Heartleaf houttuynia herb with widespread pharmacological actions. For instance, relaxation of intestinal smooth muscle could relieve enterospasm, prolong the retention time of intestinal contents, alleviate and eliminate the symptoms of diarrhea and abdominal pain^[8,24,25]. Quercitrin and isoquercitrin can ameliorate capillary fragility for haemostasis, which lead to the stoppage of bloody stool. Pathological changes, such

as swollen mitochondria with depleted ridge, shortened microvilli, maldevelopment of goblet cells and increased epithelial cell apoptosis could be found on the surface of mucous membrane and recess prior to Heartleaf houttuynia herb injection treatment. All these results in malabsorption of water with symptoms of diarrhea, while the increase of epithelial cell apoptosis can lead to the formation of ulcer due to damage of the colonic mucous membrane barrier. The expression of CD54 can further promote the inflammatory reaction. After treatment with Heartleaf houttuynia herb injection, epithelial cell apoptosis^[11], swollen mitochondria, shortened microvilli and the expression of CD54 could recover to normal gradually, which led to plerosis of colonic mucous membrane and healing of ulcer, the effect was superior to that of SASP. Heartleaf houttuynia herb is not only a medicine, but also a safe edible plant. The pH and osmotic pressure of the injection are close to those of intrinsic human environment, so there are no adverse reactions in Heartleaf houttuynia herb therapy, while SASP therapy may have side effects such as the heartburn, increased ALT, decrease WBC and rash.

UC patients often have symptoms of diarrhea, abdominal pain and tenesmus. Are these symptoms related to colonic motility disturbance? In this study, compared with the normal persons, the mean promotive speed of contraction wave stepped up and the mean amplitude of wave decreased in active UC patients, which led to diarrhea. The gastrocolic hyperreflex resulted in awareness of defecation and abdominal pain after eating that could be relieved after defecation. These two indexes improved significantly after treatment with Heartleaf houttuynia herb ($P < 0.05$). In normal persons, the postprandial pressure of sigmoid was higher than that of descending colon and splenic flexure, the pressure gradient and segmental construction made the colonic contents mixed and milled to expose to the colonic mucous membrane fully. Reabsorption of water and electrolytes were thus promoted. In active UC patients, the colonic pressure was significantly decreased ($P < 0.05$), and there was no pressure gradient in different colonic loci which could lead to disturbance of reabsorption of water and electrolytes. Diarrhea occurred due to the decrease of segmental construction and also inflammation of colonic mucosa occurred. The pain threshold of distant colon in active UC patients decreased significantly compared with that of normal persons, indicating that the distant colonic sensibility was increased. So, a small amount of intestinal contents could stimulate defecation reflex, leading to symptoms of diarrhea^[23], abdominal pain and tenesmus. After treatment with Heartleaf houttuynia herb, the colonic pressure and pain threshold recovered to normal due to the following reasons. Heartleaf houttuynia caused relaxation of intestinal smooth muscle which could relieve the enterospasm, prolong the retention time of intestinal contents, alleviate and eliminate the symptoms of diarrhea and abdominal pain. Our prophase study proved that Heartleaf houttuynia herb could improve the colonic motility disturbance of UC rats. In this study, the remission of diarrhea and abdominal pain might be partly related to this. Heartleaf houttuynia herb also has anti-inflammatory actions as we have proven in our previous animal study, which led to the remission of symptoms.

The main component of Kangshuangling sublingual tablets is low molecular mass (molecular mass ranged from 5-15 ku, peak ranged from 5-8 ku) heparin substance. Each tablet contains 1 200IU LMWH, which can be absorbed by the sublingual mucosa, so it not only has no first-pass effects by the liver compared with oral LMWH used in our previous study^[29], but also has no inconvenience of injection. Heparin, a group of sulphated glycosaminoglycans, in addition to its physiological effects and anticoagulant, antithromboembolic, antiallergic, antiviral, antiendotoxic and immunoregulative biological activities, has been found with a wide range of potentially anti-

inflammatory effects, including inhibition of neutrophil elastase and inactivation of chemokines^[40]. Compared with heparin, LMWH has higher antithromboembolic effects, longer half life period, less bleeding tendency, higher bioavailability, easier absorption by sublingual administration, as well as anti-inflammatory effects^[29,41]. Previous reports^[29] on improvement of UC patients treated with heparin prompted us to perform a pilot study of Kangshuangling sublingual tablets to find a more convenient and effective drug for patients with refractory UC. The observed response to Kangshuangling sublingual tablets was paradoxical. Sixteen of 18 patients with refractory UC unresponsive to high-dose prednisolone and sulfasalazine therapy for more than 4 wk achieved clinical remission and became asymptomatic after treatment of Kangshuangling sublingual tablets in combination with sulfasalazine. Contrary to the traditional idea that heparin could enhance bleeding, rectal bleeding was the first symptom to be improved by Kangshuangling sublingual tablets. The results were similar to other reports of heparin treatment^[42,43].

If Kangshuangling sublingual tablets have a therapeutic effect on UC, their mechanism of action should shed some lights on the elusive pathogenesis of this disease. Several thrombophilic features of UC that suggest the effect of Kangshuangling sublingual tablets on colitic symptoms may be attributable to their anticoagulant and antithrombotic properties. Evidences of a thrombotic process in UC included: reports of a hypercoagulable state^[20,22], an increased incidence of thromboembolic event^[44], and ischemic complications such as toxic megacolon and pyoderma gangrenosum. In this study, the membrane marks of platelet activity CD62p and CD63 were increased significantly, and the derivative of active platelet TXA2 was also elevated, suggesting that blood platelet TXA2 was in an active state, which not only led to a hypercoagulable state and an increased incidence of thromboembolic events, but also enhanced inflammatory reaction^[20,22]. Activated hyperaggregable platelets in the mesenteric circulation could amplify the inflammatory cascade by promoting neutrophil recruitment and chemotaxis. P-selectin has an established action as the adhesion molecule for neutrophils, and circulating platelet aggregates may contribute to ischemic damage and infarction by occluding the intestinal microvasculature. Platelets derived thromboxane A₂ may also contribute to ischemia by inducing local vasoconstriction. After treatment with Kangshuangling sublingual tablets, all these parameters dropped markedly, suggesting that the therapeutic effect of LMWH was partly related to inhibition of platelet activity, and improvement of hypercoagulable state, leading to the remission of clinical symptoms. But the membrane marks of platelet CD62p and CD63 were still higher than those of the normal controls. Whether it has predictive value for recurrence or prognosis should be further studied.

CD54 antigen could react with 85-110 ku integral membrane glycoprotein, and it is also known as an intercellular adhesion molecule-1 (ICAM-1) expressed on endothelial cells and both resting (weak) and activated (moderate) lymphocytes and monocytes^[15]. CD54 is ligand for the leukocyte function antigen-1 (CD11a). Its expression was up-regulated upon stimulation by inflammatory mediators such as cytokines and LPS, and it was involved in B cell-T cell co-stimulatory interactions. In this study, CD54 elevated significantly in blood and tissues of UC patients, being higher in tissues than in blood. Therefore, it could reflect the inflammation of intestinal mucosa. After treatment with Kangshuangling sublingual tablets, CD54 dropped significantly in both blood and tissues, indicating that Kangshuangling sublingual tablets could relieve the inflammatory activity in refractory UC patients who received high-dose prednisolone and sulfasalazine therapy for a long period (more than 4 wk) without significant improvement and

were regarded as corticosteroid-resistant refractory cases of UC. It was reported that heparin could also inhibit c-reactive protein (CRP), tumor necrosis factor (TNF) and L-selectin of UC patients. The detailed mechanisms by which anti-inflammatory properties of oral L MWH are mediated in UC remain to be elucidated further.

The multidrug resistance (MDR) gene coding for a drug efflux pump P-glycoprotein 170(Pgp-170) expressed on the surface of lymphocytes and intestinal epithelial cells^[38,39]. In this study, Pgp-170 was elevated significantly in blood and tissues of refractory UC patients. Poor response to medical therapy of certain UC patients might be related to MDR expression because glucocorticoids are known Pgp-170 substrates. There was no difference of Pgp-170 in tissues and blood, indicating that peripheral blood lymphocyte (PBL) MDR remained stable over time and was not influenced by disease activity or glucocorticoid therapy, both PBL and mucosal MDR expression appeared independent of disease activity, and there was a significant correlation between PBL and MDR expression and intestinal epithelial lymphocyte and epithelial cell expression^[38,39]. After treatment with Kangshuangling sublingual tablets, Pgp-170 dropped significantly in both blood and tissues, indicating that Kangshuangling sublingual tablet could inhibit the expression of MDR, but Pgp-170 was still higher than that of the normal controls, indicating that PBL and mucosal MDR may play an important role in determining the response of refractory UC patients to glucocorticoid therapy. From these results, we conclude that Kangshuanling sublingual tablets may play a role in treating refractory UC with activated platelets, the mechanism is partly related to the inhibition of platelet activity, hypercoagulable state, MDR expression, and its anti-inflammatory effects. No complications are found to be associated with the use of Kangshuanling sublingual tablets. It is still the focus of study in treating refractory UC with the Chinese features^[3].

REFERENCES

- 1 **Jiang XL**, Wang ZK, Qin CY. Current research and strategy on ulcerative colitis in China. *Shijie Huaren Xiaohua Zazhi* 2000; **8**: 610-613
- 2 **Jiang XL**, Quan QZ, Liu T, Dong XC. Recent advances in research of ulcerative colitis. *Shijie Huaren Xiaohua Zazhi* 2000; **8**: 216-218
- 3 **Jiang XL**, Cui HF. An analysis of 10218 ulcerative colitis cases in China. *World J Gastroenterol* 2002; **8**: 158-161
- 4 **Jiang XL**, Cui HF. Features of ulcerative colitis cases in China: An analysis of 10218 cases. *Shijie Huaren Xiaohua Zazhi* 2001; **9**: 869-873
- 5 **Jiang XL**. Strength the analysis of digestive diseases. *Shijie Huaren Xiaohua Zazhi* 2001; **9**: 864-868
- 6 **Jiang XL**, Cui HF. A new chronic ulcerative colitis model produced by combined methods in rats. *World J Gastroenterol* 2000; **6**: 742-746
- 7 **Jiang XL**, Quan QZ, Wang D, Sun ZQ, Wang YJ. A new ulcerative colitis model induced by compound method and the change of immune and ultrastructure. *Shijie Huaren Xiaohua Zazhi* 1999; **7**: 381
- 8 **Jiang XL**, Quan QZ, Wang D, Sun ZQ, Wang YJ, Qi F. Experimental study of heartleaf houttuynia herb on ulcerative colitis. *Shijie Huaren Xiaohua Zazhi* 1999; **7**: 786
- 9 **Jiang XL**, Quan QZ, Sun ZQ, Wang YJ, Qi F, Wang D, Zhang XL. Expression of lymphocyte apoptosis in patients with ulcerative colitis. *Shijie Huaren Xiaohua Zazhi* 1999; **7**: 903-904
- 10 **Jiang XL**, Quan QZ, Cheng GR, Sun ZQ, Wang YJ, Wang YP. Expression of apoptosis on biopsy tissue in patients with ulcerative colitis. *Shijie Huaren Xiaohua Zazhi* 2000; **8**: 107-108
- 11 **Jiang XL**, Pan BR, Ma JY, Ji ZH, Ma LS. Review for the 20th century and prospect for the 21st century of digestology. *Shijie Huaren Xiaohua Zazhi* 2000; **8**: 1161-1176
- 12 **Xu NZ**. Expression of adhesion molecules in tissues and pe-

- ripheral lymphocyte of patients with ulcerative colitis. *Huaren Xiaohua Zazhi* 1998; **6**(Suppl 7): 54-55
- 13 **Jiang XL**, Quan QZ, Sun ZQ, Wang YJ, Qi F, Wang D, Zhang XL. Detection of soluble CD44v6 in patients with inflammatory bowel disease. *Shijie Huaren Xiaohua Zazhi* 1999; **7**: 1028
 - 14 **Jiang XL**, Quan QZ, Chen GR, Sun ZQ, Wang YJ, Qi F, Wang D. Detection of CD44v6 on biopsy tissue can't differ ulcerative colitis from Chron's disease. *Zhonghua Xiaohua Neijing Zazhi* 2000; **19**: 298-299
 - 15 **Jiang XL**, Quan QZ, Chen GR, Yin GP, Sun ZQ, Wang YJ. Detection of CD54, CD44 on biopsy tissues in patients with ulcerative colitis. *Zhonghua Xiaohua Neijing Zazhi* 1998; **15**: 292-294
 - 16 **Jiang XL**, Quan QZ, Sun ZQ, Wang YJ, Qi F, Yin GP, Sun XM. Detection of adhesion molecules in tissues and peripheral blood of patients with ulcerative colitis. *Zhonghua Weishengwu He Mianyixue Zazhi* 1998; **18**: 156
 - 17 **Jiang XL**, Quan QZ, Sun ZQ, Wang YJ, Qi F. Effect of glucocorticoid on lymphocyte adhesion molecule phenotype expression in patients with ulcerative colitis. *Zhongguo Weizhongbing Jijiu Yixu* 1998; **10**: 366-368
 - 18 **Jiang XL**, Quan QZ, Sun ZQ, Wang YJ, Qi F, Chen GR, Gao TS, Pan X. Detection of P-selectin and CD63 in peripheral blood of patients with ulcerative colitis. *Zhongguo Weizhongbing Jijiu Yixue* 1998; **10**: 174-175
 - 19 **Jiang XL**, Quan QZ, Sun ZQ, Wang YJ. Detection of P-selectin and CD63 in patients with ulcerative colitis. *Shanghai Mianyixue Zazhi* 1998; **18**: 230
 - 20 **Jiang XL**, Quan QZ, Liu TT, Wang YJ, Sun ZQ, Qi F, Ren HB, Zhang WL, Zhang L. Detection of blood platelet activation in patients with ulcerative colitis. *Xin Xiaohuabingxue Zazhi* 1997; **5**: 736
 - 21 **Jiang XL**, Quan QZ, Wang D, Sun ZQ, Wang YJ. One case report of ulcerative colitis accompanied with acute myocardial infarction. *Shijie Huaren Xiaohua Zazhi* 1999; **7**: 963
 - 22 **Jiang XL**, Quan QZ, Sun ZQ, Wang YJ, Qi F. Relationship between syndrome-typing of ulcerative colitis and activation of platelet. *Zhongyi Zazhi* 1997; **38**: 730-731
 - 23 **Jiang XL**, Quan QZ, Wang YJ, Sun ZQ, Wang D, Qi F. Measurement of rectual and annual motility in patients with ulcerative colitis. *Zhonghua Xiaohua Neijing Zazhi* 2000; **17**: 170-171
 - 24 **Jiang XL**, Quan QZ, Dong XC, Liu T. Effects of houttuynia herb on rectual and annual motility in patients with ulcerative colitis. *Zhongyiyao Xubao* 2000; **4**: 43-44
 - 25 **Jiang XL**, Quan QZ, Wang D, Sun ZQ, Wang YJ, Qi F. Effect of heartleaf houttuynia herb on colonic pressure in rats with ulcerative colitis. *Shijie Huaren Xiaohua Zazhi* 1999; **7**: 639
 - 26 **Zhang ZD**, Chen J, Zhong YW, Zhang ST. Strength the diagnosis and treatment of ulcerative colitis. *Shijie Huaren Xiaohua Zazhi* 2003; **11**: 1027-1028
 - 27 **Jiang XL**. Diagnosis and treatment of ulcerative colitis. *Shijie Huaren Xiaohua Zazhi* 2000; **8**: 332
 - 28 **Jiang XL**, Quan QZ, Wang ZK. Diagnosis, typing and effect criteria of ulcerative colitis. *Shijie Huaren Xiaohua Zazhi* 2000; **8**: 332-334
 - 29 **Cui HF**, Jiang XL. Treatment of corticosteroid resistant ulcerative colitis with oral low molecular weight heparin. *World J Gastroenterol* 1999; **5**: 448-450
 - 30 **Jiang XL**, Qin CY, Li GQ. Special treatment for ulcerative colitis. *Shijie Huaren Xiaohua Zazhi* 2000; **8**: 341-342
 - 31 **Jiang XL**, Liu T. Treatment of refractory ulcerative colitis with heparin. *Shijie Huaren Xiaohua Zazhi* 1999; **7**: 694
 - 32 **Jiang XL**, Quan QZ, Sun ZQ, Wang YJ, Shang RL, Qi F. Clinical study on ulcerative colitis treated with Heartleaf houttuynia herb injection. *Shijie Huaren Xiaohua Zazhi* 2003; **11**: 1207-1210
 - 33 **Jiang XL**, Quan QZ, Sun ZQ, Wang YJ, Shang RL, Qi F. A control study on ulcerative colitis treated with olsalazine sodium. *Shijie Huaren Xiaohua Zazhi* 2003; **11**: 1211-1213
 - 34 **Jiang XL**, Quan QZ, Sun ZQ, Wang YJ, Shang RL, Qi F. Treatment of refractory ulcerative colitis with Kangshuangling. *Shijie Huaren Xiaohua Zazhi* 2003; **11**: 1214-1218
 - 35 **Chinese Society of Gastroenterology**. Suggestion on the diagnosis and treatment of inflammatory bowel diseases. *Zhonghua Neike Zazhi* 2001; **40**: 138-141
 - 36 **Gaffney PR**, Doyle CT, Gaffney A, Hogen J, Hayes DP, Annis P. Paradoxical response to heparin in 10 patients with ulcerative colitis. *Am J Gastroenterol* 1995; **90**: 220-223
 - 37 **Collins CE**, Cahill MR, Newland AC, Rampton DS. Platelets circulate in an activated state in inflammatory bowel disease. *Gastroenterology* 1994; **106**: 840-845
 - 38 **Farrell RJ**, Murphy A, Long A, Donnelly S, Cherikuri A, O'Toole D, Mahumd N, Keeling PW, Weir DG, Kelleher D. High multidrug resistance (P-glycoprotein 170) expression in inflammatory bowel disease patients who fail medical therapy. *Gastroenterology* 2000; **118**: 279-288
 - 39 **Yacyszyn B**, Maksymowycz W, Bowen-Yacyszyn MB. Differences in P-glycoprotein -170 expression and activity between Chron's disease and ulcerative colitis. *Hum Immunol* 1999; **60**: 677-687
 - 40 **Tyrrell DJ**, Kilfeather S, Page CP. Therapeutic uses of heparin beyond its traditional role as an anticoagulant. *Trends Pharmacol Sci* 1995; **16**: 198-204
 - 41 **Jiang XL**, Cui HF, Wang YJ, Quan QZ, Sun ZQ. Effects of oral low molecular weight heparin on hemorrheology of rabbit liver damaged by D-galactosamine. *Xin Xiaohuabingxue Zazhi* 1997; **5**: 355-356
 - 42 **Folwaczny C**, Frike H, Endres S, Hartmann G, Jochum M, Loeschke K. Anti-inflammatory properties of unfractionated heparin in patients with highly active ulcerative colitis: a pilot study. *Am J Gastroenterol* 1997; **92**: 911-912
 - 43 **Evans RC**, Wong VS, Morris AI, Rhodes JM. Treatment of corticosteroid-resistant ulcerative colitis with heparin: a report of 16 cases. *Aliment Pharmacol Ther* 1997; **11**: 1037-1040
 - 44 **Koenigs KP**, Mcphedran P, Spiro HM. Thrombosis in inflammatory bowel disease. *J Clin Gastroenterol* 1987; **9**: 627-631

Edited by Wang XL Proofread by Xu FM

• CLINICAL RESEARCH •

Effects of probiotic on intestinal mucosa of patients with ulcerative colitis

Hai-Hong Cui, Cun-Long Chen, Ji-De Wang, Yu-Jie Yang, Yong Cun, Jin-Bao Wu, Yu-Hu Liu, Han-Lei Dan, Yan-Ting Jian, Xue-Qing Chen

Hai-Hong Cui, Cun-Long Chen, Ji-De Wang, Yu-Jie Yang, Yong Cun, Jin-Bao Wu, Yu-Hu Liu, Han-Lei Dan, Yan-Ting Jian, Xue-Qing Chen, Chinese PLA Institute of Digestive Medicine, First Military Medical University, Guangzhou 510515, Guangdong Province, China

Correspondence to: Dr. Cun-Long Chen, Department of Gastroenterology, Chinese PLA Institute of Digestion Medicine, First Military Medical University, Guangzhou 510515, Guangdong Province, China. cunlong@fimmu.edu.cn

Telephone: +86-20-61641544 **Fax:** +86-20-61641530

Received: 2003-05-11 **Accepted:** 2003-06-27

Abstract

AIM: To investigate the effects of probiotic on intestinal mucosae of patients with ulcerative colitis (UC), and to evaluate the role of probiotic in preventing the relapse of UC.

METHODS: Thirty patients received treatment with sulphasalazine (SASP) and glucocorticoid and then were randomly administered bifid triple viable capsule (BIFICO) (1.26 g/d), or an identical placebo (starch) for 8 wk. Fecal samples were collected for stool culture 2 wk before and after the randomized treatments. The patients were evaluated clinically, endoscopically and histologically after 2 mo of treatment or in case of relapse of UC. p65 and I κ B expressions were determined by Western blot analysis. DNA-binding activity of NF- κ B in colonic nuclear extracts was detected by electrophoretic mobility shift assay (EMSA). mRNA expressions of cytokines were identified by semi-quantitative assay, reverse transcriptase-polymerase chain reaction (RT-PCR).

RESULTS: Three patients (20%) in the BIFICO group had relapses during 2-mo follow-up period, compared with 14 (93.3%) in placebo group ($P < 0.01$). The concentration of fecal lactobacilli, bifidobacteria was significantly increased in BIFICO-treated group only ($P < 0.01$). The expressions of NF- κ B p65 and DNA binding activity of NF- κ B were significantly attenuated in the treatment group than that in control ($P < 0.05$). The mRNA expression of anti-inflammatory cytokines was elevated in comparison with the control group.

CONCLUSION: The probiotic could impede the activation of NF- κ B, decrease the expressions of TNF- α and IL-1 β and elevate the expression of IL-10. These results suggest that oral administration of this new probiotic preparation is effective in preventing flare-ups of chronic UC. It may become a prophylactic drug to decrease the relapse of UC.

Cui HH, Chen CL, Wang JD, Yang YJ, Cun Y, Wu JB, Liu YH, Dan HL, Jian YT, Chen XQ. Effects of probiotic on intestinal mucosa of patients with ulcerative colitis. *World J Gastroenterol* 2004; 10(10): 1521-1525

<http://www.wjgnet.com/1007-9327/10/1521.asp>

INTRODUCTION

Ulcerative colitis (UC) is a chronic disease and easy to relapse, its etiology and pathogenesis have not been definitively elaborated^[1]. Primary therapy for UC is usually a combination of sulfasalazine and glucocorticoids. Sulfasalazine can be given alone or in combination with other drugs. However, a large number of patients are resistant or intolerant to sulfasalazine. Glucocorticoids suppress active inflammation very effectively, but its long-term use is associated with high rates of relapse and unacceptable toxicities. Recently, probiotic has been recommended to ameliorate the milieu of intestine and prolong the time of relapse^[2-14]. This study intended to evaluate the role of bifidobacteria in remission of UC.

MATERIALS AND METHODS

Sample collection and processing

Thirty active UC patients were recruited for this study from 2001 to 2002 at Nanfang Hospital. Severity of the disease in colon and rectum was assessed by one gastroenterologist with an endoscope. These patients on sulphasalazine (SASP) and glucocorticoid had clinical and endoscopic remission and were randomized to receive either bifid triple viable capsule (BIFICO) (1.26 g/d), or an identical placebo (starch) for 8 wk. Biopsy specimens were obtained with standard biopsy forceps to include the most macroscopically inflamed site with UC and immediately frozen in liquid nitrogen and stored at -80 °C for RNA and protein extraction. Meanwhile, fecal samples were collected for stool culture before and after 2 wk of treatments. Patients were assessed clinically, endoscopically and histologically after a 2-mo period of treatment or in case of relapse of UC.

Fecal analysis

Fecal samples were collected for microbiological examinations. We prepared the selective medium to incubate ten strains of luminal resident bacteria in large intestine. *Enterobacteria* (EMB), *Enterococcus* (EC), *Staphylococcus* (SP) and *Saccharomyces* (yeast) (SB) are aerobes. *Bacteroides* (BD), *Bifidobacterium* (BL), *Lactobacillus* (LC), *Peptococcus* (PS), *Eubacterium* (ES) and *Clostridium* (CD) are anaerobes. 0.5 g feces in a small bottle containing 4.5 mL diluted solution and 4-5 beads were concussed 1 min on a vortex agitator, 1.8 mL diluted solution was added to each of other 7 bottles. The solution was diluted in series as 10⁻², 10⁻³, ...10⁻⁸, respectively. Aerobes and anaerobes were observed 24 h and 72 h after incubation at 37 °C.

Preparation of cytoplasmic and nuclear extracts

Nuclear extracts from biopsy tissues were prepared by the method of Deryckere and Gannon^[15]. Frozen tissue was ground with a mortar in liquid nitrogen and transferred to a tissue homogenizer. Protease inhibitor cocktail (Sigma) was added and centrifuged at 2 000 r/min for 30 s. Supernatant was incubated on ice for 5 min and then centrifuged at 5 000 r/min for 5 min. The final supernatant containing cytoplasmic extracts was collected and stored at -80 °C. Pelleted nuclei were then resuspended in 50-100 μ L of buffer G and incubated on ice for 20 min.

The lysed nuclei were then transferred to a microcentrifuge tube, centrifuged at 12 000 r/min for 10 min, and the supernatant containing the nuclear extracts was collected and stored at -80 °C. Protein concentration was determined with BCA-protein estimation kit.

Western blot analysis

For each sample, an equal amount (50 µg) of protein lysates was analyzed on 100 g/L or 120 g/L sodium dodecyl sulfate-polyacrylamide gel. Proteins were electroblotted onto Immobilon PVDF membranes (Millipore, Bedford, MA), blocked in 50 g/L dry skim milk for 1 h, and then incubated with the indicated antibodies. The antibodies used were 1:700 rabbit polyclonal anti-NF-κB and IκB antibodies, the secondary antibodies used were provided in an enhanced chemiluminescence detection kit (Santa Cruz, CA). Exposure time (5-60 s) varied with the antibodies used.

Electrophoretic mobility shift assays

DNA-binding activity of NF-κB in colon nuclear extracts was determined by electrophoretic mobility shift assay (EMSA). The sequence of NF-κB probe was 5' -AGT TGA GGG GAC TTT CCC AGG C-3' [16], 10 µg of nuclear protein was incubated at room temperature for 20 min with radiolabeled [γ -³²P] ATP using T4 polynucleotide kinase. A 20 µL reaction buffer contained 2 µg poly dI-dC (Sigma), 10 mmol/L tris-HCl (pH7.5), 100 mmol/L NaCl, 10 mmol/L EDTA, 20 mmol/L MgCl₂, 10 mmol/L DTT, 3 µL of 250 mL/L glycerol and 1 µL of labeled probe. For competition assays, 100-fold molar excess of unlabeled oligonucleotide was added to the binding reaction. Nucleoprotein- oligonucleotide complexes were resolved by electrophoresis on a 50 g/L non-denaturing polyacrylamide gel (PAGE; acrylamide/bisacrylamide at 30:1) in 0.1×TBE buffer at 150 V for 2 h at 4 °C. The gel was dried and autoradiographed with intensifying screen at -80 °C for 72 h. The radioactivity of appropriate bands was counted using a BAS2000 phosphorimage analyzer (Fuji Film, Minamiasigara, Japan).

Proinflammatory and inhibitive factor mRNA detected by RT-PCR

Total RNA was isolated from biopsies using TRIzol reagent (Life Technologies). cDNA was generated from 1 µg of total RNA in a reaction volume of 20 µL, using M-MLV reverse transcriptase (MBI). PCR was performed in the linear range of amplification (determined for each primer pair-cDNA combination). Standard PCR reactions were performed with 1 µL of the cDNA solution, 50 µmol/L of each primer solution, 10 mmol/L of each Dntp, 25 mmol/L MgCl₂, 10× Goldstar DNA polymerase reaction buffer, and 0.5 units of Goldstar DNA polymerase (Eurogentec, Seraing, Belgium). Each PCR cycle was performed at 94 °C for 1 min, at 56 °C for 1 min, and at 72 °C for 1 min, respectively. Following sense / antisense primers were designed to amplify cDNA fragments^[17,18]: glyceraldehyde-3-phosphate dehydrogenase (G3PDH): sense primer: 5' -ACCACAGTCCATGCCATCAC-3', antisense: 5' -TCCACCACCTGTGCTGTGTA-3' (452 bp); TNF-α: sense primer: 5' -CTGTA GCCATGTTGTAGC-3', antisense: 5' -CAATGATCCCAAAGTAGACCT-3' (467 bp); IL-1β: sense primer: 5' -CAGCCATGGCAGAAGTACCT-3', antisense: 5' -GGCCACAACAAGTACG C-3' (223 bp); IL-10: sense primer: 5' -CTGAGGCGCTGTCATCG ATT-3', antisense: 5' -AGGTCCTGGAGTCCAGCAGA-3' (328 bp). The PCR products were then visualized on a 10 g/L agarose gel by ethidium bromide (5 µg/mL) staining.

Statistical analysis

All results were expressed as mean±SD. Statistical differences between means were determined using independent-sample *t* test and paired-sample *t* test by SPSS 10.0 statistical software.

A *P* value ≤0.05 was considered statistically significant.

RESULTS

Fecal analysis

The number of fecal bacteria before treatment in these 2 groups had no significant difference. After treatment, the fecal specimens of the patients on BIFICO were obviously different from the patients on placebo. The number of Gram-positive Bacilli and Enterococci was significantly higher than that in control group. The number of *Enterococci*, *Bacteroides* and *Bifidobacteria* was obviously less than that in control group (*P*<0.05). In control group, the number of *Bifidobacteria* (6.44 ± 0.25 , *P*<0.01) and Lactobacilli (6.67 ± 0.43 , *P*<0.05) was less than that in treatment group (Table 1).



Figure 1 Expressions of NF-κBp65 and IκB in nuclei and cytoplasm. A: Expression of NF-κBp65 in nuclei, B: Expression of IκB in cytoplasm, Lanes1-2: expression before treatment, Lanes3: expression after probiotics treatment, Lanes4: expression in control.

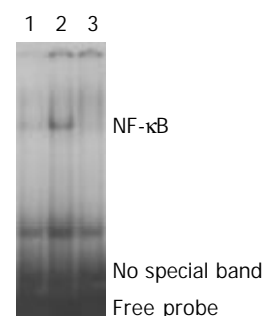


Figure 2 Inhibition of NF-κB binding DNA by BIFICO. 1, Cool probe; 2, Activation NF-κB before treatment; 3: Probiotic significantly inhibited activation of NF-κB.

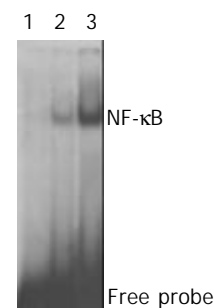


Figure 3 Activation of NF-κB in. Placebo group 1, Cool probe; 2, Activation of NF-κB before treatment; 3, Placebo did not obviously inhibit the activation of NF-κB.

NF-κB and IκB examination

The degradation of IκB in cytoplasm was obviously inhibited by BIFICO and NF-κB in nuclei was less expressed after treatment (*P*<0.05) (Figures 1, Table 2).

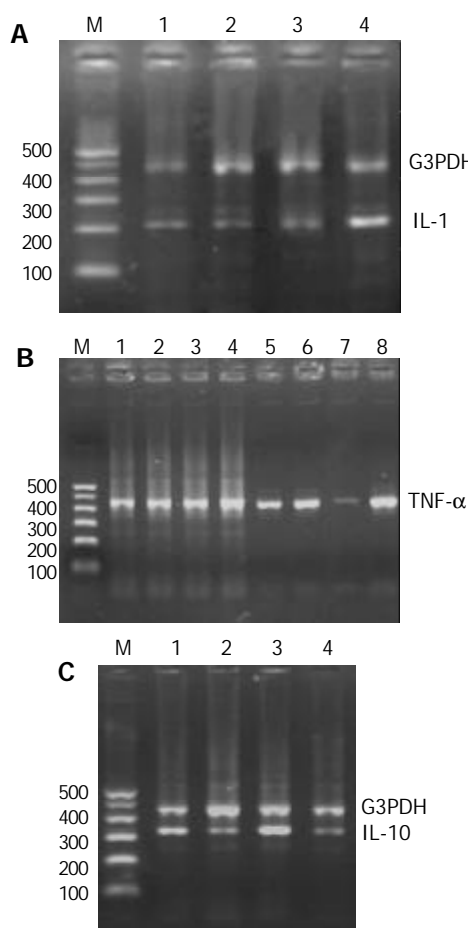


Figure 4 Expressions of IL-1 mRNA, TNF- α mRNA and IL-10 mRNA. A: Expression of IL-1 mRNA, Lanes 1,2: IL-1 mRNA expression before treatment; lane 3: BIFICO inhibited IL-1 mRNA expression; lane 4: IL-1 mRNA expression in placebo group. B: Expression of TNF- α mRNA, Lanes 1,2,3,4 G3PDH; lanes 5,6: TNF- α mRNA expression before treatment; Lane 7: BIFICO inhibited significantly mRNA expression of TNF- α ; lane 8: TNF- α mRNA expression in placebo group. C: Expression of IL-10 mRNA, Lanes 1,2: IL-10 mRNA before treatment; lane 3: BIFICO enhanced IL-10 mRNA expression; lane 4: IL-10 mRNA in placebo group.

Table 1 Flora analysis (mean \pm SD, Lg10ⁿ/g)

Index	BIFICO group		Placebo group	
	Pretreatment (n=15)	Post-treatment (n=15)	Pretreatment (n=15)	Post-treatment (n=15)
EMB	8.21 \pm 0.69	8.11 \pm 0.29	8.23 \pm 0.42	8.93 \pm 0.62 ^{ac}
EC	6.63 \pm 0.21	7.20 \pm 0.31 ^a	6.71 \pm 0.39	6.67 \pm 0.48 ^c
SP	3.55 \pm 0.96	3.61 \pm 0.19	3.65 \pm 0.41	3.72 \pm 0.30
SB	3.45 \pm 0.83	3.09 \pm 0.25 ^a	3.36 \pm 0.35	3.47 \pm 0.96
BD	6.79 \pm 0.29	7.26 \pm 0.03 ^a	6.77 \pm 0.88	6.81 \pm 0.35
BL	6.92 \pm 0.34	7.69 \pm 0.34 ^b	7.03 \pm 0.34	6.44 \pm 0.25 ^{bd}
PS	7.26 \pm 0.61	7.32 \pm 0.74	6.78 \pm 0.59	6.93 \pm 0.52
LC	6.95 \pm 0.52	7.39 \pm 0.72 ^a	7.07 \pm 0.97	6.67 \pm 0.43 ^c
ES	5.91 \pm 0.92	5.45 \pm 0.25	5.45 \pm 0.67	5.68 \pm 0.80
CD	6.18 \pm 0.78	6.13 \pm 0.66	6.19 \pm 0.72	6.37 \pm 0.96

^a P <0.05, ^b P <0.01 vs post-treatment; ^c P <0.05, ^d P <0.01 vs control. EMB: *Enterobacter*; EC: *Enterococcus*; SP: *Staphylococcus*; SB: *Saccharomyces* (yeast); BD: *Bacteroides*; BL: *Bifidobacterium*; LC: *Lactobacillus*; PS: *Peptococcus*; ES: *Eubacterium*; CD: *Clostridium*.

Activation of NF- κ B in nuclei

The results of EMSA showed that activation of NF- κ B was

elevated in patients who did not take BIFICO in comparison with pretreatment, more NF- κ B was combined with special recognition sites of DNA (P <0.05, Figures 2,3).

Table 2 Expression of NF- κ B (nucleus) and I κ B (cytoplasm) before and after therapy (mean \pm SD)

Index	BIFICO group		Placebo group	
	Pretreatment	Post-treatment	Pretreatment	Post-treatment
I κ B (cytoplasm)	0.99 \pm 0.11	0.97 \pm 0.07	0.89 \pm 0.08	0.43 \pm 0.15 ^{bd}
NF- κ B (nucleus)	0.82 \pm 0.05	0.31 \pm 0.05 ^b	0.79 \pm 0.14	0.97 \pm 0.09 ^d

^a P <0.05, ^b P <0.01 vs post-treatment; ^c P <0.05, ^d P <0.01 vs control.

Expression of IL-1- β , TNF- α , IL-10 mRNA

IL-1- β , TNF- α , IL-10 mRNAs in both groups were determined with RT-PCR. In control group, the level of IL-1- β , TNF- α mRNA at intestinal epithelial mucosa did not significantly decrease. (P <0.05, Figures 4, Table 3).

Table 3 mRNA expression of cytokines before and after therapy (OD value, mean \pm SD)

Index	BIFICO group		Placebo group	
	Pretreatment	Post-treatment	Pretreatment	Post-treatment
IL-1	0.41 \pm 0.09	0.53 \pm 0.11	0.38 \pm 0.12	1.20 \pm 0.08 ^d
TNF- α	0.79 \pm 0.06	0.35 \pm 0.12 ^b	0.86 \pm 0.05	1.40 \pm 0.18 ^d
IL-10	0.76 \pm 0.32	1.11 \pm 0.21 ^b	0.54 \pm 0.26	0.45 \pm 0.04 ^d

^a P <0.05, ^b P <0.01 vs post-treatment; ^c P <0.05, ^d P <0.01 vs control.

DISCUSSION

The pathogenesis of UC remains unknown. Genetic and environmental factors are obviously contributory. Luminal bacteria could play a major role in the initiation and perpetuation of chronic UC^[14,19-21]. Thousand of endogenous bacteria live in the large intestine and may be an essential factor in certain pathological disorders. Animal models of UC showed that colitis did not occur in a germ-free environment. In human UC, inflammation is present in parts of the gut housing the highest concentration of bacteria. Moreover, terminal ileum, caecum and rectum are relatively static, providing prolonged mucosal contact with luminal contents. Enhanced mucosal permeability may play a pivotal role in maintaining a chronic inflammatory state due to a genetic predisposition or direct contact with bacteria or their products. So far, no specific micro-organism has been directly associated with the pathogenesis of UC. Analysis of the luminal enteric flora, however, has revealed differences in the composition of this flora to healthy controls. In UC, concentrations of *Bacteroides*, *Eubacteria*, *Peptostreptococci* and facultative anaerobic bacteria are increased, whereas the number of *Bifidobacteria* is significantly reduced. Over the past few years, use of probiotics in IBD and other intestinal disorders has gained attention. Manipulation of the colonic bacteria with antibiotics and probiotics proved to be more effective and tolerable than immunosuppressants^[11,22]. Probiotics and prebiotics have a role in prevention or treatment of some diseases. The mechanisms through which dysregulation may play a central role in initiation and perpetuation of inflammatory bowel disease were discussed^[23]. BIFICO probiotic capsule was used for *Enterococci*, *Bifidobacteria*, *Lactobacilli* triple viable bacteria, probiotics such as VSL#3 could also be used to maintain clinical remission and prevent relapse in patients with

relapsing or chronic pouchitis. Therapy with anti-inflammatory agents and immunomodulators were often required for patients with chronic pouchitis resistant to antibiotics^[24,25]. Probiotic *Lactobacillus rhamnosus* GG (LGG) has proved to be beneficial to the treatment of viral- and antibiotic-associated diarrhea. Nitric oxide (NO) is involved in the protective mechanisms in the gastrointestinal tract and may contribute to some of the beneficial effects of probiotics. LGG induces NO production in J774 macrophages and in human T84 colon epithelial cells through induction of iNOS by a mechanism involving activation of transcription factor NF- κ B. Induction of iNOS and low-level synthesis of NO might be involved in the protective actions of LGG in the gastrointestinal tract^[26]. Recent results supported the concept that intestinal bacteria could induce endogenous signals that play a pathogenic role in hepatic insulin resistance and NAFLD and suggest novel therapies for these common conditions^[27,28]. We discovered that the high concentration of Gram-positive bacteria in luminal flora could effectively prolong the time of relapse of ulcerative colitis.

It is well known that transcriptional factor NF- κ B plays a pivotal role in expression of LPS-induced inflammatory factors. Because NF- κ B activation could lead to enhanced expression of proinflammatory cytokines, chemokines, inflammatory enzymes such as inducible NO synthase (iNOS) and cyclooxygenase (COX-2), adhesion molecules and inflammatory receptors^[29], modulation of NF- κ B activation might provide a direct way to inhibit inflammatory mediators^[30]. Activation of NF- κ B is triggered by phosphorylation of an inhibitory subunit, I κ B. In unstimulated cells, NF- κ B is sequestered in the cytoplasm through interaction with I κ B α and I κ B α inhibitory proteins. In response to proinflammatory stimuli, I κ B is first phosphorylated in its N-terminal domain by a large multi-kinase complex, then polyubiquitinated, and finally degraded by the proteasome. The released NF- κ B complex could translocate into the nuclei where it initiates gene transcription upon binding to its cognate DNA motifs in regulatory segments of TNF- α gene and other target genes involved in inflammatory and immune process^[31]. At the same time, we also detected the effect of probiotics on the initiation and perpetuation of inflammation. The expressions of I κ B in cytoplasm and NF- κ B in nuclei were detected by Western blot. The result manifested that probiotics efficaciously inhibited the degradation of I κ B protein. Less NF- κ B translocation into nuclei could be detected by Western blot in treatment group. Activation of NF- κ B was analyzed by EMSA, the result likewise manifested that much more NF- κ B proteins were significantly activated in control group than in probiotics group.

Recent data have demonstrated that mucosal immune response is involved in patients with IBD. The nuclear transcription factor NF- κ B is a key regulator of inducible expressions of many genes involved in immune and inflammatory responses in the gut. Stimuli like oxidative stress, cytokines (IL-1, IL-6, TNF- α), bacteria and viruses can release NF- κ B from their inactive cytoplasmatic form to the nuclei. Inhibitory cytokines can prevent the activation of NF- κ B. More potent and selective treatment strategies with anti-sense p65, proteasome inhibitors and viral I kappa B α expression vectors have been aimed to prevent NF- κ B activation in mucosal macrophages and T lymphocytes. However, NF- κ B regulated genes are also involved in survival responses of epithelial cells. Selective inhibition of NF- κ B activation in inflammatory cells could be an option in management of IBD^[32-35]. In our study, the expression of proinflammatory cytokines such as TNF- α , IL-1 β influenced by the activation of NF- κ B obviously were inhibited by probiotics and mRNA expression of anti-inflammatory cytokine IL-10 was elevated by the effect of probiotics.

In conclusion, supplementation with probiotics is helpful in maintaining remission and preventing the relapse of UC.

REFERENCES

- 1 **Rampton DS.** Management of difficult inflammatory bowel disease: where are we now? *World J Gastroenterol* 2000; **6** (Suppl 3): 8
- 2 **Mitsuyama K,** Toyonaga A, Sata M. Intestinal microflora as a therapeutic target in inflammatory bowel disease. *J Gastroenterol* 2002; **37**(Suppl 14): 73-77
- 3 **Schultz M,** Sartor RB. Probiotics and inflammatory bowel diseases. *Am J Gastroenterol* 2000; **95**(1 Suppl): S19-21
- 4 **Shanahan F.** Probiotics and inflammatory bowel disease: is there a scientific rationale? *Inflamm Bowel Dis* 2000; **6**: 107-115
- 5 **Gionchetti P,** Rizzello F, Venturi A, Brigidi P, Matteuzzi D, Bazzocchi G, Poggioli G, Miglioli M, Campieri M. Oral bacteriotherapy as maintenance treatment in patients with chronic pouchitis: a double-blind, placebo-controlled trial. *Gastroenterology* 2000; **119**: 305-309
- 6 **Baert FJ,** Rutgeerts PJ. Medical therapies for ulcerative colitis and crohn's disease. *Curr Gastroenterol Rep* 2000; **2**: 446-450
- 7 **Gionchetti P,** Amadini C, Rizzello F, Venturi A, Palmonari V, Morselli C, Romagnoli R, Campieri M. Probiotics-role in inflammatory bowel disease. *Dig Liver Dis* 2002; **34**(Suppl 2): S58-62
- 8 **Fooks LJ,** Gibson GR. Probiotics as modulators of the gut flora. *Br J Nutr* 2002; **88**(Suppl 1): S39-49
- 9 **Hanauer SB.** Update on medical management of inflammatory bowel disease: ulcerative colitis. *Rev Gastroenterol Disord* 2001; **1**: 169-176
- 10 **Madsen KL.** The use of probiotics in gastrointestinal disease. *Can J Gastroenterol* 2001; **15**: 817-822
- 11 **Linskens RK,** Huijsdens XW, Savelkoul PH, Vandenbroucke-Grauls CM, Meuwissen SG. The bacterial flora in inflammatory bowel disease: current insights in pathogenesis and the influence of antibiotics and probiotics. *Scand J Gastroenterol Suppl* 2001; **234**: 29-40
- 12 **Steidler L.** Microbiological and immunological strategies for treatment of inflammatory bowel disease. *Microbes Infect* 2001; **3**: 1157-1166
- 13 **Madsen K,** Cornish A, Soper P, McKaigney C, Jijon H, Yachimec C, Doyle J, Jewell L, De Simone C. Probiotic bacteria enhance murine and human intestinal epithelial barrier function. *Gastroenterology* 2001; **121**: 580-591
- 14 **Campieri M,** Gionchetti P. Bacteria as the cause of ulcerative colitis. *Gut* 2001; **48**: 132-135
- 15 **Deryckere F,** Gannon F. A one-hour miniprep preparation technique for extraction of DNA-binding proteins from animal tissues. *Biotechniques* 1994; **16**: 405
- 16 **Xu L,** Fidler IJ. Acidic pH-induced elevation in interleukin 8 expression by human ovarian carcinoma cells. *Cancer Res* 2000; **60**: 4610-4616
- 17 **Haller D,** Bode C, Hammes WP, Pfeifer AM, Schiffrin EJ, Blum S. Non-pathogenic bacteria elicit a differential cytokine response by intestinal epithelial cell/leucocyte co-cultures. *Gut* 2000; **47**: 79-87
- 18 **Todt J,** Sonstein J, Polak T, Seitzman GD, Hu B, Curtis JL. Repeated intratracheal challenge with particulate antigen modulates murine lung cytokines. *J Immunol* 2000; **164**: 4037-4047
- 19 **Karban A,** Eliakim R, Brant SR. Genetics of inflammatory bowel disease. *Isr Med Assoc J* 2002; **4**: 798-802
- 20 **Duerr RH.** The genetics of inflammatory bowel disease. *Gastroenterol Clin North Am* 2002; **31**: 63-76
- 21 **Hendrickson BA,** Gokhale R, Cho JH. Clinical aspects and pathophysiology of inflammatory bowel disease. *Clin Microbiol Rev* 2002; **15**: 79-94
- 22 **Guarner F,** Malagelada JR. Gut flora in health and disease. *Lancet* 2003; **361**: 512-519
- 23 **Kanai T,** Iiyama R, Ishikura T, Uraushihara K, Totsuka T, Yamazaki M, Nakamura T, Watanabe M. Role of the innate immune system in the development of chronic colitis. *J Gastroenterol* 2002; **37**(Suppl 14): 38-42
- 24 **Shen B.** Diagnosis and treatment of patients with pouchitis. *Drugs* 2003; **63**: 453-461
- 25 **Gionchetti P,** Amadini C, Rizzello F, Venturi A, Campieri M. Review article: treatment of mild to moderate ulcerative coli-

- tis and pouchitis. *Aliment Pharmacol Ther* 2002; **16**(Suppl 4): 13-19
- 26 **Korhonen R**, Korpela R, Saxelin M, Maki M, Kankaanranta H, Moilanen E. Induction of nitric oxide synthesis by probiotic *Lactobacillus rhamnosus* GG in J774 macrophages and human T84 intestinal epithelial cells. *Inflammation* 2001; **25**: 223-232
- 27 **Li Z**, Yang S, Lin H, Huang J, Watkins PA, Moser AB, Desimone C, Song XY, Diehl AM. Probiotics and antibodies to TNF inhibit inflammatory activity and improve nonalcoholic fatty liver disease. *Hepatology* 2003; **37**: 343-350
- 28 **Folwaczny C**. Anti-inflammatory effects of apathogenic salmonellas: relevance for therapy with probiotics? *Z Gastroenterol* 2001; **39**: 329-332
- 29 **Christman JW**, Lancaster LH, Blackwell TS. Nuclear factor kappa B: a pivotal role in the systemic inflammatory response syndrome and new target for therapy. *Intensive Care Med* 1998; **24**: 1131-1138
- 30 **Naik S**, Kelly EJ, Meijer L, Pettersson S, Sanderson IR. Absence of Toll-like receptor 4 explains endotoxin hyporesponsiveness in human intestinal epithelium. *J Pediatr Gastroenterol Nutr* 2001; **32**: 449-453
- 31 **Cong B**, Li SJ, Yao YX, Zhu GJ, Ling YL. Effect of cholecystokinin octapeptide on tumor necrosis factor alpha transcription and nuclear factor-kappaB activity induced by lipopolysaccharide in rat pulmonary interstitial macrophages. *World J Gastroenterol* 2002; **8**: 718-723
- 32 **Dijkstra G**, Moshage H, Jansen PL. Blockade of NF- κ B activation and donation of nitric oxide: new treatment options in inflammatory bowel disease? *Scand J Gastroenterol Suppl* 2002; **236**: 37-41
- 33 **Hanada T**, Yoshimura A. Regulation of cytokine signaling and inflammation. *Cytokine Growth Factor Rev* 2002; **13**: 413-421
- 34 **Haddad JJ**. Recombinant TNF-alpha mediated regulation of the I kappa B-alpha/NF-kappa B signaling pathway: evidence for the enhancement of pro- and anti-inflammatory cytokines in alveolar epithelial cells. *Cytokine* 2002; **17**: 301-310
- 35 **Iwadou H**, Morimoto Y, Iwagaki H, Sinoura S, Chouda Y, Kodama M, Yoshioka T, Saito S, Yagi T, Tanaka N. Differential cytokine response in host defence mechanisms triggered by gram-negative and gram-positive bacteria, and the roles of gabexate mesilate, a synthetic protease inhibitor. *J Int Med Res* 2002; **30**: 99-108

Edited by Ren SY and Wang XL **Proofread by** Xu FM

Rat liver transplantation without preservation of “phrenic ring” using double cuff method

Yong Jiang, Yu-Dong Qiu, Xiao-Ping Gu, Xin-Hua Zhu, Yi-Tao Ding

Yong Jiang, Yu-Dong Qiu, Xiao-Ping Gu, Xin-Hua Zhu, Yi-Tao Ding, Department of Hepatobiliary Surgery, Gulou Hospital, Medical Department of Nanjing University, Nanjing, 210008, Jiangsu Province, China

Yong Jiang, Department of Hepatobiliary Surgery, Changzhou 1st People's Hospital, Changzhou, 213003, Jiangsu Province, China

Supported by the Medical Administration Bureau of Jiangsu Province, No. SZ9902

Correspondence to: Dr. Yong Jiang, Department of Hepatobiliary Surgery, Changzhou 1st People's Hospital, Changzhou, 213003, Jiangsu Province, China. yyjiang8888@hotmail.com

Telephone: +86-519-6102280 **Fax:** +86-519-6621235

Received: 2003-09-06 **Accepted:** 2003-10-07

Abstract

AIM: To develop a double cuff method for rat liver transplantation without preservation of “phrenic ring” to shorten the portal vein clamping time.

METHODS: “Phrenic ring” was completely excluded from the donor liver, and end to end anastomosis of suprahepatic inferior vena cava was performed.

RESULTS: The portal vein clamping time was shortened to 10.6 min, the successful rate was 83.1%.

CONCLUSION: This method can simplify the operation and shorten the portal vein clamping time.

Jiang Y, Qiu XD, Gu XP, Zhu XH, Ding YT. Rat liver transplantation without preservation of “phrenic ring” using double cuff method. *World J Gastroenterol* 2004; 10(10): 1526-1527

<http://www.wjgnet.com/1007-9327/10/1526.asp>

INTRODUCTION

The orthotopic rat liver transplantation (ORLT) model was first described by Lee *et al.* in 1973^[1], and subsequently modified by Kamada and Calne in 1979^[2]. This model has been widely accepted and used in current scientific researches^[3-13]. In order to study the ischemia/reperfusion injury after liver transplantation, we modified the ORLT model established by Jiang *et al.*^[14]. We constructed a double cuff ORLT model without preservation of “phrenic ring”. This model can simplify the operation and shorten the portal vein clamping time.

MATERIALS AND METHODS

Animals

Male Sprague Dawley rats weighing 200-250 g were used as donors and recipients respectively. The body mass of donors was generally lower than that of corresponding recipients. The rats were housed in pathogen-free conditions with a 12 h light-dark cycle and had free access to water and were fasted for 14 h before operation. All experiments were performed in compliance with the standards for animal use and care set by Institutional Animal Care Committee.

Surgical procedures

All surgical procedures were performed under the naked eye. On the basis of the procedures described by Kamada *et al.*^[2], we made the following modifications. (1) The harvested liver from the donor was placed in a 4 °C saline bath measuring 6 cm in diameter and 3 cm in depth. The whole “phrenic ring” was removed from the suprahepatic inferior vena cava (IVC), leaving the vessel wall of suprahepatic IVC. After the double-cuff preparation was finished, the liver was perfused with cold lactated Ringer's solution through the portal vein and infrahepatic IVC. The liver was preserved in 4 °C University of Wisconsin (UW) solution for 24 h (in order to study cold preservation/reperfusion injury). (2) Instead of anastomosis of the donor “phrenic ring” with the receptor's suprahepatic IVC, the donor suprahepatic IVC was anastomosed end-to-end with the receptor suprahepatic IVC using a 7/0 continuous nylon suture.

RESULTS

Seventy-two ORLTs were performed without preservation of “phrenic ring” in rats. Of which, 59 were successful (success rate 83.1%). The rats survived over 24 h. One rat had survived more than 2 mo. One-week survival rate was not obtained because specimens were taken for study. Our criteria for operative success were as follows. After ORLT, the receptor rat could turn over, and run about actively. The rats were agile to the surrounding and could drink water. The portal vein clamping time (PVCT) was shortened (10.6 ± 1.36 min), and the shortest PVCT reached 8 min. The cause of death included a number of contributing factors: anesthesia too deep and respiratory failure (4/13); thrombosis of the portal vein (1/13); wound bleeding of the right adrenal gland area (1/13); failure of the portal vein anastomosis (2/13); stenosis or obstruction of suprahepatic IVC (4/13); and failure of the infrahepatic IVC anastomosis (1/13). Failure to control ether anesthesia and narrowing or obstruction of the outflow tract was the main cause of operative failure. In the latter case, most of them occurred at the initial stage.

DISCUSSION

Original intention of establishing the model

The author has been engaged in the research of ischemia/reperfusion injury of liver transplantation. In this process, PVCT needs to be shortened in order to reduce the interference with a too long period of splanchnic congestion. PVCT should be shortened to less than 14 min, otherwise a lethal endotoxin like syndrome induced by splanchnic congestion might play the central role which might bring about a noted systemic error in research^[15]. In the beginning by following Kamada's method, we found that the repair of “phrenic ring” and eversion anastomosis were the “bottleneck” of PVCT. Thus we established the double cuff method for ORLT without preservation of “phrenic ring”. In the early stage, suprahepatic IVC was sometimes lacerated. But on the basis of improved microsurgery and vascular anastomosis technique, this method can not only avoid laceration of the suprahepatic IVC, but also shorten PVCT. A more scientific model is thus provided for

the research of ischemia-reperfusion and rejection-tolerance in liver transplantation.

Good exposure is the key point of a successful operation

As other surgical operations, good exposure is also the key point of liver transplantation. As “phrenic ring” is not preserved, anastomosis of suprahepatic IVC becomes more important. Good exposure was achieved in the following ways. Full-length median incision on the abdomen was dragged to both sides and fixed, xiphoid process was dragged cephalad with our designed apparatus, a small pillow underlied the rat chest to raise the suprahepatic IVC stoma. By this method, no suprahepatic IVC was lacerated, PVCT was shortened to nearly 10 min. Not only the disturbance of respiratory and circulation was reduced, but also splanchnic congestion induced endotoxin like syndrome was reduced, which was hard to be attained by “triple-cuff” or conventional “double-cuff” liver transplantation.

Other relevant experiences concerning anaesthesia of donor and receptor rats

Donor livers were anaesthetized by ketamine. Kamada *et al.* recommended a dosage of 100 mg/5 Kg body mass^[2], but actually 40 to 50 mg ketamine was administrated to rats weighing 180-230 g. Receptor rats were maintained by ether inhalation anaesthesia. Steadiness of this anaesthesia is also crucial to a successful ORLT. The shallow anaesthesia would result in difficulty of operation and even bleeding, but too deep anaesthesia would lead to depression of breath and difficulty in postoperative recovery or even death. Out of control of the depth of ether anaesthesia was the main reason of postoperative respiratory failure, and also one of the main causes of death of the receptor rats (30.8%, 4/13). Our experience is “deep induction, shallow maintenance”. In the induction period, a bigger dosage of ether was given, but a low density of ether in mask was maintained during operation.

Turning over of the donor liver during its harvest

We adopted the methods recommended by Wang *et al.*^[16]. After a midline abdominal incision was made, the liver was freed from surrounding ligaments, the left infraphrenic vein and para-oesophagus vein were ligated and divided. Then the right renal vein and right adrenal vein were ligated. The suprahepatic vein was freed. Hepatoportal structure was dissected and freed. The common duct was cannulated. The donor liver was thus harvested. It was turned over only once. So this method can not only protect the donor liver, but also shorten the heat ischemic time.

REFERENCES

- 1 **Lee S**, Charters AC, Chandler JG, Orloff MJ. A technique for orthotopic liver transplantation in the rat. *Transplantation* 1973; **16**: 664-669
- 2 **Kamada N**, Calne RY. Orthotopic liver transplantation in the rat. Technique using cuff for portal vein anastomosis and biliary drainage. *Transplantation* 1979; **28**: 47-50
- 3 **Zhu XH**, Qiu YD, Shen H, Shi MK, Ding YT. Effect of matriline on Kupffer cell activation in cold ischemia reperfusion injury of rat liver. *World J Gastroenterol* 2002; **8**: 1112-1116
- 4 **Xu MQ**, Yao ZX. Functional changes of dendritic cells derived from allogeneic partial liver graft undergoing acute rejection in rats. *World J Gastroenterol* 2003; **9**: 141-147
- 5 **Svensson G**, Fjalling M, Gretarsdottir J, Jacobsson L, Holmberg SB. Kupffer cell and hepatocyte function in rat transplanted liver. *Transpl Int* 1992; **5**(Suppl 1): S417-419
- 6 **Tashiro H**, Fudaba Y, Itoh H, Mizunuma K, Ohdan H, Itamoto T, Asahara T. Hepatocyte growth factor prevents chronic allograft dysfunction in liver-transplanted rats. *Transplantation* 2003; **76**: 761-765
- 7 **Kataoka M**, Margenthaler JA, Ku G, Eilers M, Flye MW. “Infectious tolerance” develops after the spontaneous acceptance of Lewis-to-Dark Agouti rat liver transplants. *Surgery* 2003; **134**: 227-234
- 8 **Fujino M**, Adachi K, Kawasaki M, Kitazawa Y, Funeshima N, Okuyama T, Kimura H, Li XK. Prolonged survival of rat liver allograft with adenoviral gene transfection of human immunodeficiency virus type 1 nef. *Liver Transpl* 2003; **9**: 805-813
- 9 **Kato Y**, Shimazu M, Kondo M, Uchida K, Kumamoto Y, Wakabayashi G, Kitajima M, Suematsu M. Bilirubin rinse: A simple protectant against the rat liver graft injury mimicking heme oxygenase-1 preconditioning. *Hepatology* 2003; **38**: 364-373
- 10 **Fernandez L**, Heredia N, Peralta C, Xaus C, Rosello-Catafau J, Rimola A, Marco A, Serafin A, Deulofeu R, Gelpi E, Grande L. Role of ischemic preconditioning and the portosystemic shunt in the prevention of liver and lung damage after rat liver transplantation. *Transplantation* 2003; **76**: 282-289
- 11 **Li XL**, Man K, Liu YF, Lee TK, Tsui SH, Lau CK, Lo CM, Fan ST. Insulin in University of Wisconsin solution exacerbates the ischemic injury and decreases the graft survival rate in rat liver transplantation. *Transplantation* 2003; **76**: 44-49
- 12 **Lehmann TG**, Wheeler MD, Froh M, Schwabe RF, Bunzendahl H, Samulski RJ, Lemasters JJ, Brenner DA, Thurman RG. Effects of three superoxide dismutase genes delivered with an adenovirus on graft function after transplantation of fatty livers in the rat. *Transplantation* 2003; **76**: 28-37
- 13 **Sun Z**, Klein AS, Radaeva S, Hong F, El-Assal O, Pan HN, Jaruga B, Batkai S, Hoshino S, Tian Z, Kunos G, Diehl AM, Gao B. *In vitro* interleukin-6 treatment prevents mortality associated with fatty liver transplants in rats. *Gastroenterology* 2003; **125**: 202-215
- 14 **Jiang Y**, Gu XP, Qiu XD, Sun XM, Chen LL, Zhang LH, Ding YT. Ischemic preconditioning decreases C-X-C chemokine expression and neutrophil accumulation early after liver transplantation in rats. *World J Gastroenterol* 2003; **9**: 2025-2029
- 15 **Urata K**, Nguyen B, Brault A, Lavoie J, Rocheleau B, Huet PM. Decreased survival in rat liver transplantation with extended cold preservation: role of portal vein clamping time. *Hepatology* 1998; **28**: 366-373
- 16 **Wang X**, Yang JM, Yan YQ, Yao XP, Wu MC. Studies on the ways of orthotopic liver transplantation in rats. *Zhonghua Qiguan Yizhi Zazhi* 1998; **19**: 76-78

Edited by Xu JY and Wang XL Proofread by Xu FM

mRNA expression profiling reveals a role of *Helicobacter pylori* vacuolating toxin in escaping host defense

Jian-Ping Yuan, Tao Li, Zhen-Hong Li, Gui-Zhen Yang, Bao-Yu Hu, Xiao-Dong Shi, Tie-Liu Shi, Shan-Qing Tong, Xiao-Kui Guo

Jian-Ping Yuan, Tao Li (equal contributor), Zhen-Hong Li, Gui-Zhen Yang, Bao-Yu Hu, Xiao-Dong Shi, Shan-Qing Tong, Xiao-Kui Guo, Department of Medical Microbiology and Parasitology, Shanghai Second Medical University, Shanghai 200025, China
Tie-Liu Shi, Shanghai Institutes for Biological Sciences, Chinese Academy of Sciences, Shanghai 200025, China

Supported by the State Ministry of Education Research Foundation for Returned Overseas Chinese Scholars Abroad (2001) 498

Correspondence to: Xiao-Kui Guo, Department of Microbiology and Parasitology, Shanghai Second Medical University, 280 Chongqingnan Road, Shanghai 200025, China. xkguo@shsmu.edu.cn

Telephone: +86-21-64671226 **Fax:** +86-21-64671226

Received: 2003-10-31 **Accepted:** 2004-02-01

Abstract

AIM: To study the immune response of host to *Helicobacter pylori* VacA.

METHODS: The monocyte/macrophage-like U937 cells were infected with *Helicobacter pylori* vacA-positive strain NCTC 11638 or isogenic vacA-negative mutant. Differentially expressed genes were identified at 2, 6, 10, and 24 h post-infection by cDNA microarray. Differential expressions of some genes were confirmed by Northern blot.

RESULTS: More than 100 genes altered their mRNA expression at different time points respectively, many of which were identified to be related to immune evasion.

CONCLUSION: VacA is a crucial element for *H pylori* to escape from host immune defense by means of differentially regulating the expression of some related genes. These genes, previously known or unknown to be involved in the mechanism of immune evasion, deserve further investigation to unearth much more information complicated in the immune response.

Yuan JP, Li T, Li ZH, Yang GZ, Hu BY, Shi XD, Shi TL, Tong SQ, Guo XK. mRNA expression profiling reveals a role of *Helicobacter pylori* vacuolating toxin in escaping host defense. *World J Gastroenterol* 2004; 10(10): 1528-1532

<http://www.wjgnet.com/1007-9327/10/1528.asp>

INTRODUCTION

Helicobacter pylori infects about half of the world's population. Despite the induction of an immunological reaction, the infection of *H pylori* is commonly life-long, suggesting that this pathogen has evolved mechanisms to evade protective immune responses to achieve the state of host-microbial equilibrium^[1]. Some products of *H pylori* have been determined to have immunosuppressive effects for prolonging the infection. A 100 ku *H pylori* protein inhibits proliferation of T-cell and macrophage^[2], and VacA, a cytotoxin that has been found to cause massive vacuolation in several mammalian cell lines and in the gastric epithelia of patients with active chronic

gastritis associated with *H pylori* infection^[3], may perform targeted action to disable T cells. VacA interferes with proteolytic processing of tetanus toxin and toxoid and specifically inhibits the Ii-dependent pathway of antigen presentation mediated by newly synthesized major histocompatibility complex (MHC) class II, suggesting that VacA may contribute to the persistence of *H pylori* by interfering with protective immunity^[4]. However, to the author's knowledge, the exact mechanism of such an immunosuppression effect has not been fully studied. Hence, in this study, we performed a large scale measurement of gene expression alteration in host cells using gene microarray technology, which provided the crucial information for interpreting the mechanisms of immunosuppression.

MATERIALS AND METHODS

Bacterial strains and growth conditions

H pylori NCTC 11638 strain positive for vacA was given as a gift by Dr. Shi (Shanghai Institute of Gastroenterology). Isogenic vacA-negative mutant 11638-Δ vacA was constructed by substitution of a kanamycin resistant gene for a short fragment of vacA through homologous recombination, as described previously^[5]. *H pylori* strains were cultured routinely on brain heart infusion (BHI) agar plates with 5% sheep blood in mixed air containing 100 ml/L CO₂, 50 ml/L O₂, and 850 ml/L N₂ at 37 °C.

H pylori infection of monocyte/macrophage-like cell line U937

The U937 cells were maintained in RPMI 1640 medium (Gibco BRL, USA) with 2 mmol/L L-glutamine, 1.5 g/L sodium bicarbonate, 4.5 g/L glucose, 10 mmol/L HEPES, 1.0 mmol/L sodium pyruvate and 100 ml/L fetal bovine serum. The day before *H pylori* infection, fresh medium with 20 ml/L fetal calf serum was substituted. Eighteen hours later, the cells grown to 90% confluency were cocultured with *H pylori* isogenic strains at a multiplicity of infection of 10 in culture medium for 2, 6, 10, and 24 h.

Total RNA Isolation

U937 cells cocultured with NCTC 11638 and 11638-Δ vacA were collected at 2, 6, 10, and 24 h after the infection for mRNA extraction. Total RNA was isolated using TRIZOL reagent (Invitrogen, USA) according to the manufacturer's instruction.

cDNA microarrays

The cDNA microarrays were designed by Shanghai BioStar Genechip Inc. In this study, microarrays with 8 464 human cDNAs were used, including full-length and partial complementary DNAs representing novel, known, and control genes.

Preparation and hybridization of fluorescent-labeled cDNA

Aliquots of 30 μg of total RNA were fluorescently labeled with Cy5- or Cy3-dCTP (Amersham Pharmacia, Sweden) by reverse transcription in the presence of 5 μg of oligo(dT) and 1 μL of SuperScriptII (Gibco-BRL, USA). The labeled cDNAs were purified using MicroSpin S-200 columns (Amersham

Pharmacia, Sweden) and lyophilized. The probes were resuspended in 20 μ L hybridization solution containing 8 μ g of poly(dA), 2 μ g of yeast tRNA, 10 μ g of human *Cot* I DNA (Gibco-BRL, USA). After heated to 95 °C for 2 min and then cooled to room temperature, the mixture was applied to the slides and covered by a coverslip. The slides were incubated in a humid cabinet of an incubator for 16–18 h at 42 °C. Then the slides were washed at 60 °C for 10 min in solutions of 2 \times SSC with 2 g/L SDS, 0.1 \times SSC with 2 g/L SDS, and 0.1 \times SSC sequentially, and then dried at room temperature.

Array scanning and data processing

Each slide was scanned at 10 μ m resolution on a GenePix 4000B scanner (Axon Instruments, Inc., Foster City, CA) at variable PMT voltage to obtain maximal signal intensities with no more than 1% probe saturation. The images were processed with GenePix Pro 3.0. Ratios were normalized by a linear regression between ln(Cy5) and ln(Cy3) of all the genes' background-corrected signal intensities on the microarray. Genes exhibited a 2-fold or greater change in expression level and exceeded 200 in signal intensity were considered true outliers.

Preparation of ³²P-labeled probes

The plasmids containing cDNA clone used for preparing probes were provided by Shanghai BioStar Genechip Inc. A total amount of 200 ng plasmids were used as templates for PCR amplification. PCR products were purified using QIAquick Gel Extraction Kit (Qiagen, Germany). The probes were labeled using random primed Strip-EZ DNA Kit (Ambion, Austin, TX). A total amount of 25 ng purified DNA diluted in 9 μ L TE (10 mmol/L Tris-HCl, pH8, 1 mmol/L EDTA) was denatured at 95 °C for 5 min and then immediately frozen in liquid nitrogen, thawed, microfuged, and placed on ice. Afterwards, the following reaction was assembled as follows and mixed gently: A 9.0 μ L of denatured DNA, 2.5 μ L of 10 \times Decamer solution, 5.0 μ L of 5 \times buffer-dATP/-dCTP, 2.5 μ L of 10 \times dCTP, 5.0 μ L of [α -³²P]dATP (3 000 Ci/mmol,

10 mCi/mL), 1.0 μ L of exonuclease-free Klenow, and nuclease-free water to 25 μ L. After 20 min incubation at 37 °C, 1 μ L of 0.5 mol/L EDTA was added to stop the reaction.

Northern blot analysis

A 10 μ g sample of total RNA per lane was subjected to electrophoresis on 12 g/L agarose gels containing 2.2 mol/L formaldehyde. RNAs were transferred onto Zeta-probe blotting membranes (Bio-Rad Laboratories, Hercules, CA) using Vacuum Blotter (model 785, Bio-Rad Laboratories) and baked under vacuum at 80 °C for 2 h. Membranes were hybridized for 16 h at 60 °C with ULTRArray hybridization solution (Ambion, Austin, TX) containing cDNA probes labeled with [α -³²P] dCTP by random priming (Strip-EZ DNA labeling system, Ambion). The hybridized membranes were serially washed at 55 °C using 2 \times SSC with 1 g/L SDS solution, then exposed to a phosphorimager. Blots were scanned and quantified by a phosphorimager in combination with Optiquant software v. 2.50 (Cyclone Storage Phosphor System, Packard Instruments).

RESULTS

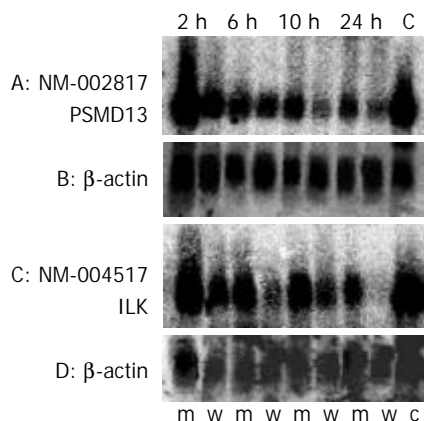
The mRNA expression in U937 cells was compared at 2, 6, 10, and 24 h after the infection with NCTC 11638 or 11638- Δ vacA. More than 100 genes altered their mRNA expression at different time points respectively, among which, the genes related to immune evasion were selected (Table 1). To confirm the differential expression profiling of the cDNA microarrays, two genes: *PSMD13* and *ILK* were chosen for northern blot analysis. As shown in Figure 1, the expression levels of these 2 genes were lower in the cells treated with *H pylori* NCTC11638 than those treated with 11638- Δ vacA. In addition, in both cases, the fold ratio changes detected by the microarray were confirmed by Northern blot (Table 2). The level of β -actin transcript was present at approximately the same level in both samples, providing an assessment of RNA content in each sample used for Northern blot analysis.

Table 1 Differentially expressed genes related to immune evasion

GeneBank_ID	Definition	Fold change			
		2 h	6 h	10 h	24 h
NM_004517	Integrin-linked kinase (ILK)	0.717	0.218	0.245	0.454
NM_001964	Early growth response 1 (EGR1)	3.184	1.149	—	—
NM_022555	Major histocompatibility complex, class II, DR beta 3 (HLA-DRB3)	1.000	0.448	0.518	0.621
NM_002116	Major histocompatibility complex, class I, A (HLA-A)	0.584	0.322	0.336	—
NM_002124	Major histocompatibility complex, class II, DR beta 1 (HLA-DRB1)	—	0.661	0.485	0.567
NM_002817	Proteasome (prosome, macropain) 26S subunit, non-ATPase, 13 (PSMD13)	0.445	0.122	0.333	0.402
NM_004159	Proteasome (prosome, macropain) subunit, beta type, 8 (large multifunctional protease 7) (PSMB8)	0.573	0.150	0.304	0.254
NM_000616	CD4 antigen (p55) (CD4)	0.855	0.560	0.317	0.831
NM_015953	eNOS interacting protein (NOSIP),	0.857	0.517	0.450	0.463
NM_020998	Macrophage stimulating 1 (hepatocyte growth factor-like) (MST1)	0.690	0.562	0.353	—
NM_005944	Antigen identified by monoclonal antibody MRC OX-2 (MOX2)	1.514	1.027	2.042	—
NM_021138	TNF receptor-associated factor 2 (TRAF2)	0.817	0.773	0.713	0.465
NM_004001	Fc fragment of IgG, low affinity IIb, receptor for (CD32) (FCGR2B)	0.581	0.569	0.467	—
NM_001100	Actin, alpha 1, skeletal muscle (ACTA1)	0.368	0.266	0.139	—
NM_001615	Actin, gamma 2, smooth muscle, enteric (ACTG2)	0.419	0.229	0.191	—
NM_005718	Actin related protein 2/3 complex, subunit 4 (20 ku) (ARPC4)	0.461	0.362	0.370	0.611
NM_020040	Tubulin, beta polypeptide 4, member Q (TUBB4Q)	0.462	0.345	0.335	0.573
NM_006009	Tubulin, alpha 3 (TUBA3)	1.062	0.710	0.484	0.885
NM_001665	ras homolog gene family, member G (<i>rho G</i>) (ARHG)	0.590	0.445	0.524	0.590
AB055890	<i>c-lbc</i> mRNA for guanine nucleotide exchange factor Lbc	1.065	0.315	0.701	0.433
NM_006400	Dynactin 2 (p50) (DCTN2)	0.865	0.361	0.334	—
NM_005428	vav 1 oncogene (VAV1)	0.510	0.421	0.387	—
NM_005993	Tubulin-specific chaperone d (TBCE)	0.770	0.485	0.524	—
NM_001747	Capping protein (actin filament), gelsolin-like (CAPG)	0.512	0.213	0.191	0.323

Table 2 Ratio of expression values obtained in U937 cells cocultured with *H pylori* NCTC11638 versus those cocultured with 11638- Δ vacA as assessed by microarray analysis and Northern blot

GeneBank ID	Gene product	Microarray ratio				Northern blot ratio			
		2 h	6 h	10 h	24 h	2 h	6 h	10 h	24 h
NM_002817	PSMD13	0.445	0.122	0.333	0.402	0.07	0.71	0.25	0.33
NM_004517	ILK	0.717	0.218	0.245	0.454	0.57	0.19	0.43	0.15

**Figure 1** Northern blot analysis result. RNA from U937 cells cocultured with *H pylori* NCTC11638 (wild type, w) or 11638- Δ vacA (mutant type, m) or RNA from normal cells (c) were separated by agarose electrophoresis, transferred onto nylon membranes, and probed with the human cDNAs as follows: NM_002817 (PSMD13), and NM_004517 (ILK). Control blots with human β -actin were provided.

DISCUSSION

Helicobacter pylori has found its own way to thrive within host cells, despite the presence of a well-functioning immune system. In the present study, differential expression of macrophage upon stimulation of VacA gives clear evidence that this vacuolating cytotoxin has evolved with various tricks to escape from the innate and adaptive immunity of the host.

Recognition of pathogen-infected host cells by effector T lymphocytes requires intracellular processing of microbial antigens and their presentation on the surface of the antigen-presenting cells (APCs) in association with MHC molecules. To avoid immune recognition, many kinds of microorganisms have evolved mechanisms which interfere with antigen presentation pathways. These mechanisms may be pivotal, especially for those pathogens causing persistent infections. The present differential expressions provide clear evidence that VacA downregulates the expression of MHC class I and class II molecules in macrophage. Thus, specific T lymphocytes may not be activated, resulting in the evasion of *H pylori* from the host's immune response and colonization of the bacteria in gastric mucosa persistently, remaining "invisible" to both CD8⁺ and CD4⁺ T cells. Interference with the class II antigen presentation pathway by *Listeria monocytogenes* has been shown to result in a reduced proliferation of CD4⁺ T lymphocytes in response to heterologous antigens^[6]. Interactions between MHC class I and human immunodeficiency virus (HIV) resulted in down-regulation of MHC-I surface expression, contributing to pathogenesis by suppressing the host's immune response^[7]. The role of MHC class I and class II-restricted functions in *H pylori* infection and immunity upon oral immunization has also been examined *in vivo*. It was found that experimental challenge with *H pylori* resulted in significantly greater colonization in MHC class I and class II mutant mice than in wild-type mice^[8]. MHC class II-deficient mice were unable to respond to oral antigenic stimulation and

remained persistently infected with *H pylori*^[8].

Nitric oxide (NO) is an important mediator of biological processes including inflammatory response. It is synthesized from L-arginine by a family of nitric oxide synthases (NOS), in which, endothelial NOS (eNOS) is a constitutively expressed isoform present in vascular endothelial cells, cardiac myocytes, and blood platelets^[9]. eNOS interacting protein (NOSIP) is a 34 ku protein specifically binds to the carboxylterminal region of the human eNOS oxygenase domain, overexpression of which in eNOS-expressing cells has been demonstrated to inhibit NO synthase activity^[10]. Thus, down-regulation of this protein upon stimulation of VacA may relieve such inhibition, leading to more NO production. The original concept that the small quantities of NO generated in a pulsatile fashion by constitutive eNOS mainly fulfil regulatory functions required for normal homeostatic function of the vasculature, while the high amount of NO produced by inducible NOS (iNOS) exerts antimicrobial and cytotoxic effects in the immune system, has recently been modified^[11]. The expression of eNOS is not restricted to endothelial cells, as it has been found to be present in monocytes/macrophages and in B and T lymphocytes^[12]. eNOS can also assume typical immunological functions previously assigned to iNOS, such as the induction of apoptotic cell death and the control of viruses^[11]. NO endows macrophages with cytostatic or cytotoxic activity against microbes and tumor cells^[13]. Nevertheless, more and more evidences have demonstrated a role for NO in the induction of immunosuppression by inhibiting T-cell proliferation during G1/S transition^[14-16]. In mouse models of T-cell-mediated autoimmunity, such as myelin antigen-induced EAE, the disease was exacerbated by genetic deletion of iNOS, indicating that NO suppressed T-cell-mediated immunity *in vivo*^[17]. In addition, NO induces apoptosis, which, the ubiquitin/proteasome and NF- κ B pathway have been determined to be involved in^[18].

In eukaryotic cells, degradation of many proteins involves their initial modification by conjugation of ubiquitin (Ub). Ubiquitinated proteins are rapidly degraded by the 26S proteasome^[19]. NO can inhibit the activities of the 20S and 26S proteasomes, providing a likely mechanism for the accumulation of NO-induced pro-apoptotic proteins p53 and Bax, the substrates of the ubiquitin/proteasome system^[18]. Apart from the indirect effect via NO functioning, the mRNA expression of proteasomes shows a significant downregulation as the result of being directly stimulated by VacA. Ub/proteasome pathway can catalyze the proteolytic processing of inactive 105 ku NF- κ B precursor into 50 ku subunit. p50 is then maintained in the cytosol conjugated with the p65 subunit in an inactive complex bound to I κ B. In addition, Ub/proteasome is involved in proteolytic digestion of I κ B, which is required for NF- κ B activation^[19]. Therefore, decreased proteasome activity should inhibit the proteolysis of NF- κ B precursor and inhibit I κ B degradation, thus blocking NF- κ B activation. Another involved protein, integrin-linked kinase (ILK), which has been determined to upregulate NF- κ B activity^[20], also shows decreased expression in this study. It might be the result of VacA induction, and moreover, ILK mRNA expression was found to be downregulated by NO^[21], corresponding to the above speculation that more NO may be produced due to downregulation of NOSIP. NF- κ B is known to be important

to cell survival. Fibroblasts and macrophages from Rel A (p65 subunit of NF- κ B) (-/-) mice were sensitive to TNF- α -induced cell death, and reintroduction of Rel A enhanced cell survival^[22]. Activation of NF- κ B is required for inflammatory cytokine release by macrophages during infection^[23]. Consequently, inhibition of NF- κ B activation may be responsible for decreased cytokine release from macrophages and the resulting immunosuppression. Additionally, because ILK is an apoptosis suppressor^[24], decreased production of this protein in macrophage may accelerate apoptosis of the cell that plays important roles in innate host defense and antigen presentation, leading to the evasion from host immunity against *H pylori*.

The capability of degrading proteins by the proteasome accounts for another important function to generate peptides presented on MHC-class I molecules to circulating lymphocytes. The presentation of these peptides enables the immune system to screen for and destroy cells expressing unusual polypeptides^[19]. Selective proteasome inhibitors were determined to prevent MHC-class I presentation of the antigenic peptide^[25]. Moreover, LMP2 and LMP7, two subunits of the proteasome, were found to be encoded in the major histocompatibility complex (MHC)^[26-28]. The experiment using specific antibodies against LMP2 and LMP7 showed that they were co-expressed with MHC-class I molecules^[29]. The levels of MHC-class I expression were shown to coincide perfectly with the LMP levels in different tissues, corresponding to the result in the present study, which shows simultaneous downregulation of MHC-class I and LMP7.

MSP, also known as HGF-like protein, is a serum protein belonging to the plasminogen-related growth factor family. It was originally discovered by Leonard and Skeel as a serum protein that stimulates shape change, movement, chemotaxis and phagocytosis of mouse peritoneal resident macrophages^[30,31]. The other important effect of MSP on macrophages was to inhibit endotoxin- or cytokine-stimulated NO production^[32]. Thereby, the decreased expression of MSP may contribute to deactivating macrophage and producing more NO, which, as described above, functions as an immunosuppressor.

The early growth response 1 (EGR1), a zinc-finger transcription factor that was shown to be significantly upregulated by 2 h postinfection in the present study, has been determined to induce downregulation of copper-zinc superoxide dismutase and manganese superoxide dismutase and stimulate the generation of reactive oxygen species (ROS) via the NADH/NADPH-oxidase system^[33]. In addition to NO, ROS produced by NADPH oxidase also have the ability to inhibit the proliferation of lymphocytes by a mechanism that suppressor macrophages impair the proliferative response of T lymphocytes to antigens or mitogens^[11]. Otsuji *et al.*^[34] demonstrated that the oxidative stress from tumor-derived macrophages mediated the decrease of CD3 ζ chain within T cells, which suppressed the antigen-specific T-cell responses. Pre-treatment of CTL or NK cells with nontoxic concentrations of H₂O₂ severely reduced their cytotoxic activity, leading to the speculation that macrophage-derived reactive oxygen metabolites contribute directly to alterations in signal transducing molecules of T cells and NK cells and to the mechanism of immunosuppression^[35]. Furthermore, the defective expression of CD3 ζ on lymphocytes has been related to some kind of carcinoma, including gastric adenocarcinoma^[36,37].

From Table 1, we may find up-regulation of MRC OX-2 (the antigen identified by monoclonal antibody, MOX2), a broadly expressed membrane glycoprotein, which has been shown to be important for regulation of the macrophage lineage. In the OX-2-deficient spleens, the number of macrophages was nearly twice the number of those in normal spleens^[38], implying a role of OX-2 in suppressing the activation of macrophage. The immunosuppression effects of OX-2 could be further

determined by many other studies. For example, several studies reported that increased expression of OX-2 in mice receiving renal allografts was associated with immunosuppression leading to increased graft survival, along with the polarization of cytokine production to type 2 cytokines in lymphocytes harvested from the transplanted animals^[39-41]. Furthermore, infusion of a mAb to OX-2 blocks both the increased graft survival and the altered cytokine production^[42]. All these data make clear that upregulation of OX-2 does favor to the immune evasion of *H pylori*.

Table 1 also demonstrates significant downregulation of many cytoskeleton-related gene expression. For example, RhoG is a member of the Rho family of GTPases, which signals to actin assembly during phagocytosis^[43]. Vav1 serves as a guanine nucleotide exchange factor (GEF) for Rho proteins, and establishes an essential and direct link between receptors with intrinsic or associated tyrosine kinase activity and the mitogenic and cytoskeletal pathways regulated by Rho proteins^[44]. Cytoskeleton has been known to be an important structural basis for phagocytosis since cytochalasin B, a toxin that blocks actin polymerization, was shown to inhibit uptake of IgG-coated erythrocytes by mouse macrophages^[45]. Phagocytosis is a process by which macrophages and leukocytes could ingest microbial pathogens to accomplish two essential immune functions, *i.e.*, to initiate the microbial death pathway, and to direct antigens to both MHC I and MHC II compartments. That is to say, phagocytosis serves not only as an innate immune effector but as a bridge between the innate and acquired immune responses^[1]. Thus, to destruct cytoskeleton may be another trick of VacA to evade host immune response.

In conclusion, we have shown that *H pylori* VacA induces the alteration of a series of genes related to immune evasion in macrophage, which ultimately establishes a state of host-microbial equilibrium. Some of these genes are for the first time made an association with VacA stimulation. Further investigations of the previously uncharacterized genes should be made to help us see through the underlying mechanisms utilized by *H pylori* to escape host immunity.

REFERENCES

- 1 **Ibraghimov A**, Pappo J. The immune response against *Helicobacter pylori*—a direct linkage to the development of gastroduodenal disease. *Microbes Infect* 2000; **2**: 1073-1077
- 2 **Knipp U**, Birkholz S, Kaup W, Opferkuch W. Partial characterization of a cell proliferation-inhibiting protein produced by *Helicobacter pylori*. *Infect Immun* 1996; **64**: 3491-3496
- 3 **Telford JL**, Ghiara P, Dell' Orco M, Comanducci M, Burroni D, Bugnoli M, Tecce MF, Censini S, Covacci A, Xiang Z. Gene structure of the *Helicobacter pylori* cytotoxin and evidence of its key role in gastric disease. *J Exp Med* 1994; **179**: 1653-1658
- 4 **Molinari M**, Salio M, Galli C, Norais N, Rappuoli R, Lanzavecchia A, Montecucco C. Selective inhibition of li-dependent antigen presentation by *Helicobacter pylori* toxin VacA. *J Exp Med* 1998; **187**: 135-140
- 5 **Yuan JP**, Li T, Shi XD, Hu BY, Yang GZ, Tong SQ, Guo XK. Deletion of *Helicobacter pylori* vacuolating cytotoxin gene by introduction of directed mutagenesis. *World J Gastroenterol* 2003; **9**: 2251-2257
- 6 **Leyva-Cobian F**, Unanue ER. Intracellular interference with antigen presentation. *J Immunol* 1988; **141**: 1445-1450
- 7 **Kamp W**, Breij EC, Nottet HS, Berk MB. Interactions between major histocompatibility complex class II surface expression and HIV: implications for pathogenesis. *Eur J Clin Invest* 2001; **31**: 984-991
- 8 **Pappo J**, Torrey D, Castriotta L, Savinainen A, Kabok Z, Ibraghimov A. *Helicobacter pylori* infection in immunized mice lacking major histocompatibility complex class I and class II functions. *Infect Immun* 1999; **67**: 337-341
- 9 **Michel T**, Feron O. Nitric oxide synthases: which, where, how, and why? *J Clin Invest* 1997; **100**: 2146-2152

- 10 **Dedio J**, Konig P, Wohlfart P, Schroeder C, Kummer W, Muller-Esterl W. NOSIP, a novel modulator of endothelial nitric oxide synthase activity. *FASEB J* 2001; **15**: 79-89
- 11 **Bogdan C**, Rollinghoff M, Diefenbach A. Reactive oxygen and reactive nitrogen intermediates in innate and specific immunity. *Curr Opin Immunol* 2000; **12**: 64-76
- 12 **Reiling N**, Kroncke R, Ulmer AJ, Gerdes J, Flad HD, Hauschildt S. Nitric oxide synthase: expression of the endothelial, Ca²⁺/calmodulin-dependent isoform in human B and T lymphocytes. *Eur J Immunol* 1996; **26**: 511-516
- 13 **MacMicking J**, Xie QW, Nathan C. Nitric oxide and macrophage function. *Annu Rev Immunol* 1997; **15**: 323-350
- 14 **Albina JE**, Abate JA, Henry WL Jr. Nitric oxide production is required for murine resident peritoneal macrophages to suppress mitogen-stimulated T cell proliferation. Role of IFN-gamma in the induction of the nitric oxide-synthesizing pathway. *J Immunol* 1991; **147**: 144-148
- 15 **Eisenstein TK**, Huang D, Meissler JJ Jr, al-Ramadi B. Macrophage nitric oxide mediates immunosuppression in infectious inflammation. *Immunobiology* 1994; **191**: 493-502
- 16 **Liew FY**. Regulation of lymphocyte functions by nitric oxide. *Curr Opin Immunol* 1995; **7**: 396-399
- 17 **van der Veen RC**. Nitric oxide and T helper cell immunity. *Int Immunopharmacol* 2001; **1**: 1491-1500
- 18 **Glockzin S**, von Knethen A, Scheffner M, Brune B. Activation of the cell death program by nitric oxide involves inhibition of the proteasome. *J Biol Chem* 1999; **274**: 19581-19586
- 19 **Coux O**, Tanaka K, Goldberg AL. Structure and functions of the 20S and 26S proteasomes. *Annu Rev Biochem* 1996; **65**: 801-847
- 20 **Tan C**, Mui A, Dedhar S. Integrin-linked kinase regulates inducible nitric oxide synthase and cyclooxygenase-2 expression in an NF- κ B-dependent manner. *J Biol Chem* 2002; **277**: 3109-3116
- 21 **Beck KF**, Walpen S, Eberhardt W, Pfeilschifter J. Downregulation of integrin-linked kinase mRNA expression by nitric oxide in rat glomerular mesangial cells. *Life Sci* 2001; **69**: 2945-2955
- 22 **Beg AA**, Baltimore D. An essential role for NF-kappaB in preventing TNF-alpha-induced cell death. *Science* 1996; **274**: 782-784
- 23 **Baeuerle PA**, Henkel T. Function and activation of NF-kappa B in the immune system. *Annu Rev Immunol* 1994; **12**: 141-179
- 24 **Attwell S**, Roskelley C, Dedhar S. The integrin-linked kinase (ILK) suppresses anoikis. *Oncogene* 2000; **19**: 3811-3815
- 25 **Rock KL**, Gramm C, Rothstein L, Clark K, Stein R, Dick L, Hwang D, Goldberg AL. Inhibitors of the proteasome block the degradation of most cell proteins and the generation of peptides presented on MHC class I molecules. *Cell* 1994; **78**: 761-771
- 26 **Brown MG**, Driscoll J, Monaco JJ. Structural and serological similarity of MHC-linked LMP and proteasome (multicatalytic proteinase) complexes. *Nature* 1991; **353**: 355-357
- 27 **Martinez CK**, Monaco JJ. Homology of proteasome subunits to a major histocompatibility complex-linked LMP gene. *Nature* 1991; **353**: 664-667
- 28 **Yang Y**, Waters JB, Fruh K, Peterson PA. Proteasomes are regulated by interferon gamma: implications for antigen processing. *Proc Natl Acad Sci U S A* 1992; **89**: 4928-4932
- 29 **Fruh K**, Yang Y, Arnold D, Chambers J, Wu L, Waters JB, Spies T, Peterson PA. Alternative exon usage and processing of the major histocompatibility complex-encoded proteasome subunits. *J Biol Chem* 1992; **267**: 22131-22140
- 30 **Leonard EJ**, Skeel A. A serum protein that stimulates macrophage movement, chemotaxis and spreading. *Exp Cell Res* 1976; **102**: 434-438
- 31 **Leonard EJ**, Skeel AH. Isolation of macrophage stimulating protein (MSP) from human serum. *Exp Cell Res* 1978; **114**: 117-126
- 32 **Wang MH**, Cox GW, Yoshimura T, Sheffler LA, Skeel A, Leonard EJ. Macrophage-stimulating protein inhibits induction of nitric oxide production by endotoxin- or cytokine-stimulated mouse macrophages. *J Biol Chem* 1994; **269**: 14027-14031
- 33 **Bek MJ**, Reinhardt HC, Fischer KG, Hirsch JR, Hupfer C, Dayal E, Pavenstadt H. Up-regulation of early growth response gene-1 via the CXCR3 receptor induces reactive oxygen species and inhibits Na⁺/K⁺-ATPase activity in an immortalized human proximal tubule cell line. *J Immunol* 2003; **170**: 931-940
- 34 **Otsuji M**, Kimura Y, Aoe T, Okamoto Y, Saito T. Oxidative stress by tumor-derived macrophages suppresses the expression of CD3 zeta chain of T-cell receptor complex and antigen-specific T-cell responses. *Proc Natl Acad Sci U S A* 1996; **93**: 13119-13124
- 35 **Kono K**, Salazar-Onfray F, Petersson M, Hansson J, Masucci G, Wasserman K, Nakazawa T, Anderson P, Kiessling R. Hydrogen peroxide secreted by tumor-derived macrophages down-modulates signal-transducing zeta molecules and inhibits tumor-specific T cell and natural killer cell-mediated cytotoxicity. *Eur J Immunol* 1996; **26**: 1308-1313
- 36 **Kono K**, Ichihara F, Iizuka H, Sekikawa T, Matsumoto Y. Expression of signal transducing T-cell receptor zeta molecules after adoptive immunotherapy in patients with gastric and colon cancer. *Int J Cancer* 1998; **78**: 301-305
- 37 **Takahashi A**, Kono K, Amemiya H, Iizuka H, Fujii H, Matsumoto Y. Elevated caspase-3 activity in peripheral blood T cells coexists with increased degree of T-cell apoptosis and down-regulation of TCR zeta molecules in patients with gastric cancer. *Clin Cancer Res* 2001; **7**: 74-80
- 38 **Hoek RM**, Ruuls SR, Murphy CA, Wright GJ, Goddard R, Zurawski SM, Blom B, Homola ME, Streit WJ, Brown MH, Barclay AN, Sedgwick JD. Down-regulation of the macrophage lineage through interaction with OX2 (CD200). *Science* 2000; **290**: 1768-1771
- 39 **Gorczynski L**, Chen Z, Hu J, Kai Y, Lei J, Ramakrishna V, Gorczynski RM. Evidence that an OX-2-positive cell can inhibit the stimulation of type 1 cytokine production by bone marrow-derived B7-1 (and B7-2)-positive dendritic cells. *J Immunol* 1999; **162**: 774-781
- 40 **Gorczynski RM**, Yu K, Clark D. Receptor engagement on cells expressing a ligand for the tolerance-inducing molecule OX2 induces an immunoregulatory population that inhibits alloreactivity *in vitro* and *in vivo*. *J Immunol* 2000; **165**: 4854-4860
- 41 **Gorczynski RM**, Chen Z, Hu J, Kai Y, Lei J. Evidence of a role for CD200 in regulation of immune rejection of leukaemic tumour cells in C57BL/6 mice. *Clin Exp Immunol* 2001; **126**: 220-229
- 42 **Gorczynski RM**, Cattral MS, Chen Z, Hu J, Lei J, Min WP, Yu G, Ni J. An immunoadhesin incorporating the molecule OX-2 is a potent immunosuppressant that prolongs allo- and xenograft survival. *J Immunol* 1999; **163**: 1654-1660
- 43 **Vigorito E**, Billadeu DD, Savoy D, McAdam S, Doody G, Fort P, Turner M. RhoG regulates gene expression and the actin cytoskeleton in lymphocytes. *Oncogene* 2003; **22**: 330-342
- 44 **Bustelo XR**. Regulatory and signaling properties of the Vav family. *Mol Cell Biol* 2000; **20**: 1461-1477
- 45 **Kaplan G**. Differences in the mode of phagocytosis with Fc and C3 receptors in macrophages. *Scand J Immunol* 1977; **6**: 797-807

Edited by Kumar M and Xu FM

• BRIEF REPORTS •

Effect of c-myc, Ki-67, MMP-2 and VEGF expression on prognosis of hepatocellular carcinoma patients undergoing tumor resection

Jun Cui, Bao-Wei Dong, Ping Liang, Xiao-Ling Yu, De-Jiang Yu

Jun Cui, Bao-Wei Dong, Ping Liang, Xiao-Ling Yu, De-Jiang Yu,
Department of Ultrasound, Chinese PLA General Hospital, Beijing
100853, China

Supported by the Medical and Health Science Foundation of PLA
during the 10th Five-year plan period, No.01Z038

Correspondence to: Dr. Jun Cui, Department of Gastroenterology,
Yu Huang Ding Hospital, Yantai, 264000, Shandong Province,
China. cuijun89@hotmail.com

Telephone: +86-535-7062606

Received: 2003-11-27 **Accepted:** 2003-12-16

Abstract

AIM: To explore the effect of c-myc, Ki-67, MMP-2 and VEGF expression on prognosis of hepatocellular carcinoma (HCC) patients undergoing tumor resection.

METHODS: Primary HCC patients underwent tumor resection were retrospectively analysed. The maximum size of the tumor was less than 5 cm, there was only one nodule in each patient. No chemoembolization was performed before resection. They were followed up after resection, and the time of recurrence was recorded. They were divided into 2 groups: group A (15 cases): tumor recurrence within 1 year after tumor resection, and group B (15 cases): with or without tumor recurrence 2 years after tumor resection. Pathological slices were made with tumor wax-sample. Immunohistochemistry staining was performed with c-myc, Ki-67, MMP-2 and VEGF monoclonal antibodies. Staining intensity was quantitatively analysed with a pathological diagram-writing analyzing system. The expressing intensity differences of stained molecules in cancer tissue and para-cancer were analysed.

RESULTS: c-myc, Ki-67, MMP-2 and VEGF expressing intensities in cancer tissue in group A were higher than those in group B (*P* values were 0.010, 0.030, 0.022 and 0.004, respectively), but they were not significantly different in para-cancer tissue in groups A and B (*P* values were 0.334, 0.343, 0.334 and 0.334, respectively).

CONCLUSION: The expression of c-myc, Ki-67, MMP-2 and VEGF in cancer tissue is related to the recurrence of HCC after tumor resection.

Cui J, Dong BW, Liang P, Yu XL, Yu DJ. Effect of c-myc, Ki-67, MMP-2 and VEGF expression on prognosis of hepatocellular carcinoma patients undergoing tumor resection. *World J Gastroenterol* 2004; 10(10): 1533-1536
<http://www.wjgnet.com/1007-9327/10/1533.asp>

INTRODUCTION

Recurrence is the main factor influencing prognosis of hepatocellular carcinoma (HCC) after tumor resection. The therapeutic measures for patients before and after operation are similar, but their prognosis after operation differs largely.

Some patients had tumor recurrence within 1 year after operation, while others had or did not have tumor recurrence 2 years after operation. The reason why there is such a difference is not clear. Researches on molecular biology have demonstrated that the prognosis of HCC is related to the activation of proto-oncogene, inactivation of tumor suppressor gene, abnormal expression of growth factors and/or their receptors^[1]. Four kinds of molecules related to biologic characteristics of HCC were studied in this experiment to clarify their relationship with recurrence of HCC after resection.

MATERIALS AND METHODS

Patients

Thirty primary HCC patients undergoing resection at Department of Hepatobiliary Surgery in General Hospital of PLA (301 Hospital) were retrospectively analysed. All resected samples were proved as HCC with pathologic examination. The selecting standards were as follows: solitary nodule with its maximum size less than 5 cm, no transarterial chemoembolization (TACE) or local thermal therapy (such as microwave coagulation or radiofrequency) before resection, no other specific treatment after resection. There were 28 males and 2 females. Their mean age was 51.5 (range, 27-75) years. The mean size of tumors was 3.0 cm. The patients were divided into two groups according to follow-up results: group A, which had tumor recurrence within 1 year after resection, group B, had or did not have tumor recurrence 2 years after resection. 15 cases were in group A (14 males and 1 female) and 15 cases in group B (14 males and 1 female). The differences of clinical data (sex, age, tumor size, liver function, serum AFP, transaminase, HBV infection) were not significant (Table 1).

Table 1 Clinical data of patients in groups A and B

Item	Group A (n=15)	Group B (n=15)
Sex	14 males, 1 female	14 males, 1 female
Age (yr)	54.7±14.3	48.2±8.4
Mean diameter (cm)	3.2±1.0	2.9±1.1
Tumor volume (cm ³)	22.0±21.4	18.2±17.6
Liver function	grade A	grade A
Serum AFP ^a (grade)	0.9±1.0	0.6±1.0
ALT (U/L)	58.0±54.1	64.9±56.6
AST (U/L)	49.9±46.8	42.0±37.7
HBV infection rate	87% (13/15)	100 (15/15)

^aserum AFP was graded as follows: 0: 0-200 µg/L, 1: 201-400 µg/L, 2: >400 µg/L.

Instrument and reagent

HPIAS-1000 high acuity color pathologic diagram-writing analyzing system (produced by Wuhan Champion Image Technology Corporation Limited). SP and DAB kit, monoclonal antibodies of c-myc, Ki-67, MMP-2 and VEGF were all purchased from Beijing Zhongshan Biological Technology Corporation Limited. The characteristics of antibodies are listed in Table 2.

Table 2 Characteristics of antibodies used in this study

Name of antibody	Specificity	Dilution	Secondary antibody
c-myc	Monoclonal Mouse anti human	1:50	Goat anti mouse
Ki-67	Monoclonal Mouse anti human	1:50	Goat anti mouse
MMP-2	Monoclonal Mouse anti human	1:50	Goat anti mouse
VEGF	Monoclonal Mouse anti human	1:50	Goat anti mouse

Immunohistochemistry staining

Serial 4 μ m thick sections were made with wax sample of resected tumors. Immunohistochemistry staining was performed with SP three-step method using the monoclonal antibodies listed in Table 2.

Quantitative analysis of positive cells

Quantitative analysis of the examined molecules was performed with HPIAS-1000 high acuity color pathologic diagram-writing analyzing system. Molecules in cancer and para-cancer tissues were analysed. Three fields of view (FOV) were randomly selected in cancer and para-cancer tissues to quantitatively analyse the expressing intensity. One hundred cells were observed in each FOV, positively stained cells were calculated, finally the average positively stained cells in 100 observed cells were determined. The cells were determined as positive-staining only if they were stained without considering their staining intensity. The medium optical density(MOD) of plasma or nuclei in positively stained cells was calculated with a pathologic diagram-writing analyzing system. The product of multiplication of average positively stained cells and MOD was calculated, which was considered as the expressing intensity of positively stained molecules.

Comparison of staining

The difference of expressing intensity of examined molecules in cancer and para-cancer tissues was compared in the same group (group A or B), the difference of expressing intensity in groups A and B was compared in the same tissue (cancer tissue or para-cancer tissue).

Statistical analysis

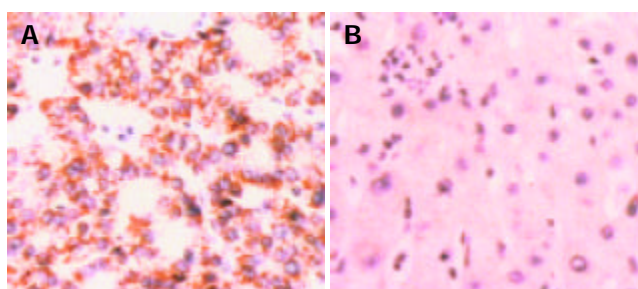
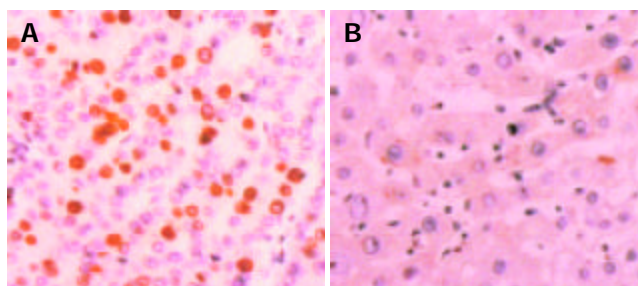
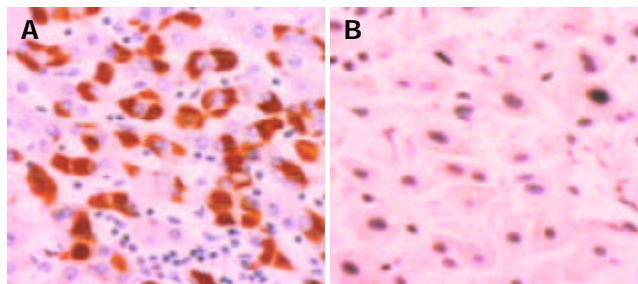
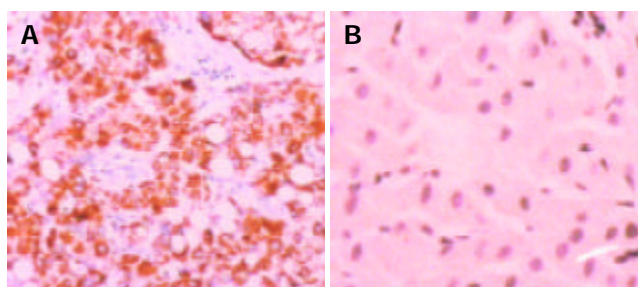
Data were presented as mean \pm SD. Paried-sample *t* test was used to compare the difference, the statistic software SPSS 10.0 was used. *P*<0.05 was considered statistically significant.

RESULTS

Expressing rate and intensity of examined molecules in cancer and para-cancer tissues in group A (Table 3)

Table 3 Expressing rate(%) and intensity of examined molecules in cancer and para-cancer tissues in group A

Item	Cancer tissue	Para-cancer tissue
c-myc	80 (12/15) ^b ; 3.95 \pm 2.81 ^b	0 (0/15); 0.00 \pm 0.00
Ki-67	60 (9/15) ^b ; 1.57 \pm 2.20	7 (1/15); 0.57 \pm 2.21
MMP-24	7 (7/15) ^a ; 3.70 \pm 4.13 ^a	7 (1/15); 0.80 \pm 3.10
VEGF	67 (10/15) ^b ; 5.44 \pm 4.20 ^b	7 (1/15); 0.04 \pm 0.15

^a*P*<0.05, ^b*P*<0.01 vs Para-cancer tissue.

Figure 1 Positive and negative c-myc, A: Positive c-myc; B: Negative c-myc.

Figure 2 Positive and negative Ki67, A: Positive Ki67; B: Negative Ki67.

Figure 3 Positive and negative MMP-2, A: Positive MMP-2; B: Negative MMP-2.

Figure 4 Positive and negative VEGF, A: Positive VEGF; B: Negative VEGF.

Expressing rate and intensity of examined molecules in cancer and para-cancer tissues in group B (Table 4)

Table 4 Expressing rate (%) and intensity of examined molecules in cancer and para-cancer tissues in group B

Item	Cancer tissue	Para-cancer tissue
c-myc	40 (6/15); 1.34 \pm 2.74	7 (1/15); 0.26 \pm 1.00
Ki-67	40 (6/15); 0.18 \pm 0.38	7 (1/15); 0.01 \pm 0.04
MMP-2	20 (3/15); 0.61 \pm 1.70	0 (0/15); 0.00 \pm 0.00
VEGF	27 (4/15); 1.04 \pm 3.38	0 (0/15); 0.00 \pm 0.00

Expressing rate and intensity of examined molecules in cancer tissues in groups A and B (Table 5)

Table 5 Expressing rate (%) and intensity of examined molecules in cancer tissues in groups A and B

Item	Group A	Group B
<i>c-myc</i>	80 (12/15); 3.95±2.81 ^b	40 (6/15); 1.34±2.74
Ki-67	60 (9/15); 1.57±2.20 ^a	40 (6/15); 0.18±0.38
MMP-2	47 (7/15); 3.70±4.13 ^a	20 (3/15); 0.61±1.70
VEGF	67 (10/15); 5.44±4.20 ^b	27 (4/15); 1.04±3.38

^a*P*<0.05, ^b*P*<0.01 vs Group B.

Expressing rate and intensity of examined molecules in para-cancer tissues in groups A and B (Table 6)

Table 6 Expressing rate (%) and intensity of examined molecules in para-cancer tissues in groups A and B

Item	Group A	Group B
<i>c-myc</i>	0 (0/15); 0.00±0.00	7 (1/15); 0.26±1.00
Ki-67	7 (1/15); 0.57±2.21	7 (1/15); 0.01±0.04
MMP-2	7 (1/15); 0.80±3.10	0 (0/15); 0.00±0.00
VEGF	7 (1/15); 0.04±0.15	0 (0/15); 0.00±0.00

Micrographs of *c-myc*, Ki-67, MMP-2 and VEGF

The micrographs of *c-myc*, Ki-67, MMP-2 and VEGF positive and negative expression were listed in figures 1-4.

DISCUSSION

Relationship of *c-myc* expression with prognosis of HCC

Activation of *c-myc* oncogene plays important role in cancer occurrence, gene location on chromosome of 8q24. *c-myc* oncogene can be activated through two ways. One is that it is confluent by light chain sequence of immunoglobulin through chromosomal translocation, the other is through DNA amplification. The protein coded by *c-myc* oncogene contains 439 amino acids, and can be combined specifically with intranuclear DNA to play transcription regulating function. *c-myc* oncogene is not expressed in the resting phase of cells, while it is rapidly expressed under the induction of mitoses, then it promotes cell proliferation and infiltration. It was reported in literature^[2] that HBV interpolation could promote amplification and over-expression of *c-myc* oncogene, then normal cellular genetic regulation was disturbed. Genetic mutation related with cancer occurrence could be induced through this mechanism, it was related with occurrence of HCC. *c-myc* oncogene codes phosphoric acid protein whose molecular weight is 62 KD. The protein is located in the nuclei of normal hepatocytes and HCC cells, as well as in plasm of some cells. It was demonstrated *in vitro* that the blockage of *c-myc* expression could suppress the growth of HCC cells^[3-5]. Some researchers demonstrated that the expression of *c-myc* in HCC tissue was related with the prognosis of HCC patients^[6]. Wang *et al.*^[7] reported that amplification of *c-myc* oncogene was correlated with a poor prognosis of HCC. Niu *et al.*^[8] reported that the positive expressing rate of *c-myc* in HCC was correlated with the histological differentiation, and was significantly higher in the poorly differentiated samples than in well differentiated samples. Zhang *et al.*^[9] reported that *c-myc* gene amplification was closely related to the development and progression of HCC. This study showed that *c-myc* expressing rate and intensity in cancer tissue in patients of group A were higher than those in para-cancer tissue, while the *c-myc* expressing rate and intensity in cancer tissue in patients of group B were not significantly

different from those in para-cancer tissue. *c-myc* expressing intensity in cancer tissue in patients of group A was higher than that in patients of group B. It demonstrated that the expression of *c-myc* in cancer tissue could reflect the malignancy of HCC. HCC with high *c-myc* expression in cancer tissue had a high recurrence rate. *c-myc* expressing rates in cancer tissue in the two groups of patients were significantly different, suggesting that *c-myc* over-expression occurs in HCC, its expressing intensity is related to the prognosis of HCC.

Relationship of Ki-67 expression with prognosis of HCC

Tumor cells consist of proliferating cells (S, G2, M, G1 stage), temporarily non-proliferating cells (G0) and non-proliferating cells. Ki-67 can label proliferating cells in any stage except those in stage G0, while it is not expressed in cells in silent stage. Ki-67 is rapidly degraded or its antigenic determinant is disappeared after mitosis. So Ki-67 is considered as a kind of objective marker reflecting proliferating activity of cells. Ki-67 is located in cell nuclei, and always in particle shape in immunohistochemistry staining. Ki-67 labelling index has been considered as a marker of cellular proliferative activity, the higher the Ki-67 labelling index, the lower the cellular differentiation and the poorer the prognosis of HCC^[10-16]. It was demonstrated in this study that Ki-67 expressing rate in cancer tissue in group A was higher than that in para-cancer tissue, while the expressing intensity was not significantly different. Ki-67 expressing rate and intensity in cancer tissue in group B were not significantly different from those in para-cancer tissue. Ki-67 expressing intensity in cancer tissue in group A was much higher than that in group B, suggesting that Ki-67 expression could reflex malignancy of HCC. HCC with a high Ki-67 expression had a high recurrence rate. Ki-67 expressing rate in cancer tissue of the two groups was not significantly different, suggesting that Ki-67 is abnormally expressed in HCC, its expressing intensity is related to the prognosis of HCC.

Relationship of MMP-2 expression with prognosis of HCC

A main step of invasion and metastasis of malignant tumor is to degrade extracellular matrix (ECM) and basement membrane. There are much collagen IV in ECM and basement membrane, collagen IV is very important for maintaining the integrity of ECM and basement membrane. Collagenase IV could degrade collagen IV and destroy the integrity of basement membrane. Matrix metalloproteinase II (MMP-2) is a kind of collagenase IV, its expression is related to tumor recurrence and metastasis. Positive particles of MMP-2 are located in cell plasm. Some researchers reported that MMP-2 expression in cancer tissue was related with prognosis of HCC, HCC with high MMP-2 expression had high malignancy, easy recurrence and metastasis^[17-23]. This study showed that MMP-2 expressing rate and intensity in cancer tissue in group A were higher than those in para-cancer tissue, MMP-2 expressing rate and intensity in cancer tissue in group B were not significantly different from those in para-cancer tissue. MMP-2 expressing intensity in cancer tissue in group A was much higher than that in group B, suggesting that MMP-2 expression could reflex malignancy of HCC. HCC with a high MMP-2 expression had a high recurrence rate. MMP-2 expressing rate in cancer tissue of the two groups was not significantly different, suggesting that MMP-2 is abnormally expressed in HCC, its expressing intensity is related to the prognosis of HCC.

Relationship of VEGF expression with prognosis of HCC

Vascularization is an important link in tumor growth, invasion and metastasis. Tumor blood vessels not only provide nutrition needed for tumor growth, but also provide pathways for spreading tumor cells. Vascular endothelial growth factor (VEGF) could promote cell proliferation and vascularization, and is

closely related to growth, invasion and metastasis of HCC. Expression of VEGF in HCC tissue is positively correlated with growth and metastasis of HCC, it could be a marker for determining the prognosis of HCC. Positive particles of VEGF are located in plasm of tumor cells. Some researchers reported that HCC patients with high VEGF expression had poor prognosis^[24-28]. This study showed that VEGF expressing rate and intensity in cancer tissue in group A were higher than those in para-cancer tissue, VEGF expressing rate and intensity in cancer tissue in group B were not significantly different from those in para-cancer tissue. VEGF expressing intensity in cancer tissue in group A was much higher than that in group B, suggesting that VEGF expression could reflex malignancy of HCC. HCC with a high VEGF expression had a high recurrence rate. VEGF expressing rate in cancer tissue of the two groups was not significantly different, suggesting that VEGF is abnormally expressed in HCC, its expressing intensity is related to the prognosis of HCC.

Clinical value of this study

Ultrasound guided biopsy becomes a kind of mature diagnostic technique for HCC. It was shown in this study that characters of HCC with recurrence within 1 year after tumor resection were *c-myc*, Ki-67, MMP-2 and VEGF high expression in cancer tissue. If prognosis of HCC patients could be determined through quantitative analysis of biopsied tissue stained with immunohistochemistry before treatment, then theoretical fundamentals for HCC patients to select therapy method could be provided.

REFERENCES

- 1 **Qin LX**, Tang ZY. The prognostic molecular markers in hepatocellular carcinoma. *World J Gastroenterol* 2002; **8**: 385-392
- 2 **Wu CG**, Salvay DM, Forgues M, Valerie K, Farnsworth J, Markin RS, Wang XW. Distinctive gene expression profiles associated with Hepatitis B virus x protein. *Oncogene* 2001; **20**: 3674-3682
- 3 **Cheng J**, Luo J, Zhang X, Hu J, Hui H, Wang C, Stern A. Inhibition of cell proliferation in HCC-9204 hepatoma cells by a *c-myc* specific ribozyme. *Cancer Gene Ther* 2000; **7**: 407-412
- 4 **Zhang H**, Lin C, Shao Y. Experimental therapy of adenovirus-transferred antisense *c-myc* on hepatocellular cancer cell. *Zhonghua Yixue Zazhi* 2001; **81**: 673-676
- 5 **Ebinuma H**, Saito H, Kosuga M, Wakabayashi K, Saito Y, Takagi T, Nakamoto N, Okuyama T, Ishii H. Reduction of *c-myc* expression by an antisense approach under Cre/loxP switching induces apoptosis in human liver cancer cells. *J Cell Physiol* 2001; **188**: 56-66
- 6 **Fang Y**, Huang B, Liang Q, Li H, Huang C. Clinical significance of *c-myc* oncogene amplification in primary hepatocellular carcinoma by interphase fluorescence *in situ* hybridization. *Zhonghua Binglixue Zazhi* 2001; **30**: 180-182
- 7 **Wang Y**, Wu MC, Sham JS, Zhang W, Wu WQ, Guan XY. Prognostic significance of *c-myc* and AIB1 amplification in hepatocellular carcinoma. A broad survey using high-throughput tissue microarray. *Cancer* 2002; **95**: 2346-2352
- 8 **Niu ZS**, Li BK, Wang M. Expression of p53 and *C-myc* genes and its clinical relevance in the hepatocellular carcinomatous and pericarcinomatous tissues. *World J Gastroenterol* 2002; **8**: 822-826
- 9 **Zhang J**, Wang K, Cong S, Qiu F, Wang X, Wang P. Correlation of *c-myc* gene amplification, MTS1/p16 gene alternation, and HBV infection in human hepatocellular carcinoma. *Zhonghua Ganzhangbing Zazhi* 2001; **9**: 294-296
- 10 **Schmitt-Graff A**, Ertelt V, Allgaier HP, Koelble K, Olschewski M, Nitschke R, Bochaton-Piallat ML, Gabbiani G, Blum HE. Cellular retinol-binding protein-1 in hepatocellular carcinoma correlates with beta-catenin, Ki-67 index, and patient survival. *Hepatology* 2003; **38**: 470-480
- 11 **Aoki T**, Inoue S, Imamura H, Fukushima J, Takahashi S, Urano T, Hasegawa K, Ogushi T, Ouchi Y, Makuuchi M. EBAG9/RCAS1 expression in hepatocellular carcinoma: correlation with tumour dedifferentiation and proliferation. *Eur J Cancer* 2003; **39**: 1552-1561
- 12 **Daveau M**, Scotte M, Francois A, Coulouarn C, Ros G, Tallet Y, Hiron M, Hellot MF, Salier JP. Hepatocyte growth factor, transforming growth factor alpha, and their receptors as combined markers of prognosis in hepatocellular carcinoma. *Mol Carcinog* 2003; **36**: 130-141
- 13 **Shirahashi H**, Sakaida I, Terai S, Hironaka K, Kusano N, Okita K. Ubiquitin is a possible new predictive marker for the recurrence of human hepatocellular carcinoma. *Liver* 2002; **22**: 413-418
- 14 **Tamano M**, Sugaya H, Oguma M, Iijima M, Yoneda M, Murohisa T, Kojima K, Kuniyoshi T, Majima Y, Hashimoto T, Terano A. Serum and tissue PIVKA-II expression reflect the biological malignant potential of small hepatocellular carcinoma. *Hepatol Res* 2002; **22**: 261-269
- 15 **Inagawa S**, Itabashi M, Adachi S, Kawamoto T, Hori M, Shimazaki J, Yoshimi F, Fukao K. Expression and prognostic roles of beta-catenin in hepatocellular carcinoma: correlation with tumor progression and postoperative survival. *Clin Cancer Res* 2002; **8**: 450-456
- 16 **Ito Y**, Takeda T, Sakon M, Monden M, Tsujimoto M, Matsuura N. Expression and prognostic role of cyclin-dependent kinase 1 (*cdc2*) in hepatocellular carcinoma. *Oncology* 2000; **59**: 68-74
- 17 **Ishii Y**, Nakasato Y, Kobayashi S, Yamazaki Y, Aoki T. A study on angiogenesis-related matrix metalloproteinase networks in primary hepatocellular carcinoma. *J Exp Clin Cancer Res* 2003; **22**: 461-470
- 18 **Liu Z**, Yan L, Xiang T, Jiang L, Yang B. Expression of vascular endothelial growth factor and matrix metalloproteinase-2 correlates with the invasion and metastasis of hepatocellular carcinoma. *Shengwu Yixue Gongchengxue Zazhi* 2003; **20**: 249-250
- 19 **McKenna GJ**, Chen Y, Smith RM, Meneghetti A, Ong C, McMaster R, Scudamore CH, Chung SW. A role for matrix metalloproteinases and tumor host interaction in hepatocellular carcinomas. *Am J Surg* 2002; **183**: 588-594
- 20 **Giannelli G**, Bergamini C, Marinosci F, Fransvea E, Quaranta M, Lupo L, Schiraldi O, Antonaci S. Clinical role of MMP-2/TIMP-2 imbalance in hepatocellular carcinoma. *Int J Cancer* 2002; **97**: 425-431
- 21 **Niu Q**, Tang Z, Ma Z, Qin L, Bao W, Zhang L. Relationship between serum matrix metalloproteinase-2 and metastasis and recurrence following radical hepatic resection in hepatocellular carcinoma. *Zhonghua Ganzhangbing Zazhi* 2001; **9**(Suppl): 58-60
- 22 **Sawada S**, Murakami K, Murata J, Tsukada K, Saiki I. Accumulation of extracellular matrix in the liver induces high metastatic potential of hepatocellular carcinoma to the lung. *Int J Oncol* 2001; **19**: 65-70
- 23 **Maatta M**, Soini Y, Liakka A, Autio-Harmainen H. Differential expression of matrix metalloproteinase (MMP)-2, MMP-9, and membrane type 1-MMP in hepatocellular and pancreatic adenocarcinoma: implications for tumor progression and clinical prognosis. *Clin Cancer Res* 2000; **6**: 2726-2734
- 24 **Xiong ZP**, Yang SR, Xiao EH, Zhou SK, Zhang ZS, Liang ZY. Relation between vascular endothelial growth factor and reoccurrence-metastasis after transcatheter arterial chemoembolization in hepatocellular carcinoma. *Zhonghua Zhongliu Zazhi* 2003; **25**: 562-565
- 25 **Zhao ZC**, Zheng SS, Wan YL, Jia CK, Xie HY. The molecular mechanism underlying angiogenesis in hepatocellular carcinoma: the imbalance activation of signaling pathways. *Hepatobiliary Pancreat Dis Int* 2003; **2**: 529-536
- 26 **Zhao J**, Hu J, Cai J, Yang X, Yang Z. Vascular endothelial growth factor expression in serum of patients with hepatocellular carcinoma. *Chin Med J* 2003; **116**: 772-776
- 27 **Moon WS**, Rhyu KH, Kang MJ, Lee DG, Yu HC, Yeum JH, Koh GY, Tarnawski AS. Overexpression of VEGF and angiopoietin 2: a key to high vascularity of hepatocellular carcinoma? *Mod Pathol* 2003; **16**: 552-557
- 28 **Chao Y**, Li CP, Chau GY, Chen CP, King KL, Lui WY, Yen SH, Chang FY, Chan WK, Lee SD. Prognostic significance of vascular endothelial growth factor, basic fibroblast growth factor, and angiogenin in patients with resectable hepatocellular carcinoma after surgery. *Ann Surg Oncol* 2003; **10**: 355-362

Effects of bile reflux and intragastric microflora changes on lesions of remnant gastric mucosa after gastric operation

Chao Zhang, Zhan-Kui Liu, Pei-Wu Yu

Chao Zhang, Zhan-Kui Liu, Pei-Wu Yu, Department of General Surgery, Southwest Hospital, Third Military Medical University, Gaotan Yan, Chongqing 400038, China

Correspondence to: Professor, Dr. Chao Zhang, M.D., Department of General Surgery, Southwest Hospital, Third Military Medical University, Gaotan Yan, Chongqing 400038, China. meizhang6688@yahoo.com
Telephone: +86-23-68773074

Received: 2003-06-06 **Accepted:** 2003-10-22

Abstract

AIM: To investigate the effects of bile reflux and intragastric microflora changes on lesions of remnant gastric mucosa after gastric operation.

METHODS: Concentration of bile acid and total bacterial counts (TBC) in gastric juice were measured in 49 patients with peptic ulcer before and after gastrectomy. One year after the operation, sample of gastric mucosa taken from all the patients were used for histological examination.

RESULTS: The concentration of gastric bile acid was significantly increased in group B-I, or B-II and SV+A than that in group HSV ($P < 0.05-0.01$). The abnormal histological changes in the remnant gastric mucosa were more common in the first 2 groups than in the last group.

CONCLUSION: The type of gastrectomy can affect bile reflux. The abnormal histological changes in the remnant gastric mucosa are closely related to the elevation of bile acid concentration and increase of TBC in gastric juice. HSV can effectively prevent bile reflux and keep the gastric physiological functions stable.

Zhang C, Liu ZK, Yu PW. Effects of bile reflux and intragastric microflora changes on lesions of remnant gastric mucosa after gastric operation. *World J Gastroenterol* 2004; 10 (10): 1537-1539

<http://www.wjgnet.com/1007-9327/10/1537.asp>

INTRODUCTION

Bile reflux was usually found after routine operation in the treatment of peptic ulcer, and for some patients, it could be found very serious complications, such as epigastric causalgia, obstinate bilious vomiting, body mass descent and so on, its incidence is 5-35%^[1-4]. Forty-nine patients with gastric resection in treating peptic ulcer were observed in order to investigate the effects of bile reflux and intragastric microflora changes on lesions of remnant gastric mucosa after gastrectomy gastric resection.

MATERIALS AND METHODS

A total of 49 patients with peptic ulcer (32 male, 17 female, average age 44.3 years) including 14 patients with gastric ulcer, 28 patients with duodenal ulcer and 7 patients with compound

ulcer were investigated in a retrospective manner. These patients were divided into 4 groups according to the operation kind: 10 patients with Billroth I (B-I), 14 patients with Billroth II (B-II), 12 patients with selected vagotomy plus antrectomy (SV+A), 13 patients with High selected vagotomy (HSV).

Gastric juice on an empty stomach was been extracted at 3-5 d pre-operation, 7 d post-operation, 3 wk and 1 year post-operation, the bile acid concentration was measured by radio-immunity analysis (RIA), obtained from Wuzhou Institute of Isotope.

A 0.5 mL gastric juice plus 5 mL broth was put into sterilization test tube and cultured at 37 °C for 24-48 h, it was defined sterile growth if it had no bacteria growth through observation of 48 h, if bacteria were found, it were separated and evaluated by means of platinum loop.

For pro-operation annual patients, 2 samples of gastric mucosa were fixed by formaldehyde solution, then were observed through light microscope. Diagnosis of gastric ulcer was based on the detection standard of gastric mucosal disease formulated by gastric cancer co-operation group in 1981. The result was indicated by count scores as follow: the normal gastric mucosa was equal to 0; slight-degree, medium-degree, and sever-degree superficial gastritis were 1, 2, and 3; slight -degree, medium-degree, and sever-degree atrophic gastritis were 4, 5, and 6; if gastritis plused slight-degree, medium-degree and severe-degree intestinal metaplasia, the scores would be plus 1, 2, 3.

RESULTS

Bile acid concentration at post-operation 3 wk and 1 year was significantly increased than that at pre-operation in group B-II ($P < 0.05$), and is the same in group B-I ($P < 0.05$) and in group SV+V ($P < 0.05$); Bile acid concentration at post-operation was slight increased ($P > 0.05$). From post-operation 3 wk, bile acid concentration in B-II, B-I and group SV+V were significantly increased than that in group HSV, especially in group B-II (Table 1).

After operation, total bacterial count of gastric juice in group B-II, B-I and group SV+V were significantly increased than that in group HSV ($P < 0.05-0.01$). In this study, 204 samples of gastric juice were cultivated, 88 samples were found bacteria growing in 92 samples that pH was > 4.0 and the count of bacteria will be more along the higher of pH ($r = 0.784$, $P < 0.01$). Gram-Negative bacillus were always found after operation, and associated with the level of bile reflux. The rate of finding Gram-Negative bacillus was 64.1% in group B-II, 25.81% in group B-I, 29.62% in SV+A, and 10.25% in group HSV and significantly lower than that in 3 groups ($P < 0.01$, $P < 0.05$, $P < 0.05$). *Escherichia coli* and *Bacillus proteus* were common in group B-II, B-I and group SV+V, but, *Streptococcus* and *Lactobacillus* were common in group HSV.

During 1 year after operation, the incidence of atrophic gastritis was 35.7% in group B-II, 30% in group B-I, 33.3% in SV+A, 15.4% in group HSV. The incidence of Intestinal metaplasia was 28.6% in group B-II, 20% in group B-I, 25% in SV+A, 7.8% in group HSV. It was found by statistics analysis that the degree of change of gastric remnant

Table 1 Changes of bile acid concentration of gastric juice in different group($C_B/\text{nmol} \cdot \text{mL}^{-1}$, mean \pm SD)

Group	n	Pre-operation	Post-operation		
			1 wk	3 wk	1 yr
B-I	14	21.15 \pm 9.36	36.50 \pm 25.27	76.60 \pm 48.38 ^b	59.75 \pm 29.80 ^b
B-II	10	22.17 \pm 7.74	45.13 \pm 19.08 ^a	52.98 \pm 25.04 ^a	43.79 \pm 9.89 ^b
SV+A	12	22.43 \pm 10.15	39.04 \pm 18.72	54.84 \pm 27.49 ^a	46.33 \pm 14.52 ^b
HSV	13	23.54 \pm 11.56	30.12 \pm 17.24	28.02 \pm 16.18	27.68 \pm 15.44

^a $P < 0.05$, ^b $P < 0.01$ vs HSV.**Table 2** Changes of total bacterial count of gastric juice in different groups (log10/mL, mean \pm SD)

Group	n	Pre-operation	Post-operation		
			1 wk	3 wk	1 yr
B-II	14	1.27 \pm 2.14	3.83 \pm 2.09 ^a	4.86 \pm 0.38 ^b	3.97 \pm 1.97 ^b
B-I	10	1.77 \pm 2.35	4.30 \pm 1.64 ^a	4.33 \pm 1.55 ^a	3.82 \pm 1.99 ^b
SV+A	12	1.84 \pm 2.27	3.90 \pm 1.79 ^a	4.13 \pm 1.68 ^a	3.85 \pm 2.04 ^b
HSV	13	1.26 \pm 2.07	2.41 \pm 2.35	2.59 \pm 2.78	1.56 \pm 2.13

^a $P < 0.05$, ^b $P < 0.01$ vs HSV.**Table 3** Results of histological examination of remnant gastric mucosa 1 year after operation

Group	n	Normal	Superficial gastric	Atrophic gastritis			Intestinal metaplasia		
				Slight	Medium	Severe	Slight	Medium	Severe
B-II	14	0	9	2	2	1	1	1	2
B-I	10	0	7	2	1	0	1	0	1
SV+A	12	0	8	1	1	1	1	1	1
HSV	13	0	10	1	1	0	1	0	0

histological abnormality alteration in group B-II, B-I and group SV+V was significantly higher than that in group HSV (t values separately were 2.047, 2.025, 2.029, $P < 0.05$), and the change of gastric remnant histological abnormality alteration associated with increasing of concentration of gastric juice cholic acid.

DISCUSSION

Bile reflux was common in gastric post-operation and the mod of operation could affect the degree of bile reflux, generally speaking, it was slight after high selected vagotomy, it was severe after gastrectomy, and it was very common in Billroth II^[1]. In our study, the concentration of gastric juice cholic acid was significantly increased in group B-II, it was higher in group B-I and group SV+V than that in group HSV. There was no significant difference between pre-operation and post-operation in group HSV although it was slight higher after operation, so it suggested that HSV could reduce bile reflux. Traditional gastrectomy and SV+A destructed the normal gastric dissection and deleted the function of Pyloric and innervation, these factors resulted in gastric emptying disorder and dodecadactylon increased reversed peristalsis, so bile reflux was increased and it could lead to the lesion of gastric mucosa. HSV remained the Pyloric dissection and innervation, it maintained the usual diet passage, and the function of Pyloric is normal, so it could prevent intestines and stomach reflux^[2].

Alkaline reflux gastritis was a complex complication after gastric operation, and its mechanism is not yet fully understood. We think when mod of operation was selected, we should excerpt the mod in coincidence to normal physiology function and based on the patient's specific situation in order to reduce the complication.

The effect of bile reflux on total bacterial count and the

changes of remnant gastric mucosa histological Current concepts suggest that gastric acid possesses strongly germicidal effect, the count of bacteria of gastric acid was only $10^5/\text{mL}$, and the denomination of bacteria was similar to that in buccal cavity. Oxyntic cell was deleted or its innervation was broken after gastric operation, so the ability of stomach excreting acid was decreased, the data of pH were creasing, if the small intestinal juice including bile reflux to stomach, the data of pH would be more increased. These factors are advantageous to bacteria growth and breeding, resulted in intragastric bacterial over-growth (IBO), the flora in Lower digestive tract (especially Gram-Negative bacillus and Anaerobe) could reflux to stomach and reproduced here^[5-10]. Because of these bacteria, the conjugate cholic acid changed to free cholic acid which has a strongly toxic effect, and the following could damaged the integrity of gastric mucosa, certain cationic permeability could increased, such as H^+ could contra-direction diffuse, and these changes can resulted in Mast cell releasing histamine and 5-serotonin, so it could be found capillary telangiectasia, mucosa hyperemia, edema, bleeding, and superficial Ulceration^[11,12].

In our study, the concentration of cholic acid in gastric juice was higher, the bacterial count of gastric juice was more, and the denomination of flora in intestinal tract was more. Pathological examination found that flaming cell infiltration, atrophic gastritis, and intestinal metaplasia, all these could indicate that the abnormal histological changes of gastric mucosa associated with the increasing concentration of cholic acid in gastric juice and increasing total bacterial count of gastric juice.

The role of dodecadactylon regurgitation resulting in gastric mucosa precancerous lesion and gastric cancer was though highly, Houghton *et al.* found that follicle cell and DNA count was increased if rat was raised by carcinogens (MNNG) and

at the same time reinforced regurgitation from dodecadactylon to stomach, so the ratio of gastric carcinoma was significantly increased. Freeing cholalic acid was confirmed as carcinogen, it could result in stomach carcinoma if it was higher in a long term^[13-17]. For patients with higher concentration of cholalic acid in gastric juice, intragastric bacterial over-growth (IBO), and pathological examination finding abnormal changes, should be thought highly of the occurrence of stomach carcinoma.

REFERENCES

- 1 **Madura JA**. Primary bile reflux gastritis: which treatment is better, Roux-en-Y or biliary diversion? *Am Surg* 2000; **66**: 417-423
- 2 **Barrett MW**, Myers JC, Watson DI, Jamieson GG. Detection of bile reflux: *in vivo* validation of the Bilitec fibreoptic system. *Dis Esophagus* 2000; **13**: 44-50
- 3 **Menges M**, Muller M, Zeitz M. Increased acid and bile reflux in Barrett's esophagus compared to reflux esophagitis, and effect of proton pump inhibitor therapy. *Am J Gastroenterol* 2001; **96**: 331-337
- 4 **Dixon MF**, Neville PM, Mapstone NP, Moayyedi P, Axon AT. Bile reflux gastritis and Barrett's oesophagus: further evidence of a role for duodenogastro-oesophageal reflux? *Gut* 2001; **49**: 359-363
- 5 **Johnnesson KA**, Hammar E, Stael von Holstein C. Mucosal changes in the gastric remnant: long-term effects of bile reflux diversion and *Helicobacter pylori* infection. *Eur J Gastroenterol Hepatol* 2003; **15**: 35-40
- 6 **Sundbom M**, Hedenstrom H, Gustavsson S. Duodenogastric bile reflux after gastric bypass: a cholescintigraphic study. *Dig Dis Sci* 2002; **47**: 1891-1896
- 7 **Dixon MF**, Mapstone NP, Neville PM, Moayyedi P, Axon AT. Bile reflux gastritis and intestinal metaplasia at the cardia. *Gut* 2002; **51**: 351-355
- 8 **Talley NJ**, Abeygunasekera S. Bile reflux and Barrett's oesophagus: innocent bystander or sinister companion? *Dig Liver Dis* 2002; **34**: 246-248
- 9 **Konturek PC**, Brzozowski T, Kania J, Konturek SJ, Hahn EG. Nitric oxide-releasing aspirin protects gastric mucosa against ethanol damage in rats with functional ablation of sensory nerves. *Inflamm Res* 2003; **52**: 359-365
- 10 **Zhou L**, Sung JJ, Lin S, Jin Z, Ding S, Huang X, Xia Z, Guo H, Liu J, Chao W. A five-year follow-up study on the pathological changes of gastric mucosa after *H pylori* eradication. *Chin Med J* 2003; **116**: 11-14
- 11 **Penagini R**. Bile reflux and oesophagitis. *Eur J Gastroenterol Hepatol* 2001; **13**: 1-3
- 12 **Blackstone M**. Pancreatitis from bile reflux-again? *Gastroenterology* 2003; **124**: 863-864
- 13 **Shi X**, Zhao F, Dai X, Dong X, Fang J, Yang H. Effects of san qi on gastric secretion and protective factors of gastric mucosa in the rat with precancerous lesion of stomach. *J Tradit Chin Med* 2003; **23**: 220-224
- 14 **Qiu GB**, Gong LG, Hao DM, Zhen ZH, Sun KL. Expression of MTLN gene in gastric carcinoma. *World J Gastroenterol* 2003; **9**: 2160-2163
- 15 **Chen BQ**, Yang YM, Gao YH, Liu JR, Xue YB, Wang XL, Zheng YM, Zhang JS, Liu RH. Inhibitory effects of c9, t11-conjugated linoleic acid on invasion of human gastric carcinoma cell line SGC-7901. *World J Gastroenterol* 2003; **9**: 1909-1914
- 16 **Du JJ**, Dou KF, Peng SY, Xiao HS, Wang WZ, Guan WX, Wang ZH, Gao ZQ, Liu YB. cDNA suppression subtraction library for screening down-regulated genes in gastric carcinoma. *World J Gastroenterol* 2003; **9**: 1439-1443
- 17 **Zhu XD**, Lin GJ, Qian LP, Chen ZQ. Expression of survivin in human gastric carcinoma and gastric carcinoma model of rats. *World J Gastroenterol* 2003; **9**: 1435-1438

Edited by Chen WW and Wang XL Proofread by Xu FM